YB-1 oncoprotein in cancer and drug resistance

Michael Algie

a thesis submitted for the degree of

Doctor of Philosophy

at the University of Otago, Dunedin,

New Zealand

March 2018

Abstract

Y-box-binding protein 1 (YB-1) is a biomarker that is predictive of poor prognosis in cancer. Various molecular functions of YB-1 in cancer have been proposed, including the transcriptional regulation of gene expression. YB-1 also binds to RNA transcripts to influence gene expression.

In the present study, the status of YB-1 as a biomarker was confirmed by immunohistochemistry using two antibodies against YB-1. However, the prognostic sensitivity of these two antibodies differed. The observed difference in antibody affinity was most likely due to the tertiary structure or protein-protein interactions (PPI) associated with various functions of YB-1 *in situ*.

To gain further insights into the molecular functions and potential mechanisms of YB-1 in cancer biology the state of phosphorylation of YB-1 and the PPI were investigated in the cytoplasm and nucleus of two cancer cell lines. The YB-1 from the cytoplasm and nucleus of the cell lines was extensively phosphorylated. These experiments identified >250 proteins. These binding partners confirmed the multifunctionality of YB-1 as the proteins that co-purify with YB-1 participate in glycolysis, RNA splicing, RNA stabilization, translation, mitochondrial localisation, and chromosomal association. These data suggest that the bulk of YB-1 function may be explained by non-transcriptional mechanisms.

Mechanisms of drug resistance were also investigated. Depleting YB-1, using siRNA duplexes, reduced MDA-MB231 cell growth and increased cell death. The loss of YB-1 sensitised MDA-MB231 cells to cisplatin exposure by increasing cell death. Cisplatin exposure altered the distribution of YB-1 protein to perinuclear spots and to foci in the nucleus of many cells.

The molecular basis of YB-1 mediated cisplatin resistance was analysed by examining the alterations of YB-1 PPI during cisplatin exposure using co-immunoprecipitation of YB-1 binding partners and mass spectrometry-based protein identification. Quantitative analyses of the co-immunoprecipitated proteins from MDA-MB231 cells indicated that a subset of the proteins, such as TRIM28 and FAM120A, increased markedly after 48 and 96 hours of cisplatin exposure. The chromosomal proteins that interacted with YB-1 were disproportionately affected by cisplatin exposure.

The importance of FAM120A, TRIM28, and C1QBP, three YB-1 binding partners identified here, during cisplatin exposure was studied. The subcellular distribution of FAM120A was most similar that of YB-1 in MDA-MB231 cells. Depleting

YB-1 or FAM120A, but not TRIM28 or C1QBP, sensitised MDA-MB231 cells to cisplatin exposure. Depleting YB-1 alongside either FAM120A or C1QBP partially restored the growth of MDA-MB231 cells. YB-1 does not appear to participate in the repair of double-strand DNA breaks during cisplatin exposure as depleting YB-1 had no effect on the number of γH2AX foci that formed during cisplatin exposure.

This is the first report that integrates findings of protein-binding partners, state of phosphorylation, and subcellular localisation of endogenous YB-1 to understand the complex functions of YB-1. These results confirm the importance of RNA binding to the molecular function of YB-1. The interaction of YB-1 with FAM120A, a novel finding, increases during cisplatin exposure and both proteins together, via an unknown molecular pathway, confer cisplatin resistance to breast cancer cells.

Declaration

I declare that the immunohistochemistry presented in Figure 3.2, 3.3, and 3.4 was performed and analysed by Dr Adele Woolley.
I performed all other work that is presented herein.

Michael Algie

Acknowledgements

I would like to thank my supervisors, Professor Antony Braithwaite, Dr Adele Woolley, and Dr Torsten Kelffmann for their guidance, advice, and support during my studies. I would like to extend a special thank you to Torsten for generously sharing his knowledge of mass spectrometry. Learning to use the machines has been an absolute highlight of my PhD studies.

I am very grateful for the help I have received from the administrative staff in the Department of Pathology. Also, a big thanks to the other staff in the department and my friends and colleagues in the lab. A particular thanks needs to go to Igor Ruza who provided a lot of the levity that makes working in laboratories enjoyable.

Thank you to all my friends and family for their fantastic support over the last few years. I am lucky to be surrounded by such wonderful people who can distract me when I need it.

I would like to say how grateful I am for the ongoing support from my wife Louie and our three amazing boys, Matt, Toby, and Ned. As well as being a patient proofreader, Louie has gone above and beyond to ensure our household has remained a happy and joyful one. The arrival of Toby and Ned during my PhD has been a great gift and I thank Louie for agreeing that it was the right time for them to arrive.

These boys have provided plenty of laughs and hugs. Finally, a big thanks to Matt who has shown great patience, a positive attitude, and an inspiring curiosity in addition to being great company as we walk to school each morning.

Contents

List of Figures

List of Tables

Glossary

β-actin . . . . . β-actin

γH2AX . . . . . Histone H2AX phosphorylated on S140

4E-BP . . . . . eukaryotic translation initiation factor 4E-binding protein

ABCB1 . . . . . ATP-binding cassette, sub-family B [MDR/-TAP], member 1 (also known as multidrug resistance gene 1/MDR1)

AKT . . . . . RAC-alpha serine/threonine-protein kinase

ALYREF . . . . . THO complex subunit 4

AP2A . . . . . Transcription factor AP-2-alpha

APE1 . . . . . apurinic/apyrimidinic (AP) endonuclease 1

BAX . . . . . BCL2 associated X, apoptosis regulator

BN-PAGE . . . . . blue-native PAGE

BRCA1 . . . . . Breast cancer type 1 susceptibility protein

BSA . . . . . bovine serum albumin

C1QBP . . . . . Complement component 1 Q subcomponent-binding protein, mitochondria

CCL5 . . . . . CC motif chemokine 5 [also known as regulated upon activation, normal T cell expressed and secreted [RANTES]]

CCND1 . . . . . cyclin D1

CD95 . . . . . Tumor necrosis factor receptor superfamily member 6 [also known as the fas receptor]

CSD . . . . . cold-shock domain

DAVID . . . . . Database for Annotation, Visualization, and Integrated Discovery

DBPA . . . . . DNA-binding protein A [also known as YBX3 and CSDA]

DDX6 . . . . . Probable ATP-dependent RNA helicase DDX6

DHX9 . . . . . ATP-dependent RNA helicase A

DNA . . . . . deoxyribonucleic acid

DNLI3 . . . . . DNA ligase 3

DPOD1 . . . . . DNA polymerase subunit δ-1

DPOG1 . . . . . DNA polymerase subunit γ-1

DPOLB . . . . . DNA polymerase β

DSP . . . . . dithiobis[succinimidyl propionate]

DTT . . . . . dithiothreitol

EDTA . . . . . Ethylenediaminetetraacetic acid

EGFR . . . . . epidermal growth factor receptor [also known as HER-1 or Receptor tyrosine-protein kinase erbB-1]

eIF2 . . . . . Eukaryotic initiation factor 2

eIF4B . . . . . Eukaryotic translation initiation factor 4B

eIF4E . . . . . Eukaryotic translation initiation factor 4E

eIF4F complex . . . . . Eukaryotic translation initiation factor 4F complex

eIF4H . . . . . Eukaryotic translation initiation factor 4H

ENO1 . . . . . Alpha-enolase

EP300 . . . . . Histone acetyltransferase p300

ERBB2 . . . . . Receptor tyrosine-protein kinase erbB-2 [also known as HER-2]

ERK . . . . . extracellular signal-regulated kinase

EWS . . . . . Ewings Sarcoma proto-oncoprotein

EZH2 . . . . . Enhancer of Zeste Homolog 2

FAC . . . . . Focal adhesion kinase 1

FAM120A . . . . . Constitutive coactivator of PPAR-gamma-like protein 1 [also known as OSSA]

FBX33 . . . . . F-box only protein 33

FOXK2 . . . . . Forkhead box protein K2

FOXQ1 . . . . . Forkhead box protein Q1

FSH . . . . . follicle stimulating hormone

G3BP1 . . . . . Ras GTPase-activating protein-binding protein 1

GAPDH . . . . . Glyceraldehyde-3-phosphate dehydrogenase

GATA1 . . . . . Erythroid transcription factor

GM-CSF . . . . . Granulocyte-Macrophage Colony-Stimulating factor

GSK3β . . . . . Glycogen synthase kinase-3 beta

HLA . . . . . Human leukocyte antigen [also known as Major Histocompatibility complex]

HNRNPA2B1 . . . . . Heterogeneous nuclear ribonucleoproteins A2/B1

hnRNP-L . . . . . Heterogeneous nuclear ribonucleoprotein L

hnRNP-K . . . . . Heterogeneous nuclear ribonucleoprotein K

hnRNP-C . . . . . Heterogeneous nuclear ribonucleoproteins C1/C2

hnRNP-A1 . . . . . Heterogeneous nuclear ribonucleoprotein A1

HNRNPU . . . . . Heterogeneous nuclear ribonucleoprotein U

HNRPQ . . . . . Heterogeneous nuclear ribonucleoprotein Q [also known as Synaptotagmin-binding, cytoplasmic RNA-interacting protein]

hNTH1 . . . . . human endonuclease III

hr . . . . . hour

HR23B . . . . . UV excision repair protein RAD23 homolog B

HRAS . . . . . GTPase HRas

IF . . . . . immunofluorescence

IF4A3 . . . . . Eukaryotic initiation factor 4A-III [P38919]

IGF2BP1 . . . . . Insulin-like growth factor 2 mRNA-binding protein 1 [Q9NZI8]

IGF2BP3 . . . . . Insulin-like growth factor 2 mRNA-binding protein 3 [O00425]

IHC . . . . . immunohistochemistry

IL-1β . . . . . Interleukin-1 beta

IL13R . . . . . IL13 receptor subunit-2

IL2 . . . . . Interleukin-2

IL6 . . . . . interleukin 6

ILF3 . . . . . Interleukin enhancer-binding factor 3

IP . . . . . immunoprecipitation

IRES . . . . . internal ribosome entry site

KRAS4A . . . . . GTPase KRas, isoform 1

KRAS4B . . . . . GTPase KRas, isoform 2

LC-MS/MS . . . . . liquid chromatography-coupled tandem mass spectrometry

MAPK1 . . . . . Mitogen-activated protein kinase 1 [also known as ERK2]

MAX . . . . . Protein max

MDR-1 . . . . . Multidrug resistance protein 1

MEK . . . . . Ras-Raf-mitogen-activated and extracellular-signal regulated kinase

min . . . . . minute

MMP2 . . . . . 72 kDa type IV collagenase (also known as gelatinase A)

MPC . . . . . multi-protein complex

mRNP . . . . . messenger ribonucleoprotein

MSH2 . . . . . DNA mismatch repair protein Msh2

MT1-MMP . . . . . Membrane type 1 matrix metalloproteinase

mTOR . . . . . mammalian target of rapamycin

mTORC1 . . . . . mTOR complex 1

Myc proto-oncogene . . . . . MYC

NAP1L1 . . . . . Nucleosome assembly protein 1-like 1

NAP1L4 . . . . . Nucleosome assembly protein 1-like 4

NDF6 . . . . . Neurogenic differentiation 6 [also known as MATH2]

NDRG1 . . . . . Protein NDRG1

NEIL1 . . . . . Endonuclease 8-like 1

NEIL2 . . . . . Endonuclease 8-like 2

NF-κB . . . . . Nuclear factor NF-κ-B

NF1 . . . . . Neurofibromin

NONO . . . . . Non-POU domain-containing octamer-binding protein

NPM1 . . . . . Nucleophosmin

NRAS . . . . . GTPase NRas

NTH . . . . . Endonuclease III-like protein 1

OGFOD . . . . . 2-oxoglutarate and Fe(II)-dependent oxygenase domain containing 1

p16INK4A . . . . . Cyclin dependent kinase inhibitor 2A (also known as *CDKN2A*)

p21(Cip1) . . . . . Cyclin-dependent kinase inhibitor 1

p53 . . . . . p53 tumor suppressor

PABP . . . . . polyadenylate-binding protein

PABP1 . . . . . polyadenylate-binding protein 1 [P11940]

PABP2 . . . . . polyadenylate-binding protein 2 [Q86U42]

PABP3 . . . . . polyadenylate-binding protein 3 [Q9H361]

PABP4 . . . . . polyadenylate-binding protein 4 [Q13310]

PARP1 . . . . . poly(ADP-ribose)polymerase 1

PBS . . . . . phosphate-buffered saline, pH 7.4

PCNA . . . . . proliferating cell nuclear antigen

PDCD . . . . . programmed cell death protein 4

PI3K . . . . . phosphatidylinositol 3-kinase

PIK3CA . . . . . Phosphatidylinositol 4,5-bisphosphate 3-kinase

PLEC . . . . . Plectin

PPI . . . . . protein-protein interactions

PTB . . . . . polypyrimidine tract binding protein

PTM . . . . . post-translational modification

PURA . . . . . Pur-α

PURB . . . . . Pur-β

RALY . . . . . RNA-binding protein Raly

RB . . . . . Retinoblastoma-associated protein

RBBP6 . . . . . retinoblastoma binding protein 6

RIPA . . . . . radioimmunoprecipitation assay buffer

RL27A . . . . . 60S ribosomal protein L27a [P46776]

RS27A . . . . . Ubiquitin-40S ribosomal protein S27a [P62979]

RS3 . . . . . 40S ribosomal protein S3

RSK . . . . . p90 ribosomal S6 kinase

RTCB . . . . . tRNA-splicing ligase RtcB homolog [Q9Y3I0]

SDS-PAGE . . . . . Sodium dodecyl sulfate Polyacrylamide gel electrophoresis

sec . . . . . second

SNAT1 . . . . . Sodium-coupled neutral amino acid transporter 1

SND1 . . . . . Staphylococcal nuclease domain-containing protein 1

SREK1 . . . . . Splicing regulatory glutamine/lysine-rich protein 1

SRSF9 . . . . . Serine/arginine-rich splicing factor 9

STAT3 . . . . . Signal transducer and activator of transcription 3

TBS . . . . . tris-buffered saline, pH 7.6

TGF-β . . . . . Transforming growth factor beta-1

TLS . . . . . translocation liposarcoma protein

TNBC . . . . . triple-negative breast cancer

TOP2A . . . . . DNA topoisomerase II

TP53 . . . . . Cellular tumor antigen p53

TP73 . . . . . tumor protein 73

TRIM28 . . . . . Transcription intermediary factor 1-beta [also known as TIF1B or KAP1]

TWIST . . . . . Twist homolog 1

UTR . . . . . untranslated region

VEGF . . . . . Vascular endothelial growth factor

VIM . . . . . Vimentin

WRN . . . . . Werner syndrome ATP-dependent helicase

XIC . . . . . extracted ion chromatogram

XPC . . . . . DNA repair protein complementing XP-C cells

XRCC5 . . . . . X-ray repair cross-complementing protein 5 [also known as Ku80]

XRCC6 . . . . . X-ray repair cross-complementing protein 6 [also known as Ku70]

YBX1 . . . . . Y-box binding protein 1 (Entrez Gene: 4904)

YAP1 . . . . . Transcriptional coactivator YAP1 [Yes-associated protein 1]

YB-1 . . . . . Nuclease-sensitive element-binding protein 1 (P67809; also known as Y-box-binding protein 1)

$YB1^{C}$ . . . . . antibody, raised in rabbit, against C-terminus of YB-1

Chk-YB-1b . . . . . chicken YB-1 homologue

$^{N}YB1$ . . . . . antibody, raised in rabbit, against N-terminus of YB-1

$^{N}YB1_{sheep}$ . . . . . antibody, raised in sheep, against N-terminus of YB-1

YWHAB . . . . . Transcriptional coactivator YAP1 [Yes-associated protein 1]

YWHAZ . . . . . 14-3-3 protein zeta/delta

Chapter 1

YB-1 a multifunctional protein: a review

1.1 Biology of cancer

Biological systems are self-maintaining and very complex. In general, complex multicellular organisms, such as vertebrates, begin as a single cell that was the result of the fusion of one oocyte and one spermatozoan. Many divisions are required before this cell, and its daughter cells, can form a mature organism that is ready to reproduce. While dividing, these cells must also differentiate to create the specialised cell-types and tissues that the organism will require to function. Furthermore, the fully-grown organism will need to replace cells as they die. The process described above is known as homeostasis (reviewed in Pellettieri & Sánchez Alvarado 2007). The systems that guide the growth, differentiation, and maintenance of homeostasis in eukaryotes are robust (Yan et al. 2010). Many molecular pathways are involved in homeostasis but three main functions are central to its maintenance; cell differentiation, cell survival (this includes cell division and cell death), and genome maintenance (Vogelstein et al. 2013).

Perturbation of the mechanisms that maintain homeostasis can lead to unregulated cell division and clusters of cells, known as tumours, may form if the errantly dividing cells are not removed. In general, tumours that remain within their tissue of origin are known as benign tumours. Cancerous tumours arise when a group of cells with uncontrolled cell division also have the potential to grow into and penetrate other tissues.

At the cellular level, the genome, encoded using deoxyribonucleic acid (DNA),

contains the primary code for the components of the homeostatic systems. Cancer is predominantly thought to be caused by alterations to the genome, which are known as mutations, and the cells in most cancers contain multiple mutations (Knudson 1986, Renan 1993, Vogelstein et al. 2013). Mechanisms that act at the organism and tissue levels, such as inflammation via the immune system, are also important to the development of cancer (reviewed in Hanahan & Weinberg 2011). However, the primary focus of this thesis is on events at or below the cellular level.

Tumour suppressor genes encode proteins are critical to maintaining homeostasis. The ability of tumour suppressors to monitor for loss of homeostasis is frequently modified or lost in cancer cells. Many tumour suppressors control the transition of cells through key points in mitosis, known as cell cycle checkpoints, to ensure that only normal cells may complete mitosis (Sager 1989, Hanahan & Weinberg 2000). The p53 tumor suppressor is encoded by the Cellular tumor antigen p53 (*TP53*) gene which is mutated in ∼50% of cancers (Braithwaite et al. 2005, Levine & Oren 2009, Bieging et al. 2014). p53 exercises control over the stress response of cells through an ability to control the cell cycle and to direct DNA damage response signalling (**Figure 1.1**). p53 can induce cell cycle arrest, senescence, or apoptosis. Mutations to p53 reduce or remove its capabilities in cancer cells to induce cell cycle arrest, senescence, or apoptosis (Braithwaite et al. 2005, Levine & Oren 2009). In addition to controlling cell death, many tumour suppressors, like p53, may also be tied to metabolic processes that allow cancerous cells to survive in rapidly growing tumours (Levine & Puzio-Kuter 2010). Retinoblastoma-associated protein (*RB*) is another tumour suppressor with a key role in controlling the cell cycle (**Figure 1.1**). RB can inhibit mitosis at the transition of cells from the gap 1 (G_1) phase, which consists of cells that have completed mitosis, to S-phase, where cells begin to synthesise a copy of their genome (Classon & Harlow 2002, Manning & Dyson 2012). This regulatory role is supported by the ability of RB to negatively regulate the E2F-family transcription factors, as some of these transcription factors can positively regulate the cell cycle (Classon & Harlow 2002, Manning & Dyson 2012). Cyclin-dependent kinase inhibitor 2A (*CDKN2A*, also known as *p16INK4A* which is used throughout) is another tumour suppressor gene which also inhibits the transition of cells from G_1/S through its ability to inhibit cyclin-dependant kinases which inactivate RB (**Figure 1.1**; Liggett & Sidransky 1998, Rayess et al. 2012). Genome instability, which further weakens or removes homeostatic mechanisms, can be a consequence of the loss of *TP53* or *RB* gene functions (Rausch et al. 2012, Manning & Dyson 2012). Breast cancer type 1 susceptibility protein (*BRCA1*) is involved in

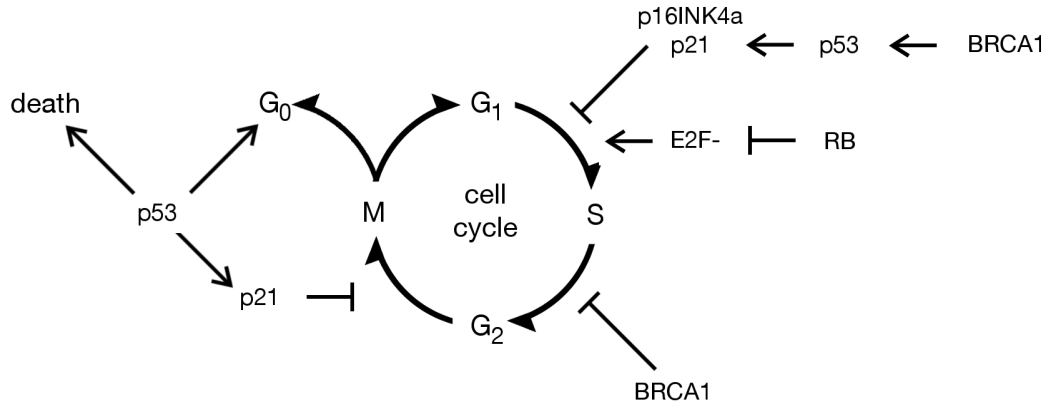

Figure 1.1: Tumour suppressor genes control the passage of cells through the cell cycle. Gap 1 (G_1) is followed by the synthesis of DNA (S), gap 2 (G_2), and then mitosis (M). Cells can exit the cell cycle (G_0) or die.

monitoring for DNA integrity. *BRCA1* can also influence mitosis, specifically during the S-phase, the following gap 2 (G_2) phase, and through to mitosis checkpoint (M; **Figure 1.1**; Roy et al. 2012). Mutation of *BRCA1*, or the related *BRCA2* gene, accounts for most inheritable cases of breast and ovarian cancer. Therefore, tumour suppressor proteins generally monitor for modification of the genome and have the ability to control cell fate by inhibiting their division or initiating cell death.

Other genes and their protein products can also promote the features of cancerous cells. These genes and proteins, known as oncogenes and oncoproteins respectively, promote cancer development and maintenance through gain-of-function mutations or overexpression (reviewed in Shortt & Johnstone 2012). Like tumour suppressors, many oncogenes encode proteins that influence cell division and cell death. In general, their deregulation or mutation leads to the promotion of cell division, inhibition of cell death, or senescence (Vita & Henriksson 2006, Shortt & Johnstone 2012). The Myc proto-oncogene (*MYC*) is an oncogene that functions as a transcription factor for many genes that promote mitosis (Vita & Henriksson 2006). A number of oncogenes transduce mitogenic signals from the extracellular environment through their positions as critical parts of cell-surface receptors. Two proteins that exemplify this class of oncogene are the Receptor tyrosine-protein kinase erbB-2 (*ERBB2*, also known as HER-2; Moasser 2007) and epidermal growth factor receptor (*EGFR*, also known as HER-1 or Receptor tyrosine-protein kinase erbB-1; Ciardiello & Tortora 2008). These proteins become deregulated in cancers and begin to provide mitogenic signals irrespective of the presence of their ligands. The four Ras family genes, *HRAS*, *NRAS*, *KRAS4A* and *KRAS4B*, are another group of oncogenes that

respond to extracellular signals to activate kinase signalling pathways to support mitosis and cell survival (Schubbert et al. 2007). Mutation or deregulation of ras genes leads to constitutive activation of the ras signalling pathway, the key downstream targets of the ras genes are the Ras-Raf-mitogen-activated and extracellular-signal regulated kinase (MEK) extracellular signal-regulated kinase (ERK) pathway. The overlap in function between tumour suppressors and oncogenes reflects the importance of this redundancy of function to maintaining homeostasis and it explains why multiple modifications are required for cancer to form (Hanahan & Weinberg 2000).

In addition to unregulated cell division, many aggressive cancers possess, or have the potential to gain, the ability to spread from their tissue of origin to other areas of the body (reviewed in Weigelt et al. 2005). This process is known as metastasis and it accounts for up to 90% of cancer deaths (Hanahan & Weinberg 2011). Metastatic cancers possess the ability to move through tissues. However, the epithelial cells, from which many cancers arise, have limited capacity to move as they adhere tightly to adjacent cells (Hanahan & Weinberg 2011). The acquisition of metastatic capability is correlated with the acquisition of mesenchymal markers in a process known as epithelial-mesenchymal transition (Kalluri 2009, Singh & Settleman 2010). Mesenchymal cells are elongated, polarised, and move more easily through tissues than epithelial cells. The difference in the mobility of epithelial and mesenchymal cells is in part explained by the types of connections that they maintain with other cells. The connections between epithelial cells are stronger than those between the more mobile mesenchymal cells, with an epithelial cell marker, E-cadherin, indicating strong connections between cells (Hanahan & Weinberg 2000, Singh & Settleman 2010). N-cadherin and vimentin are often used as markers of a mesenchymal phenotype that is more invasive with a greater potential to metastasise (Hanahan & Weinberg 2000, Singh & Settleman 2010). Other proteins that are present in some invasive and metastatic cancers can degrade the extracellular matrix, such as those from the matrix metalloproteinase family (Weigelt et al. 2005).

This brief review attempts to summarise the key processes in cancer. These processes are the loss of homeostasis, the inactivation of tumour suppressors, and, the activation of oncogenes. The hallmarks of cancer provides a more complete framework for understanding the development of cancer (Hanahan & Weinberg 2000, Hanahan & Weinberg 2011). Therefore, these fundamental processes are important to the research that is reported in this thesis.

1.2 Biology of breast cancer

The focus of this thesis is a protein called Nuclease-sensitive element-binding protein 1 (P67809; also known as Y-box-binding protein 1) (YB-1) and YB-1 is discussed extensively in the rest of this literature review. A number of the chapters deal specifically with the function and importance of YB-1 in breast cancer. Therefore, further information about breast cancer is included in this introduction to provide an expanded example of cancer.

Within the breast, the mammary glands are specialised structures that produce milk during lactation. The breast ducts and lobules, of which the mammary gland is comprised, are the source of the majority of breast cancers (**Figure 1.2.A** Li et al. 2003a, Weigelt et al. 2008). Ductal carcinoma *in situ* and lobular carcinoma *in situ* are comprised of abnormal cells that are confined completely within their tissue of origin (**Figure 1.2.B**: Ward et al. 2015). Lobular carcinoma *in situ* is considered to be a neoplasia rather than a cancer. However, the diagnosis includes an increased risk of breast cancer. Ductal carcinoma *in situ* are more common than lobular carcinoma *in situ* and there is potential for ductal carcinoma *in situ* to become invasive. Around 90% of diagnosed breast cancers are invasive, which means that they are not confined to the breast ducts or lobules (Li et al. 2003a, Weigelt et al. 2008). Of this 90%, approximately 70% are ductal carcinomas, 10% lobular carcinomas, 6% mixed ductal and lobular carcinoma, and 15% lobular and mixed ductal-lobular carcinoma (Li et al. 2003a). In addition to the classification relating to the tissue of origin, breast cancers are also classified based on histological markers for the rate of proliferation. Grade I indicates low levels of proliferation and grade III represents high levels of proliferation.

Molecular information is also important to breast cancer classification as the molecular sub-type of breast cancers has a significant bearing on which treatments are appropriate. Three broad groups of breast cancer have been identified in the literature; luminal, HER2-positive (*ERBB2*), and basal-like breast cancers (**Figure 1.2.B**; Perou et al. 2000, Blows et al. 2010). In luminal breast cancers, either or both of the estrogen receptor (ER) and the progesterone receptor (PR) are present and these receptors transduce growth signals to support tumour growth (ER^{-ve}/PR^{-ve}; Blows et al. 2010). HER2-positive breast cancers are those with an amplification of the *ERBB2* gene, which is also known as HER-2. *ERBB2* promotes cell division and inhibits cell death, and *ERBB2* amplification leads to the overexpression of the ERBB2 protein which supports the growth of tumours. HER2-positive breast

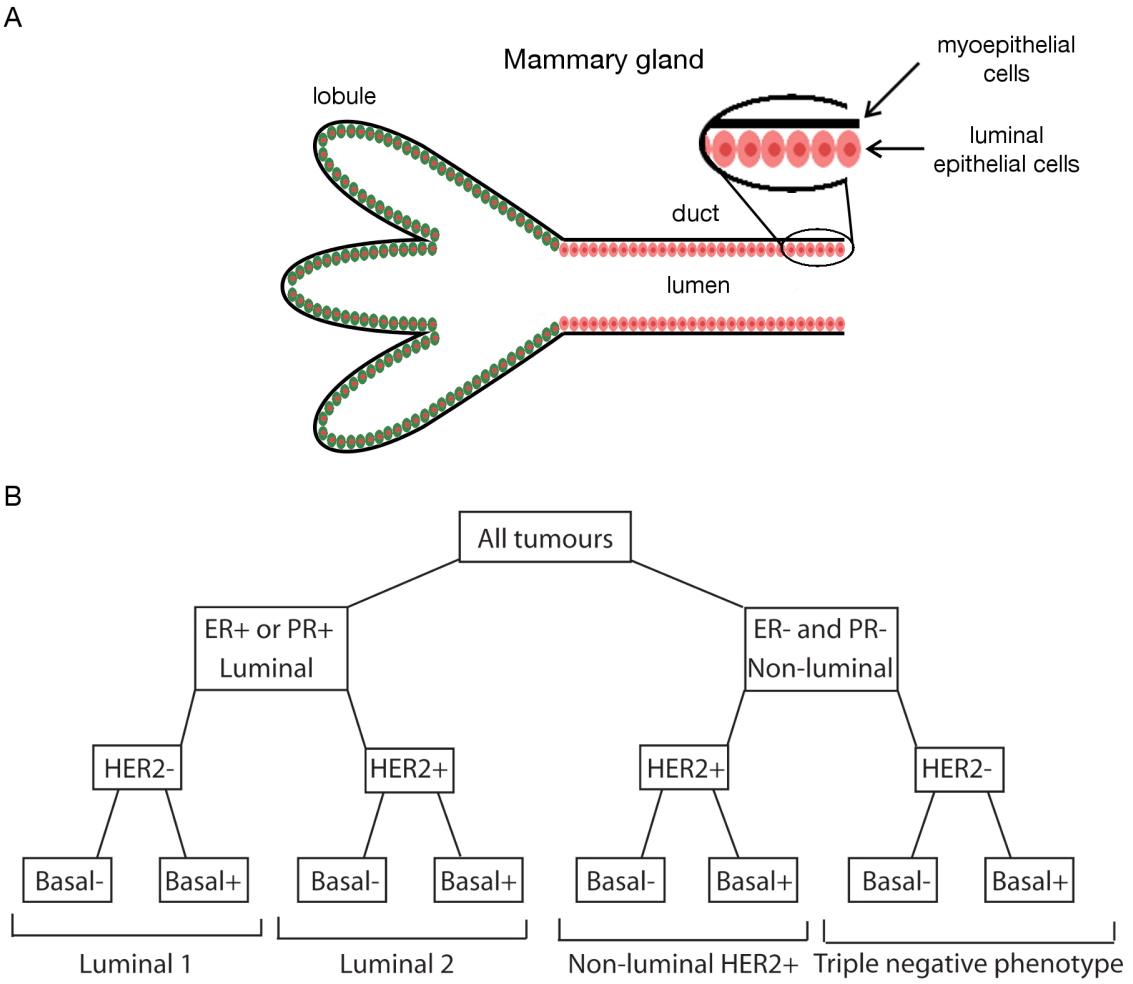

Figure 1.2: Breast cancers have differing pathological and molecular features. **A**, the mammary gland is the primary unit of breast tissue. **B**, breast tumours are characterised by their tissue of origin, mitotic potential and their molecular subtype. Reproduced from Blows et al. (2010).

cancers account for 15 - 25% of all breast cancers (Pauletti et al. 1996, Ross & Fletcher 1998). Another sub-class is luminal 2, which comprises any luminal cancers that are either positive for *ERBB2* or exhibit elevated proliferation (grade III). Basal-like cancers do not express estrogen or progesterone receptors and they lack amplification of the *ERBB2* gene. Basal-like cancers are categorised according to expression of basal and myoepithelial cell markers; Epidermal growth factor receptor (*EGFR*) and cytokeratins 5 and 6 (Perou et al. 2000, Nielsen et al. 2004, Carey et al. 2006). Another sub-type is referred to as (triple-negative breast cancer (TNBC); Blows et al. 2010). TNBCs do not express estrogen or progesterone receptors and do not over-express *ERBB2* (**Figure 1.2.B**). Therefore, many TNBCs are also part of the basal-like molecular subtype, although some TNBC tumours are excluded due to their lack of basal cell markers. TNBC tumours account for 15 - 20% of all breast cancers and this group includes cancers with mutations to BRCA1 (Griffiths & Olin 2012, Shah et al. 2012).

The breast cancer subtypes influence which treatment options are appropriate. Many treatments are given in combination, either concurrently or sequentially. There are two primary methods of treatment for invasive breast cancers and ductal carcinoma *in situ*s. The first is the surgical removal of tumour tissue, or the whole breast and lymph nodes. The second is the use of radiation to destroy the cancer cells. A variety of chemotherapy drugs are often used in combination with one another (summarised in Table 1 of Mauri et al. 2005). Treatments that target critical aspects of the molecular subtypes are used in addition to chemotherapeutic drugs. Targeted treatments for patients with luminal cancers include agents that aim to reduce the availability of estrogen within the body or to inhibit the response of cells to estrogen (Horwitz & McGuire 1975, Mauri et al. 2006, Early Breast Cancer Trialists' Collaborative Group (EBCTCG) et al. 2015). Where the ERBB2 is over-expressed, targeted treatments interfere with ERBB2 signalling to slow the growth, or kill, these cancer cells (reviewed in Foulkes et al. 2010).

TNBC and basal-like sub-types currently lack targeted treatments. Both sub-types are also aggressive as they contribute disproportionately to breast cancer cases that progress to metastatic disease and also to breast cancer deaths (Dent et al. 2007, Foulkes et al. 2010, Griffiths & Olin 2012). However, this aggression may be transient and survival rates improve in cases where initial chemotherapeutic treatment results in complete pathologic response. Molecular sub-typing of TNBCs highlights the presence of TNBC subtypes that are sensitive to different drugs (Lehmann et al. 2011). However, surgical resection and a variety of chemotherapeutic agents remain

the primary treatments for TNBC (André & Zielinski 2012, Griffiths & Olin 2012).

1.3 YB-1 is overexpressed in cancer

The research presented in this thesis focuses on the YB-1 protein which is encoded by the Y-box binding protein 1 (Entrez Gene: 4904) (*YBX1*) gene. The published reports contain contradictions relating to which tissues contain *YBX1* mRNA and YB-1 protein; some studies suggest that YB-1 is largely, or entirely, absent in normal tissue (Bargou et al. 1997, Dahl et al. 2009, Janz et al. 2002). Irrespective of this ambiguity in normal tissues, a primary reason for researching YB-1 is that many studies indicate that the functions of YB-1 are significant in cancer. Elevated levels of YB-1, or of *YBX1* mRNA, have been identified in a wide range of cancers. YB-1 levels are elevated in colorectal cancer (Shibao et al. 1999, Jürchott et al. 2010, Yan et al. 2014), non-small cell lung carcinoma (Gu et al. 2001, Shibahara et al. 2001, Gessner et al. 2004), adenocarcinoma (Shibahara et al. 2001), synovial sarcoma (Oda et al. 2003), androgen resistant prostate cancers (Giménez-Bonafé et al. 2004), ovarian cancer (Kamura et al. 1999, Huang et al. 2004a, Basaki et al. 2007) and breast cancer (Bargou et al. 1997, Lee et al. 2008, Woolley et al. 2011, Stratford et al. 2012, Reipas et al. 2013). Furthermore, YB-1 levels are positively correlated with cancer aggression and negatively correlated with disease-free or recurrence-free survival (Janz et al. 2002, Habibi et al. 2008, Dahl et al. 2009, Lasham et al. 2012).

In addition to overexpression, the subcellular localisation of YB-1 appears to be important (Kamura et al. 1999). For example, an immunohistochemistry (IHC) study reported that YB-1 was not present in normal breast tissue but found clear evidence of both nuclear and cytoplasmic staining in tumour tissues (Janz et al. 2002). This study also found that elevated levels of YB-1 were associated with tumour progression. Increased levels of YB-1 in the nuclei of tumour cells is also correlated with lymph node metastasis in patients with non-small cell carcinoma (Gessner et al. 2004, Shibahara et al. 2001). Furthermore, nuclear YB-1 staining is also associated with increased expression of Multidrug resistance protein 1 (MDR-1) in patients with poor prognosis (Bargou et al. 1997, Dahl et al. 2009). The ATP-binding cassette, sub-family B [MDR/TAP], member 1 (also known as multidrug resistance gene 1/MDR1) (*ABCB1*) gene encodes an ATP-dependant drug efflux pump that is responsible for drug resistance in many cancer cells (Modok et al. 2006). Other reports rarely detect YB-1 in the nucleus however, increased levels of YB-1 in the cytoplasm have still been associated with poor patient prognosis (Wu et al. 2006).

Therefore, the distribution of YB-1 in cancer cells varies from study to study even among those that have examined the same cancer type.

To summarise, the accumulated evidence supports the conclusions that YB-1 is elevated in a wide range of cancers and that elevated YB-1 is linked to aggressive cancers. These results confirm that YB-1 is an oncoprotein (Astanehe et al. 2009, Cohen et al. 2010).

1.4 The functions of YB-1 in cancer

The functional significance of the elevation of YB-1 in cancer cells does not appear to be singular. Rather, the elevation of YB-1 in a range of cancers has been attributed to the participation of YB-1 in multiple functions in cancer cells. The following sub-sections outline these functions. The molecular mechanisms that allow YB-1 to participate in these functions are provided at a later stage in the review.

1.4.1 YB-1 promotes the early stages of cancer development

A number of studies implicate YB-1 in the early development of breast cancers through the ability to promote genome stability. Overexpressing the YB-1 homologue in murine mammary tissue leads to the development of breast carcinomas (Bergmann et al. 2005). The breast carcinomas appear to develop because YB-1 increases mitosis rates and the presence of cells with two nuclei indicates that mitotic checkpoints are being breached. Bergmann et al. (2005) conclude that the breast carcinomas are caused by genetic instability that was the result of mitotic failure and the amplification of centrosomes. Centrosomes are a structure that mediates the partitioning of genetic material during the M-phase of mitosis.

More recent work has affirmed that YB-1 also directly promotes genetic instability in human cells. The overexpression of YB-1 in human breast epithelial cells also leads to centrosome amplification and aneuploidy (Davies et al. 2011). Subsequent work from the same authors confirms that YB-1 promotes genetic instability and they propose that YB-1 is a driver of tumour initiating stem cells (Davies et al. 2014). Other research supports a link between YB-1 and genetic instability. In DT40 cells, a chicken B cell line (Baba & Humphries 1984), disrupting one allele of the chicken YB-1 homologue (*Chk-YB-1b*) led to genetic abnormalities (Swamynathan et al. 2002). However, this work is difficult to interpret as it correlates the depletion of YB-1 with genetic abnormalities. The differing cellular context may explain the difference from

results in murine and human cells, or it could be an example of the goldilocks effect, where too much or too little of an allele is suboptimal (Cohen et al. 2004, Boothby & Williams 2012).

Not all research supports the role of YB-1 in the development of cancer. Overexpression of YB-1 blocks the oncogenic transformation of chicken embryo fibroblasts by phosphatidylinositol 3-kinase (PI3K) or RAC-alpha serine/threonine-protein kinase (AKT) (Bader et al. 2003, Bader & Vogt 2008). Furthermore, the AKT in these cells remained functional, indicating that YB-1 does not inactivate AKT. These observations remain difficult to link to other work on YB-1.

In summary, YB-1 may contribute to genetic instability. Increased proliferation accompanies this genetic instability and the ability of YB-1 to promote the proliferation of cancer cells is a fundamental function of YB-1.

1.4.2 Role of YB-1 in mitosis

Many studies have shown that YB-1 promotes cell division (mitosis; Ladomery & Sommerville 1995) and YB-1 is correlated with elevated rates of mitosis in cancer cells (Sabath et al. 1990). Furthermore, overexpression of YB-1 stimulates tumour growth in cultured breast cells (Sutherland et al. 2005) and also in non-small cell lung carcinomas (Harada et al. 2014). The ability of the murine YB-1 homologue to increase proliferation indicates that this function of YB-1 is conserved in other species (discussed above; Bergmann et al. 2005). Furthermore, the expression of *YBX1* mRNA is positively correlated with an E2F1 cell proliferation signature in breast cancer tumours (Lasham et al. 2012). Confirmation of a functional link between YB-1, mitosis, and the E2F-transcription factors comes from observations that depleting YB-1 in various cell lines perturbs transcripts from the E2F1 pathway while also inhibiting mitosis and tumour formation in a mouse xenograft model (Lasham et al. 2012). Therefore, the ability of YB-1 to promote mitosis has been confirmed by studies showing that overexpression of YB-1 has a positive effect on mitosis and that depletion of YB-1 has a negative effect.

The literature includes conflicting reports relating to the point of the cell cycle that is promoted by YB-1. However, recent work appears to provide some clarification. A number of studies have found that depleting YB-1 arrests tumour cells in $G1_1$ of the cell cycle (**Figure 1.3**; Shiota et al. 2008a, Basaki et al. 2010, Yu et al. 2010, Kawaguchi et al. 2015). Overexpression of YB-1 has the opposite effect, in that it increases the number of cells that are in G_2 and undergoing mitosis (Davies

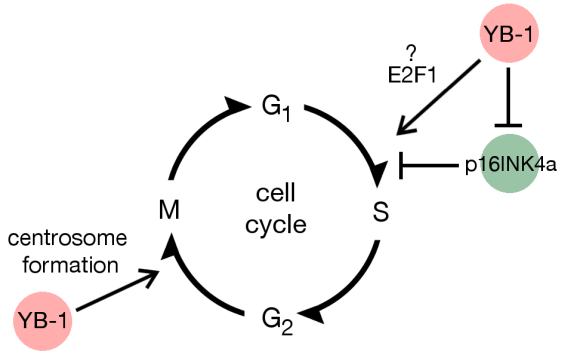

Figure 1.3: YB-1 can promote the passage of cells through the cell cycle at the G_1-S boundary and during mitosis (M).

et al. 2011). YB-1 has been proposed to promote the progress of cells through G_1/S by repressing the expression of *p16INK4A* (**Figure 1.3**; Basaki et al. 2010, Yu et al. 2010, Kotake et al. 2013).

YB-1 also appears to participate in the maturation of the centrosomal microtubule array during mitosis (**Figure 1.3**; Davies et al. 2011, Kawaguchi et al. 2015). Depleting YB-1 disrupts the organisation of microtubules in relation to the centrosome during telophase which in turn, leads to defects in the reformation of the nuclear membrane (Kawaguchi et al. 2015). Despite the microtubule abnormalities, cells lacking YB-1 have been shown to pass through the G_2/M checkpoint and then accumulate in G_1. It has been proposed that spindle assembly occurring via a chromatin-mediated pathway allows the cells to complete mitosis, and the defects in the resulting nuclear envelope then hold the cells in G_1 (Kawaguchi et al. 2015). Kawaguchi et al. (2015) found no indication of aneuploidy.

In other species YB-1 also appears to be linked to mitosis. Disruption of one allelle of the chicken YB-1 homologue slowed the growth of DT40 cells via an apparent blockade of G_2/M of the cell cycle (Swamynathan et al. 2002). In this study the disruption of a single allele had no effect on the levels of *YBX1* mRNA or YB-1 and the effects were proposed to be due to the remaining disrupted allele. Support for this hypothesis comes from a study of the N-terminus of the rat YB-1 homologue. Khandelwal et al. (2009) observed that the N-terminus fragment slowed the growth of rat hepatoma cells via an apparent blockade of the G_2/M of cell cycle. The N-terminus fragment, located in the cytoplasm of the cells, was proposed to block the G_2/M cell cycle checkpoint by sequestering cyclin D1 (Khandelwal et al. 2009).

Therefore, YB-1 promotes the proliferation of a variety of cells. The ability to

promote mitosis may explain the contributions of YB-1 to the growth of tumours. It is however, important to note that YB-1 can also promote the survival of cells (Lasham et al. 2000, Capowski et al. 2001, Lu et al. 2005) and this may be a critical feature of tumour development (Hanahan & Weinberg 2000). The ability of YB-1 to promote mitosis by facilitating passage through cell cycle checkpoints appears to explain in part, the role of YB-1 in genetic instability.

1.4.3 YB-1 promotes drug resistance

The ability of YB-1 to promote the survival of cells became evident through research into the role of YB-1 in the cellular response to a number of stressors. The overexpression of YB-1 has been correlated with drug resistance in a number of different cancers, including breast cancers (Janz et al. 2002, Huang et al. 2005), synovial sarcomas (Oda et al. 2003), and in a murine melanoma model (Zaidi et al. 2015). Furthermore, YB-1 has been implicated in the resistance of a number of cancers to specific compounds. For example, elevated levels of YB-1 are present in recurrent breast cancers that were treated with anthracycline, a drug that blocks DNA replication (Huang et al. 2005).

The overexpression of YB-1 in cancers also correlates with other proteins that are known to promote drug resistance. The overexpression or nuclear localisation of YB-1 has been correlated with MDR-1 expression or activity in prostate cancer (Giménez-Bonafé et al. 2004), ovarian cancer (Huang et al. 2004a), colon cancer (Vaiman et al. 2007), and lymphoma (Xu et al. 2009). However, in non-small cell lung cancer there is no correlation between YB-1 and MDR-1 expression although elevated expression of YB-1 does positively correlate with proliferating cell nuclear antigen (PCNA) and DNA topoisomerase IIα (TOP2A; Gu et al. 2001). Both PCNA and TOP2A participate in DNA repair rather than drug efflux. Another study implicates YB-1 in the stress response through the correlation of elevated YB-1, mutated p53, and negative patient outcomes (Gessner et al. 2004). Therefore, analyses of clinical samples links YB-1 to drug resistance via multiple pathways.

In addition to the correlation of YB-1 with drug resistance in general, a number of biochemical studies also confirm that YB-1 has a direct role. Depleting YB-1 sensitises cells to a range of stressors and drugs; UV irradiation (Guay et al. 2008b), platinum compounds (Guay et al. 2008b), etoposide (Ohga et al. 1996, Ohga et al. 1998, Schittek et al. 2007, Tsofack et al. 2013), and doxorubicin (Bargou et al. 1997). The opposite is also true as overexpression of YB-1 contributes to cisplatin resistance

(Ohga et al. 1996, Ohga et al. 1998, Shibahara et al. 2004). YB-1 has been implicated in a stress response to the inhibition of RNA synthesis via actinomycin D (Asakuno et al. 1994). Depleting one allele of the mouse YB-1 homologue sensitises cells to cisplatin and mitomycin C (Shibahara et al. 2004). *YBX1*$^{-/-}$ mouse fibroblasts are sensitive to oxidative stress due to high levels of the cell cycle checkpoint inhibitors P16INK4A and p21Cip1 (Lu et al. 2005). In breast cancer, YB-1 is also implicated in resistance to targeted therapies. YB-1 may promote resistance to antihormonal therapies for breast cancer by stimulating TGFβ pathways (Popp et al. 2013). YB-1 may also promote resistance to the primary therapy for HER2-positive breast cancers, Trastuzumab (also known as Herceptin; Astanehe et al. 2012). The role of YB-1 in the resistance to these therapies is likely to rely on the ability of YB-1 to encourage cell division despite the loss of hormonal or *ERRB2* growth signals (**Figure 1.3**).

YB-1 levels are correlated with resistance to a wide range of stressors, including chemotoxic drugs and inhibitors of proliferation. The breadth of these agents appears to favour a general mechanism for YB-1 during stress that inactivates cell death signalling. Support for such a general mechanism comes from observations that YB-1 can inhibit the function of p53 (Homer et al. 2005, Lasham et al. 2003) in addition to the ability of YB-1 to promote the passage of cells through the cell cycle. However, multiple molecular functions have been proposed to explain the activity of YB-1 in protecting cells from stress. Many of these, such as the modulation of drug efflux pumps and interaction with DNA repair proteins, seem to indicate that YB-1 has multiple functions during stress.

Mechanistic explanations for the molecular role of YB-1 in the stress response are provided later in this literature review. Furthermore, the research that is reported in **Chapters 5 - 7** focuses on the role of YB-1 during drug exposure.

1.4.4 YB-1 facilitates an invasive phenotype

YB-1 is also known to promote the metastasis of cancer cells. The correlation of elevated YB-1 with aggressive tumours and survival in breast cancers was discussed in **Chapter 1.3**. YB-1 levels are also positively correlated with metastasis in colorectal cancer (Yan et al. 2014) and gastric cancers (Wu et al. 2012).

The importance of YB-1 in the development of metastatic features has been confirmed in cell culture experiments following YB-1 overexpression. The overexpression of YB-1 causes cells to develop mesenchymal and metastatic features (Evdokimova

et al. 2009a, Evdokimova et al. 2009b). YB-1 overexpression increases cell motility in a wound healing assay, and also rates of invasion in a matrigel invasion assay (Castellana et al. 2015). Overexpressing YB-1 in adenocarcinoma cells (MCF-7) leads to an invasive phenotype which is attributed in part to the interaction of YB-1 with Membrane type 1 matrix metalloproteinase (MT1-MMP) at the cell membrane, in structures referred to as invadopodia (Lovett et al. 2010). This interaction appears to promote cell motility in three-dimensional culture as the addition of a monoclonal antibody against MT1-MMP reverses the invasive phenotype. Depleting YB-1 in an invasive breast cancer cell line with metastatic potential, MDA-MB231, promotes an epithelial-like phenotype (Castellana et al. 2015). Indirect evidence for the ability of YB-1 to influence cell migration and invasion comes from experiments that show that inhibiting the activity of mammalian target of rapamycin (mTOR) reduces the levels of YB-1 while also reducing the migration and invasion of prostate cancer cells (PC-3) in three dimensional culture (Hsieh et al. 2012). Therefore, a number of studies have confirmed that YB-1 can promote metastatic characteristics.

YB-1 may increase the levels of many mesenchymal cell proteins while also reducing epithelial cell proteins. YB-1 promotes the expression of the mesenchymal cell markers (SNAI1 and TWIST) in breast cancer (Evdokimova et al. 2009a, Castellana et al. 2015) and bone osteosarcoma cells (U2OS; Lyons et al. 2016). Overexpression of YB-1 can also reduce the levels of the epithelial cell marker E-cadherin in breast cancer cells (Castellana et al. 2015). Similar results were obtained from colorectal cancers where YB-1 was inversely correlated with E-cadherin expression and positively correlated with N-cadherin and vimentin (Yan et al. 2014). There was an inverse correlation of YB-1 with the epithelial cell marker E-cadherin in prostate cancer cells (Khan et al. 2014).

Therefore, a number of studies have found that YB-1 correlates with metastasis in cancers. Furthermore, the results from *in vitro* culture experiments confirm that YB-1 promotes invasive behaviour and the expression of numerous protein markers of metastatic potential.

1.4.5 Functions of YB-1 in cancer; summary

The levels of YB-1 are elevated in many cancers and the functional consequences of this appear to include; the promotion of genomic instability, mitosis, drug resistance, and, metastasis. Promoting chromosome instability, mitosis, and cell survival during drug exposure, may rely on general interactions of YB-1 with cellular pathways that

control cell survival and check-point control mechanisms (p53, p16INK4a, E2F-family members). The role of YB-1 in promoting an invasive phenotype is less likely to be linked to these survival and check-point control mechanisms. Instead, it appears to rely on the ability of YB-1 to promote the expression of mesenchymal markers and to interact with membrane receptors. The diverse functions that have been attributed to YB-1 in cancer make it difficult to produce a cohesive model that incorporates all of these functions in a consistent way. The following sections review the details of the *YBX1* gene. The molecular activities of YB-1 are then reviewed as these appear to explain the functions of YB-1 in cancer.

1.5 The *YBX1* gene

The *YBX1* gene (Gene ID: 4904) is located on chromosome 1p34.2 (Qian et al. 1995, Makino et al. 1996) and it codes for a multifunctional protein that is 324 amino acids long. The *YBX1* gene comprises 8 exons that span 7 introns and covers 19 kilobases of genomic sequence (Toh et al. 1998). The processed *YBX1* mRNA (GI: 109134359) is 1561 bp in length and nucleotides 172 - 1146 encode the YB-1 protein. Ensembl (ENSG00000065978, GRCh38.p7) indicates the potential for multiple *YBX1* splice variants but they have not been reported in the literature which instead consistently confirms the existence of full-length *YBX1* mRNA (Kudo et al. 1995, Ohga et al. 1996). However, the use of alternative transcriptional start sites can vary the length of the 5′-untranslated region (UTR) of *YBX1* mRNA without altering the protein coding region of the transcript (Fukuda et al. 2004, Lyabin et al. 2014). Therefore, the *YBX1* gene appears to produce mRNA that codes for a single protein and if alternative splicing occurs it is a rare event.

Human *YBX1* is very similar to the homologous Y-box genes in other species (**Figure 1.4**; Wolffe 1994). Furthermore, *Homo sapiens* possesses four *YBX1* pseudogenes, located on 9p13.1, 14q23.3, 7q22.3, and 7q36.1. These were most likely generated by gene duplication events (Toh et al. 1998) and, excepting the pseudogene on 7q22.3 (YBX1P2), the *YBX1* pseudogenes lack introns. Processed *YBX1* pseudogenes are also found in *Bos Taurus* (Ozer et al. 1993b), rat (Ozer et al. 1993a), and mouse (Familari et al. 1994). None of these pseudogenes are believed to be translated to protein but it cannot be excluded as some intronless pseudogenes do produce protein (Rusk 2011).

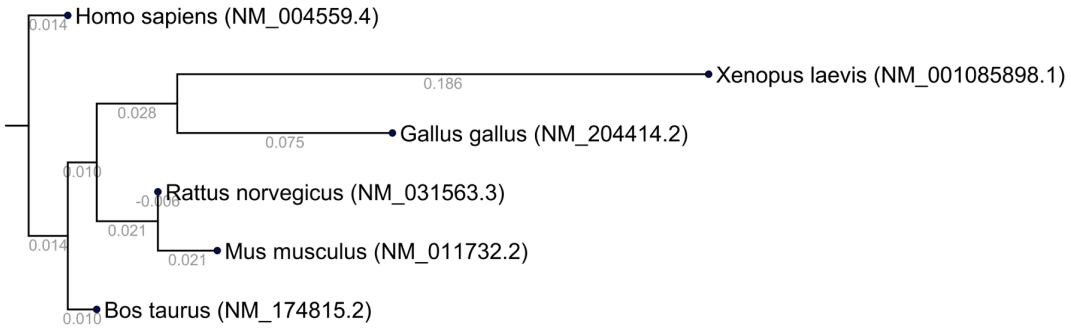

Figure 1.4: The *YBX1* gene is highly conserved in vertebrates. A phylogenetic tree showing the similarity of the sequences for *YBX1* mRNA in various mammals. The phylogenenetic tree was produced in CLC Sequence Viewer 8.0 from an alignment of the YBX1 mRNA sequences from a range of vertebrates (gap open cost = 10; gap extension cost = 1.1, End gap cost = as any other, Alignment mode = very accurate). The phylogenetic tree was produced using the neighbour joining algorithm with Kimura 80 as the distance measure. Distance measures are shown below each branch.

1.6 The structure of YB-1

The high level of conservation of the *YBX1* gene loci most likely relates to the membership of YB-1 in the super-family of cold-shock domain (CSD) proteins. In human YB-1 the CSD is encoded by amino acids 55 - 128 (**Figure 1.5**). Members of the cold-shock protein superfamily possess the ability to bind RNA, single stranded DNA (ssDNA) and double stranded DNA (dsDNA). Homologues are known to exist in prokaryotes and in eukaryotes from plants (Chaikam & Karlson 2010) to mammals (reviewed in Wolffe 1994, Kohno et al. 2003). Multiple regions of YB-1 have been implicated in binding to single-stranded DNA, and the region from 15 - 77 aa is important for binding to single-stranded nucleic acids (Kloks et al. 2002). There are two ribonucleoprotein motifs, RNP-1 at 70 - 77 aa and RNP-2 at 84 - 87 aa, within the CSD which also promote binding to nucleic acids (**Figure 1.5**; Kolluri et al. 1992, Landsman 1992, Wang et al. 2000). *Escherichia coli* cold-shock proteins consist of only the CSD. Many other eukaryotic CSD genes share amino terminus (N-terminus) or the carboxyl terminus (C-terminus) domains that are homologous to human YB-1 (**Figure 1.5**).

While the CSD is highly structured, both the N-terminus and the C-terminus of YB-1 appear to be intrinsically unstructured (Selivanova et al. 2010). Proteins containing unstructured domains are proposed to form hubs within biological networks due to their ability to form transient structures that can interact with a large number of other proteins (Dunker et al. 2005). Hence, the unstructured N-terminus and C-terminus of YB-1 may, in part, explain the wide range of functions and interactions

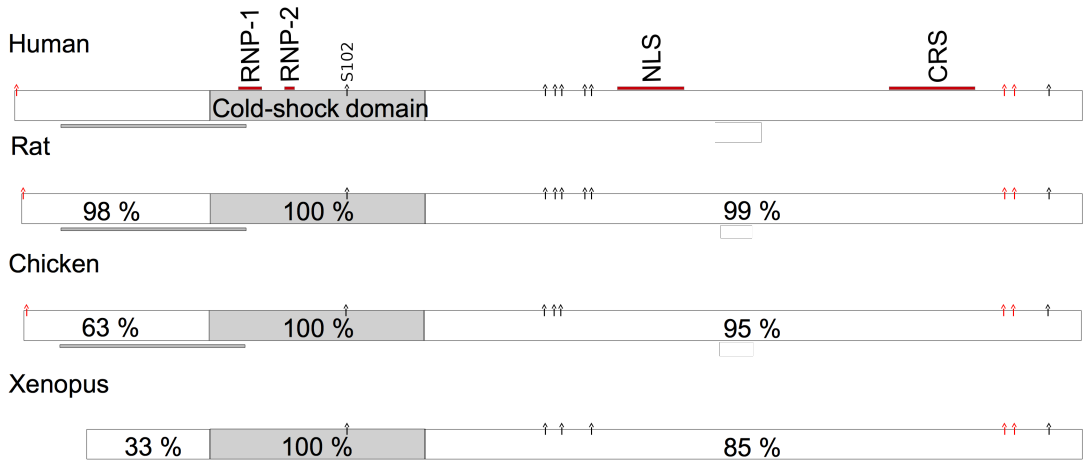

Figure 1.5: The protein structure of YB-1. Percentage figures are identity scores from Clustal alignments (CLUSTALO, `http://www.uniprot.org/help/sequence-alignments`). Red arrows above the protein diagrams indicate the positions of amino acid side chain acetylation and black arrows indicate the positions of amino acid side chain phosphorylation. Red bars above the protein diagrams represent reported structural motifs. The grey bar represents the region of YB-1 that interacts with ssDNA. CSD = cold-shock domain; RNP = RNA recognition motif; NLS = nuclear localisation signal; cleave = proteolytic cleavage site; CRS = cytoplasmic retention signal; S102 = serine 102 phosphorylation site.

that have been observed from YB-1.

The N-terminus (1 - 54 aa) of YB-1 contains a high proportion of alanine and proline residues and of the 3 domains on YB-1, the N-terminus has the fewest functions attributed to it. The C-terminus of YB-1 is comprised of $\sim$ 30 aa stretches where alternatively either acidic or basic amino acids predominate (Murray et al. 1992). The C-terminus of YB-1 also confers the protein with the ability to non-specifically bind to DNA and RNA (reviewed in Wolffe 1994, Ladomery & Sommerville 1994). In keeping with a role in binding to RNA, the C-terminus of YB-1 is required for YB-1 to incorporate into messenger ribonucleoprotein (mRNP)s (Matsumoto et al. 1996) and it is also required for YB-1 to promote translational repression of mRNA transcripts (Izumi et al. 2001). Furthermore, a cytoplasmic retention signal is also located in the C-terminus of YB-1 (267 - 293 aa; **Figure 1.5**).

Cleavage of the C-terminus of YB-1 between Glu-219 and Gly-220 is proposed to act as a signal for the N-terminus and CSD containing fragment to translocate to the nucleus. Here YB-1 can act as a transcription factor (Stenina et al. 2001, Sorokin et al. 2005). However, this cleavage event is not a prerequisite for the nuclear localisation of YB-1 following genotoxic stress (Cohen et al. 2010). Furthermore, some YB-1 antibody preparations produce a cross-reactive signal from HNRNP-A1

which localises to the nucleus of cells following stress. A recent publication proposes that there are two further nuclear localisation signals within YB-1 (van Roeyen et al. 2013). The C-terminus YB-1 fragment that is produced by proteasomal cleavage localises to the nucleus of cells following genotoxic stress to block the transcriptional activity of full-length YB-1. These conflicting reports are difficult to reconcile. With regards to post-translational cleavage of YB-1 a single point is certain, full-length YB-1 can translocate to the nucleus following stress (Cohen et al. 2010).

1.7 Regulation of *YBX1* gene expression and YB-1 function

1.7.1 Regulation of *YBX1* transcript

Many proteins and mechanisms can regulate the levels of *YBX1* mRNA and YB-1 in cells. A number of proteins can transactivate the *YBX1* gene (**Figure 1.6**). MYC can transcriptionally activate the *YBX1* gene in multiple myeloma cells (Bommert et al. 2013). A feedback loop exists between these two proteins as YB-1 also regulates the levels of MYC via the ability to promote translation of *MYC* mRNA (**Figure 1.6.B**; Cobbold et al. 2008, Cobbold et al. 2010). YB-1 and interleukin 6 (IL-6) also appear to mutually regulate one another. In keeping with a role for YB-1 in invasion and metastasis, the transcriptional control of the *YBX1* gene in cancers can be promoted by interleukin 6 (IL6) via the STAT3 pathway (Castellana et al. 2015). YB-1 has also been shown to promote the production of *IL-6* mRNA (Castellana et al. 2015) Furthermore, in macrophages YB-1 binds to and promotes the secretion of *IL-6* mRNA (Kang et al. 2014). Therefore, some of the trans-acting proteins for the *YBX1* gene form regulatory loops.

E(nhancer)-boxes in the promoter of the *YBX1* gene appear to be important to the transcriptional regulation of the *YBX1* gene (**Figure 1.6.C**; Makino et al. 1996). The E-box sequence (CANNTG) is most commonly found as the sequence CACGTG (Murre et al. 1989). A number of proteins interact with the E-box in the promoter of the *YBX1* gene. Following cisplatin exposure, tumor protein 73 (TP73) has been found to aid in the recruitment of a complex of MYC and Protein max (MAX) to the E-box upstream of *YBX1* to promote transcription from the *YBX1* gene (**Figure 1.6.B**; Uramoto et al. 2002). Neurogenic differentiation 6 (aka MATH2) also promotes transcription from *YBX1* in the brain of post-natal mice via an E-box

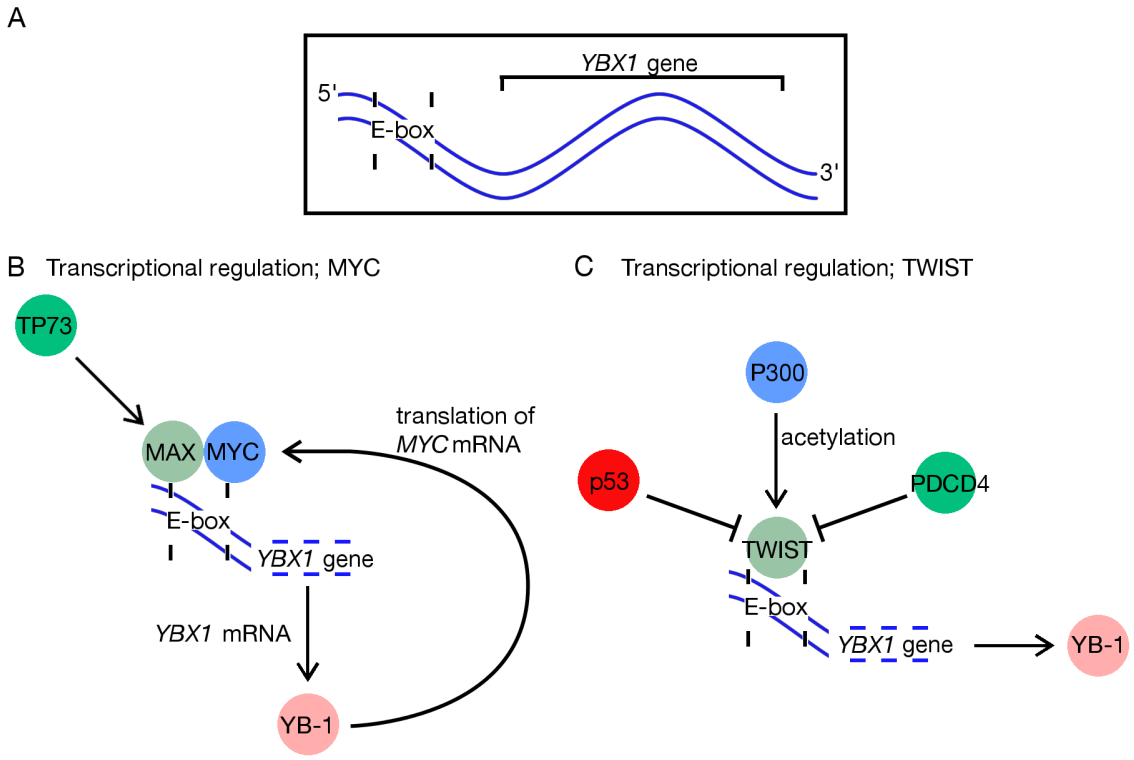

Figure 1.6: The *YBX1* gene is regulated by multiple transcription factors. **A**, a simplified cartoon of the *YBX1* gene loci showing the E-box that is in the 5′ promoter region. **B**, the MYC transcription factor binds to the E-box in the promoter of *YBX1* gene to promote the production of *YBX1* mRNA and YB-1. **C**, the TWIST transcription factor binds to the E-box in the promoter of *YBX1* gene to promote the production of *YBX1* mRNA and YB-1.

in the 5′ UTR of *YBX1* (Ohashi et al. 2009).

Twist homolog 1 (TWIST), a transcription factor, also binds to E-boxes and a number of studies highlight its ability to promote transcription of the *YBX1* gene (**Figure 1.6.C**). The initial reports link the regulation of *YBX1* by TWIST to the role of YB-1 in drug resistance by showing that TWIST can transactivate the *YBX1* gene in cisplatin-resistant cell lines (Shiota et al. 2008a).

A number of proteins and interactions appear to facilitate the transactivation of the *YBX1* gene by TWIST. For example, TWIST requires acetylation by histone acetyltransferase p300 (p300), an acetyltransferase that can regulate transcription through chromatin remodelling, before it can function as a transcription factor for *YBX1* (**Figure 1.6.C**; Shiota et al. 2010a). The transactivation of the *YBX1* gene by TWIST is inhibited by programmed cell death protein 4 (PDCD), a tumour suppressor protein with roles influencing transcription and translation, binding to the DNA-binding domain of TWIST (**Figure 1.6.C**; Shiota et al. 2009). p53 can also inhibit the ability of TWIST to transactivate the *YBX1* gene (**Figure 1.6.C**; Shiota et al. 2008b). Furthermore, overexpression of either YB-1 or TWIST blocks the ability of p53 to induce cell arrest. The relationship between YB-1 and TWIST appears to influence the function of YB-1 in cancer as a promoter of invasion and metastasis (Shiota et al. 2010b, Iwanami et al. 2014, Song et al. 2014). This is consistent with independent observations that TWIST also drives the formation of invadopodia in metastatic tumour cells (Eckert et al. 2011). Furthermore, the ability of TWIST to transactivate the *YBX1* gene may impact on the role of YB-1 in drug resistance and survival as well as in cell division (Shiota et al. 2010b).

The expression of the *YBX1* gene is regulated post-transcriptionally through the interaction of proteins with *YBX1* mRNA. Some of these proteins interact with the 5′-UTR region of *YBX1* mRNA (Yokoyama et al. 2003, Thoreen et al. 2012, Lyabin et al. 2012, Zaccara et al. 2014). YB-1 functions as a developmental protein during the maturation of haematopoeitic cells (Yokoyama et al. 2003). The expression of YB-1 is reduced by Erythroid transcription factor (GATA1) binding to an element in the 5′-UTR region (Yokoyama et al. 2003).

The 5′-UTR of *YBX1* mRNA also allows the mTOR pathway to promote the translation of *YBX1* mRNA (**Figure 1.7**; Thoreen et al. 2012, Lyabin et al. 2012, Zaccara et al. 2014, Lyabin & Ovchinnikov 2016). An oligopyrimidine motif (ATT CTCGCT) in the 5′-UTR of mouse *YBX1* mRNA subjects it to translational suppression following the inhibition of the mTOR pathway (Thoreen et al. 2012). The 5′-UTR of *YBX1* mRNA in humans contains a pyrimidine-rich translation element,

also known as a TOP-like motif, which allows the mTOR pathway to promote the translation of *YBX1* mRNA (Hsieh et al. 2012, Lyabin et al. 2012). The mTOR pathway promotes the translation of *YBX1* mRNA through the ability of the mTOR complex 1 (mTORC1) to inhibit the eukaryotic translation initiation factor 4E-binding protein (4E-BP) which itself inhibits translational initiation by binding to eIF4E, or other 4F-group proteins (**Figure 1.7**; translational initiation is reviewed in **Chapter 1.8.3.2**; Thoreen et al. 2012, Hsieh et al. 2012, Lyabin et al. 2012). Lyabin & Ovchinnikov (2016) suggest that 4E-BP and 4F-group proteins are dispensable to the action of the mTOR pathway on *YBX1* mRNA translation. Irrespective of this suggestion, the study does confirm the ability of mTOR to promote the translation of *YBX1* mRNA. The ability of the mTOR pathway to increase levels of YB-1 may support features of metastatic cancers (**Chapter 1.4.4**; Hsieh et al. 2012). During stress, induced by doxorubicin exposure, p53 can reduce the translation of *YBX1* mRNA by inhibiting the mTOR pathway (**Figure 1.7**; Zaccara et al. 2014). Lyabin et al. (2012) also provides indirect support for the importance of the interaction of YB-1 and the mTOR pathway by showing that as the confluence of both mouse embryonic fibroblast cells (3T3) and human embryonic kidney cells (HEK293) increases, mTOR signalling leads to reduced levels of YB-1 which in turn may slow cell division (**Chapter 1.4.2**). Therefore, the mTOR signalling pathway can increase levels of YB-1 by promoting the translation of *YBX1* mRNA. The interaction of mTOR pathway with YB-1 translation appears to be relevant to the functions of YB-1 that relate to drug resistance and metastatic cancer.

In addition to regulation by other genes and proteins, YB-1 has also been found to autoregulate the translation of *YBX1* mRNA. The *YBX1* promoter lacks a CAAT-box or TATA-box in the 10 kilobases that are upstream of the gene; thus ruling out autoregulation of *YBX1* transcription via a Y-box sequence (Makino et al. 1996). However, this same 5′ promoter sequence is composed of 70% G and C nucleotides which could attract YB-1 binding (see **Chapter 1.8.1**). YB-1 negatively regulates the translation of *YBX1* mRNA via two binding elements. Translational inhibition is caused by the binding of YB-1 to an element in the 3′ UTR of *YBX1* mRNA. This excludes polyadenylate-binding protein (PABP) from binding to and promoting the translation of the *YBX1* mRNA (Skabkina et al. 2005, Lyabin et al. 2013). The second YB-1 binding element is in the 5′ UTR of *YBX1* mRNA. This also inhibits the translation of *YBX1* mRNA although the mechanisms are unknown (Fukuda et al. 2004). However, the *YBX1* 5′ UTR that was cloned by Fukuda et al. (2004) is 160bp longer than the canonical *YBX1* mRNA sequence and only one of the studies

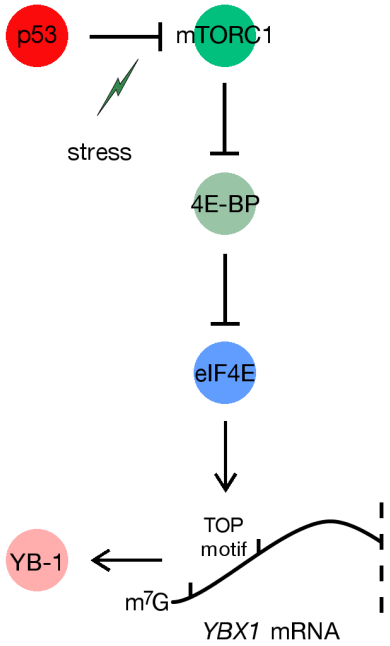

Figure 1.7: mTORC1, from the mTOR pathway, can promote the translation of *YBX1* mRNA. The TOP motif, shown above *YBX1* mRNA, can also be a pyrimidine-rich translation element. 4E-BP and eIF4E may be dispensable for mTORC1 regulation of *YBX1* mRNA translation.

elements lies within the commonly observed 5′ UTR (Lyabin et al. 2011). This makes the results difficult to interpret.

YBX1 gene expression is known to be modulated by a variety of proteins. A negative feedback loop exists whereby the translation of *YBX1* mRNA can be inhibited by YB-1. TWIST also appears to be an important regulator of the *YBX1* gene. The post-transcriptional regulation of *YBX1* mRNA by the mTOR pathway also appears to be a significant positive regulator of *YBX1* gene expression.

1.7.2 Regulation of YB-1 activity

The concentration of YB-1 affects the activity of the protein. For example, the loss of one or both *YBX1* alleles sensitizes mouse fibroblasts to DNA damage from mitomycin C and cisplatin; this shows that *YBX1* is haploinsufficient (Shibahara et al. 2004, Lu et al. 2005). Therefore, it appears possible that mechanisms that alter the concentration of YB-1 molecules in the cell, impact indirectly on the activity(s) of YB-1 at the molecular level. The apparent shift in YB-1 function that occurs when levels of YB-1 increase may be driven by changes in the rate of post-translational modification (PTM) on YB-1 as competition for kinases may alter the PTM of

YB-1 This shift could also be n effect of the alteration of YB-1:RNA ratios in RNP complexes (see **Chapter 1.8.3.2**). Some PTMs such as the acetylation of S2 and K81 have unknown effects on YB-1 function (Choudhary et al. 2009, Gauci et al. 2009). Similarly, a single study indicates that following DNA damage, YB-1 may become poly(ADP-ribosyl)ated by poly(ADP-ribose)polymerase 1 (PARP1; Alemasova et al. 2015). However, as discussed below, various PTMs have known effects on YB-1 function.

1.7.2.1 Regulation of YB-1 activity; phosphorylation

Phosphorylation is the addition of a phosphate group (HPO_3) mainly to serine, threonine or tyrosine residues by a kinase. Phosphorylation is a common post-translational modification that can alter protein function (Rubin & Rosen 1975). YB-1 has many potential phosphorylation sites. Most of these are conserved in the YB-1 homologues in other species, supporting the idea that they are important to YB-1 function (**Figure 1.5** and **Table 1.1**).

Table 1.1: The YB-1 residues that have been shown to be phosphorylated in human samples are conserved in other species.

Human	Rabbit	Rat	Mouse	Chicken	Xenopus
S2	y	y	y	y	y
T7	y	y	y	y	y
S102	y	S100	S100	S99	S80
Y158	y	Y156	Y156	Y155	Y136
Y162	y	S160	S160	S159	Y140
S165	y	S163	S163	S162	-
S167	y	S165	S165	S164	S145
S174	y	S172	S172	-	
S176	y	S174	S174	-	S152
S313	y	S311	S311	T310	T292
S314	y	S312	S312	S311	S293

"y" indicates that the residue bears the same exact position in the protein as the human YB-1 residue. "-" indicates that the residue is not present in the protein. **Abbreviations**; S = serine, T = threonine, Y = tyrosine.

High-throughput studies have revealed that many serine and threonine residues on YB-1 are commonly phosphorylated. These studies show that YB-1 is phosphorylated at residues spanning the length of the protein across a range of cell types and growth conditions (S2, T7, S102, Y158, Y162, S165, S167, S174, S176, S313,

and S314; Molina et al. 2007, Sugiyama et al. 2007, Dephoure et al. 2008, Kyono et al. 2008, Ruse et al. 2008, Sui et al. 2008, Tsai et al. 2008, Brill et al. 2009, Gauci et al. 2009, Nagano et al. 2009, Van Hoof et al. 2009, Han et al. 2010, Olsen et al. 2010). Phosphorylation of the residues from S165 to S176 and of S314 has been detected by a minimum of 8 studies for each site, indicating that these modifications are common. However, S102 (Pan et al. 2009, Brill et al. 2009) and S313 (Gauci et al. 2009, Olsen et al. 2010) have only been detected by two studies respectively. This disparity may indicate that YB-1 sequences containing phosphorylation at S102 or S313 are difficult to detect using the method of liquid chromatography-coupled tandem mass spectrometry (LC-MS/MS) or, that it is rare for YB-1 to be phosphorylated at these residues. The former appears to be most likely for YB-1 peptides that are phosphorylated at S102 as the phosphorylation of S102 has been confirmed by numerous biochemical studies (discussed below).

There is limited information regarding the functional consequences of YB-1 being phosphorylated at most of the known sites. However, phosphorylation in general has been shown to influence the activity of YB-1. For example, phosphorylation of the *Xenopus* YB-1 homologue affects its ability to bind to nucleic acids (Tafuri & Wolffe 1993, Murray et al. 1991, Kick et al. 1987) and phosphorylated rabbit YB-1 is incorporated into free and polysomal mRNPs in ribosome-free rabbit reticulocytes (Minich et al. 1993). YB-1 requires phosphorylation by Mitogen-activated protein kinase 1 (MAPK1, also known as ERK2) and Glycogen synthase kinase-3 beta (GSK3β) to bind to single-stranded DNA in the hypoxia responsive region that is downstream of the Vascular endothelial growth factor (*VEGF*) gene. This binding also inhibits the transcription of *VEGF* (Coles et al. 2005). These studies indicate that phosphorylation enhances the ability of YB-1 to bind to nucleic acids. The phosphorylated YB-1 residues and the kinases involved remain unidentified.

The functional significance of phosphorylation at two specific sites on YB-1 has been described. Prabhu et al. (2015) found that treating HEK293 cells with Interleukin-1 beta (IL-1β) leads to the phosphorylation of ectopically expressed YB-1 at S165. It should be noted that the authors have failed to fully annotate the MS/MS spectra (T. Kleffmann, personal communication). Examination of the MS/MS spectra for the fragment ions that indicate the presence of HPO_3, or a loss of H_3PO_4, on an amino acid side chain shows that the MS/MS spectra comes from two peptides each with a single phosphorylation, one at S165 and the other at S167 (see **Supplementary A.1 - A.1.1** for notes on MS/MS fragmentation and the analysis of phosphorylated peptides). Prabhu et al. (2015) found that the phosphorylation

of YB-1 at S165 is necessary for NF-κB activation which in turn is likely to facilitate the development of colon tumours. Therefore, the function of phosphorylation at S165 seems to impact on the ability of YB-1 to promote the early stages of cancer development (Prabhu et al. 2015).

The phosphorylation of S102 on YB-1 appears to be an important marker of the activity of YB-1 in cancer cells. It is thought to influence the ability of YB-1 to bind to nucleic acids as S102 resides within the CSD and, as such, this region is involved in DNA binding (Wu et al. 2006). Phosphorylation of YB-1 at S102 has been observed in breast cancer cells (Sutherland et al. 2005, Evdokimova et al. 2006b, Bader & Vogt 2008, Law et al. 2010, Toulany et al. 2011), monocytes (Alidousty et al. 2014), and the granulosa cells that surround ovaries (Donaubauer & Hunzicker-Dunn 2016). Furthermore, phosphorylation of YB-1 at S102 has been correlated with aggression and metastasis in melanomas (Sinnberg et al. 2012) and with epithelial to mesenchymal transition in prostate cancer cells (Khan et al. 2014). Therefore, phosphorylation of YB-1 at S102 appears to be common in a wide range of cancers and it is also important to YB-1 function.

Multiple kinases can phosphorylate YB-1 at S102. Expression of AKT is correlated with YB-1 in breast tumours and AKT can phosphorylate S102 of YB-1 (Sutherland et al. 2005, Evdokimova et al. 2006b, To et al. 2007). p90 ribosomal S6 kinase (RSK) also phosphorylates YB-1 at S102, and it appears to do so with a greater efficiency than AKT (Stratford et al. 2008, Aronchik et al. 2014). Furthermore, a point mutation of the *K-ras* gene at codon 13 (Hollestelle et al. 2007), which activates the PI3K/AKT pathway and is common in some cancer, leads to constitutive phosphorylation of YB-1 at S102 (Toulany et al. 2011). The phosphorylation of YB-1 at S102 was increased in granulosa cells following exposure to follicle stimulating hormone (FSH) via the ERK/RSK-2 signaling pathway (Donaubauer & Hunzicker-Dunn 2016). The authors showed that RSK-2 does not phosphorylate S102 but it inhibits the activity of a phosphatase, Serine/threonine-protein phosphatase PP1-beta catalytic subunit (PP1β), that dephosphorylates S102 on YB-1 (Donaubauer & Hunzicker-Dunn 2016). YB-1 is also phosphorylated in monocytic cells where it promotes maturation to macrophages by binding to the promoter of C-C motif chemokine 5 (*CCL5*, also known as regulated upon activation, normal T cell expressed and secreted [RANTES]). Calcineurin acts as a phosphatase and removes the phospo-group from S102 of YB-1 late in the process of macrophage maturation (Raffetseder et al. 2012, Alidousty et al. 2014). Therefore, the phosphorylation of YB-1 at S102 appears to be regulated via multiple kinases and phosphatases.

Multiple alterations to the function of YB-1 have been linked to its phosphorylation at S102. The phosphorylation of YB-1 at S102 appears to play a role in mitosis. However, phosphorylation of YB-1 at S102 has no significant effect on mitosis in adherent cells. Instead, it promotes the growth of a range of cells in soft-agar (Anchorage independant growth; Sutherland et al. 2005, Aronchik et al. 2014). A decoy that partially prevents the phosphorylation of S102 without lowering cellular levels of YB-1 protein inhibits the growth of cancer cells and also sensitises them to trastuzumab, a monoclonal antibody that inhibits the HER2 receptor from activating the MAPK and the PI3k/AKT pathways (Law et al. 2010). Depleting YB-1 or inhibiting the phosphorylation of YB-1 at S102 reduces the expression of HER-2 and EGFR in breast cancer cells (Sutherland et al. 2005, Wu et al. 2006, Law et al. 2010). Furthermore, the role of YB-1 in promoting cytokinesis failure in normal breast epithelial cells (HUMEC) is reliant on phosphorylation of S102 and only YB-1 that is phosphorylated at S102 localises to the centrosomes (Davies et al. 2011, Davies et al. 2014, Kawaguchi et al. 2015). Currently, it is unclear how phosphorylation of YB-1 at S102 links the promotion of anchorage independent growth with cytokinesis failure.

The phosphorylation of YB-1 at S102 is also important to DNA damage response signalling. YB-1 that is phosphorylated at S102 promotes the survival of cells following UV irradiation, most likely due to the involvement of this phosphorylated form of YB-1 in the repair of double-stranded DNA breaks (Toulany et al. 2011). Increased levels of phosphorylated YB-1 were also observed in the renal and inflammatory cells of a murine model for acute peritonitis (Hanssen et al. 2013). The phosphorylation of YB-1 at S102 is also required for Follicle stimulating hormone exposure to increase the levels of a range of mRNA transcripts involved in steroidogenesis (Donaubauer & Hunzicker-Dunn 2016). The effects of phosphorylation of YB-1 at S102 appear to be important to the function of YB-1 but the research presents a paradox as phosphorylation at S102 is critical to DNA binding but also critical to the interaction of YB-1 with the mircotubules of the centrosome that are specifically separate from DNA.

Summary

To date the effects of phosphorylations of YB-1 at two sites (S102 and S165) have been studied. Phosphorylation of YB-1 at both of these sites leads to significant changes in the function of YB-1.

Other serine, threonine, and tyrosine residues in YB-1 appear to be phosphory-

lated in a number of cell types (reviewed above). These phosphorylation sites are conserved in a range of YB-1 homologues in vertebrates (**Table 1.1**). Therefore, phosphorylation of YB-1 at these sites is conserved across a range of cell types and also between species. This infers that any alterations to the function of YB-1 that result from these phosphorylations are also likely to be conserved across a range of cell-types and between species. Currently, the effects of phosphorylation at these sites on the functions of YB-1 are uncharacterised. Furthermore, few studies have focused on the systematic characterisation of the phosphorylation states of YB-1. The work presented in **Chapter 4** provides a systematic survey of YB-1 phosphorylation in two cancer cell lines. The elucidation of the prevalence of phosphorylation at other YB-1 residues should be a priority given their potential to also confer multifunctionality to YB-1. Multiple phosphorylation of YB-1 at S102 and another site may explain the paradoxical alterations of YB-1 function that are currently ascribed solely to the phosphorylation of YB-1 at S102.

1.7.2.2 Regulation of YB-1 activity; ubiquitin and the proteasome.

YB-1 has been shown to be subject to regulation by ubiquitination and the proteasome (discussed in **Chapter 1.6**; Stenina et al. 2000, Stenina et al. 2001, Sorokin et al. 2005, Lutz et al. 2006, Chibi et al. 2008, van Roeyen et al. 2013). The interaction of YB-1 with the proteasome appears to be regulated at various levels. RBBP6 (retinoblastoma binding protein 6), a putative E3 ubiquitin ligase, binds to and ubiquitinates the C-terminus of YB-1 leading to its degradation by the proteasome (Chibi et al. 2008). The N-terminus of YB-1 can also be polyubiquitinated by F-box 33 prior to its proteasomal degradation (Lutz et al. 2006). The conditions under which these two proteins ubiquitinate YB-1 are not fully characterised.

The ability of proteasomal cleavage of YB-1 to modify the function of YB-1 was discussed in **Chapter 1.6**. The proteasomal cleavage of YB-1 between Glu-219 and Gly-220 may lead to the truncated protein accumulating in the nucleus (Sorokin et al. 2005). However, this mechanism is not evident in human cancer cell lines (Cohen et al. 2010). Thrombin has also been shown to cleave YB-1 in endothelial cells and this cleaved YB-1 is also transcriptionally active (Stenina et al. 2000). Furthermore, thrombin treatment of epithelial cells appears to inhibit the ability of YB-1 to bind to mRNA (Stenina et al. 2001). Thrombin cleaves purified YB-1 protein via a non-canonical site *in vitro* making the mechanism and relevance of thrombin treatment difficult to interpret (unpublished data, Algie and Braithwaite).

Therefore, the significance of the proteasomal cleavage of YB-1 is unclear as it is not a requirement for stress induced nuclear localisation of YB-1 (Cohen et al. 2010).

The nuclear localisation of YB-1 has been discussed in **Chapter 1.6**. In general, ∼90% of YB-1 is located in the cytoplasm of cells where it binds to mRNA and promotes the formation of mRNPs (Evdokimova et al. 2006a). However, studies have observed YB-1 accumulating, or being present, in the nucleus of cells in response to adenoviral infection (Holm et al. 2002), hyperthermia (Stein et al. 2001), and DNA damage (Koike et al. 1997, Kamura et al. 1999). YB-1 can require p53 to translocate to the nucleus following cellular stress (Zhang et al. 2003, Homer et al. 2005, Guay et al. 2006). The accumulation of YB-1 in the nucleus is presumed to relate primarily to the increased activity of YB-1 as a transcription factor. The C-terminus of YB-1 contains a cytoplasmic retention signal (Koike et al. 1997) and, as mentioned previously, proteasomal cleavage of the C-terminus of YB-1 causes the truncated N-terminus plus CSD protein to accumulate in the nucleus (Sorokin et al. 2005). Phosphorylation of S102 has also been posited as a requisite for nuclear localisation of YB-1 in ovarian cancer (Basaki et al. 2007). YB-1 is also reported to localise to the nucleus of cells during the G_1/S phases of mitosis (Jurchott et al. 2003). Therefore, the subcellular localisation of YB-1 appears to be dynamic, with the YB-1 localising throughout the cell depending on its function.

1.8 Mechanisms of YB-1 activity

YB-1 takes part in a variety of cellular processes. Many of those processes occur because YB-1 can promiscuously bind to nucleic acids. This section will outline those nucleic acid binding properties and the cellular processes in which YB-1 plays a important role.

1.8.1 Nucleic acid binding

YB-1 binds to nucleic acids in both a sequence non-specific and a sequence specific manner (Wolffe 1994). Nucleic acid binding is integral to the ability of YB-1 to influence the transcription of genes and the splicing, translation, and stability of RNA transcripts. Therefore, knowledge of which nucleic acid sequences YB-1 binds is important to understanding the function of the protein.

The study of the nucleic acid binding affinity of YB-1 is complicated by three factors. The first is that YB-1 has a general affinity for nucleic acids (Bouvet

et al. 1995). Furthermore, it can be difficult to assess the applicability of nucleic acid binding studies that use YB-1 homologues from other species. However, the strong homology of the protein in many species indicates that most homologues are likely to share binding preferences with YB-1. Finally, the extensive phosphorylation of YB-1 may alter the nucleic acid binding characteristics of YB-1 (**Chapter 1.7.2**). The phosphorylation of YB-1 is likely to vary with the cellular context. Some studies also use YB-1 that has been produced by bacteria and this YB-1 will lack the extensive phosphorylation of endogenously produced YB-1 (**Chapter 1.7.2**).

YB-1 binds to inverted Y-boxes (CAAT-boxes) *in vitro* (Dorn et al. 1987, Ozer et al. 1990). For example, YB-1 binds to the Y-boxes in the promoters of Human leukocyte antigen (HLA; also known as Major Histocompatibility complex) class II genes (Didier et al. 1988, Rakoff-Nahoum et al. 2001). Subsequent studies have shown that YB-1 does not bind to and reduce the melting temperature of the classic Y-box sequence (ATTG) any more aggressively than other sequences. Instead, the alternative Y-box sites GGTC and TGGT were strongly bound by YB-1 (Zasedateleva et al. 2002). Therefore, the general DNA and RNA binding preferences of YB-1 are varied.

While studies of individual binding sites are informative, there have also been attempts to deduce global rules for the interaction of YB-1 with nucleic acids. YB-1 binds DNA sequences that are rich in pyrimidines (C/T; Kolluri et al. 1992). It has been shown that there are two pyrimidine rich YB-1 binding sites in the 5′ UTR of the *VEGF* mRNA and YB-1 appears to mediate the incorporation of polypyrimidine tract binding protein (PTB) to these complexes (Coles et al. 2004). However, high-throughput studies indicate that YB-1 preferentially binds to ssDNA and RNA 7-mer sequences that are enriched with guanine (Minich et al. 1993, Zasedateleva et al. 2002). Furthermore, a recent and exhaustive RNA-binding screen confirms that YB-1 possesses both of the preceding preferences by showing that YB-1 strongly binds to both pyrimidine rich and G-rich sequences. In this study, the top 5 YB-1 binding motifs are comprised of 60% pyrimidines (C/U) without any adenines meaning that the sequences are also enriched (40%) for guanine (Ray et al. 2009). Another study shows that YB-1 has an affinity for GC rich sequences (Dong et al. 2009). Endogenous rabbit YB-1 can inhibit the translation of its own mRNA via a UCCA(G/A)CAA motif in the *YBX1* mRNA (Skabkina et al. 2005). The differences in the RNA binding motifs that have been identified in these studies may be explained, as is noted above, by inherent differences between YB-1 homologues or by the phosphorylation of YB-1 altering the nucleic acid binding prefer-

ences of YB-1. The two high-throughput studies utilise recombinant YB-1 which will have different PTMs to endogenous YB-1 (see **Chapter 1.7.2**). Furthermore, as discussed in subsequent sections of this review, other proteins interact with YB-1 to modulate the effects of its nucleic acid binding.

YB-1 binds double-stranded DNA but possesses a higher affinity for ssDNA (Tafuri & Wolffe 1992, Izumi et al. 2001). For example, YB-1 binds preferentially, and in a sequence specific manner, to x-box sequences in promoters as ssDNA, and less so to dsDNA in Y-box sequence (MacDonald et al. 1995, Zasedateleva et al. 2002). YB-1 can also separate strands to create ssDNA in both Y-boxes and x-boxes (MacDonald et al. 1995). The RNP-1 motif is thought to be responsible for the ssDNA binding activities of YB-1 (Kolluri et al. 1992). The N-terminus and C-terminus of YB-1 also contribute to the ability of YB-1 to bind RNA (Bouvet et al. 1995).

YB-1 may recognise DNA structure, mismatched bases, and modified nucleic acids (see **Chapter 1.8.2.2** below) in addition to its sequence specific preferences (reviewed in Swamynathan et al. 1998). YB-1 preferentially binds a ssDNA sequence that forms an intramolecular triplex (Horwitz et al. 1994). However, a high-throughput screen of structured and unstructured 7-mer RNA sequences found that the sequence specific binding of YB-1 to RNA is unaffected by tertiary RNA structure (Ray et al. 2009). YB-1 decreases the melting temperature of dsDNA (MacDonald et al. 1995, Zasedateleva et al. 2002). One exception to this is dsDNA sequences containing poly-G runs; here YB-1 increases the melting temperature (Zasedateleva et al. 2002). Furthermore, YB-1 also separates dsDNA and RNA sequences that contain mismatches and facilitates the annealing of strands of complimentary DNA and RNA (Skabkin et al. 2001, Gaudreault et al. 2004).

The involvement of YB-1 in epigenetics is implied via the ability of YB-1 to preferrentially bind to methylated cytosines (Dürnberger et al. 2013). Notably, this research found that YB-1 did not display enriched RNA binding. The evidence for YB-1 participating in epigenetic processes has also come via the observation that in renal cell carcinomas, YB-1 and Enhancer of Zeste Homolog 2 (EZH2), a polycomb histone methyltransferase that modifies epigenetic code are positively correlated with one another (Wang et al. 2015a). However, Wang et al. (2015a) links the correlation to the ability of YB-1 to promote transcription of *EZH2* mRNA rather an interaction of YB-1 and EZH2 while binding to methylated DNA.

Summary

YB-1 has a strong general affinity for all nucleic acids. The interaction of YB-1 with RNA and DNA has been studied in multiple situations. The results show that YB-1 has a range of preferences for nucleic acid binding which will be reviewed in a functional context in the following sections.

1.8.2 DNA-binding protein

The ability to bind to DNA appears to be central to the functions of YB-1 in cancer (**Chapter 1.4**). The nuclear localisation of YB-1 has been correlated with cancer progression (Bargou et al. 1997, Janz et al. 2002) which has led to a focus on the role of YB-1 in modulating transcription in cancer. This focus is reinforced by the correlation of nuclear localisation of YB-1 and drug resistance via the transcription of the *ABCB1* gene (Bargou et al. 1997). The ability to bind DNA provides YB-1 with two mechanistic pathways to participate in cancer progression. The first is by acting as a transcription factor and the second is participating in DNA repair. The details of these two mechanisms are reviewed in the following sections.

1.8.2.1 Transcription factor

The ability of YB-1 to act as a transcription factor has been confirmed repeatedly; **Table 1.2** includes a subset of known YB-1 transcriptional target genes. Notably, YB-1 can transactivate, and also repress, target genes to influence many of the functions that YB-1 has in cancer (these functions are reviewed in **Chapter 1.4**). YB-1 is capable of acting as a transcription factor for genes containing Y-box elements in their promoters (Spitkovsky et al. 1992, Gronostajski et al. 1984).

The ability of YB-1 to act as a transcription factor may allow it to promote drug resistance. By binding to an inverted CCAAT-box in the *ABCB1* gene promoter, YB-1 can stimulate *ABCB1* transcription during cellular stress (Asakuno et al. 1994, Ohga et al. 1996, Ohga et al. 1998, Sengupta et al. 2011, Chattopadhyay et al. 2008). Cofactors may be required for YB-1 to transactivate *ABCB1* as acetylated human apurinic/apyrimidinic (AP) endonuclease 1 (APE1) acts as a cofactor for YB-1 during the regulation of MDR-1 transcription (Sengupta et al. 2011).

YB-1 does not activate the transcription of *ABCB1* in all contexts. Overexpression of YB-1 in prostate cancer cell lines has no effect on the levels of MDR-1 (Saupe et al. 2014). Furthermore, depleting YB-1 has no effect on the levels of *ABCB1* mRNA and MDR-1 or, on the survival of a human pancreatic carcinoma cell line that is reliant on MDR-1 for resistance to the DNA-intercalculating drug

Table 1.2: A subset of the genes that YB-1 can influence at the transcriptional level.

Gene	Activated	Repressed	Interaction via Y-box	Citation
ABCB1	x		x	Asakuno et al. (1994)
Fas receptor/CD95		x		Lasham et al. (2000)
Thymidine kinase	x			Dorn et al. (1987)
Cyclin A	x		x	Jurchott et al. (2003)
Cyclin B1	x		x	Jurchott et al. (2003)
DNA topoisomerase 11 α	x			Shibao et al. (1999)
Major vault protein	x		x	Stein et al. (2005)
myosin light-chain 2v	x		x	Zou & Chien (1995)
MMP2	x	x	x	Mertens et al. (1997)
HER2	x		x	Sakura et al. (1988)
EGFR	x		x	Sakura et al. (1988)
Tyrosine-protein phosphatase non-receptor type 1	x			Fukada & Tonks (2003)
MHC class II		x	x	Didier et al. (1988)
collagen-α *1*		x	x	Higashi et al. (2003)
GM-CSF		x		Diamond et al. (2001)

Daunorubicin (Kaszubiak et al. 2007). It has been postulated recently that YB-1 does not bind to the inverted CCAAT-box *in vivo* as there is little evidence that YB-1 binds to Y-boxes in sequencing data from chromatin immunoprecipitation of YB-1 (Dolfini & Mantovani 2013a, Dolfini & Mantovani 2013b). Many studies correlate *ABCB1* mRNA, or MDR-1, and YB-1 in cancer (**Chapter 1.4.3**). Therefore, the relationship between the two appears to be important. However, it appears that YB-1 influences the transcription of *ABCB1* in specific contexts.

There are other genes that YB-1 is known to transactivate via a Y-box in their promoter region. The ability of YB-1 to promote metastatic features may relate the transactivation of matrix metalloproteinase 2 (*MMP2*) and the subsequent secretion of the protein that MMP2 encodes, 72 kDa type IV collagenase (also known as gelatinase A; Mertens et al. 2002). Exposure to ionizing radiation leads to YB-1 promoting the transcription and secretion of MMP2, and p53 and Transcription factor AP-2-alpha are required as cofactors (Mertens et al. 2002). The ability of YB-

1 to transactivate the *MMP2* gene has been confirmed in a variety of cell lineages (van Roeyen et al. 2013, Schittek et al. 2007, Shinkai et al. 2016). Lovett et al. (2010) shows that overexpressing YB-1 in MCF-7 cells promotes an invasive phenotype which occurs because, rather than a strong transactivation of the *MMP2* gene, YB-1 overexpression leads to the presentation of 2 kDa type IV collagenase at the surface of migrating cells. The increased levels of MMP2 promote invasive features in cells which links to the role of YB-1 in invasion.

YB-1 also activates and represses the transcription of genes that lack Y-boxes in their promoters. By binding to single-stranded DNA, YB-1 can repress the transcription of Tumor necrosis factor receptor superfamily member 6 (*CD95*, also known as the fas receptor; Lasham et al. 2000). The CD95 protein is capable of inducing apoptosis and this inhibition may impact on the ability of YB-1 to promote apoptosis. Other work has shown that YB-1 may inhibit p53 from transactivating target genes (Homer et al. 2005).

YB-1 can also transactivate genes that promote mitosis. YB-1 binds the promoter of *ERBB2* and *EGFR in vitro* (Sakura et al. 1988) and has more recently been found to enhance the expression of both *ERBB2* and *EGFR* mRNA (Wu et al. 2006). YB-1 elevates the levels of other transcripts in the MAPK pathway and poor survival of patients from colorectal cancer has been correlated with both a MAPK pathway gene signature and YB-1 (Jürchott et al. 2010). YB-1 levels are positively correlated with *ERBB2* and *EGFR* expression in breast tissue (Turashvili et al. 2011) and ER/PR negative breast tumours that include the HER-2 positive tumours (Woolley et al. 2011).

YB-1 promotes the progress of cells through G_1/S by inhibiting the expression of cyclin-dependent kinase inhibitors, p21(Cip1) and p16(INK4A), that prevent cell cycle progression and may induce senescence (Basaki et al. 2010, Yu et al. 2010, Davies et al. 2014). YB-1 binds to a Y-box located in the promoter of the *CDC6* gene, which promotes DNA synthesis during the S-phase of the cell cycle, and the levels of *CDC6* mRNA reduced when YB-1 was depleted (Basaki et al. 2010). Depleting YB-1 also led to decreased levels of mRNA transcripts for other genes that promote passage through the cell cycle (cyclin D1 [*CCND1*], *CDK1* and *CDK2*). In non-small cell lung carcinomas, YB-1 may promote mitosis via transcriptional activation of genes associated with mitosis; *CCND1* and an associated protein CDC6 (Harada et al. 2014).

Summary

YB-1 can act as a transcription factor for a number of genes with functions that are consistent with the roles of YB-1 in cancer (**Chapter 1.4**). The ability of YB-1 to act as a transcription factor is promoted as the mechanistic link to many of its functions in cancer. This is one of the reasons that the nuclear localisation is considered to be an important feature of YB-1 in cancer.

1.8.2.2 DNA repair

The importance of YB-1 to cell survival during exposure to a range of DNA damaging drugs is reviewed in **Chapter 1.4.3**. The ability of YB-1 to bind to DNA provides YB-1 with the opportunity to directly participate in DNA repair. YB-1 is involved in DNA repair via a role in base excision repair, a pathway that repairs DNA sites that are abasic, apurinic/apyrimidinic. YB-1 has a greater binding affinity for depurinated DNA than for undamaged DNA (Hasegawa et al. 1991). Besides effectively binding nucleic acid sequences containing apurinic/apyrimidinic bases, YB-1 also preferentially binds to cisplatin, mitomycin C, and UV modified DNA (Ohga et al. 1996, Ise et al. 1999). YB-1 has not only been implicated in the repair of genomic DNA but also in mismatch repair in mitochondrial DNA (de Souza-Pinto et al. 2009).

YB-1 interacts directly with damaged DNA and the C-terminus of YB-1 is thought to help to target and recruit DNA repair proteins to damaged DNA (Ise et al. 1999, Gaudreault et al. 2004, Skabkin et al. 2001). A number of DNA repair proteins have been shown to interact with YB-1 during DNA repair, for example glycosylase, Endonuclease 8-like 2 (NEIL2), DNA polymerase beta and gamma, DNA ligase II, APE1, DNA mismatch repair protein Msh2 (MSH2), X-ray repair cross-complementing protein 5 (XRCC5 also known as Ku80), Werner syndrome ATP-dependent helicase (WRN), and endonuclease III (Das et al. 2007, Gaudreault et al. 2004, Marenstein et al. 2001). PCNA is a protein that is involved in targeting a DNA polymerase that replaces excised DNA fragments during base excision repair (Sancar et al. 2004). PCNA interacts with the C-terminus of YB-1 both *in vitro* and *in vivo* (Ise et al. 1999). Furthermore, YB-1 interacts with human endonuclease III (hNTH1) following the exposure of YB-1 overexpressing cells to cisplatin or UV which may indicate the two proteins interact to carry out base excision repair (Guay et al. 2008b). *In vitro* assays show that YB-1 and APE1 stimulate the activity of hNTH1 in base excision repair (Marenstein et al. 2003). Of particular note, in addition to APE1 participating with YB-1 during base excision repair, it also acts as a

co-factor for YB-1 in its role as a transcription factor for *ABCB1* (Chattopadhyay et al. 2008).

Summary
YB-1 can bind to damaged DNA. YB-1 also interacts with DNA repair machinery, in particular, the components that are involved in nucleotide excision repair or base excision repair.

1.8.3 RNA-binding protein

While YB-1 can act as a transcription factor for a number of genes, YB-1 can also bind to RNA. Through the ability to bind to RNA, YB-1 has been found to participate in RNA splicing, translation of RNAs, and the protection of RNAs from degradation. Emerging research has also shown that YB-1 can interact with non-coding RNAs (Blenkiron et al. 2013, Liu et al. 2015) but currently the full significance of these interactions is unclear and as such, they will not be discussed further. Furthermore, the potential for YB-1 to accompany RNAs throughout their lifecycle makes it very difficult to deduce the level(s) at which YB-1 regulates gene expression. It is clear that the nuclear localisation of YB-1 that has been observed in some cancers, and following stress, is a prerequisite for YB-1 to act as a transcription factor. However, while in the nucleus YB-1 may also participate in the post-transriptional regulation of gene expression by binding to RNA to stabilise transcripts and to participate in splicing pre-mRNA transcripts.

1.8.3.1 Splicing

RNA splicing is a multistep process that creates translatable mRNA transcripts from the RNA gene products (pre-mRNA transcripts) that are transcribed by RNA polymerase II (reviewed in Chen & Manley 2009). While newly transcribed RNA contains exons, nucleic acid sequences that code for amino acids, they also contain introns, nucleic acid sequences that do not code for amino acids. This intronic sequence needs to be removed (spliced) to produce a mature mRNA. Before becoming a mature mRNA, pre-mRNAs undergo further modifications, such as the addition of a 7-methylguanylate cap to the 5′ terminus and polyadenylation of the 3′ end. The spliceosomal machinery comprises specialised RNA and protein complexes, small nuclear ribonuclear particles, and other proteins that promote or inhibit splicing via motifs and elements on immature RNAs. The spliceosome is one of the largest

biomolecular machines in the cell (Chen & Manley 2009) and hence the assembly and regulation of its function comprises many regulated steps. The formation of spliceosome components on the pre-mRNA and catalysis of splicing are outside of this review (for a review of this topic see Chen & Manley 2009).

Besides the role of the spliceosome in processing pre-mRNA to mature mRNA transcripts, the spliceosome also contributes to protein diversity by regulating alternate splicing; the inclusion or exclusion of exons from the mRNA. The primary signals for the splicing machinery are the splice site and the branch point, these sequence motifs are located near the 5′ and 3′ ends of intronic sequences that are adjacent to the exons (reviewed in Chen & Manley 2009). Approximately 95% of multi-exon containing genes are thought to be alternately spliced (Pan et al. 2008). Co-factors interact with RNA and spliceosomal proteins to modulate the inclusion and exclusion of RNA sequence by binding to enhancer sequences. In general, proteins from the Serine-arginine family appear to promote splice-site recognition by the spliceosome while the inhibition of splice site recognition frequently occurs via hnRNP proteins. YB-1 interacts with a number of hnRNP proteins, for example hnRNP-K in the nucleus of human cells (Shnyreva et al. 2000). The regulation of splicing is also known to occur as RNA is transcribed by Polymerase II, cotranscriptionally, and the speed of transcription is thought to greatly affect the eventual splicing of the RNA (Muñoz et al. 2009).

YB-1 has been detected in human prespliceosomes (also known as A complexes; Hartmuth et al. 2002, Wolf et al. 2009) and also in spliceosomes (also known as B complexes; Deckert et al. 2006). YB-1 and a YB-1 homologue in the midge, *Chironomus tentans*, associate with newly transcribed RNA (Chansky et al. 2001, Soop et al. 2003). These data all indicate that YB-1 associates with RNA as it is transcribed and that YB-1 is present when pre-mRNA transcripts are processed to mature mRNA transcripts (**Figure 1.8.A**). The broad RNA affinities that YB-1 possesses may promote this early association. However, YB-1 does not interact directly with the splicing machinery by binding to splice sites or branch points. The role of YB-1 in splicing appears to rely predominantly on YB-1 binding to exon sequences on pre-mRNA transcripts.

YB-1 acts as an exonic splicing enhancer by binding to, and then promoting the inclusion of, exons (**Figure 1.8.B**). YB-1 has been shown to bind to exon v4 of *CD44* (Stickeler et al. 2001, Watermann et al. 2006). The binding of YB-1 to a splicing motif, known as an A/C-rich exon enhancer, in exon 4 of *CD44* pre-mRNA *in vitro*, enhances the inclusion of this exon (Stickeler et al. 2001, Watermann

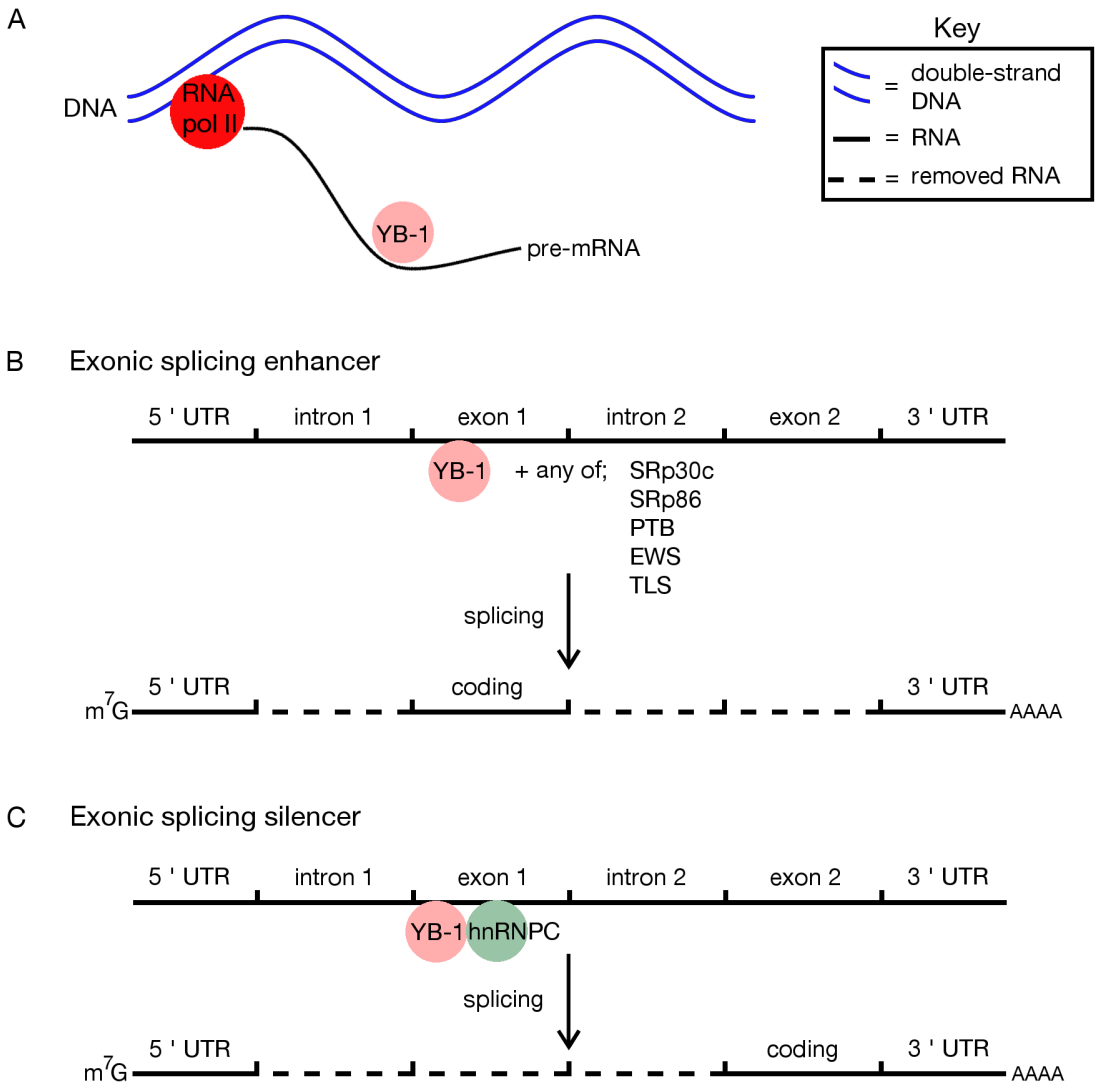

Figure 1.8: YB-1 influences the outcome of splicing events. **A**, YB-1 can bind to pre-mRNA transcripts as they are transcribed. **B**, YB-1, through interactions with a number of proteins, can act as an exonic splicing enhancer to promote the inclusion of exons during splicing events. **C**, by binding to motifs in intronic regions, YB-1 and hnRNPC can act as an exonic splicing silencers to promote the exclusion of exons during splicing.

et al. 2006). This alternative splicing event is one of a number that have been implicated in metastatic development of a range of cancers, including breast cancers (Prochazka et al. 2014). YB-1 is also known to interact with splicing factors from the Serine Arginine family, SRp30c and SRp86, and others such as PTB (**Figure 1.8.B**; Raffetseder et al. 2003, Li et al. 2003b, Coles et al. 2004). This further implies that YB-1 has a consistent role in promoting the inclusion of exons. Elevated levels of YB-1 alter RNA splicing with and without SRp30c, indicating that YB-1 may generally facilitate interactions of splicing factors with RNA (Raffetseder et al. 2003). Heat-stress disrupts both the co-localisation of YB-1 with SRp30c and their promotion of splicing. YB-1 facilitates appropriate splicing of the Neurofibromin (*NF1*) gene, a negative regulator of the Ras-Raf-MEK-ERK signalling pathway, by binding to an exonic splicing enhancer (ACAAC) in exon 37 of *NF1* mRNA (Skoko et al. 2008). Mutation of the first cytosine of this exonic splicing enhancer disrupts the binding of YB-1 and leads to exon-skipping via the recruitment of hnRNP-A1 and hnRNP-A2 to the mutated *NF1* mRNA. Therefore, YB-1 promotes the inclusion of exons in pre-mRNAs.

Much of the research mentioned above used mini-gene *in vitro* systems to study the influence of YB-1 on splicing. The importance of YB-1 to splicing the same pre-mRNA transcripts *in vivo* was often attenuated compared to that in the mini-gene *in vitro* systems. This highlights the importance sequence context to splicing (Stickeler et al. 2001, Raffetseder et al. 2003, Skoko et al. 2008). Therefore, despite the affinity of YB-1 for RNA cofactors appear to be critical to the ability of YB-1 to participate in splicing. Indeed, the association of YB-1 with the C-terminus of either translocation liposarcoma protein (TLS) or Ewings Sarcoma proto-oncoprotein (EWS) has repeatedly been shown to influence pre-mRNA splicing (**Figure 1.8.B**; Chansky et al. 2001, Rapp et al. 2002). Both TLS and EWS are prone to fusion with other proteins. These fusion proteins do not interact with YB-1 and this disrupts the exonic splicing enhancer activity of YB-1. The association of YB-1 and EWS with newly transcribed *MDM2* pre-mRNA also promotes its splicing to mature *MDM2* mRNA (Dutertre et al. 2010). The introduction of a stressor, exposure to camptothecin, disrupts the association of YB-1 and EWS and results in exon-skipping, mis-splicing, of *MDM2* mRNA (Dutertre et al. 2010). This exon-skipping allows the deregulation of p53 driven transcription of the *MDM2* gene from MDM2 protein production. This is due to the exon-skipping significantly reducing the amount of appropriately spliced *MDM2* mRNA for the duration of exposure to the stressor. The removal of camptothecin restores appropriate splicing of *MDM2* mRNA.

Translation of MDM2 from these transcripts can then proceed thus allowing the activities of p53 to be attenuated. The ability to inhibit the production of a negative regulator of p53 would promote many of the functions of YB-1 in cancer. It is currently unclear as to how many transcripts exhibit exon-skipping when YB-1 binding is disrupted. However, Dutertre et al. (2010) found a number of other genes where exon-skipping occurrs during camptothecin treatment and, importantly, also following depletion of YB-1. Therefore, YB-1 may have wide-ranging function in the promotion of exon inclusion which appears to occur in a number of cellular contexts.

YB-1 can also silence splicing by binding to specific sequences to promote exon skipping. This function as an exonic splicing silencer requires YB-1 to interact with other proteins (**Figure 1.8.C**). By binding to an exonic splicing silencer motif (TTTT) in exon 10 of the muscle specific receptor tyrosine kinase pre-mRNA, hnRNP-C can mediate the binding of YB-1 to "CATC/CACC" motifs that are adjacent to the "TTTT" motif. This promotes the production of mature mRNA that lacks exon 10 (Nasrin et al. 2014). The alternatively spliced transcript is important to the development of neuromuscular junctions in human myocytes. While the function of enhancing exon exclusion appears to conflict with the previously reported function of YB-1 as an exonic splicing enhancer, the sequence composition of the motifs involved are similar with high A/C content. More than 300 RNA transcripts in the human genome contain similar motifs, TTTT adjacent to CATC or CACC (Nasrin et al. 2014). A screen of 6% of these (24/378 candidate sequences) detected alternative exon inclusion or exclusion in almost 40% of the candidate sites (9 out of 24) when YB-1 or hnRNP-C was depleted with three transcripts requiring the depletion of both hnRNP-C and YB-1 to promote alternative splicing. YB-1 overexpression repressed splicing at a C/A-rich motifs (CACACCA; Wang et al. 2013). Depleting YB-1 represses this effect as does depleting hnRNP-L or hnRNP-C (Wang et al. 2013). However, the former effect is the stronger of the two.

Summary

YB-1 binds to sequences dominated by C/A to promote or suppress the splicing of exons. This contrasts with high-throughput studies where YB-1 was found to prefer binding to pyrimidine (C/U) and guanine rich RNA sequences (Dong et al. 2009, Ray et al. 2009). The use of recombinant proteins or the absence of cofactor proteins, which may alter the binding of YB-1 in the high-throughput screens, may account for this discrepancy. Importantly, while the ability of YB-1 to influence splicing of a small number of transcripts has been confirmed, two large screens indicate that YB-

1 may influence the splicing of many more transcripts (Dutertre et al. 2010, Nasrin et al. 2014).

1.8.3.2 Translation

Requiring a significant metabolic investment, the translation of mRNA transcripts into polypeptide chains is one of the final steps in the synthesis of proteins from genes (gene expression). As such, translation is a highly regulated process with the regulation of translation accounting for as much as 40% of the titre of individual proteins (Schwanhäusser et al. 2011). The uncoupling of mRNA levels from protein levels is highly context specific. A recent study into the influence of p53 in translation found that 70% of the genes that were differentially regulated by doxorubicin or nutlin-3a exposure, a group that included *YBX1*, displayed uncoupling of the levels of translated proteins from mRNA levels (Zaccara et al. 2014).

Defining the complexity and steps of translation falls outside the scope of this review. Only the steps of cap-dependent translation initiation, which YB-1 is involved in, will be outlined (**Figure 1.9.A**; for a comprehensive review of translation initiation see Jackson et al. 2010). The PABP family are important in translational initiation as they bind to the 3′ poly(A) tail of mRNAs and facilitate the recruitment of the eIF4F complex to the 7-methylguanylate cap at the 5′ end of the mRNA. The eIF4F complex, eIF4B, or, eIF4H are required to melt secondary structures within the 5′ UTR of the mRNA. At this point the 43S preinitiation complex can be recruited to the mRNA whereupon it scans the mRNA 5′ to 3′ to locate the initiation codon. The following steps involve the maturation of a translation ready ribosome and creation of a polypeptide chain from the mRNA transcript. Importantly, translation initiation is the step that limits the production of protein from mRNA transcripts (Jackson et al. 2010).

YB-1 is located in mRNPs, which are complexes that comprise RNA and protein, and YB-1 is known to be critical to the formation of mRNPs (Minich & Ovchinnikov 1992, Evdokimova et al. 1995). YB-1 can inhibit or promote the translation of mRNA transcripts. Generally, when the amount of YB-1 in an mRNP is low, translation of the mRNA transcript is promoted and when YB-1 is present in an RNP in abundance, translation of the bound transcript is repressed (Minich & Ovchinnikov 1992, Evdokimova et al. 1998, Pisarev et al. 2002). YB-1 is thought to primarily promote translation initiation by increasing the efficiency of 5′ to 3′ scanning by the 43S preinitiation complex as YB-1 masks stretches of sequence that

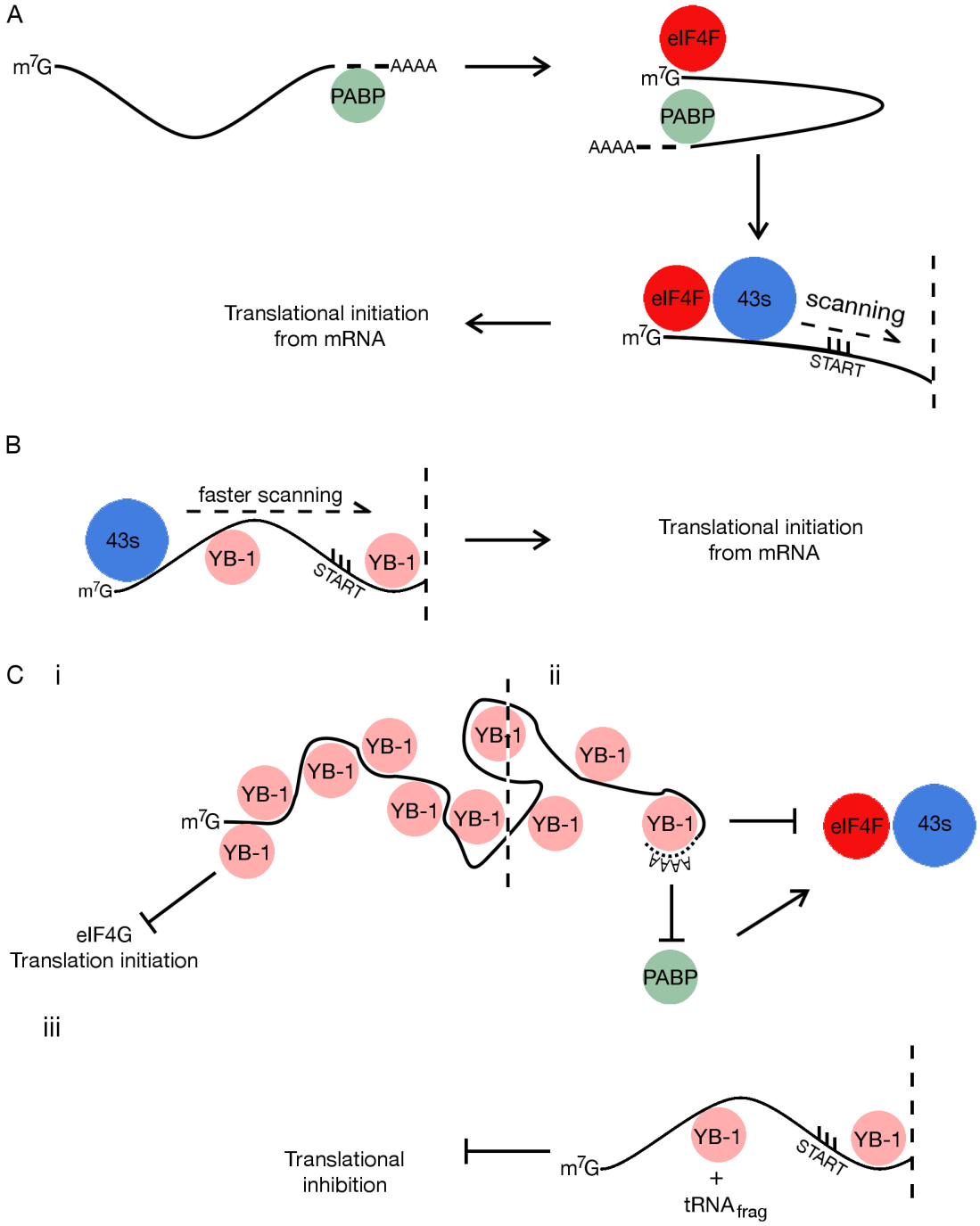

Figure 1.9: YB-1 influences the initiation of cap-dependent translation. **A**, the main steps in the initiation of cap-dependent translation from mRNA transcripts. **B**, YB-1 can improve the scanning rate of the 43s initiation complex to promote translational initiation. **C**, YB-1 can inhibit translation by (i), inhibiting the binding of eIF4G at the 5′-UTR, (ii), by blocking the binding of PABP to the poly-A tail on the 5′-UTR, or (iii), by interacting with 5′ fragments of tRNA through an unkown mechanism. The 5′ methyl guanidine cap (m^7G) and poly-adenylated tail at the 3′ of mRNA transcripts(AAA) are shown. The start codon is also highlighted (START).

do not contain the initiation codon (**Figure 1.9.B**; Svitkin et al. 1996, Kovrigina et al. 1996, Evdokimova et al. 1998). The general ability of YB-1 to promote translation has been verified for a small number of specific transcripts. The interaction of YB-1 with DEAD box RNA helicase (DDX6) promotes the translation of factors that allow self-renewal of epidermal progenitor cells (Wang et al. 2015b). YB-1 promotes the cap-independent translation of the mesenchymal cell markers *SNAI1* and *TWIST* (Evdokimova et al. 2009a). Therefore, YB-1 appears to promote the translation of transcripts that are involved in metastasis.

Increasing the YB-1:RNA ratio, reminiscent of that in free mRNPs, inhibits translation from mRNA transcripts *in vitro* (Nekrasov et al. 2003) and *in vivo* (**Figure 1.9.C i**; Davydova et al. 1997). The interaction of YB-1, via its C-terminus (Izumi et al. 2001), and PABP is the primary mechanism via which YB-1 inhibits translation (Minich & Ovchinnikov 1992, Skabkina et al. 2003, Skabkina et al. 2005, Kedersha & Anderson 2007, Chernov et al. 2008a, Svitkin et al. 2009, Maher-Laporte et al. 2010). The PABP family includes many homologues which most studies assume have conserved function, however, recent studies indicate that the many members of the PABP family possess unique functionality (Gorgoni et al. 2011). The differences between the interaction of YB-1 and the PABP family homologues have not been studied.

Inhibition of translation by YB-1 in free mRNPs seems to occur as YB-1 displaces the translation initiation factor eIF4G, a component of the eIF4F complex, from mRNA (**Figure 1.9.C ii**; Nekrasov et al. 2003). In rabbit reticulocyte translation systems, YB-1 has been shown to be central to preventing translation in free mRNP (Minich & Ovchinnikov 1992). The translational inhibition that characterised free mRNPs remains following the removal of most proteins, other than YB-1, from the mRNP.

YB-1 inhibits the translation of *YBX1* mRNA (**Chapter 1.7.1**) by binding to two elements in the transcript. The first element is in the 3′ UTR of *YBX1* mRNA (UCCA[A/G]CAA; **Figure 1.9.C ii**; Skabkina et al. 2005, Lyabin et al. 2011). By binding to this element, YB-1 excludes PABP from the poly(A) tail of *YBX1* mRNA. PABP can alleviate this inhibition by binding to an element (1149 - 1204 nucleotides) that overlaps with the YB-1 binding elements (Lyabin et al. 2011). YB-1 can also bind to elements in the 5′ UTR of *YBX1* mRNA to inhibit its translation (Fukuda et al. 2004). YB-1 also influences the translation of other transcripts, such as *TGF*-β mRNA which encodes a signalling protein that can promote an invasive phenotype in cells (Singh & Settleman 2010). The 5′ UTR of the *TGF*-β mRNA

contains a strong and a weak YB-1 binding site. In tubular kidney cells, YB-1 allows translation by binding to the former while binding to the latter inhibits translation (Fraser et al. 2008). Therefore, the regulation occurring via binding to the 5′ UTR element likely represents an alternative mechanism by which YB-1 can influence translation.

An alternative mechanism for YB-1 inhibiting translation relates to the interaction of YB-1 with fragments from tRNAs. During or following stress, YB-1 interacts with the 5′ fragments from tRNAs that have been cleaved by angiogenin (Ivanov et al. 2011, Ivanov et al. 2014, Lyons et al. 2016). The interaction of YB-1 and tRNA fragments appears to inhibit translation but the mechanism is not fully elucidated (**Figure 1.9.C iii**; Ivanov et al. 2011, Lyons et al. 2016). The importance of the interaction between YB-1, fragments of tRNAs, and translational inhibition in cells that have undergone stress, is also currently unknown.

To date, the translational inhibition caused by YB-1 has been shown to be relevant to oncogenic transformation. The chicken YB-1 homologue appears to block the oncogenic transformation of cells by inhibiting translation of specific genes (Bader & Vogt 2004, Bader & Vogt 2005, Bader & Vogt 2008).

In mammals, proteins containing selenocysteines function in redox reactions and these proteins may be important in some cancers (reviewed in Lu & Holmgren 2009). YB-1 may facilitate the inclusion of selenocysteine during translation. As such, YB-1 has the potential to regulate a small group of 25 proteins in humans (Arnér 2010). YB-1 interacts with glutathione peroxidase transcripts at a selenocysteine insertion sequence in the 3′ UTR to allow UGA codons to insert selenocysteine rather than a translation termination (Shen et al. 1998, Shen et al. 2006). The relevance of this observation to YB-1 and its role in cancer is currently unclear.

Translation via an internal ribosome entry site (IRES), provides an alternative mechanism to cap-dependent translation during stress and mitosis (Subkhankulova et al. 2001, Grover et al. 2008). Research has confirmed that YB-1 can promote translation from IRESs although our current knowledge of YB-1 interactions with IRESs is limited to a small number of transcripts and the mechanism is yet to be fully elucidated. However, rather than being a general mechanism for translation via IRESs, the mechanism is sequence specific, as YB-1 does not promote translation from all mRNA transcripts that contain IRESs (Cobbold et al. 2010).

YB-1 enhances translation via IRESs from transcripts that are consistent with YB-1 promoting mitosis and cell survival during stress. YB-1 can promote the translation of *MYC* mRNA via an IRES and a mutation that occurs within the IRES

in multiple myeloma, further increases the ability of YB-1 to promote translation via the mutated IRES (Cobbold et al. 2008, Cobbold et al. 2010). During hypoxia YB-1 promotes the translation of *p16INK4a* mRNA by binding to an IRES in its 5′ UTR (Bisio et al. 2015). A mutation in the 5′ UTR of *p16INK4a* mRNA, which is common in melanomas, reduces the binding efficiency of YB-1 with the IRES, and this may lessen the ability of p53 and YB-1 to control senescence and cell cycle checkpoints (Bisio et al. 2015). The presence of YB-1 in a complex with PTB during apoptosis, activates the translation of a number of apoptotic proteins via IRESs (King et al. 2014). The rules surrounding this interaction are yet to be elucidated but the role for YB-1 in facilitating the apoptotic signalling cascade seems to conflict with YB-1 inhibiting apoptosis and other cell death programs. However, the ability of YB-1 to inhibit the initiation of apoptosis may be separate from its role in the apoptotic signalling cascade once it has been triggered.

Phosphorylation may provide YB-1 with the ability to interact with different aspects of the translational machinery. Phosphorylated YB-1 can bind to the 7-methylguanylate cap at the 5′ end of mRNA but it does not inhibit cap-dependent translation (Evdokimova et al. 2006b). However, this phosphorylated YB-1 could still inhibit the use of an IRES on a poliovirus (Evdokimova et al. 2006b). Chicken YB-1 that is phosphorylated at S99 also lacks the ability to inhibit cap-dependent translation (Bader & Vogt 2008).

Summary

YB-1 can promote and inhibit the translation of mRNA transcripts. YB-1 appears to promote translation of mRNA transcripts through two mechanisms. The first is to improve the scanning rate of the 43S initiation complex during the initiation of cap-dependent translation (**Figure 1.9.B**). The second mechanism relies on YB-1 interacting with IRESs. The ability of YB-1 to inhibit translation appears to require multiple YB-1 molecules to bind to mRNA transcripts. This inhibits the interaction of proteins that initiate cap-dependent translation (**Figure 1.9.C**). Therefore, there is little evidence to suggest that protein interactions are integral to the recruitment of YB-1 to mRNA transcripts during translation initiation. Instead, the ability of YB-1 to bind to RNA (**Chapter 1.8.1**) appears to be central to its ability to participate in translation.

1.8.3.3 mRNA stability

YB-1 is likely to bind to pre-mRNA transcripts during their transcription (**Chapter 1.8.3.1**). YB-1 also appears to be present when mRNA transcripts are degraded. *In vitro* assays indicate that YB-1 possesses endoribonuclease (Moraes et al. 2003) and exonuclease (Izumi et al. 2001, Gaudreault et al. 2004) activities. However, these observations are inconsistent with the vast majority of research which indicates that YB-1 forms stable associations with RNA and DNA. This section highlights the role of YB-1 in protecting RNA from degradation.

The ability of YB-1 to protect RNA from degradation is integrally linked to its multiple roles in translation. The recruitment of YB-1 to mRNA transcripts leads to mRNP formation and translational inhibition (**Chapter 1.8.3.2**), while also protecting the mRNA transcripts in these translationally quiescent mRNPs from degradation (**Figure 1.10.A**; Evdokimova et al. 2001, Evdokimova et al. 2006a, Evdokimova et al. 2009a). This protection is maximal when the number of YB-1 molecules that bind to an mRNA reaches sufficient density for YB-1 to homodimerise and form a tight structure which excludes other factors from accessing the RNA (Skabkin et al. 2004). Therefore, when sufficient YB-1 molecules are available, YB-1 can protect RNA from degradation though its general ability to bind RNA.

YB-1 can also protect capped-mRNA from degradation by binding to specific motifs (**Figure 1.10.B**; Chen et al. 2000, Capowski et al. 2001, Coles et al. 2004). YB-1 protects Granulocyte-Macrophage Colony-Stimulating factor (*GM-CSF*) mRNA from degradation by binding to an AU-rich element in the 3′ UTR (Capowski et al. 2001). YB-1 can also transactivate the *GM-CSF* gene by binding to its promoter (Diamond et al. 2001). Therefore, YB-1 regulates the *GM-CSF* gene at multiple levels. The ability of YB-1 to protect RNA from degradation is also highlighted by research showing that during hypoxia, tRNA may be cleaved to produce fragments that can bind to YB-1. Thereby displacing YB-1 from other transcripts which may then be at risk of degradation (Goodarzi et al. 2015).

The importance of YB-1 as a protector of mRNA is not fully defined but YB-1 has been observed to act in concert with other proteins. Nucleolin and YB-1 bind to a response element in the 5′ UTR of *IL-2* mRNA and facilitate the formation of a mRNP complex that is stabilized in T-cells (**Figure 1.10.C i**; Chen et al. 2000). YB-1 and other proteins, including hnRNP-K, protect human preprorenin mRNA via 3′ UTR binding (**Figure 1.10.C ii**; Skalweit et al. 2003). YB-1, IGF2BP1, HNRNPU, SYNCRIP, and DHX9 associate with a coding region instability determinant

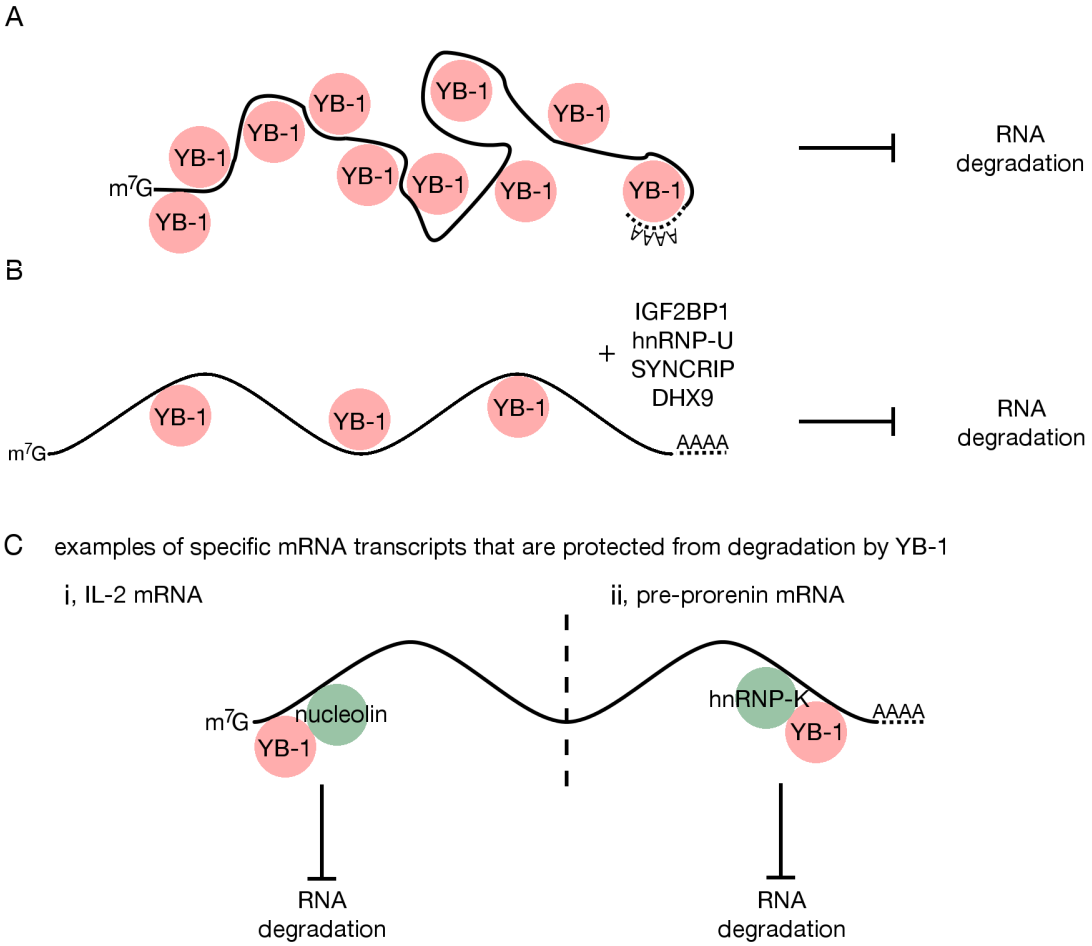

Figure 1.10: YB-1 protects mRNA transcripts from degradation. **A**, many YB-1 molecules binding to a single mRNA transcript leads to a translationally silenced mRNP that is also protected from degradation. **B**, YB-1, in addition to other RNA-binding proteins, can protect mRNA transcripts from degradation. **C**, selected mRNA transcripts that YB-1 is known to protect from degradation. **i**, the IL-2 mRNA transcript can be protected from RNA degradation when YB-1 and nucleolin bind to a response element in its 5′ UTR. **ii**, the pre-prorenin mRNA transcript can be protected from RNA degradation when YB-1 and hnRNP-K bind to the 3′ UTR.

in the *MYC* mRNA to hold the transcript in the non-polysomal, or translationally quiescent, fraction and block translation coupled degradation of *MYC* mRNA (Weidensdorfer et al. 2009). These examples show YB-1 stabilising RNA transcripts by binding to them and aiding mRNP formation. It must be also noted that YB-1 is a component of larger cellular structures that are involved in RNA stability.

In addition to facilitating the translation of a suite of mRNA transcripts during stress, many via IRESs, YB-1 is also a constituent of RNA and protein foci that form in the cytoplasm of cells following stress (**Figure 1.11**; reviewed in Anderson et al. 2015). Processing bodies are foci that form in the cytoplasm of mammalian cells which are thought to degrade RNA that has been primed for degradation (Anderson et al. 2015). Processing bodies are more frequent in the cytoplasm of cells following stress and while YB-1 is found in processing bodies, its function within them is currently uncharacterised (Yang & Bloch 2007, Kato et al. 2010, Bann et al. 2014).

Stress granules also form in the cytoplasm of cells in response to stress and they are enriched for RNA, RNA binding proteins, and proteins from translationally stalled mRNA transcripts (**Figure 1.11**; Kedersha & Anderson 2007, Anderson et al. 2015). Part of the function of stress granules appears to be the preservation of cellular resources when translation stalls during stress. The mRNA transcripts from the stalled ribosomes are protected from degradation while in stress granules, and this allows translation to rapidly resume once the stress has passed. The composition of stress granules is highly dynamic with their constituents in a constant state of flux (Kedersha & Anderson 2007, Anderson et al. 2015, Bounedjah et al. 2014). However, YB-1 is a consistent component of stress granules (Kedersha & Anderson 2007), and gold-immunostaining of YB-1 in transmission electron microscopy confirms that the density of YB-1 is elevated in stress granules compared to the rest of the cytoplasm (**Figure 1.11**; Bounedjah et al. 2014). While in stress granules YB-1 appears to have unique protein interactions (Tanaka et al. 2014). Therefore, YB-1 is aggregated in stress granules while the remaining cytoplasmic YB-1 is more diffuse.

Despite YB-1 being a component of stress granules, an abundance of YB-1 in the cytoplasm directly inhibits the formation of stress granules (**Figure 1.11**; Bounedjah et al. 2014, Tanaka et al. 2014). Stress granules form from the aggregated remains of polysomes that have disassociated during stress. The presence of an excess of YB-1 in the cytoplasm may stabilise the mRNA and proteins from disassociated polysomes so that they form mRNPs rather than stress granules (Bounedjah et al. 2014). The role and function are currently unclear for this pool of cytosplamic

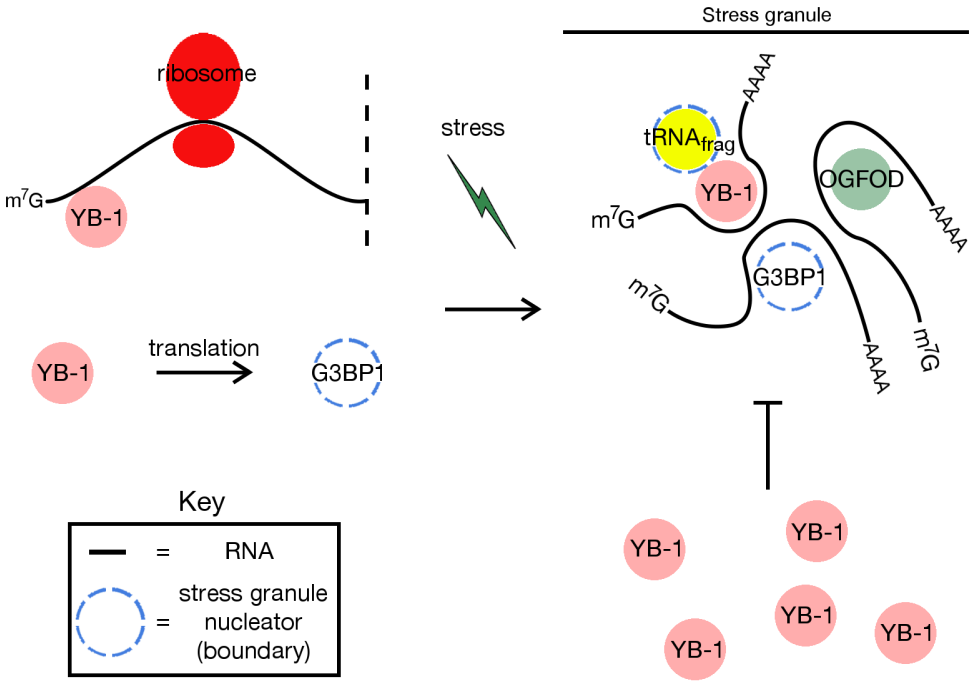

Figure 1.11: YB-1 can promote or inhibit the formation of stress granules during stress events.

YB-1 that does not appear to be bound to RNA.

YB-1 has also been shown to promote the formation of stress granules. It has been suggested that YB-1 can aid in their formation by moving mRNPs along microtubules, termed microtubule-mediated stirring, to stress granules (Chernov et al. 2009). However, this directly contradicts the findings from Bounedjah et al. (2014) which show that the formation of mRNPs following stress inhibits the formation of stress granules. Irrespective, YB-1 appears to promote stress granule formation by maintaining cellular levels of Ras GTPase-activating protein-binding protein 1 (G3BP1; **Figure 1.11**). YB-1 promotes the translation of G3BP1 by binding to the 5′ UTR of *G3BP1* mRNA (Somasekharan et al. 2015). This is critical, as G3BP1 is thought to be the "nucleator" protein around which stress granules form. Depleting YB-1 in human sarcoma cells inhibits the formation of stress granules via reductions in G3BP1 (Somasekharan et al. 2015). Therefore, in excess, YB-1 is a competitor for stress granule formation while also indirectly promoting their formation by maintaining levels of G3BP1 around which stress granules nucleate.

The interaction of YB-1 with short RNA sequences, such as miRNA (Yuan et al. 2014) and cleaved tRNA sequences (Ivanov et al. 2011, Ivanov et al. 2014, Goodarzi et al. 2015, Lyons et al. 2016), may also influence the formation and function of stress granules. By binding to tRNA fragments, YB-1 appears to promote stress

granule formation (**Figure 1.11**; Lyons et al. 2016). Goodarzi et al. (2015) proposes that the significance of YB-1 in stress granule formation is directly influenced by the production of stress-induced tRNA fragments. In the absence of these fragments, YB-1 remains bound to transcripts that promote metastatic characteristics during hypoxia. In contrast, the presence of stress-induced tRNA fragments during hypoxia attract YB-1 and the metastatic transcripts are at risk of degradation during hypoxia.

Within stress granules, a subset of mRNAs that encode critical proteins still need to be translated. The dynamic nature of stress granules appears to allow mRNA transcripts that are critical to cell survival to exit the stress granule so that translation can resume (Anderson et al. 2015). YB-1 in stress granules has also been directly implicated in facilitating the translation of heat-shock protein 70 mRNA, which is involved in protein folding (Tanaka et al. 2014). mTORC1 is also thought to recruit proteins to stress granules to specifically translate mRNA transcripts with 5′ terminus oligopyrimidine motifs, such as the one in *YBX1* mRNA which is known to be under control of mTORC1 signalling (**Chapter 1.7.2.1**). Therefore, *YBX1* mRNA in stress granules is likely to be preferentially translated by translational machinery that is activated by the mTORC1 signalling pathway.

Stress granules appear to be important to cell survival. Overexpression of 2-oxoglutarate and Fe(II)-dependent oxygenase domain containing 1 (OGFOD), which YB-1 associates with in stress granules, promotes the phosphorylation of eIF2α without aiding in the formation of stress granules during stress (Wehner et al. 2010). Following the removal of the stressor, overexpression of OGFOD causes phosphorylation of eIF2α to remain for longer and this contributes to a lag in the resumption of cellular translational activity. The survival of cells is lowered as they recover from stress (Wehner et al. 2010). RNA stability, particularly during stress, also appears to be important in cancer. The expression of YB-1 and G3BP1 is highly correlated in human sarcomas, and like YB-1, elevated G3BP1 expression correlates with poor survival (Somasekharan et al. 2015).

Summary

YB-1 promotes RNA stability through general and specific mechanisms. The importance of the ability of YB-1 to promote RNA stability has not been extensively researched in cancer. However, the research that has been performed indicates that the molecular function of YB-1 to stabilise RNA has the potential to be important to cancer biology.

1.9 Summary

The key points from this literature review are summarised as:

- Increased levels of YB-1 are correlated with aggressive cancers;
- This correlation appears to relate to four main functions of YB-1 in cancers;
    1. YB-1 can drive cancer development by promoting genetic instability.
    2. YB-1 promotes cell division.
    3. YB-1 promotes cell survival during stress, such as chemotherapy.
    4. YB-1 promotes an invasive phenotype in cancer cells.
- YB-1 can affect these functional changes in cancer cells via multiple mechanisms.

The correlation of elevated YB-1 with poor patient survival has been made in a wide range of cancers (**Chapter 1.3**). The functional reasons for this correlation appear to be multiple (**Chapter 1.4**) as observations from clinical samples indicate that YB-1 has the ability to influence events at the cellular and tumour level. Broadly, the research has shown that YB-1 can promote the development of cancer, the rate at which cancer cells divide, the survival of cancer cells in response to a variety of stresses, and the development of invasive phenotypes in cancer cells. At the molecular level the ability of YB-1 to bind to RNA and DNA, in a general and also a sequence-specific manner, supplies multiple mechanisms to explain the influence of YB-1 at the cellular and tissue level in cancer. This review attempted to summarise the functions of YB-1, however, the ability of YB-1 to act as a transcription factor has been widely reported. As a result, this aspect of YB-1 biology has been heavily condensed for this review. In contrast, the activities of YB-1 that is binding RNA have been given a greater relative focus for this review.

The contrast between the depth of reports for YB-1 as a transcription factor and its other roles may reflect the reality of YB-1 function. An alternative, and compelling, viewpoint, is that the importance of YB-1 as an RNA binding protein is under-appreciated (Dolfini & Mantovani 2013a, Dolfini & Mantovani 2013b). The primacy that transcriptional effects are given in relation to gene expression is not limited to YB-1 research. However, recent work quantifying the concentration, production, and stability of mRNAs and proteins for ∼5000 genes in single samples,

found that RNA transcription and concentration predicts less than half of the variation in protein concentrations (Schwanhäusser et al. 2011, Vogel et al. 2010). These studies also confirm that the levels of many proteins are highly uncoupled from the levels of their mRNA transcripts. Therefore, post-transcriptional regulation of gene expression (splicing, RNA stability, translational silencing, translation activation) is a critical factor influencing the cellular levels of proteins. The ability of YB-1 to regulate post-transcriptional gene expression could be more important than is currently appreciated.

In most cases, the effects of YB-1 at the cellular level may be explained by multiple molecular capabilities of YB-1. One explanation for the multiple molecular functions of YB-1 may relate to phosphorylation of YB-1. High-throughput studies confirm that YB-1 is phosphorylated at multiple locations in many cellular contexts while numerous reports that focus on YB-1 highlight that, in general, phosphorylation can modulate the function of YB-1 (**Chapter 1.7.2.1**). However, the function of only two of these phosphorylation sites, S102 and S165, is partially characterised and there is currently a single article that focuses on phosphorylation of YB-1 at S165 (Prabhu et al. 2015). The importance of phosphorylation at S102 in cancer is supported by numerous studies. However, the phosphorylation of YB-1 at S102 has been shown to activate YB-1 as a transcription factor, as a binding factor of microtubules that interact with the centrosome, and as a promoter of translational initiation. Therefore, a specific function of a single YB-1 molecule which bears a phosphorylation at S102 is unclear. The presence of phosphorylation at other sites, in addition to S102, may more accurately explain the functional states of YB-1. Furthermore, phosphorylation of YB-1 at these other sites is likely to modify the function of the protein. Therefore, the functional consequences of phosphorylation at these other sites warrants further investigation.

1.10 Thesis scope

The research that is presented in this thesis primarily focuses on YB-1 in breast cancer or a breast cancer cell line (MDA-MB231). The chapter titles are:

- **Chapter 3**, Immunohistochemical analysis of YB-1 in breast tumours;
- **Chapter 4**, Identification of YB-1 interacting proteins in the cytoplasm and nucleus;

- **Chapter 5**, YB-1 confers resistance to genotoxic stress treatment of MDA-MB231 cancer cells;
- **Chapter 6**, Identification of YB-1 interacting proteins during cisplatin exposure;
- **Chapter 7**, Analysis of functional interactions between YB-1, FAM120A, TRIM28, and C1QBP.

The reports that YB-1 is elevated in cancers are consistent. **Chapter 3**, addresses the contradictory reports regarding the presence of YB-1 in normal tissues. It then uses IHC to examine the subcellular localisation and levels of YB-1 in cancerous tissues. The subcellular localisation of YB-1 in tumours is important. This is due to the molecular functions that YB-1 is proposed to perform requiring that YB-1 be in either the nucleus or the cytoplasm. Furthermore, the tertiary structure and protein interactions of YB-1 appear to alter the prognostic sensitivity of IHC. This led to an interest in the protein-protein interactions (PPI) of YB-1.

In **Chapter 4** an affinity-purified antibody against YB-1 has been used to examine the PPI and phosphorylation state of endogenous YB-1 in the cytoplasm and nucleus of cancer cell lines. This work highlights that YB-1 is phosphorylated at multiple sites while it is in the cytoplasm and nucleus of cultured cells. The PPI of YB-1 also provide evidence that YB-1 is likely to participate in most of the molecular mechanisms that have been reported in this review.

The remaining chapters focus on the role of YB-1 in drug sensitivity in a breast cancer cell line, MDA-MB231. The importance of YB-1 to MDA-MB231 cells during exposure to chemotherapeutic drugs is researched in **Chapter 5**. Using the knowledge gained in **Chapter 5**, the experiments in **Chapter 6** assess how cisplatin exposure alters the PPI of YB-1 in MDA-MB231 cells. The results confirm that the PPI, and most likely the function, of YB-1 alters in subtle rather than coarse ways during cisplatin exposure. Finally, **Chapter 7** tests selected proteins that copurify with YB-1 during cisplatin exposure to see whether they also influence the response of MDA-MB231 cells to cisplatin exposure.

Chapter 2

Materials and methods

2.1 Cell Culture

Unless otherwise stated, the cells used in this thesis were grown in DMEM media (Life Technologies) supplemented with 10% heat-inactivated and sterile-filtered bovine foetal calf serum (Moregate, New Zealand). The cell lines were adherent and passaged when 75 - 90% confluent using 0.25% Trypsin-Ethylenediaminetetraacetic acid (EDTA), pH 7.2 - 8.0 (Life Technologies) for up to 5 minute (min). Growing cells were discarded once their passage reached 22. Following retrieval from storage in $N_2(l)$, the growing cells were maintained at 37°C for a minimum of 4 days before being used in experiments. The seeding ratios that were used for the A549 and MDA-MB231 cell lines are shown in **Table 2.1**.

When proteins were required from cells that were being cultured, they were lifted from the cell culture vessel using 0.25% Trypsin-EDTA for up to 5 min. A small aliquot (30 - 50 µl) was set aside and the remainder of the cells sedimented using centrifugation at 220 g for 5 min at room temperature. The cells in the aliquots were counted using a haemocytometer and the sedimented cells were then resuspended and sedimented again in 37°C phosphate-buffered saline (PBS). The cells were then lysed in 1 × radioimmunoprecipitation assay buffer (RIPA) at a concentration of 10 000 cells per µl RIPA (**Table 2.2**). To allow the Benzonase to act, the DNA and RNA was removed from the lysates via an incubation step, on ice for 30 min. The insoluble cellular debris was removed from lysates by centrifugation at 12 000 g for 10 min at 4°C. The lysates were then frozen at ⁻20 - ⁻80°C or immediately used for downstream applications.

Table 2.1: The number of MDA-MB231 or A549 cells that were seeded for various growth vessel formats and also for different experiment types.

Vessel	Surface area (cm^2)	Proliferation ($+ 10^5$)	50% Confluence ($+ 10^5$)	Transfection ($+ 10^5$)
	1	0.691	1.057	2.083
T175	175	121	185	364.6
T75	75	51.8	79	156.3
6-well	9.6	6.63	10.15	20
24-well	2	1.38	2.1	4.167
96-well	0.32	0.22	0.342	0.667

The columns to the right of the double lines highlight three experiment types. Proliferation was used for the expansion of cell stocks. 50% confluence was used for experiments where the cells were required to be $\sim$ 90% confluent within 48 hrs. Transfection was used for experiments that involved the depletion of mRNA transcripts using silencing RNA duplexes (**Chapter 2.8**).

2.2 Antibodies

The antibody preparations that were used are summarised in **Table 2.3**. Multiple antibodies were utilised to detect YB-1 and three of these were produced in-house. The first was an antibody, raised in rabbit, against C-terminus of YB-1 ($YB1^C$). The second was an antibody, raised in rabbit, against N-terminus of YB-1 (^{N}YB1). The third and final antibody was antibody, raised in sheep, against N-terminus of YB-1 ($^N YB1_{sheep}$). The first 12 amino acids in the N-terminal of YB-1 were used as the immunising peptide for ^{N}YB1 and $^N YB1_{sheep}$ (MSSEAETQQPPA). $YB1^C$ was raised against 299 - 313 aa of YB-1 (CDGKETKAADPPAENS). These polyclonal antibodies were affinity-purified and their use has been validated in Cohen et al. (2010) and Woolley et al. (2011).

Table 2.2: Recipes for two cell lysis buffers that were used to lyse cells.

Stock	**5×RIPA**	**5×conc.**	**1×RIPA**	**Final Conc.**
Standard				
1 M Tris-HCl, pH 7.5	500µl	250 mM	←	**50 mM**
5 M NaCl	300µl	750 mM	←	**150 mM**
20% NP40	500µl	5%	←	**1%**
10% Deoxycholate	500µl	2.5%	←	**0.5%**
10% SDS	200µl	0.5%	←	**0.1%**
ultrapure H_2O			8ml	
Low detergent				
1 M Tris-HCl, pH 7.5			500µl	**50 mM**
5 M NaCl			300µl	**150 mM**
20% NP40			250µl	**0.5%**
10% Deoxycholate			100µl	**0.1%**
ultrapure H_2O			8833µl	

The first listed recipe is for a standard RIPA. The **Low detergent** variant that is listed was used for immunoprecipitation (IP). The 5 × RIPA was often frozen immediately after preparation and it was used once thawed or discarded. Once diluted to the working concentration (1 × RIPA), the buffer was discarded after 12 hrs. Benzonase was added to 1 × RIPA at a rate of 100 U per mL immediately prior to use. Complete Protease Inhibitor EDTA-free and PhosStop were also added to 1 × RIPA following the manufacturers reccomendations.

Table 2.3: A list of the antibody preparations that were used for immunofluorescence and immunoblotting.

Target	Ab.Cat.No	Species	IF Dilution	IB Dilution
^{N}YB1	in house	rabbit	1:800	1:3333
YB1^{C}	in house	rabbit		1:1500
^{N}YB1$_{sheep}$	in house	sheep	1:333	
YB1^{S102}	C34A2	rabbit*		1:1500
YB-1 [59-Q]	sc-101198	mouse*	1:250	
C1qBP	ab24733	mouse*	1:500	1:10000
FAM120A	HPA019734	rabbit	1:80	1:500
TRIM28	A300-274A	rabbit	1:1000	1:5000
γH2AX	JBW301	mouse	1:800	
γH2AX	AB2893	rabbit	1:1000	
pan H3 [A3S]	05-928	rabbit*		1:5000
β-Actin [AC-15]	ab6276	mouse*		1:20000
β-Tubulin [E7]	E7	mouse*		1:2000
p53^{S15}	#9284	rabbit		1:1000

Abbreviations; * = monoclonal, IF = immunofluoresence, IB = immunoblot, in house = affinity purified antibodies prepared in the laboratory.

2.3 Polyacrylamide gel electrophoresis and immunoblotting

2.3.1 SDS-PAGE

Protein lysates were prepared in RIPA buffer (see **Table 2.2**). Denaturation and reduction was carried out by the addition of denaturing loading buffer containing dithiothreitol (DTT) and the samples were placed in boiling water for 5 min (final concentration; 50 mM Tris-HCl, 0.1% bromophenol blue, 10% glycerol, 100 mM DTT; modified from Weber & Osborn 1969). Sodium dodecyl sulfate Polyacrylamide gel electrophoresis (SDS-PAGE) gels, 15 cm long and 0.75 mm thick, were prepared with 6% to 10% polyacyrlamide depending on the size of the proteins that were being resolved. These SDS-PAGE gels were used to separate proteins using electrophorsis at 125 V for approximately 2 hrs in SDS-PAGE buffer (25 mM Tris, 192 mM glycine, 0.1% SDS, pH 8.3 Laemmli 1970). The Precision Plus Protein Dual Color Standard (Biorad) was used to monitor the migration of proteins. When required, proteins were stained in-gel by incubation for 4 - 24 hrs in 30 ml of a colloidal coommassie G-250 stain (34% methanol, 17% [w/v] $(NH_4)_2SO_4$, 3% phosphoric acid,

0.1% coomassie G-250 [Biorad]). The gels were destained in ultrapure H_2O.

2.3.2 Non-reducing SDS-PAGE

Non-reducing SDS-PAGE was undertaken as outlined in **Chapter 2.3.1**, however, DTT was omitted from the loading buffer and the samples were kept on ice during sample preparation. Non-reducing SDS-PAGE was necessary due to the presence of reducible cross-links (for details see **Figure 2.2)** in lysates containing cross-linked proteins. Samples that were not cross-linked were loaded in each gel. These samples ensured that any altered migration in cross-linked samples was due to *in vitro* chemical modification with cross-linker, rather than the omission of the reducing agent.

2.3.3 Blue-native-PAGE

Blue-native PAGE (BN-PAGE) was developed following Swamy et al. (2006). Precast 4 - 16% polyacrylamide gels and buffers were purchased from Invitrogen. Following optimisation, 1% digitonin and 2 units Benzonase per 100µl of lysis buffer were included in the lysis buffer. Coomassie G-250 was added to the sample loading buffer. The addition of Benzonase resulted in the removal of both RNA and DNA from the lysates.

2.3.4 Immunoblotting

Proteins separated by PAGE were transferred to nitrocellulose or polyvinylidene fluoride membrane using Towbin's buffer (20% MeOH, 25 mM Tris, 192 mM glycine, 0.1% SDS, pH 8.3; Towbin et al. 1979, Renart et al. 1979). The successful transfer of proteins was confirmed by incubating the membranes in Ponceau S staining solution (0.1%(w/v) Ponceau S in 5%(v/v) acetic acid) for 5 min. The proteins were detected using the Western Breeze kit (Life Technologies) and the chemiluminescent signal was recorded using Medical X-Ray Film General Purpose Blue (MXB, Kodak). The migration of proteins was confirmed using either the Precision Plus Protein Dual Color Standard (Biorad) or MagicMark XP (Life Technologies). When $YB1^{S102}$ or shrimp alkaline phosphatase treatment (see **Chapter 2.5**) was used, the proteins were transferred to nitrocellulose membrane and non-specific antibody binding was inhibited by a blocking buffer (1% bovine serum albumin, 0.1% Tween20, 50 mM Tris-Cl, pH 7.6, 150 mM NaCl). For these experiments, a secondary antibody that

was conjugated to anti-horseradish peroxidase was used at 1:10 000 in 0.5% bovine serum albumin in tris-buffered saline, pH 7.6 (TBS) with 0.1% Tween20 for 30 min.

To prepare digital images of films, a white-light transilluminator in a Gel Doc XR Gel Documentation System provided illumination and the images were captured using the 4 megapixal charge-coupled device camera that was provided with the Gel Doc XR (Biorad). Densitometry was performed using Quantity One 1-D analysis software (Biorad).

2.4 Northern blotting

Northern blotting were used to detect *YBX1* mRNA. To prevent RNases from degrading the RNA RNase contamination was controlled by the following measures:

- All glassware and metalware was baked at 180°C for 3 hrs;
- Lids from bottles and stirring bars were treated with RNase-away (Thermo Scientific);
- All plasticware was RNase-free;
- All solutions were prepared using Diethylpyrocarbonate-treated ultrapure H_2O;
- The gel electrophoresis tank was washed with detergent, rinsed well, and soaked in 3% H_2O_2 for 10 min at room temperature. Diethylpyrocarbonate-treated water was then used to rinse the tank.

Messenger RNA was extracted from the cell lines using the Dynabeads mRNA direct kit as per the manufacturer's instructions (Invitrogen). The mRNA concentration was measured using a Nanodrop (Thermo-Scientific). Five-hundred nanograms of mRNA was denatured in loading buffer (50% deionised formamide, 6% formaldehyde, 1*MOPS, 0.05% bromophenol blue, 1% glycerol) at 65°C for 10 minutes. The denatured DNA was separated on a 25 × 15 cm 1% agarose denaturing RNA gel at 120 V until the marker dye was 2 - 3 cm from the end of the gel. The mRNA was then blotted to a positively-charged nylon membrane (Roche) overnight using a semi-dry transfer. The mRNA cross-linked to the membrane using 120 mJ/cm^2 240 nm UV.

A digoxigenin-labelled probe was synthesised using a PCR DIG probe synthesis kit (Roche) and primers directed against 734 - 943 nucleotides of *YBX1* mRNA (5'-TATGCAGCAGACCGTAACCA-3' and 5'-GCACAGGAGGGTTGGAATAC

-3'). The incorporation of digoxigenin into the PCR fragment was confirmed by the retardation of its migration compared to an unlabelled PCR fragment. This probe binds to full-length *YBX1* mRNA (ENST00000321358) as well as three other proposed splice variants (ENST00000436427, ENST00000332220, ENST00000467957). The probe was hybridised at 50°C in DIG easy Hyb buffer (Roche) with 1 µl per 6 ml of buffer for 6 hrs. The DIG label was detected using a chemiluminescent enzyme immunoassay (DIG Luminescent Detection Kit, Roche) and Medical X-Ray Film General Purpose Blue (MXB, Kodak). To control for variance in mRNA loading, a DIG-labelled probe was prepared against 787 - 917 nucleotides of β-actin mRNA. The *YBX1* mRNA digoxigenin-labelled probe was stripped from the membrane using two incubations at 80°C for 60 min in 50 mM Tris-HCl, pH 7.5, with 50% deionized formamide and 4.5% SDS. Following two 5 min incubations in 2 × Saline-Sodium Citrate buffer (pH 7.0) the membrane was then ready for a new probe to be hybridised.

2.5 De-phosphorylation of proteins from cultured cells

Two approaches were taken to remove phosphate groups from phosphorylated proteins. The first used lysates that were prepared in 1 × RIPA (**Chapter 2.1**). Shrimp alkaline phosphatase was added so that the lysates had 5000 cells per µL and 0.25 U of shrimp alkaline phosphatase per µl (Fermentas, #EF0511; 1 × RIPA, 1 × EDTA-free Complete, 10 mM $MgCl_2$). phosSTOP was added at a 2 × concentration as required during the experiments. These lysates were incubated at room temperature for 1 hr prior to being used for immunoblotting.

The second approach included preparing and separating protein lysates for immunoblotting (**Chapter 2.1** and **Chapter 2.3**). Following the inhibition of non-specific antibody binding, the membranes were rinsed twice for 5 min in double-distilled H_2O. The membranes were then incubated for 1 hr at room temperature in a buffer containing 20 U per ml shrimp alkaline phosphatase (10 mM Tris-HCl [pH 7.5 at 37°C], 10 mM $MgCl_2$, 1 mg/ml bovine serum albumin (BSA)). The immunoblotting protocol resumed following a further two 5 min washes in TBS with 1% bovine serum albumin and 0.1% Tween20 (Sigma-Aldrich).

2.6 DNA-affinity purification of YB-1

The interaction of YB-1 with DNA was investigated using a biotinylated DNA probe (5'-Biotin-CCTCCCACCCTCCCCACCCTCCCCACCCTCCC-3'). Cells were trypsinised, rinsed twice with phosphate-buffered saline, pH 7.4 (PBS), and then diluted in RIPA buffer (see **Table 2.2**) at 1×10^4 cells per µl. The cells were passed through a 22 gauge needle 10 times and incubated on ice for 30 min before the debris was removed by centrifugation at 30 000 g for 20 min. Five hundred microlitres of lysate was dispensed into tubes with biotinylated DNA probe that had been dispensed at the indicated concentration and gently mixed at room temperature for 30 min. The biotinylated probe was recovered by adding 20 µl of streptavidin beads, which had been rinsed twice in RIPA, to each sample and mixed at room-temperature for 1 hr. The beads were immobilised, the supernatant removed, and the streptavidin-DNA probe conjugate was rinsed gently 4 times in RIPA buffer. The DNA probe, and any proteins that were bound to it, were recovered using two different methods. The first involved the denaturation of samples in 60 µl of denaturing sample buffer in RIPA. This was boiled for 5 min, immediately placed on a magnet, and the supernatant, which contained the sample, was collected in a fresh tube. The other recovery method sought to recover proteins that had interacted with the DNA probe. This was carried out by digesting the probe using 1 U of benzonase per µl of RIPA buffer which was incubated at room-temperature for 1 hr before being placed on a magnet. The supernatants were then collected in a fresh tube and the samples stored at $^{-}20^{o}$C.

2.7 Subcellular fractionation of cultured cells

The subcellular fractionation was performed by swelling trypsinized cells in a hypotonic solution prior to passing them through a dounce to rupture the outer cell membrane (Mermoud et al. 1992). Adherent cells were harvested and resuspended in PBS. An aliquot was counted on a haemocytometer. Cells were spun at 220 g for 5 min at 4°C, resuspended in a hypotonic buffer at a concentration of 1×10^4 cells per µl (10 mM HEPES, pH 7.9, 1.5 mM $MgCl_2$, 10 mM KCl, 0.5 mM, DTT, 1 × Complete EDTA-free), and incubated for 5 min at 4°C. 2×10^6 cells were added to a dounce homogeniser (Kontes, 885300-0002, 2 ml, tight pestle; 0.013 - 0.064 mm clearance) and the dounce was applied for 20 strokes. Following the 20 strokes aliquots were then taken after every 3 strokes, placed in a haemocytometer

and inspected on a microscope. The douncing was stopped when $\sim$ 95% of the cell membranes were ruptured. The sample was removed from the dounce and spun at 220 g for 5 min at 4°C. The supernatant (cytoplasm) was removed and 12.5 µl of 5 $\times$ RIPA was added for every 50 µl cytoplasm fraction.

Contaminating cytoplasmic proteins were removed from the nuclei using centrifugation through sucrose gradients. The pelleted nuclei were resuspended in 5 ml of chilled S1 buffer (0.25 M Sucrose,10 mM $MgCl_2$) and gently layered over 5 ml of chilled S3 buffer (0.88 M Sucrose,10 mM $MgCl_2$)). The nuclei were spun at 2800 g for 10 min at 4°C. The nuclear pellet was resuspended in PBS, pelleted, and then lysed in 1 $\times$ RIPA.

2.8 Transfecting cells with exogenous nucleic acids

Target mRNA and proteins were depleted using siRNA duplexes (**Table 2.4**). **Table 2.4** outlines the gene targets, target sequences, suppliers, and concentration range at which each duplex was used. The duplexes supplied by Life Technologies were Stealth RNAi duplexes while those supplied by Dharmacon were SmartPool duplexes that included three siRNA duplexes. Unless otherwise stated, reverse transfections were performed with cells dispensed into tissue culture vessels in the presence of the siRNA duplex. The siRNA duplex had been complexed with RNAiMax (Life Technologies) transfection reagent in 5% bovine foetal calf serum media for 24 hrs. Following this, experiments were undertaken as outlined in other sections.

Table 2.4: The specific details of the duplex RNA(s) that were used to deplete RNA and proteins during this thesis.

Target	Supplier	Ab.Cat.No	Sequence (5' - 3')
siCTRL	LifeTech.	N/A	CCACACGAGUCUUACCAAGUUGCUU
YB-1	LifeTech.	HSS166994	GGUCCUCCACGCAAUUACCAGCAAA
YB-1	LifeTech.	HSS166995	GACCCUAUGGGCGUCGACCACAGUA
C1QBP	LifeTech.	HSS101146	
C1QBP	LifeTech.	HSS186347	
C1QBP	LifeTech.	HSS101148	
siCTRL2	Dharmacon		
FAM120A	Dharmacon	L-014186-01	
TRIM28	Dharmacon	L-005046-00	

Abbreviations; siCTRL = non-targeting sequence.

To express exogenous gene products, DNA plasmids were transfected into cells. The cells were transfected when they were ~ 80 - 85% confluent. To transfect one well in a 6-well plate, the cells were incubated with 2 μg of plasmid DNA. The plasmid DNA had been complexed with 5 μl Lipofectamine 2000 in bovine foetal calf serum-free DMEM media for 24 hrs before being returned to media that contained 10% bovine foetal calf serum.

2.9 Assays for monitoring cell growth and viability

The growth and viability of adherent cells was monitored in up to 360 wells per experiment using an InuCyte FLR (Essen Biosciences). The general structure of these experiments is summarised by **Figure 2.1**. Cells that had grown to a confluence of 70 - 85% in media with 10% bovine foetal calf serum were harvested and the depletion of mRNA and proteins took place as outlined in **Chapter 2.8**. Specifically, 2,200 cells were seeded into each well of a 96-well plate; all outer wells on the 96-well plate were filled with 200 μl PBS to minimise evaporation. After 24 hrs, the media were changed to a standard media plus or minus any treatments that were required for the experiment. When cell viability was also monitored, YOYO-1 Iodide dye (Life Technologies) was added at 1 μl per 10 ml of media (discussed below; O'Clair & Appledorn 2011). All treatments were dispensed from this pool.

Cell confluence was monitored by collecting phase-contrast images every 2 or 3 hrs for the duration of the experiment using the InuCyte FLR. Confluence was calculated by the Confluence algorithm (v1.5), which is included with the InuCyte FLR software. The maximal growth-rate for each well was derived from the confluence data using the *grofit* package (Kahm et al. 2010) in R (v3.1.1 (2014-07-10)). Following optimisation of the parameters, the spline fitting function was used to estimate the maximal growth-rate from maximum slope (μ) and the maximum cell growth (A). The following settings were used for curve-fitting of the confluence data by *grofit*;

```
opt_bt_rt <- grofit.control(smooth.gc = 0.7, smooth.dr = 0.4, parameter
    = 28, neg.nan.act = TRUE, fit.opt = "b", nboot.gc = 100, nboot.dr
    = 100)
```

The *DRC* package in R (version 3.1.1 (2014-07-10) – "Sock it to Me" Ritz & Streibig 2005, Ritz et al. 2015) was used to create dose-response curves that were

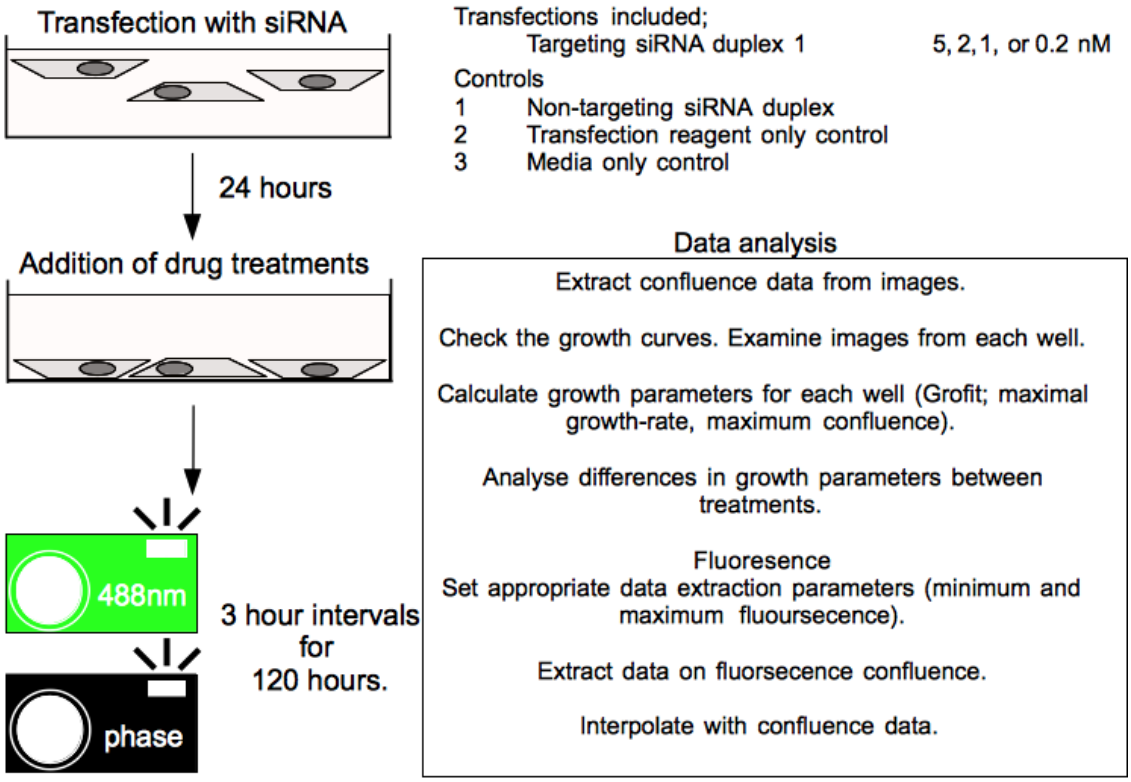

Figure 2.1: The general outline for experiments investigating the role of YB-1 in the sensitivity of MDA-MB231 cells to various drugs. Fluorescence measurements came from YOYO-1 Iodide, which has excitation/emission maxima at 491 nm and 509 nm, using the fluorescence channel on the InuCyteFLR l which has an excitation of 470 nm max (450 - 490 nm) and an emission of 515 nm max (500 - 530 nm).

created from the maximal slope data. A number of the inbuilt parametric regression models were tested including a five-parameter log-logistic dose-response model, Weibull I, and Weibull II. The testing also included an analysis of the residuals from each fit, a comparison of each fit to a fit from an analysis of variance, and, finally, the amount of variation explained by each model was compared using the Akaike information criterion (Ritz et al. 2015). When drugs were used in sufficient concentration to reduce total cell survival to 0%, the growth measurements were scaled to the control and the top-most drug dose (μ - $\mu_{\text{maximum drug}}$)/($\mu_{\text{media only}}$-$\mu_{\text{maximum drug}}$). Each experiment was analysed using the same models and fixed parameters. Optimisation revealed that analysing the scaled data, and using a 2-parameter log-logistic calculation, provided the most accurate and consistent fitting to the data. The lower and upper asymptotes for the models were set to 0 and 1 respectively, while the slope and effective dose were calculated for each combination of siRNA duplex at each concentration.

In experiments where cell viability was monitored, fluorescent images from an excitation of 470 nm max (450 - 490 nm) and an emission of 515 nm max (500 - 530 nm) were obtained alongside the phase contrast images using the InuCyte FLR. YOYO-1 Iodide is cell-impermeant and produces fluorescence when it intercalculates with DNA from cells where the cell membrane is no longer intact.

Autofluorescence, primarily from the riboflavin in the DMEM (Essen Bioscience 2009), was evident for the first 24 hrs of each experiment, by which time the autofluorescence was bleached. Analysis of the fluorescence data began with images taken 24 hrs after the YOYO-1 Iodide was added to the media. The fluorescence data were extracted with the following parameters fixed; Background Intensity = 20 fluorescence arbitrary units (A.U.), Foreground Intensity 200 A.U., Manual Adjustment 50 A.U. Cell viability data were originally intended to be analysed as live/dead counts. To produce these measurements, the number of dead cells was derived from the number of fluorescent particles at the end of the experiments. The number of total cells was calculated from fluorescent images following the permeabilisation of cells with Triton-X100 at the end of the experiment. However, consistent permeabilisation did not occur and counting fluorescent particles following permeabilisation did not provide an accurate assessment of the total number of cells in each field of view. In the absence of a viable end-point measurement the data from fluorescence were reported as death index. Death index is; log-transformed[(confluence of the fluorescent signal / confluence of the cells)].

The effects of drug exposure on cell death are reported as Relative death index.

This measurement is normalised two ways. The first way is similar to the death index, as it controls for cell number by dividing YOYO-1 Iodide signal by confluence. The second controls for the general effects of the siRNA duplex on cell viability by normalising the measures to cells that were incubated without drugs for that siRNA duplex and siRNA duplex concentration. Therefore, relative death index is the measure of change in non-viable cells and it was calculated as; log-transformed + 1 ([confluence of the fluorescent signal /confluence of the cells]$^{\text{media}}$ - [confluence of the fluorescent signal / confluence of the cells]$^{\text{cisplatin}}$).

2.10 Immunofluorescence

To prepare a 2% Paraformaldehyde solution, 1 g of EM-grade paraformaldehyde was dissolved into 20 ml of 65°C double-distilled water with 4 drops of 1 M NaOH. One molar NaOH was added slowly until the paraformaldehyde was in solution and the volume adjusted to 25 ml using double-distilled water. One hundred millilitres of 0.2 M phosphate buffer (pH 7.3) was prepared from 23 ml 0.2 M NaH_2PO_4 and 77 ml of 0.2 M Na_2HPO_4. 25 ml of 0.2 M phosphate buffer (pH 7.3) was added to the paraformaldehyde to give a 2% paraformaldehyde solution which was used immediately or stored at 4°C for up to 4 days.

Cells were grown on poly-L-lysine coated coverslips in 24-well plates. Cells were fixed using paraformaldehyde solution for 15 min at room temperature. The cells were washed twice with ice cold PBS and at this point stored at 4 °C. Cells were permeabilsed by incubation with 200 µl PBS containing 0.25 % Triton X-100 for 10 min and then washed, with PBS, three times for 5 min. The non-specific reaction of the primary and secondary antibodies was reduced by a 30 min incubation in 200 µl PBS containing 0.2% cold water fish skin gelatin (Sigma) in 1% BSA with 10% heat-inactivated serum from the species in which the secondary antibody was raised. The cells were then incubated at 4°C in a humidified chamber overnight with the diluted antibody in 200 µl 1% bovine serum albumin, 0.2% cold water fish skin gelatin in PBS. See **Table 2.3** for antibody specific dilutions. Every run included controls for each secondary antibody. The only alteration in this step was that the primary antibody was omitted. The following morning the primary antibody solution was decanted and the cells washed three times for 5 min using PBS plus 0.25% tween20.

The cells were incubated for 1 hr at room temperature in the dark with 200 µl PBS that included 1:2000 of the appropriate secondary antibody, 1% BSA, 0.2% cold-fish skin gelatin (Alexa Fluor 488, F(ab')2 fragment of goat anti-rabbit IgG (H

+ L) [A11070]; Alexa Fluor 488, F(ab')2 fragment of goat anti-mouse IgG (H + L) [A11017]; lexaFluor 568, F(ab')2 fragment of goat anti-mouse IgG (H + L) [A11019]; Alexa Fluor 568 donkey anti-sheep IgG (H + L) [A21099]). To visualise nuclei, the double strand DNA binding dye Hoescht was included at 0.5 mg per ml (excitation/emission maxima at 350 nm and 461 respectively; Life Technologies). The secondary antibody solution and Hoescht was decanted and the coverslips washed in the dark three times for 5 min in 160 µl PBS with 0.25% Tween20. The slides were prepared by placing small dots of ProlongGold (Life Technologies), an antifade mountant, to appropriately labelled slides. The coverslips were then recovered and eased, cell side down, onto the dots of mountant. The slides were placed upside down on a flat surface before being weighted to ensure that the coverslips cured flat.

For fluorescence microscopy, the slides were imaged using a Zeiss fluorescent microscope with SPOT-RT CCD camera (Diagnostic Instruments). Confocal microscopy was performed using a Nikon C2+ Confocal Eclipse Ni-E Microscope (Channels; 405 nM, 488 nM, 561. nM) objective; Plan Apo λ 40x. During imaging, the control containing no primary antibody, and a selection of the slides, was used to set exposure conditions that encompassed the intensity range for each primary antibody. Once the settings were set, they remained static for imaging of each channel for that set of slides.

2.10.1 Extraction of cytoplamic proteins and RNA

Cytoplasmic proteins and mRNAs were extracted from MDA-MB231 cells using two 5 min incubations in Cytoskeleton buffer that had been pre-heated to 37°C (10 mM Pipes, pH 7.0, 100 mM NaCl, 300 mM sucrose, 3 mM $MgCl_2$, 0.7% Triton X-100, 0.3 mg/ml RNase A; Britton et al. 2013). The cells were gently washed in PBS and fixed immediately. Fixation and immunofluorescence (IF) then proceeded as outlined in **Chapter 2.10**.

2.10.2 Analysis of micrographs

The images from IF were analysed using the FIJI distribution of ImageJ (Version, 2.0.0-rc-49/1.51a; Schindelin et al. 2012). Confocal images were imported into FIJI using the Bio-Formats library plugin (version, 5.1.10; The Open Microscopy Environment 2016). To ensure accurate assessment of the subcellular distribution, two-dimensional images that bisected the centre of the nucleus of the imaged cells were created. To do this, two-dimensional images, or Z-projections, were produced

from the maximum signal intensity of the three Z-slices where the Hoechst dye (DNA) produced its peak signal. Fluorescence data (gray values) were displayed using an enhanced false colour lookup table (Green hot, ImageJ). This allows better visualisation of low intensity signals from YB-1. To provide an accurate summary of the results, where appropriate the gray values are plotted in R (see **Chapter 2.15** for details). Gamma H2A foci were counted using the pzFociez macro in ImageJ (Znojek 2012). The macro was used in a semi-supervised fashion where, following masking of the nuclei channel, nuclei that were too close to be separated by the mask were removed from the analysis. The γH2AX foci in the nuclei of a minimum of 200 cells were counted for each treatment.

2.11 Immunohistochemistry

Sections fixed in neutral-buffered-formalin and embedded in paraffin wax were processed using a standard citrate buffer antigen-retrieval protocol. Three rabbit polyclonal primary antibodies were used to detect YB-1, (see above). These were diluted in 1%BSA in PBS as follows: ^{N}YB1; 1:1200 and YB1^{C}; 1:1000 and incubated overnight at 4°C. Detection of the primary antibody was carried out using the EnVisionTM+ Dual Link system (Dako) according to the manufacturers protocol. Specimens were counterstained in Gills haematoxylin and mounted in Entellan (ProSciTech). Staining pattern and intensity was visualized using a Zeiss Axioplan compound microscope, and photographed with a SPOT-RT CCD camera. Immunohistochemistry was the work of Dr Adele Woolley.

2.11.1 Immunohistochemistry Assessment

100 cells in each specimen were scored according to the presence and intensity of staining. Negative staining was scored as zero, weak as one, moderate as two and strong as three. The intensity of staining within the tumour was compared to at least three regions of adjacent normal tissue. Identification and assessment of immunohistochemical staining of diagnostic breast tissue was carried out in consultation with registered pathologists. Immunohistochemistry assessment was the work of Dr Noelyn Hung and Dr Adele Woolley.

2.12 Immunoprecipitation

Proteins were immunoprecipitated from cellular lysates using either protein G dynabeads (Invitrogen) or Protein G Mag Sepharose (GE healthcare). Lysates were prepared for IP at standard concentrations, the equivalent of 1×10^4 cells per µl, or in the case of IP from nuclei, 5×10^4 cells per µl. A low detergent RIPA buffer was used for all IP (**Table 2.2**). To create this buffer in 5 ml cytoplasmic preparations (**Chapter 2.7**), the following was added; 1 phosSTOP tablet, 55 µl 10% deoxycholate, 137.5 µl 20% NP40, 275 µl 1M Tris-HCL, pH 7.5. The low detergent RIPA buffer was added to nuclei pellets, passed through a 22 gauge needle 10 times, and incubated on ice for 20 min. Debris was cleared from lysates by centrifugation at 13 000 g for 10 min.

During these steps, the beads were prepared for use. At this point in the experiment, the protein G dynabeads and Protein G Mag Sepharose protocols differ from one another. Protein G dynabeads were immobilised on a magnet and washed three times with 300 µl of lysis buffer. Antibody preparations were added to the lysates and they were rotated for 1 hr at 4°C. Twenty-five µl of protein G beads were then added for every 20 µg of antibody and incubated on a rotator for 30 min at 4°C. The bead:antibody:YB-1 complexes were then immobilised by a magnet, the lysate removed, and the bead:antibody:YB-1 complex was taken to the next step.

The Protein G Mag Sepharose beads were used at a concentration of 75 µl for every 50 µg of antibody. For these IPs, the antibody and Protein G Mag Sepharose beads were complexed together in 500 µl of low-detergent RIPA for 30 min, immobilised, and then rinsed once with another 500 µl of soft buffer. The lysate was then added to the immobilised antibody plus Protein G Mag Sepharose beads and rotated for 1 hr at 4°C.

From this point the experiments, the protocols were the same. Samples were washed three times in 200 µl soft buffer at 4°C. The samples were inverted gently for mixing and carefully transferred to a new tube for the last wash. The interaction of the antibody with the protein G beads was disrupted using competitive elution. The peptide to which ^{N}YB1 was raised was added to each sample at a concentration of 100-fold to nativePAGE buffer (Life Technologies) with 1% Digitonin (Sigma), 1 × phosSTOP (Roche) and 1 × complete EDTA- (Roche). The samples were incubated at room temperature for two hrs with gentle mixing. Following this, the supernatant was collected and stored at -80°C to await analysis.

2.13 Mass Spectrometry

LC-MS/MS has been used to identify the proteins that copurify with immunoprecipitated YB-1. Identifying proteins using LC-MS/MS identification requires that the proteins are reduced to peptides that can be efficiently retained and specifically eluted by the liquid chomatography system that supplies the mass spectrometer with peptides. An overview of the key elements for analysing peptides using LC-MS/MS are reviewed in more detail in **Supplementary information A.1**.

2.13.1 Sample preparation

The proteins that were recovered using IP were separated using SDS-PAGE and the gel was stained using colloidal coommassie staining (**Chapter 2.3.1**). Protein bands and fractions were excised and subjected to in-gel digestion with trypsin using a robotic workstation for automated protein digestion. The protocol for automated in-gel digestion was based on the method of Shevchenko et al. (1996) and the eluted peptides were dried using a centrifugal concentrator. To perform LC-MS/MS on phosphorylated peptides, the phosphorylated peptides from the YB-1 bands were enriched using TiO_2 Mag sepharose beads (GE Healthcare).

To generate peptides from cross-linked proteins (see **Chapter 2.13.5**), the bands were excised from non-reducing SDS-PAGE gels and processed manually. Peptides were generated from proteins using trypsin but reduction was omitted. Gel pieces were buffered by three rounds of dehydration and swelling in 80% acetonitrile and then 50 mM $NH_4)HCO_3$ for 5 min each. Following a final dehydration step in 80% acetonitrile, the proteins were alkylated in 20 mM idoacetamide in 50 mM $NH_4)HCO_3$ for 15 min in the dark. Two more rounds of dehydration and swelling were followed by the addition of 200 ng of trypsin to the dehydrated gel pieces and incubation overnight at 37°C. The following morning, another 100 ng of trypsin was added and left at 37°C for another two hrs. The peptides were then collected by two rounds of dehydration and rehydration in 80% acetonitrile with 0.2% formic acid and 0.2% formic acid in ultrapure H_2O for 30 min at each step. The sample was then split with the peptides with intact cross-links, these were not reduced and dried to a 2 - 5 µl volume in a centrifugal concentrator to await prompt analysis. The remainder of the sample was dehydrated in 80% acetonitrile and then reduced via a 45 min incubation at 45°C in 200 mM DTT in 50 mM ammonium bicarbonate. 200 mM idoacetamide was added and the samples incubated for a further 15 min in the dark and at room temperature. DTT and idoacetamide were removed from the

peptide mixtures using C18 filled zip-tips.

2.13.2 LC-MS/MS of tryptic peptides

Following tryptic digestion, the samples were re-solubilised in 1% (v/v) acetonitrile, 0.2% (v/v) formic acid in ultrapure H_2O, and injected onto an Ultimate 3000 nano-flow LC-System (Dionex Co, CA) that was in-line coupled to the nano-electrospray source of a LTQ-Orbitrap XL hybrid mass spectrometer (Thermo Scientific, San Jose, CA). Peptides were separated on an in-house packed emitter-tip column (75 µm ID fused silca tubing packed with C-18 material on a length of 8 - 9 cm). The gradient for liquid chromatography was modified depending on the sample. Generally, the gradient developed from 1% [v/v] acetonitrile, 0.2% (v/v) formic acid to 80% (v/v) acetonitrile, 0.2% (v/v) formic acid in ultrapure H_2O at a flow rate of 400 nl/min.

Full MS (MS^1) in a mass range between m/z 400 - 2000 was performed in the Orbitrap mass analyser with a resolution of 60,000 at m/z 400 and an AGC target of 2^e5. Preview mode for FTMS master scan was enabled to generate precursor mass lists. The strongest 5 signals, with a charge state $\geq [M + 2H]^{2+}$, were selected for CID (collision induced dissociation)-MS/MS (MS^2) in the LTQ ion trap at a normalised collision energy of 35% using an AGC target of 1^e5 and two microscans. CID and higher-energy collisional dissociation (HCD) were used to fragment peptides with intact cross-links and only precursors with a charge state $\geq [M + 4H]^{4+}$ were selected for MS^2 scans. Dynamic exclusion was enabled with 2 repeat counts during 30 second (sec)s and an exclusion period of 180 secs. The exclusion mass width was set to 0.01.

2.13.3 Data Analysis

For protein identification, MS/MS data were searched against the Human Swiss-Prot amino acid sequence database using the Mascot search engine (http://www.matrixscience.com) and Sequest using Proteome Discoverer (v1.4). The search was set up for full tryptic peptides with a maximum of 3 missed cleavage sites. Carboxyamidomethyl cysteine, oxidized methionine, deamidation (N, Q), and phosphorylation (S, T, Y) were included as variable modifications as appropriate. The precursor mass tolerance threshold was 10 ppm and the maximum fragment mass error 0.8 Da.

Peptides were accepted as identified if their score was above the score threshold for the false discovery rate of 1:100, as assessed by the Percolator algorithm (Käll

et al. 2007). Proteins were considered identified when they were assigned ≥ 2 unique peptides above the aforementioned score threshold. To improve the accuracy of protein identification, the peptide search files were loaded together. This makes all peptides that were identified interacting with YB-1 available to provide more information about which proteins were present. Information about splice variants was removed prior to bioinformatic analyses.

Proteins that included peptides with CAMthiopropanoyl on a lysine were collated and a database containing all potential cross-linked peptides from the proteins was created using the xComb software (for details of cross-linking see **Chapter 2.13.5** and **Figure 2.2**; Panchaud et al. 2010). To analyse cross-linked peptides, aliquots of the cross-linked peptides were reduced and alkylated (see above) and subjected to LC-MS/MS analysis. The CAMthiopropanoyl (K) modification, which corresponds to a DSP adduct that has been reduced and alkylated, was added to the searches (**Figure 2.3**).

2.13.4 Relative quantification of proteins by mass spectrometry

The semi-quantitative analysis of the protein levels used the top three peptides method (Silva et al. 2006) and was executed using Proteome Discoverer (v1.4). When more accurate quantification was required, each sample was injected onto the LC-MS/MS three times.

Skyline was used to create a spectral library from the Proteome Discoverer search files (.msf) from each phosphopeptide run (c2.6; Schilling et al. 2012). Precursor ions from MS^1 scans were analysed using the workflow described by Schilling et al. (2012). Each peak assignment was confirmed by manual inspection. Care was taken to remove precursors ions where the peak area assessment was incorrect due to the presence of ions from other precursors that interfered with the quantification. Precursors where the ratio of the precursor isotopes was outside the expected range (idotp <0.90; Schilling et al. 2012) were also removed from the analyses (isotope peaks are reviewed in **Supplementary information A.1**).

2.13.5 *In vivo* cross-linking of proteins

Proteins were cross-linked *in vivo* by treating intact cells with dithiobis[succinimidyl propionate] (DSP) or paraformaldehyde buffered in PBS. Cross-linking using DSP

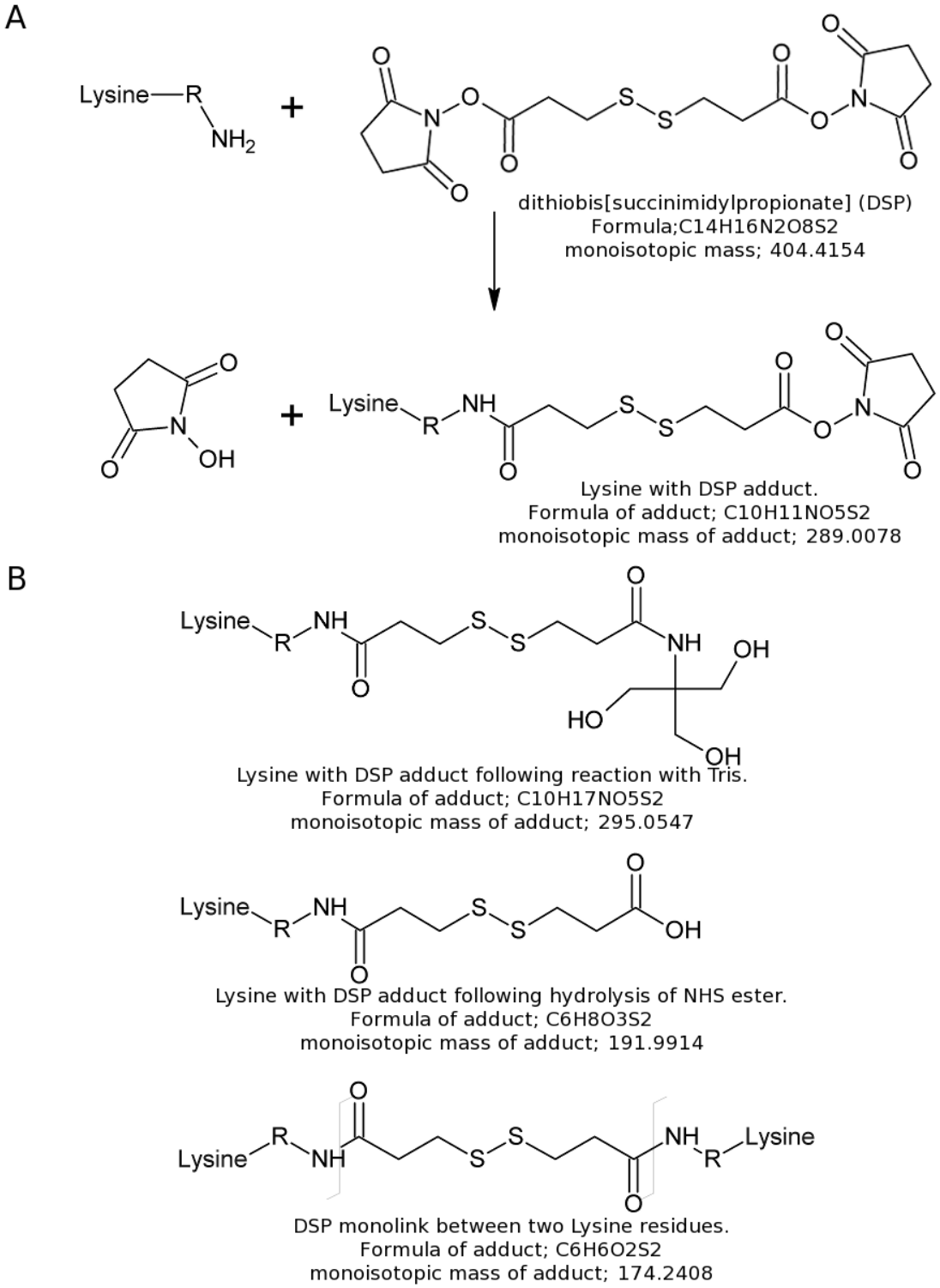

Figure 2.2: **A**, The interaction of dithiobis[succinimidylpropionate] (DSP) with the free amino group (NH_2) of lysine. Potential reactions of the remaining N-hydroxysuccinimide (NHS) group of DSP following the formation of an adduct with a lysine. **B**, the remaining NHS group can interact with Tris during the quenching reaction, it can be hydrolised, or it can form a cross-link by interacting with another lysine residue. The name, chemical formula, and monoisotopic mass of each adduct is noted below each structure.

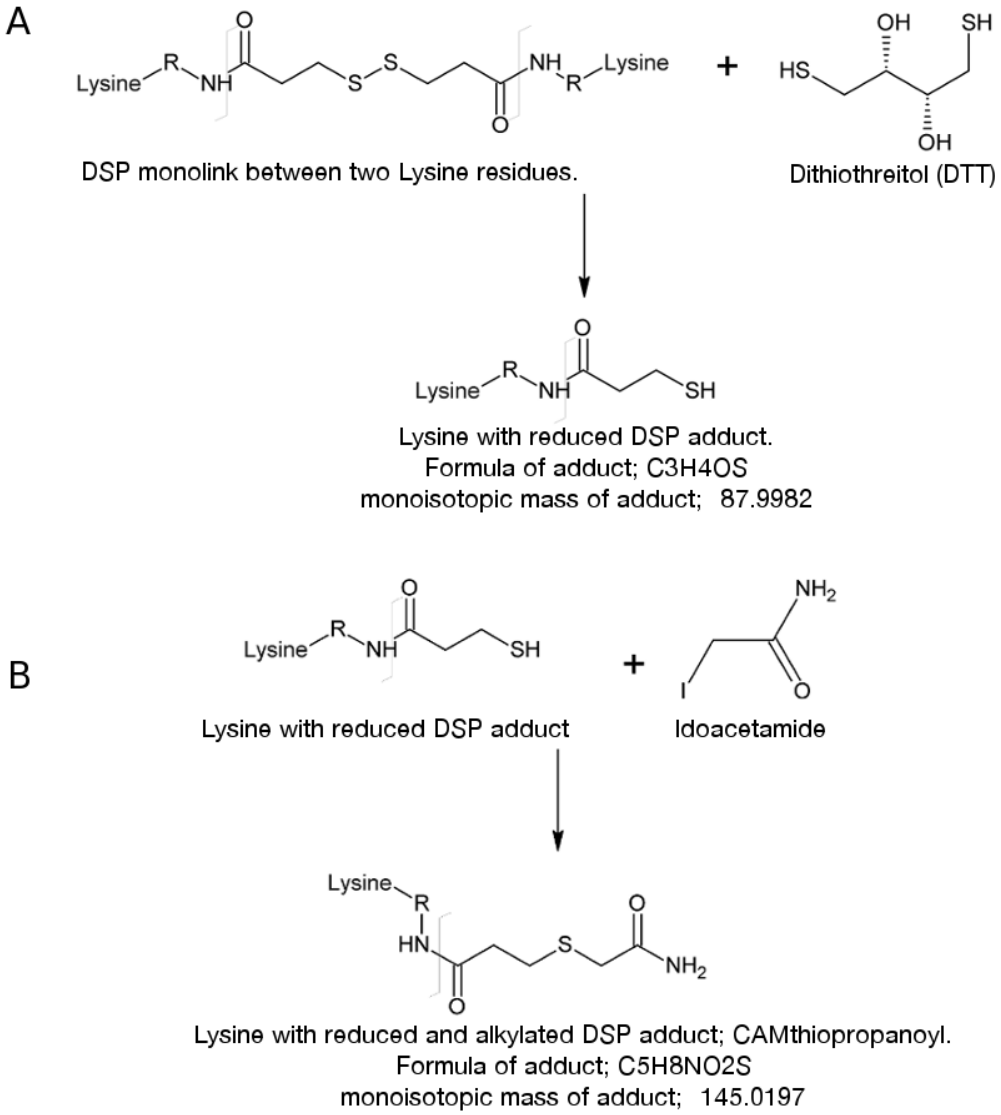

Figure 2.3: The disulfide bond at the centre of DSP was cleaved using DTT to separate the cross-linked peptides. **A**, following reduction with DTT, the cross-links were **B** alkylated using idoacetamide. The name, chemical formula, and monoisotopic mass of each adduct is noted below each structure.

creates cross-links on the amino groups of lysine residues and N-termini (**Figure 2.2**). Cells were tripsinized, counted, and rinsed twice with PBS. Immediately prior to its use, a 25 mM DSP solution was prepared in DMSO ($[CH_3]s_2SO$). The cells were diluted to 10 000 cells per µl in PBS and the 25 mM DSP solution was added to the cell suspension at a ratio of 1:25. Cross-linking took place with gentle mixing at room-temperature for 45 min. The cells were spun and the supernatant removed. The remaining cross-linker was then quenched by the addition of 100 mM Tris in PBS which was added in a stoichiometry of at least 1:1 with the cross-linking reagent and incubated at room-temperature for 10 min. This step was repeated once before the cells were lysed at 10 000 cells per µl in RIPA, snap frozen, and placed into $^{-}$20°C. Cross-linked IP samples were concentrated using centrifugation at 15 000 g at room temperature in a Vivaspin 500, 30 000 MWCO column (Sartorius) until their volume was 25 µl.

To assess which peptides had interacted with DSP, the cross-linked peptides were reduced and alkylated and subjected to LC-MS/MS (**Figure 2.3**; **Chapter 2.13**).

2.13.6 Size exclusion chromatography

Size exclusion chromatography was performed using a Thermo Finnegan Spectra System SN4000 controller, SpectraSYSTEM Solvent Degasser, SpectraSYSTEM solvent pump, and AS3000 UV6000. Cross-linked lysates were run three times through a Vivaspin 20 100 kDa MWCO filter (GE Lifesciences) to the deadstop and then refilled with 150 mM NaCl; 50 mM Tris-HCl (pH 8.0). The concentrated and detergent depleted samples were directly loaded on a Superdex 200 10/300GL (GE lifesciences) column at a flow-rate of 0.7 ml per min. The mobile phase was 150 mM NaCl:50 mM Tris-HCl (pH 8.0). Initial calibration of the elution range was performed using Blue Dextran (Sigma) and vitamin B12 (Sigma). Fractions from the sample were collected from two min before the estimated start of the elution phase and through to completion as determined by spectroscopy. Fractions were stored at $^{-}$20°C.

2.14 Bioinformatics

The enrichment of terms amongst proteins was assessed using the functionally annotated clusters from Database for Annotation, Visualization, and Integrated Discovery (DAVID) (version 6.7; Huang et al. 2009a, Huang et al. 2009b). The clas-

sification stringency was set to medium. The background settings for enrichment analyses were the human genome background which is built into DAVID. However, in some instances the background was set to the total proteins that were identified in immunoprecipitations of YB-1 from the work reported here. This alteration is highlighted when reported.

Protein-protein interactions (PPI) were recovered from searches of the *Experiments* and *Databases* evidence prediction methods in String (version 9.1; Snel et al. 2000, von Mering et al. 2003, Franceschini et al. 2013, Szklarczyk et al. 2015). The PPI networks were visualised and examined using Cytoscape (v3.1). The networks were arranged using the Spring-electric layout provided by the AllegroLayout plug-in (Yoon 2015). Markov clustering (Yan et al. 2010, Yu et al. 2007) was performed using a cytoscape plug-in CytoNCA (Tang et al. 2015). The enrichment of gene ontology terms (Ashburner et al. 2000) was further assessed using the Bingo cytoscape plug-in (version 3.0.3; Maere et al. 2005). Bingo gene ontology enrichment used the generic GOSlim with hypergeometric testing with benjamini and Hochberg false discovery rate correction. The background was set to genome from the *Homo sapiens* annotation file. Statistical significance was set to $p \leq 0.05$.

2.15 Statistical analyses

Statistical analyses were carried out using R, version 3.1.1 (2014-07-10) – "Sock it to Me". Data handling was primarily carried out using dplyr (version 0.5.0; Wickham & Francois 2016) and reshape2 (version 1.4.1: Wickham 2007). Graphing was performed using ggplot2 (version 2.1.0; Wickham 2009) except for heatmaps which were created using the `heatmaps()` function from the gplots package (version 3.0.1; Warnes et al. n.d.).

T-tests were performed using the R base function `t.test()`. Paired t-tests were used where appropriate and this is noted. T-tests for the dose-response curves were performed using the `compPam()` function within the DRC package. General linear models, such as analysis of variance, were produced using the `aov()` command. Post-hoc testing for the factors in these linear models was performed using the `TukeyHSD()` command with *conf.level = 0.95*.

Chapter 3

Tertiary structure and protein interactions may influence the prognostic sensitivity of antibodies against YB-1

3.1 Introduction

Observations have consistently shown that the levels of YB-1 are elevated in aggressive breast cancers (reviewed in **Chapter 1.3**). However, the subcellular localisation of YB-1 in these cancers is not reported consistently. The variable YB-1 immunostaining patterns between studies may be explained by variations in the immunoreactivity of the antibodies that were used. Work from our laboratory has highlighted that many YB-1 antibodies either have a low affinity for YB-1 or they exhibit non-specific binding (Cohen et al. 2010). To date, the majority of YB-1 antibodies used in immunohistochemical studies have been generated to residues within the N-terminus (Bargou et al. 1997, Dahl et al. 2009, Janz et al. 2002) or to the C-terminus of YB-1 (Fujita et al. 2005, Habibi et al. 2008, Wu et al. 2006).

Variations in the immunoreactivity of YB-1 antibodies were hypothesised to explain the conflicting reports, as well as the variable subcellular localisation of YB-1. To test this hypothesis, the presence of YB-1 in normal breast tissues and cancerous breast tissues was assessed using immunohistochemistry (IHC) with two antibodies. The two affinity-purified antibodies target the N-terminus (amino acids 1-12; ^{N}YB1) or the C-terminus (amino acids 299 - 313; YB1^{C}) of YB-1. The

specificity of ^{N}YB1 and YB1^{C} to YB-1 was verified in Cohen et al. (2010). Both ^{N}YB1 and YB1^{C} have matching binding affinities for denatured YB-1 and recognise a single band on immunoblots.

The work detailed in this chapter addresses the contradictory reports of YB-1 in normal tissues by assessing the presence and expression of *YBX1* mRNA and YB-1 in normal human tissues. Following this, an assessment was made of the correlation of staining from ^{N}YB1 or YB1^{C} in IHC of breast samples to prognostic markers. The results demonstrate that both antibodies have significant prognostic value. However, ^{N}YB1 shows more sensitivity. The biochemical reasons for the differences between ^{N}YB1 and YB1^{C} were explored. The protein-protein interactions, or the secondary/tertiary structure of YB-1 in its native conformation, appear to affect the binding of ^{N}YB1 and YB1^{C} to YB-1. Portions of the work reported here were included in Woolley et al. (2011).

3.2 Results

3.2.1 *YBX1* mRNA and YB-1 are present in normal human tissue and human cancer cell lines

The levels of *YBX1* mRNA across a range of normal tissues were assessed to address contradictory reports about the presence of *YBX1* mRNA in normal tissues. To carry out this assessment, the RNAseq Atlas was downloaded (Krupp et al. 2012). Data relating to *YBX1* mRNA were extracted and analysed. This analysis shows that *YBX1* mRNA is present in a wide range of normal tissues (**Figure 3.1.A**). The levels of *YBX1* mRNA are in the top quartile of the measured mRNA transcripts in all tissues. To highlight how the levels of *YBX1* mRNA compare with those of other transcripts, a selection of gene products was included in the heatmap. Two of these transcripts come from the lowest quartile of mRNA expression levels (*TP53* and the α catalytic subunit of Phosphatidylinositol 4,5-bisphosphate 3-kinase [*PIK3CA*]) and three are from the highest quartile of mRNA transcript measurements (Vimentin [*VIM*], β-actin [*β-actin*], and Glyceraldehyde-3-phosphate dehydrogenase [*GAPDH*]). Therefore, *YBX1* mRNA is present and robustly expressed in a wide range of normal tissues.

The presence of *YBX1* mRNA in cancer cell lines of varying lineages was also assessed using northern blotting. The northern blot confirms that *YBX1* mRNA is present in all of the cell lines that were analysed (**Figure 3.1.B**). Levels of

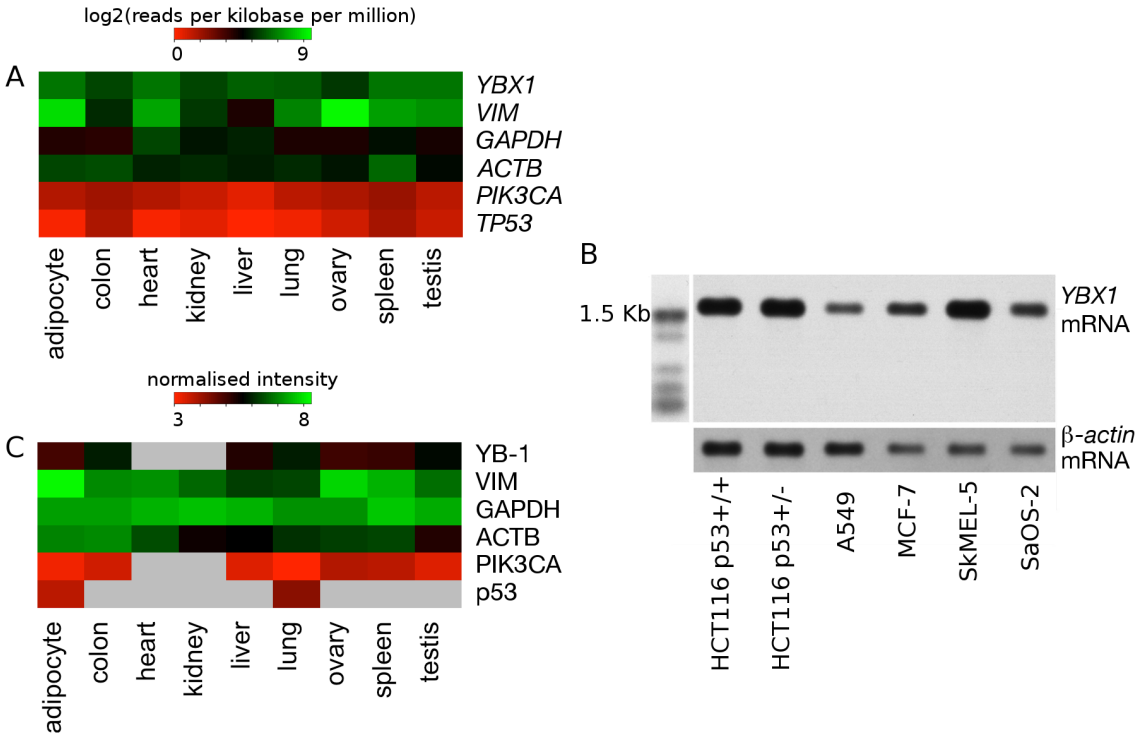

Figure 3.1: *YBX1* mRNA and YB-1 are present in a wide range of normal tissues. **A**, *YBX1* mRNA was detected and quantified using sequencing. The levels of highly expressed (*VIM*, *GAPDH*, *ACTB*) and lowly expressed gene products (*PIK3CA*, *TP53*) provide a reference. **B**, *YBX1* mRNA was also detected in 500ng of mRNA from 6 cancer cell lines using northern blotting. **C**, YB-1 was also detected in the same tissues using mass spectrometry. Sequencing data for the analysis in **A** were collected from RNAseqatlas on 16.07.2014 and are presented as log2(reads per kilobase per million). The data for **C** were collected from proteomicsDB on 21.06.2014 and are presented as normalised intensity. Grey panels indicate that the protein is not detected in this tissue. *Abbreviations*; *VIM* = vimentin, *GAPDH* = Glyceraldehyde-3-phosphate dehydrogenase, *ACTB* = β-actin, *PIK3CA* = Phosphatidylinositol 4,5-bisphosphate 3-kinase catalytic subunit alpha isoform, *TP53* = Cellular tumor antigen p53.

YBX1 mRNA are lowest in A549 cells derived from a lung carcinoma and highest in SkMEL-5 cells derived from melanoma. The cDNA probe that was used to detect *YBX1* mRNA should also bind to three of the four proposed *YBX1* splice variants (**Chapter 2.4**). In all cases, a single band is present and the alignment of these bands with the mass ladder indicates that the signals come from full-length *YBX1* mRNA. Therefore, northern blotting confirms the presence of only full-length *YBX1* mRNA in a range of cancer cell lines.

To confirm that YB-1 is a feature of normal tissues, LC-MS/MS data was downloaded from the ProteomicsDB (Wilhelm et al. 2014). Analysis of these data confirms the presence of moderate to high levels of YB-1 in most of the tissues (**Figure 3.1.C**). This shows that the *YBX1* mRNA in normal tissues is translated to its protein YB-1 and that YB-1 is a feature of most normal tissues. In general, the levels of YBX1 mRNA and YB-1 are concordant. However, despite adequate *YBX1* mRNA levels, YB-1 was not detected in the heart and kidney tissue samples (**Figure 3.1.C**). This may reflect the variance that is inherent in samples from different sources, or it could be due to a specific limitation of mass spectrometry. The limitation being the ability of interfering signals to cause false negative results. The LC-MS/MS data apply to the tissue level and lack critical information about proteins at the cellular and subcellular levels. Histological techniques, such as IHC or immunofluorescence (IF), provide information about proteins at the cellular and subcellular levels.

The levels of YB-1 and its subcellular distribution in normal breast tissues (reduction mammoplasties) were assessed using IHC. Staining for YB-1 with ^{N}YB1 is present in all of the reduction mammoplasties (**Figure 3.2**). The IHC confirms that YB-1 is present in normal breast tissue. This work also highlights the variation of YB-1 within normal breast tissue. YB-1 is present in both lobular and ductal mammary structures. Consistently strong staining is present in columnar alterations with prominent apical snouts and secretions; which share some features with premalignant lesions, such as elevated proliferation (arrowheads in **Figure 3.2.ii and iv**; Dessauvagie et al. 2007). At the subcellular level, staining for YB-1 is present primarily in the cytoplasm of cells. There are no cells where YB-1 was only localised to the nucleus. A small number of cells appear to have YB-1 in their nuclei but the thickness of the tissue sections (5µm) prevents the definitive confirmation of this nuclear signal (see insets **Figure 3.2.i, iii, iv and vi**).

In summary, these results confirm the presence of YB-1 in normal breast tissue. IHC shows that YB-1 is primarily localised to the cytoplasm in normal breast tissue.

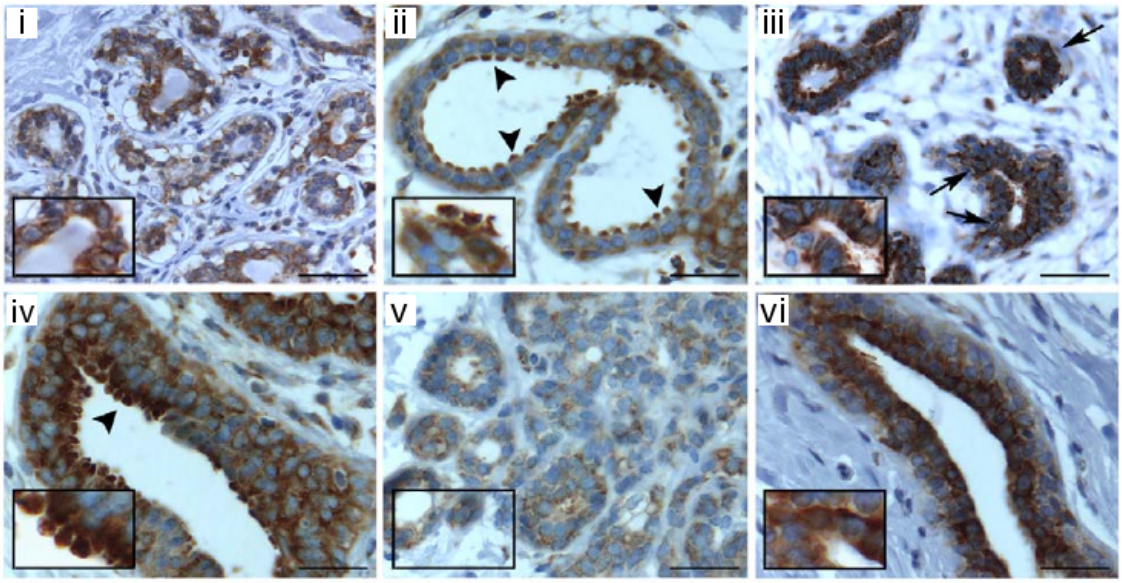

Figure 3.2: YB-1 is detected by ^{N}YB1 in the cytoplasm and perinuclear region of normal lobular (i, iii and v) and ductal (ii, iv and vi) breast tissue by IHC. Insets show staining at a higher magnification. Arrowheads (panels ii and iv) depict high levels of YB-1 in columnar alterations with prominent apical snouts and secretions. Immunohistochemistry, analysis, and this image is the work of Adele Woolley. Scale bars 20 μM.

Furthermore, the levels of YB-1 in normal breast tissue vary between individuals as well as within individual breast tissue samples.

3.2.2 YB-1 is elevated in breast cancer tissue

The strong YB-1 staining in IHC from some reduction mammoplasties indicates that high levels of YB-1 do not generally signify cancer. However, YB-1 has been reported to be elevated in breast cancer (Janz et al. 2002, Habibi et al. 2008, Dahl et al. 2009, Lasham et al. 2012) and the signals from ^{N}YB1 and YB1^{C} that are detected using IHC are hypothesised to differ from that of normal tissues. IHC was used to examine the levels and distribution of YB-1 in histological sections from breast tumours. Two cohorts of tumours were analysed. The first cohort came from the Dunedin Public Hospital, in New Zealand, and all of the images that are included here are from this cohort. A second cohort of samples was supplied as tissue microarrays by the Singapore General Hospital in Singapore. The summarise results from this second cohort are included here. The levels of YB-1 in breast cancer sections have been assessed using ^{N}YB1 and YB1^{C} . Both ^{N}YB1 and YB1^{C} detect YB-1 in all sections and both show that YB-1 levels vary between the breast tumour samples (**Figure 3.3**). Staining for YB-1 is predominantly in the cytoplasm

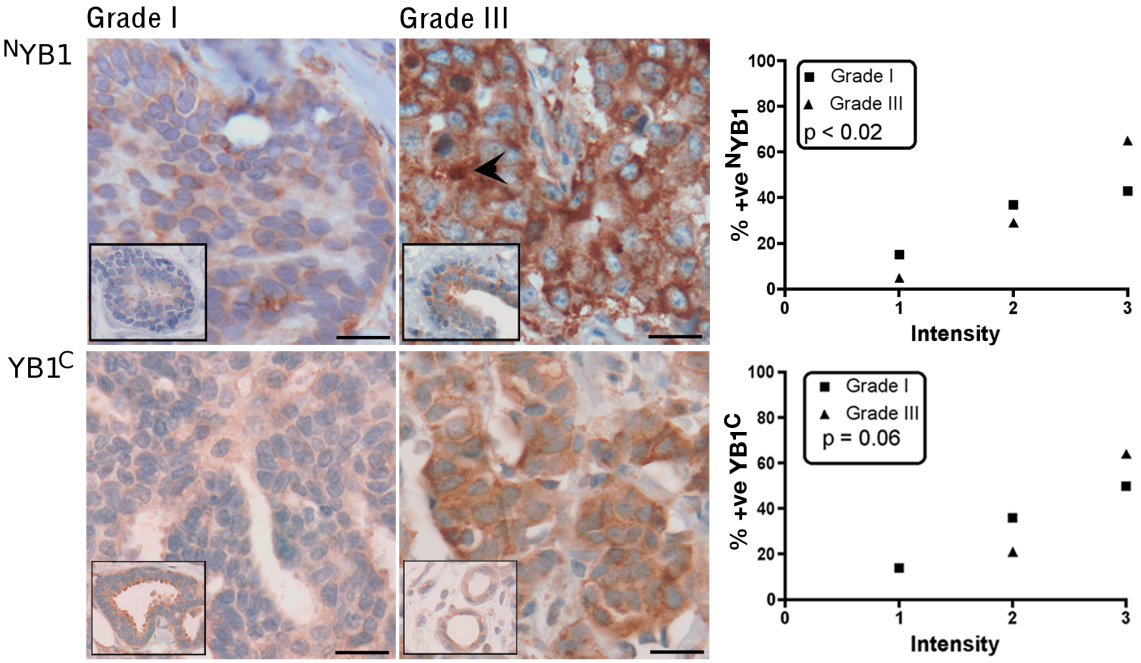

Figure 3.3: Levels of YB-1 are increased in grade III breast tumours as detected by ^{N}YB1, but not YB1^{C} . IHC was carried out on formalin-fixed paraffin-embedded breast tumours (n = 90) from the New Zealand cohort using two antibodies targeting different epitopes and compared to adjacent normal tissue (insets). Staining patterns and levels of expression are shown for each antibody. Differences in staining intensity as detected by ^{N}YB1 were significant (p = 0.02) whereas those detected by YB1^{C} were not (p = 0.06). Nuclear YB-1, as detected by ^{N}YB1, was evident in < 3% of cases (arrowhead, upper middle panel). Immunohistochemistry, analysis, and this image is the work of Adele Woolley. Scale bars 10 µM.

of cells. Nuclear YB-1 is only detected with ^{N}YB1 and only observed in < 3% of cases.

To formally assess the variability of YB-1 staining from ^{N}YB1 and YB1^{C} , the intensity of staining from cytoplasmic YB-1 was assessed on a scale of 0 (none) to 3 (high). The low number of reduction mammoplasty samples means they could not be used as a normal breast tissue control for the levels of YB-1 (n = 10). Instead, histological grade I (n = 32) and grade III (n=28) breast tumors were compared. Grade II tumors have been excluded as their gene expression profile is not distinct and appears to be a mixture of grade I and III tumours (Ignatiadis & Sotiriou 2008). The second cohort included 42 grade I and 82 grade III tumours from the Singapore General Hospital. Only ^{N}YB1 discerns a difference between grade I and grade III breast tumours in the tumours from the Dunedin cohort (^{N}YB1, p < 0.02; YB1^{C} , p = 0.06; Fisher's exact). In IHC performed with ^{N}YB1, the maximum intensity of staining is seen in ∼ 40% of grade I tumours and ∼ 60% of grade III tumours. The

results from the Singapore cohort show that both ^{N}YB1 and YB1^{C} detect stronger staining for YB-1 in grade III tumours than in grade I (grade I = 42, grade III = 82, ^{N}YB1, $\chi^2 = 35.95$, p,0.005; YB1^{C} , $\chi^2 = 8.623$, p,0.02). Therefore, breast tumours with advanced histological grade are more likely to show intense staining for YB-1 and ^{N}YB1 is more sensitive to this subset of breast tumours than YB1^{C} .

To examine in greater detail the importance of YB-1 in breast cancers, the tumour data were further analysed based on hormone receptor status. One group contains ER^{+ve}/PR^{+ve} cancers (n = 68; the significance of ER^{+ve}/PR^{+ve} is reviewed in **Chapter 1.2**). The second grouping of ER^{-ve}/PR^{-ve} tumours includes aggressive basal-like tumours and ERBB^2 (HER2)$^+$ tumours (n = 22). The results show that ^{N}YB1 staining has an intensity of 2 or 3 in the ER^{-ve}/PR^{-ve} tumours and that ^{N}YB1 staining is more likely to be elevated in the ER^{-ve}/PR^{-ve} tumours compared to the ER^{+ve}/PR^{+ve} tumours (**Figure 3.4**; p,0.007; Fisher's exact). YB1^{C} detects no difference in the levels of YB-1 between the two tumour subsets. In the larger Singapore cohort, the levels of YB-1 are elevated with both ^{N}YB1 ($\chi^2 = 40.71$, p,0.005) and YB1^{C} ($\chi^2 = 28.17$, p,0.015).

In summary, variable levels of YB-1 are a feature of normal breast tissues (**Figure 3.2**). This variability is also a feature of cancerous breast tissues. However, the highest levels of YB-1 were observed more frequently in aggressive breast cancers, as predicted by histological grade and also by hormone receptor status. The two antibodies used to detect YB-1 produce broadly similar staining but ^{N}YB1 is more sensitive when detecting elevated YB-1 in aggressive breast cancers.

3.2.3 YB-1 is present in the cytoplasm and nucleus of cells

In breast tumour samples, the staining from ^{N}YB1 in the cytoplasm confirms that the levels of YB-1 are elevated in a subset of cancers (high histological grade and/or ER^{-ve}/PR^{-ve}; **Chapter 3.2.2**). The prognostic sensitivity of ^{N}YB1 is derived from increased levels of YB-1 in the cytoplasm of breast cancer cells. This observation appears to support the notion that the ability of YB-1 to influence RNA stability and translation is important to the role of YB-1 in cancer.

The thickness of the sections that were used for IHC precludes the definitive confirmation of how YB-1 is distributed in tumour cells. Therefore, confocal microscopy was used to gain further information about the distribution of the YB-1 that is detected by ^{N}YB1. The MDA-MB231 breast cancer cell line was chosen for this work. MDA-MB231 cells are ER^{-ve}/PR^{-ve} making them a good model cell

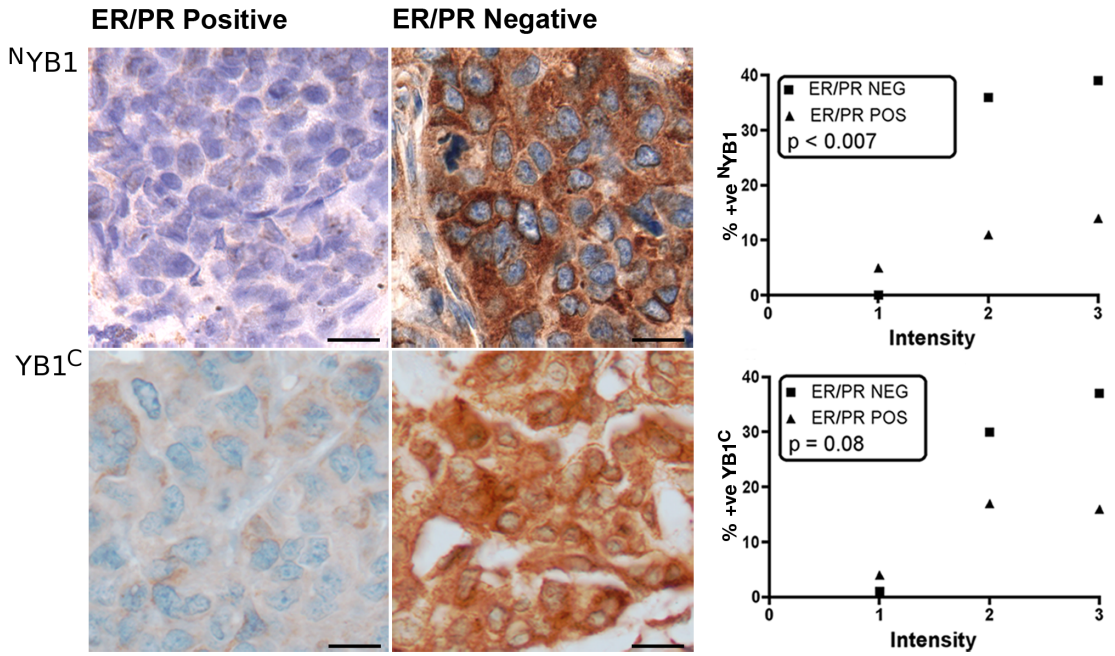

Figure 3.4: Levels of YB-1 are increased in ER^{-ve}/PR^{-ve} breast tumours as detected by ^{N}YB1, but not YB1^{C} . IHC was carried out on formalin-fixed paraffin-embedded tumours (n = 90) from the New Zealand cohort using two antibodies targeting different epitopes. Staining patterns and levels of expression are shown for representative sections for each antibody: ER^{+ve}/PR^{+ve} tumours are represented in the left hand column; ER^{-ve}/PR^{-ve} tumours in the central column. Differences in staining intensity, as detected by ^{N}YB1, were significant (p,0.007) whereas those detected by YB1^{C} were not (p = 0.08). Immunohistochemistry and analysis is the work of Adele Woolley. Scale bars 10 µM.

line for the subset of breast cancers that have increased levels of YB-1 (**Chapter 3.2.2**). MDA-MB231 cells were grown on coverslips and fixed after 72 hours. Following IF labelling with ^{N}YB1, the cells were imaged using confocal microscopy. The results highlight that YB-1 is located primarily in the cytoplasm of MDA-MB231 cells (**Figure 3.5.A**). The signal from cytoplasmic YB-1 is granular with prominent YB-1 signal in the perinuclear region. This perinuclear YB-1 is shown on the profile plots for all three cells in **Figure 3.5.A**. Notably, in many cells this perinuclear aggregation of YB-1 signal is polar (**Figure 3.5.A**, Cell 2).

The signal from ^{N}YB1 in the nucleus of MDA-MB231 cells is low. The nuclei of most MDA-MB231 cells contain weak punctate fluorescence. The profile plots from cross-sections of Cell 2 and Cell 3 show the signal peaks from YB-1 in the nuclei of these MDA-MB231 cells (**Figure 3.5.A**). A second pattern of YB-1 signal is present in the nuclei of many MDA-MB231 cells. It consists of fine filaments that often traverse most of the nucleus (**Figure 3.5.A**, Cell 1). This work confirms that YB-1 is present in the cytoplasm and nuclei of MDA-MB231 cells. Furthermore, ^{N}YB1 can detect YB-1 in both subcellular compartments.

The literature indicates that the YB-1 in the nuclei of MDA-MB231 cells can interact with RNA and also with DNA (**Chapter 1.8.1**). To confirm that some of the YB-1 in the nucleus of MDA-MD231 cells interacts with DNA, cytoplasmic proteins and RNA were removed prior to fixation. Cytoplasmic proteins were extracted using a cytoplasmic extraction buffer and the RNA was digested by RNase A (**Chapter 2.10.1**). IF was performed using ^{N}YB1. The results from confocal microscopy confirm that most of the cytoplasmic YB-1 is removed from these MDA-MB231 cells. However, a weak fluorescent signal is still present outside the nucleus of most cells (see profile plots for all cells in **Figure 3.5.B**). The polarity of this signal suggests that it could come from the polar, perinuclear YB-1 maxima that are present in many MDA-MB231 cells. The efficiency of the extraction for this perinuclear YB-1 may be reduced due to a membrane bound organelle, such as the golgi apparatus or the endoplasmic reticulum, that hinders its clearance. In the absence of cytoplasmic proteins and RNA, the signal from YB-1 within the nucleus is revealed as foci in most MDA-MB231 nuclei (**Figure 3.5.B**). Furthermore, upon removal of cytoplasmic proteins and RNA, filaments of YB-1 were no longer observed in the nuclei of MDA-MB231 cells. This suggests that these filaments were YB-1 associating with RNA in the nucleus.

The results show that a small amount of cellular YB-1 is located in the nucleus of MDA-MB231 cells. When in the nucleus, YB-1 is evident as filaments that are likely

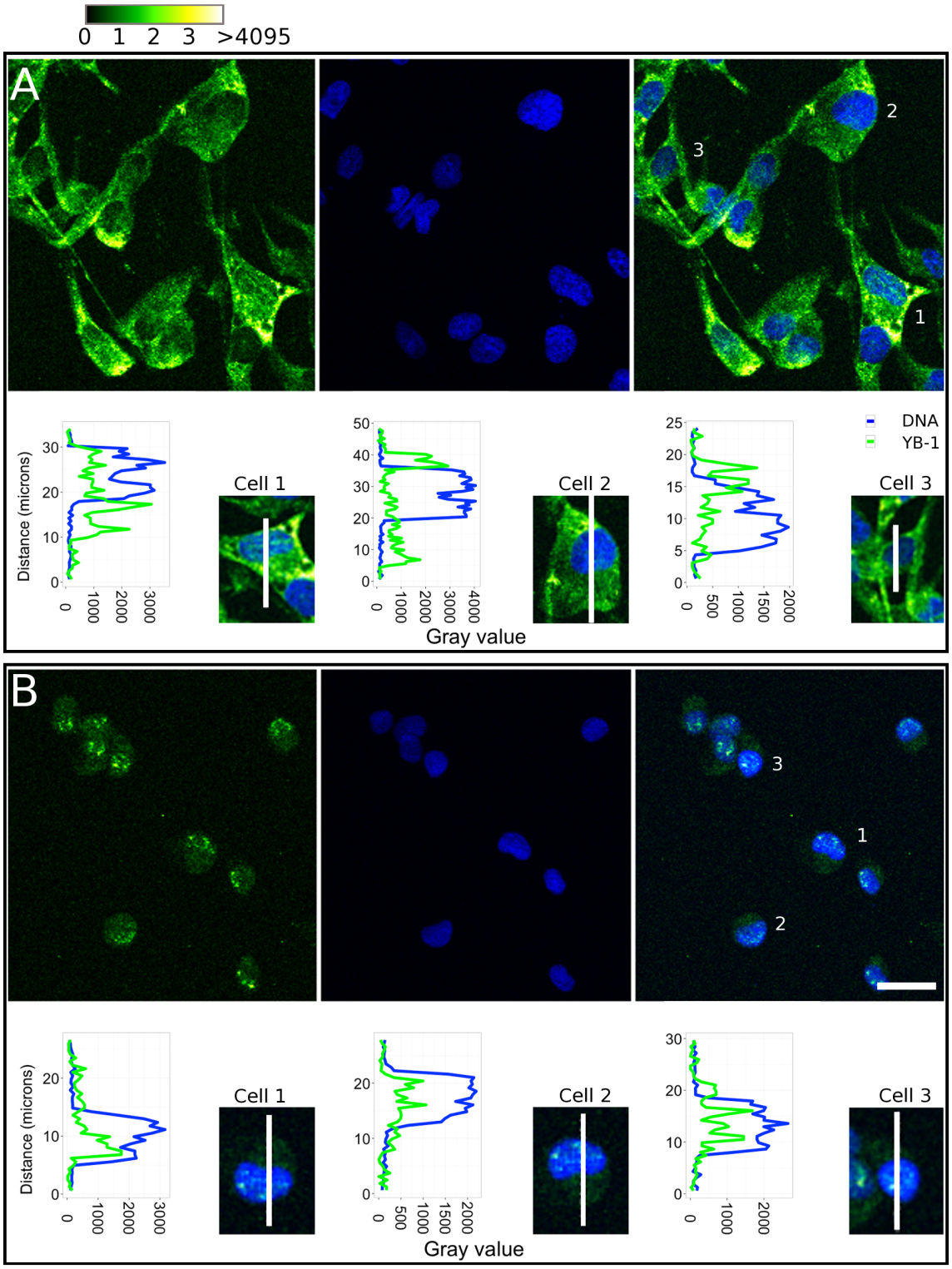

Figure 3.5: YB-1 is present in the cytoplasm and nucleus of MDA-MB231 cells. **A**, IF signal from ^{N}YB1 in MDA-MB231 cells was assessed using confocal microscopy. **B**, Cytoplasmic proteins and RNA were removed from MDA-MB231 cells and the YB-1 that remained was assessed using confocal microscopy. All images are Z-projections of the maximal signal from three Z-slices across the nuclei of MDA-MB231 cells. The profile plots show the signal intensity from the line across each cell to the right of the graph. ^{N}YB1 was labelled with AlexaFluor 488 and gray values are represented using the Green Hot LUT (ImageJ). DNA labelled with Hoechst is represented as blue. Scale bar is 25 μM.

to be associated with RNA. YB-1 is also present as foci that appear to be interacting with DNA or to be bound to RNA in bodies that are refractory to RNase. These results broadly support those from the IHC in tumour samples where ^{N}YB1 appears to be able to bind to YB-1 in the cytoplasm and nuclei of breast tumour cells.

3.2.4 ^{N}YB1 and YB1^{C} detect denatured YB-1 with equal efficiency

The results from IHC in breast cancer samples show that ^{N}YB1 possesses greater sensitivity as a prognostic marker than YB1^{C} . The differences between the two antibodies in IHC may be explained by a post-translational modification of YB-1 that is both specific to YB-1 in the nucleus of cells and that also inhibits the binding of YB1^{C} to YB-1. There are 4 known post-translational modifications (PTMs) that fall within the immunising peptide sequence for YB1^{C} on YB-1 (299 - 313 aa); acetylation on K301 and K304 (Frye et al. 2009) and phosphorylation of S313 or S314. The acetylation of K301 and K304 have been implicated in the excretion of YB-1 and as such, are unlikely to be an important modification for breast cancer cells.

Phosphorylation of YB-1 at S313 or S314 was hypothesised to inhibit the binding of YB1^{C} to YB-1. A phosphatase, shrimp alkaline phosphatase, was used to study the influence of phosphorylation on the binding of YB1^{C} and ^{N}YB1 to YB-1. YB-1 is correlated with drug resistance in lung cancers (Kashihara et al. 2009). To promote any PTM of YB-1 that relate to this role in drug resistance (**Chapter 1.4.3**), lysates were prepared from A549 cells that were cultured in 30 μM cisplatin for 0, 5, or 24 hours. Immunoblotting was performed with these lysates. Prior to the addition of primary antibodies, a portion of each blot was incubated with shrimp alkaline phosphatase to remove phosphate groups from the blotted proteins. The results show that shrimp alkaline phosphatase has no effect on the binding of ^{N}YB1 to YB-1 (**Figure 3.6.A**, ^{N}YB1; n = 3). Phosphatase appears to reduce the binding of YB1^{C} to YB-1 from lysates prepared from MDA-MB231 cells that have been exposed to cisplatin for 5 hours (**Figure 3.6.A**, YB1^{C}). However, this effect is only evident in the blot that is shown. A positive control was included in these experiments to confirm the successful removal of phosphate groups from YB-1. YB1^{S102} is a monoclonal antibody that binds specifically to YB-1 that is phosphorylated at S102. YB1^{S102} should cease to bind YB-1 following shrimp alkaline phosphatase treatment. However, signal YB1^{S102} is not reliably detected in these experiments

(**Figure 3.6.A**, $YB1^{S102}$).

Shrimp alkaline phosphatase reacts with the chemiluminescent detection system for secondary antibodies that are conjugated with the alkaline phosphatase used for the other immunoblots in this thesis. This alkaline phosphatase-conjugated secondary antibody provides adequate signal from $YB1^{S102}$ and an antibody against p53 that is phosphorylated at S15 (**Figure 3.6.B**, AP lanes). A horseradish peroxidase secondary antibody was used in **Figure 3.6.A** and this secondary exhibits poor signal to noise ratios on two phosphospecific antibodies that were used as positive controls for these experiments (**Figure 3.6.B**, HRP lanes). The non-specific binding by $YB1^{S102}$ is observed at approximately 60 kDa. The specificity of the $YB1^{S102}$ antibody is confirmed by the specific depletion of only the $\sim$ 50 kDa band in samples where YB-1 had been depleted (A. Braithwaite, personal communication). Titration of the horseradish peroxidase antibody, and freshly ordered antibody and detection reagents, did not improve the detection of either antibody. Therefore, the failure of the $YB1^{S102}$ as a positive control is due in part to the poor sensitivity of the horseradish peroxidase detection system for $YB1^{S102}$.

In the following step, shrimp alkaline phosphatase was used to remove the phosphate groups from YB-1 in solution, rather than from YB-1 that was immoblised on a nitrocellulose membrane. The lysates from A549 cells that were at $\sim$ 75% confluence were prepared with and without phosphatase inhibitors. Once the lysates had been cleared of cellular debris, shrimp alkaline phosphatase was added to aliquots of each sample which were then incubated at room temperature for 1 hour prior to being separated using SDS-PAGE. In the presence of the phosphatase inhibitors, the intensity of the signal from $YB1^{C}$ is reduced in the sample that was incubated with shrimp alkaline phosphatase (**Figure 3.6.C**). However, in the absence of phosphatase inhibitors, shrimp alkaline phosphatase has no effect. The results from this experiment show that shrimp alkaline phosphatase does not alter the intensity of signal from $YB1^{S102}$ (**Figure 3.6.C**). Therefore, either $YB1^{S102}$ is not specific to YB-1 that is phosphorylated at S102 or, the shrimp alkaline phosphatase failed to remove the phosphate group from S102.

These experiments failed to produce a consistent alteration to the binding of $YB1^{C}$ to YB-1. The successful removal of phosphate groups was not confirmed in these experiments. This was in part due to poor detection of the positive control $YB1^{S102}$ by the horseradish peroxidase secondary. Horseradish peroxidase was only used in the immunoblots for these experiments. Therefore, the results from these experiments are inconclusive.

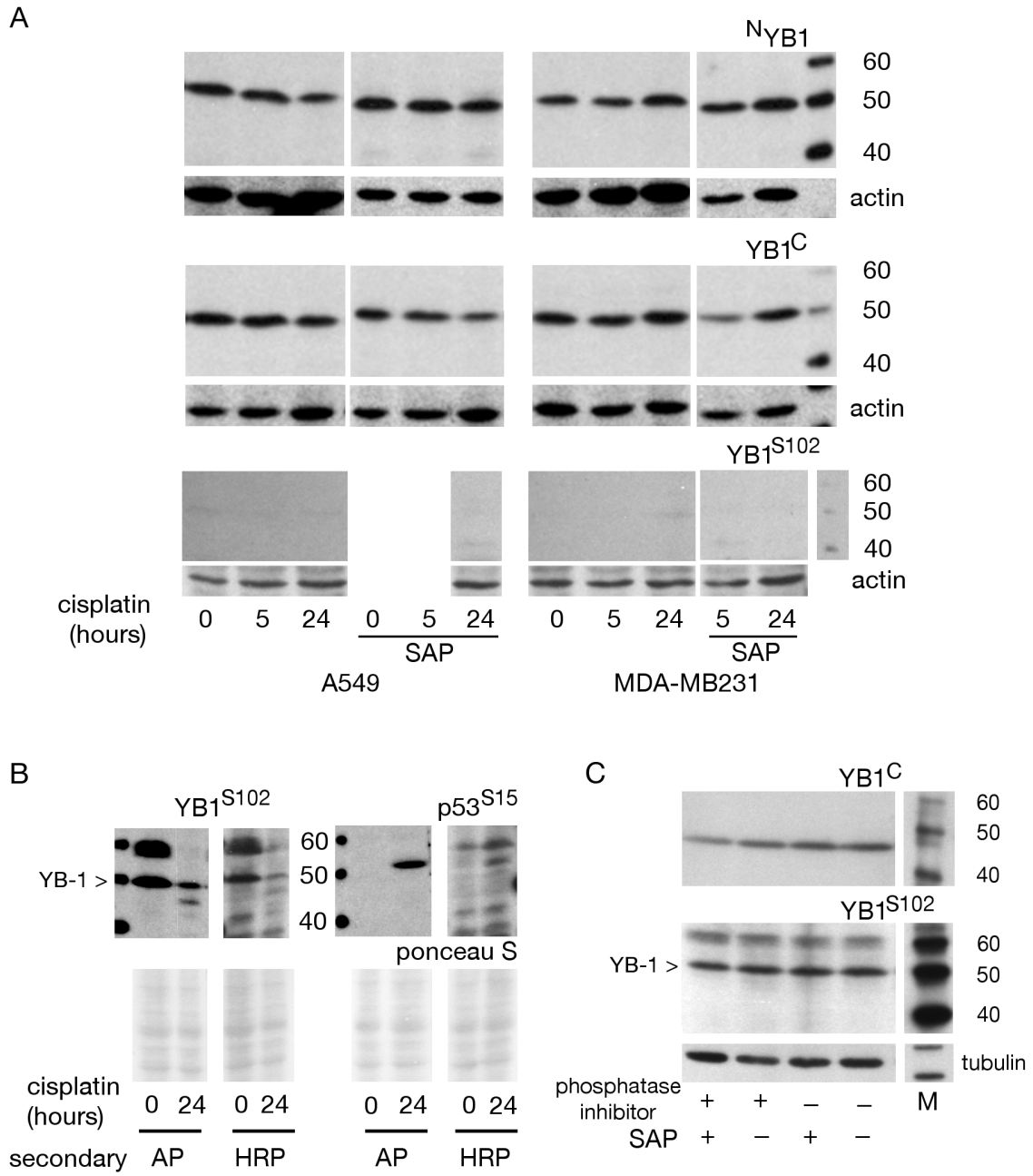

Figure 3.6: The binding of ^{N}YB1 and YB1^{C} to YB-1 does not appear to be influenced by phosphorylation of YB-1. **A**, immunoblots of lysates from A549 cells that were incubated in 30 μM cisplatin for 0 - 24 hours. Prior to detection with primary and horseradish peroxidase (HRP) secondary antibodies, a portion of the membrane was cut and incubated with shrimp alkaline phosphatase to remove phosphorylations from the separated proteins. Immunoblots were exposed to ^{N}YB1, YB1^{C} and YB1^{S102}. **B**, immunoblots of lysates from A549 cells that were exposed to 30 μM cisplatin for 0 or 24 hours. The signal from YB1^{S102} and p53^{S15} was detected with HRP and alkaline phosphatase (AP) secondary antibodies. Efficient loading of proteins is confirmed using ponceau S staining. **C**, immunoblots of two lysates prepared from the same A549 cells but phosphatase inhibitors were only included in one. Shrimp alkaline phosphatase was also added to an aliquot of each lysate prior to SDS-PAGE. **Abbreviations**; M = marker, SAP = shrimp alkaline phosphatase, AP = alkaline phosphatase, HRP = horseradish peroxidase.

An alternative approach was taken to assess whether phosphorylation of YB-1 at S313 or S314 could inhibit the binding of $YB1^{C}$ to YB-1. Immunoprecipitation with $YB1^{C}$ was used to test the ability of $YB1^{C}$ to bind YB-1 that is phosphorylated at S313 or S314. The tyrptic peptides derived from the YB-1 that was immunoprecipitation with $YB1^{C}$ are subjected to LC-MS/MS analysis. Analysis of the data from LC-MS/MS shows that the YB-1 recovered by $YB1^{C}$ produces peptides that were phosphorylated at S314 (the work of W. Ma and V. Valova, reported in Woolley et al. 2011). The presence of YB-1 peptides phosphorylated at S314 appears to confirm that $YB1^{C}$ can bind to YB-1 that is phosphorylated at S314.

In conclusion, phosphorylation of YB-1 at S314 does not appear to affect the binding of $YB1^{C}$. This indicates that phosphorylation of YB-1 at S314 is unlikely to be the direct cause of the difference between the two antibodies in IHC analyses of breast tumours.

This study sought other explanations for the differing prognostic sensitivity of $YB1^{C}$ and ^{N}YB1. Previous research on the function of YB-1 in breast cancer has highlighted the importance of the ability of YB-1 to bind to DNA and act as a transcription factor (**Chapter 1.8.2.1**). Therefore, it was hypothesised that ^{N}YB1 is superior to $YB1^{C}$ in its ability to bind to YB-1 that has an increased affinity for DNA; an affinity that allows YB-1 to function as a transcription factor. This hypothesis is consistent with the observation that IHC using ^{N}YB1, but not $YB1^{C}$, detects YB-1 in the nucleus of breast cancer cells (**Figure 3.3**). It is also consistent with the results from IF which confirm that YB-1 is likely to interact with DNA (**Figure 3.5**).

The hypothesis has been tested by examining the ability of $YB1^{C}$ and ^{N}YB1 to bind to YB-1 that is captured by a single-stranded DNA probe (**Chapter 2.6**). The ability of YB-1 (Cohen et al. 2010) and a YB-1 homologue (Horwitz et al. 1994) to bind to this sequence has already been confirmed. The YB-1 that was captured by the DNA-probe was recovered and then visualised using immunoblotting. The results from both ^{N}YB1 and $YB1^{C}$ reveal that a small proportion of total cellular YB-1 is recovered by the DNA probe as the majority of YB-1 remained in the flow-through fraction (**Figure 3.7.A**, flow compared to DNA). Phosphorylation of YB-1 at S102 has been implicated in activating YB-1 as a transcription factor (Sutherland et al. 2005, Wu et al. 2006, Davies et al. 2011). Thus, $YB1^{S102}$ is the ideal positive control to confirm the recovery of transcriptionally active YB-1. Immunoblotting using $YB1^{S102}$ indicates that YB-1 that is phosphorylated at S102 does not bind to the DNA probe (**Figure 3.7.A**). The signal from YB-1 that is recovered by the

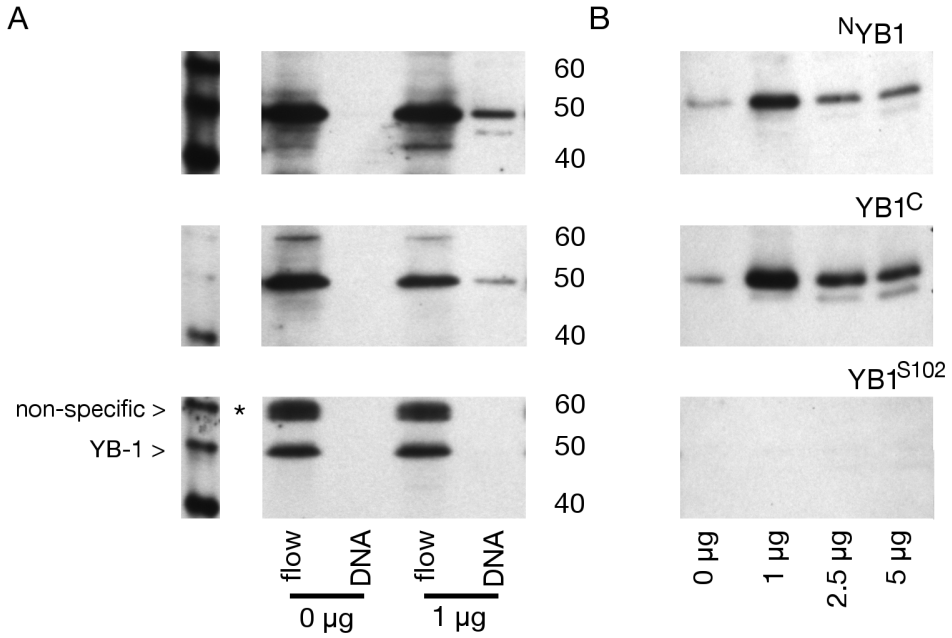

Figure 3.7: YB1^{C} and ^{N}YB1 both detect the YB-1 that binds to a single-stranded DNA probe. **A**, a representative image showing the proportion of YB-1 that was captured from A549 cell lysates using a DNA-affinity probe and detected on immunoblots using ^{N}YB1, YB1^{C} and YB1^{S102}. **B**, the YB-1 that was captured by 0 - 5 µg of DNA-affinity probe. These samples came from the experiment shown in **A** but they were loaded without the flow-through fraction. The regions of the YB1^{S102} immunoblots where YB-1 and non-specfic signals were observed are noted. **Abbreviations**; flow = flow-through fraction, DNA = protein captured by single-stranded DNA probe.

DNA probe makes it difficult to compare the amount of recovered YB-1 when the flow-through is loaded alongside each sample. Loading only the DNA-captured YB-1 samples provides a clearer picture of the YB-1 that is bound to the DNA probe. The representative immunoblots highlight the negative relationship between YB-1 recovery and the concentration of DNA probe (**Figure 3.7.B**). This is consistent across all experiments (n = 4). The bead-only control purifications, where DNA probe was not added, indicate that YB-1 has an intrinsic affinity for the streptavidin beads that were used for these experiments (**Figure 3.7.B**, 0µg lane).

These experiments show that only a small amount of the YB-1 in A549 cells was able to bind to DNA. Surprisingly, there is no support for YB-1 having an affinity for DNA when it is phosphorylated at S102. The differences in the prognostic sensitivity between ^{N}YB1 and YB1^{C} do not appear to be related to the ability of either antibody to bind to a subset of the total cellular YB-1 that has an increased affinity for DNA.

A final approach was taken to compare the intrinsic binding properties of YB1^{C} and ^{N}YB1 to YB-1. The results from IF confirmed that most of the YB-1 was in

the cytoplasm of MDA-MB231 cells but they were not quantitative. Subcellular fractionation, followed by immunoblotting, was performed to gain quantitative data for the distribution of YB-1 between the cytoplasm and nucleus of cells. The A549 cell line, which is derived from a lung adenocarcinoma, was used for these experiments. The subcellular fractionation was performed as outlined in **Chapter 2.7**. The IF experiments indicate that there is less YB-1 in the nucleus of cells than the cytoplasm (**Figure 3.5**). Therefore, contamination of the nuclear fraction by YB-1 from the cytoplasm is the most likely weakness for these experiments. An antibody to β-tubulin, which is present in cells at high levels but only in the cytoplasm, was used to ensure that the nuclear fraction does not contain any cytoplasmic proteins. All data presented here comes from experiments where there was no signal from β-tubulin in the nuclear fraction (see **Figure 3.8.A**, left panel).

The distribution of YB-1 between the cytoplasm and nuclei of A549 cells has been assessed using densitometry. The percentage of signal in each fraction is calculated by dividing the density measurement for that fraction from the pooled sum of the densities of the cytoplasmic and nuclear fractions. The results confirm that, at any given time, most of the YB-1 in asynchronous A549 cells is in the cytoplasm (78 ± 7.6% YB-1 in the cytoplasm; **Figure 3.8.A**). Therefore, YB-1 is predominantly in the cytoplasm of a wide range of cells types.

The densitometry measurements from these experiments were also used to test for differences in the intrinsic affinity of ^{N}YB1 and YB1^{C} for the YB-1 in the cytoplasm and nucleus of A549 cells. The results show that there is no difference in the affinity of ^{N}YB1 and YB1^{C} for YB-1 from the nucleus of A549 cells (paired t-test, $t = 2.1733$, $df = 5$, $p = 0.0818$; **Figure 3.8.B**). These experiments also show that $\sim$ 20% of YB-1 is in the nucleus of these cells. Furthermore, both ^{N}YB1 and YB1^{C} detect YB-1 in the cytoplasm and the nucleus of cells with a similar efficiency.

In summary, the results in this section are derived from the detection of denatured YB-1 on immunoblots with the aim of separating a sub-species of YB-1 that would explain the increased sensitivity of ^{N}YB1 as a prognostic marker in IHC of breast cancer (**Chapter 3.2.2**). Three approaches were used to separate this hypothesised sub-species of YB-1. The results show that none of the approaches reveal differences between ^{N}YB1 and YB1^{C} on immunoblots. This indicates that ^{N}YB1 and YB1^{C} are likely to bind to denatured and reduced YB-1 with an equal efficiency.

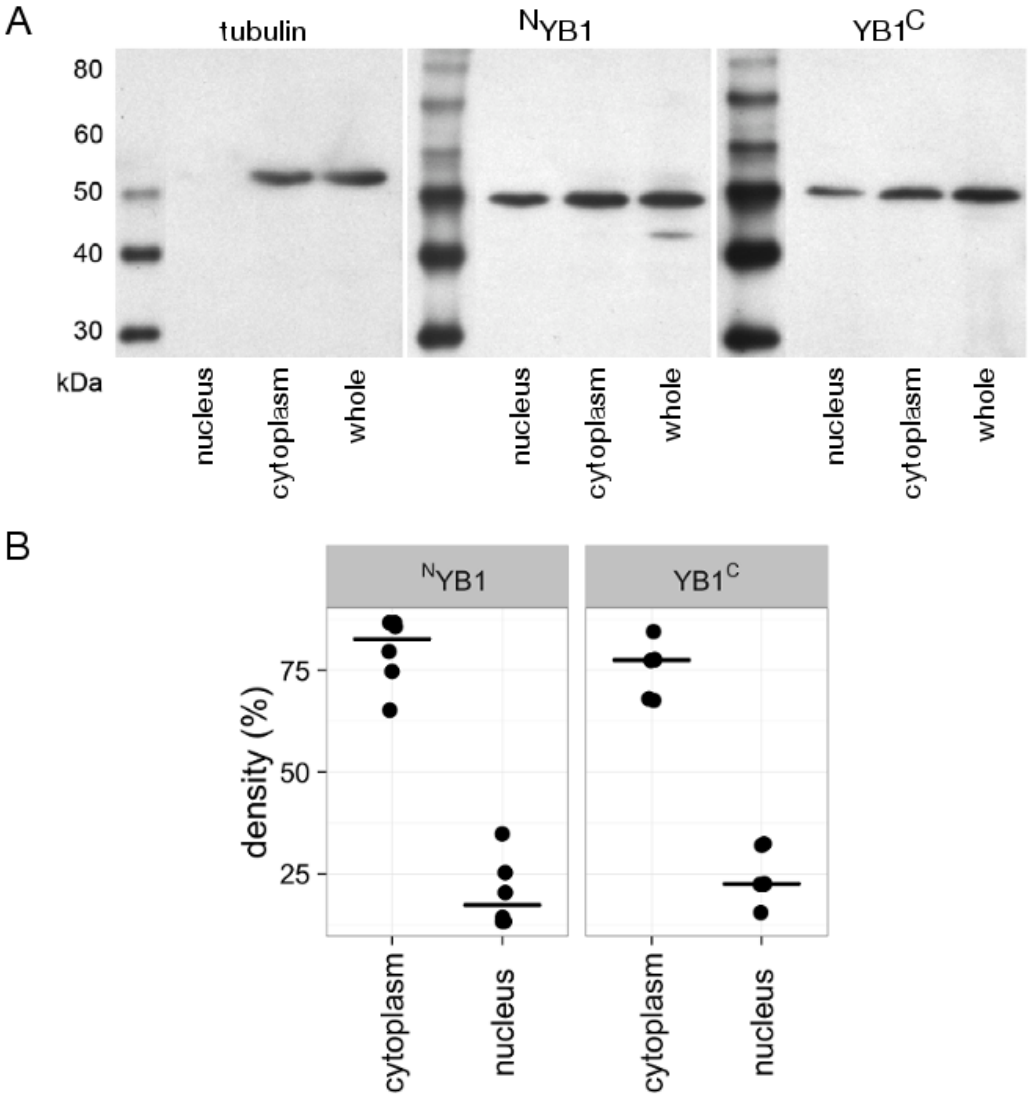

Figure 3.8: ^{N}YB1 and YB1^{C} have equal affinity for YB-1 from the cytoplasm and nucleus of A549 cells. Immunoblot analysis of A549 cells that were separated into cytoplasmic and nuclear fractions. **A**, the presence of cytoplasmic proteins was confirmed using β-tubulin and YB-1 was detected using antibodies to ^{N}YB1 and YB1^{C} . **B**, the amount of YB-1 in the cytoplasm and nucleus of A549 cells was estimated by analysis of the density of the signal from immunoblots (n = 8). A paired t-test found no difference in the levels of YB-1 that were detected by ^{N}YB1 and YB1^{C} ($t = 2.1733$, $df = 5$, $p = 0.0818$).

3.2.5 ^{N}YB1 and YB1^{C} detect YB-1 in a number of multi-protein complexes

The PPI or secondary/tertiary structure of YB-1 were hypothesised to affect the binding of ^{N}YB1 and YB1^{C} to YB-1. To research this hypothesis, protein lysates from A549 cells were separated under native conditions using BN-PAGE. RNA and DNA were removed from the lysates prior to their separation. The immunoblots from BN-PAGE reveal that YB-1 is found in multiple complexes in A549 cells (**Figure 3.9.A**). Both ^{N}YB1 and YB1^{C} bind to multiple bands containing YB-1 on these immunoblots. However, the signals from ^{N}YB1 and YB1^{C} are different, with the antibodies binding to multi-protein complex (MPC)s with differing mobilities (**Figure 3.9.A** for a representative gel). Specifically, a band is detected by both ^{N}YB1 and YB1^{C} at $\sim$ 720 kDa. However, ^{N}YB1 always detects a sharp band at this mobility while the signal at $\sim$ 720 kDa from YB1^{C} is diffuse. Both ^{N}YB1 and YB1^{C} detect different bands between 250 - 450 kDa. In this region of the gel, YB1^{C} exhibits signal (band 2) in only the cytoplasm while the signal from ^{N}YB1 is observed in both nuclear and cytoplasmic fractions (band 3). Band 4 is most likely to be monomeric YB-1, as denatured YB-1 runs with the same mobility (**Figure 3.9.B**). Unlike the other protein species that are discussed, its appearance on immunoblots from BN-PAGE varies between runs indicating that it may be a result of technical variation.

The immunoblots from BN-PAGE in this section indicate that protein-protein interactions or the secondary/tertiary structure of YB-1, is most likely to be responsible for the differing performance of ^{N}YB1 and YB1^{C} . Therefore, the differences in the performance of ^{N}YB1 and YB1^{C} in IHC appear to relate to variable detection of YB-1 when it is incorporated in various MPCs and, to reflect that, ^{N}YB1 detects a functionally distinct subset of complexes that contain YB-1.

3.3 Discussion

The data presented in this chapter confirm that:

- YB-1 is present in normal human tissues;
- Elevated levels of cytoplasmic YB-1 staining from ^{N}YB1 and YB1^{C} in IHC are correlated with high histological grade and ER^{-ve}/PR^{-ve} breast cancers;

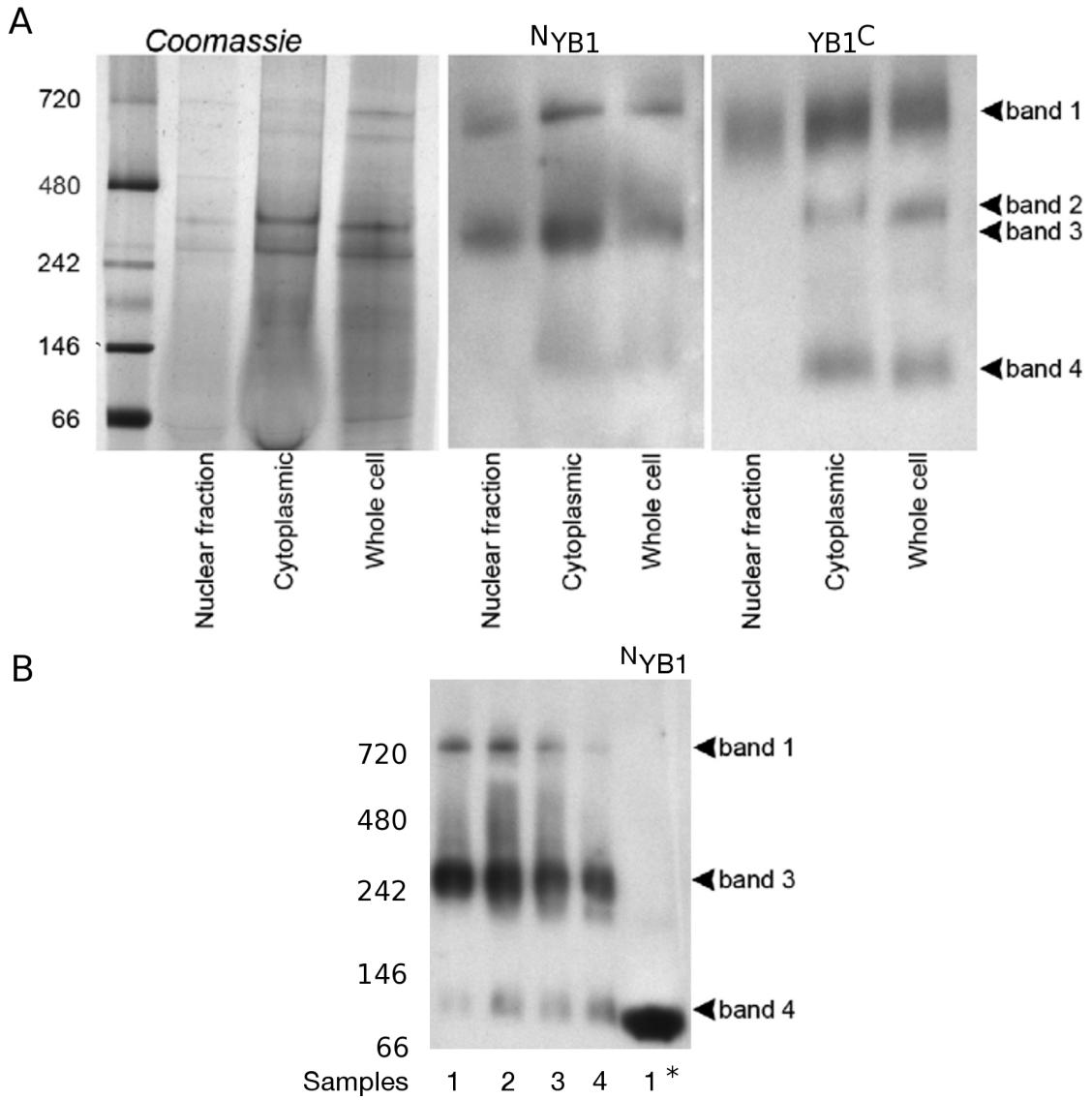

Figure 3.9: ^{N}YB1 and YB1^{C} bind to multiple MPCs that are resolved in BN-PAGE. **A**, following subcellular fractionation (confirmed using SDS-PAGE in **Figure 3.8**) lysates from A549 cells were separated using blue-native PAGE and the separated proteins blotted onto a membrane. YB-1 protein was detected using YB1^{C} and ^{N}YB1. **B**, lysates from A549 cells. *, indicates that prior to separation, the lysate had denaturing sample buffer added (containing SDS and DTT) and was heated to 100°C for 5 minutes. The arrows highlight the location of the main bands that were observed in repeated experiments.

- The YB-1 in A549 and MDA-MB231 cells is primarily present in the cytoplasm;
- Denaturation and reduction resistant PTM are unlikely to affect the binding of ^{N}YB1 and YB1^{C} ;
- ^{N}YB1 and YB1^{C} bind to multiple multiprotein complexes that do not entirely overlap.

The results presented here confirm that *YBX1* mRNA and YB-1 are present in most normal adult tissues (**Chapters 3.2.1 - 3.2.2**). The studies that failed to detect YB-1 in normal tissues utilise IHC (Bargou et al. 1997, Dahl et al. 2009, Gunasekaran & Ganeshan 2014). Therefore, IHC appears to have variable success in detecting YB-1.

The data from IHC presented in this chapter show that YB-1 is present in breast tissue. IHC confirms the presence of YB-1 in all ductal breast tissue from reduction mammoplasties. Notably, cytoplasmic YB-1 is present in all normal breast tissue. The presence of YB-1 in normal breast tissue differs from previous findings (Bargou et al. 1997, Dahl et al. 2009). Dahl et al. (2009) detected very weak staining for YB-1 in normal breast tissue. This discrepancy appears to relate to the antibody used in that study that does not bind to endogenous YB-1 on immunoblots. Dahl et al. (2009) proposes that the antibody can only bind to YB-1 when it maintains a specific conformation. Bargou et al. (1997) also reported that YB-1 was not detected in normal breast tissue. This is difficult to reconcile with the results reported here as the antibody was produced from the same epitope as ^{N}YB1. Technical considerations may explain this discrepancy. Antigen retrieval, that can improve the signal from target proteins in IHC by reversing some modifications that occur during formalin fixation and paraffin embedding (Shi et al. 2001), and the blocking conditions, which can decrease the signal from non-specific proteins, may differ between Bargou et al. (1997) and the work presented here. The buffer conditions, duration and temperature of the antigen retrieval steps were not reported in Bargou et al. (1997). The discrepancy between the results that are reported here and previous studies may also relate to the difficulty of accurately assessing the location of signal in IHC, which is discussed in the following paragraph.

This work also aimed to determine whether IHC in breast tumours using two antibodies, generated to either end of YB-1, would provide the same conclusions about the value of YB-1 as a prognostic tool. Two performance characteristics

are important in relation to the prognostic value of YB-1; the ability to detect the levels of YB-1 and the subcellular localisation of YB-1. With the N-terminus antibody (^{N}YB1), the staining intensity of cytoplasmic YB-1, although variable, tends to be highest in grade III tumours and in the more aggressive ER^{-ve}/PR^{-ve} negative tumours. Other research is supportive of the importance of cytoplasmic YB-1 staining in breast cancer (Mylona et al. 2014). These findings confirm previous reports that were carried out with an antibody generated to the same N-terminus epitope (Bargou et al. 1997, Dahl et al. 2009, Janz et al. 2002). Unlike these previous reports,this study found that strong YB-1 staining in the nucleus is rare ($\sim$ 3% of tumours). Confocal immunofluorescence microscopy shows that ^{N}YB1 detects punctate nuclear staining in most grade III tumours that is not discernible by IHC (Woolley et al. 2011). The localisation and distribution of YB-1 in MDA-MB231 cells is similar to previous reports of YB-1 distribution in A549 cells (Cohen et al. 2010). Many cells exhibit staining in the cytoplasmic region directly adjacent to the nucleus (perinuclear). Previous reports may have interpreted this increased perinuclear intensity as nuclear staining due to the plane of section.

Cytoplasmic YB-1 detected with YB1^{C} is also highest in grade III and ER^{-ve}/PR^{-ve} negative tumours. It does not reach statistical significance in the smaller New Zealand cohort but does show a significant difference in the Singapore cohort. However, this is of lesser magnitude than that found with ^{N}YB1 (Woolley et al. 2011). As with ^{N}YB1, the increase in cytoplasmic staining is most notable in the perinuclear region. These findings are in agreement with elevated YB-1 levels, that are detected by an antibody generated to the same C-terminus peptide sequence, previously reported in breast (Wu et al. 2006, Habibi et al. 2008), non-small cell lung (Shibahara et al. 2001) and prostate cancers (Giménez-Bonafé et al. 2004). However, unlike some of these reports, confocal immunofluorescence microscopy using this antibody finds no evidence of nuclear YB-1 staining (Woolley et al. 2011).

Multiple studies show that increased *YBX1* mRNA levels provide sufficient information to detect aggressive breast cancers by highlighting the negative correlation of *YBX1* mRNA with survival (Yu et al. 2010, Turashvili et al. 2011, Lasham et al. 2012). Similar observations, including those outlined in this chapter, have been made for YB-1. Together, these data strongly indicate that increased levels of YB-1 in breast tumours reduce the odds of survival for people with cancer. However, the significant variance in the levels of YB-1, which is observed in IHC of both normal breast tissue and breast tumours, highlights important issues relating to the use of YB-1 in prognostic assessments. Highly elevated levels of YB-1 are observed

in some normal breast epithelial cells (**Figure 3.2**). Therefore, the role of YB-1 in aggressive breast cancer cells must require some changes in the function of YB-1.

The increased sensitivity of ^{N}YB1 compared to YB1^{C} may relate to the function of a second element of YB-1 biology that is present in cancer cells. ^{N}YB1 detects this second element with greater sensitivity. The utility of cytoplasmic YB-1 as a prognostic marker may highlight the importance of the functions that are undertaken by YB-1 in the cytoplasm. However, an alternative explanation is that the high levels of cytoplasmic YB-1 are a secondary effect of increased levels of YB-1. Increased levels of YB-1 may allow a small amount of YB-1 to interact with DNA and influence the transcription of target genes that promote an aggressive breast cancer phenotype.

To explain the difference between ^{N}YB1 and YB1^{C}, a number of possibilities have been considered. The most obvious is that the antibodies have different binding affinities to YB-1. However, the K_d of each antibody, as measured by immunoprecipitation, is approximately 5 nM (Woolley et al. 2011), making this explanation unlikely. Another explanation is that the fixation of clinical samples prior to IHC renders the epitope for YB1^{C} unavailable in YB-1 that is located in the nucleus (Habibi et al. 2008, Wu et al. 2006). However, this also seems unlikely. YB-1 is not detected in the nucleus of cultured cells by YB1^{C} when fixation and tissue thickness is not an issue (Woolley et al. 2011). Another possibility is that the C-terminus epitope is obscured by PTMs that are important when YB-1 is in its native conformation. YB-1 peptides with phosphorylation to serine 314, adjacent to the epitope for YB1^{C}, were identified in both ^{N}YB1 and YB1^{C} immunoprecipitated YB-1. Therefore, phosphorylation of YB-1 on serine 314 also seems to be an unlikely explanation.

The apparent differences in epitope availability may be explained by steric inhibition caused by protein-protein interactions. When protein lysates are separated in the absence of reducing or denaturing agents to preserve protein:protein interactions moieties, this study shows that ^{N}YB1 and YB1^{C} bind to YB-1 with different mobilities. This suggests that ^{N}YB1 and YB1^{C} differ in their ability to detect specific protein complexes containing YB-1. The detection of YB-1 in the nuclear fraction by YB1^{C} in BN-PAGE contradicts the findings that YB1^{C} is unable to detect YB-1 in the nuclei of fixed cells (Woolley et al. 2011). This discrepancy may be explained by YB-1 binding RNA to form homodimeric YB-1:RNA complexes (Skabkin et al. 2004). The formation of these YB-1:RNA complexes involves the CSD and the C-terminus region (Izumi et al. 2001) and could render the epitope of YB1^{C} inaccessible in YB-1 molecules that are integrated into the YB-1:RNA complexes. The

role of the C-terminus region in forming these YB-1:RNA multimers increases as the YB-1:mRNA ratio increases (Skabkin et al. 2004). Other unknown interactions, particularly within the spliceosome which contains many proteins (**Chapter 1.8.3.1**), may also allow heterodimers to form within the spliceosome. IHC results correlate elevated YB-1 levels with grade and negative ER^{-ve}/PR^{-ve} status. Therefore, the increased sensitivity of ^{N}YB1, relative to YB1^{C} , may be due to a reduction in the availability of the C-terminus epitope caused by the effects of increasing YB-1:RNA ratio on YB-1:RNA multimer formation.

3.3.1 Summary

The results from this chapter demonstrate the potential for the tertiary structure and protein interactions of YB-1 to influence the prognostic sensitivity of antibodies against YB-1 in IHC. Furthermore, the lack of strong nuclear localisation in IHC highlights the potential importance of the function of YB-1 as an RNA binding protein in aggressive breast cancers.

Chapter 4

Identification of YB-1 interacting proteins in the cytoplasm and nucleus

4.1 Introduction

The ability of YB-1 to influence cell biology via a wide range of molecular mechanisms, most of which require interaction with either RNA or DNA, is thought to explain the role(s) of YB-1 in cancer (**Chapter 1.8**). Previous reports have identified the most prominent molecular mechanism of YB-1 in cancer as the process of binding to DNA to influence gene transcription (**Chapter 1.8.2.1**). The specific ability of YB-1 to transactivate genes with CAAT boxes in their promoters is hypothesised to be important to the function of YB-1 in cancer. However, the chromatin purified by chromatin immunoprecipitation of endogenous YB-1 (Astanehe et al. 2012) showed no evidence that YB-1 binds to CAAT boxes (Dolfini & Mantovani 2013b). A review that followed this observation concluded that YB-1 may act via post-transcriptional regulation in cancer cells (Dolfini & Mantovani 2013a). It is flawed to equate the lack of clear interaction between YB-1 and inverted y-boxes with a lack of transcriptional effects for YB-1. However, the importance of gene regulation at the RNA level should not be discounted.

Translation may have a dominant influence on protein abundance as only $\sim$ 40% of the variation in protein levels was explained by mRNA abundance in murine fibroblasts (Schwanhäusser et al. 2011). **Chapter 3** also shows that most of the YB-1 in breast cancer cells is in the cytoplasm which provides support for the importance

of molecular mechanisms of YB-1 besides transcription. YB-1 in the cytoplasm may influence the biology of cancer cells by binding to RNA and altering gene expression via a number of post-transcriptional mechanisms (**Chapter 1.8.3**). When in the cytoplasm, YB-1 is present in mRNPs and, as a core constituent of mRNPs, YB-1 can promote translational initiation or inhibit translation (**Chapter 1.8.3.2**). The other potential function of YB-1 in the cytoplasm of cells is to stabilise mRNA transcripts (**Chapter 1.8.3.3**).

Given the predominant cytoplasmic localisation of YB-1 in breast cancers (**Chapter 3**), the work in this chapter aims to clarify the function(s) of YB-1 in cancer cells. Phosphorylation is likely to alter the function of YB-1 and high-throughput studies indicate that YB-1 is phosphorylated along its length (**Chapter 1.7.2.1**). This work aimed to deduce the phosphorylation state of YB-1 in cancer cells. The phosphorylation was hypothesised to differ depending on the subcellular localisation of YB-1. A second hypothesis was that the function of YB-1 changes with its subcellular localisation. This has been examined by studying the protein-protein interactions (PPI) of YB-1 in the cytoplasm and nucleus. The work in this chapter uses ^{N}YB1 for immunoprecipitating YB-1 in an attempt to include the interactions of the subset of YB-1 that ^{N}YB1 detected in IHC.

4.2 Results

4.2.1 Over-expression of YB-1 is a poor strategy for studying the protein interactions of YB-1

YB-1 constructs were produced to determine the suitability of using exogenously expressed YB-1 to study the protein interactions of YB-1. A large tag protein, such as FLAG or GST, was hypothesised to influence the structure of the intrinsically disordered domains at either end of YB-1. Altering the confirmation of these domains may alter the function and protein interactions of the expressed YB-1. Therefore, two constructs were produced with a small tag protein, Human influenza haemagglutinin (HA), at either the N-terminus (HA-YB-1) or the C-terminus (YB-1-HA; Dr Rhodri Harfoot, St. Judes Children's Hospital, Memphis, USA, performed the cloning). A549 cells were transfected with the two YB-1 constructs for 72 hours at which time lysates were produced and then separated using SDS-PAGE. The results from immunoblotting show that YB-1 with HA at the N-terminus is poorly expressed (**Figure 4.1.A**, arrow). This poor expression was due to an error which

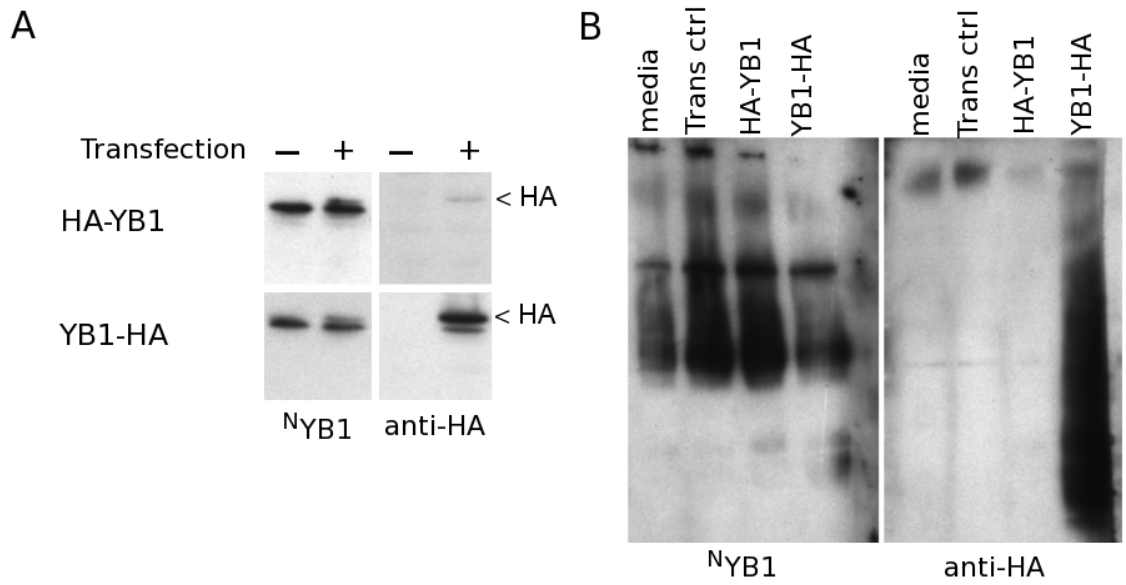

Figure 4.1: YB-1-HA does not behave like endogenous YB-1 on immunoblots from BN-PAGE. **A**, immunoblots of protein lysates from A549 cells expressing YB-1 with HA tags (HA-YB1 and YB1-HA) for 72 hours show the signal from ^{N}YB1 and anti-HA. **B**, immunoblots from blue-native PAGE of HA YB-1 constructs that were transfected for 48 hours. The signal on the immunoblots comes from either ^{N}YB1 or from anti-HA. **Abbreviations**; media = media-only cells, Trans ctrl = transfection control, <HA = position of HA-tagged YB-1.

led to the initiator methionine being included at the start of the coding sequence of the construct. However, YB-1 with HA at the C-terminus is detected as a fine band above endogenous YB-1 by ^{N}YB1 (**Figure 4.1.A**, arrow). The presence of YB-1-HA is further confirmed by the signal produced by anti-HA on immunoblots.

The effect of the over-expression of HA-tagged YB-1 on the multi-protein complex (MPC)s that are detected by ^{N}YB1 was tested. Two wild-type HA-tagged YB-1 constructs were over-expressed for 48 hours in A549 cells. The results show that over-expression of YB-1-HA does not greatly alter the pattern of signal produced by ^{N}YB1 on BN-PAGE (**Figure 4.1.B**). However, the signal from anti-HA does not resemble the pattern of endogenous YB-1 produced by ^{N}YB1. This result highlights that the PPI of exogenous YB-1 are likely to differ from those of endogenous YB-1. The PPI and phosphorylation of endogenous YB-1 became the focus of further investigation into the PPI of YB-1.

4.2.2 The purification of endogenous YB-1 protein

The aim of this work was to identify separate fractions of YB-1 that were involved in different cellular processes using cancer cell lines. To do so, A549 and MDA-

MB231 cells were separated into cytoplasmic and nuclear fractions prior to the immunoprecipitation of YB-1 using ^{N}YB1. Total YB-1 from these two cell lines was hypothesised to be separated into functionally distinct groupings of YB-1. The first of these groupings influences RNA stability and translation in the cytoplasm. The second grouping was the YB-1 that influences transcription and RNA splicing in the nuclear fraction. Cytoplasmic lysates were prepared from 5×10^7 cells at a concentration of 1×10^4 cells per μL. Previous observations indicated that $\sim 20\%$ of the total cellular YB-1 resided in the nucleus of A549 and MDA-MB231 cells (refer to **Chapter 3**; **Figures 3.5** and **3.8**). Therefore, nuclei from 5×10^8 cells were used for nuclear immunoprecipitations (n = 2 for each cell line and subcellular compartment). Tissue culture and nuclei preparation took place in batches. Following purification, an aliquot of nuclei was lysed and used to screen for cytoplasmic contaminants. The remainder was snap-frozen in liquid nitrogen and stored at ⁻80°C. Each YB-1 immunoprecipitation used 100 μg of ^{N}YB1 (outlined in **Chapter 2.12**).

The purified YB-1 was separated using 10% SDS-PAGE and stained using colloidal coommassie staining. The band in each lane with the greatest density migrated at around 45 kDa, an appropriate mass to be YB-1 (**Figure 4.2.A**, <YB-1). The lanes were cut from the gel, digested with trypsin, and the composition of the tryptic peptides was analysed using LC-MS/MS (**Chapter 2.13**). Analysis of the LC-MS/MS runs confirmed the purification of YB-1. The peptides assigned to YB-1 from all LC-MS/MS runs cover $\sim 90\%$ of YB-1 sequence (**Figure 4.2.B**). Furthermore, the sequence coverage from individual YB-1 immunoprecipitation samples provides coverage across most of the linear YB-1 sequence with only the N-terminus exhibiting inconsistent coverage. This inconsistent coverage is due to a paucity of lysine and arginine residues in this region and, as a result, trypsin creates fewer, and longer, peptides from the N-terminus of YB-1.

The amount of YB-1 that was captured by each immunoprecipitation has been estimated using the data from LC-MS/MS. The LC-MS/MS runs were performed to maximise peptide identifications rather than provide quantitative data. The YB-1 bands were cut from the coommassie gel for phosphopeptide analysis which further impairs the accuracy of estimates of YB-1 levels.

The results from the LC-MS/MS data indicated that there was 4-fold less YB-1 recovered from the nucleus of MDA-MB231 cells (peak area under the curve; 2×10^7 arbitrary units (A.U.) and 2×10^7 A.U.) than from the cytoplasm (peak area under the curve; 7×10^7 A.U. and 9×10^7 A.U.). In A549 cells, the loading appears more even with the YB-1 recovered from the nuclei (peak area under the curve; $4 \times$

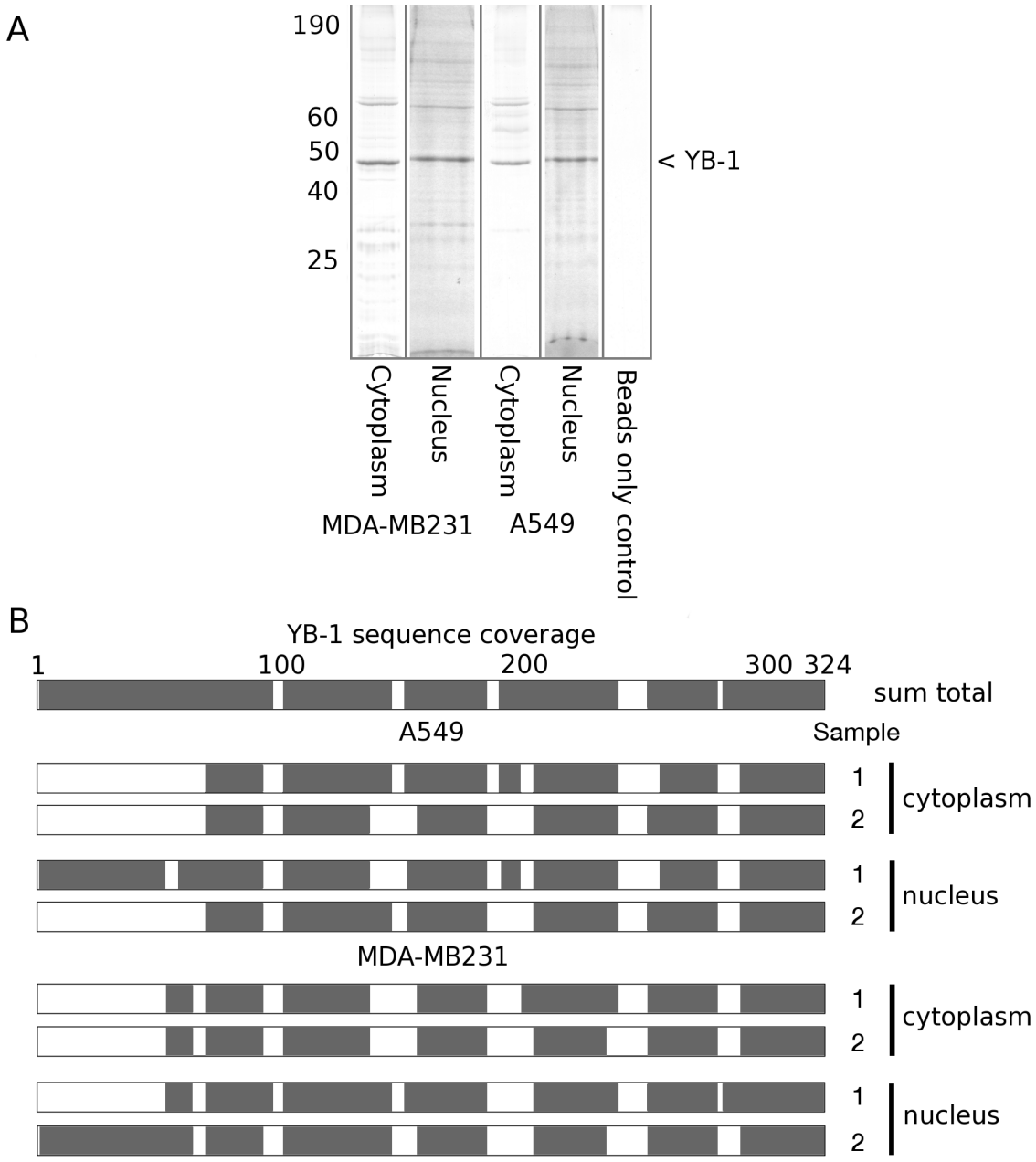

Figure 4.2: YB-1 was purified from the cytoplasm and nuclei of A549 and MDA-MB231 cells using ^{N}YB1. **A**, representative coommassie stain of YB1 from the cytoplasm and nuclei of A549 and MDA-MB231 cells. **B**, the sequence coverage from peptides for YB-1 that were identified using LC-MS/MS. The peptide identifications from all runs (sum total) and each replicate sample (Sample = 1 or 2) from the cytoplasm and nuclei of A549 and MDA-MB231 cells are shown.

10^8 A.U. and 7×10^6 A.U.) being 80% of that from the cytoplasm (peak area under the curve; 4×10^8 A.U. and 3×10^7 A.U.). Inter-run variation was evident between the replicates from A549 cells. The highest values are from a pair of samples from A549 cells that were analysed in the first YB-1 immunoprecipitation experiment. These estimates of YB-1 levels from the LC-MS/MS are at odds with the intensity of coomassie staining from the YB-1 bands (**Figure 4.2.A**). The staining intensity of these YB-1 bands appears to be approximately equivalent, if not slightly greater in the nuclear fractions where 10-fold more cells were used. This disparity is likely to be due to inaccurate quantification from the LC-MS/MS as a result of the aforementioned focus on maximising peptide identifications in addition to the YB-1 peptides that were lost during phosphopeptide enrichment.

It was hypothesised that the differing functions of YB-1 in the cytoplasm and nucleus would lead to the YB-1 in the cytoplasm and nucleus bearing phosphorylation(s) at different sites. To assess whether the phosphorylation of YB-1 varies with cell line and subcellular compartment, the phosphorylated peptides from each YB-1 band were enriched using TiO_2 beads. The captured peptides were analysed using LC-MS/MS.

Analysis of the MS/MS (MS^2) spectra measured by LC-MS/MS indicates that YB-1 is phosphorylated at multiple locations in both A549 and MDA-MB231 cells (**Table.4.1**; notes relating to the detection of phosphorylated peptides in LC-MS/MS are included in **Supplementary figure A.1.1**). The most commonly detected phosphorylation is at S165 of YB-1. Phosphorylation of S165 is detected in the nucleus and cytoplasm of both A549 and MDA-MB231 cells. In the cytoplasm, phosphorylation of S165 is reliably identified by two distinct peptides that incorporate up to 4 serine residues (S165, S167, S174, and S176). There is strong evidence that the phosphorylation is at S165 (**Figure 4.3** - **Figure 4.5**).

A short peptide that includes S165 and S167 (NYQQNYQNSESGEK) was reliably detected in the LC-MS/MS runs for 3 of the 4 cytoplasmic samples (a representative MS^2 spectrum is shown in **Figure 4.3** and the presence or absence of the peptide in each sample is confirmed in **Figure 4.4**). The phosphorylation was localised to S165 using fragment ions which carried the C-terminus, known as y-series ions, which ended at S167 (y-4) and E166 (y-5) and lacked any mass shift to indicate the presence of HPO_3 (**Figure 4.3**). However, the C-terminal fragment ending at S165 (y-6), was shifted by 80 Da indicating the presence of HPO_3. The spectra attributed to this peptide also had fragments from the N-terminus (b-ions) ending at S165 (b-9) with a neutral loss of H_3PO_4 (representative spectra is shown

Table 4.1: A summary of the phosphorylated YB-1 residues that were detected here in YB-1 from the cytoplasm and nucleus of A549 and MDA-MB231 cells.

Phosphorylation	MDA-MB231				A549			
	cytoplasm		nucleus		cytoplasm		nucleus	
S165	+	+	+	+	+	+	+	+
(S165 or S167)*				+			+	
(S165 or S167)* and (S174 or S176)*		+						
S174 also S176 [two]	+				+		+	
S314	+	+	+		+		+	

n = 2 for each cell line and subcellular compartment. Two "+" signs indicate that this peptide was found in both sample replicates. * = the phosphorylation site could not be localised unambiguously. [two] = MS^2 scans indicated the presence of two peptides with HPO_3 at the indicated locations.

in **Figure 4.3**).

The presence of the peptide in each sample was further tested using information about the chemical composition of the peptides and the natural abundance of heavy stable isotopes. This information was used to predict the relative abundance of isotope peaks in the MS^1 scans (outlined in **Chapter 2.13.4** and see **Supplementary figure A.1** for an explanation of isotope peaks in LC-MS/MS). The peaks from peptides that included heavy stable isotopes were included in the analysis to improve the accuracy of the identification of phosphorylated peptide precursors (Schilling et al. 2012).

The MS^1 scans were used to assess the levels of phosphorylated NYQQNYQNSESGEK generated from YB-1 from the cytoplasm and nuclei of A549 and MDA-MB231 cells. The results show that NYQQNYQNSESGEK was most abundant in the two samples from the cytoplasm of MDA-MB231 cells (**Figure 4.4**). One MDA-MB231 nuclear replicate sample lacks an MS^2 measurement of the precursor. However, the MS^1 scan provides evidence that the peptide was present but failed to reach the intensity threshold that was required to trigger an MS^2 scan (**Figure 4.4.A - B**). YB-1 peptides with phosphorylated S165 were conservatively estimated to be at least five-fold more prevalent on cytoplasmic YB-1 (**Figure 4.4.B**).

Longer YB-1 peptides encompassing S165 - S176 (NYQQNYQNSESGEKNE GSESAPEGQAQQR) were also phosphorylated at S165 (**Figure 4.5**). In some MS^2 spectra, single and doubly-charged y-ions from C-terminal fragments ending at E166 (Y-19) were present. This confirms that HPO_3 was not present after E166.

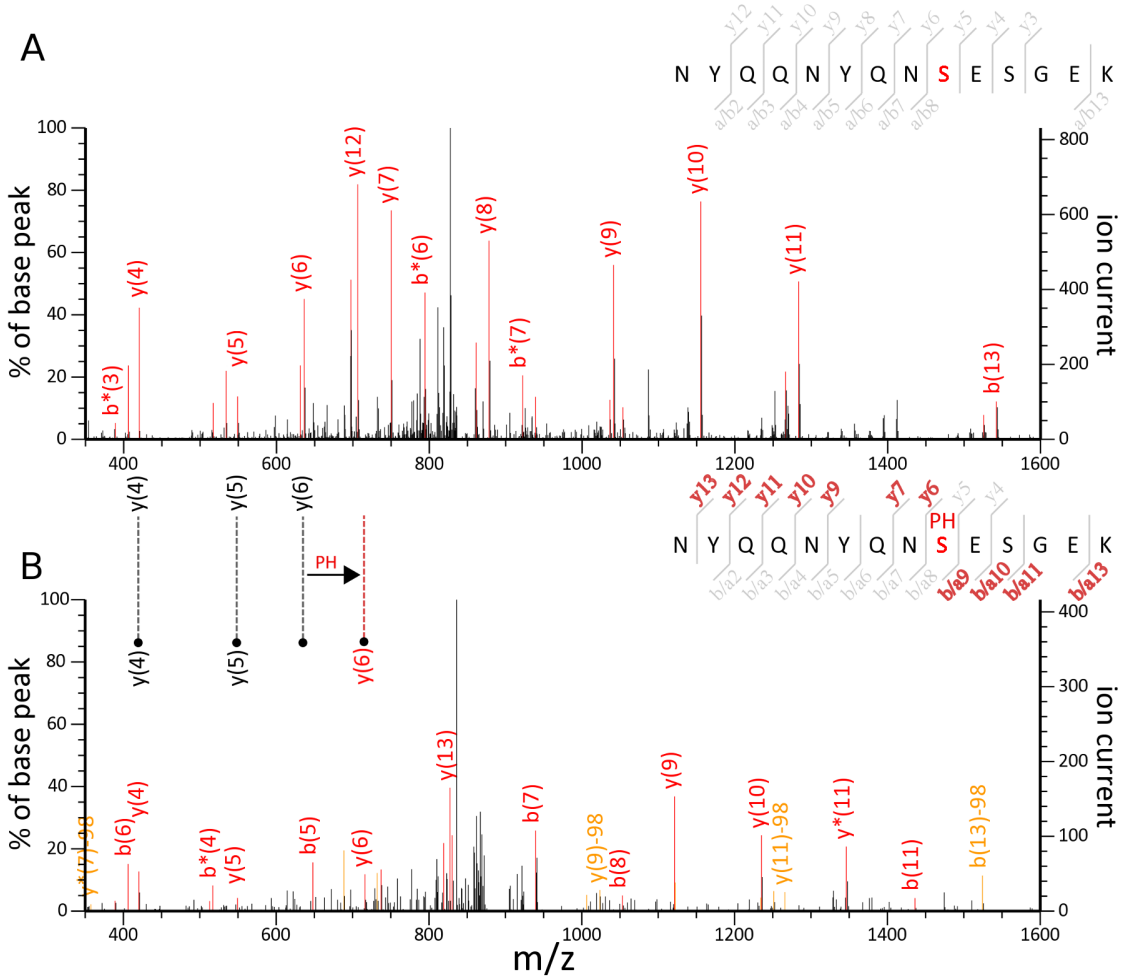

Figure 4.3: Immmunopurified YB-1 from A549 and MDA-MB231 cells is phosphorylated at S165. MS^2 spectra from NYQQNYQNSESGEK, a YB-1 peptide that spans serine 165 (red) and S167. MS^2 spectra of representative unmodified (**A**, monoisotopic mass of 1687.7074: m/z = 844.8641 of doubly charged parent ion: Mascot ion score = 60) and phosphorylated (**B**, monoisotopic mass of 1767.6737 , m/z = 884.8478 of doubly charged parent ion: Mascot ion score = 38) peptides are shown. The fragment ions that were detected by the Mascot search engine to identify the sequence are highlighted in red or yellow; yellow denotes a neutral loss of 98 Da (H_3PO_4) from phosphorylated fragment ions. y-ions and b-ions represent fragments containing the C-terminus and the N-terminus respectively. The fragment ions that contain HPO_3 (+79.9663) or show a neutral loss of H_3PO_4 (- 97.9769; shown in yellow) are highlighted as red in the sequence cartoon and the location of the phosphorylation is denoted by "PH". The ions that were used to identify the site of phosphorylation are shown between the spectra from unmodified (**A**) and phosphorylated (**B**).

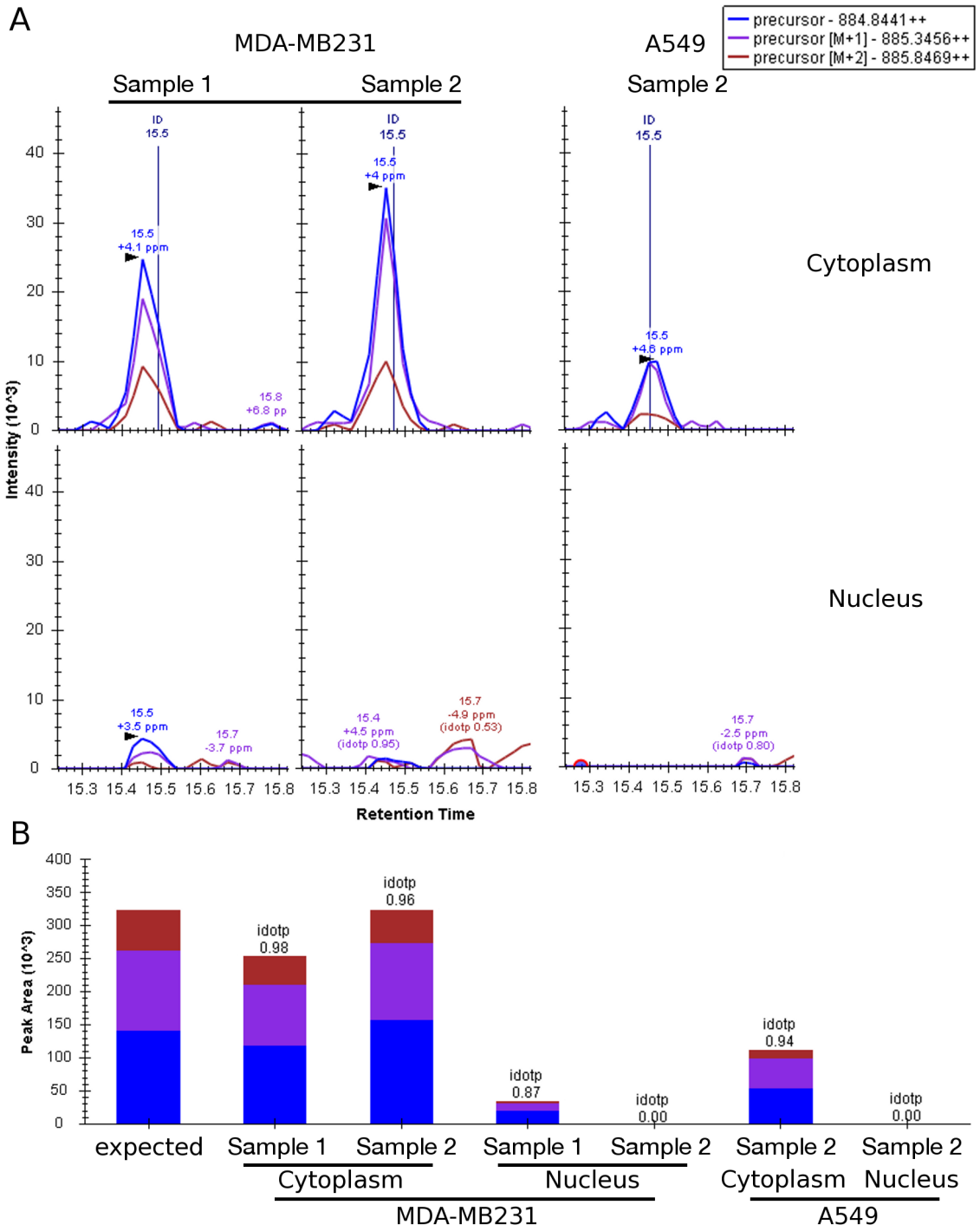

Figure 4.4: Peptides confirming the phosphorylation of YB-1 at S165 are present in YB-1 from the cytoplasm from A549 and MDA-MB231 cells. **A**, extracted MS^1 ion chromatogram plots showing the peak area under the curve of the monoisotopic (M), M+1, and M+2 precursor ions for phosphorylated NYQQNYQNSESGEK from the YB-1 purified from the cytoplasm and nuclei of A549 and MDA-MB231 cells (replicates = Sample 1 or 2). The positive identification of the peptide from MS^2 scans is indicated by **ID** above the plots. **B**, plots showing the calculated peak area under the curve derived from the extracted ion chromatograms shown in **A**. The isotope dot product (idotp) values indicate how closely the ratio of the three precursor ions matches the **expected** ratio (idotp range = 0 - 1; reliable identifications $\geq$ 0.90).

N-terminal fragments, known as a-ions, ending with S165 (a^{++}-9) and E166 (a^{++}-10-98) were also shifted to indicate the presence of HPO_3 and a neutral loss of of H_3PO_4 respectively. Other peptides with this sequence were detected in the cytoplasm and nucleus of A549 and MDA-MB231 cells. However, artificial or endogenous modifications (deamidations) inhibit high confidence in assigning the phosphorylation to S165. The modifications also makes quantification using MS^1 scans ineffective.

Phosphorylation of the peptide AADPPAENSSAPEAEQGGAE at S313 or S314 appears to be a common phosphorylation of YB-1 (**Table 4.1**). Peptides bearing this modification were present on YB-1 from the cytoplasm of cells while phosphorylated S314 was only detected on YB-1 from a single replicate for the nuclei of MDA-MB231 cells (**Figures 4.6 - 4.6**). Of the peptides detected, most lacked fragment ions to precisely identify whether the phosphorylation was at S313 or S314. However, one peptide containing a y-ion indicated that S314 was the site of phosphorylation (Y-11 in **Figure 4.6**). This mirrors the experience of previous work described in Woolley et al. (2011) where phosphorylation was either localised to S314 or the spectra were ambiguous. Therefore, YB-1 is phosphorylated at S314 and the phosphorylation state of S313 is uncertain.

MS^2 spectra also identified a peptide with the sequence NEGSESAPEGQAQQR and a single phosphorylation (**Figure 4.8.A**). Two serine residues, S174 and S176, lie within this peptide. The MS^2 scan indicated that two peptides were present, one was phosphorylated at S174 and the other was phosphorylated at S176 respectively (**Figure 4.8.B**). The evidence for this came from the identification of two sets of y-ions 10 and 11 that confirmed both phosphorylation sites. Therefore, YB-1 was phosphorylated at S174 and at S176.

The other phosphopeptides lacked consistent detection or the exact site of phosphorylation was undetermined (**Table 4.1**). The purified YB-1 from the nuclear samples produced a group of peptides with phosphorylation at either S165 or S167. However, they are only observed in one replicate for immunoprecipitated YB-1 from the nuclei from each cell line. These peptides appear to be a different population to the S165 peptides.

In a single replicate from the cytoplasm of MDA-MB231 cells, a peptide with an amino acid sequence matching **Figure 4.5** (NYQQNYQNSESGEKNEGSESAP EGQAQQR) was phosphorylated at two sites. Analysis of the fragments provided evidence that one HPO_3 was at either S165 or 167 and the other at either S174 or S176. The mascot scores range from 33.8 - 37.3 depending on how the phosphorylation sites are arranged. Manual analysis of the raw data indicated that mass signals

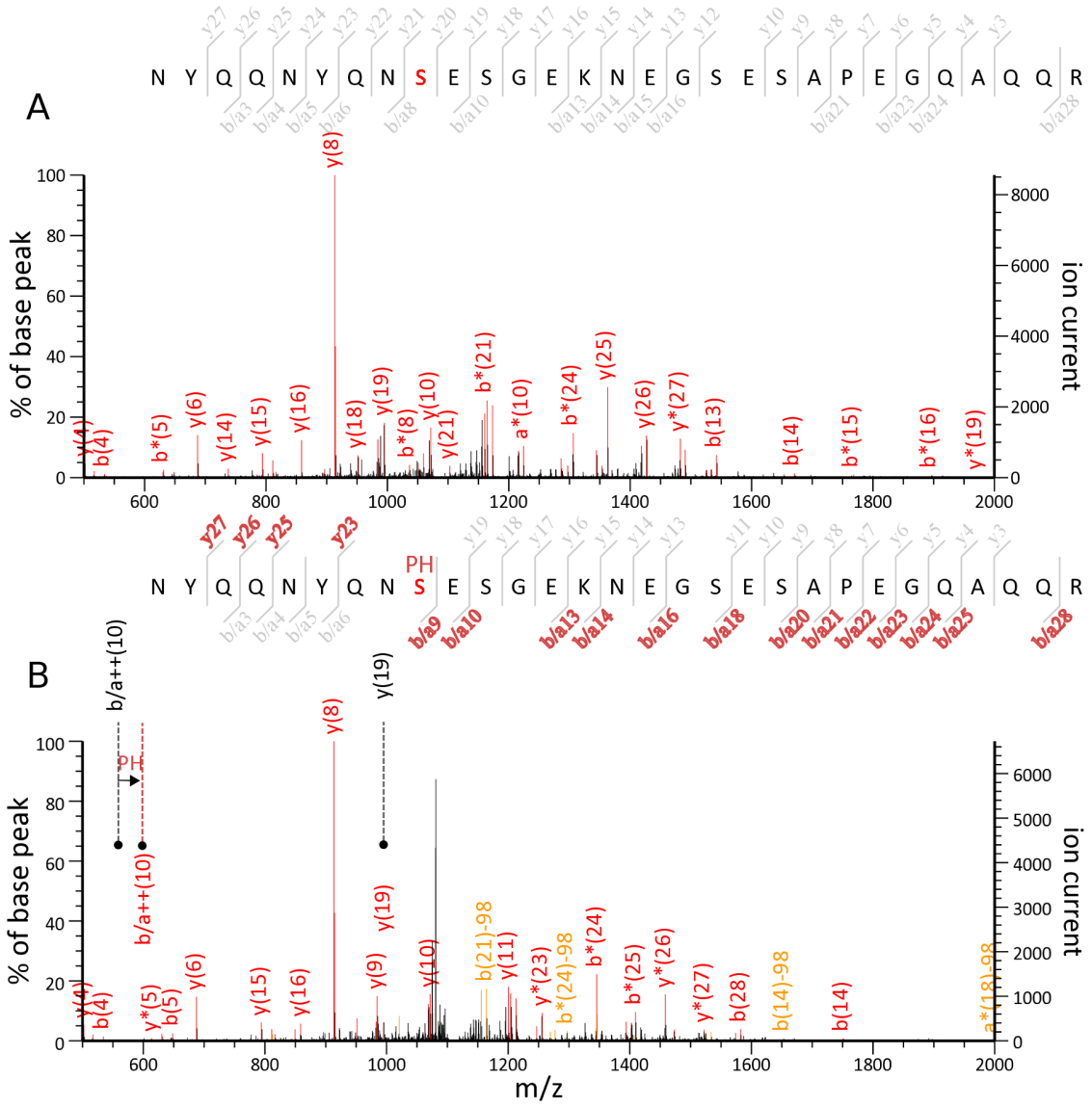

Figure 4.5: Immmunopurified YB-1 from A549 and MDA-MB231 cells is phosphorylated at S165. MS^2 spectra from NYQQNYQNSESGEKNEGSESAPEGQAQQR, a YB-1 peptide that spans serine 165 (red), S167, S174, and S176. MS^2 spectra of representative unmodified (monoisotopic mass of 3256.3889: m/z = 1086.4749 of triply charged parent ion: Mascot ion score = 85, **A**) and phosphorylated (monoisotopic mass of 3336.3704: m/z = 1113.1307 of triply charged parent ion: Mascot ion score = 64, **B**) peptides are shown. The fragment ions that were detected by the Mascot search engine to identify the sequence are highlighted in red or yellow; yellow denotes a neutral loss of 98 Da (H_3PO_4) from phosphorylated fragment ions. y-ions and b-ions represent fragments containing the C-terminus and the N-terminus respectively. The fragment ions that contain HPO_3 (+ 79.9663) or show a neutral loss of H_3PO_4 (- 97.9769; shown in yellow) are highlighted as red in the sequence cartoon and the location of the phosphorylation is denoted by "PH". The ions that were used to identify the site of phosphorylation are shown between the spectra from unmodified (**A**) and phosphorylated (**B**).

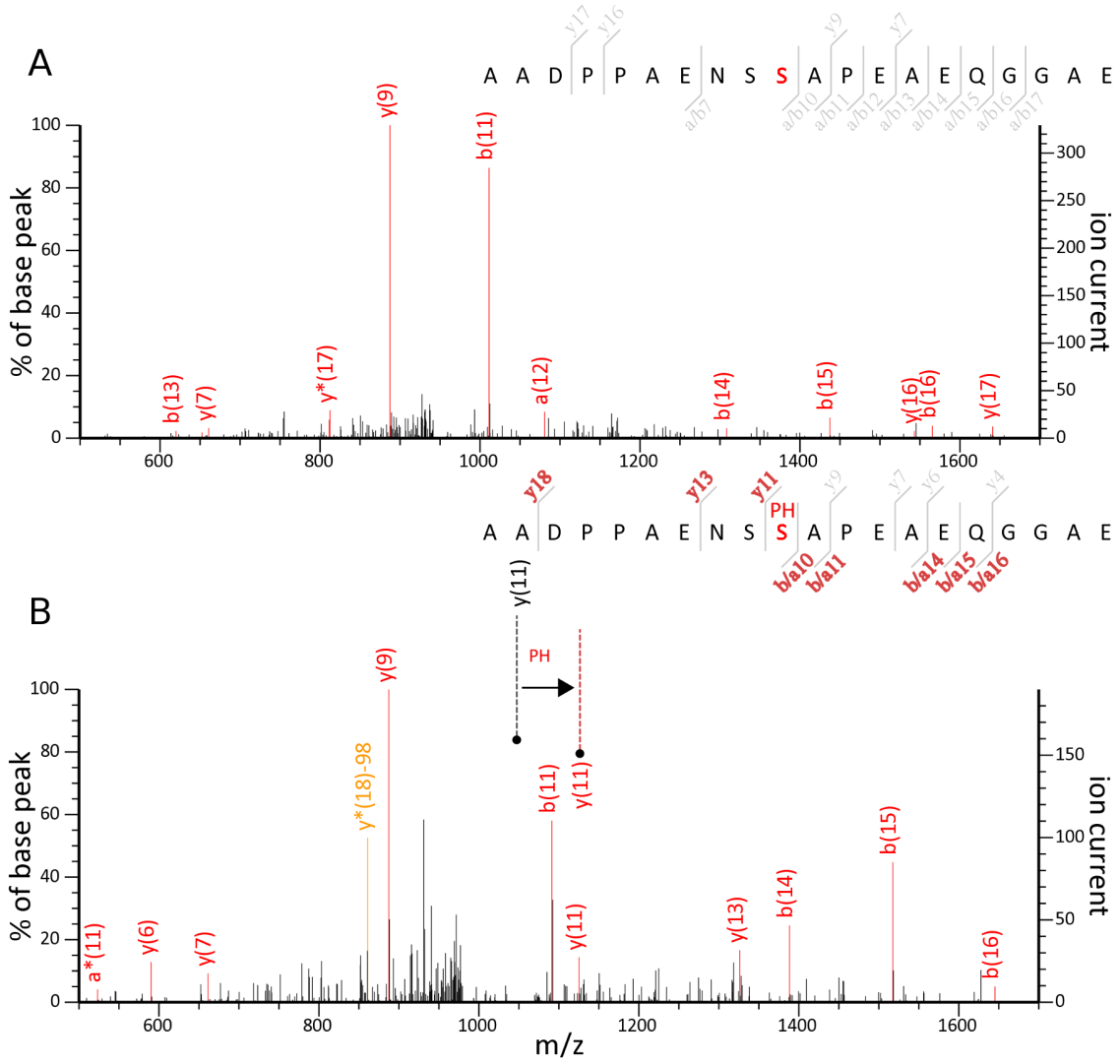

Figure 4.6: Immmunopurified YB-1 from A549 and MDA-MB231 cells is phosphorylated at S314. MS^2 spectra from AADPPAENSSAPEAEQGGAE a YB-1 peptide that spans serine 313 and S314. MS^2 spectra of representative unmodified (monoisotopic mass of 1896.7973: m/z = 949.4113 of doubly charged parent ion: Mascot ions score = 11, **A**) and phosphorylated (monoisotopic mass of 1976.7636: m/z = 989.3947 of doubly charged parent ion: Mascot ion score = 39, **B**) peptides are shown. The fragment ions that were detected by the Mascot search engine to identify the sequence are highlighted in red or yellow; yellow denotes a neutral loss of - 98 Da (H_3PO_4) from phosphorylated fragment ions. y-ions and b-ions represent fragments containing the C-terminus and the N-terminus respectively. The fragment ions that contain HPO_3 (+ 79.9663) or show a neutral loss of H_3PO_4 (- 97.9769; shown in yellow) are highlighted as red in the sequence cartoon and the location of the phosphorylation is denoted by "PH". The ions that were used to identify the site of phosphorylation are shown between the spectra from unmodified (**A**) and phosphorylated (**B**).

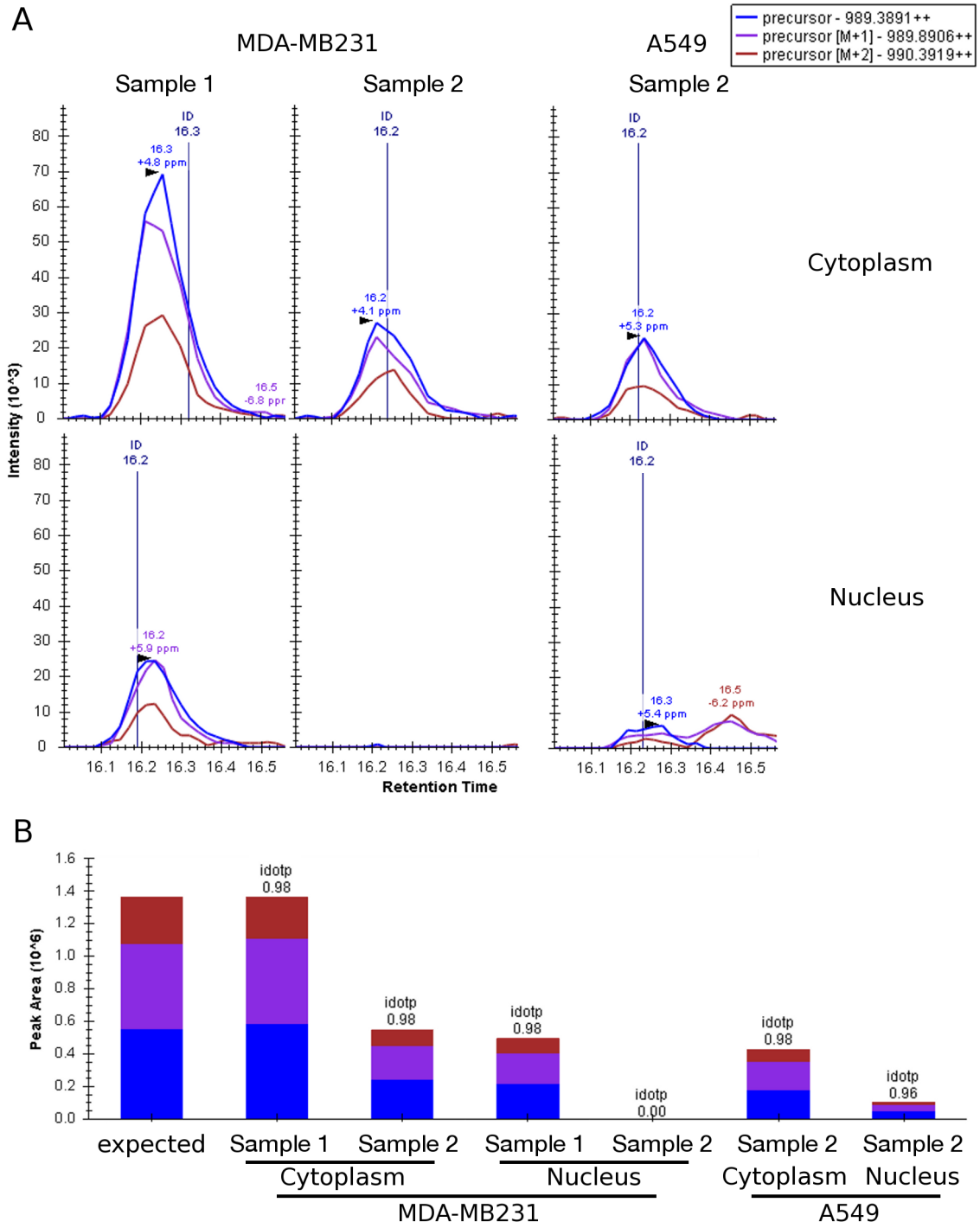

Figure 4.7: Peptides confirming the phosphorylation of YB-1 at S314 are present in YB-1 from the cytoplasm and nuclei of A549 and MDA-MB231 cells. **A**, extracted MS^1 ion chromatogram plots showing the peak area under the curve of the monoisotopic (M), M+1, and M+2 precursor ions for phosphorylated AADPPAENSSAPEAEQGGAE from the YB-1 purified from the cytoplasm and nuclei of A549 and MDA-MB231 cells. The positive identification of the peptide from MS^2 scans is indicated by **ID** above the plots. **B**, plots showing the calculated peak area under the curve derived from the extracted ion chromatograms shown in **A**. The isotope dot product (idotp) values indicate how closely the ratio of the three precursor ions matches the **expected** ratio (idotp range = 0 - 1; reliable identifications $\geq$ 0.90).

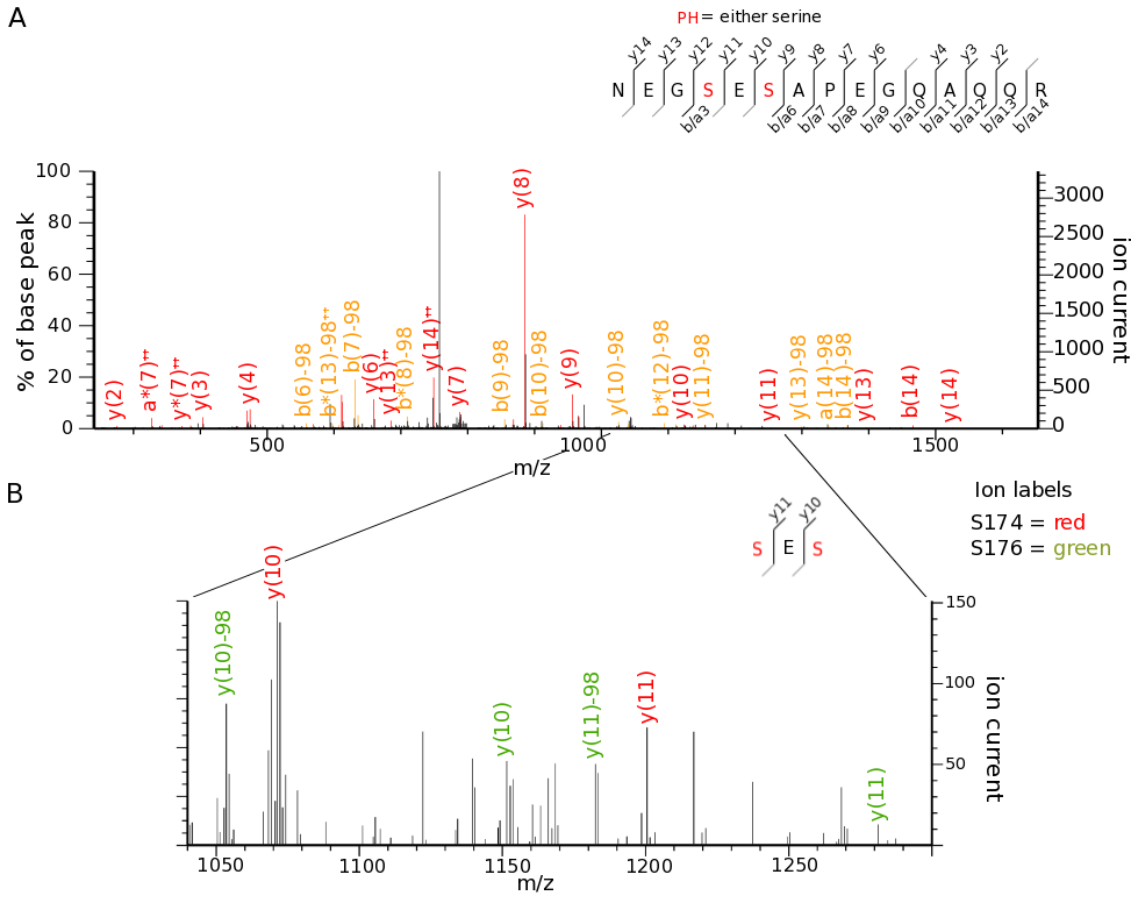

Figure 4.8: Immmunopurified YB-1 from A549 and MDA-MB231 cells is phosphorylated at S174 and S176. MS^2 spectra from NEGSESAPEGQAQQR indicates the presence of two YB-1 peptides with a single HPO_3 at either S174 or S176. **A**, MS^2 spectra of representative phosphorylated peptides is shown (monoisotopic mass of 1666.6663: m/z = 834.3405 of doubly charged parent ion: Mascot ion score = 59 [for assignment of HPO_3 to S174] or 54 [for assignment of HPO_3 to S176]). The fragment ions that were detected by the Mascot search engine to identify the sequence are highlighted in red or yellow; yellow denotes a neutral loss of 98 Da (H_3PO_4) from phosphorylated fragment ions. y-ions and b-ions represent fragments containing the C-terminus and the N-terminus respectively. The fragment ions that contain HPO_3 (+ 79.9663) or show a neutral loss of H_3PO_4 (-97.9769; shown in yellow) are highlighted as red in the sequence cartoon. **B**, ions from 1025 - 1300 m/z of the spectrum that highlights the presence of y-ions that support the presence of two peptides with a single HPO_3 at either S174 (labels in red) or S176 (labels in green).

for the intact phosphorylated peptides were present in the other replicate IP from the cytoplasm of MDA-MB231 cells as well as in one of the runs from MDA-MB231 nuclei. In both instances, no fragmentation information for the localisation of the phosphorylation site was acquired as the precursors failed to reach the intensity threshold that was required to trigger the acquisition of MS^2 scans.

Chapter 3.2.4 highlighted the presence of YB-1 phosphorylated at S102 in both A549 and MDA-MB231 cells. Information about the subcellular localisation of YB-1 phosphorylated at S102 has been sought although peptides exhibiting phosphorylation at S102 are absent from the LC-MS/MS. Unphosphorylated peptides including S102 are present in all samples showing that without modification this peptide species ionises and fragments efficiently during LC-MS/MS. There are 5 arginine and lysine residues in the 10 amino acids that precede S102. Phosphorylation can interfere with trypsin cleavage at nearby lysine and arginine residues (Benore-Parsons et al. 1989, Molina et al. 2007). To accommodate any localised reduction in the efficiency of trypsin cleavage, the data were searched allowing up to 7 missed trypsin cleavage sites. This did not yield measurements from any peptides with phosphorylated S102. Therefore, tryptic peptides that include phosphorylation at S102 of YB-1 have poor compatibility with LC-MS/MS.

This work showed that the YB-1 in A549 and MDA-MB231 cells was phosphorylated at multiple sites (S165, S174, S176, and S314). Phosphorylation of S165 was detected in all samples but was present at elevated levels in YB-1 from the cytoplasm. Phosphorylation at S314 appears to be present on YB-1 that is distributed throughout A549 and MDA-MB231 cells. Other phosphorylated peptides did not yield sufficient information to localise the HPO_3 to a specific residue. These results confirm that phosphorylation is not an event that is exclusive to YB-1 that resides in the nucleus of cells.

4.2.3 The protein-protein interactions of YB-1

The PPI of YB-1 were hypothesised to change when YB-1 moves between the cytoplasm and nucleus of cultured cells. To study this hypothesis, the PPI of YB-1 that was immunopurified from the cytoplasm and nuclei of A549 and MDA-MB231 cells was surveyed. Immunoprecipitated YB-1 was separated on a 10% SDS-PAGE gel (**Figure 4.2.A**; n = 2 for each cell line and sub-cellular compartment). The lanes were cut from the gel, digested with trypsin, and the composition of the tryptic peptides was analysed using LC-MS/MS (**Chapter 2.13**). LC-MS/MS was used to

measure the proteins that had been co-precipitated with the YB-1 in each immunoprecipitation sample. The results showed that the protein interactions of YB-1 in the cytoplasm and nuclei of A549 and MDA-MB231 cells were extensive. 295 proteins were identified in all LC-MS/MS runs using the strict filtering criteria and significance thresholds described in **Chapter 2.13** (For the full list see; **Table B.1** and `CD/Chapter_4/MS_subcell_sum_sht.xlsx`).

The distribution of proteins across subcellular compartments and cell lines has been assessed. Proteins were considered to be identified in the subcellular compartment of a cell line if they satisfied either of the following rules;

Rule A = the protein was detected in both replicates for the subcellular compartment in that cell line.

OR

Rule B = the protein was detected in one replicate for the subcellular compartment in that cell line and assigned to that subcellular compartent using **Rule A** in the other cell line.

Using these rules, 267 of the 295 proteins that were identified have been assigned to the cytoplasm and/or nucleus of each cell line. The YB-1 interacting proteins from A549 and MDA-MB231 cells were very similar with $\sim$ 80% of proteins copurifying with YB-1 from both cell lines (**Figure 4.9.A**; these proteins are listed in `CD/Chapter_4/MS_subcell_sum_sht.xlsx`, rows 4 - 270). There were more unique protein identifications made in the MDA-MB231 cell line (43 or 16.1% of proteins identified). Of the 267 proteins that have been identified, more than one third were detected in both the nucleus and the cytoplasm (94/36%) while 118 (44%) proteins were uniquely identified in nuclear fractions.

The protein interactions that are shared between the two cell lines are likely to contain PPI of YB-1 that are relevant in other biological contexts. There are 201 proteins that were present in the same subcellular locations in both cell lines (**Figure 4.9.B**). From this initial group of 201 proteins, 85 (42.3%) were detected in both the cytoplasm and the nucleus. In both cell lines, 29 proteins (14.4%) were identified solely in the cytoplasm while 87 (43.3%) proteins were exclusively detected interacting with YB-1 in the nucleus of both cell lines. The interactions were consistent between the two cell lines. While YB-1 is in the nucleus it appears to interact with a large number of proteins.

The similarity of the detected protein interactions of YB-1 was assessed by comparing them to previous publications. To do so, all of the first order protein interac-

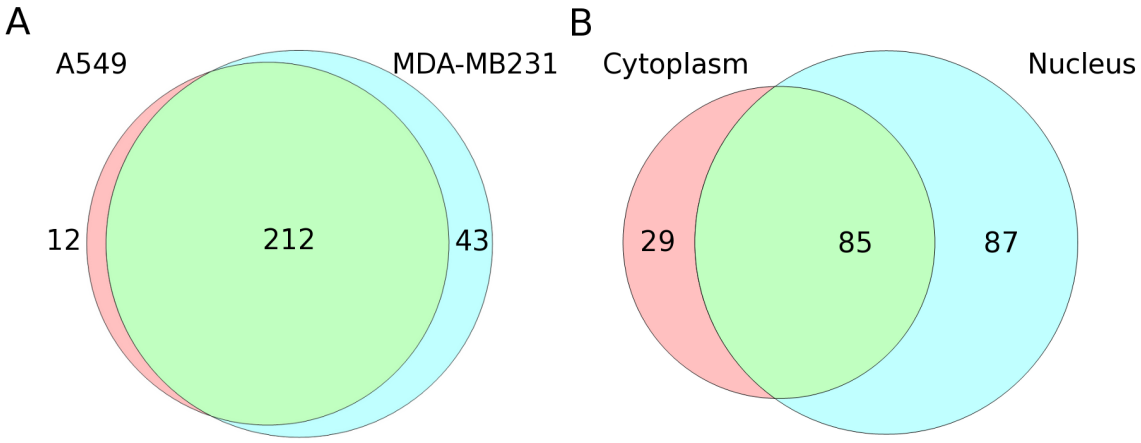

Figure 4.9: Venn diagrams showing the proteins that are detected in IP YB-1 from the cytoplasm and nucleus of A549 and MDA-MB231 cells. **A**, the distribution of protein identifications between A549 (pink) and MDA-MB231 (turquoise) cells. **B**, the distribution of protein identifications between the cytoplasm (pink) and nucleus (turquoise). The number of protein identifications are indicated in each quadrant.

tions of the identified proteins with one another were retrieved from the *Experiments* and *Databases* fields in the String database (for details see **Chapter 2.14**). Forty-two (24%) of the 178 first order protein interactions of YB-1 in String were also detected in this experiment. Other known protein interactions of YB-1 were present as homologous proteins. In this experiment, the polyadenylate-binding proteins were resolved as polyadenylate-binding protein 1 (PABP1; P11940) and Polyadenylate-binding protein 4 (Q13310). YB-1 was listed in the String database as interacting with two other members of this protein family; Polyadenylate-binding protein 2 (Q86U42) and Polyadenylate-binding protein 3 (Q9H361). Insulin-like growth factor 2 mRNA-binding protein 1 (Q9NZI8) was also found in both this experiment and the String database. This experiment also detected the presence of Insulin-like growth factor 2 mRNA-binding protein 3 (O00425). Other proteins that YB-1 is known to interact with, such as p53, AKT, and GSK3β, were not detected in this experiment.

Ribosomal proteins, cytoskeletal proteins, keratins were detected but proteins from these groups can be recovered due to non-specific interactions during immunoprecipitation. YB-1 that is bound to RNA may interact with ribosomes and cytoskeletal proteins and these interactions are in keeping with YB-1 biology. Contaminating proteins that interact non-specifically with the beads should not be present due to the specific recovery of YB-1 via competitive elution with the immunising peptide (**Figure 4.2** No antibody lane). However, there was no viable control for proteins that interact transiently with YB-1, or its interaction partners, during the

immunoprecipitation. Non-specific interactions may have a physiochemical specificity to YB-1 complexes under *ex vivo* conditions and thus may be reproducible.

The area of the top three peptides for each protein assignment were used to test for concordance of the replicate LC-MS/MS runs for each cell line and subcellular compartment. In spite of the low quality quantification, dendrograms supervise 6 of the immunoprecipitation samples into nuclear and cytoplasmic groupings and then cell line groupings (**Figure 4.10**). The A549 cytoplasmic and nuclear fraction that are not arranged with their replicates were processed separately from the other samples. In the intervening months, the LC-MS/MS method had been optimised and the levels of detergent in the immunoprecipitation buffers lowered. A group of 23 proteins with ubiquitous expression are grouped together and this group is likely to represent contaminants. It includes keratins, cytoskeletal proteins (*VIM*, Plectin), miscellaneous proteins (tRNA-splicing ligase RtcB homolog [Q9Y3I0], Complement component 1 Q subcomponent-binding protein, mitochondrial [C1QBP; Q07021], Eukaryotic initiation factor 4A-III [P38919], Ubiquitin-40S ribosomal protein S27a [P62979], 60S ribosomal protein L27a [P46776]), YB-1 and the YB-1 homologue DNA-binding protein A (DBPA; P16989). Due to its ubiquitous presence in each sample, YB-1 was also assigned to this group along with most of the keratins in the sample.

This work indicates that YB-1 interacts with a large number of proteins. The use of two cell lines highlights that the PPI of YB-1 are consistent between A549 and MDA-MS231 cells. Furthermore, the PPI of YB-1 in the cytoplasm and nucleus suggests that a number of proteins are likely to move between the two subcellular compartments with YB-1.

4.2.4 Bioinformatic analyses of co-immunoprecipitating proteins

The potential function of YB-1 in the two cell lines and in each subcellular compartment can be inferred through the PPI of YB-1. The molecular functions of YB-1 are presumably represented by the functions and processes of the PPI of YB-1. Bioinformatics was used to elucidate the range of functions that could be deduced from the PPIs. To do this, the proteins that interacted with YB-1 were tested for the enrichment of bioinformatic terms using DAVID (retrieved from v6.7 on 24.02.2014; Huang et al. 2009a, Huang et al. 2009b). DAVID contains the collated data, such as gene ontology, KEGG, and protein functional domains, for genes and

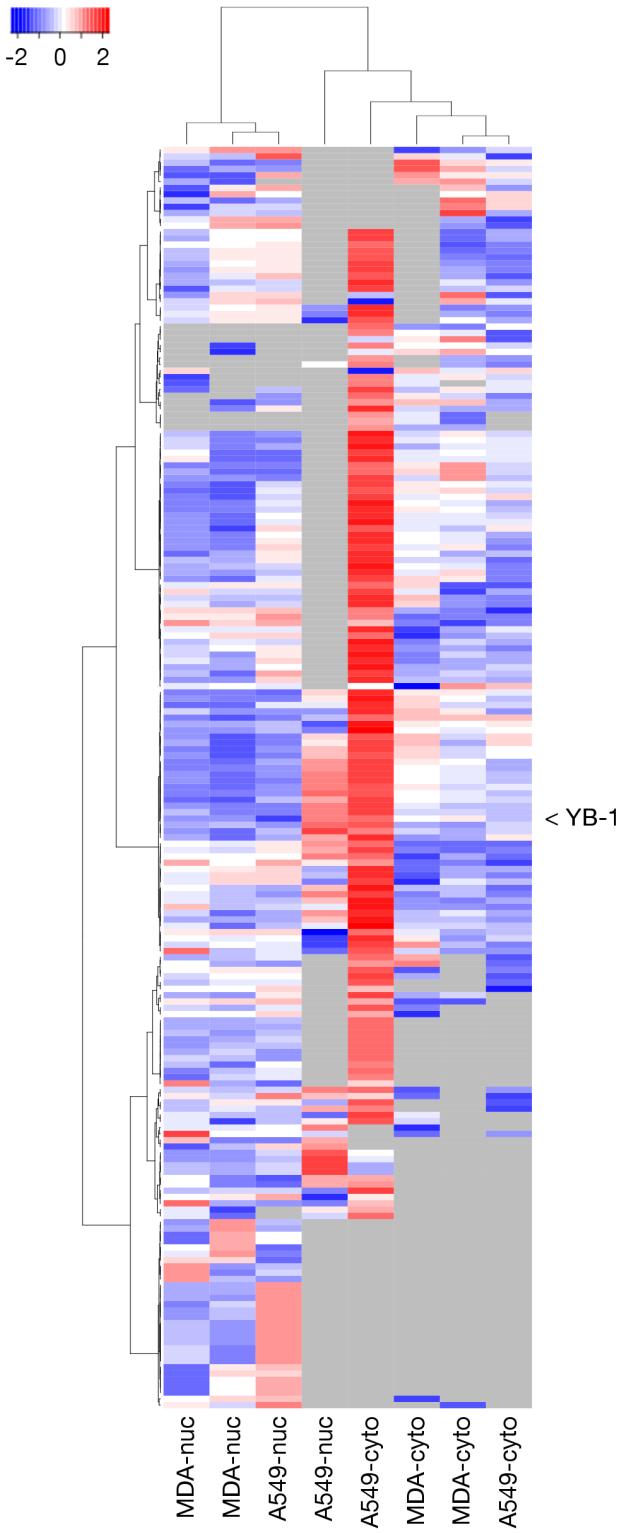

Figure 4.10: Heatmap showing binding partners of endogenous YB-1 in the cytoplasm and nucleus of A549 and MDA-MB231 cells. Label-free quantification was log-transformed for clustering and the colour was scaled across each row. Each row represents a protein that was identified with a consistent subcellular localisation. Grey panels indicate that the protein was not detected. Label-free quantifications from the top three peptides method (Silva et al. 2006) are provided in `CD/Chapter_4/MS_subcell_sum_Top3.xlsx`.

proteins from a wide variety of sources (terms). This approach assessed whether any terms are overrepresented in the list of submitted proteins compared to a control, or background, list; an enrichment score ≥ 1.3 was taken to indicate a significant enrichment compared to the background (Huang et al. 2009a, Huang et al. 2009b). The whole genome was used as the background list for this work. Similar terms were clustered together, to remove the redundancy that is inherent in a database like DAVID, which has been collated from many sources.

The results indicate that YB-1 participates in many processes (**Table 4.2**, All identified; full results in `CD/Chapter_4/DAVID_files/All_conserv_DAVID.txt`). RNA binding and processing are the most common processes attributed to the proteins interacting with YB-1. The enrichment of terms associated with RNA binding and the ribosome (Enrichment = 64.3) infers the involvement of YB-1 in translation and possibly RNA stability in A549 and MDA-MB231 cells. A large group of proteins interacting with YB-1 appears to be involved in RNA processing and splicing (Enrichment = 33). Another small group of proteins is also involved in RNA stability (Enrichment = 6.9). A group of nuclear encoded proteins that localise to the mitochondrial matrix were also present (Enrichment = 2.9). Finally, a smaller group of proteins with DNA-associated terms are enriched (Enrichment = 2).

Table 4.2: Enriched terms in YB-1 IP proteins from A549 and MDA-MB231 cells.

Cluster description	All identified	Cytoplasm	Nuclear
ribosome:ribonucleoproteins:RNA binding	64.3 (23-145)	33.7 (13-73)	61.1 (28-121)
RNA processing:spliceosome	33.0 (28-82)	11.8 (13-32)	26.5 (24-67)
organelle lumen:nuclear lumen:nucleolus	28.2 (63-116)	6.2 (21-45)	28.7 (50-90)
DNA/RNA helicase activity	11.3 (30-31)	4.5 (5-15)	8.1 (9-22)
ubiquitin conjugation:isopeptide bond	8.7 (25-29)	6.7 (13 - 16)	7.9 (17-23)
mitochondrial matrix	2.9 (3-18)	0.35 (4-12)	3.6 (7-26)
regulation of mRNA stability	6.9 (8)	4.7 (5-13)	6.2 (6-7)
Translational initiation	5.9 (7-11)	8.2 (7-11)	-
Protein-DNA complex:chromosome	2 (3-14)	-	1.4 (3-10)

Data for Functional Annotation Clustering were retrieved from DAVID, v6.7 on 24.02.2014. The columns provide the enrichment score for the clustered functional annotation from amongst a total of 296 proteins for **All identified** column, 114 proteins in the **Cytoplasm** column, and 214 proteins in the **Nuclear** column. Enrichment scores ≥ 1.3 are significant. The bracketed numbers show the minimum and maximum number of proteins that were associated with terms within the cluster.

The terms associated with the detected proteins can also be used to test for the specific enrichment of cytoplasmic and nuclear proteins in each fraction. The enrichment of terms associated with translational initiation amongst the 112 proteins from the cytoplasmic fraction was consistent with YB-1 being present in protein:RNA complexes during the initiation of translation (Enrichment = 8.2; **Table 4.2**, Cytoplasm; full results in `CD/Chapter_4/DAVID_files/unv_cyto_DAVID.txt`). YB-1 is known to participate in translation specifically at translational initiation (**Chapter 1.8.3.2**). Furthermore, the lack of proteins associated with translational initiation confirmed that the nuclear fractions were only contaminated with cytoplasmic proteins at very low levels. Information about the function of YB-1 in the nucleus of A549 and MDA-MB231 cells came from terms associated with RNA processing:spliceosome (**Table 4.2**, Nuclear; full results in `CD/Chapter_4/DAVID_files/unv_nuc_DAVID.txt`). These terms were more enriched in the proteins that interact with YB-1 in the nucleus (Enrichment = 26.5) than in the cytoplasm (Enrichment = 11.8). The specific enrichment of proteins interacting with DNA and chromatin in the nuclear fraction (Enrichment = 1.4) confirms that nuclear proteins were enriched amongst the proteins recovered with YB-1 from nuclei.

The bioinformatics appear to confirm the predominance of the activities of binding or interacting with RNA in YB-1 biology. However, a small number of the proteins recovered using immunoprecipitation of YB-1 indicate that YB-1 also interacts with DNA. These results confirm the multifunctionality of YB-1.

The analysis of enriched terms provide an indication of the processes that the detected proteins can participate in. However, most biochemical tasks, such as splicing RNA, building a protein polypeptide, or transcribing DNA, require the coordination of many processes. An *in silico* PPI network was built to gain further insight into which proteins are likely to form functional units. The data sources for building the *in silico* PPI differed from those used for the enrichment of terms analysis. Therefore, this second approach provides independent evidence for the protein groupings from the enrichment of terms. The interactions between the YB-1 binding proteins with consistent subcellular localisation were retrieved from a database of PPI (String, v9.1) and imported into Cytoscape (v3.1) for analysis and visualisation. The *in silico* PPI network that resulted from this work was highly connected with 3505 connections (edges) between the 265 proteins (nodes; **Figure 4.11**). This was significantly more edges than the average of 850 edges from 265 proteins that were randomly sampled from the human genome ($p < 0.001$; String v9.1). The connectivity of proteins that form complexes with one another

should be greater than the connectivity of proteins with unrelated functions (Ge et al. 2001, von Mering et al. 2002). *In silico* protein interaction networks were also prepared using the proteins that were uniquely identified in the cytoplasm (**Supplementary figure C.1**), proteins that were identified in the cytoplasm and nucleus (**Supplementary figure C.2**), and those that were unique to the nucleus of both cell lines (**Supplementary figure C.3**).

In an *in silico* PPI network, the proteins that reside together in MPCs should form groups of proteins that are strongly connected to one another. These groups of proteins are referred to as clusters. The presence of protein clusters in the network was tested using decompositional clustering via the Markov Cluster Algorithm (mcl-edge software Enright et al. 2002, Van Dongen 2012, Van Dongen 2000). The Markov Cluster Algorithm separates sets of nodes that share a high density of edges from one another (for more details see Van Dongen 2012). The clustering indicated that there were 10 groups of connected proteins with 4 or more members (**Figure 4.11**; full results in `CD/Chapter_4/DAVID_files/DAVID_clusters`). Six of these 10 groups of proteins were enriched for some aspect of RNA biology. The three largest clusters represent different aspects of RNA biology. The largest grouping (Cluster 1, red nodes) in the network included the translational machinery as it was dominated by proteins involved in translation (61/67 proteins, translation [GO:0006412]). The second largest group (Cluster 2, brown nodes) contains YB-1 along with other RNA-binding proteins. Together these proteins include parts of the spliceosome (37/62 proteins, RNA splicing [GO:0008380]). The proteins in Cluster 3 (blue nodes) cover a wide range of functions associated with RNA processing (17/36 proteins, RNA metabolic processes [GO:0016070]). Cluster 3 also included proteins that were likely to be involved in ribonucleoprotein complex biogenesis (16/36 proteins, GO:0022613) and ribosomal or non-coding RNA processing (7/36 proteins, rRNA processing [GO:0006364]; 8/36 proteins, non-coding RNA processing [GO:0034660]). There was also a group of 6 helicases in Cluster 3 (Probable ATP-dependent RNA helicase DDX5 [P17844], ATP-dependent RNA helicase DDX24 [Q9GZR7], Pre-mRNA-splicing factor ATP-dependent RNA helicase DHX15 [O43143], Probable ATP-dependent RNA helicase DDX17 [Q92841], Putative ATP-dependent RNA helicase DHX30 [Q7L2E3], 5'-3' exoribonuclease 2 [Q9H0D6]). Two groups of proteins contain cytoskeletal proteins and keratins (Cluster 4, 14 proteins, light green nodes; Cluster 6, aqua blue nodes). The function of the fifth group of proteins was unclear (Cluster 5, yellow nodes). This group included Polyadenylate-binding protein 1 and other RNA-binding proteins that are

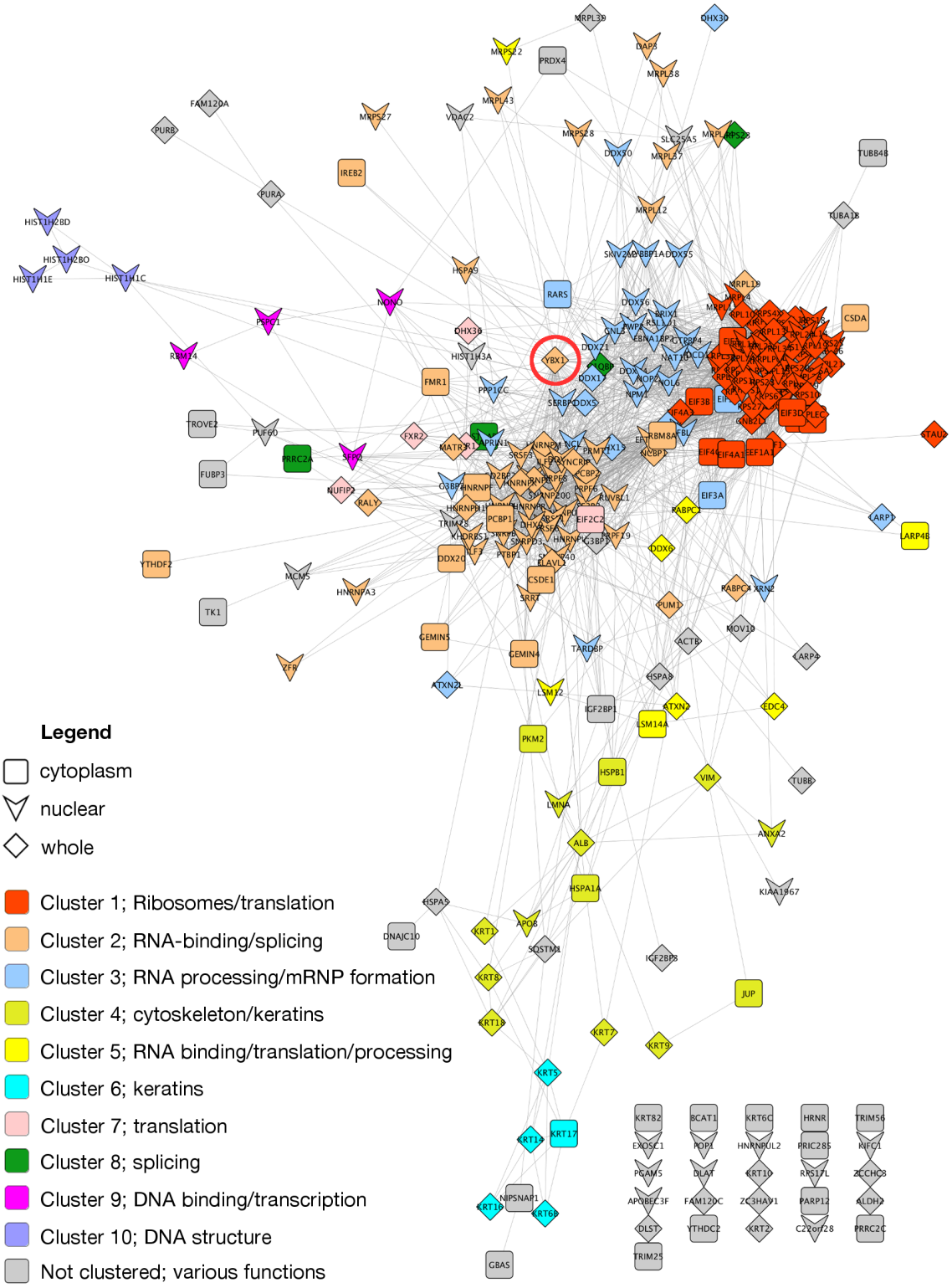

Figure 4.11: Binding partners of endogenous YB-1 in the cytoplasm and nucleus of A549 and MDA-MB231 cells. A network of *in silico* interactions between the proteins that were identified interacting with YB-1 (String, v9.1). Markov clustering has been applied and the network was visualised in Cytoscape (v3.2). The network layout was performed using the Allegro spring electric plugin. The nodes that were grouped together by the MCL algorithm are coloured according to the key on the bottom left-hand side of the image. This key also notes the primary function of the proteins in each cluster. The location of YB-1 is highlighted by a red circle.

involved in RNA processing (3/8 proteins, cytoplasmic mRNA processing body assembly [GO:0033962]; 3/8 proteins, nuclear-transcribed mRNA catabolic process, deadenylation-dependent decay [GO:0000288]) and the regulation of translation (4/8 proteins, regulation of translation [GO:0006417]). A small group of proteins (Cluster 7, pink nodes) appeared to be involved in the negative regulation of translation (3/5 proteins, GO:0017148) and another small group (Cluster 8, green nodes) were most likely involved in mRNA splicing (2/3 proteins, RNA splicing [GO:0008380]; 2/3 proteins, ribonucleoprotein complex assembly [GO:0022618]).

Two small groups of proteins were comprised of proteins that interact with DNA. One of these groups (Cluster 9, pink nodes) contains proteins that were implicated in DNA recombination (3/4 proteins, GO:0006310), histone deacetylation (2/4 proteins, GO:0016575), DNA repair (3/4 proteins, GO:0006281), and also transcription (4/4 proteins, Transcription DNA-templated [GO:0006351]). Three of these proteins (Paraspeckle component 1 [Q8WXF1], Non-POU domain-containing octamer-binding protein [Q15233], and Splicing factor, proline- and glutamine-rich [P23246]) can form a complex to influence transcription. However, while it is not included in the gene ontology for these proteins, all 4 are also known to locate to paraspeckles and participate in splicing (Fox et al. 2005, Marko et al. 2010). The final group of proteins with 4 or more members (Cluster 10, purple nodes) consists of histone proteins that are involved in chromatin structure (2/4 proteins, nucleosome positioning [GO:0016584]; 4/4 proteins, chromatin organization [GO:0006325]).

The *in silico* PPI network revealed a number of the functions already reported for YB-1. The principle functions of YB-1 were confirmed by the interaction of YB-1 with proteins that participate in RNA splicing (Clusters 2 and 8), RNA processing (Cluster 3, 5), and translation (Clusters 1, 5, and 7). There were also protein groups present that can interact with DNA to influence chromatin structure (Cluster 10) and gene transcription (Cluster 9).

The connections (edges) within the network highlight groups of proteins that are likely to act together (clusters; **Figure 4.11**). It was also hypothesised that in addition to direct participation in these multiple processes, a critical function of YB-1 was to regulate processes. To test this hypothesis, the flow of information through the *in silico* PPI has been examined by calculating betweenness centrality (Yan et al. 2010, Yu et al. 2007). Betweenness centrality assesses the likelihood that a node regulates the flow of information to and from the groups of proteins in the network. The shortest path that links every pair of nodes in the network is assessed to calculate the betweenness centrality. For every protein a tally is then made for

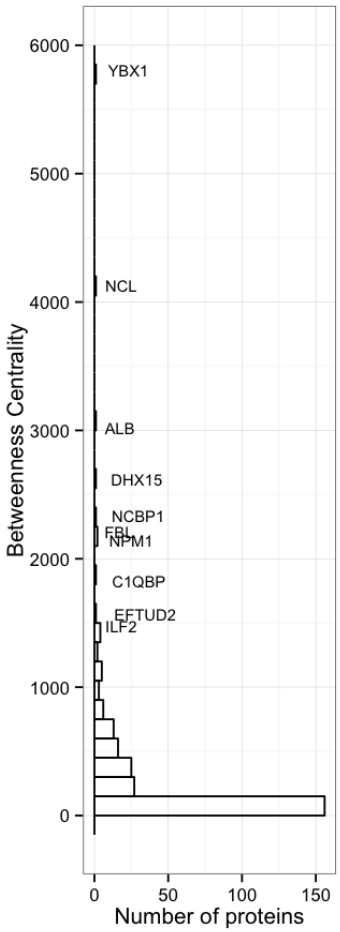

Figure 4.12: Betweenness centrality of the binding partners of endogenous YB-1 in the cytoplasm and nucleus of A549 and MDA-MB231 cells. The betweenness centrality of all protein pairs in the *in silico* PPI network was calculated using CytoNCA plugin in Cytoscape. The betweenness centrality measurement for each protein in the network has been graphed. The betweenness centrality measures have been graphed in intervals of 150 and the 10 proteins with the highest calculated betweenness centrality are highlighted in the graph.

the number of times the protein is part of one of these shortest paths. By controlling the flow of information between clusters, proteins with a high betweenness centrality can regulate the behaviour of the network (Yan et al. 2010, Yu et al. 2007).

Betweenness centrality was calculated for all nodes in the *in silico* PPI network (Tang et al. 2015). The results reveal that YB-1 has the highest betweenness centrality of any protein in the network (**Figure 4.12**). This indicates that YB-1 has the potential to link and regulate the multiple functional groups that are detected interacting with YB-1.

Using bioinformatics to study the large number of proteins interacting with YB-1 revealed functions that were primarily related to the ability of YB-1 to bind to RNA.

Groups of proteins with functions specific to every step in the lifecycle of RNA are present. In the nucleus of both cell lines, YB-1 interacted with a small number of proteins that influence chromatin. The placement of YB-1 within the *in silico* PPI network indicates that YB-1 is well placed to control the activity of the functional groupings contained within the network.

4.3 Discussion

The data presented in this chapter confirm that:

- The protein interactions of exogenous YB-1 are likely to differ from those of endogenous YB-1;
- YB-1 is phosphorylated at S165, S174, S176, and S314 in MDA-MB231 and A549 cells;
- The PPI of YB-1 indicate that YB-1 has similar functions in MDA-MB231 and A549 cells;
- The PPI of YB-1 in MDA-MB231 and A549 cells highlight the importance of YB-1 in the regulation of RNA transcripts.

The work presented in this chapter characterises the phosphorylations of YB-1 in the cytoplasm and nucleus of A549 and MDA-MB231 cells. It also analyses the PPI of YB-1 that was purified using ^{N}YB1 in the cytoplasm and nucleus of A549 and MDA-MB231 cells. RNA binding appears to be central to the molecular functions of YB-1 in these two cell lines.

4.3.1 Over-expression of YB-1 and protein-protein interactions

The forced expression of exogenous YB-1 in A549 cells shows that the mobility of HA-tagged YB-1 in A549 cells on BN-PAGE differed from that of endogenous YB-1. The differing mobility of YB-1 is likely to be caused by endogenous and exogenous YB-1 having different PPI. These results prompted this study to rely solely on endogenous YB-1 to assess the PPI of YB-1.

The mobility difference in BN-PAGE also highlights that recombinant proteins differ from the molecules that they are supposed to mimick. The most obvious

structural and biochemical differences are often the presence of a 'tag' protein on the N-terminal or C-terminal of the studied protein. These tags commonly have useful characteristics, such as the availability of high-affinity purification tools (Glutathione-S-trasnferase; Moron et al. 1979, Smith & Johnson 1988) or the ability to visualise the protein in live cells (Green-fluorescent protein; Morin & Hastings 1971, Chalfie et al. 1994). However, tags can affect the tertiary structure of proteins (Kapust & Waugh 1999, Smyth et al. 2003). The tertiary structure of intrinsically disordered domains, such as that on either end of YB-1 (Selivanova et al. 2010, Guryanov et al. 2012), may be influenced by tag proteins. Dahl et al. (2009) demonstrated that a monoclonal antibody targeting YB-1 detected denatured recombinant YB-1 but not endogenous YB-1 on immunoblots. The authors proposed that the tag stabilised recombinant YB-1. This may be correct, however, the ability to move between multiple structures is a functional feature of intriniscally disordered protein domains.

There are other biochemical differences that distinguish recombinant proteins from endogenous proteins. The RNA for recombinant proteins lack the processing cues, 3'UTR, 5'UTR, and introns, that are present on endogenous RNA transcripts. These elements influence the transport and translation of RNA transcripts (Andreassi & Riccio 2009, Moore & Proudfoot 2009). Also potentially problematic is the introduction of a recombinant protein without feedback mechanisms that slow the rate of protein production into an otherwise regulated molecular environment. In A549 cells the molecular functions of YB-1 were already performed by endogenous YB-1. Overexpression of YB-1 has been shown to swamp regulatory signals (Bader & Vogt 2008) and importantly, for an RNA binding protein like YB-1, other studies have shown that mRNP function was greatly affected by the stoichiometry of their constituents (Riley & Steitz 2013).

These experiments were performed to establish tools planned for use during this PhD study. Exogenous YB-1 fused to tags has been used frequently to study the functions of YB-1 (Toulany et al. 2011, Davies et al. 2011, Garand et al. 2011, Castellana et al. 2015). The results presented here indicate that the PPI of exogenous and endogenous YB-1 may differ. Therefore, over-expression of YB-1 is best suited as a confirmatory method for the results gained from experiments using endogenous protein.

4.3.2 Phosphorylation of YB-1 in MDA-MB231 and A549 cells

Multiple phosphorylation sites were identified on the YB-1 that was purified from the cytoplasm and nuclei of both A549 and MDA-MB231 cells. The phosphorylation of YB-1 has been confirmed specifically at S165, S174, S176, and S314. This work also shows that a single YB-1 molecule can be phosphorylated at two locations, once at S165 or S167 and once at S174 or S176. The use of subcellular fractionation indicates that the phosphorylation of YB-1 at S165 is more common in the cytoplasm of A549 and MDA-MB231 cells while phosphorylation of YB-1 at S314 occurs throughout the cells. The other phosphorylation events (**Table 4.1**) require further work to confirm their distribution through A549 and MDA-MB231 cells.

These phosphorylation events have been reported in high-throughput studies (see **Chapter 1.7.2.1**). However, in the absence of manual curation of MS^2 spectra as was performed here, the results from the high-throughput studies are not definitive about the location of the phosphorylated residue on peptides that include multiple phosphorylation sites. The phosphorylation of YB-1 from the cytoplasm and nucleus of A549 has also been studied by Al Jabry (2016) and the results were concordant with those presented here.

The results presented in this thesis indicate that the phosphorylation of YB-1 at other sites is common in A549 and MDA-MB231 cells and highly likely to alter the activity of YB-1. The phosphorylation of rabbit YB-1 at unspecified sites led to its incorporation into free and polysomal mRNPs (Minich et al. 1993). Phosphorylation also impeded the ability of YB-1 to inhibit cap-dependant translation (Evdokimova et al. 2006b). In this study, the PPI of YB-1 indicated that YB-1 was interacting with RNA to influence splicing, RNA transport, and translation. The identification of multiple phosphorylations highlights their potential to influence the molecular function of YB-1. In HEK293 cells, the phosphorylation of YB-1 at S165 has been shown to occur following IL-1β exposure (Prabhu et al. 2015). This phosphorylation may promote the early stages of cancer development by contributing to the activation of NF-κB (Prabhu et al. 2015). The means by which phosphorylation alters the molecular function of YB-1 are still unclear and the work presented here also shows that S165 can be phosphorylated in the absence of IL-1β exposure in some cell types. Extensive work has been carried out to characterise the functional implications of YB-1 being phosphorylated at S102. However, multiple molecular functions, which are somewhat discordant, have been attributed to this phospho-

rylation event (**Chapter 1.7.2.1**). The phosphorylation of another site on YB-1 alongside phosphorylation at S102 may explain the diverse functions that have been attributed solely to YB-1 that is phosphorylated at S102.

The implications for the function of YB-1 have been not been confirmed for these phosphorylation events. The initial plan for this experiment was to separate purified YB-1 using BN-PAGE to describe the phosphorylation and PPI of YB-1 for each MPC. However, purified YB-1 separates as a monomer in BN-PAGE (**Supplementary figure C.4**). This meant that the phosphorylation of YB-1, and the protein composition of the MPCs, was not determined. The PPI of YB-1 did, however, provide some general insights into the function of YB-1 that is phosphorylated at these residues.

4.3.3 Protein interactions of YB-1 in MDA-MB213 and A549 cells

The work reported here examined the PPI of YB-1 in two cancer cell lines. The protein interactions of YB-1 were extensive and bioinformatic analyses indicated that they were consistent with the known molecular functions of YB-1 (**Chapter 1.8**). Furthermore, the identified proteins had specific functions that were appropriate for their location in the cells. The high betweenness centrality of YB-1 within the *in silico* network also indicates that YB-1 is well placed to control the function of the proteins in the network.

The proteins that interact with endogenous YB-1 were consistent across the two cell lines ($\sim$ 80%). The *in silico* PPI network corroborated the results from analysis of terms enrichment by showing that the reported multifunctionality of YB-1 was reflected by specific groups of proteins within the network. Most research effort into YB-1 necessarily focuses on a specific aspect of YB-1 function. This can leave the impression that YB-1 neatly switches between functions in response to stimuli. While this may be true for some of the processes that YB-1 participates in, it is unlikely to be the case for many of the functions of YB-1. YB-1 is present in stress granules where it interacts with Trinucleotide repeat-containing gene 6A protein (GW182) and PABP1 (Kedersha & Anderson 2007). In this work, YB-1 was found to interact with PABP1 but not GW182. YB-1 and PABP1 are likely to join mRNPs once a transcript has been processed to mRNA. GW182 is likely to be recruited to mRNPs, and to interact with YB-1 and PABP1, upon stress activation (Braun et al. 2013). Therefore, many protein interactions of YB-1 will not be

present in these experiments as the experimental conditions were not conducive to these interactions occurring.

More generally, the proteins that interact with YB-1 imply that in A549 and MDA-MB231 cells rather than switching from one function to another, YB-1 participates in a large number of processes concurrently at the cellular level. The central importance of RNA binding in YB-1 biology is confirmed by the interaction of YB-1 primarily with RNA-binding proteins. However, there is also evidence that YB1 interacts with DNA-associated proteins. This is consistent with the observations from IHC on breast cancer sections, and IF from MDA-MB231 cells, where YB-1 is primarily in the cytoplasm but a small amount interacts with DNA (**Chapter 3**).

The molecular functions of YB-1 in mRNA transport and translation meant that YB-1 was expected to interact with cytoskeletal proteins (Davies et al. 2011, Hutchins et al. 2010, Maher-Laporte et al. 2010, Chernov et al. 2008b) and ribosomal proteins (**Chapter 1.8.3.2**). Both of these groups of proteins are often considered to be contaminants of immunoprecipitation experiments. IP will recover proteins that interact non-specifically with protein complexes that contain YB-1. The use of endogenous YB-1 precluded the use of tandem-affinity purifications which can identify contaminants more effectively (Mellacheruvu et al. 2013).

The recovery of non-specific proteins was minimised in two ways. Eluting YB-1 from the bead-^{N}YB1 complex using competition with the ^{N}YB1 peptide should avoid contamination of the samples by proteins that interact non-specifically with the bead-^{N}YB1 complex. Coommassie staining of the bead-only control confirmed that negligible contamination came from the bead-^{N}YB1 complex. However, proteins that interact non-specifically with YB-1, or its interaction partners, will be present in these samples. Keratins can accrue after IP and the keratins that were detected are likely to be of no relevance to the function of YB-1. Subcellular fractionation mitigated another source of non-specific contamination of immunoprecipitations; proteins that have a high affinity for one another but that never come into contact due to their subcellular localisation (Mellacheruvu et al. 2013). However, contaminating proteins will be present through non-specific interactions with YB-1, or its binding partners, and these are difficult to identify. These contaminating proteins may also behave like transient binding partners. However, the interaction of YB-1 with ribosomes and cytoskeletal proteins was consistent with the known functions of YB-1.

These observations are consistent with the findings that YB-1 adheres to newly transcribed RNAs (Hartmuth et al. 2002, Wolf et al. 2009, Dutertre et al. 2010).

Many of the proteins that are detected interacting with YB-1 are RNA-binding proteins that will also adhere to RNAs at some point in their lifecycles (for more discussion see **Chapter 1.8.3**). Therefore, many of the protein interactions may be mediated by the shared interaction of a protein and YB-1 with another protein or the same RNA transcript.

YB-1 that is binding to RNA in the nucleus should interact with the large number of proteins that comprise the protein machinery that processes nascent RNA to mRNA; spliceosomes are some of the biggest macromolecular complexes in the cell (Chen & Manley 2009). Most of the PPI of YB-1 from nuclei appeared to reflect the role of YB-1 in splicing and RNA processing. Many of these PPI were also found in YB-1 from the cytoplasm, indicating the recovery of other RNA binding proteins that remain with RNA transcripts throughout their lifecycle.

The components of the transcriptional machinery were not unambiguously identified, the presence of proteins that associate with chromatin (**Table 4.2**, Protein-DNA complex:chromosome) confirmed the interaction of YB-1 with DNA. A small amount of YB-1 was found in the nucleus of cancer cells where it appears to interact with DNA as well as RNA (**Figure 3.5**). Therefore, these data do not necessarily support the notion that YB-1 only influences cancer via RNA mechanisms.

There have been reports that YB-1 is capable of influencing chromatin structure (Davies et al. 2014). Two mechanisms have been proposed although both require further validation. The first mechanism is that YB-1 stabilises the histone acetyltransferase p300 through AKT that leads to chromatin remodelling (Davies et al. 2014). Davies et al. (2014) also proposes that YB-1 can increase the chromatin remodelling activity of p300 which in turn, allows YB-1 to function as a transcription factor for target genes. p300 was not detected in this work.

Although DNA-associated proteins represented a small proportion of interacting proteins, the small percentage of YB-1 that interacts with DNA could still have a significant effect. YB-1 that is binding to DNA is expected to interact with far fewer proteins as transcription can be initiated by <35 proteins (Murakami et al. 2013). An enrichment of annotations can provide insights into the function of protein groups although it does not rank the biological importance of each functional group. For YB-1, the processes that it participates in while binding to RNA (splicing, translation) require the cooperation of many proteins.

Concentrating on the expression of a single gene can illustrate how the relatively weak enrichment of annotations for chromatin, amongst the proteins that are detected, could still be influential. As a transcription factor, YB-1 may bind to the

promoter of this gene to create many transcripts through its action as a dominant transacting factor. As an RNA binding protein, many YB-1 molecules need to bind to many RNA transcripts from this same gene to have a dominant transacting influence. Furthermore, it is likely that multiple YB-1 molecules per RNA transcript are required.

4.3.4 Summary

The work outlined here supports the notion that YB-1 is a multifunctional protein that is highly likely to participate in many processes in a single population of cells. The majority of these processes are related to RNA metabolism and this is consistent with the localisation of YB-1 in MDA-MB231 cells (**Chapter 3.5**). A small subset of the proteins that copurified with YB-1 interact with DNA but they do not provide strong evidence that YB-1 interacts with DNA as a transcription factor.

YB-1 has many functions in cancer (**Chapter 1.4**) and the subsequent research in this thesis focuses on the function of YB-1 in drug resistance. Exposure to a chemotherapuetic agent, where cells require YB-1 to survive the exposure, is hypothesised to modulate the function of YB-1 to a process that promotes survival.

Chapter 5

YB-1 confers resistance to genotoxic stress treatment of MDA-MB231 cancer cells

5.1 Introduction

The protein interactions of YB-1 in MDA-MB231 and A549 cells indicated that YB-1 was participating in a wide range of processes in dividing cancer cells (**Chapter 4**). Notably, the protein interactions of the YB-1 in the nucleus of these cells indicated that the critical function of YB-1 in the nucleus most likely relied on YB-1 binding to RNA. The well documented role of YB-1 as a transcription factor (**Chapter 1.8.2.1**) did not receive direct support, as YB-1 only interacted with a small number of proteins that were associated with DNA binding in the nucleus (**Chapter 4**). This led to interest in the function of YB-1 during other events that were relevant to cancer. Exposure to chemotherapeutic drugs was chosen as YB-1 can protect cells during chemotherapy and this protection appears to require the interaction of YB-1 with DNA (**Chapter 1.4.3**; discussed below). However, a wide range of drugs and drug concentrations have been used to assess the functions of YB-1 during drug exposure (Fujii et al. 1994, Chattopadhyay et al. 2008, Guay et al. 2008a, Garand et al. 2011). Therefore, it was not clear how to select the appropriate drug and exposure conditions to assess the molecular functions of YB-1 during drug exposure.

This chapter examined the importance of YB-1 to the survival of a TNBC cell line, MDA-MB231, during exposure to a variety of chemotherapeutic agents. As previously noted (**Chapter 1.4.3**), the biochemical activity of YB-1 in cancers dur-

ing their exposure to chemotherapeutic agents is still unclear. However, the of YB-1 activity could functions as a transcription factor or a DNA repair protein. YB-1 may directly interact with DNA to repair damage from DNA damaging agents. Therefore, initially four common chemotherapeutic drugs with different mechanisms of action were studied; paclitaxel, doxorubcin, camptothecin, and cisplatin. Paclitaxel is a microtubule-stabilizing agent (Blagosklonny & Fojo 1999) and members of this drug family are used to treat TNBC. Doxorubicin is also used to treat TNBCs. Doxorubicin can intercalculate with DNA to block DNA replication. The ability of doxorubicin to kill cancer cells is thought to be mediated by its stabilisation of DNA topoisomerase II on DNA which blocks DNA replication (Tacar et al. 2013). Camptothecin inhibits the progression of cells through S-phase by stabilising DNA topoisomerase I that is complexed with DNA (Liu et al. 2000). The stabilised complex then has potential to collide with replication forks during S-phase. Camptothecin is not currently used to treat TNBC but analogues are used for colon, ovarian, cervical, and small cell lung cancers. Cisplatin interacts with DNA and can cross-link DNA base-pairs to one another. The mode of action for cisplatin is not fully understood. Cisplatin is not a common treatment for breast cancers but there is renewed interest in using platinum-based therapies, cisplatin and carboplatin, to treat TNBC (Byrski et al. 2014, Petrelli et al. 2014). TNBC appear to benefit specifically from the inclusion of cisplatin in neoadjuvant therapy, as measured by pathologic complete response (Petrelli et al. 2014). Recent work has highlighted that cisplatin may be an effective treatment for drug-resistant TNBCs that carry amplification of the BRCA1 gene (Byrski et al. 2014).

The work in this chapter aimed to confirm the importance of YB-1 to the drug resistance of MDA-MB231 cells. The role of YB-1 in the drug resistance of MDA-MB231 cells was tested using depletion of *YBX1* mRNA and YB-1 followed by exposure to chemotherapeutic drugs. The central motivation of this work was to define drug exposure conditions in which MDA-MB231 cells could only survive when YB-1 was present. These conditions would be ideal for a robust assessment of how drug exposure alters the molecular functions of YB-1 by assessing the PPI of YB-1 during cisplatin exposure. Portions of this work are included in Lasham et al. (2016) and were also presented at *The DNA damage response in cell physiology and disease* (EMBO conference, October 2013, Greece).

5.2 Results

5.2.1 Depleting YB-1 impairs the growth and survival of MDA-MB231 cells

To assess the role of YB-1 in drug resistance YB-1 was depleted from MDA-MB231 cells prior to the addition of drugs. These experiments provided data about the effects of depleting YB-1 on the growth and viability of MDA-MB231 cells. This section focuses on these data. The design of the experiments in this chapter was outlined in **Chapter 2.9** and **Figure 2.1**. Briefly, MDA-MB231 cells were allowed to settle for 24 hr in the presence of a non-targeting siRNA duplex (siCTRL) or one of two siRNA duplexes directed against YB-1 (siYB1_1 and siYB1_2). The transfection media were replaced with media containing 10% bovine foetal calf serum and the confluence of each well was monitored every 2 - 3 hrs for 120 hrs using an Incucyte FLR.

Immunoblotting confirmed that YB-1 was depleted 72 hrs after transfection with siYB1_1 and siYB1_2 (**Figure 5.1.A**). The siRNA duplex siYB1_1 appeared to deplete YB-1 more efficiently than YB1_2, which was consistent with previous observations for these siRNA duplexes (A. Braithwaite, personal communication). Transfecting MDA-MB231 cells with 5 nM siYB1_2 had a similar effect on YB-1 levels as the transfection with 1 nM siYB1_1. Ponceau S staining of the membranes indicated even loading of proteins. However, the resolution of the immunoblots did not provide sufficient resolution to quantify the degree of YB-1 depletion from the siRNA duplexes and the transfection efficiency was not confirmed.

The confluence of MDA-MB231 cells following transfection with siCTRL, or either of the transfection controls (media-only and transfection reagent only), reached plateaus after 55 - 96 hrs (representative plot showing cell confluence following transfection with 5 nM siRNA duplexes is shown in **Figure 5.1.B**). Depleting YB-1 with either siYB1_1 or siYB1_2 reduced the confluence of MDA-MB231 cells throughout the 120 hrs of monitoring (representative plot showing cell confluence following transfection with 5 nM siRNA duplexes is shown in **Figure 5.1.B**).

The maximal growth-rate of the MDA-MB231 cells was estimated using the confluence data that was collected every 2 hours during the experiments (outlined in **Chapter 2.9**). Using confluence data to derive the growth-rate means that the growth-rate measurements represent the maximum rate of expansion of the cell population. The maximal growth-rate may reflect changes in the rate of cell

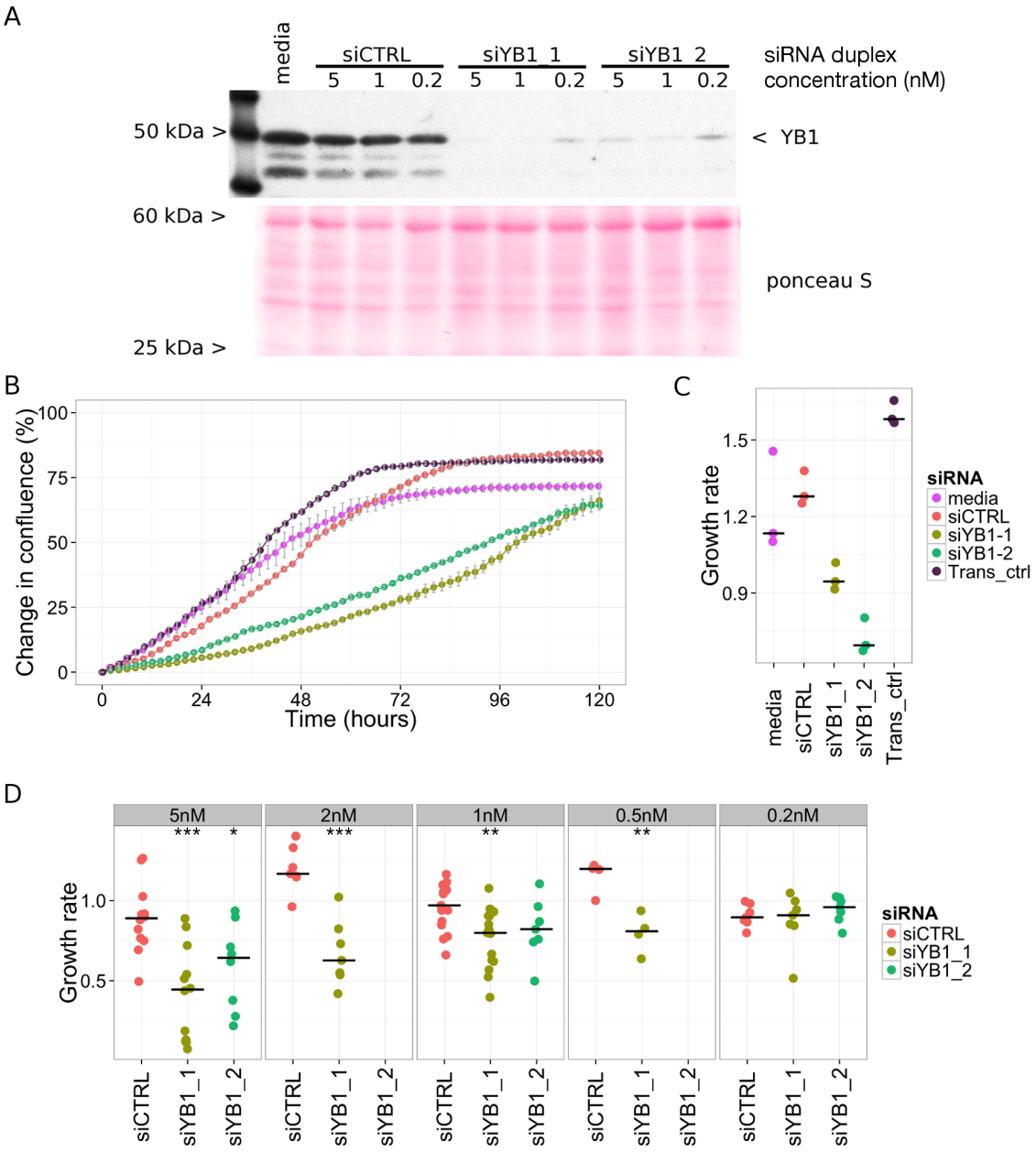

Figure 5.1: Depleting YB-1 reduces the growth-rate of MDA-MB231 cells. **A**, representative immunoblot showing the depletion of YB-1 in MDA-MB231 cells 72 hrs after the transfection with either of two siRNA duplexes directed against YB-1 (siYB1_1 and YB1_2) but not when a scrambled siRNA duplex is used (siCTRL). **B**, plot showing the change in confluence from the MDA-MB231 cells following transfection over 120 hrs (n = 1). **C**, maximal growth-rates that were derived from the confluence data in **C**. **D**, plot showing the maximal growth-rates from all experiments where YB-1 was depleted in MDA-MB231 cells during experimental work for this thesis. The siRNA duplexes are non-targeting or directed against YB-1 and used at a concentration ranging from 0.2 - 5nM as indicated above each panel. One-tailed t-tests were used to compare the growth-rates of MDA-MB231 cells following transfection with siCTRL and siYB1 each concentration of siRNA duplex. The hypothesis used for the test was that depleting YB-1 reduced the growth-rate of MDA-MB231 cells; * =p <0.05, ** = p <0.01, *** = p <0.001. **Abbreviations**; media = no transfection reagents, Trans_ctrl = transfection reagent control, siCTRL = scrambled siRNA duplex, siYB1_1 or 2 = two siRNA duplex directed against YB-1.

Table 5.1: Depleting YB-1 reduced the growth-rate of MDA-MB231 cells.

siRNA	Concentration (nM)	Reps	Growth-rate ± S.E.	p-value (t-value)
siCTRL	5	12	0.895 ± 0.063	-
siYB1_1	5	12	**0.418 ± 0.085**	**0.0001142 (-4.4654)**
siYB1_2	5	8	**0.588 ± 0.096**	**0.04634 (-1.8407)**
siCTRL	2	7	1.195 ± 0.053	
siYB1_1	2	7	**0.673 ± 0.077**	**<0.0001 (-5.5869)**
siCTRL	1	15	0.958 ± 0.038	
siYB1_1	1	15	**0.762 ± 0.048**	**0.001842 (-3.1836)**
siYB1_2	1	7	0.822 ± 0.072	0.1485 (-1.0936)
siCTRL	0.5	4	1.153 ± 0.051	
siYB1_1	0.5	4	**0.798 ± 0.062**	**0.002431 (-4.4171)**
siCTRL	0.2	7	0.905 ± 0.026	
siYB1_1	0.2	7	0.872 ± 0.066	0.3267 (-0.4667)
siYB1_2	0.2	7	0.943 ± 0.031	0.8178 (0.9439)

One-tailed t-tests, Welch Two Sample t-tests, were used to compare the growth-rate of MDA-MB231 cells following the depletion of YB-1. The hypothesis used for the test was that depleting YB-1 reduced the growth-rate of MDA-MB231 cells. Significant differences are shown as bold text (p-value <0.05). **Abbreviations**; Reps = replication. S.E. = standard error of the mean.

division, changes in cell survival, and/or changes in cell size. The images from each experiment were carefully inspected to monitor for changes in cell morphology and any apparent changes in the morphology of cells have been highlighted in the results. The maximal growth-rates that are derived from the confluence data in **Figure 5.1.B** show that depleting YB-1 appears to reduce the growth-rate of MDA-MB231 cells (**Figure 5.1.C**). To confirm this observation the maximal growth-rates from all of the experiments in this thesis were compared between non-targeting and YB-1 siRNA duplexes (**Figure 5.1.D**. The results from statistical comparisons and replication are shown in **Table 5.1**). The results show that depleting YB-1 using siYB1_1 (0.5 - 5 nM) or siYB1_2 (5 nM) reduces the growth-rate of MDA-MB231 cells. Therefore, it was confirmed that depleting YB-1 does reduce the growth-rate of MDA-MB231 cells.

The experiments described in **Chapter 5.2.3** and **Chapter 5.2.4** also monitored the death of cells. This was carried out by including YOYO-1 Iodide in the growth media and the acquisition of fluorescent images with an excitation of 470 nm max and emission of 515 nm every 3 hrs for 120 hrs. YOYO-1 Iodide is cell-impermeant and produces fluorescence when it intercalculates with DNA from cells

where the cell membrane is no longer intact (outlined in **Chapter 2.9**). The data from YOYO-1 Iodide fluorescence are were normalised to produce a measure that is termed death index (Death index is; log-transformed[(confluence of the fluorescent signal / confluence of the cells)]; further details in **Chapter 2.9**).

Representative images show that depleting YB-1 appeared to increase the number of non-viable cells (green signal in **Figure 5.2.A**). The death index of MDA-MB231 cells 120 hrs after transfection with siCTRL, siYB_1 or siYB_1 (0.2 - 5 nM) was compared to confirm that depleting YB-1 increased the rate of cell-death. The results show that the death index was increased in MDA-MB231 cells 120 hrs after depleting YB-1 using either siYB1_1 or siYB1_2 at one or 5 nM (**Figure 5.2.B**). Therefore, the results from these experiments show that depleting YB-1 increased rates of cell death in MDA-MB231 cells.

Depleting YB-1 reduces the growth-rate of MDA-MB231 cells. Data from a fluorescent marker of non-viable cells indicated that this reduction was in part explained by increased levels of cell death, or reduced cell viability, following the depletion of YB-1. The results in the following sections focus specifically how depleting YB-1 alters the response of MDA-MB231 cells to drug exposures.

5.2.2 Depleting YB-1 impairs the growth of MDA-MB231 cells during exposure to chemotherapeutic drugs

YB-1 has an affinity for modified DNA and has been reported to protect cells during events that alter DNA (Ohga et al. 1996). In this thesis, YB-1 was hypothesised to contribute to the resistance of MDA-MB231 cells to chemotherapeutic drugs that modify DNA. The contribution of YB-1 to the tolerance of MDA-MB231 cells to various drugs was tested by depleting YB-1 in MDA-MB231 cells prior to their exposure to the drugs. The design of this experiment was outlined in **Chapter 2.9** and **Figure 2.1**. Briefly, MDA-MB231 cells were allowed to settle for 24 hr in the presence of a non-targeting siRNA duplex (siCTRL) or one of two siRNA duplexes directed against YB-1 (siYB1_1 and siYB1_2). The transfection media were removed and replaced with media containing drugs. Four drugs were added in dilution series; cisplatin (7.5, 12.5, 25, 50, or 100 μM), camptothecin (0.1, 1, 2.5, 5, or 10 μM), paclitaxel (0.1, 1, 10, 100 nM, 1, or 10 μM), and doxorubicin (0.1, 1, 5, 10, 20 μM). The confluence of each well was monitored every two hrs for 120 hrs using an Incucyte FLR.

This experiment focussed on the importance of YB-1 to MDA-MB231 cells dur-

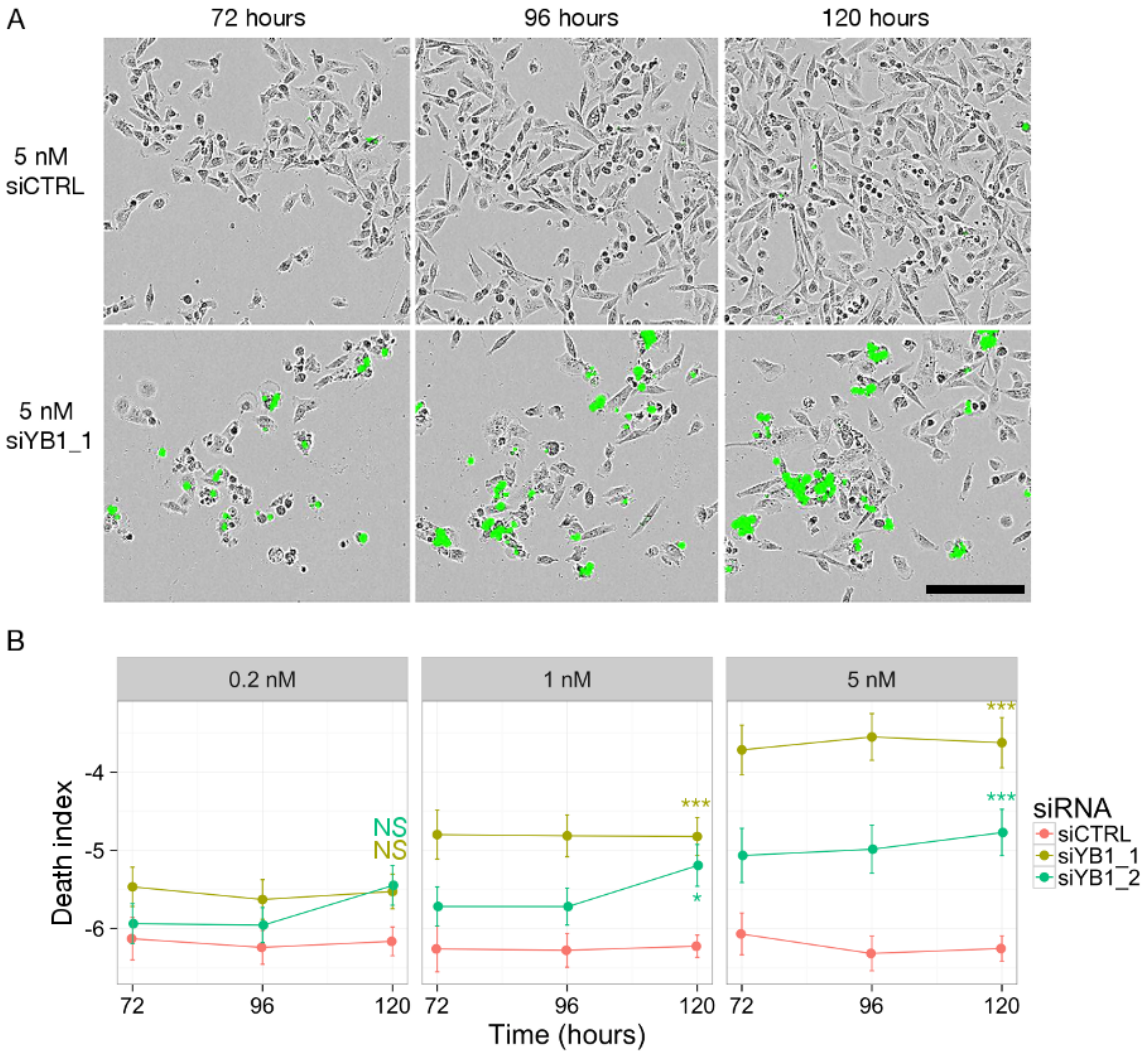

Figure 5.2: YB-1 promotes the viability of MDA-MB231 cells. **A**, representative composite images show phase-contrast and YOYO-1 Iodide fluorescence from MDA-MB231 cells 72 - 120 hrs after transfection with siRNA duplexes. **B**, the effects of transfection with a scrambled siRNA duplex (siCTRL) or one of two siRNA duplexes directed against YB-1 (siYB1_1 or siYB1_2) on the death index of MDA-MB231 cells (n = 7). Death index = log-transformed[(confluence of the fluorescent signal / confluence of the cells)]. ANOVA was used to compare siCTRL to siYB1_1 or siYB1_2 at 120 hrs, Tukeys honestly significant differences were used to compare the effects of changing the concentration of siRNA duplexes on cell viability; NS = non-significant, * = p <0.05, *** = p <0.001. Scale bar represents 200 μm.

ing exposure to 4 drugs. The results from the drug exposures indicate that YB-1 participates in a process, or several processes, that protect MDA-MB231 cells from all 4 chemotherapeutic drugs that were tested. To compensate for the reduction in growth-rate that resulted from depleting YB-1 (**Figure 5.1.C**), the response of the cells was calculated by normalising the maximal growth-rates for each transfection (described in **Chapter 2.9**). Supplementary figures D.1 - D.4 provide plots showing the change in confluence during the 120 hr monitoring period as well as response plots showing how individual wells respond to drug exposure.

Depleting YB-1 sensitises MDA-MB231 cells to the microtubule-stabilizing agent paclitaxel (**Figure 5.3.A**). The results highlight that at 0.1 μM paclitaxel, the lowest concentration of paclitaxel used, depleting YB-1 with either siRNA duplex reduced the growth of MDA-MB231 cells below 50% response (0.55 ± 0.06 for siCTRL compared to 0.02 ± 0.01 for siYB1_1 and 0.35 ± 0.01 for siYB1_2; **Figure 5.3.A**). The absence of lower concentrations of paclitaxel in the experiment made the ED_{50} estimates from the log-logistic models unreliable.

The other drugs in this experiment derive their toxicity through their ability to inhibit DNA synthesis. Each drug achieves this via different mechanisms. The results show that depleting YB-1 sensitises MDA-MB231 cells to camptothecin (**Figure 5.3.B**). Depleting YB-1 reduced the growth-rate of MDA-MB231 cells in the presence of as little as 0.1 μM camptothecin. This contrasts with the control MDA-MB231 cells where the maximal growth-rate was unaffected by exposure to 0.1 μM camptothecin (**Figure 5.3.B**). However, after 72 hrs of exposure to 0.1 μM camptothecin the confluence of the control cells ceased to increase before reducing, possibly indicating cell death (**Supplementary figure D.2.A** siCTRL).

The results also indicate that depleting YB-1 sensitised MDA-MB231 cells to the presence of cisplatin (**Figure 5.3.C**). The maximal growth-rate of the control MDA-MB231 cells had a response of 0.58 ± 0.03 in the presence of 7.5 μM cisplatin. Depleting YB-1 reduced the growth-rate of MDA-MB231 cells in all concentrations of cisplatin, reducing to 0.05 ± 0.08 and 0.37 ± 0.02 for siYB1_1 and siYB1_2 respectively in the presence of 7.5 μM cisplatin. Therefore, YB-1 does play a role in protecting MDA-MB231 cells from cisplatin.

The results from this experiment also showed that depleting YB-1 sensitised MDA-MB231 cells to doxorubicin exposure (**Figure 5.3.D**). Exposure to 0.1 μM doxorubicin reduced the response of siCTRL-transfected MDA-MB231 cells to 0.80 ± 0.17. Depleting YB-1 reduced the response of these cells to 0.12 ± 0.07 and 0.35 ± 0.02 for the siYB1_1 and siYB1_2 siRNA duplexes respectively.

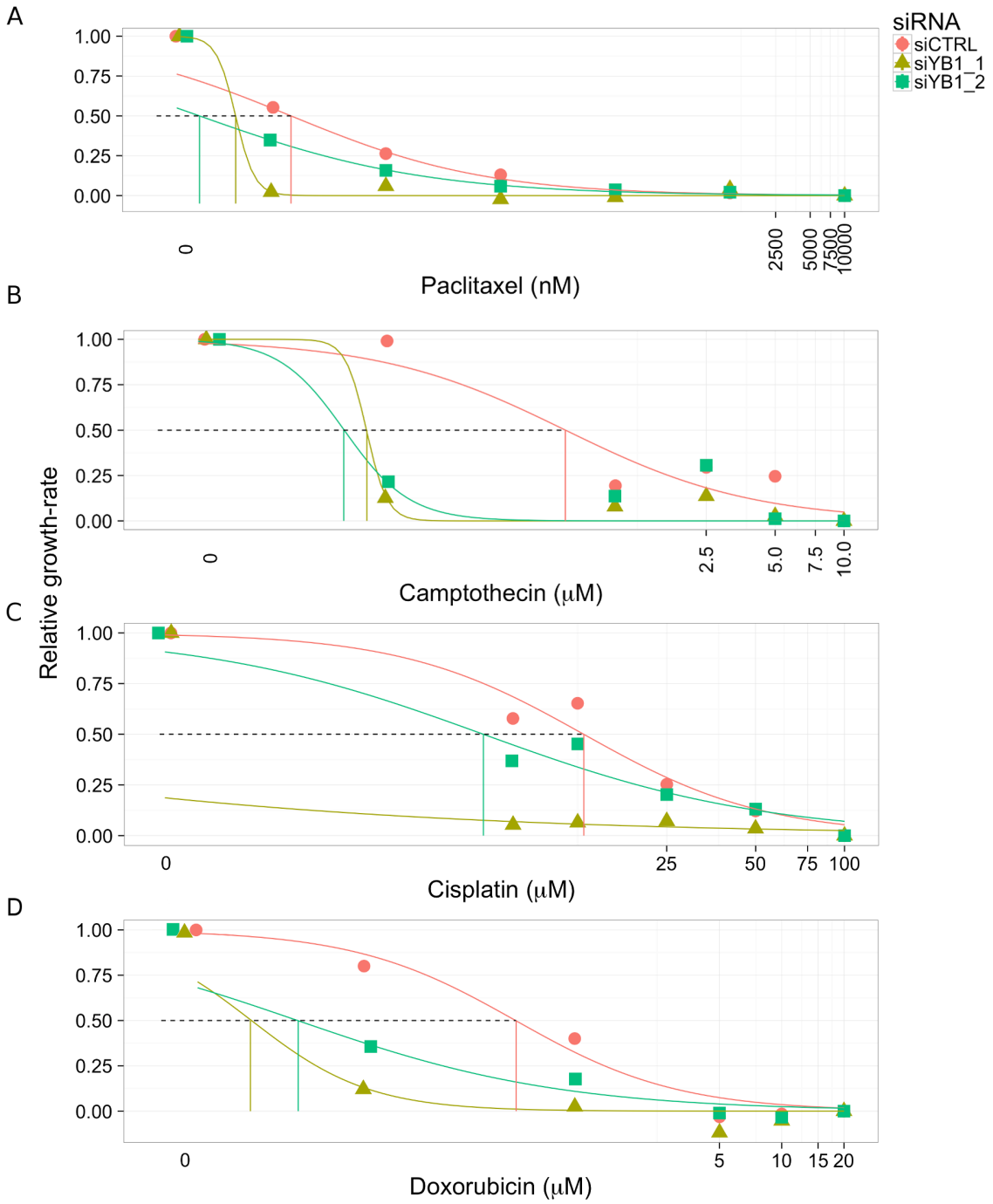

Figure 5.3: Depleting YB1 increases the sensitivity of MDA-MB231 cells to drugs with a range of mechanisms of action. MDA-MB231 cells were transfected with a non-targeting siRNA duplex (siCTRL) or one of two siRNA duplexes directed against YB-1 (siYB1_1 and siYB1_2; n = 1). The maximal growth-rate of the cells in paclitaxel (0.1, 1, 10, 100 nM, 1, 10 μM); **A**), camptothecin (0.1, 1, 2.5, 5, 10 μM; **B**), cisplatin (7.5, 12.5, 25, 50, or 100 μM; **C**), and doxorubicin (0.1, 1, 5, 10, 20 μM; **D**) was derived using the confluence of the MDA-MB231 cells that were monitored for 120 hrs. The response to drug was calculated as outlined in **Chapter 2.9**. Dotted horizontal lines indicates a 50% reduction in relative growth-rate. Vertical lines show the drug concentration where this 50% reduction occurred.

In summary, depleting YB-1 sensitises MDA-MB231 cells to all of the compounds that were tested. Therefore, YB-1 appears to protect MDA-MB231 cells during exposure to a range of toxic compounds despite each possessing a different mechanism for killing cells. The ability of YB-1 to support cellular survival during exposure to a range of threats does not appear to be consistent with the primary role of YB-1 during drug exposure being to participate in processes that repairing the damage caused by drugs. It is more consistent with YB-1 having a regulatory role during drug exposure. Of the chemotherapeutic drugs that were tested in this experiment, doxorubicin and cisplatin were selected for further examination. Doxorubicin was selected as it is a common chemotherapeutic for TNBC. Cisplatin was selected due to the renewed evidence that it may be an effective treatment for a subset of TNBCs in conjunction with previous reports that YB-1 promotes the survival of cells during cisplatin exposure (**Chapter 1.4.3**).

5.2.3 Sensitivity of MDA-MB231 cells to doxorubicin

The preceding experiment led to the hypothesis that YB-1 helps to maintain the viability of MDA-MB231 cells during doxorubicin exposure. The experiments used to test this hypothesis was similar to those outlined in **Chapter 5.2.2** but they differed as each siRNA duplex (siCTRL, siYB1-1, and siYB1-2) was used at three concentrations; 0.2 nM, 1 nM, and 5nM (outlined in **Chapter 2.1**). Doxorubicin was included as a 1:1 dilution series starting at 10 μM and ending at 0.165 μM. Cell death was monitored via the inclusion of YOYO-1 Iodide in the media.

These experiments assessed the importance of YB-1 to MDA-MB231 cells during doxorubicin exposure. The response curves and confluence plots indicate that depleting YB-1 slows the growth-rate of MDA-MB231 cells in doxorubicin (**Supplementary figures D.5 - D.8**). However, careful examination of the phase-contrast images highlighted that the MDA-MB231 cells ceased to divide within the first 48 hrs of exposure to $\geq$ 0.156 μM doxorubicin. Therefore, during doxorubicin exposure the maximal growth-rate data represented the expansion of cells rather than cell-division.

The increased confluence of MDA-MB231 cells in doxorubicin was caused by the cells expanding, which began to occur after 48 hrs exposure to doxorubicin (**Figure 5.4**, *media* inset shows normal size of MDA-MB231 cells). For the final 72 hrs of the experiments, the morphology of MDA-MB231 cells, which were transfected with siCTRL siRNA duplex, remained enlarged (**Figure 5.4**). Furthermore, the lack of

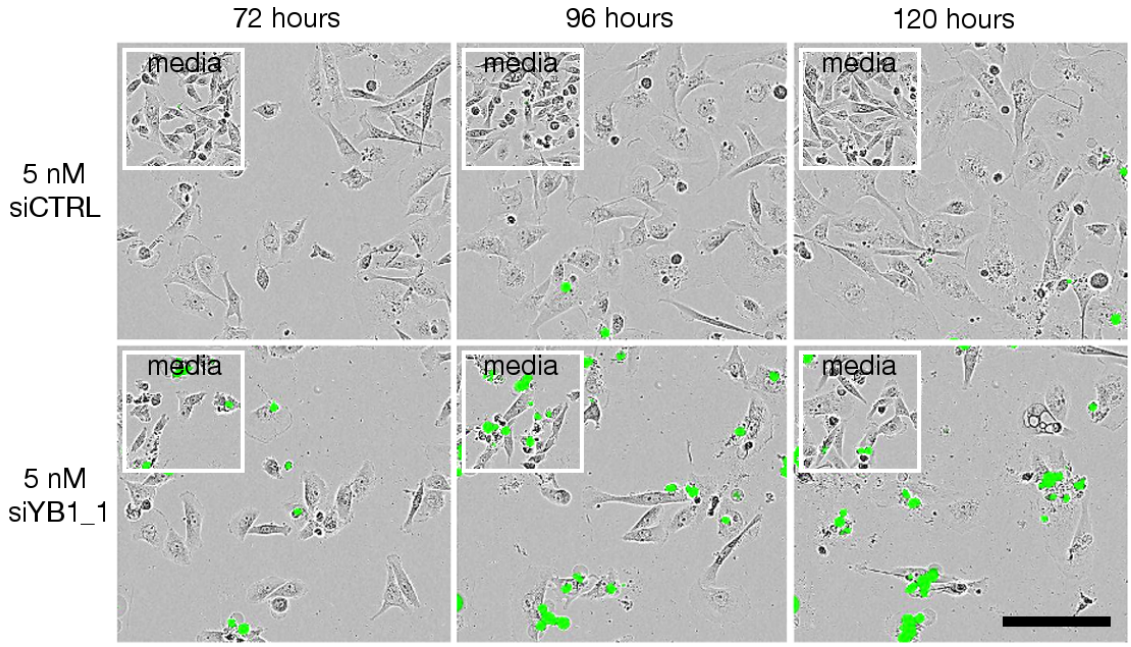

Figure 5.4: YB-1 contributes to the survival of MDA-MB231 cells during doxorubicin exposure. Representative composite images show MDA-MB231 cells 72 - 120 hrs after transfection with a scrambled siRNA duplex (siCTRL) or one of two siRNA duplexes directed against YB-1 (siYB1_1) are grown in the presence of 0.156 μM doxorubicin. The images are merged phase-contrast and fluorescence (excitation, 470 nm max; 450 - 490 nm/emission, 515 nm max; 500 - 530 nm) taken with a 10 × objective lens that are representative of those from the three replicate experiments (n= 3). The insets, labelled "media", show the transfected cells grown in media at a matching magnification. Scale bar represents 200 μm.

fluorescent signal above most cells indicates that the majority of these cells had intact membranes and were probably still viable. The absence of cell division, in addition to the morphology and apparent viability of the cells in 0.165 μM doxorubicin, suggested that these cells were senescent. However, the cells would need to progress through the cell cycle in the presence of doxorubicin to enter a senescent state and this was not confirmed.

The depletion of YB-1 did not stop MDA-MB231 cells from becoming larger while in the presence of 0.156 μM doxorubicin (**Figure 5.4**, *media* inset shows normal size of MDA-MB231 cells). However, depletion of YB-1 did lead to cells disappearing after 72 hrs of exposure to 0.156 μM doxorubicin. Fluorescence from YOYO-1 Iodide above many of the cells highlighted that death was occurring (**Figure 5.4**). The disparity between the size of the control and YB-1 depleted MDA-MB231 cells precluded the reliable normalisation of the fluorescence data. Therefore, a qualitative analysis was performed. Depleting YB-1 appears to cause most MDA-MB231 cells to die during doxorubicin exposure. The focus of further work in this thesis is limited to the role of YB-1 during cisplatin exposure (see following section).

The concentration and duration of doxorubicin exposure meant that exposing MDA-MB231 cells to doxorubicin caused them to cease dividing, although cell death was relatively infrequent. Depleting YB-1 prior to doxorubicin exposure strongly reduced the viability of MDA-MB2331 cells. Therefore, YB-1 participates process(es) that maintains the viability of the MDA-MB231 cells during exposure to doxorubicin.

5.2.4 Sensitivity of MDA-MB231 cells to cisplatin

For these experiments, YB-1 was hypothesised to protect MDA-MB231 cells during exposure to cisplatin. The use of cisplatin (0, 1.56, 3.125, 6.25, 12.5, 25, 50 μM), rather than doxorubicin, is the only modification to the experimental protocol from the previous section (**Chapter 5.2.3**).

It has already been noted that depleting YB-1 reduces the growth-rate of MDA-MB231 cells (**Figure 5.1.D** and **Figure 5.2**). Plots of the confluence data highlight the negative effects of YB-1 depletion and of cisplatin exposure on the growth of MDA-MB231 cells (all growth plots in **Supplementary figures D.9 - D.11**). The confluence data from experiment three highlighted that growth can be reduced to almost zero when transfections are performed with 5 nM siYB1_1 and siYB1_2 (**Figure D.9**, experiment 3). In that experiment, the strong impairment of survival

that accompanied transfection with 5 nM siYB1_1 or siYB1_2 meant that there were no cells to assess the effects of cisplatin exposure. This reduced the replication to two experiments for the 5 nM transfections. Therefore, statistical comparisons were not made at the 5 nM level.

YB-1 was hypothesised to protect MDA-MB231 cells during cisplatin exposure. To examine the effects of YB-1 depletion on the growth-rate of MDA-MB231 cells in the presence of cisplatin, the change in growth-rate from the media only for that siRNA duplex and siRNA duplex concentration was calculated (response). These response curves were used to derive an estimate of the median effective dose (ED_{50}), an estimate of a concentration where 50% of the cells would die (for further details see **Chapter 2.9**). The results show that depleting YB-1 reduces the ED_{50} estimates for MDA-MB231 cells in cisplatin (**Figure 5.5**; statistics summarised in **Table 5.2**). Included in this analysis are the results from a separate series of experiments where YB-1 was depleted using 2 nM siYB1_1. This experiment included a narrower range of cisplatin concentrations (1.56 - 12.5 μM cisplatin). The reduced range of cisplatin concentrations lowered the ED_{50} estimates but the estimates were consistent within the experiment. Depleting YB-1 with 2 nM siYB1_1 reduced the ED_{50} estimate for MDA-MB231 cells in cisplatin by 1.85 ± 0.69 μM cisplatin (p-value, 0.0087; **Table 5.2**). Similarly, depleting YB-1 with 1 nM siYB1_1 reduced the ED_{50} estimate to 1.81 ± 0.68 μM cisplatin (p-value, 0.0001; **Table 5.2**). The ED_{50} estimates for cisplatin following the depletion of YB-1 with 1 nM or 0.2 nM siYB1_2 or 0.2 nM siYB_1, was significantly lower than the ED_{50} estimates for equivalent controls (**Table 5.2**). These experiments show that depleting YB-1 inhibits the growth-rate of MDA-MB231 cells during cisplatin exposure.

Representative images from these experiments highlight the negative effects of depleting YB-1 in MDA-MB231 cells prior to cisplatin exposure. The MDA-MB231 cells that continued to divide in the presence of 1.56 μM cisplatin had a similar phenotype and size to normal MDA-MB231 cells (**Figure 5.6.A**). Depleting YB-1 prior to cisplatin exposure altered the phenotype of MDA-MB231 cells so that many were shorter, with most cells showing signs of cell death. The size of MDA-MB231 cells in cisplatin was similar irrespective of YB-1 depletion (**Figure 5.6.A**, compared to insets).

The normalised data from YOYO-1 Iodide fluorescence, expressed as death index, were used to quantify the effects of YB-1 depletion on cell viability during cisplatin exposure. Depleting YB-1 increased levels of cell death in MDA-MB231 cells (**Figure 5.2**). The plotted cell viability data appears to confirm that cisplatin

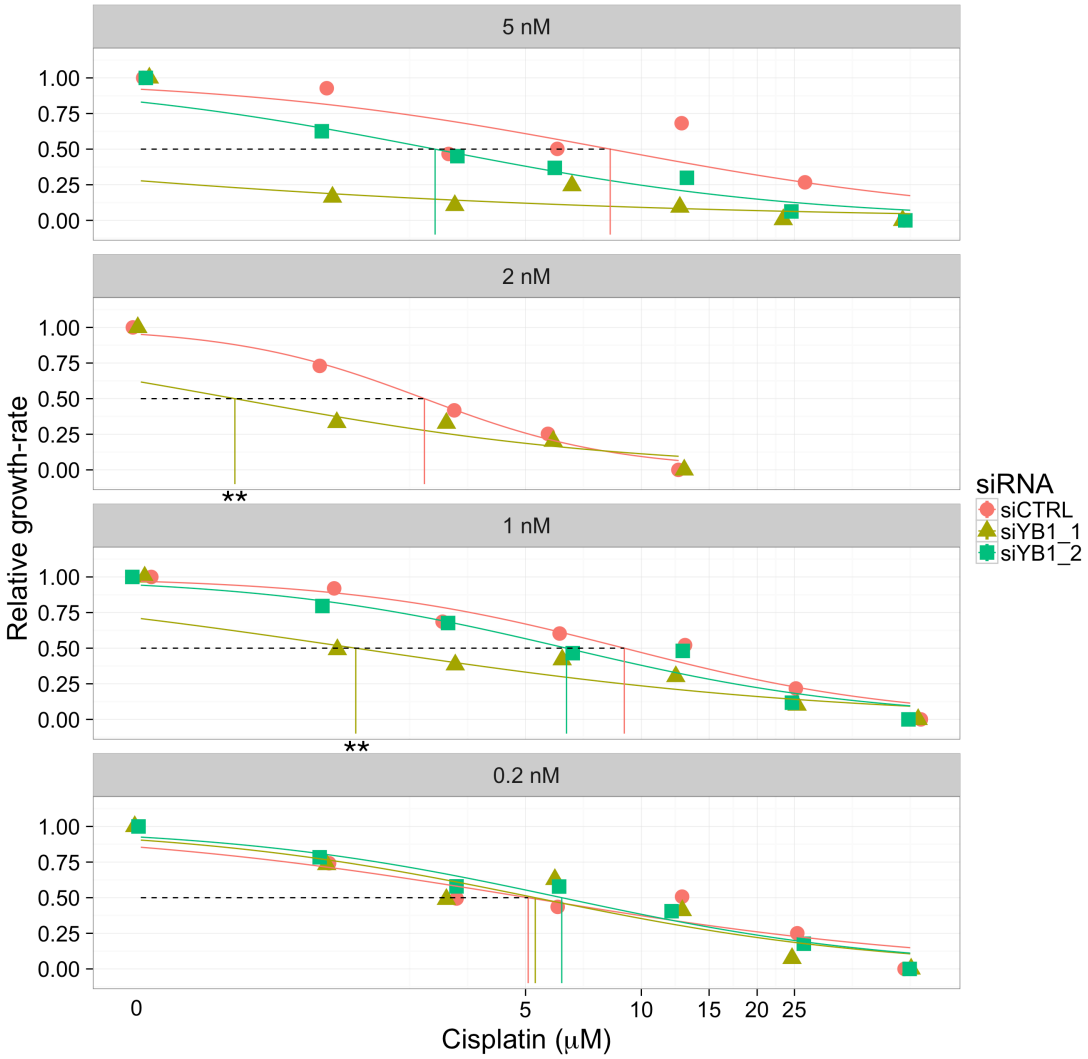

Figure 5.5: Depleting YB-1 reduces the growth-rate of MDA-MB231 cells during cisplatin exposure. The effects of varying concentrations of cisplatin (0, 1.56, 3.125, 6.25, 12.5, 25, 50 μM) on the growth-rate of MDA-MB231 cells with and without YB1 protein present. YB-1 was depleted using two siRNA duplexes directed against YB-1 (siYB1_1 and YB1_2) or the MDA-MB231 cells were transfected using a scrambled siRNA duplex (siCTRL). The maximal growth-rate was calculated using the confluence data and for each siRNA duplex, the response to drug is calculated as outlined in **Chapter 2.9**. See **Table 5.2** for further explanation of the statistical analysis. Dotted horizontal lines indicates a 50% reduction in relative growth-rate. Vertical lines show the drug concentration where this 50% reduction occurred. **Replication**; 5 nM, n= 2; 2 nM, n = 4; 1 nM and 0.2 nM n = 3. **Abbreviations**; ** = p <0.01, *** = p <0.001.

Table 5.2: Depleting YB-1 reduced the growth-rate of MDA-MB231 cells during exposure to cisplatin (0 - 50 μM).

siRNA	Concentration	Reps	ED_{50} ± S.E. (μM)	Delta ± S.E. (μM)	p-value (t-value)
siCTRL	5	2	8.30 ± 2.12	-	-
siYB1_1	5	2	0.06 ± 0.21	-	-
siYB1_2	5	2	2.91 ± 0.80	-	-
siCTRL	2	4	2.73 ± 0.42	-	-
siYB1_1	2	4	0.88 ± 0.55	**-1.85 ± 0.69**	**0.0087 (2.690)**
siCTRL	1	4	9.03 ± 1.50	-	-
siYB1_1	1	3	1.81 ± 0.68	**-7.22 ± 1.64**	**0.0001 (4.3986)**
siYB1_2	1	3	6.39 ± 1.13	-2.64 ± 1.87	0.1640 (1.4107)
siCTRL	0.2	3	5.08 ± 1.47	-	-
siYB1_1	0.2	3	5.30 ± 1.08	0.22 ± 1.82	0.9039 (0.1214)
siYB1_2	0.2	3	6.21 ± 1.19	1.13 ± 1.89	0.5506 (-0.6010)

The dose-response curves were fitted using log-logistic regression. Estimates are for effective doses where 50% of the cells were killed by cisplatin (ED_{50}). T-tests were used to compare the ED_{50} following the depletion of each protein to the ED_{50} of the siCTRL RNA duplex, significant differences shown as **bold text** (p-value <0.05). 2 nM transfections were from a separate set of experiments with a reduced range of doses (1.56 - 12.5 μM cisplatin). Reps = replication. S.E. = standard error of the mean.

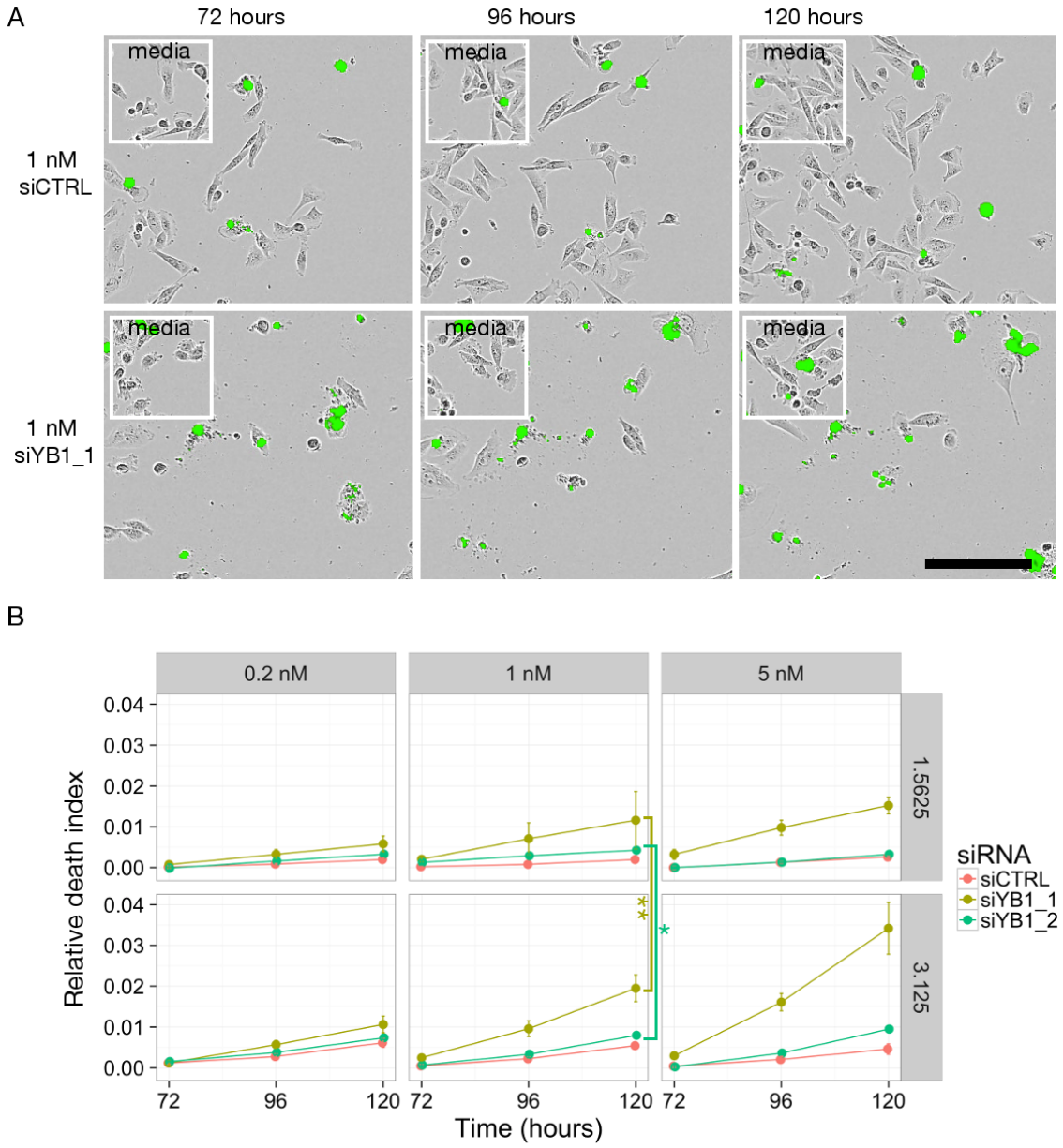

Figure 5.6: Depleting YB-1 impairs the survival of MDA-MB231 cells during cisplatin exposure. **A**, representative composite images show MDA-MB231 cells which have been maintained in media that included 1.56 µM for up to 120 hrs after transfection with 1 nM scrambled siRNA duplex (siCTRL) and siYB1_1, one of two siRNA duplexes directed against YB-1 (the other was siYB1_2). **B**, the change in the viability of MDA-MB231 cells during cisplatin exposure relative to cells in media. Relative death index was calculated as described in **Chapter 2.9**. The hypotheses that depleting YB-1 increased Relative death index during cisplatin exposure was tested using two-way analysis of variance; model = Relative death index ~ siRNA.concentration + drug. The images shown are merged phase-contrast and fluorescence (excitation, 470 nm max; 450 - 490 nm/emission, 515 nm max; 500 - 530 nm) that are representative of those from the three replicate experiments (n= 3 except for 5 nM siRNA duplexes where n = 2). The insets, labelled "media", show the transfected cells grown in media at a matching magnification. Scale bar represents 200 µM. **Abbreviations**; * = p <0.05, ** = p <0.01.

exposure further reduces the viability of MDA-MB231 cells (**Supplementary figure D.12**). There was a strong increase in the death index measurements following transfection with siCTRL MDA-MB231 cells and 120 hrs of exposure to 25 - 50 μM cisplatin. However, the growth-rate data indicates that depletion of YB-1 sensitises MDA-MB231 cells to much lower concentrations of cisplitin (1.56 - 3.13 μM).

The effects of depleting YB-1 were examined in greater detail using the cell viability measurements from cells that were exposed to the two lowest concentrations of cisplatin (1.56 and 3.125 μM cisplatin) for 120 hrs. The levels of cell death were assessed using Relative death index. This normalisation controls for the effects of YB-1 depletion on death index to provide a measure of the cell death that was induced by drug exposure (explained in detail in **Chapter 2.9**). The results confirm that exposing cells to 3.125 μM cisplatin increases cell death compared to cells exposed to 1.56 μM cisplatin (see rows *siYB1_1; 1.56 vs 3.13 μM* and *siYB1_2; 1.56 vs 3.13 μM* in **Table 5.3**; **Figure 5.6.B**). Depleting YB-1 also alters the Relative death index measurements (see rows *siYB1_1; transfections* and *siYB1_2; transfections* in **Table 5.3**; **Figure 5.6.B**).

The specific source of differences between the siRNA duplexes were examined using Tukey's honest significance tests. All possible combinations of the siRNA duplexes and concentrations were included in the post-hoc tests, but only the results from control versus YB-1 depletion that match in concentration are presented here (**Table 5.3**). Insufficient replication (n = 2) meant that post-hoc statistical comparisons were not made for 5 nM siRNA duplexes. Depleting YB-1, using either siYB_1 or siYB1_2, prior to cisplatin exposure increased the Relative death index measurements relative to siCTRL transfected cells (**Table 5.3**; **Figure 5.6.B**). The Relative death index measurements were unaffected when YB-1 was depleted with 0.2 nM siYB_1 or siYB1_2 (**Table 5.3**; **Figure 5.6.B**). Therefore, depleting YB-1 further impairs the viability of MDA-MB231 cells during cisplatin exposure.

The data from YOYO-1 Iodide signal indicates that depleting YB-1 reduces the viability of MDA-MB231 cells and that cisplatin exposure leads to further losses in viability. The cell viability data, expressed as Relative death index, from these experiments indicates that the reduced growth-rate that occurs following YB-1 depletion and cisplatin exposure, can in part be explained by elevated levels of cell death.

Another set of experiments were performed to assess how depleting YB-1 influences the survival of cells as they recover from a two hr exposure to cisplatin. This brief exposure should limit the damage in each cell to a discrete point in the mitotic

Table 5.3: Depletion of YB-1 increases Relative death index following 120 hrs exposure to cisplatin (1.56 - 3.13 μM; n = 3).

Comparison	Relative death index ± S.E.	p-value (F/t-value)
siYB1_1; 1.56 vs 3.13 μM	**0.0065 ± 0.0040**	**0.00247 (11.32)**
siYB1_1; transfections	-	**0.000008 (11.52)**
1 nM; siYB1_1 - siCTRL	**0.0120 ± 0.0097**	**0.0096255**
0.2 nM; siYB1_1 - siCTRL	0.0042 ± 0.0097	0.7667320
siYB1_2; 1.56 vs 3.13 μM	**0.0039 ± 0.0008**	**<0.000001 (95.701)**
siYB1_2; transfections	-	**0.000856 (6.034)**
1 nM; siYB1_2 - siCTRL	**0.0024 ± 0.0020**	**0.0120597**
0.2 nM; siYB1_2 - siCTRL	0.0013 ± 0.0020	0.3976222

The hypotheses that depleting YB-1 increased Relative death index during cisplatin exposure was tested using two-way analysis of variance; model = Relative death index ∼ siRNA.concentration + drug. Separate 2-way ANOVAs were performed for siYB_1 and siCTRL and and YB_2 and siCTRL. The main effects from the 2-way ANOVAs are shown in *italics*. Post-hoc tests were performed using Tukey multiple comparisons of means with selected tests shown. Significant differences are shown as **bold text**. S.E. = standard error of the mean.

cycle. Following the cisplatin exposure, the cells had the opportunity to recover from cisplatin-induced damage in the absence of the added stress of new damage occurring. For these experiments, YB-1 was depleted in MDA-MB231 cells (siRNA duplexes at 0.5, 1, 2 nM). Forty-eight hrs later the cells were exposed to 3.125 - 25 μM cisplatin for 2 hrs. The confluence of each well was monitored for 96 hrs after cisplatin exposure.

The results confirm that depleting YB-1 reduces the survival of MDA-MB231 cells following a two-hr exposure to cisplatin (n = 4; **Figure 5.7**; the statistical analyses are summarised in **Table 5.4**). Irrespective of the concentration used for the siRNA duplexes, depleting YB-1 reduced the ED_{50} estimates by half from ∼ 10 μM to ∼ 6 μM cisplatin (**Table 5.4**).

Together the data from these experiments supports the conclusion that loss of YB-1 reduces the viability of MDA-MB231 cells during or after cisplatin exposure. These experiments also indicated that 1.56 - 3.13 μM cisplatin is an appropriate concentration range to assess the molecular function of YB-1 during cisplatin exposure. Depletion of YB-1 with 0.2 nM siYB_1, or ≤1 nM siYB_2, did not sensitise MDA-MB231 cells to cisplatin exposure. This indicates that a small amount of YB-1 could still improve the viability of MDA-MB231 cells during cisplatin exposure.

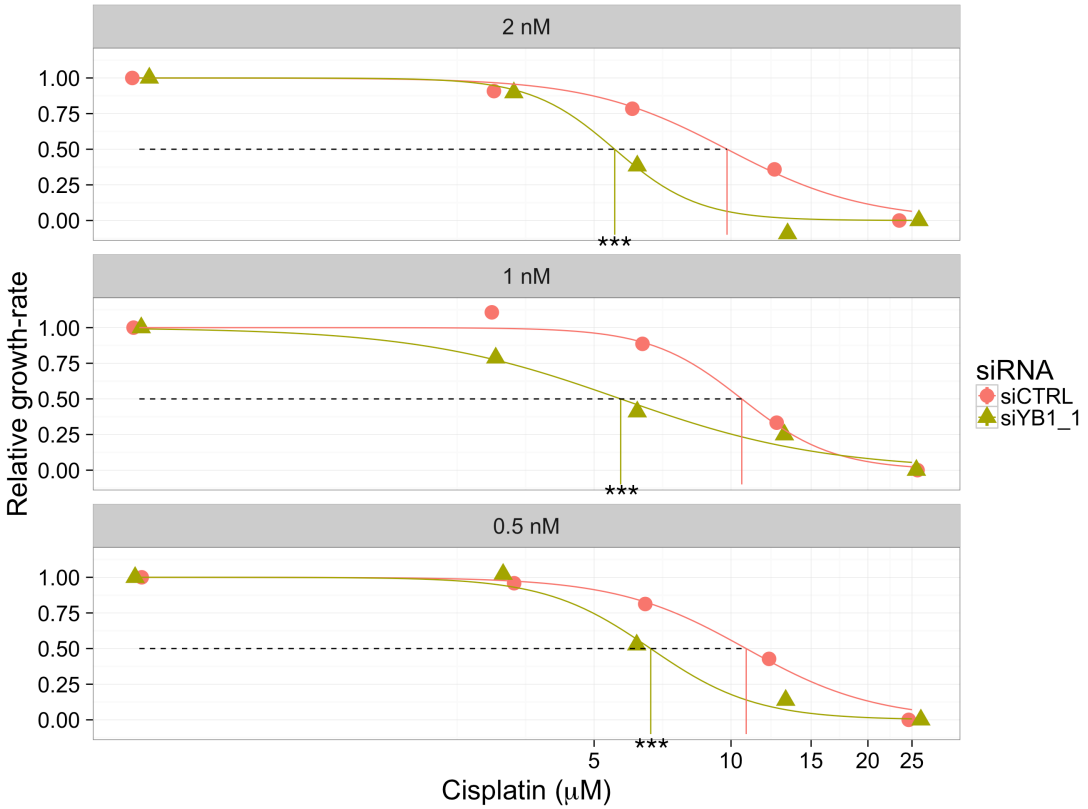

Figure 5.7: Depleting YB-1 reduces the growth-rate of MDA-MB231 cells following a two hr exposure to cisplatin (0, 3.125, 6.25, 12.5, 25 μM, n = 4). YB-1 was depleted using siYB1_1 (0.5, 1, 2 nM) and 48 hrs later media that contained cisplatin was added for two hrs. The confluence of the cells was then monitored for 96 hrs. The maximum growth-rate was used to estimate the ED_{50} for each treatment during 120 hrs to cisplatin. *** = p-value <0.001.

Table 5.4: Depleting YB-1 reduces the growth-rate of MDA-MB231 cells following two hrs of exposure to cisplatin (0 - 25 μM; n = 4).

siRNA	Concentration (nM)	ED_{50} ± S.E.	Delta ± S.E.	p-value (t-value)
siCTRL	2	9.80 ± 0.73	-	-
siYB1_1	2	5.55 ± 0.37	**-4.26 ± 0.82**	**<0.0001 (5.169)**
siCTRL	1	10.56 ± 0.87	-	-
siYB1_1	1	5.72 ± 0.68	**-4.84 ± 1.10**	**<0.0001 (4.394)**
siCTRL	0.5	10.80 ± 0.78	-	-
siYB1_1	0.5	6.66 ± 0.43	**-4.14 ± 0.89**	**<0.0001 (4.634)**

The dose-response curves were fitted using log-logistic regression. Estimates for the effective doses where 50 % of the cells were killed by cisplatin (ED_{50}) are given. T-tests were used to compare the ED_{50} following the depletion of each protein to the ED_{50} of the siCTRL RNA duplex, significant differences shown as **bold text**. S.E. = standard error of the mean.

5.2.5 Cisplatin exposure alters the subcellular distribution of YB-1

Challenging cells with various stressors has been shown to cause YB-1 to relocalise to the nucleus (Koike et al. 1997, Stein et al. 2001, Fujita et al. 2005, Cohen et al. 2010). It was hypothesised that YB-1 would translocate to the nucleus of MDA-MB231 cells that were grown in media with 1.56 μM cisplatin. This translocation was hypothesised to be prompted by the participation of YB-1 in either the repair of cisplatin damage to DNA or the activity of YB-1 acting as a transcription factor for genes that are involved in the cellular survival response to cisplatin exposure (reviewed in **Chapter 1.4.3**). This hypothesis was tested using IF. MDA-MB231 cells were grown on coverslips with or without 1.56 μM cisplatin for 48 hrs prior to fixation. The subcellular localisation of YB-1 was analysed using confocal microscopy. The distribution of YB-1 in the cells matched that discussed in **Chapter 3.2.3** and **Figure 3.5**. Briefly, most of the YB-1 was in the cytoplasm of the cells and many cells had low levels of punctate signal from YB-1 in the nucleus (**Figure 5.8.A**, overlapping YB-1 and DNA signals in profile plots for cells 1 - 3).

During cisplatin exposure, YB-1 was hypothesised to translocate to the nucleus of MDA-MB231 cells. However, the results showed that YB-1 remained primarily in the cytoplasm of all cells after 48 hrs of exposure to 1.56 μM cisplatin (**Figure 5.8.B**). Cisplatin exposure did lead to more intense YB-1 signal in the nucleus and an accumulation of YB-1 signal at the perinuclear boundary in the cells (**Figure 5.8.B**, profile plots for cells 2 - 3). The alterations in the cellular distribution of YB-1 that occurred following cisplatin exposure were consistent (comparing media only; **Figure 5.8.A** and cisplatin exposure; **Figure 5.8.B**).

Experiments presented in this chapter also show that YB-1 promotes the survival of MDA-MB231 cells following a short, two hr, exposure to cisplatin. YB-1 was hypothesised to relocalise to the nucleus of cells following a two hr exposure to cisplatin (**Chapter 1.4.3**). To test this hypothesis, $\sim$ 75% confluent MDA-MB231 cells, on glass coverslips, were exposed to 12.5 μM cisplatin for two hrs. The medium was changed and, following a two hr recovery period, the cells were processed for confocal microscopy. The results show an increase in the intensity of YB-1 signal around the nucleus of MDA-MB231 cells (**Figure 5.9.A - B**). This signal partially obscures the YB-1 signal in the nucleus of the cells.

The effect of cisplatin exposure on the residence of YB-1 in the nucleus was tested using the extraction of cytoplasmic proteins and RNA from MDA-MB231

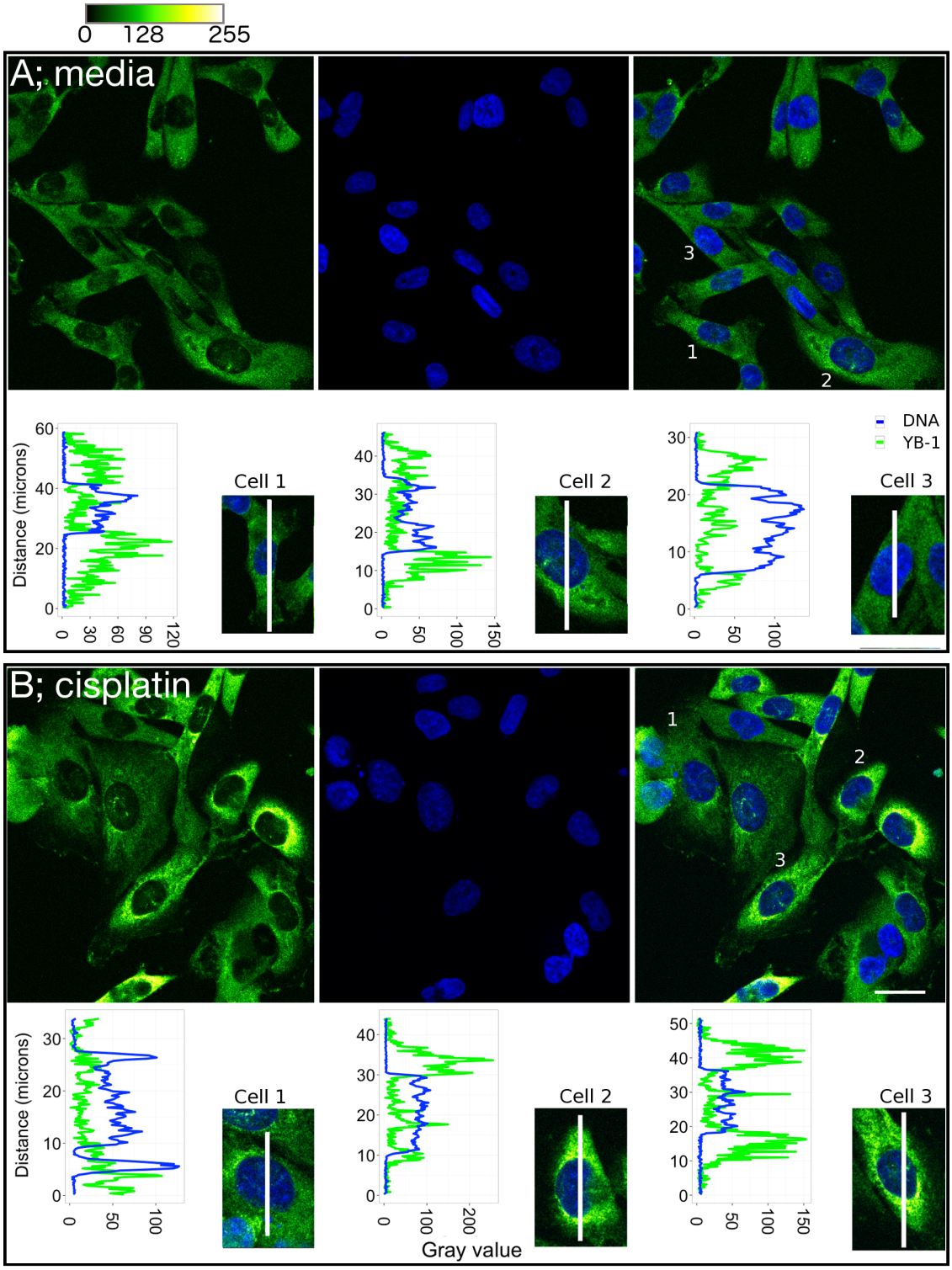

Figure 5.8: Cisplatin exposure increases the levels of YB-1 at the perinuclear boundary in MDA-MB231 cells. IF signal from ^{N}YB1 in MDA-MB231 cells after in media (**A**) or after 48 hrs of exposure to 1.56 µM cisplatin (**B**). Images are Z-projections of the maximal signal from 3 Z-slices across the nuclei of MDA-MB231 cells. Profile plots show the signal intensity from the line across each cell to the right of each graph. ^{N}YB1 is labelled using AlexaFluor 488 and gray values are represented using the Green Hot LUT (ImageJ). DNA labelled with Hoechst is represented as blue. Scale bar is 25 µM.

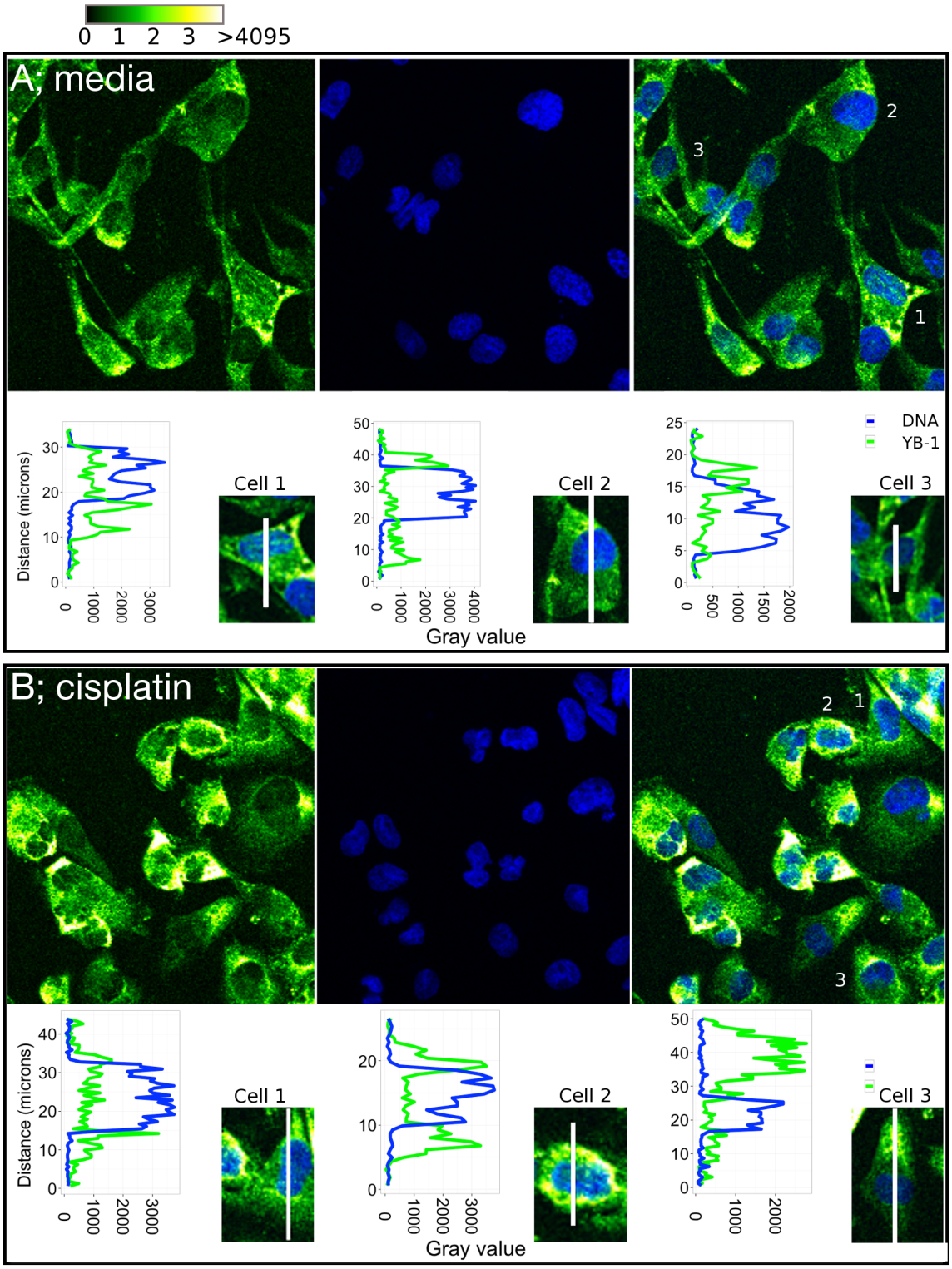

Figure 5.9: Brief exposure of MDA-MB231 cells to 12.5 μM cisplatin increases the intensity of YB-1 staining. **A**, confocal microscopy shows the signal from ^{N}YB1 in MDA-MB231 cells (also shown in **Figure 3.5.A**). **B**, IF signal from ^{N}YB1 in MDA-MB231 cells two hrs after a two hr exposure to 12.5 μM cisplatin. Images are Z-projections of the maximal signal from 3 Z-slices across the nuclei of MDA-MB231 cells. Profile plots show the signal intensity from the line across each cell to the right of each graph. ^{N}YB1 is labelled with AlexaFluor 488 and gray values are represented using the Green Hot LUT (ImageJ). DNA labelled with Hoechst is represented as blue. Scale bar is 25 μM.

cells following two-hrs of exposure to 12.5 μM cisplatin and another two hr recovery period (**Chapter 2.10.1**). The results from confocal microscopy showed that the signal from YB-1 that was interacting with DNA formed foci which increased in intensity following the brief exposure to cisplatin (**Figure 5.10.A - B**, profile plots for intensity). Therefore, these experiments further confirm the presence of YB-1 in the nucleus. They also confirm that YB-1 interacts with DNA, or nuclear structures containing RNA that are refractory to RNase digestion, and this interaction increases following a brief exposure to cisplatin.

The results from two sets of experiments show that during and following cisplatin exposure, YB-1 is distributed throughout MDA-MB231 cells. Exposing MDA-MB231 cells to cisplatin leads to YB-1 signal increasing at the periphery of the nucleus. YB-1 levels also appear to increased in the nucleus during cisplatin exposure. The results from IF following the extraction of cytoplasmic proteins and RNA confirm that YB-1 interacts with DNA in the nucleus of MDA-MB231 cells.

5.3 Discussion

The results presented in this chapter show that:

- Loss of YB-1 reduces the growth-rate and increases the death index of MDA-MB231 cells;
- Loss of YB-1 increases the sensitivity of MDA-MB231 cells to paclitaxel, camptothecin, cisplatin, and doxorubicin;
- Loss of YB-1 increases a measure of cell death in MDA-MB231 cells during exposure to cisplatin;
- Cisplatin exposure leads to the accumulation of YB-1 at the perinuclear boundary;
- The interaction of YB-1 with the DNA of MDA-MB231 cells appears to increase following cisplatin exposure.

5.3.1 Loss of YB-1 reduces the growth and viability of MDA-MB231 cells

Depleting YB-1 in MDA-MB231 cells was a starting point for many of the experiments that are presented in this chapter. The results indicate that depleting YB-1

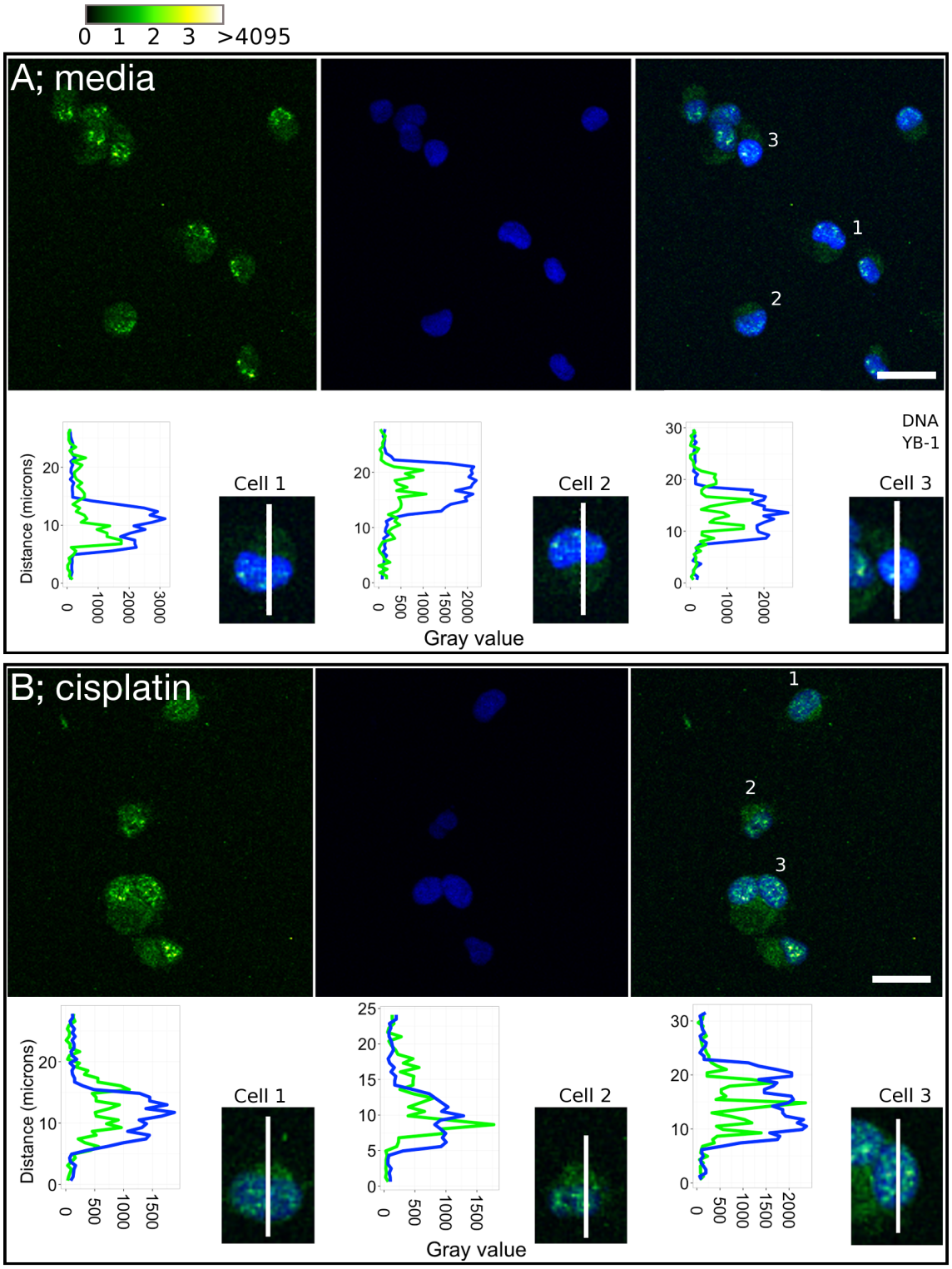

Figure 5.10: YB-1 interacts with DNA before and after a two hr exposure to 12.5 μM cisplatin. **A**, IF signal from ^{N}YB1 in the nucleus of MDA-MB231 cells (also shown in **Figure 3.5.B**). **B**, the signal from ^{N}YB1 in the nucleus of MDA-MB231 cells two hrs after a two hr exposure to 12.5 μM cisplatin. Images are Z-projections of the maximal signal from 3 Z-slices across the nuclei of cells. Profile plots show the signal intensity from the line across each cell to the right of each graph. ^{N}YB1 is labelled with AlexaFluor 488 and gray values are represented using the Green Hot LUT (ImageJ). DNA labelled with Hoechst is represented as blue. Scale bar is 25 μM.

reduces the growth-rate of MDA-MB231 cells. Increased levels of death are also shown to accompany the depletion of YB-1 from MDA-MB231 cells. Depleting YB-1 with 5 nM siYB1_1 or siYB1_2 occasionally led to an almost complete inhibition of cell growth.

The use of confluence data to estimate growth-rate meant that the relative contribution of cell-division and death was not confirmed. However, others studies indicate that YB-1 depletion may influence mitosis as depleting YB-1 can lead to an accumulation of cells in the G_1 phase of the mitotic cycle (**Chapter 1.4.2**). MDA-MB231 cells accumulate in G_1 following the depletion of YB-1 (Yu et al. 2010). Therefore, the results from Yu et al. (2010) indicate that the reduced growth-rate that accompanies the depletion of YB-1 from MDA-MB231 cells is likely to result from the influence of YB-1 on both the cell-cycle and cell viability.

Robust depletion of YB-1 was required before the growth and viability of MDA-MB231 cells was strongly reduced. Therefore, the results presented here indicate that in MDA-MB231 cells low levels of YB-1 can promote cell survival. This appears to contradict the findings from other studies which found that over-expression of YB-1 promoted many of the functions of YB-1 in cancer, including increased cell division (**Chapter 1.3 - 1.4**). Therefore, it appears likely that only a small amount of YB-1 is required to perform the tasks that maintain viability in MDA-MB231 cells. A post-translationally modified form of YB-1 could also be responsible for the promotion of the survival of MDA-MB231 cells. There are multiple phosphorylation sites on YB-1 and many of these sites are phosphorylated in MDA-MB231 cells (**Chapter 4.2.2**, Toulany et al. 2011). Small amounts of specifically phosphorylated YB-1 may be retained in MDA-MB231 cells where it can positively influence cell survival.

5.3.2 YB-1 supports cell survival during a range of stress events

The results presented in this chapter confirm that depleting YB-1 decreases the growth-rate of MDA-MB231 cells during exposure to a range of cytotoxic drugs (paclitaxel, camptothecin, doxorubicin, cisplatin). These drugs kill cells via multiple mechanisms. It is not currently clear if YB-1 has a single molecular function that promotes cell survival during exposure to these agents.

These results indicate that depleting YB-1 sensitises cells to camptothecin. The is potentially the first observation that indicates a protective role for YB-1 in MDA-MB231 cells during camptothecin exposure. The breast cancer cell line, MCF-

7, was also sensitised to camptothecin exposure by the depletion of YB-1 (Guay et al. 2008b). However, the importance of YB-1 to cell survival during camptothecin exposure appears to vary with cell type. Depleting YB-1 had no effect on the sensitivity of epidermoid cancer (KB) cells to camptothecin (Ohga et al. 1996). In prostate cancer cells (PC-3), which have mutant p53 (Isaacs et al. 1991, Carroll et al. 1993), depleting YB-1 had the opposite effect to that observed in this study, as it improved resistance to camptothecin (Wu et al. 2014). Therefore, YB-1 is only important to camptothecin resistance in specific cellular contexts.

The results from the current work also confirm a number of studies which have shown that YB-1 can protect cells from paclitaxel. YB-1 has been shown to improve the survival of prostate, breast, and ovarian cancer cell lines during or following paclitaxel exposure (Shiota et al. 2009, Shiota et al. 2011, Kang et al. 2013, Shiota et al. 2014). Decreasing levels of YB-1 sensitised breast cancer cell lines, including MDA-MB231 cells, to paclitaxel (Lee et al. 2008, To et al. 2010, Lasham et al. 2016). However, as with camptothecin, YB-1 was not critical to paclitaxel resistance in all breast cell lines as depleting YB-1 did not sensitise BT-549 cells to paclitaxel (Lasham et al. 2016).

In this study doxorubicin exposure is shown to cause MDA-MB231 cells to enlarge and, it appears, to cease dividing (**Chapter 5.2.3**). The phenotype of these cells could have indicated senescence. Depleting YB-1 altered the response of MDA-MB231 cells to doxorubicin exposure so that the majority died. These observations are consistent with a previous report which found that YB-1 inhibited the ability of P53 to induce cell death without interfering with the ability of P53 to induce cell cycle arrest via transactivation of the *CDKN1A* gene (Homer et al. 2005). The efficiency of P53 at inducing cell death could explain how a small amount of cellular YB-1 can inhibit cell-death during doxorubicin exposure. However, the p53 in MDA-MB231 cells exhibits a gain-of-function mutation which can promote the survival of MDA-MB231 cells during serum starvation (Hui et al. 2006). Previous research has shown that following doxorubicin exposure, MDA-MB231 cells undergo delayed apoptosis (Elmore et al. 2002). Due to the presence of functional p53, MCF-7 cells became senescent following doxorubicin exposure (Elmore et al. 2002). Therefore, it is unlikely that the phenotype of the MDA-MB231 cells during doxorubicin exposure reflects senescence (**Figure 5.4**). Irrespective of this, depleting YB-1 strongly reduces the viability of MDA-MB231 cells during doxorubicin exposure.

Other studies also indicate that YB-1 protects cells during doxorubicin exposure. Doxorubicin resistance is accompanied by increased levels of YB-1 in HT1080

fibrosarcoma cells (Levenson et al. 2000) and MCF-7 cells (Yang et al. 2010). Multiple myeloma cells with, elevated levels of YB-1, are highly proliferative and over-expression of YB-1 conferred resistance to apoptosis following doxorubicin exposure (Chatterjee et al. 2008). In bladder cancer cell lines, YB-1 promoted resistance to doxorubicin (Shiota et al. 2010b). Kim et al. (2013) reported that ectopic expression of YB-1 protects NIH3T3 fibroblasts during doxorubicin exposure. The ability of YB-1 to promote resistance to doxorubicin may vary with cell type. Depleting YB-1 had no effect on the sensitivity of KB cells to doxorubicin (Ohga et al. 1996).

Therefore, the initial experiment in this chapter (**Chapter 5.2.2**) indicates that YB-1 depletion sensitises MDA-MB231 cells to all four drugs that were tested. This may indicate that in MDA-MB231 cells, YB-1 functions to generally promote cell survival. This would also be consistent with the negative effect of depleting YB-1 on MDA-MB231 cell growth-rate and their survival in the absence of drug exposure. Lasham et al. (2016) proposed that the ability of YB-1 to reduce levels of EGR-1 in paclitaxel resistance could be a general mechanism for YB-1 to promote cell survival.

5.3.3 YB-1 supports cell survival during cisplatin exposure

The wide variation in the results from other studies was a significant factor that prompted the experiments in this chapter. The central aim of this work was to define drug exposure conditions where MDA-MB231 cells survived only when YB-1 was present. The results reported here confirm that depleting YB-1 sensitises MDA-MB231 cells to cisplatin exposure between 1.56 - 3.13 μM. Furthermore, the drug response curves utilise a derived response to cisplatin which separates the general decreases MDA-MB231 cell survival following YB-1 depletion from the effects of cisplatin exposure on survival. Therefore, the absolute reduction in survival that accompanies YB-1 depletion and cisplatin exposure was cumulative, and it encompasses the reduced survival that was solely derived from depleting YB-1 in addition to the effects of cisplatin exposure.

A number of previous studies have also focussed on the role of YB-1 in cisplatin resistance but their exposure conditions, specifically the timing and concentrations of cisplatin, varied greatly. This variation may reflect differences in the intrinsic resistance of different cell lines to cisplatin. A cisplatin resistant KB cell line, KCP-4, has an IC_{50} of 25 μM compared to 0.4 μM cisplatin in the parental KB cell line (Fujii et al. 1994). However, some of the studies that focus on YB-1 have used cisplatin at doses where cell survival is unlikely. For example, a study that showed

YB-1 interacting with the MDR-1 promoter to increase the levels of MDR-1 in the colorectal cancer cell line, HCT-116, exposed the cells to 133 μM cisplatin for 6 hrs (Chattopadhyay et al. 2008).

Two previous studies from the same research group are directly relevant to the results presented in this chapter. They focused on the importance of YB-1 to the survival of two breast cancer cell lines (MCF-7 and MDA-MB231) during cisplatin exposure. The results are difficult to reconcile with one another and also with those from this research. In one study, the EC_{50} for MDA-MB231 and MCF-7 cells following 96 hrs of cisplatin exposure was estimated to be 284 μM cisplatin and 84 μM cisplatin respectively (Garand et al. 2011). These dosage ranges are exceedingly high compared to those used in this chapter. However, the same lab group also used a clonogenic assay where cells were exposed to cisplatin and then seeded at a low density so that they formed colonies that could be counted (Guay et al. 2008a). This clonogenic assay also demonstrated that depleting YB-1 impaired the survival of MCF-7 and MDA-MB231 cells. However, both cell lines were very sensitive to cisplatin. Eighteen hrs of exposure to 0.5 μM cisplatin reduced the survival of MDA-MB231 cells by >90% (Guay et al. 2008a). The manner of cisplatin exposure can alter the apparent sensitivity of cells to cisplatin but the variation in the results from Garand et al. (2011) and Guay et al. (2008a) appear to be improbable. The results from the current study provided robust evidence that, irrespective of the duration of exposure, MDA-MB231 cells do not survive exposure to >25 μM cisplatin. Furthermore, unlike previous studies, there is clear evidence that the MDA-MB231 cells continued to divide in the presence of 1.56 - 3.13 μM cisplatin while depleting YB-1 rendered many cells unviable.

Coarse changes in the localisation of a protein within the cell in response to drug exposure are likely to indicate that the function of this protein has been altered by the drug exposure. IF was performed to ensure that this low level of cisplatin exposure, 1.56 μM cisplatin, had an effect on the subcellular localisation of YB-1. However, cisplatin exposure did not lead to a strong redistribution of YB-1 in MDA-MB231 cells. YB-1 did not translocate to provide diffuse signal in the nucleus as Guay et al. (2008a) observed with ectopically expressed GFP-YB-1 during cisplatin exposure. Instead, most of the YB-1 remained in the cytoplasm of MDA-MB231 cells during cisplatin exposure, with strong signal in the cytoplasm adjacent to the nucleus. This perinuclear signal may come from the formation of stress granules that contain YB-1 (Kedersha & Anderson 2007, Bounedjah et al. 2014, Anderson et al. 2015). There was also an increase in the levels of YB-1 in the nucleus of MDA-

MB231 cells following cisplatin exposure. The extraction of cytoplasmic proteins and RNA provided, to the best of my knowledge, the first images of YB-1 interacting with DNA within cultured cells in the absence of an interfering signal from YB-1 interacting with RNA. The extraction of cytoplasmic and RNA bound proteins prior to IF shows great promise for studying the interactions of YB-1 with DNA in cultured cells.

5.3.4 Summary

The results presented in this chapter confirm that in MDA-MB231 cells, YB-1 promotes survival during normal cell culture conditions and also during exposure to a number of drugs. The finding that MDA-MB231 cells require YB-1 to survive chronic exposure to 1.56 - 3.13 μM, satisfies the central aim of this chapter. YB-1 remained primarily in the cytoplasm of MDA-MB231 cells during exposure to 1.56 μM cisplatin. This cisplatin exposure lead to YB-1 accumulating at the perinuclear boundary and there was an increased intensity of YB-1 foci in the nucleus. The molecular function of YB-1 in MDA-MB231 cells during exposure to 1.56 μM cisplatin is unknown. The following chapter examined the PPI of YB-1 during cisplatin exposure to gain further information about the molecular function of YB-1 in MDA-MB231 cells during exposure to 1.56 μM cisplatin.

Chapter 6

Identification of YB-1 interacting proteins during cisplatin exposure

6.1 Introduction

The ability of YB-1 to support the survival of MDA-MB231 cells during cisplatin exposure (**Chapter 5**) is consistent with previous reports. These reports showed that in a range of cells, YB-1 contributes to resistance to a variety of chemotherapeutic agents (**Chapter 5.3.3**). However, YB-1 interacts with many proteins from diverse biochemical pathways (**Chapter 4**).

Research highlights that YB-1 may contribute to the survival of cells during genotoxic stress via any of the following pathways. YB-1 has been reported to respond to cellular stress by binding RNA to influence splicing (Dutertre et al. 2010), by forming stress granules (Onishi et al. 2008, Chernov et al. 2009, Wehner et al. 2010, Salleron et al. 2014, Tanaka et al. 2014, Somasekharan et al. 2015), and by translation via the promotion of the internal ribosome entry pathway (Evdokimova et al. 2006b, King et al. 2014, Bisio et al. 2015). YB-1 can also bind to DNA at which point it may induce or inhibit transcription. Furthermore, by binding to modified DNA, YB-1 may influence the cellular response to DNA damage (**Chapter 1.4.3**). The results of the previous chapter indicate that YB-1 increases its interaction with DNA during and following cisplatin exposure (**Chapter 5.2.5**).

When cells are exposed to cisplatin, the activity of YB-1 as a transcription factor appears to be important. Specifically, YB-1 has been shown to protect a variety of cancer cells by driving transcription from the MDR-1 gene (Ohga et al. 1996, Ohga et al. 1998, Sengupta et al. 2011, Chattopadhyay et al. 2008). The

transcriptional activation of MDR-1 has been shown to rely on YB-1 binding to an inverted CCAAT-box in the MDR-1 gene promoter (Ohga et al. 1996, Ohga et al. 1998, Sengupta et al. 2011). However, other reports show that YB-1 does not alter the levels of MDR-1 mRNA or protein (Kaszubiak et al. 2007). Recently, it has been postulated that YB-1 does not bind to the inverted CCAAT-box *in vivo* (Dolfini & Mantovani 2013a, Dolfini & Mantovani 2013b).

Other research into the function of YB-1 during cisplatin exposure centres around YB-1 binding to double-stranded DNA that is modified by cisplatin (Ise et al. 1999, Izumi et al. 2001, Gaudreault et al. 2004). The functional outcome of this binding has not been confirmed, but the research to date has provided support for two scenarios. Firstly, YB-1 may be part of the DNA damage sensing and repair machinery. YB-1 appears to be directly involved in DNA-strand separation in preparation for its repair by the base excision repair pathway (Gaudreault et al. 2004). YB-1 interacts with the DNA repair protein complementing XP-C cells (XPC) - UV excision repair protein RAD23 homolog B (HR23B) complex (Fomina et al. 2015). This complex is a damage sensing component of the nucleotide excision repair pathway and the interaction of YB-1 has a synergistic effect on the binding of both to bulky DNA lesions (Fomina et al. 2015). YB-1 has also been shown to participate in nucleotide excision repair via an interaction with human endonuclease III (Guay et al. 2008b). The second scenario is that YB-1 allows DNA synthesis to continue in the presence of DNA damage by interacting with PCNA to facilitate the initiation of a DNA damage tolerant synthesis pathway (Ise et al. 1999).

The work presented in this chapter is based around the hypothesis that a cohort of the proteins that interact with YB-1 in MDA-MB231 cells will be modulated during exposure to cisplatin. This cohort of proteins should highlight the biochemical process via which YB-1 contributes to the resistance of MDA-MB2331 cells during cisplatin exposure.

An alternative YB-1 purification strategy was used to test this hypothesis. Proteins have been cross-linked *in vivo* prior to the immunoprecipitation of YB-1 and LC-MS/MS analyses. Portions of the work in this chapter have been presented at the *The DNA damage response in cell physiology and disease* (EMBO conference, October 2013, Greece).

6.2 Results

6.2.1 Optimising strategies for cross-linking YB-1 complexes

To study the PPI of YB-1 during cisplatin exposure, MDA-MB231 cells were cross-linked to stabilise PPI *in situ* prior to IP (**Chapter 2.13.5**). Cross-linking stabilises many transient and weak PPI in cells while also creating adducts between polypeptide sequences that are proximal (**Figure 2.2**). These adducts remain when reduction and alkylation are omitted from the tryptic digestion, ensuring that pairs of linked peptides are present in the tryptic digestion. LC-MS/MS can be used to gain information about the peptides that are linked by the cross-links.

The suitability of two cross-linking agents were assessed in this thesis using formaldehyde (in the form of paraformaldehyde) and dithiobis[succinimidyl propionate] (DSP). Formaldehyde favours reaction with primary amines (R-NH_2) but it may also react with secondary amines (R-NH_2-R; reviewed variously in Sutherland et al. 2008, Klockenbusch & Kast 2010, Leitner et al. 2010). DSP has greater specificity for the primary amines on lysines or the N-termini of proteins. The cross-linkers were tested at various concentrations, temperatures, and on adherent cells or cell suspensions. Following cross-linking, the lysates were separated using non-reducing SDS-PAGE. The criteria for assessing the efficacy of the cross-linkers was their ability to slow the migration of YB-1 on non-reducing SDS-PAGE gels.

The results from immunoblotting confirm that both DSP and formaldehyde cross-links alter the migration of YB-1 in non-reducing SDS-PAGE (**Figure 6.1**). In the absence of cross-linking, the YB-1 from MDA-MB231 cells had identical migration irrespective of whether they had been reduced with DTT (**Figure 6.1**, lanes 1 - 2). Therefore, the absence of reduction prior to SDS-PAGE did not alter the migration of YB-1. Cross-linking MDA-MB231 cells using DSP shifted the migration of some YB-1 signal so that it ranged between $\sim$ 90 kDa and the top of the gel. DSP caused this mass shift irrespective of concentration (1 mM or 2 mM) and temperature (4°C or room temperature). Reducing and heating aliquots of lysates that were cross-linked with 2 mM DSP caused most YB-1 to migrate as a monomer (slightly below 50 kDa **Figure 6.1**, DSP = lane 9). The loss of mass-shifted YB-1 that accompanied the reduction and breaking of the di-sulfide bond on DSP confirmed that DSP cross-links caused the observed mass-shifts in YB-1 signal on immunoblots.

Cross-linking MDA-MB231 cells with paraformaldehyde also altered the migration of YB-1. When paraformaldehyde was used as a cross-linker, the maximal

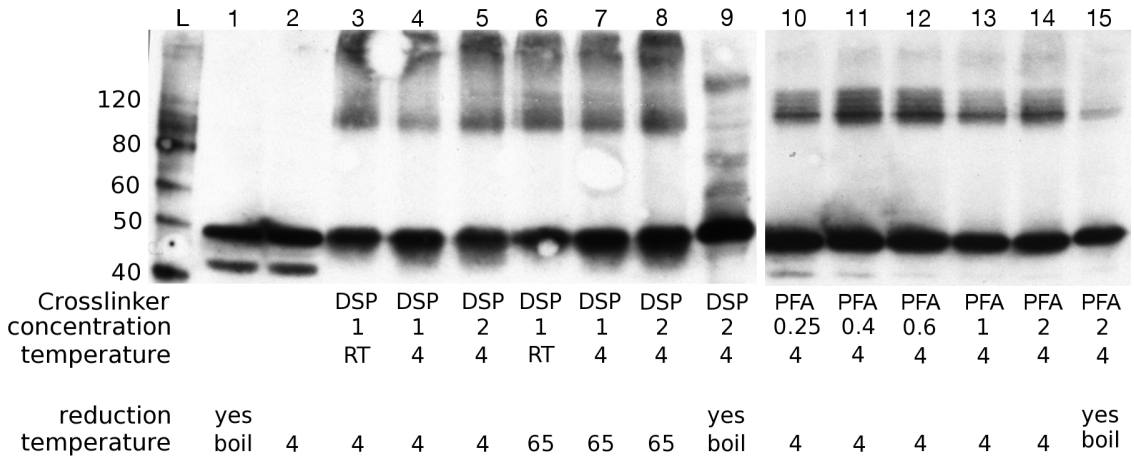

Figure 6.1: The mobility of YB-1 on non-reducing SDS-PAGE alters following the exposure of MDA-MB231 cells to cross-linking agents. Paraformaldehyde and DSP were used to cross-link the proteins in MDA-MB231 cells to one another prior to their lysis. Immunoblotting was performed using ^{N}YB1. **Abbreviations**; DSP = dithiobis-succinimidylpropionate (concentration = mM); PFA = paraformaldehyde (concentration = %); RT = room-termperature; L = molecular ladder.

mass-shifted signal migrated between 90 and 120 kDa (**Figure 6.1**, lanes 10 - 14). Cross-linking MDA-MB231 cells with paraformaldehyde between 0.4 and 0.6% at 4°C produced the most consistent alterations in the migration of YB-1. Heating paraformaldehyde samples breaks the paraformaldehyde cross-links (Jackson 1999). Heating an aliquot of lysates from MDA-MB231 cells that were cross-linked with 2% paraformaldehyde at 4°C removed most of the mass-shifted YB-1 signal (**Figure 6.1**, paraformaldehyde = lane 15). The negative effects of formaldehyde on protein solubility are likely to explain these observations. The absence of mass-shifted YB-1 following reduction with DTT confirmed that formaldehyde cross-links caused the mass-shift.

Both of the cross-linking agents that were tested successfully cross-link YB-1. DSP produced the widest range of mass-shifted YB-1. Furthermore, DSP offered the advantage of creating adducts with consistent masses when intact (**Figure 2.2**) and also following reduction and alkylation (**Figure 2.3**). Information from reduced and alkylated peptides is critical to searching for cross-linked peptide pairs with LC-MS/MS. The linking distance of formaldehyde is $\sim$ 2Å compared to 12 Å for DSP. However, paraformaldehyde contains polymers of formaldehyde that retain cross-linking activity at either end; this means that the cross-linking distance can vary. Therefore, DSP was used as the cross-linker in subsequent experiments.

The immunoblots of lysates from DSP cross-linked MDA-MB231 cells revealed the presence of monomeric YB-1 (**Figure 6.1**, migrating slightly below 50 kDa).

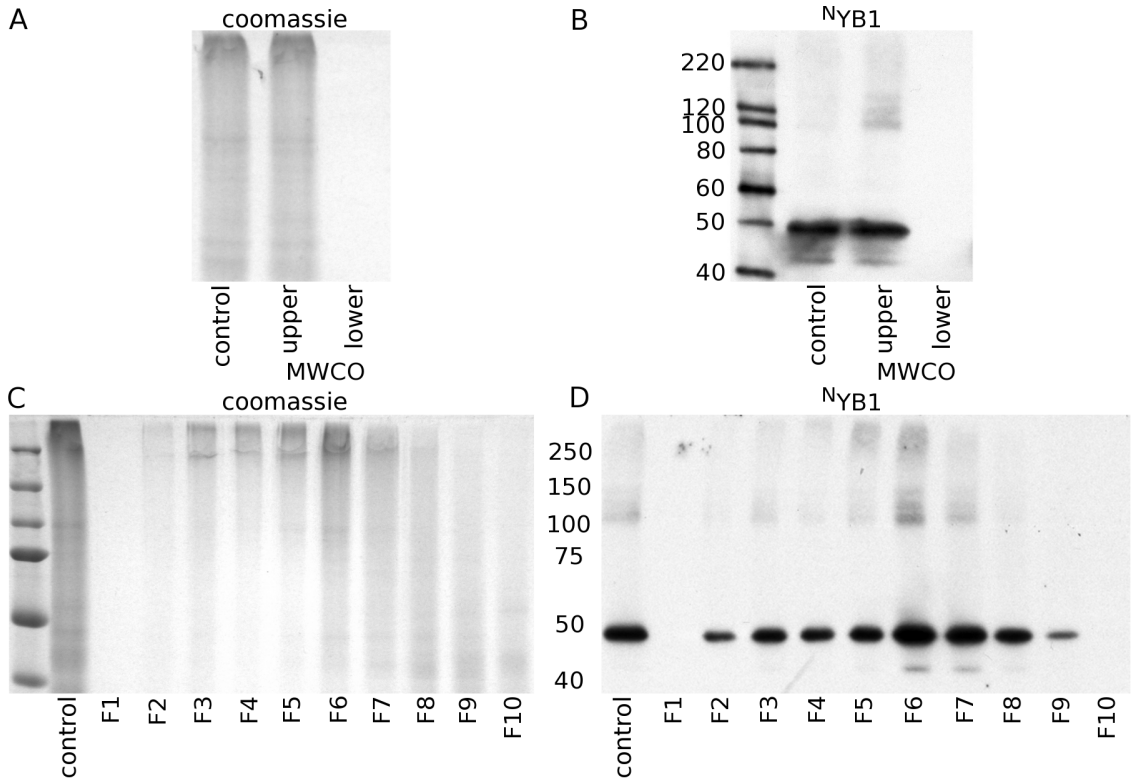

Figure 6.2: Cross-linked YB-1 from MDA-MB231 cells cannot be separated from monomeric YB-1 prior to its separation by non-reducing SDS-PAGE. **A**, lysates from cross-linked MDA-MB231 cells were passed through a 100 kDa molecular weight cut-off spin filter (MWCO). A 10% non-reducing SDS-PAGE was used to separate the proteins from the upper (upper) and lower (lower) chambers of the MWCO filter and half of the gel stained with colloidal commassie G250. **B**, the other half of the gel in **A** was used for immunoblotting with ^{N}YB1. Size exclusion chromatography was performed on lysates from cross-linked MDA-MB231 cells and the fractions collected. The fractions were separated using non-reducing 10% SDS-PAGE. The gels were stained with colloidal coomassie G-250 (**C**) or blotted to a nylon membrane and YB-1 detected using ^{N}YB1 (**D**).

This monomeric YB-1 could not be cross-linked to YB-1 interaction partners. During IP, the monomeric YB-1 competes with YB-1 that is cross-linked to its interaction partners to bind the antibody against YB-1. As the monomeric YB-1 would reduce the recovery of YB-1 that was cross-linked to its interaction partners, attempts were made to remove it from the cross-linked lysates.

To remove monomeric YB-1, the cross-linked MDA-MB231 cell lysates were passed through a 100 kDa molecular weight cutoff filter. These lysates were then separated using non-reducing SDS-PAGE. Coommassie staining and immunoblotting of the 100 kDa flow-through fraction (lower chamber with molecules <100 kDa) revealed the absence of monomeric YB-1 (**Figure 6.2 A - B**). Therefore, YB-1 does not pass through 100kDa molecular cut-off filters.

Size exclusion chromatography was used as an alternative strategy to separate monomeric YB-1 from the YB-1 protein complexes in cross-linked MDA-MB231 cell lysates. Coommassie staining of non-reducing SDS-PAGE from size exclusion chromatography confirmed that the fractions were sorted by size (**Figure 6.2 C**). However, the immunoblot from these samples confirmed the presence of monomeric YB-1 in all fractions that contain YB-1 (**Figure 6.2 D**). Therefore, monomeric YB-1 was still observed on non-reducing SDS-PAGE following size exclusion chromatography.

These results led to the conclusion that most of the monomeric YB-1 that was observed on non-reducing SDS-PAGE was absent before and during size exclusion chromatography. It was hypothesised that the SDS in the SDS-PAGE buffers releases YB-1 from larger molecular assemblages whereupon the released YB-1 migrates as monomeric YB-1. No further attempts were made to purify solely YB-1 that exhibited a mass shift on non-reducing SDS-PAGE.

6.2.2 The mobility of cross-linked YB-1 following cisplatin and doxorubicin exposure

The distribution of YB-1 in MDA-MB2331 cells was altered following 48 hrs of cisplatin exposure (**Figure 5.8**). Changes in the cellular distribution of YB-1 are likely to indicate changes to the function of YB-1 and also its PPI. However, the point(s) when YB-1 begins to protect MDA-MB231 cells during cisplatin exposure remain unknown. It was important to purify YB-1 at the point when it was involved in protecting MDA-MB231 cells from the effects of cisplatin. Therefore, coarse temporal information about the response of YB-1 to cisplatin may be used to inform decisions about when to assess the PPI of YB-1.

It was hypothesised that exposing MDA-MB231 cells to cisplatin and to doxorubicin would alter the mobility of cross-linked YB-1 on non-reducing SDS-PAGE. To test this hypothesis, MDA-MB231 cells at ∼30% confluence were cultured in media containing cisplatin (1.56, 3.125, or 6.25 μM) or doxorubicin (0.156 or 0.3125 μM) for up to 120 hrs (**Figure 6.3**, n = 3). These data highlighted that exposure to neither cisplatin nor doxorubicin disrupted the signals from cross-linked YB-1 at a coarse level. Exposure of MDA-MB231 cells for 4 or 24 hrs did not induce reliable alterations to the migration of YB-1 (**Figure 6.3**, lanes 1 - 12). However, following 48 hrs of exposure to cisplatin and doxorubicin there was an increase in YB-1 signal from ∼ 200 kDa to the top of the gel (**Figure 6.3**, lanes 13 - 24). This increase

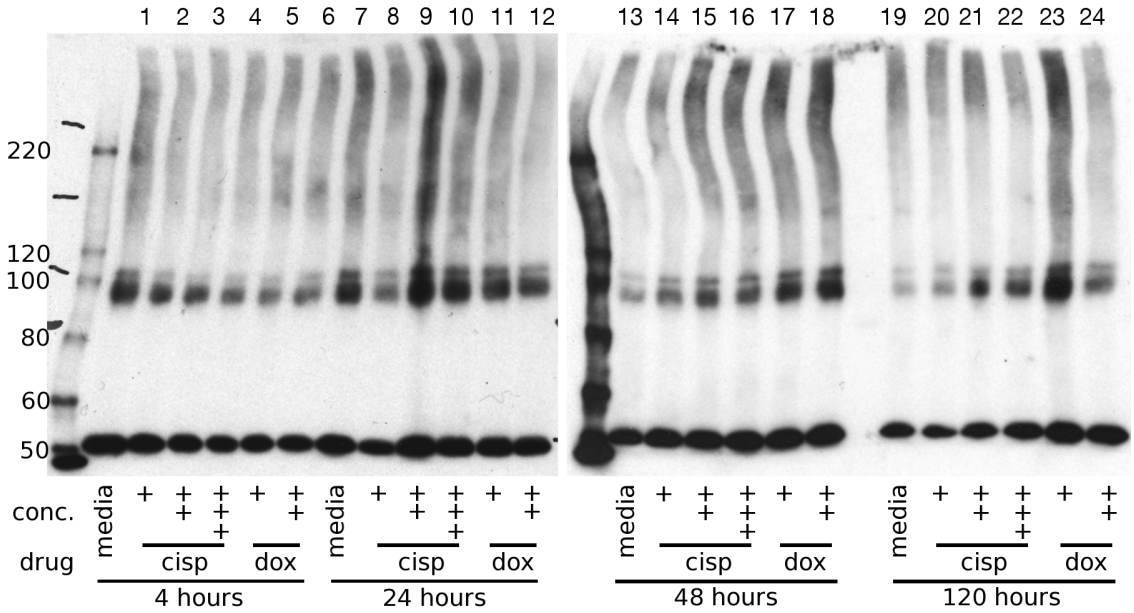

Figure 6.3: Exposure to cisplatin and doxorubicin does not cause large disruptions to the mobility of YB-1 from MDA-MB231 cells that are cross-linked using DSP. Representative immunoblots showing ^{N}YB1 signal from MDA-MB231 cells that were incubated with 1.56 - 6.125 μM cisplatin or 0.156 - 0.313 μM doxorubicin for 4 - 120 hrs (n = 3). Lysates were prepared from DSP cross-linked MDA-MB231 cells and separated using non-reducing 6% SDS-PAGE gel. **Abbreviations**; cisplatin (cisp); + = 1.56, ++, 3.13, +++ = 3.25 μM; doxorubicin (dox); + = 0.156, ++ = 0.313 μM.

was attenuated in the lysates from MDA-MB231 cells exposed to 1.56 μM cisplatin (**Figure 6.3**, lanes 14 and 20).

These results indicate that the PPI of YB-1 are most likely to be modulated following 48 - 120 hrs of cisplatin exposure. There is no evidence that the mobility of cross-linked YB-1 alters following 4 or 24 hrs of cisplatin exposure. These results, in conjunction with those from IF (**Figure 5.8**), led to the decision to collect IP YB-1 data following 48 and 120 hrs of cisplatin exposure.

6.2.3 Immunoprecipitation of cross-linked YB-1

The work in this chapter utilised a new preparation of affinity purified polyclonal antibody raised in sheep against the same sequence as ^{N}YB1 (^{N}YB1$_{sheep}$). The ability of ^{N}YB1$_{sheep}$ to purify YB-1 from DSP cross-linked MDA-MB231 lysates was tested. The binding capacity of the protein-G beads was also tested by using the protein G beads at 1 × (+) or 2 × (++) the manufacturers capacity for binding human immunoglobulin G. The results showed that using 50 μg of ^{N}YB1$_{sheep}$ for every mL of lysate at 10 000 cells per μL provided optimal recovery of YB-1 from DSP cross-linked MDA-MB231 cells (**Figure 6.4**). Using twice the volume of

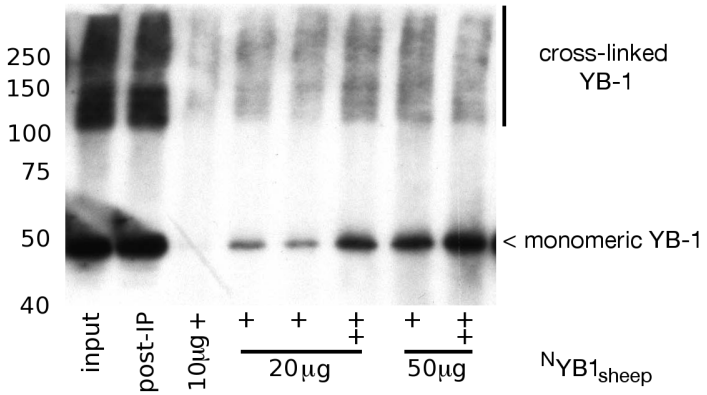

Figure 6.4: Optimising the IP of YB-1 using a sheep anti-N-terminal YB-1 ($^{N}YB1_{sheep}$). YB-1 was immunoprecipitated using $^{N}YB1_{sheep}$ from lysates prepared from 1×10^6 MDA-MB231 cells that were cross-linked using DSP. $^{N}YB1_{sheep}$ was used at concentrations ranging from 10 - 50 µg. The proteins that had bound to $^{N}YB1_{sheep}$ were recovered using protein G beads at 1 × (+) or 2 × (++) the manufacturers capacity for binding human immunoglobulin G (2.6 µg igg/µL of storage solution). The recovered proteins were separated using non-reducing 6% SDS-PAGE and YB-1 detected by immunoblotting using $^{N}YB1$.

protein-G beads further improved the recovery of YB-1 from the cell lysates. This experiment also confirmed that both monomeric YB-1 and cross-linked YB-1 were recovered using IP. Therefore, 50 µg of $^{N}YB1_{sheep}$ per mL of cross-linked cell lysate and twice the volume of protein-G beads recommended by the manufacturer was used for subsequent immunoprecipitations of YB-1.

The next set of experiments optimised the detection of DSP cross-links and reduced and alkylated DSP adducts on peptides using LC-MS/MS. This step was important, as detecting cross-linked peptide pairs is challenging and data analysis relies on knowledge of the peptide sequences that are being searched. YB-1 was precipitated from 4×10^7 DSP cross-linked MDA-MB231 cells. The purified YB-1 was separated using non-reducing SDS-PAGE and fractions were cut from above 150 kDa. Tryptic peptides were generated from these fractions, but to preserve intra- and inter-peptide cross-links the reduction and alkylation steps were omitted (**Chapter 2.3**). The similarity of intact cross-linked peptides and the reduced and alkylated peptides was maintained by splitting the peptide pool after over-night digestion. Aliquots of the peptide samples were reduced, alkylated, and analysed on LC-MS/MS. These experiments confirmed that DSP modified the peptides and also that tryptic digestion still occurred in the absence of reduction and alkylation.

These experiments were also used to optimise LC-MS/MS conditions and the data analysis of cross-linked peptide pairs. Over two experiments, various condi-

tions were tested, including collision induced disassociation (CID) and higher-energy collisional dissociation (HCD). Sites of cross-linking were not identified when searching the LC-MS/MS datasets against sequence databases containing all possible DSP cross-linked peptide pairs (**Figure 2.2 B**) of the expected YB-1 interaction partners using the xComb software (Panchaud et al. 2010).

The optimisation experiments confirmed that reduced and alkylated DSP adducts were readily detected using LC-MS/MS. Intact cross-linked peptide pairs were not detected. This failure was attributed to the low concentration of the samples. Therefore, the following experiments utilised more starting material to boost the concentration of peptides that were used for LC-MS/MS.

6.2.4 The purification of cross-linked YB-1 from MDA-MB231 cells during cisplatin exposure

It was hypothesised that the PPI of YB-1 would change while YB-1 promoted the survival of MDA-MB231 cells during cisplatin exposure. To examine this, YB-1 was purified from MDA-MB231 cells that were exposed to 1.56 μM cisplatin for 0, 48, or 96 hrs. This experiment aimed to survey the PPI of YB-1 in MDA-MB231 cells during cisplatin exposure. It also aimed to gain information about which proteins interacted directly with YB-1 by analysing cross-linked peptide pairs.

MDA-MB231 cells were grown in 1.56 μM cisplatin for 48 and 96 hrs. The cells were collected and the cross-linking reaction was performed on these intact suspension MDA-MB231 cells using 2 mM DSP. For each experimental condition 250 μg of $^{N}YB1_{sheep}$ was used to purify YB-1 from 5×10^7 MDA-MB231 cells. A control YB-1 IP came from MDA-MB231 cells that were seeded alongside the cisplatin-treated cells, grown in normal media for 48 hrs, and processed concurrently with the 48 hr cisplatin sample. It was intended that MDA-MB231 cells would be harvested following 48 and 120 hrs of cisplatin exposure. However, after 96 hrs of cisplatin exposure the cells that were intended to be harvested at 120 hrs were $\sim$ 85 - 95 confluent. The PPI of YB-1 could be affected by the division of cells slowing or ceasing in response to confluence and these changes would constitute a confounding effect. Therefore, the cells were harvested 24 hrs early, following 96 hrs of cisplatin exposure.

The proteins that purified with YB-1 from the cross-linked MDA-MB231 cells using $^{N}YB1_{sheep}$ were separated by non-reducing SDS-PAGE. The polyacrylamide gels were fixed and stained using colloidal coomassie G250. Scans of these gels

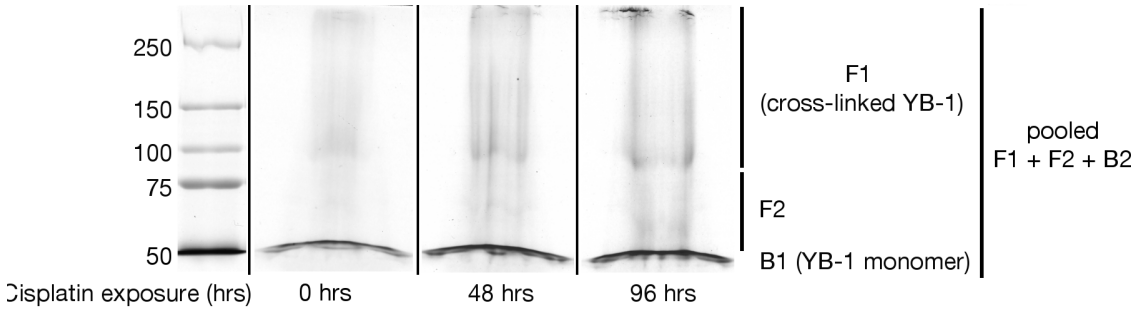

Figure 6.5: Coomassie stained non-reducing SDS-PAGE gels showing the proteins that were recovered by the IP of YB-1 from MDA-MB231 cells following 0, 48, or 96 hrs of exposure to 1.56 μM cisplatin. The regions of each gel where monomeric YB-1 migrates is referred to as **B1** and the region of the gel where cross-linked YB-1 migrated is referred to as **F1**. The region **F2** was also cut for LC-MS/MS. **Pooled** refers to data analyses that were performed using all fractions from each sample.

showed the recovery of proteins with a higher molecular weight than YB-1 (**Figure 6.5**). The main protein bands migrate with similar masses to the immunoblots that were performed using ^{N}YB1 (**Figure. 6.4**). This indicated that the majority of proteins and protein complexes that were recovered were likely to be in complex with YB-1. However, the poor resolution of these gels prompted the pooling of the region of the gel where cross-linked YB-1 migrates (**Figure 6.5**, >90 kDa; F1). The monomeric YB-1 band at the base of the gel (B1) was cut separately and the gel region between B1 and F1 was also cut as a fraction (**Figure 6.5**, F2). Analyses that incorporate LC-MS/MS data from all fractions (F1, F2, and B1) are referred to as pooled (**Figure 6.5**, pooled).

Information about the direct interaction partners of YB-1 was to be obtained using MS/MS spectra from cross-linked peptide pairs that included YB-1 and a direct interaction partner that were joined by an inter-protein cross-link (**Chapter 2.13.5**). Successful identification of these cross-linked peptide pairs required knowledge of the peptide sequences that were likely to be linked to one another. The pilot studies were deemed to have failed to resolve cross-linked peptide pairs in part because of insufficient starting material. The signal on the coomassie stained gels indicated that there was still insufficient material to reliably detect cross-linked peptides. Therefore, each peptide sample was reduced, alkylated, and then injected in triplicate for LC-MS/MS. The aim of the new approach was to collect quantitative data about the peptides to allow more accurate estimation of the protein quantities from each fraction.

The ability of DSP to cross-link YB-1 was confirmed by searching the LC-MS/MS data with the monoisotopic mass of a reduced and alkylated DSP adduct (145.0197

u; **Figure 2.3**) included as a variable modification to lysine residues. The results show that of the 22 unique peptide sequences that aligned to YB-1, 14 include either the reduced or alkylated DSP adduct. Of the 14 peptide sequences with evidence of cross-linking, 9 were only ever observed with the modification corresponding to a reduced and alkylated DSP adduct. The remaining 5 peptide sequences were detected with and without DSP adducts. YB-1 peptides with DSP adducts were detected in LC-MS/MS runs from B1 as well as from F1.

The DSP adducts from the YB-1 that migrated as a monomer, in B1, were extensive. The YB-1 in this region did not show a mass shift compared to reduced YB-1, indicating that these adducts were most likely to be the result of DSP reacting with two lysines on a single YB-1 molecule (intra-protein cross-links). The results confirmed that the DSP cross-linking reaction was highly efficient in these MDA-MB231 cells and that YB-1 was cross-linked by DSP.

6.2.5 The PPI of cross-linked YB-1 from MDA-MB231 cells during cisplatin exposure.

To gain information about the proteins that purify with YB-1, all LC-MS/MS data (pooled) from this experiment were searched against the human UniProtKB database. Pooling the searches from all runs and filtering the search data, as outlined in **Chapter 4.2.3**, resulted in the identification of 461 unique proteins (see `CD/Chapter_6/All_crosslinked_protein_ID.xlsx` for full results including Uniprot identifiers). Of these 461 proteins, 307 (67%) were observed in all three samples (**Figure 6.6.A**; protein groups shown in `CD/Chapter_6/euler_xlink_all_cisplatin.csv`). The euler diagram also highlighted that the protein identifications varied in response to cisplatin exposure without being strongly disrupted.

The altered IP protocol incorporated cross-linking and a new antibody, and this would have influenced the proteins that were recovered with YB-1. To test the consistency of the PPI of YB-1, the proteins that copurified with cross-linked YB-1 were compared to the protein identifications from previous purifications of YB-1 (**Chapter 4.2.3**). This comparison highlighted that 55% of the proteins from the MDA-MB231 cells in the subcellular experiments were shared with identifications from the cross-linked MDA-MB231 cells (140 out of 254 proteins; **Figure 6.6.B**; protein groups shown in `CD/Chapter_6/euler_xlink_all_Mcyt_Mnuc.csv`). The proteins that copurified with YB-1 from both the cytoplasm and nuclei of MDA-MB231 cells had the best coverage with 59 out of 89 proteins identified in the YB-1

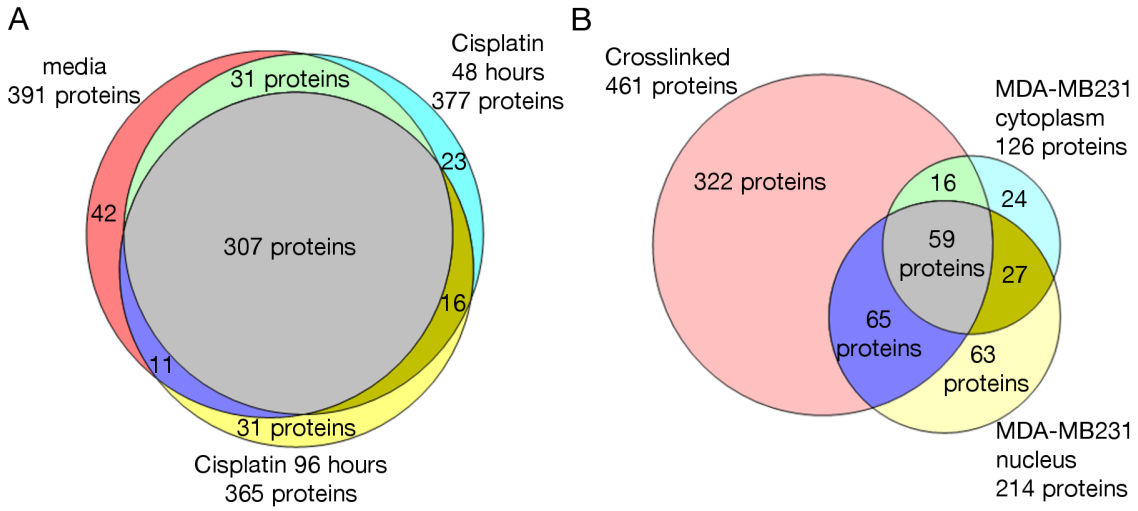

Figure 6.6: Euler diagrams showing all proteins (pool) that copurify with YB-1 from cross-linked MDA-MB231 cells and in the cytoplasm and nucleus of MDA-MB231 cells. **A**, the distribution of pooled protein identifications between media (red), 48 hrs of cisplatin exposure (turquoise), and 96 hrs of cisplatin exposure (pale yellow). **B**, the distribution of all protein identifications from cross-linked MDA-MB231 cells (red) and the cytoplasm (turquoise) and nucleus (pale yellow) of MDA-MB231 cells in **Chapter 4.2.3**. The number of protein identifications are indicated in each quadrant.

immunoprecipiations from cross-linked MDA-MB231 cells (69%). Of the proteins that were identified exclusively in the cytoplasm or nucleus of MDA-MB231 cells, 40% of the cytoplasmic (16 out of 40 proteins) and 50% of the nuclear proteins (65 out of 128 proteins) were also identified in this experiment.

The PPI of YB-1 from the cytoplasmic fractions were expected to exhibit the strongest concordance with the protein list from the cross-linked IP. This is because the protein lysates were loaded to the YB-1 IP with an input ratio of 1:1 with these cross-linked immunoprecipiations. The results from the nuclear fractions were expected to include PPI that were too rare to detect, as the nuclei to cell number was 10:1 for the nuclear proteins. However, the results showed that $\sim$ 60% of the protein identifications from nuclear fractions of MDA-MB231 cells overlapped with those from YB-1 that was purified from cross-linked MDA-MB231 cells (124 out of 214 proteins; **Figure 6.6.B**; protein groups shown in `CD/Chapter_6/euler_xlink_all_Mcyt_Mnuc.csv`). Therefore, this experiment provided confirmatory evidence of an interaction with YB-1 for $\sim$ 60% of the proteins that were identified in **Chapter 4.2.3**.

Many of the proteins identified in this experiment were absent in cytoplasmic or nuclear fractions from MDA-MB231 cells (322 out of 461 proteins; **Chapter 4.2.3**). These protein level identifications may have been the result of weak and transient

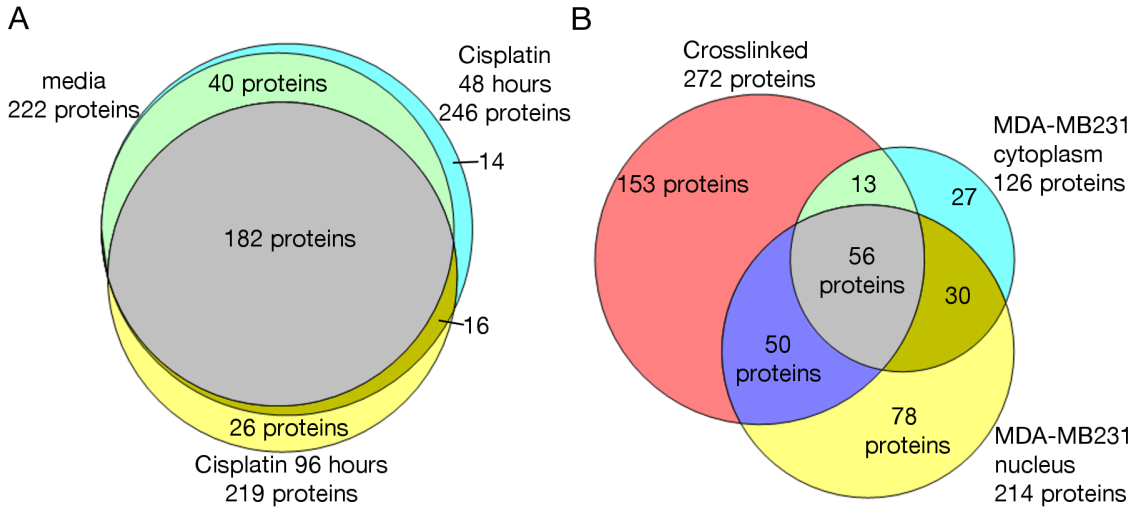

Figure 6.7: Euler diagrams showing the proteins detected in fraction 1 (F1) from immunopurified YB-1 from cross-linked MDA-MB231 cells and in the cytoplasm and nucleus of MDA-MB231 cells. **A**, the distribution of protein identifications in F1 between media (red), 48 hrs of cisplatin exposure (turqoise), and 96 hrs of cisplatin exposure (yellow). **B**, the distribution of the pooled protein identifications in F1 from cross-linked MDA-MB231 cells (red) and the cytoplasm (turquoise) and nucleus (pale yellow) of MDA-MB231 cellsin **Chapter 4.2.3**. The number of protein identifications are indicated in each quadrant.

interactions being stabilised by DSP. Alternatively, the addition of 2.5 fold more antibody may have resulted in an increased yield of YB-1 and a concomitant increase in the amount of copurified proteins.

The region of the gel that contained mass-shifted YB-1 (F1) was hypothesised to be enriched for the direct interaction partners of YB-1. In total, 272 proteins were identified in F1 (see; **Table E.1** and `CD/Chapter_6/F1_crosslinked_protein_ID.xlsx` for full results). The presence of cross-linked proteins in F1 was supported by a predominance of proteins with a molecular weight below 80 kDa, despite F1 being cut from above 90 kDa on the gels (77%; 209 of 272 proteins; **Figure 6.5**). Sixty-seven percent of the protein identifications were present in all three samples (182 out of 272 proteins; **Figure 6.7.A**; protein groups shown in `CD/Chapter_6/euler_xlink_F1_drugs.csv`). The protein identifications from F1 of the media-only IP overlapped entirely with those from F1 of the 48 hrs cisplatin exposure YB-1 IP. Twenty percent of the protein identifications in F1 were unique to the samples that were exposed to cisplatin (56 out of 272 proteins; **Figure 6.7.A**). Cisplatin exposure altered a cohort the PPI of YB-1 in MDA-MB231 cells.

The protein identifications from F1 were also compared to those from the subcellular localisation experiments (**Chapter 4.2.3**). The direct interaction partners of YB-1 were hypothesised to be enriched in F1. The presence of these direct inter-

action partners meant that the identifications that overlapped with the subcellular experiments were likely to be genuine YB-1 interaction partners. The results show that 44% of the proteins identified in F1 were also observed in the subcellular fractionation experiments (119 out of 272 proteins; **Figure 6.7.B**; protein groups shown in `CD/Chapter_6/euler_xlink_F1_Mcyt_Mnuc.csv`). Therefore, a greater proportion of the proteins that were identified in F1, the region of the gels that contained cross-linked YB-1, overlapped with the proteins that were identified in **Chapter 4.2.3** when compared to the pooled protein identifications from this experiment (30% or 139 out of 461; **Figure 6.6.B**).

Purifying YB-1 from MDA-MB231 cells that were cross-linked using DSP recovered cross-linked YB-1. The detection of peptides with reduced or alkylated DSP adducts at lysine residues confirmed that the cross-linking was successful. These adducts were detected on YB-1 peptides from B1 and F1, indicating that intra-protein and inter-protein DSP cross-links were present on YB-1. Approximately 60% of the protein identifications from **Chapter 4** were also observed copurifying with cross-linked YB-1. However, $\sim$ 70% of the protein identifications were unique to this experiment.

6.2.6 Bioinformatic analyses of PPI of cross-linked YB-1 during cisplatin exposure

The potential function(s) of YB-1 in MDA-MB231 cells during cisplatin exposure were examined by analysing the functions that were attributed to the identified proteins. These analyses were carried out using DAVID. The results from DAVID for all protein identifications are provided in `CD/Chapter_6/DAVID_files/xlink_all_DAVID_FAC_20151125.txt`. However, the proteins identifications from F1, which include quantitative data, were the basis for the analyses that follow.

The enrichment analysis presented here was performed using the 272 proteins that were identified in F1. The results from DAVID provide further support for the multifunctional nature of YB-1 (summarised in **Table 6.1**; full results in `CD/Chapter_6/DAVID_files/xlink_F1_DAVID_FAC_20151125.txt`). The proteins that coimmunoprecipitated with mass-shifted YB-1 in F1 were enriched for annotations relating to interaction with RNA, including those for ribosomal proteins (Enrichment = 55.35), RNA splicing (Enrichment = 8.63), and RNA stabilisation (Enrichment = 5.86). Other annotations, which were also observed in the previous experiments, were associated with the chromosome (Enrichment = 2.22), ubiquitin conjugation

Table 6.1: Enriched terms in the proteins that interact with cross-linked YB-1 (F1).

Cluster description	All identified	Up or down
ribosome:ribonucleoproteins:RNA binding	55.35 (54 - 93)	-
transit peptide:mitochondrion	12.7 (30 - 54)	-
ubiquitin conjugation:isopeptide bond	9.98 (21 - 29)	-
RNA processing:spliceosome	8.63 (15 - 60)	-
glycolysis	7.81 (12 - 26)	-
mRNA stabilization	5.86 (6 - 20)	-
Citrate cycle (TCA cycle)	4.83 (7 - 14)	-
Reg. of apoptosis:negative reg. of apoptosis	3.74 (17 - 34)	-
Internal ribosome entry pathway	2.49 (3 - 7)	-
14-3-3 proteins:protein targeting	2.36 (4 - 10)	-
chromatin assembly and organisation	2.22 (3 - 20)	1.71 (3 - 24)
DNA:double-stranded DNA binding	-	1.90 (4 - 8)

The **All identified** column includes the 272 proteins that were identified in F1. The **Up or down** column includes enrichment analysis from 64 proteins that increased by a ratio of ≥ 2 or decreased by ≤ 0.5 following either 48 or 96 hrs of exposure to 1.56 μM cisplatin. All 772 proteins that were identified as copurifying with YB-1 were used as a background for enrichment analysis of the **Up or down** column.

(Enrichment = 9.98), and also with mitochondrial localisation (Enrichment = 12.7). There were groups of enriched terms that were unique to this experiment. Specifically, those associated with glycolysis, the cell cycle (via the 14-3-3 proteins; Enrichment = 2.36), internal ribosome entry pathway (Enrichment = 2.49), and the citrate cycle (TCA cycle; Enrichment = 4.83) . Therefore, the functions of the proteins identified in F1 overlapped with the functionality of proteins identified in **Chapter 4.2.4**. Additional functional groupings of proteins that interact with RNA were detected via an enrichment for proteins that were involved in internal ribosome entry.

The potential function of the proteins that were detected in F1 was further examined by building an *in silico* PPI network comprised of all the protein identifications from F1 using String (v10). This network was highly enriched for edges indicating a high degree of PPI. There were 4957 edges (PPI) amongst the 268 proteins that were mapped using the String database (**Figure 6.8**). The level of PPI that would be expected from a random sample of 268 proteins from any location in the genome was 132 edges (Enrichment, protein-protein interaction, P-value = 0; String v10). Decompositional clustering using markov clustering produced two groups of proteins that incorporated 78% of the network; cluster 1 (120 proteins) and cluster

2 (91 proteins) (**Figure 6.8**; cluster 1 and 2). The *in silico* network showed that the proteins in F1 were strongly connected to one another.

More specific details about the effect of cisplatin exposure on the PPI of YB-1 were gained via label-free quantification of each protein identification from F1. The label-free quantification used the average peak area of the three most abundant peptides for each protein identified in F1 (top three peptides method described in Silva et al. 2006). These data were used to compare the levels of YB-1 in F1 from each treatment. The levels of YB-1 in the F1 from each cisplatin treatment were calculated as a ratio of the amount of YB-1 in the control sample. The ratios from the quantitative data indicated that there was less YB-1 in F1 from the 48 hrs cisplatin exposure sample (0.82-fold of media) than there was in F1 from media only cells. There was no difference in the amount of YB-1 in F1 from media MDA-MB231 cells and those following 96 hrs of cisplatin exposure (1.02-fold of media loading).

The quantification of YB-1 was confirmed using the peak area of each precursor for the YB-1 peptides that were identified in F1 (outlined in **Chapter 2.13.4, Skyline**). The results from this more detailed screen of peptide precursor areas appeared to confirm that there was less YB-1 in F1 following 48 hrs of cisplatin exposure, with the YB-1 peptide ratio dropping by 0.83 ± 0.39 relative to media-only MDA-MB231 cells. Cisplatin exposure for 96 hrs elevated the YB-1 peptides by 1.10 $\pm$ 0.23 relative to F1 from media. However, the individual peptide quantifications varied, which was highlighted by the standard errors and also the plot of individual peptide identifications (**Figure 6.9**, YBX1). Given the variance in the YB-1 peptide quantifications, the quantitative values for the proteins identified in F1 were not normalised to YB-1 loading.

From the 272 proteins that were identified in F1, the abundance of 65 proteins changed following 48 or 96 hrs of cisplatin exposure (by $>$ 2-fold or $<$ 0.5-fold; full list in `CD/Chapter_6/F1_UP_DOWN.xlsx`). An analysis of the terms that were enriched was performed on these 65 proteins, and also YB-1, using DAVID. A stringent background was used for detecting which terms were enriched amongst these 65 proteins. This background was the list of all proteins that were identified in LC-MS/MS from all purifications of YB-1 in thesis (772 proteins; full list in `CD/Chapter_6/DAVID_files/All_proteinIDs_forDAVIDbackground.xlsx`). The results showed that the enriched terms amongst the proteins that had their abundance in F1 modulated by cisplatin exposure, were associated with chromatin assembly and organisation (Enrichment = 1.71) and also double-stranded DNA binding (Enrichment = 1.90 ; **Table 6.1**; full results in `CD/Chapter_6/DAVID_files/`

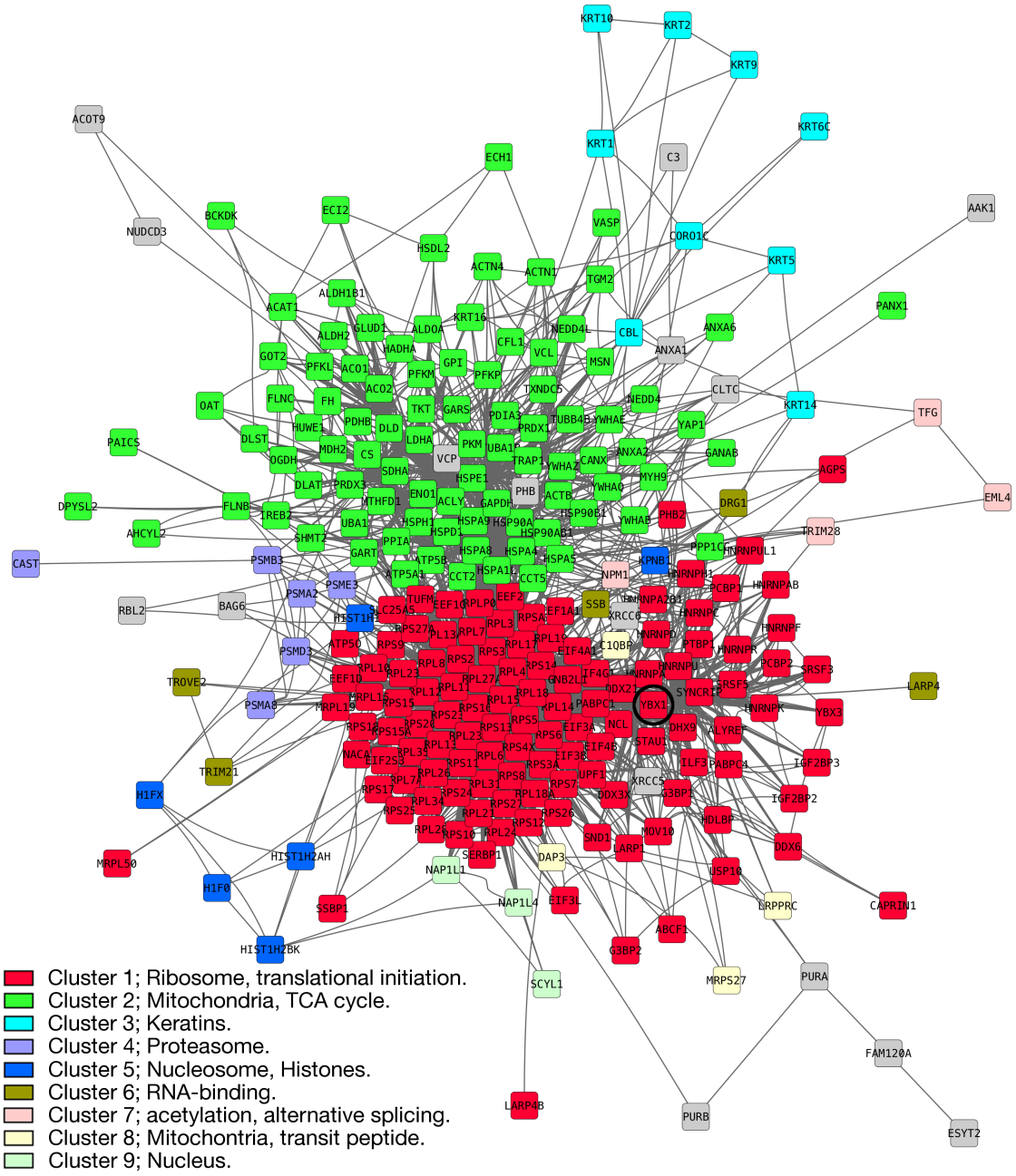

Figure 6.8: An *in silico* network of proteins that copurify with cross-linked YB-1 from cisplatin-treated MDA-MB231 cells. The predicted interactions of the proteins that were identified in F1 cross-linked YB-1 (String, v10). Markov clustering was applied and the network visualised in Cytoscape (v3.2). The network layout was performed using the Allegro spring electric plugin. The nodes that were grouped together by the MCL algorithm have been coloured according to the key on the bottom left-hand side of the image. This key also notes the primary function of the proteins in each cluster. The location of YB-1 is highlighted by a black circle.

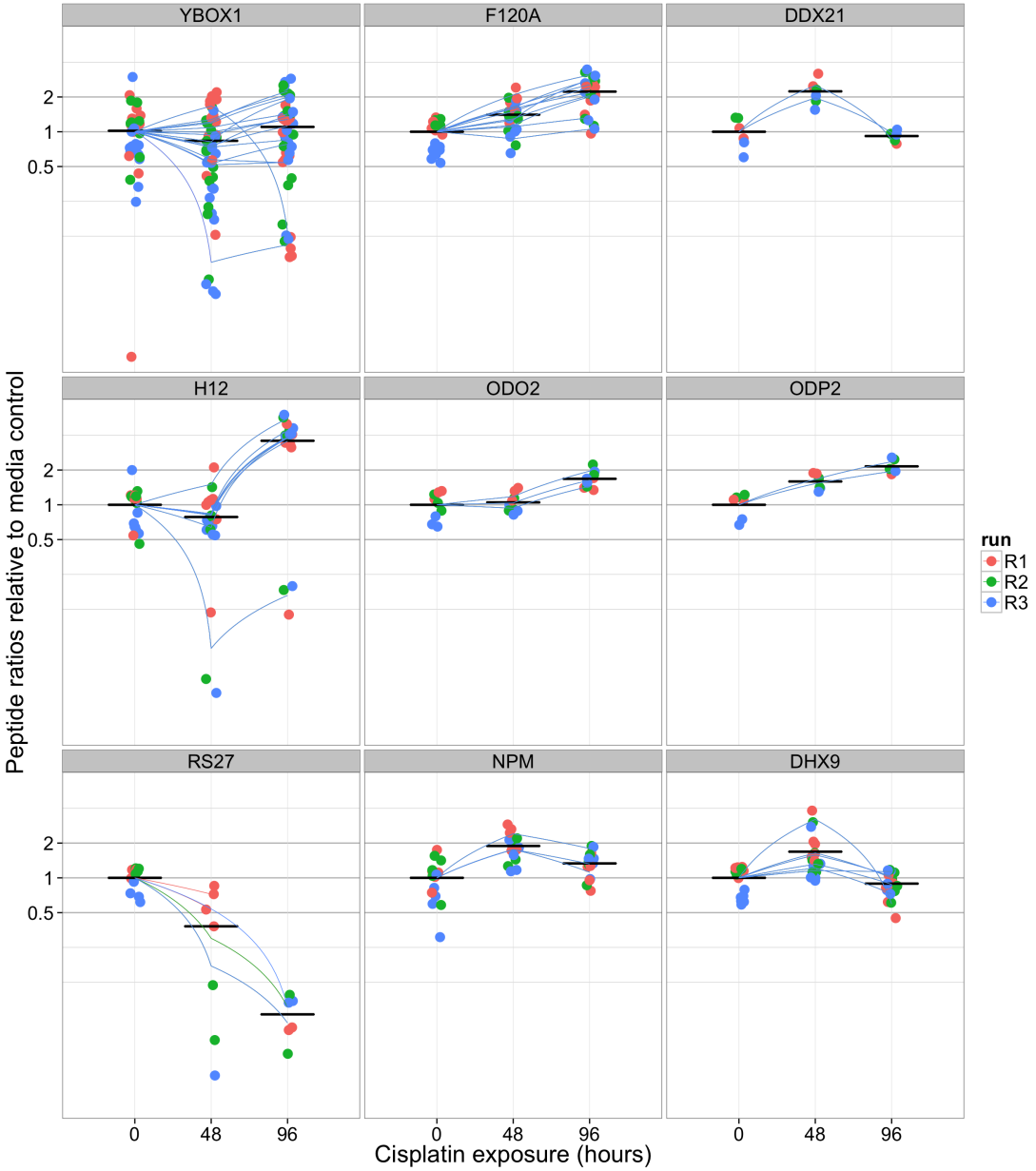

Figure 6.9: Quantitative changes in a subset of peptides for the proteins that interact with YB-1 during cisplatin exposure. These proteins were also detected in the cytoplasm or nuclei of MDA-MB231 cells in **Chapter 4.2.3** and the peptide quantification was performed using MS^1 filtering in Skyline. The y-axis was plotted in log2 and the major y-axis lines indicate a doubling (2) or halving (0.5) of the peptide quantification relative to no cisplatin exposure. The minor y-axis lines indicate successive doubling or halving of the quantifications. The mean inferred protein-level fold changes for each treatment are shown as black lines and the coloured lines linking the treatments lead to peptide-level means. The colour of the data points indicates which of the triplicate injection each peptide was detected in (R1 - R3). **Abbreviations**; YBOX = YB-1, F120A = Constitutive coactivator of PPAR-gamma-like protein 1, DDX21 = Nucleolar RNA helicase 2, H12 = Histone H1.2, ODO2 = Dihydrolipoyllysine-residue succinyltransferase component of 2-oxoglutarate dehydrogenase complex, mitochondrial, ODP2 = Dihydrolipoyllysine-residue acetyltransferase component of pyruvate dehydrogenase complex, mitochondrial, RS27 = 40S ribosomal protein S27, NPM = nucleophosmin, DHX9 = ATP-dependent RNA helicase A.

`xlink_F1_updown_2to0,5_FAC_allIPbckgrnd_20151125.txt`). These results appeared to indicate that during cisplatin exposure, a subset of cellular YB-1 became more involved in influencing transcription and/or chromatin structure. Thirty of the 65 (46%) modulated proteins included these enriched terms. The function of the other 35 proteins is highlighted in the following section.

To gain a better understanding of the relationship between the proteins that were modulated by cisplatin exposure, an *in silico* PPI network was built from the cisplatin modulated proteins. The *in silico* PPI network of the 62 proteins that String could map was enriched for edges (150 edges observed; 5.1 edges expected, P-value = 0, Enrichment, protein-protein interaction, String v10; **Figure 6.10**). Nine of the proteins lacked edges that connected them to the rest of the network.

The markov clustering algorithm was used to group the proteins in F1 that were altered in abundance by cisplatin exposure. The largest group of proteins that was modulated by cisplatin exposure were the ribosomal proteins, involved in translation (Cluster 1; 11 of 14 proteins, translation; GO:0006412; **Figure 6.10**). The second largest group included many proteins that were unique to this experiment. These proteins were involved in energy metabolism, specifically, the oxidation of carbohydrates and fatty acids (6 of 11 proteins, KEGG pathway; Citrate cycle [TCA cycle]). Other proteins from this group were mitochondrial (7 out of 11, mitochondrion; GO:0005739). Cluster 4 included proteins that were associated with the proteasome (5 of 7 proteins, proteolysis; GO:0006508, 4 of 7 associated with ubiquitin-dependent protein catabolic process; GO:0006511) while cluster 6 was dominated by cytoskeletal proteins (5 of 6 proteins, cytoskeleton; GO:0005856). The functional annotations for proteins in these clusters were not specifically enriched amongst the proteins that were modulated by cisplatin exposure (**Table 6.1**, the specific enrichments are summarised in column **Up or down**).

The proteins in the remaining groups, cluster 3 and cluster 5, included functional annotations that were specifically enriched amongst cisplatin modulated proteins (**Table 6.1**; chromatin and DNA binding). Cluster 3 was diverse. It included proteins that can shuttle between the cytoplasm and nucleus and also form mRNPs (HNRNPA2B1, ALYREF, YBX1, ILF3, NPM1, ribonucleoprotein complex; O:0030529). Proteins in this cluster, including YB-1, may also regulate transcription (YBX1, ILF3, TRIM28, NPM1; GO:0030528) and transcriptional repression (YBX1, ILF3, TRIM28; GO:0016564). Cluster 5 was connected to cluster 3 by 4 proteins (NPM1, ILF3, NAP1L1, and NAP1L4). Three of these proteins shared an annotation for nucleosome assembly (NAP1L1, NAP1L4, NPM1) with 5 of the 7

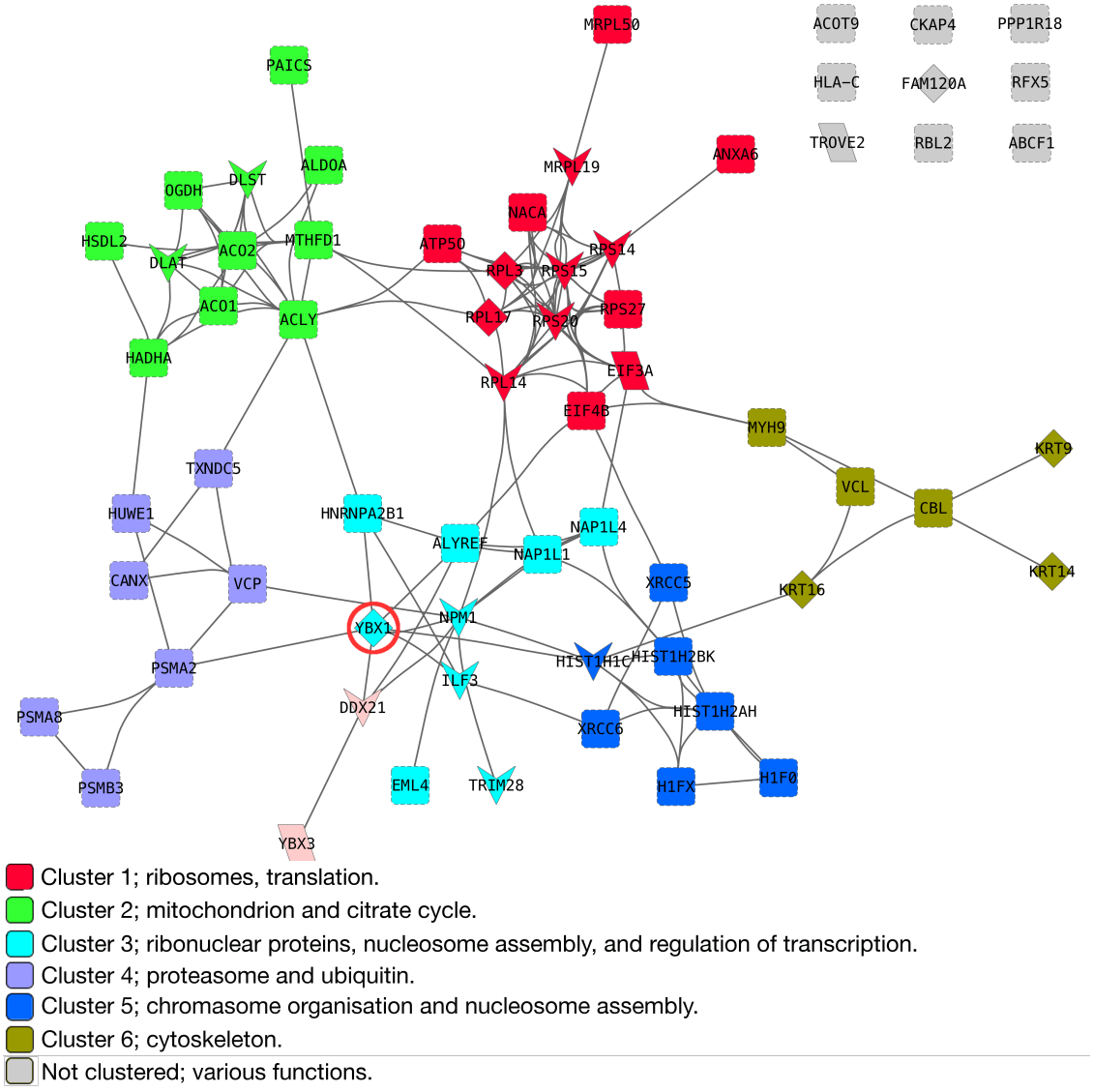

Figure 6.10: A network of proteins that copurify with cross-linked YB-1 and change their abundance in F1 in response to cisplatin exposure (by $\geq$ 2-fold or $\leq$ 0.5-fold by top 3 quantification). The predicted *in silico* interactions of the proteins that were identified interacting with cross-linked YB-1 (String, v10). Markov clustering was applied and the network visualised in Cytoscape (v3.2). Nodes that were grouped by the MCL algorithm have been coloured. The key shows the colour for each node alongside a summary of the functional annotations for proteins in the cluster. The location of YB-1 is highlighted by a red circle. The shape of the nodes indicates whether a protein was detected interacting with YB-1 in a subcellular compartment of MDA=MB231 (**Chapter 4.2.4**); Square nodes = not detected in subcellular samples, rhomboid nodes = cytoplasm, diamond nodes = cytoplasm, and nucleus, arrow = nucleus.

proteins in cluster 5 (GO:0034728). In addition to the association with nucleosome assembly, all 7 proteins in cluster 5 were associated with chromosome organization (GO:0051276).

The network analyses highlighted that two clusters in the *in silico* network included proteins associated with chromatin and DNA binding. These terms appeared to co-operate with YB-1 to protect MDA-MB231 cells during cisplatin exposure. To continue studying the process(es) by which YB-1 protects MDA-MB231 cells during cisplatin exposure, proteins needed to be selected from those that were detected interacting with YB-1. The following criteria were used to guide the selection of proteins that had the potential to be important interactions for YB-1 during cisplatin exposure;

- Proteins whose association with YB-1 was altered by cisplatin exposure;
- Proteins with terms that were enriched specifically in the cisplatin modulated group (chromatin assembly and organisation; DNA:double-stranded DNA binding);
- Proteins that functioned as effectors; proteins with enzymatic and/or regulatory functions;
- Proteins that were detected in the nucleus of MDA-MB231 cells in **Chapter 4**.

These guidelines directed research into the 65 proteins that were modulated following cisplatin exposure. As cisplatin creates DNA damage, effector molecules involved in DNA repair were of particular interest. Three proteins involved in DNA repair fit the above criteria; X-ray repair cross-complementing protein 5 [also known as Ku80] (XRCC5), X-ray repair cross-complementing protein 6 [also known as Ku70] (XRCC6), and Transcription intermediary factor 1-beta [also known as TIF1B or KAP1] (TRIM28).

XRCC5 and XRCC6 form a dimer with one another to repair double-strand breaks via non-homologous end joining (Davis & Chen 2013). Nucleotide excision repair, rather than non-homologous end joining, is the canonical pathway for the repair of DNA damage caused by cisplatin. However, cisplatin adducts that have not been repaired prior to S-phase may then give rise to double-strand breaks (Bosco et al. 2004, Huang et al. 2004b, Kaminski et al. 2008). XRCC6 was only detected in the cytoplasm of MDA-MB231 cells in **Chapter 4** while XRCC5 was only detected

following 48 hrs of cisplatin exposure. An increase in the association of YB-1 and DNA repair proteins was consistent with the recruitment of YB-1 to DNA repair machinery. However, the association of XRCC6 with YB-1 was unchanged following 48 hrs cisplatin exposure and then it reduces to 0.20-fold after 96 hrs. Therefore, the quantitative data were inconsistent with YB-1, XRCC5, and XRCC6 interacting to promote the repair of DNA damage from cisplatin via non-homologous end joining.

TRIM28 was the other DNA repair protein that was regulated by cisplatin exposure. TRIM28 can act as an effector molecule during the repair of double-stranded DNA (reviewed in Lemaitre & Soutoglou 2014). In addition to this, TRIM28 can influence transcription (Friedman et al. 1996, Wang et al. 2007). TRIM28 regulates both pathways through the ability to influence the formation of heterochromatin (reviewed in Lemaitre & Soutoglou 2014). Following 48 hrs of cisplatin exposure, TRIM28 was elevated 3.05-fold and remained slightly elevated after 96 hrs (1.38-fold). In **Chapter 4**, TRIM28 was detected in the nucleus of MDA-MB231 cells. These observations were consistent with the interaction of YB-1 and TRIM28 to influence transcription or DNA repair during cisplatin exposure. TRIM28 was chosen as a representative of the DNA interacting proteins.

The results from functional enrichment analysis indicated that proteins involved in chromatin formation (cluster 5) were important to the function of YB-1 during cisplatin exposure. However, the peptides that were identified for the proteins in cluster 5 provided poorly resolved protein identifications. For example, the peptides that provided identification of histone 1.2 were equally likely to come from histone 1.4. This low resolution was partly due to the strong sequence homology of the histone proteins. Furthermore, the histone proteins are small, which reduces their potential to produce proteotypic peptides that are appropriate for detection using LC-MS/MS. Including the mass adducts of common histone modifications, such as acetylation, in searches of the LC-MS/MS data provided no further information about the effects of cisplatin on the histone proteins that interacted with YB-1 during cisplatin exposure.

The proteins that linked cluster 3, which included YB-1, to the chromosomal proteins in cluster 5 could regulate the function of the latter group in the *in silico* network. Four proteins, Interleukin enhancer-binding factor 3 (ILF3), Nucleophosmin (NPM1), Nucleosome assembly protein 1-like 1 (NAP1L1), and Nucleosome assembly protein 1-like 4 (NAP1L4), linked these two clusters of proteins. Edges connected ILF3 to 4 out of the 8 proteins in cluster 3 (**Figure 6.10**). ILF3 was also detected in the nucleus of MDA-MB231 cells (**Chapter 4**). During cisplatin

exposure, the interaction of ILF3 with YB-1 appeared to weaken. The levels of ILF3 reducing in F1 by 48% following 48 hrs of cisplatin exposure and by 56% following 96 hrs. Furthermore, ILF3 has similar multifunctionality to YB-1, as it can bind to DNA and RNA to influence transcription, splicing, and translation (Castella et al. 2015). This made the functional significance of this interaction unclear.

NAP1L1 and NAP1L4 are involved in the formation of chromatin via roles as chaperones for histone proteins. They were reduced 0.47-fold and 0.49-fold respectively, following 96 hrs of cisplatin exposure. Neither protein was detected in **Chapter 4**. The abundance of NPM1 in F1 reduced 0.29-fold after 48 hrs and 0.44-fold after 96 hrs of cisplatin exposure. However, more accurate analysis, using Skyline, indicated that interference in one of the peptides used for quantification artificially elevated the quantification in the media samples. Without any clear candidates from this group of four proteins, or from directly within cluster 5, TRIM28 was chosen as the sole representative of the chromatin assembly proteins.

Inspection of the quantitative data also highlighted other proteins of interest. Of these, Constitutive coactivator of PPAR-gamma-like protein 1 [also known as OSSA] (FAM120A) was reliably detected in all samples. It was also detected in the nucleus of MDA-MB231 cells (**Chapter 4.2.4**). The levels of FAM120A in F1 were elevated following cisplatin exposure, increasing 1.95-fold following 48 hrs and 2.96 fold following 96 hrs of cisplatin exposure. Since its annotation in 2001 the function(s) of FAM120A have remained largely unknown. In the mouse, FAM120A appeared to be an RNA-binding protein (Kobayashi et al. 2008). A manual query of a screen of RNA-binding proteins (Baltz et al. 2012) confirmed that human FAM120A also appeared to bind RNA. FAM120A may also be an effector molecule with the ability to regulate the activity of Src kinases to protect cells from oxidative stress-induced apoptosis (Tanaka et al. 2009). As an RNA-binding protein, FAM120A could provide insight into the detection of YB-1 function during cisplatin exposure via a pathway that TRIM28 was unlikely to be part of. Therefore, FAM120A was selected for further research.

6.3 Discussion

The results from the work that was presented here revealed that:

- Cross-linking alters the migration of YB-1 on non-reducing SDS-PAGE gels;
- The PPI reveals the interaction of YB-1 with clusters of functionally distinct

proteins that are consistent with the known molecular functions of YB-1;

- Cisplatin exposure leads to distinct but not global changes to the PPI of YB-1;
- Quantitative LC-MS/MS reveals that proteins associated with chromatin assembly and organisation, and DNA binding are disproportionately altered by cisplatin exposure.

6.3.1 Cross-linking YB-1

The results confirm that cross-linking YB-1 with DSP shifts YB-1 signals on immunoblots. This indicates the successful cross-linking of YB-1 with both formaldehyde and DSP. Furthermore, multiple DSP cross-linking sites are identified on YB-1 peptides using LC-MS/MS.

Following cross-linking, some of the YB-1 from lysates that were separated using non-reducing SDS-PAGE migrated as monomers. Attempts to remove this monomeric YB-1 from the immunoblots were unsuccessful. It was hypothesised that the monomeric YB-1 on non-reducing SDS-PAGE was in complex with other proteins prior to their preparation for non-reducing SDS-PAGE. Previously, the structural arrangement of YB-1 *in situ* was postulated to explain the differences in the sensitivity of ^{N}YB1 and YB1^{C} as prognostic markers (**Chapter 3.3**; Woolley et al. 2011). The physical occlusion of some regions of multimerised YB-1 would also stop DSP from forming inter-molecular cross-links on lysine residues in these regions of YB-1. Furthermore, the model of YB-1 homo-multimerisation presented by Skabkin et al. (2004) allows monomeric YB-1 (B1) to be cross-linked variously at the N-terminus or C-terminus depending on the level of YB-1 saturation on individual RNA transcripts.

More information about the intra- and inter-molecular cross-links would have allowed further analysis of this model. However, rather than collecting cross-linked peptide data, quantitative data was obtained using F1 from gels of YB-1 that was purified from cisplatin-treated MDA-MB231 cells. This quantitative data provides critical insights into the effects of cisplatin exposure on the PPI of YB-1.

6.3.2 Protein interactions of YB-1 during cisplatin exposure

The functional enrichment and *in silico* network analyses are concordant with the results in **Chapter 4**. Amongst the proteins that copurified with YB-1, there are proteins that interact with RNA transcripts as they are transcribed through

to their translation. In both sets of experiments, there are groups of proteins that interact with DNA and also those which have functional annotations associated with mitochondria. The discussion here focuses on the effects of cisplatin exposure on the PPI of YB-1.

The data presented in this chapter indicate that YB-1 continues to participate in most functions irrespective of cisplatin exposure. Exposing MDA-MB231 cells to up to 6.125 μM cisplatin had little effect on the migration of cross-linked YB-1 on immunoblots. Analyses using LC-MS/MS show that 1.56 μM cisplatin exposure for up to 96 hrs also leads to subtle alterations to a subset of the PPI of YB-1. Therefore, this work conflicts with reports linking cisplatin resistance with almost exclusive localisation of YB-1 to the nucleus (Yahata et al. 2002, Gaudreault et al. 2004). However, the results are consistent with the localisation of YB-1 in MDA-MB231 cells during exposure to 1.56 μM cisplatin (**Chapter 5.2.5**). Specifically, IF shows that YB-1 remains in the cytoplasm during cisplatin exposure. This appears to be confirmed by the continued interaction of YB-1 with proteins with molecular functions in the cytoplasm. The increased intensity of YB-1 signal in the nucleus, and on the DNA, of MDA-MB231 cells that was observed using IF is consistent with the altered interaction of YB-1 with a subset of proteins associated with chromatin binding during cisplatin exposure.

In order to survive cisplatin exposure, cells need to decrease the amount of cisplatin that can modify DNA or become resistant to the effects of cisplatin modifying DNA (Kelland 2007). Reducing the amount of cisplatin that enters cells appears to be the primary mechanism by which cisplatin resistant cancer cells reduce the amount of cisplatin that reaches DNA (reviewed in Gately & Howell 1993). YB-1 has been reported to protect cells from cisplatin exposure via the transcriptional activation of the MDR-1 gene.

Transcription factors have diverse protein interactions and these alter when the transcription factors associate with chromatin (Mohammed et al. 2013, Li et al. 2015). The PPI of YB-1 from MDA-MB231 cells during cisplatin exposure did not provide strong support for the hypothesis that positive regulation of transcription was central to the role of YB-1 during cisplatin exposure. Only 12 of the 272 proteins that are identified in F1 were annotated with transcription factor binding (GO:0008134; SND1, PURA, DRG1, CSDA, ENO1, YAP1, YWHAB, RPS3, PURB, TRIM28, NPM1, YWHAZ). There is evidence that FAM120A interacts with two transcription factors (FOXK2 and FOXQ1) but not when either protein is binding to chromatin (Li et al. 2015). Importantly, transcriptional proteins that have

been shown to interact with YB-1 previously, P300 and RNA polymerases (Chansky et al. 2001, Sengupta et al. 2011), were not detected in the current work. Finally, despite previous work linking YB-1, cisplatin exposure, and MDR-1 expression during cisplatin exposure, the predominant drug efflux pathways associated with cisplatin resistance appear to involve copper binding pathways rather than members of the ABC-transporter family, of which MDR-1 is a member (Larson et al. 2009, Samimi et al. 2003, Katano et al. 2002). In summary, the proteins that copurify with YB-1 from MDA-MB231 cells exposed to cisplatin provide little evidence that the YB-1 in MDA-MB231 cells positively influences transcription in response to cisplatin exposure.

The bioinformatic analyses indicates that the interactions of YB-1 with proteins that influence chromatin structure were disproportionately affected when MDA-MB231 cells are exposed to cisplatin. YB-1 has been linked to a repressive chromatin complex that includes H1.2 (Kim et al. 2008). H1.2 was identified in F1 from all three samples. Besides YB-1, only one of the other 7 proteins that have been shown to interact directly with H1.2, was also detected in F1; Transcriptional activator protein Pur-alpha (PUR-α). Notably, it is these three proteins together, H1.2, YB-1, and PUR-α, that can repress P53 driven transcription of the *BAX* gene by binding specifically with P53 that is bound to the *BAX* gene promoter (Kim et al. 2008). Other researchers have also found that PUR-α can promote cisplatin resistance (Kaminski et al. 2008).

TRIM28 can also repress the transcription of genes, specifically those that are targets of the E2F- family members, through its ability to promote the formation of heterochromatin (Wang et al. 2007). By repressing the transcription of E2F1 target genes in concert with TRIM28, YB-1 could slow cell division and provide more time for cisplatin damaged DNA to be repaired before S-phase. However, in order to function as a transcriptional repressor, TRIM28 needs to interact with a Kruppel-associated box zinc finger protein (Wolf et al. 2015). Kruppel-associated box zinc finger proteins were not detected in the current work. Changes in chromatin structure, such as the ability of TRIM28 to promote the formation of heterochromatin, can influence processes besides transcriptional repression (reviewed in Lemaitre & Soutoglou 2014).

In addition to altering gene transcription during cisplatin exposure, YB-1 may protect cells due to its interaction with cisplatin damaged DNA and participation in the repair of cisplatin damage to DNA (**Chapter 1.4.3**). Cisplatin causes multiple DNA adducts and legions which can be repaired by multiple repair mechanisms (re-

viewed in Siddik 2003). Nucleotide excision repair is thought to be the main DNA repair pathway that removes intra-strand cisplatin-DNA adducts (Siddik 2003). Base excision repair may also protect cells from cisplatin damage by rapidly removing cisplatin adducts before an inter-strand cross-link can form (Caiola et al. 2015). Finally, double-strand breaks in the DNA are a secondary form of cisplatin induced DNA damage. These result from the incorrect repair of cisplatin adducts (Huang et al. 2004b) or the presence of inter-strand cross-links during DNA replication (Bosco et al. 2004, Frankenberg-Schwager et al. 2005, Brozovic et al. 2009). The inter-strand cross-links and double-strand breaks have a significant effect on cell death following cisplatin exposure (Brozovic et al. 2009).

YB-1 may remove cisplatin adducts via nucleotide excision repair or base excision repair. YB-1 interacts preferentially with damaged DNA, and this binding may promote the repair of cisplatin adducts. Some of the chromatin proteins that were modulated by cisplatin exposure have the potential to participate in DNA repair. However, few of the DNA repair proteins that are known to interact with YB-1 were detected in this work. Gaudreault et al. (2004) links YB-1 with base excision repair and mis-match repair mechanisms through the interactions of YB-1 with MSH2, DNA polymerase delta, XRCC5, and WRN. However, in this study, only XRCC5 was detected. Furthermore, nucleotide excision repair, rather than base excision repair, is the primary repair pathway for intra-strand cisplatin-DNA adducts (Kothandapani et al. 2011). None of the nucleotide excision repair proteins, XPC, HR23B, or NEIL, that have been shown to interact with recombinant YB-1 (Das et al. 2007, Fomina et al. 2015) were detected in the current work. Other researchers also failed to recover NEIL when they purify either endogenous or exogenous YB-1 (Pestryakov et al. 2012). PCNA, which has crucial roles in DNA synthesis as well as in DNA repair, has previously been shown to interact with YB-1 (Ise et al. 1999). PCNA was identified in F1 in the current work, but cisplatin exposure has no effect on the levels of PCNA that copurify with YB-1. YB-1 may already be interacting with PCNA to promote an error tolerant DNA synthesis pathway in MDA-MB231 cells, as MDA-MB231 cells are aneuploid with 57 ± 5 chromosomes (Satya-Prakash et al. 1981). Therefore, the evidence to support the participation of YB-1 in nucleotide excision repair in MDA-MB231 cells during cisplatin exposure is equivocal.

The potential for YB-1 to participate in the repair of double-strand breaks in the DNA was studied. Three proteins that are involved in repairing double-strand breaks in DNA have been identified in F1; TRIM28, XRCC5, and XRCC6 (discussed

in **Chapter 6.2.6**). The subcellular localisation and quantification of XRCC5 and XRCC6 are inconsistent with an interaction with YB-1 promoting increased DNA repair during cisplatin exposure. TRIM28 is known to participate in the repair of double-stranded DNA breaks in regions of heterochromatin, where repair rates are slower (reviewed in Lemaitre & Soutoglou 2014). Through an interaction with these proteins, YB-1 may participate in the repair of double-stranded DNA breaks in heterochromatin. **Chapter 5** indicates that following the depletion of YB-1, MDA-MB231 cells begin to die after 2 - 3 days in 1.56 μM cisplatin. This timing is consistent with YB-1 having a role in the repair of double-stranded DNA breaks in regions of heterochromatin.

6.3.3 Differences from other studies

The discrepancies between the PPI detected in this work and by other researchers have already been noted. Various factors are likely to explain these discrepancies.

The YB-1 molecules that have been studied here differ from the YB-1 that were previously used to study the PPI of YB-1. The current work used YB-1 from MDA-MB231 cells. With the exception of Pestryakov et al. (2012), the other studies used ectopically expressed YB-1 to research the PPI of YB-1 (Ise et al. 1999, Chansky et al. 2001, Gaudreault et al. 2004, Das et al. 2007, Guay et al. 2008a, Kim et al. 2008, Garand et al. 2011, Tsofack et al. 2011, Fomina et al. 2015). The poor suitability of ectopically expressed YB-1 for studying PPI was highlighted (**Chapter 4.2.1**). Therefore, the use of endogenous YB-1 may explain some discrepancies in the PPI observed here and those observed previously.

Phosphorylation of YB-1 is likely to differ with cellular context. Previous studies utilised a wide range of cell types. The YB-1 in MDA-MB231 cells was phosphorylated at multiple sites (**Table.4.1**; Toulany et al. 2011). Phosphorylation to YB-1 at atleast one of these sites, serine 102, modulates the function of YB-1. There is little information available regarding the functional consequences of phosphorylation at other amino acids in YB-1. Therefore, the PPI of YB-1 are likely to be altered by the multiple phosphorylations to YB-1 in MDA-MB231 cells (**Table 4.1**).

The proteins that are available to interact with YB-1 also vary with the cellular context. The significance of the presence of wild-type P53 has already been discussed (**Chapter 5.3.2**). Gaudreault et al. (2004) used a cell line with wild-type P53 that is expressed at very low levels, HEK 293, to detect NONO and RALY interacting with exogenously expressed, calmodulin and streptavidin tagged, YB-1 during oxaliplatin

exposure (Tsofack et al. 2011). NONO and RALY were identified in the nucleus of MDA-MB231 cells but neither protein copurified with cross-linked YB-1. The failure to detect NONO or RALY in IP from cross-linked cells also highlights that the conditions of the purification impact on the identification of PPI.

The final, and potentially critical, reason that the results from the current study may differ from previous results relates to the manner of cisplatin exposure. Other studies exposed cells to cisplatin for different durations and at different concentrations. The cisplatin exposure used in this work is tolerated by the cells when YB-1 is present. However, the cisplatin exposures used by other studies, appear to be likely to cause cell death (discussed in **Chapter 5.3.3**). It is difficult to assess the significance of the PPI of YB-1 during a lethal exposure of cisplatin.

6.3.4 Summary

The work in this chapter indicated that many of the functions of YB-1 in MDA-MB231 cells were unaffected by cisplatin exposure. This is consistent with the results from IF (**Chapter 5.2.5**) that show cisplatin exposure causing consistent, but subtle, alterations to the localisation of YB-1. In the absence of gross perturbations to the PPI of YB-1, the quantitative LC-MS/MS data were used to investigate which YB-1 functions were altered and likely to be important to the survival of MDA-MB231 cells during cisplatin exposure. The interaction of YB-1 with chromatin proteins appeared to be important. Previous publications indicated that the ability of YB-1 to promote a transcriptional response is central to its role during cisplatin exposure. However, the results presented here highlight that the PPI of YB-1 provide little evidence that this occurs in MDA-MB231 cells during cisplatin exposure. Two proteins, FAM120A and TRIM28, were selected for further analysis. TRIM28 was chosen to represent the molecular function of YB-1 in nucleus, specifically transcriptional repression and the repair of DNA damage. The molecular function of FAM120A is less clear but cisplatin exposure lead to increased levels of FAM120A copurifying with YB-1 and it may be an RNA protein.

Chapter 7

Analysis of functional interactions between YB-1, FAM120A, TRIM28, and C1QBP

7.1 Introduction

Four-hundred and sixty-one proteins copurified with cross-linked YB-1 from MDA-MB231 cells (**Chapter 6**). The levels of 65 of these proteins altered in response to cisplatin exposure. A disproportionate number of these 64 proteins had functions relating to chromatin formation and double-strand DNA binding (**Chapter 6**). Two of these proteins, TRIM28 and FAM120A, were selected for further analyses. Both proteins were hypothesised to co-operate with YB-1 to help MDA-MB231 cells to survive cisplatin exposure. However, the functions of FAM120A and TRIM28 differ (discussed below). Therefore, separate hypotheses were required to explain the interaction of each protein with YB-1 in MDA-MB231 cells during cisplatin exposure.

Two hypotheses were generated to explain how the interaction of YB-1 and TRIM28 may promote the survival of MDA-MB231 cells during cisplatin exposure. The first hypothesis was that by interacting with one another, YB-1 and TRIM28 facilitate the repair of double-strand DNA breaks in regions of heterochromatin. TRIM28 has been shown to repair double-strand breaks in heterochromatic, or compacted, DNA. These DNA lesions are repaired more slowly than other double-strand breaks (Goodarzi et al. 2008, Goodarzi et al. 2009, Noon et al. 2010, Goodarzi et al. 2010). The second hypothesis was that the interaction of YB-1 and TRIM28

down-regulates transcription of E2F-family gene targets to slow the division of MDA-MB231 cells during cisplatin exposure. This hypothesis was inconsistent with the ability of YB-1 to positively regulate E2F1 gene targets (Lasham et al. 2012). However, increased interaction with TRIM28 during cisplatin exposure, which is known repress transcription from E2F-family gene targets (Wang et al. 2007, Hu et al. 2012, Chen et al. 2012), may lead to YB-1 functioning as a repressor E2F1 gene targets.

Although the function of FAM120A is poorly characterised it is thought that FAM120A is likely to bind to RNA (Kobayashi et al. 2008, Tanaka et al. 2009). Furthermore, FAM120A can influence cell survival in response to oxidative stress (Tanaka et al. 2009, Woźniak et al. 2014). The mechanisms that explains the ability of FAM120A to promote cell survival is poorly characterised. Tanaka et al. (2009) proposes that FAM120A protects cells from oxidative stress-induced apoptosis by regulating the activity of Src kinases. The same study suggests that this molecular function of FAM120A is due to its ability to act as a scaffold for kinases (Tanaka et al. 2009). The IL13 receptor subunit α-2 (IL13Rα2) required FAM120A to activate the Focal adhesion kinase 1 and PI3K pathways (Bartolome et al. 2015). At the cellular level, the interaction of FAM120A and the IL13Rα2 also promotes the survival of two colon carcinoma cell lines. Therefore, FAM120A and YB-1 appear to be unlikely to participate in a DNA repair pathway during cisplatin exposure. Instead, FAM120A and YB-1 were hypothesised to promote the survival of MDA-MB231 cells via either the regulation of kinase activity or the ability to influence gene expression by binding to RNA (splicing, translation, or protecting RNA from degradation).

YB-1 also interacts with nuclear-encoded mitochondrial proteins. These interactions did not appear to vary during cisplatin exposure (**Chapter 6**) but mitochondria play an important role in cell survival (Sena & Chandel 2012). During cisplatin exposure the mitochondria of a prostate cancer cell line, DU-145, promote cell death by producing reactive oxygen species (Marullo et al. 2013). C1QBP was chosen to represent the group of mitochondrial proteins that copurified with YB-1. C1QBP has been shown to participate in pre-mRNA splicing (Petersen-Mahrt et al. 1999, Zheng et al. 2003, Heyd et al. 2008), to interact with the immune system (reviewed in Peerschke & Ghebrehiwet 2014) and it is also a mitochondrial protein (Muta et al. 1997, Dedio et al. 1998, Hu et al. 2013).

C1QBP was identified in all IP samples in **Chapter 6** but cisplatin exposure did not alter the levels of C1QBP (1.45-fold at 48 hrs and 1.29-fold after 96 hrs). However, elevated levels of C1QBP can promote cell death (Meenakshi et al. 2003,

Sunayama et al. 2004, Reef et al. 2007). Furthermore, cisplatin exposure led to elevated levels of C1QBP in rat and HeLa cells (Meenakshi et al. 2003, Kamal & Datta 2006). There are conflicting reports regarding the effects of depleting C1CBP on the survival of HeLa cells following cisplatin exposure. One report showed that depleting C1QBP in HeLa cells increased the levels of cell death in response to cisplatin exposure (Hu et al. 2013). Another found that cell death was reduced (Kamal & Datta 2006). Given the number of studies that show increased levels of C1QBP leading to cell death, it was hypothesised that depleting C1QBP would protect MDA-MB231 cells during cisplatin exposure.

In this chapter, the presence and subcellular localisation of TRIM28, FAM120A, and C1QBP in MDA-MB231 cells were confirmed. Following this, the effects of depleting all three proteins in MDA-MB231 cells on the sensitivity to cisplatin was tested. Finally, the effects of depleting YB-1 on γH2AX foci formation during cisplatin exposure was used to study the role of YB-1 in repairing double-strand DNA breaks.

7.2 Results

7.2.1 The depletion and detection of FAM120A, TRIM28, and C1QBP

The specificity of the antibodies against TRIM28, FAM120A, C1QBP was tested. To do this, MDA-MB231 cells were allowed to settle in the presence of transfection-ready siRNA duplexes directed against TRIM28, FAM120A, C1QBP, and YB-1 at concentrations ranging from 2 - 10 nM. Lysates were collected after 48 and 96 hrs. The signal on immunoblots for each primary antibody corresponded with the expected mass of each protein (**Figure 7.1.A - C**; TRIM28 = 89 kDa, FAM120A = 122 kDa, C1QBP = 31 kDa). Furthermore, in each instance the siRNA duplexes effectively deplete this signal. **Figure 7.1.D** shows the depletion of YB-1 by 2 nM siYB1_1 and the stable levels of YB-1 following the depletion of FAM120A and TRIM28.

These results confirmed that each antibody could bind specifically to its target protein. They also confirmed that the siRNA duplexes depleted their target proteins. Therefore, the specificity of the tools for depleting and detected FAM120A, TRIM28, and C1QBP has been confirmed.

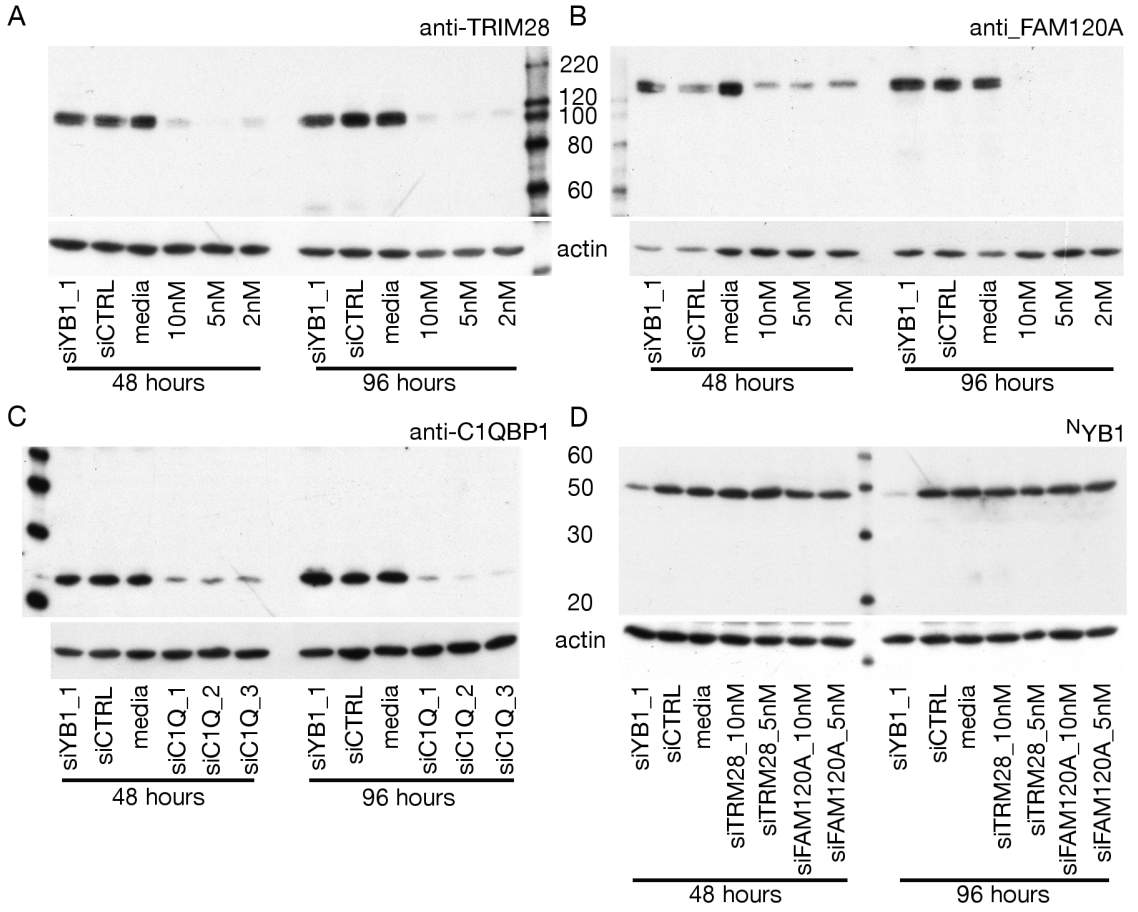

Figure 7.1: Validation of siRNA duplexes and antibodies to FAM120A, TRIM28, and C1QBP. MDA-MB231 cells were transfected with siRNA duplexes against FAM120A, TRIM28, and C1QBP at a range of concentrations (2 - 10 nM). The cells were harvested following 48 or 96 hrs and lysates prepared. Immunoblots were performed for cells transfected with each siRNA duplex and detected against the proteins that were targeted for depletion (TRIM28, **A**; FAM120A, **B**; C1QBP, **C**; ^{N}YB1, **D**). Even loading is confirmed using anti-β-actin (shown below each blot).

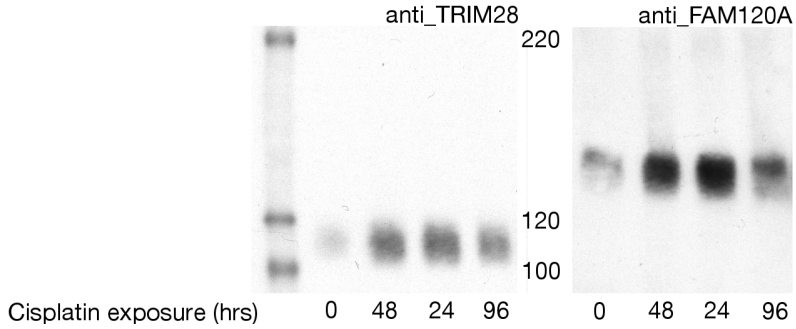

Figure 7.2: The levels of TRIM28 and FAM120A increase in MDA-MB231 cells following cisplatin exposure. MDA-MB231 cells were exposed to 1.56 μM cisplatin for 24 - 96 hrs. The lysates were separated on 6% SDS-PAGE gels prior to immunoblotting with antibodies against TRIM28 and FAM120A.

7.2.2 The effects of cisplatin exposure on TRIM28, FAM120A, and C1QBP in MDA-MB231 cells

TRIM28, FAM120A, and C1QBP copurify with YB-1 from MDA-MB231 cells during cisplatin exposure (**Chapter 6.2.5**). Cisplatin exposure did not alter the levels of C1QBP that copurified with YB-1 (**Chapter 6.2.5**). However, the levels of TRIM28 and FAM120A that copurified with YB-1 did increase in response to cisplatin exposure. Therefore, the effects of exposing MDA-MB231 cells to 1.56 μM cisplatin on the levels of TRIM28 and FAM120A were assessed. Lysates were collected from MDA-MB231 cells following 24, 48, and 96 hrs of exposure to 1.56 μM cisplatin. Immunoblots indicated that cisplatin exposure increased the amount of TRIM28 and FAM120A in MDA-MB231 cells (**Figure 7.2**). The signal from FAM120A highlighted that the protein may migrate as two separate bands but the resolution of the 10% SDS-PAGE was too low to confirm this (**Figure 7.1**). Lowering the acrylamide percentage of the gel to 6% should have provided better separation of FAM120A, however, the resolution was still insufficient to confirm the presence of two bands in the immunoblot of FAM120A (**Figure 7.2**). Therefore, these immunoblots indicated that cisplatin exposure may increase the levels of TRIM28 and FAM120A in MDA-MB231 cells.

TRIM28, FAM120A, and C1QBP were all excised from the region of gels that contained mass-shifted YB-1 that was purified from cross-linked MDA-MB231 cells (**Figure 6.5**, F1). However, TRIM28 and FAM120A migrated in the same region of the gel as mass-shifted YB-1 in the absence of cross-linking (**Figure 7.2**). Therefore, it was possible that TRIM28 and FAM120A were detected in F1 without being cross-linked to YB-1. If either protein was cross-linked to YB-1, its migration on

non-reducing SDS-PAGE will be further slowed following cross-linking.

The ability of cross-linking to alter the mobility of each protein was tested. Aliquots of MDA-MB231 cells were cross-linked using DSP and separated by non-reducing 6% SDS-PAGE. The results show that cross-linking slows the migration of FAM120A, TRIM28, and C1QBP (**Figure 7.3**). Cross-linking abolished monomeric TRIM28 from the immunoblot. FAM120A was similar, with the strongest signal migrating above the 220 kDa molecular weight marker. The presence or absence of monomeric C1QBP was unconfirmed as the mass of C1QBP was below the resolving limit of the 6% SDS-PAGE. However, the strong signal from C1QBP exhibited a mass-shift that was consistent with cross-linking. The immunoblots for all three proteins highlighted the presence of mass-shifted signal above 220 kDa (shown as bars in **Figure 7.3**). This was a region where mass-shifted YB-1 also appeared following cross-linking.

DNA and RNA were removed from aliquots of the cross-linked samples to confirm the primary importance of DSP adducts in altering the migration of YB-1, FAM120A, TRIM28, and C1QBP. Removing DNA and RNA had no effect on the migration of YB-1, TRIM28, FAM120A, or C1QBP (**Figure 7.3**). However, the removal of DNA and RNA increased the signal intensity. The improved solubility of proteins that were bound to DNA, which can precipitate with cellular debris when lysates are centrifuged, may account for these increases.

Cross-linking MDA-MB231 cells using DSP slowed the migration of FAM120A, TRIM28, and C1QBP. This signal was present in areas of gels where cross-linked YB-1 also migrated. Only a fraction of the mass-shifted FAM120A and C1QBP signals overlapped with those from YB-1, but all of the TRIM28 migrated in the same area of the gel as mass-shifted YB-1.

7.2.3 The distribution of C1QBP, TRIM28, and FAM120A in MDA-MB231 cells before and during exposure to cisplatin

In order to bind to one another, C1QBP, TRIM28, or FAM120A need to be present in the same area of MDA-MB231 cells as YB-1. IF was used to assess the distribution of each protein in MDA-MB231 cells. For this experiment, MDA-MB231 cells, grown on glass coverslips, were exposed to 1.56 μM cisplatin for 72 hrs. Following this, the cells were fixed and IF performed.

The literature indicated that C1QBP can localise to the mitochondria and nu-

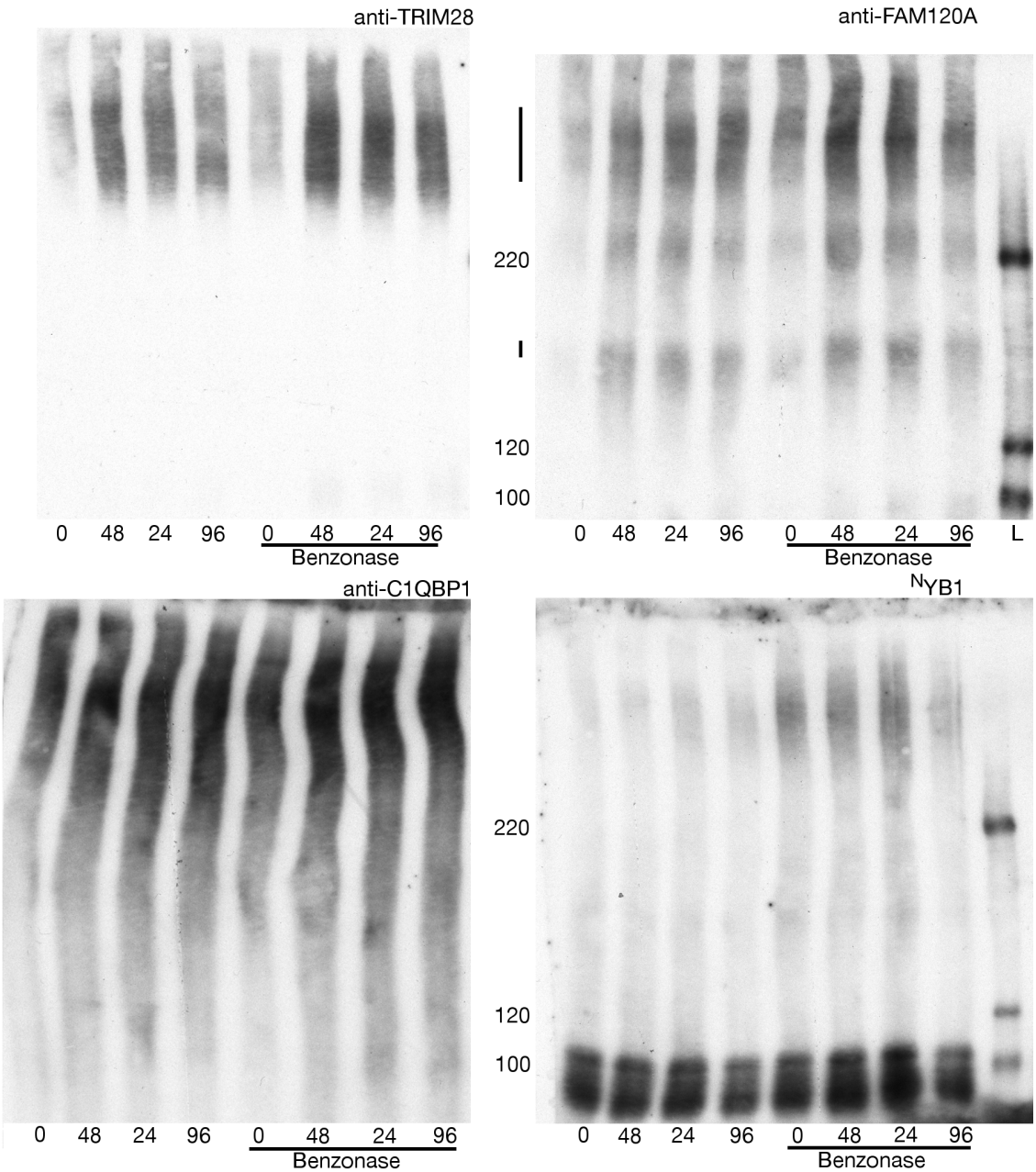

Figure 7.3: Cross-linking MDA-MB231 cells alters the migration of TRIM28, FAM120A, and C1QBP. MDA-MB231 cells were exposed to 1.56 μM cisplatin for 0 - 96 hrs prior to being cross-linked using DSP. The cross-linked lysates were separated using non-reducing 6% SDS-PAGE. Immunoblotting was performed using antibodies against TRIM28, FAM120A, C1QBP, and YB-1. The cells that were cross-linked come from an aliquot of the cells shown in **Figure 7.2**. Benzonase was used to remove RNA and DNA from aliquots of the cross-linked cells. The black bars that are adjacent to the TRIM28 and FAM120A immunoblots indicate regions where there were signals from cross-linked YB-1.

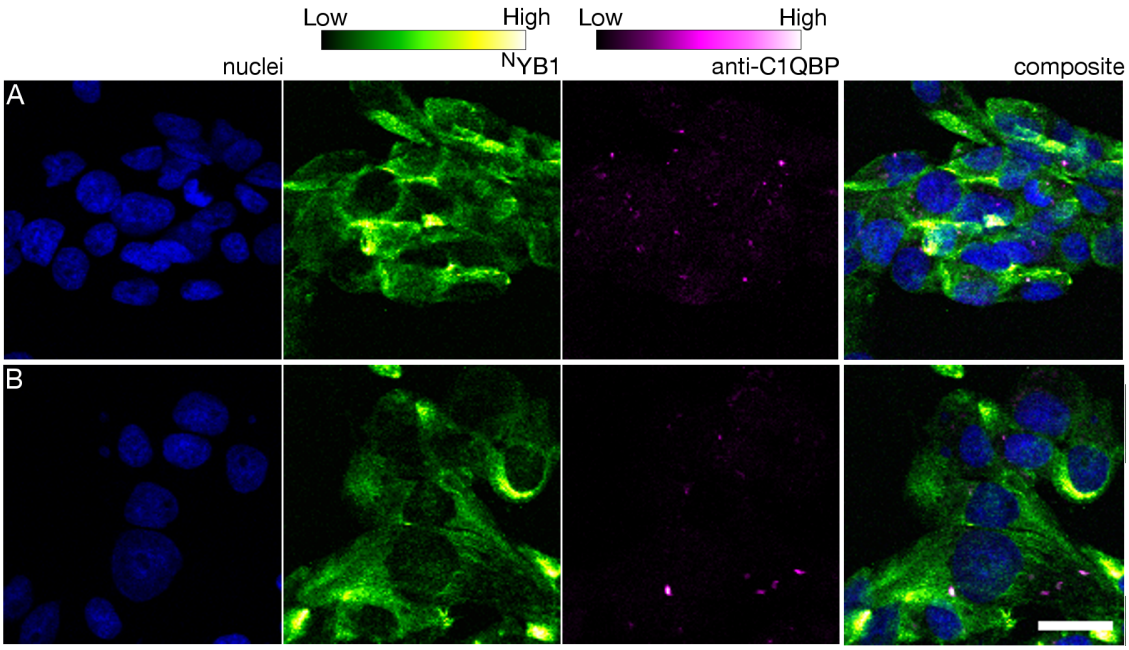

Figure 7.4: C1QBP and YB-1 in MDA-MB231 cells. IF signals from ^{N}YB1 (green) and anti-C1QBP1 (magenta) in MDA-MB231 cells in media (**A**) or after 72 hrs of exposure to 1.56 μM cisplatin (**B**) were assessed using confocal microscopy. Images are Z-projections of the maximal signal from 3 Z-slices across the nuclei of MDA-MB231 cells. ^{N}YB1 was labelled with AlexaFluor 488 and gray values are represented using the Green Hot LUT (ImageJ). C1QBP1 was labelled with AlexaFluor 568 and gray values were represented using the Magenta Hot LUT. DNA labelled with Hoechst is represented as blue. Scale bar is 25 μM.

cleus (**Chapter 7.1**). The results from IF indicated that most C1QBP localised in the cytoplasm close to the nuclear membrane, an area where it was most likely in mitochondria (**Figure 7.4.A**). Cisplatin exposure did not appear to alter the distribution of C1QBP in MDA-MB231 cells (**Figure 7.4.B**). There was signal from ^{N}YB1 in the same locations as that from C1QBP (**Figure 7.4.A - B**). Therefore, the interaction of YB-1 and C1QBP was most likely to occur in the mitochondria of MDA-MB231 cells.

The primary antibody preparations for TRIM28 and FAM120A were raised in rabbit and purchased with the aim of co-localising them with the signal from ^{N}YB1$_{sheep}$. However, the fluorescent signals from ^{N}YB1$_{sheep}$, and also an antibody against YB-1 that was raised in mouse (**Table 2.3; YB-1 [59-Q]**), were weak and diffuse. These signals were comparable to those from control cells that received no primary antibody for each secondary antibody. Therefore, the co-localisation of TRIM28 or FAM120A with YB-1 YB-1 was not confirmed.

The distribution of TRIM28 in MDA-MB231 cells was assessed. YB-1 was hypothesised to interact with TRIM28 in the nucleus. The signal from γH2AX is

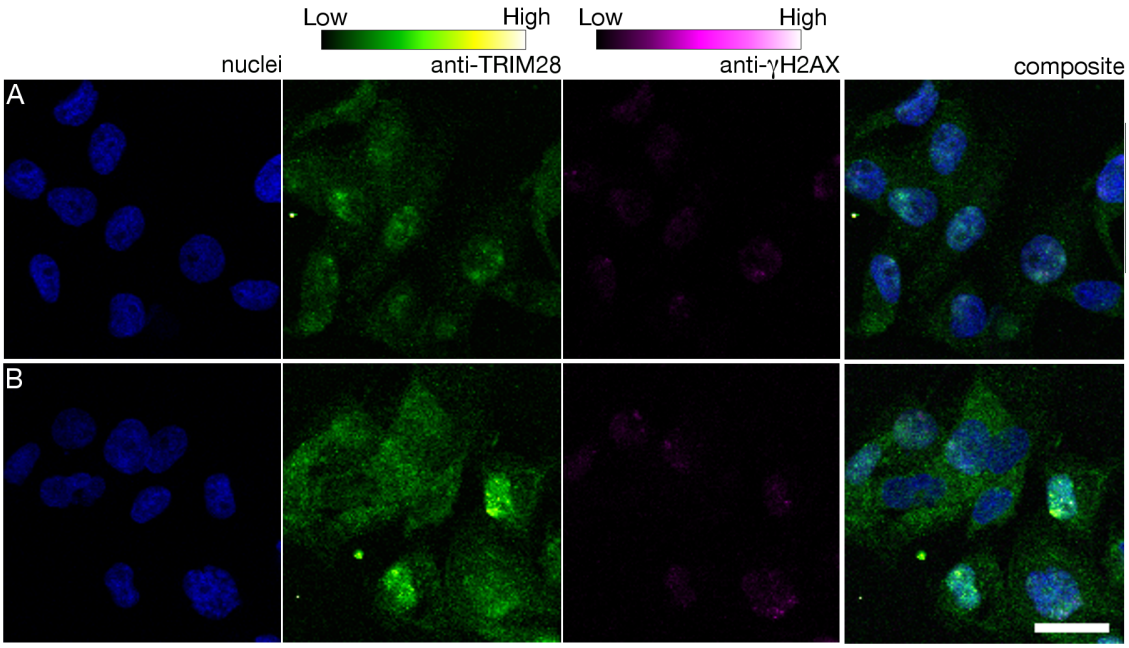

Figure 7.5: TRIM28 is distributed throughout MDA-MB231 cells and cisplatin exposure led to stronger TRIM28 signal in the nucleus. IF signal from TRIM28 (green) and anti-γH2AX (magenta) in MDA-MB231 cells in media (**A**) or after 72 hrs of exposure to 1.56 μM cisplatin (**B**) was assessed using confocal microscopy. Images are Z-projections of the maximal signal from 3 Z-slices across the nuclei of MDA-MB231 cells. TRIM28 was labelled with AlexaFluor 488 and gray values are represented using the Green Hot LUT (ImageJ). γH2AX was labelled with AlexaFluor 568 and gray values are represented using the Magenta Hot LUT. DNA labelled with Hoechst is represented as blue. Scale bar is 25 μM.

shown, as TRIM28 and YB-1 were hypothesised to interact during the repair of double-strand DNA breaks in regions of heterochromatin. γH2AX foci form around these breaks as they repair. The IF signal from TRIM28 showed that TRIM28 was distributed throughout MDA-MB231 cells (**Figure 7.5**). In many cells, the signal from TRIM28 was slightly stronger in the nucleus than the cytoplasm, and large foci were apparent in the nuclei of many cells. Following 72 hrs of exposure to cisplatin, the TRIM28 in some MDA-MB231 cells increased (**Figure 7.5.B**). Cisplatin exposure also led to a general brightening of the TRIM28 in the nuclei of many cells with more, and stronger, foci also evident in the nucleus.

The function of FAM120A is poorly characterised. Analysis of the IF signal from FAM120A highlighted that FAM120A was distributed throughout MDA-MB231 cells (**Figure 7.6.A**). The signal from FAM120A was predominantly in the cytoplasm and punctate FAM120A signal was observed in the nuclei of most cells. Seventy-two hrs of exposure to 1.56 μM cisplatin did not appear to alter the distribution of FAM120A signal in MDA-MB231 cells (**Figure 7.6.B**). The distribution

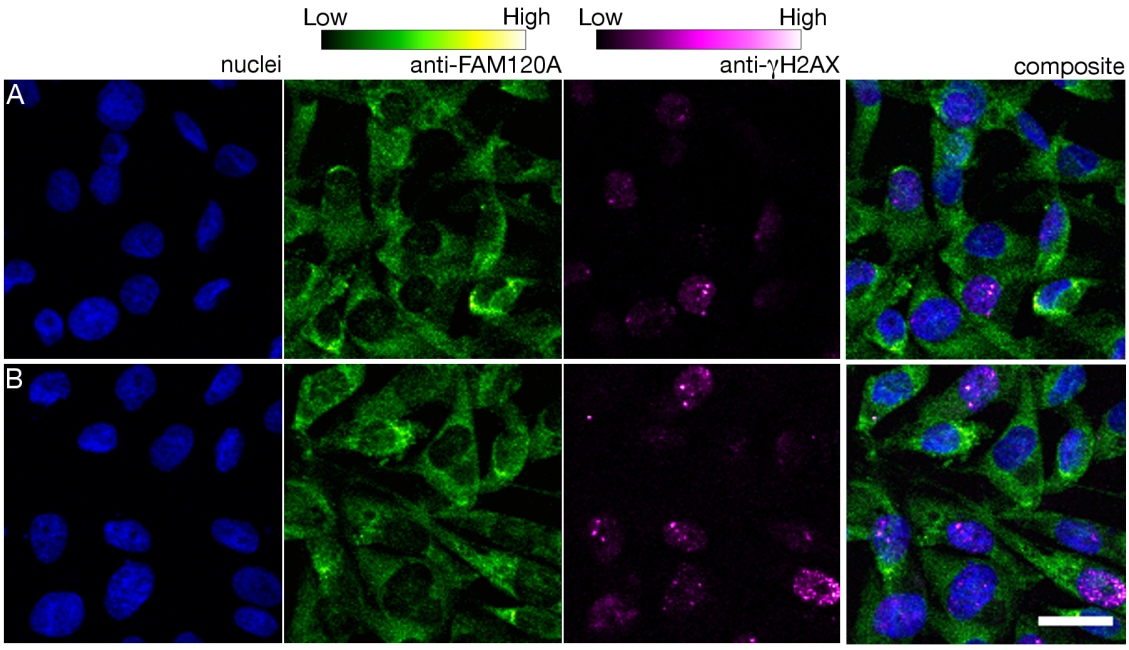

Figure 7.6: FAM120A is distributed throughout MDA-MB231 cells. IF signal from FAM120A (green) and anti-γH2AX (magenta) in MDA-MB231 cells in media (**A**) or after 72 hrs of exposure to 1.56 μM cisplatin (**B**) was assessed using confocal microscopy. Images are Z-projections of the maximal signal from 3 Z-slices across the nuclei of MDA-MB231 cells. FAM120A was labelled with AlexaFluor 488 and gray values are represented using the Green Hot LUT (ImageJ). γH2AX was labelled with AlexaFluor 568 and gray values were represented using the Magenta Hot LUT. DNA labelled with Hoechst is represented as blue. Scale bar is 25 μm.

of FAM120A in MDA-MB231 cells was similar to the distribution of YB-1 (**Figure 7.4.A - B**).

The distribution of two of the three proteins, C1QBP and TRIM28, in MDA-MB231 cells indicated that the function of each protein was only likely to overlap with discrete subsets of the functions of YB-1. These two proteins appeared to be associating with YB-1 via separate functional pathways. The distribution of FAM120A throughout MDA-MB231 cells indicated that YB-1 and FAM120A appear to be unlikely to interact at the cell-membrane as part of a kinase signal transduction network (Bartolome et al. 2015). Instead, the similarities between the distribution of signal from FAM120A and YB-1 in MDA-MB231 cells were more consistent with the hypothesis that FAM120A and YB-1 interacted with one another while binding to RNA.

7.2.4 FAM120A contributes to the survival of MDA-MB231 cells during cisplatin exposure

To examine the importance of each protein to MDA-MB231 cells during cisplatin exposure, each protein was depleted using siRNA duplexes (validated in **Chapter 7.2.1**) prior to a drug sensitivity assay being performed (the same design as **Chapter 5.2.4**). The strong reductions to cell viability that resulted from transfections using 5 nM siYB1_1 (**Figure D.9**) prompted a reduction to the maximum concentration of the siRNA duplexes from 5 nM to 2 nM. These experiments were designed to assess the functional links between YB-1 and the interacting proteins via analysis of the effect of each siRNA duplex on the growth-rates and morphology of MDA-MB231 cells. The effects of depleting a binding partner that is essential to the function of YB-1 should be similar to the effect of depleting YB-1 from the cells.

Depleting YB-1 was shown to reduce the growth-rate of MDA-MB231 cells (**Figure 5.1.D**). In these experiments, depleting YB-1 reduced the growth-rate of MDA-MB231 cells by 0.48 ± 0.40 compared to the siCTRL-treated cells (**Figure 7.7.A - B**; $t = 5.1437$, $df = 2$, p-value $= 0.03578$). The potential for the loss of FAM120A, TRIM28, or C1QBP to reduce the growth-rate of MDA-MB231 cells was assessed. The results show that depleting FAM120A, TRIM28, or C1QBP did not change the growth-rate of MDA-MB231 cells (**Figure 7.7.A - B**; for all t-tests, df=2, p-value >0.50; complete plots **Supplementary figures F.1 - F.5**). Therefore, the three proteins did not appear to be important to the function of YB-1 that leads to reduced growth in MDA-MB231 cells following YB-1 depletion.

The phase-contrast images from this experiment were used to assess how depleting each protein altered the morphology of MDA-MB231 cells. MDA-MB231 cells retained their normal morphology following transfection with the non-target siRNA duplex (siCTRL; **Figure 7.7.C**). Depleting YB-1 using 2 nM siYB1_1 led to increased numbers of cells with poor attachment while other cells also appeared to be unhealthy (siYB1_1; **Figure 7.7.C**).

The morphological changes of MDA-MB231 cells following the depletion of FAM120A, TRIM28, or C1QBP were also assessed. Depleting TRIM28 or C1QBP had no discernible effect on the morphology of MDA-MB231 cells (**Figure 7.7.C**, siTRIM28 and siC1Q_2). In contrast, depleting FAM120A did appear to alter the morphology of MDA-MB231 cells. Following the depletion of FAM120A, MDA-MB231 cells became less polarised and more cuboidal (**Figure 7.7.C**). Depleting FAM120A also appeared to increase the size of MDA-MB231 cells but this increase was not quan-

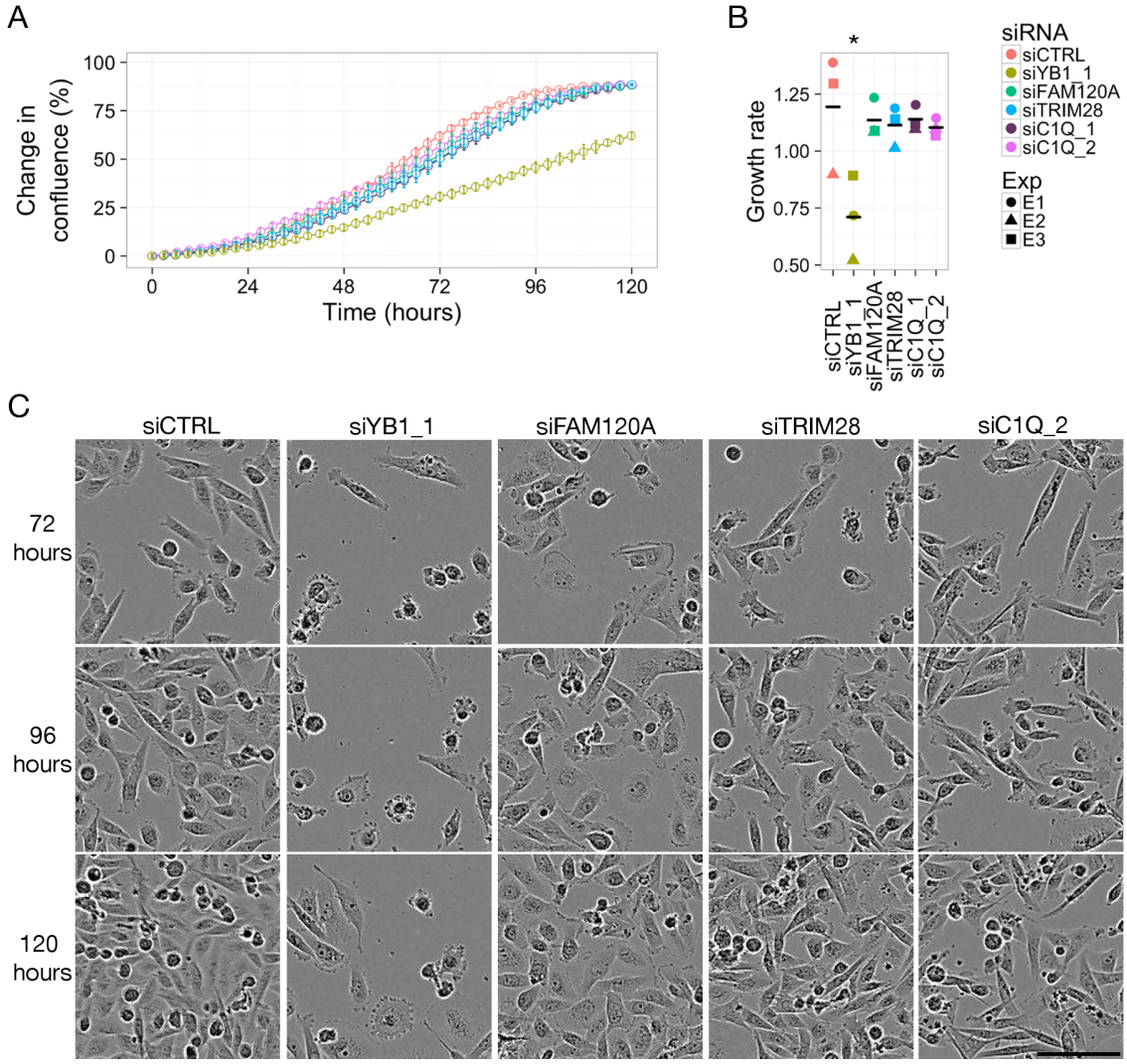

Figure 7.7: Depleting FAM120A, TRIM28, and C1QBP does not alter the growth-rate of MDA-MB231 cells. YB-1, FAM120A, TRIM28, and C1QBP have been depleted using 2 nM siRNA duplexes for 24 hrs, the media changed, and the confluence of the cells monitored using the Incucyte FLR. **A**, the confluence of each treatment from a representative experiment (Experiment 1). **B**, the maximum growth-rate that was derived from the confluence data for each experiment. **C**, representative images from Experiment 1 highlighted the morphology of MDA-MB231 cells following the depletion of YB-1, FAM120A, TRIM28, and C1QBP. A p-value of <0.05 from paired t-tests of the growth-rates of MDA-MB231 cells following transfection of siCTRL and each protein target is indicated by *. siRNA = siRNA duplexes against the indicated transcripts. Exp = experiment identifier. Scale bar is 100 µm.

tified as the margins of cells that touched one another were poorly defined. In conclusion, the results appear to show that the morphology of MDA-MB231 cells is altered following the depletion of YB-1 and FAM120A.

The varied effects that depleting FAM120A, TRIM28, or C1QBP had on the morphology of MDA-MB231 cells further highlighted that the functions of the three proteins were not entirely shared by YB-1. However, these proteins were selected due to their potential to interact with YB-1 in MDA-MB231 cells during cisplatin exposure. It was hypothesised that depleting TRIM28, FAM120A, or C1QBP would sensitise MDA-MB231 cells to cisplatin. The ED_{50} for cisplatin in each treatment was calculated (shown in **Table 7.1**). The results from these experiments confirm the importance of YB-1 to the survival of MDA-MB231 cells during cisplatin exposure. Compared to the 2 nM non-targeting siRNA duplex, depleting YB-1 using 2 nM siYB1_1 reduced the ED_{50} of MDA-MB231 cells from 2.73 ± 0.42 μM cisplatin in 2 nM siCTRL to 0.88 ± 0.55 μM cisplatin (p-value, 0.0087; **Table 7.1** and **Figure 7.8.A**).

The results from these experiments, summarised in **Table 7.1** and **Figure 7.8.A**, highlight that the estimated ED_{50} for cisplatin did not decrease when TRIM28 or C1QBP were depleted from MDA-MB231 cells. Depleting TRIM28 had no effect on the ED_{50} estimates for cisplatin. The ED_{50} estimates for cisplatin were also unchanged following the depletion of C1QBP with either siRNA duplex, with one exception. Depleting C1QBP using 1 nM siC1Q_2 elevated the ED_{50} for cisplatin in MDA-MB231 cells by 0.99 ± 0.29 μM cisplatin compared to a curve fitted to all 1 nM siRNA measurements (p-value, 0.0010; **Table 7.1**; **Figure 7.8.A**). The reasons for the discrepancy between the two siRNA duplexes against C1QBP are unknown.

The results show that depleting FAM120A reduces the ED_{50} for cisplatin in MDA-MB231 cells (**Table 7.1**; **Figure 7.8.A**). This was true when the mix of siRNA duplexes against FAM120A were used at either 2 or 1 nM. The reduction of the ED_{50} for cisplatin in MDA-MB231 cells was inversely correlated with the concentration of siFAM120A. Transfecting MDA-MB231 cells with 2 nM siFAM120A reduced the ED_{50} by 1.57 ± 0.38 μM cisplatin relative to the control (p-value, 0.0068; **Figure 7.8.A**). Compared to the ED_{50} of all 1 nM siRNA duplex transfections, using 1 nM siFAM120A reduced the ED_{50} estimate by 0.62 ± 0.29 μM cisplatin (p-value, 0.0324; **Table 7.1**; **Figure 7.8.A**). Therefore, the results from these experiments indicate that depleting either YB-1 or FAM120A reduces growth-rate of MDA-MB231 cells during cisplatin exposure.

The morphology of MDA-MB231 cells that were transfected with 2 nM siCTRL

Table 7.1: Depleting YB-1 or FAM120A reduces the ED_{50} for cisplatin in MDA-MB231 cells (0 - 12.5 μM; n = 3).

siRNA	Concentration	ED_{50} ± S.E.	Delta ± S.E.	p-value (t-value)
siCTRL	2 μM	2.73 ± 0.42	-	-
siYB1_1	2 μM	0.88 ± 0.55	**-1.85 ± 0.69**	**0.0087 (2.690)**
siFAM120A	2 μM	1.16 ± 0.38	**-1.57 ± 0.56**	**0.0068 (2.781)**
siTRIM28	2 μM	1.85 ± 0.24	-0.88 ± 0.48	0.0714 (1.828)
siC1Q_2	2 μM	2.28 ± 0.29	-0.45 ± 0.51	0.3789 (-0.885)
siC1Q_3	2 μM	3.34 ± 0.36	0.61 ± 0.55	0.2699 (1.111)
all siRNA	1 μM	2.62 ± 0.14	-	-
siFAM120A	1 μM	1.99 ± 0.25	**-0.62 ± 0.29**	**0.0324 (-2.166)***
siTRIM28	1 μM	2.54 ± -0.30	-0.08 ± 0.32	0.8145 (-0.235)*
siC1Q_2	1 μM	2.39 ± 0.22	-0.23 ± 0.26	0.3806 (-0.880)*
siC1Q_3	1 μM	3.61 ± 0.26	**0.99 ± 0.29**	**0.0010 (3.375)***
all siRNA	0.2 μM	2.87 ± 0.24	-	-
siFAM120A	0.2 μM	2.31 ± 0.35	-0.57 ± 0.45	0.1813 (-1.345)*
siTRIM28	0.2 μM	4.07 ± 0.73	1.18 ± 0.76	0.1258 (1.542)*
siC1Q_2	0.2 μM	2.97 ± 0.41	0.08 ± 0.55	0.8527 (0.186)*
siC1Q_3	0.2 μM	2.65 ± 0.46	-0.24 ± 0.52	0.6493 (-0.456)*

The dose-response curves were fitted using log-logistic regression. Estimates for the effective doses, the dose where 50% of the cells were killed by cisplatin (ED_{50}), are given. T-tests were used to compare the ED_{50} of MDA-MB231 cells to cisplatin following the depletion of each protein to the ED_{50} of the siCTRL RNA duplex, significant differences are shown as **bold text**. siCTRL and siYB1_1 were only used at 2 nM so for the 1 nM and 0.2 nM siRNA duplexes, the effects of depleting FAM120A, TRIM28 and C1QBP were compared to the ED_{50} that was calculated by fitting a log-logistic model to the pooled growth-rate data from all measurements where siRNA duplexes were used at that concentration ("all siRNA"). A "*" in the "p-value (t-value)" column indicates that comparing the ED_{50} estimate to the ED_{50} estimate from 2 nM siCTRL provided the same result (p-value <0.05). S.E. = standard error of the mean.

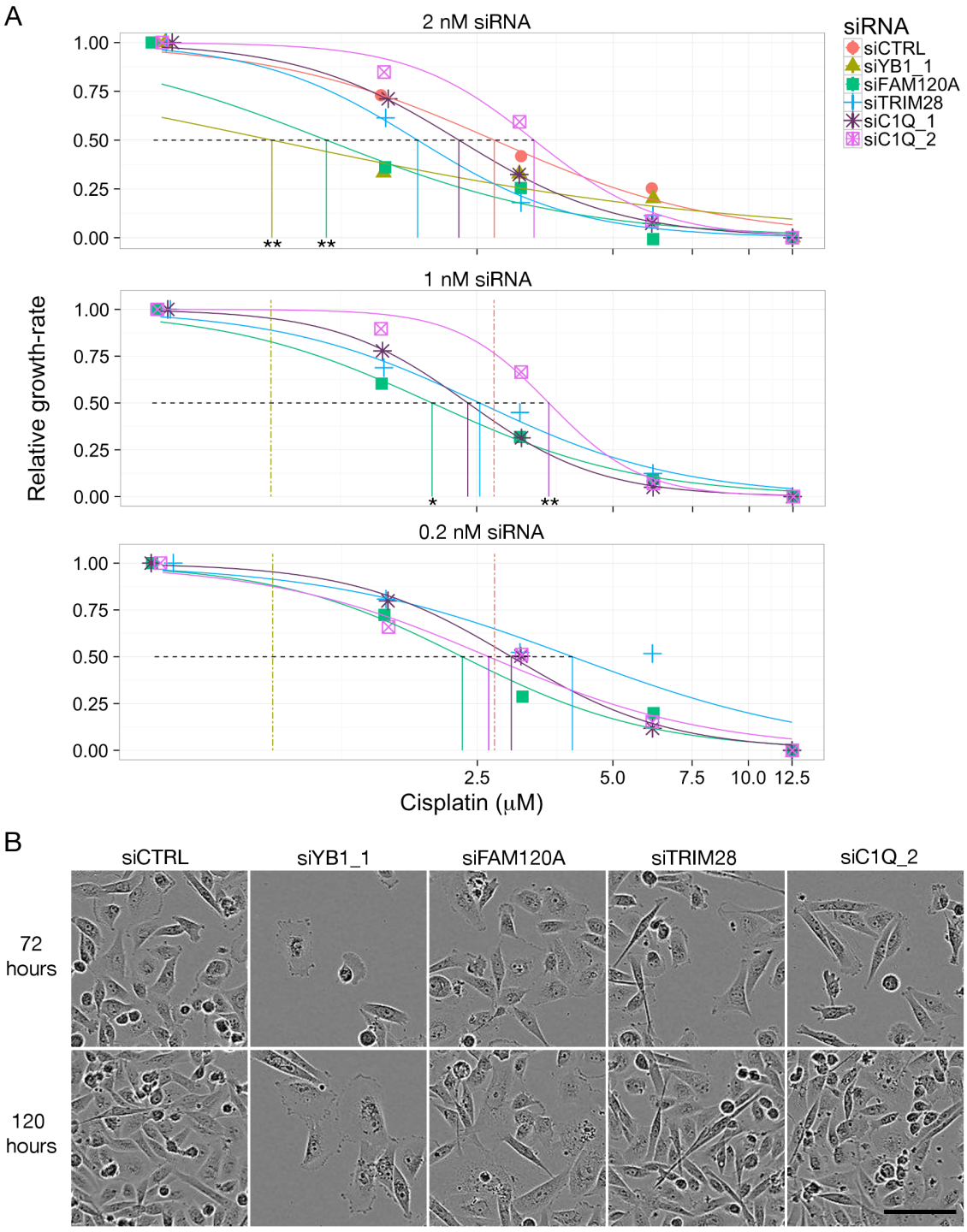

Figure 7.8: Depleting YB-1 or FAM120A reduces the growth-rate of MDA-MB231 cells during cisplatin exposure (1.56 - 12.5 μM; n = 3). YB-1, FAM120A, TRIM28, and C1QBP were depleted using siRNA duplexes at 0.2, 1, or 2 nM and the growth of the cells monitored using the Incucyte FLR. **A**, survival curves were generated from the maximum growth-rate of MDA-MB231 cells that were cultured in the presence of varying concentrations of cisplatin. **B**, images from Experiment 1 highlight the effects of 2 nM siRNA duplexes on the morphology of MDA-MB231 cells in 1.56 μM cisplatin. siRNA = siRNA duplexes against the indicated transcripts. These data were generated in the same experiments as those shown in **Figure 7.7**. * =p <0.05, ** = p <0.01. Scale bar is 100 μm.

appeared normal during exposure to 1.56 μM cisplatin (**Figure 7.8.B**). Following the depletion of YB-1 using 2 nM siYB1_1, the few MDA-MB231 cells remaining after 120 hrs of exposure to 1.56 μM cisplatin were enlarged (**Figure 7.8.B**). Depleting TRIM28 did not alter the morphology of MDA-MB231 cells during exposure to 1.56 μM cisplatin (siCTRL compared to siTRIM28, **Figure 7.8.B**). However, exposure to 1.56 μM cisplatin may result in a small increase in the prevalence of poorly attached cells following their transfection with 2 nM siC1Q_2 (**Figure 7.8.B**). The morphology of MDA-MB231 cells following the depletion of FAM120A using 2 nM siRNA duplexes appeared to be further altered during cisplatin exposure. Following 72 and 120 hrs of exposure to cisplatin, many cells appeared to increase in size and they also possessed enlarged nuclei (**Figure 7.8.B**).

In summary, the growth-rates and morphology of MDA-MB231 cells following the depletion of C1QBP, TRIM28, or FAM120A highlights that the functions of each of the three proteins were not entirely equivalent to the functions of YB-1 in MDA-MB231 cells. Unlike YB-1, depletion of any of these three proteins was not accompanied by a reduction in growth-rate. However, depleting FAM120A increased the sensitivity of MDA-MB231 cells to cisplatin. These data were consistent with the hypothesis that FAM120A and YB-1 interact co-operatively to promote the survival of MDA-MB231 cells during cisplatin exposure.

Further experiments were carried out to assess the interaction between YB-1 and each of FAM120A, TRIM28, and C1QBP. For these experiments, up to two proteins were depleted concurrently. Each transfection included either of 1 nM siCTRL or 1nM siYB1_1 (level 1). Each transfection also included one of 1 nM siCTRL, 1 nM siYB1_1, 1 nM siFAM120A, 1 nM siTRIM28, or 1 nM siC1Q_3 (level 2). Cisplatin, at concentrations ranging from 0 - 3.125 μM, was added 24 hrs after the commencement of the transfection and the confluence of the cells monitored for 120 hrs. The aim of these experiments was to highlight interactions between YB-1 and the selected proteins. One potential interaction was synthetic lethality, where the effect of depleting either protein in isolation is recoverable but depleting both together is irrecoverable.

The effects of depleting YB-1, in combination with the other proteins, on the growth-rate of MDA-MB231 cells were assessed. The results show that depleting YB-1 reduces the growth-rate of MDA-MB231 cells (level 1, two-way ANOVA, df, 1, f-value, 17.243, p-value, 0.000358; **Figure 7.9.A**). Consistent with previous results (**Figure 7.7.A - B**), the growth-rates of MDA-MB231 cells were unaffected by the depletion of any of the other proteins, irrespective of siCTRL or siYB1_1 treatment

(level 2, two-way ANOVA, df, 3, f-value, 2.58, p-value, 0.855).

The relationship between the growth-rate of MDA-MB231 cells and YB-1, FAM120A, TRIM28, and C1QBP1 was also examined in finer detail using pairwise comparisons. The comparisons were limited to a total of 10 as the growth-rates of FAM120A, TRIM28, and C1QBP1 depletions were not compared to one another (summarised in **Table 7.2**). The comparisons revealed that depleting TRIM28 and YB-1 together reduced the growth-rate of MDA-MB231 cells in a similar manner to that observed when YB-1 was depleted alone (**Table 7.2**, rows 3 - 4). Depleting FAM120A or C1QBP, in addition to YB-1, appeared to attenuate the reduction in growth-rate that was normally observed during cisplatin exposure (**Figure 7.7.A**). Pairwise comparisons revealed that the growth-rate was somewhere between that observed for depletion of C1QBP or FAM120A alone and that of MDA-MB231 cells where only YB-1 was depleted (**Table 7.2**, rows 6 - 7 and 9 - 10). Therefore, depleting FAM120A or C1QBP appeared to lessen the negative effects that depleting YB-1 had on the growth-rate of MDA-MB231 cells. However, depleting FAM120A or C1QBP did not completely abrogate the negative effects of depleting YB-1 on the growth-rate of MDA-MB231 cells. The morphology of the MDA-MB231 cells, where YB-1 was depleted alongside FAM120A, TRIM28, or C1QBP, was similar (**Figure 7.7.A**). Therefore, there is no evidence of synthetic lethality occurring when YB-1 is depleted alongside any of FAM120A, TRIM28, or C1QBP.

These experiments also included an analysis of the survival of MDA-MB231 cells during cisplatin exposure. The previous experiments provided knowledge about the critical cisplatin dose range for MDA-MB231 cells, allowing a restricted range of cisplatin doses to be used for these experiments (0 - 3.125 μM). Consistency of ED_{50} estimation was maintained by using the log-logisitic model settings from the previous work. However, the scaling was altered as some MDA-MB231 cells remained alive following 120 hrs of exposure to the maximum cisplatin dose (3.125 μM). Therefore, it was inappropriate to scale the growth-rates in each treatment to the maximum growth-rates from cells that were exposed to 3.125 μM cisplatin. Instead, each treatment was scaled to the 0 μM cisplatin measurement. The similarity of the ED_{50} estimate for 2 nM siCTRL of 2.85 ± 0.35 μM cisplatin with that from previous experiments, 2.73 ± 0.42 (**Table 7.1**), indicated that the results were consistent with the previous experiment. Furthermore, the experiments are internally consistent.

The results from these experiments show that depleting YB-1 sensitises MDA-MB231 cells to cisplatin (**Table 7.3** and **Figure 7.10.A**). The previous experiment indicates that depleting FAM120A reduced the growth-rate of MDA-MB231 cells

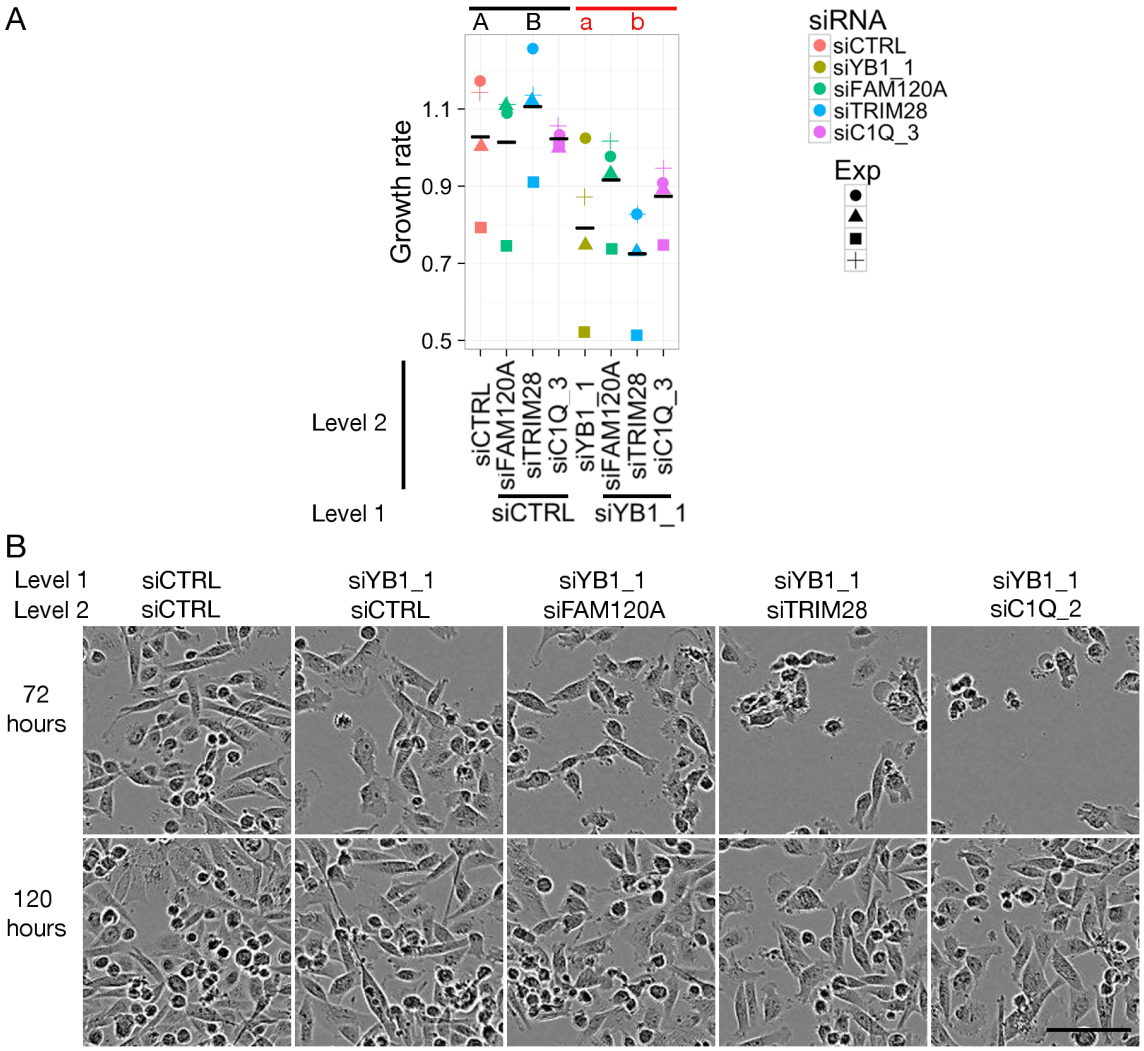

Figure 7.9: Depleting FAM120A and C1QBP counteracts the negative effects of depleting YB-1 on the growth-rate of MDA-MB231 cells (n = 4). Two levels of siRNA duplex were used in these experiments. Level 1 included 1 nM siCTRL or 1nM siYB1_1 and level 2 included 1nM siYB1_1, 1nM siFAM120A, 1nM siTRIM28, or 1nM siC1QBP (see **Table 7.3** for siRNA duplex combinations). Following transfections, the growth of the cells was monitored using the Incucyte FLR. **A**, the maximum growth-rate for each transfection was derived from the confluence data. The bar colour above the plot indicates significant main effects in a 2-way ANOVA while capital to lower case letters indicate significant differences in post-hoc t-tests. **B**, images from a single experiment show how the morphology of MDA-MB231 cells was affected by transfection with 1 nM siYB1_1 combined with siRNA duplexes against one of FAM120A, TRIM28, and C1QBP. Scale bar is 100 μm.

Table 7.2: The effects of depleting the interaction partners of YB-1 and YB-1 together on the growth-rate of MDA-MB231 cells (n = 4).

Depletion #1	Depletion #2	p-value
siCTRL + siCTRL	siYB1_1 +siCTRL	**0.0324**
siCTRL + siCTRL	siCTRL + siTRIM28	0.4588
siYB1_1 + siCTRL	siYB1_1 + siTRIM28	0.5280
siCTRL + siTRIM28	siYB1_1 + siTRIM28	**0.0012**
siCTRL + siCTRL	siCTRL + siFAM120A	0.8946
siCTRL + siFAM120A	siYB1_1 + siFAM120A	0.3569
siYB1_1 + siCTRL	siYB1_1 + siFAM120A	0.2429
siCTRL + siCTRL	siCTRL + siC1Q_3	0.9618
siCTRL + siC1Q_2	siYB1_1 + siC1Q_2	0.1652
siYB1_1 + siCTRL	siYB1_1 + siC1Q_2	0.4370

The hypotheses that depleting YB-1 and the interaction partners of YB-1 together altered the growth-rate of MDA-MB231 cells was tested using two-way analysis of variance; model = Growth-rate siRNA #1 (siCTRL, siYB1_1) + siRNA #2 (siCTRL, siTRIM28, siFAM120A, siC1Q_3. Post-hoc tests were performed as pairwise comparisons using t-tests with pooled standard deviation with selected tests shown. Significant differences are shown as bold text. S.E. = standard error of the mean.

Table 7.3: Depleting the interaction partners of YB-1 and YB-1 together further reduces the survival of MDA-MB231 cells during cisplatin exposure (0 - 3.125 μM; n = 4).

siRNA #1	siRNA #2	ED_{50} ± S.E.	Delta ± S.E.	p-value (t-value)
siCTRL	siCTRL	2.85 ± 0.35	-	-
siCTRL	siFAM120A	2.09 ± 0.21	-0.76 ± 0.41	0.0634 (1.871)
siCTRL	siTRIM28	2.10 ± 0.17	-0.75 ± 0.38	0.0542 (1.941)
siCTRL	siC1q_3	2.34 ± 0.30	-0.51 ± 0.46	0.2681 (1.112)
siCTRL	siYB1_1	1.83 ± 0.19	-1.02 ± 0.40	**0.0110 (2.575)**
siYB1_1	siFAM120A	1.16 ± 0.13	-0.66 ± 0.23	**0.0038 (2.944)**
siYB1_1	siTRIM28	1.32 ± 0.13	-0.52 ± 0.23	**0.0253 (2.261)**
siYB1_1	siC1q_3	1.28 ± 0.13	-0.55 ± 0.23	**0.0177 (2.399)**

The dose-response curves have been fitted using log-logistic regression. Estimates for the effective doses where 50% of the cells were killed by cisplatin (ED_{50}) are given. T-tests were used to compare the ED_{50} estimates. All ED_{50} estimates that include 1 nM siCTRL in "siRNA #1" were compared to the ED_{50} estimate for 2 nM siCTRL (row #1). The ED_{50} estimates that included siYB1_1 in "siRNA #1" were compared to the ED_{50} estimate for 1 nM siCTRL + 1 nM siYB1_1 (row #5). Significant differences are shown as **bold text**. S.E. = standard error of the mean.

during cisplatin exposure (**Table 7.1**). The trend in the current experiment is consistent with this, as depleting FAM120A reduces the ED_{50} estimate for cisplatin compared to the siCTRL samples, but the reduction is not significant (p,value, 0.0634; **Table 7.3**).

Depleting any of FAM120A, TRIM28, or C1QBP alongside YB-1 results in further reductions in the ED_{50} estimates for MDA-MB231 cells in cisplatin compared to MDA-MB231 cells where only YB-1 is depleted (statistical analysis summarised in **Table 7.3**; **Figure 7.10.A**). The lowest ED_{50} estimate came from MDA-MB231 cells where YB-1 and FAM120A were both depleted (1.16 $\pm$ 0.13 μM cisplatin, t-value, 2.944, p-value, 0.0038). The results from these experiments confirm the importance of YB-1 to the survival of MDA-MB231 cells during exposure to cisplatin.

Depleting FAM120A, TRIM28, or C1QBP, alongside YB-1 further sensitises MDA-MB231 cells to cisplatin. Furthermore, depleting either C1QBP or FAM120A mitigated some of the negative growth effects that resulted from depleting YB-1 (**Figure 7.7.A**). The apparent need that FAM120A, and likely C1QBP, be present for the depletion of YB-1 to have a significant effect on reducing the growth-rate of MDA-MB231 cells infers that these two proteins lie down-stream to YB-1 in a signalling pathway that is perturbed by the depletion of YB-1. From these results, it could also be inferred that the biochemical pathways underpinning the effects of YB-1 depletion on the growth-rates may be different, and possibly separate, to those promote the role of YB-1 in cisplatin sensitivity. FAM120A appears to be involved in both pathways but, in the growth pathway, FAM120A would lies downstream of YB-1. In the cisplatin pathway, FAM120A appears to be more likely to have a function that is equivalent to that of YB-1.

The effects of depleting FAM120A, C1QBP, or TRIM28 on the survival of MDA-MB231 cells following a 2 hr exposure to cisplatin were examined. Data from the siCTRL and siYB1_1 treatments are also presented in **Table 5.4** and **Figure 5.7**, although these results are not discussed further here. For these experiments, YB-1, FAM120A, TRIM28, or C1QBP were depleted in MDA-MB231 cells using reverse transfections (siRNA duplexes at 0.5, 1, 2 nM). To provide sufficient time for the proteins to be depleted, the cells were exposed to 3.125 - 25 μM cisplatin for 2 hrs 48 hrs after the commencement of the transfections. Following the two hr exposure, the media was replaced and the confluence of the cells monitored for 96 hrs.

The results from this experiment show that YB-1 depletion reduces the survival of MDA-MB231 cells following a 2 hr exposure (summarised in **Table 7.4** and **Figure 7.11**). Depleting C1QBP has no effect on estimates of the ED_{50} for cis-

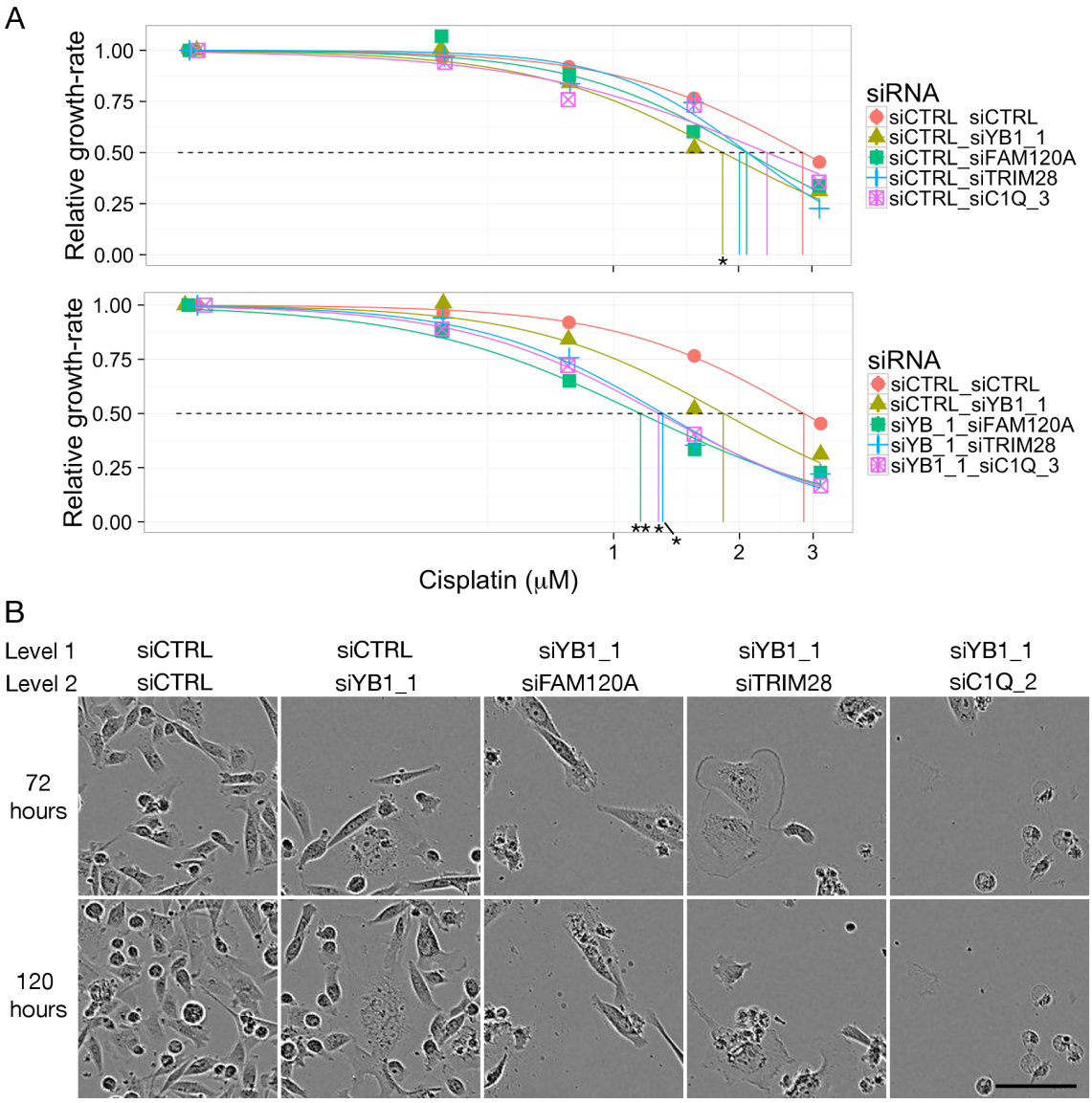

Figure 7.10: Depleting FAM120A, TRIM28, or C1QBP in conjunction with YB-1 further reduces the growth-rate of MDA-MB231 cells during cisplatin exposure (0 - 3.125 μM; n = 4). YB-1, FAM120A, TRIM28, and C1QBP were depleted using 1 nM siRNA duplexes and the growth of the cells was monitored using the Incucyte FLR (see **Table 7.3** for siRNA duplex combinations). **A**, the ED_{50} for cisplatin was estimated by fitting the maximum growth-rates using log-logistic regression. **B**, representative images from Experiment 1 highlighted how transfection altered the morphology of MDA-MB231 cells that were grown in 1.56 μM cisplatin. siRNA = siRNA duplexes against the indicated transcripts. These data were generated in the same experiments as those shown in **Figure 7.9**. * = p <0.05, ** = p <0.01. Scale bar is 100 μm.

Table 7.4: Depleting YB-1 or FAM120A reduces the growth-rate of MDA-MB231 cells following 2 hrs of exposure to cisplatin (0 - 25 μM; n = 4).

siRNA	Concentration	ED_{50} ± S.E.	Delta ± S.E.	p-value (t-value)
siCTRL	2	9.80 ± 0.73	-	-
siYB1_1	2	5.55 ± 0.37	**-4.26 ± 0.82**	**0.0000 (5.169)**
siFAM120A	2	7.36 ± 0.64	**-2.44 ± 0.97**	**0.0139 (2.510)**
siTRIM28	2	10.94 ± 0.72	1.13 ± 1.03	0.2744 (-1.100)
siC1Q_3	2	9.57 ± 0.77	-0.24 ± 1.06	0.8239 (-0.22322)
siCTRL	1	10.56 ± 0.87	-	-
siYB1_1	1	5.72 ± 0.68	**-4.84 ± 1.10**	**0.0000 (4.394)**
siFAM120A	1	8.96 ± -0.88	-1.61 ± 1.23	0.1963 (1.301)
siTRIM28	1	10.95 ± 1.02	0.39 ± 1.34	0.7743 (-0.288)
siC1Q_3	1	11.78 ± -1.19	1.22 ± 1.47	0.4106 (0.827)
siCTRL	0.5	10.80 ± 0.78	-	-
siYB1_1	0.5	6.66 ± 0.43	**-4.14 ± 0.89**	**0.0000 (4.634)**
siFAM120A	0.5	10.11 ± 0.73	-0.69 ± 1.07	0.5222 (0.643)
siTRIM28	0.5	13.75 ± 1.11	**2.95 ± 1.36**	**0.0327 (-2.169)**
siC1Q_3	0.5	10.01 ± 0.81	0.78 ± 1.13	0.4885 (-0.696)

The dose-response curves were fitted using log-logistic reggression. Estimates for the effective doses, where 50% of the cells were killed by cisplatin (ED_{50}), are given. T-tests were used to compare the ED_{50} following the depletion of each protein to the ED_{50} of the siCTRL RNA duplex, significant differences are shown as **bold text**. S.E. = standard error of the mean.

platin in MDA-MB231 cells (summarised in **Table 7.4.A**). The effects of depleting TRIM28 are more complex. Depleting TRIM28 using siTRIM28 at 2 or 1 nM has no effect on the sensitivity of MDA-MB-231 cells to cisplatin. However, transfecting MDA-MB231 cells using 0.5 nM siTRIM28 appears to decrease the sensitivity of MDA-MB231 cells to cisplatin, as the estimated ED_{50} increased by 2.95 ± 1.36 μM cisplatin compared to the ED_{50} estimate from 0.5 nM siCTRL-treated cells (**Table 7.4.A**; t-value= -2.169,p-value = 0.0327). Finally, FAM120A also appears to support the survival of MDA-MB231 cells following cisplatin exposure. Depleting FAM120A using 2 nM, reduces the ED_{50} of cisplatin by 2.44 ± 0.97 compared to the 2 nM siCTRL-treated cells (p-value, 0.0139). The sensitivity of MDA-MB231 cells to cisplatin was unaltered when less siFAM120A duplex was used (**Table 7.4** and **Figure 7.11.A**).

The morphology of MDA-MB231 cells following two hrs of exposure to 6.25 μM cisplatin was also examined. MDA-MB231 cells that were transfected with 2 nM siCTRL, siTRIM28, or siC1Q_2 displayed similar morphologies to one another,

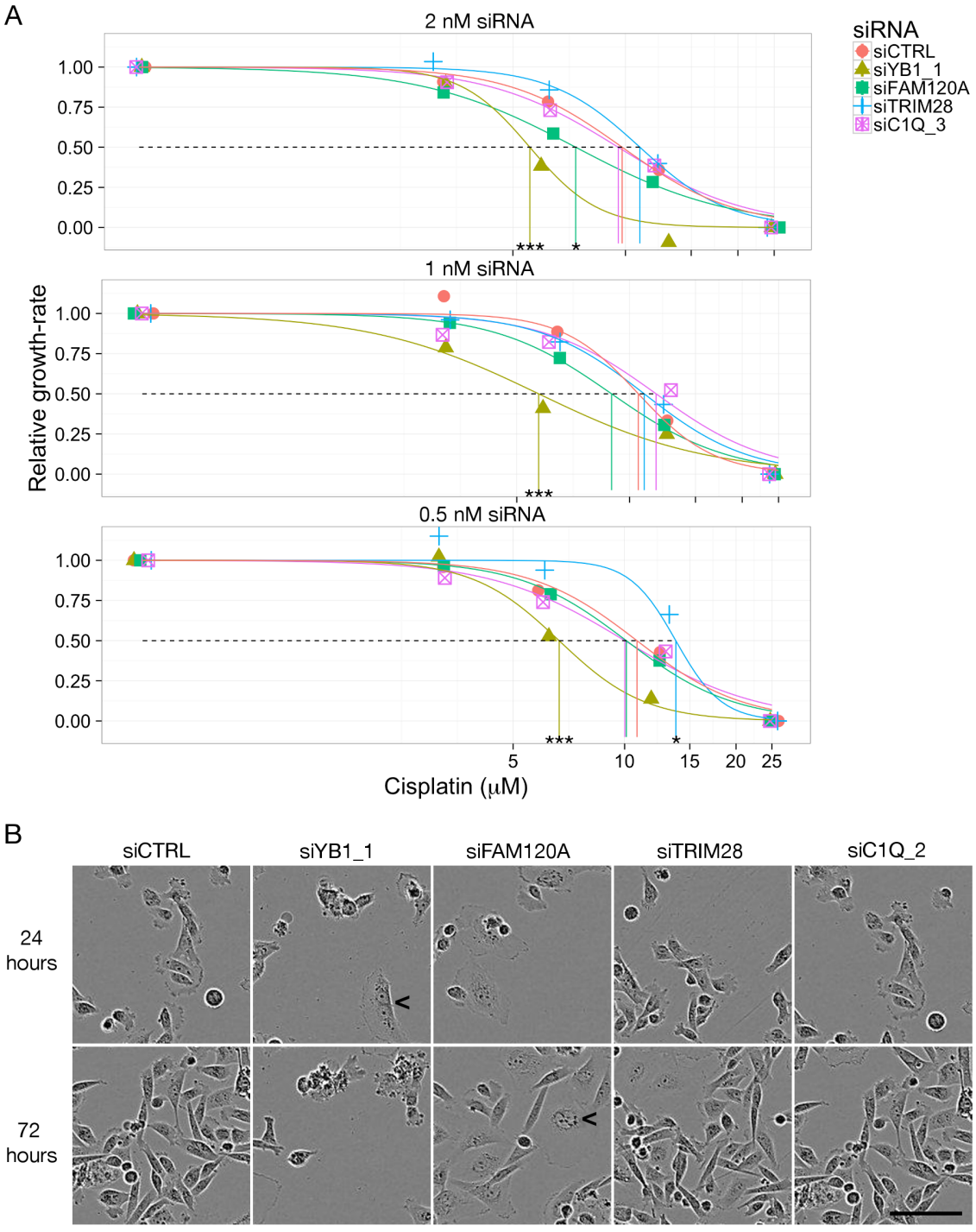

Figure 7.11: Depleting YB-1 or FAM120A reduces the survival of MDA-MB231 cells following a 2 hr exposure to cisplatin (3.125 - 25 μM, n = 4). YB-1, FAM120A, TRIM28, and C1QBP were depleted using siRNA duplexes (0.5, 1, 2 nM) and 48 hrs later media that contained cisplatin was added for two hrs. The confluence of the cells was monitored for 96 hrs. **A**, response curves were prepared from the maximum growth-rates to estimate the ED_{50} for each treatment. **B**, representative phase-contrast images of MDA-MB231 cells 24 and 72 hrs after a 2 hr exposure to 6.25 μM cisplatin. **Abbreviations**; * = p-value <0.05, *** = p-value <0.001. < = bi-nucleate cell. Scale bar is 100 μm.

24 and 72 hrs after two hrs of exposure to 6.25 μM cisplatin (**Figure 7.11.B**). Corresponding to the reductions in the ED_{50} estimates resulting from the YB-1 depletion, the cells that remained after 24 and 72 hrs using 2 nM siYB1_1 and two hrs of exposure to 6.25 μM cisplatin exhibited poor attachment (**Figure 7.11.B**, YB-1). Depleting FAM120A with 2 nM siRNA duplex resulted in some cells appearing to be enlarged 72 hrs after cisplatin exposure (**Figure 7.11.B**, FAM120A). Loss of control of mitosis following the depletion of YB-1 or FAM120A, and a brief cisplatin exposure, was also indicated by the presence of what appeared to be cells with two nuclei (**Figure 7.11.B**, <). Therefore, the effects of depleting YB-1 and FAM120A on the morphology of MDA-MB231 cells, following a 2 hr exposure to 6.25 μM cisplatin, are consistent with the two proteins supporting the viability of MDA-MB231 cells.

The results from these experiments highlight three primary points. Firstly, they further illustrate the importance of YB-1 to the survival of MDA-MB231 cells during and following cisplatin exposure. Secondly, of the three proteins that were studied, only FAM120A consistently shows the potential to interact with YB-1 to influence the survival of MDA-MB231 cells during, and following, cisplatin exposure. The final point involves the partial abrogation of the negative effects on the growth of MDA-MB231 cells that was observed following concurrent depletion of YB-1 and FAM120A or C1QBP. These observations raise the possibility that the pathway leading to reduced growth following YB-1 depletion may act in part through FAM120A and C1QBP. However, further experiments that explicitly enumerate cell division are needed to confirm this final point.

7.2.5 The repair of double-strand DNA breaks is not central to YB-1 function during cisplatin exposure

YB-1 is known to interact with DNA repair proteins that act via the nucleotide excision and base excision repair pathways (reviewed in **Chapter 1.8.1**; Gaudreault et al. 2004, Das et al. 2007, Chattopadhyay et al. 2008, Sengupta et al. 2011, Fomina et al. 2015). However, the YB-1 in MDA-MB231 cells did not appear to interact with proteins that were exclusively linked to either pathway during cisplatin exposure (**Chapter 6**). Instead, YB-1 interacted with proteins that participate in the repair of double-strand DNA breaks (TRIM28, XRCC5, and XRCC6; **Chapter 6**). Double-strand DNA breaks form as secondary lesions during cisplatin exposure (discussed in **Chapter 6.3.2** and **Chapter 7.1**). TRIM28 is known to have an

important role in the repair of double-strand breaks in regions of heterochromatin which get repaired slowly (Goodarzi et al. 2008, Noon et al. 2010, White et al. 2012). Therefore, the late onset of death in MDA-MB231 cells during cisplatin exposure (>72 hrs), and the increased levels of TRIM28 that copurified with YB-1 from cells that were exposed to cisplatin, prompted these experiments that focus on the repair of double-strand DNA breaks.

Histone H2AX (H2AX) with phosphorylation to serine 139 forms foci (γH2AX foci) around double-strand DNA breaks. It then facilitates the recruitment of DNA repair factors (Paull et al. 2000, Lowndes & Toh 2005, Löbrich et al. 2010). YB-1 was hypothesised to participate in the repair of the sub-population of double-strand DNA breaks that occur in heterochromatin during cisplatin exposure. Therefore, the number of γH2AX foci in each cell was used to indicate that double-strand DNA breaks were being repaired, including those double-strand breaks in regions of heterochromatin.

These experiments utilised 5 nM siRNA duplexes (siCTRL or siYB1_1) to deplete YB-1 in MDA-MB231 cells, grown on poly-L-lysine coated coverslips in 24-well plates, prior to 48 hrs of 1.56 μM cisplatin exposure. The cells were fixed using 2% paraformaldehyde in PBS and IF performed using anti-γH2AX. A 40 × objective lens was used to image the coverslips and multiple fields of view were selected using the signal from DNA (Hoechst). The γH2AX foci in the nuclei of a minimum of 200 cells were counted for each treatment (see **Chapter 2.10.2**).

The IF indicated that the nuclei of MDA-MB231 cells enlarged following 48 hrs of cisplatin exposure (**Figure 7.12.A**). The steps for counting γH2AX foci included the creation of a mask around all nuclei in each image. The data from these masks were used to examine how cisplatin exposure and YB-1 depletion altered the size of MDA-MB231 cell nuclei. Following 48 hrs of cisplatin exposure, the average size of nuclei increased from 2954 ± 148 nm^2 in the control media to 4037 ± 212 nm^2 in nuclei that were incubated in 1.56 μM cisplatin (**Figure 7.12.B**; Df = 1,F-value = 23.371, p-value = 0.00022). The average size of the nuclei of MDA-MB231 cells was consistent irrespective of the presence or absence of YB-1 (Df = 1, F-value -= 0.077, p-value = 0.785). Experimental variation was noticed during data analyses, so the experiment was included in the 2-way ANOVA model as a covariate. This revealed that the average size of the nuclei varied between the experiments (Df = 1, F-value = 7.468, p-value = 0.01541). The reasons for increases in nuclear size were not clear. However, chromatin dynamics can affect nuclear size (Jevtić & Levy 2014, Gasser 2002). The repair of double-strand DNA breaks in regions of

heterochromatin would constitute a disruption to chromatin dynamics.

The results from counting γH2AX foci showed that following 48 hrs of cisplatin exposure, the average number of γH2AX foci in the nuclei of MDA-MB231 cells increased from 1.45 ± 0.33 γH2AX foci per nucleus to 4.92 ± 0.87 γH2AX foci per nucleus (**Figure 7.12.A and C**; DF = 1, F-value = 15.677, P-value = 0.00126). However, depleting YB-1 had no effect on the number of γH2AX foci that were observed (**Figure 7.12.C**; Df = 1, F-value = 0.944, P-value = 0.34657). The experiment identifiers were also included in the 2-way ANOVA as covariates but no significant effect was detected (DF = 1, F-value = 0.06038,P-value=0.06038).

YB-1 depletion has no effect on the number of γH2AX foci that are present in MDA-MB231 cells during cisplatin exposure. Furthermore, the preceding section highlights that TRIM28 plays no role in the survival of MDA-MB231 cells during cisplatin exposure (**Chapter 7.2.4**). The function of TRIM28 is central to the hypothesis that YB-1 participates in the repair of double-strand DNA breaks in regions of heterochromatin during cisplatin exposure. The finding that TRIM28 has no effect on the survival of MDA-MB231 cells during cisplatin exposure (**Chapter 7.2.4**) and, that the number γH2AX foci in MDA-MB231 cells are not altered following the depletion of YB-1, means that there was no support for the hypothesis that YB-1 participates in the repair of double-strand DNA breaks in regions of heterochromatin during cisplatin exposure.

7.3 Discussion

Three proteins, C1QBP, FAM120A, and TRIM28, were hypothesised to co-operate with YB-1 to improve the survival of MDA-MB231 cells during cisplatin exposure. TRIM28 was also hypothesised to co-operate with YB-1 to influence the repair of double-strand DNA breaks or to repress the transcription of E2F- gene targets. Finally, FAM120A and C1QBP were hypothesised to co-operate with YB-1 to transduce survival signals as was C1QBP. The results that were presented in this chapter show that:

- Of the three proteins studied, the subcellular distribution of FAM120A was most similar to the distribution of YB-1 in MDA-MB231 cells;
- Depleting FAM120A increases the sensitivity of MDA-MB231 cells to cisplatin;
- Depleting FAM120A or C1QBP in conjunction with YB-1 may attenuate the

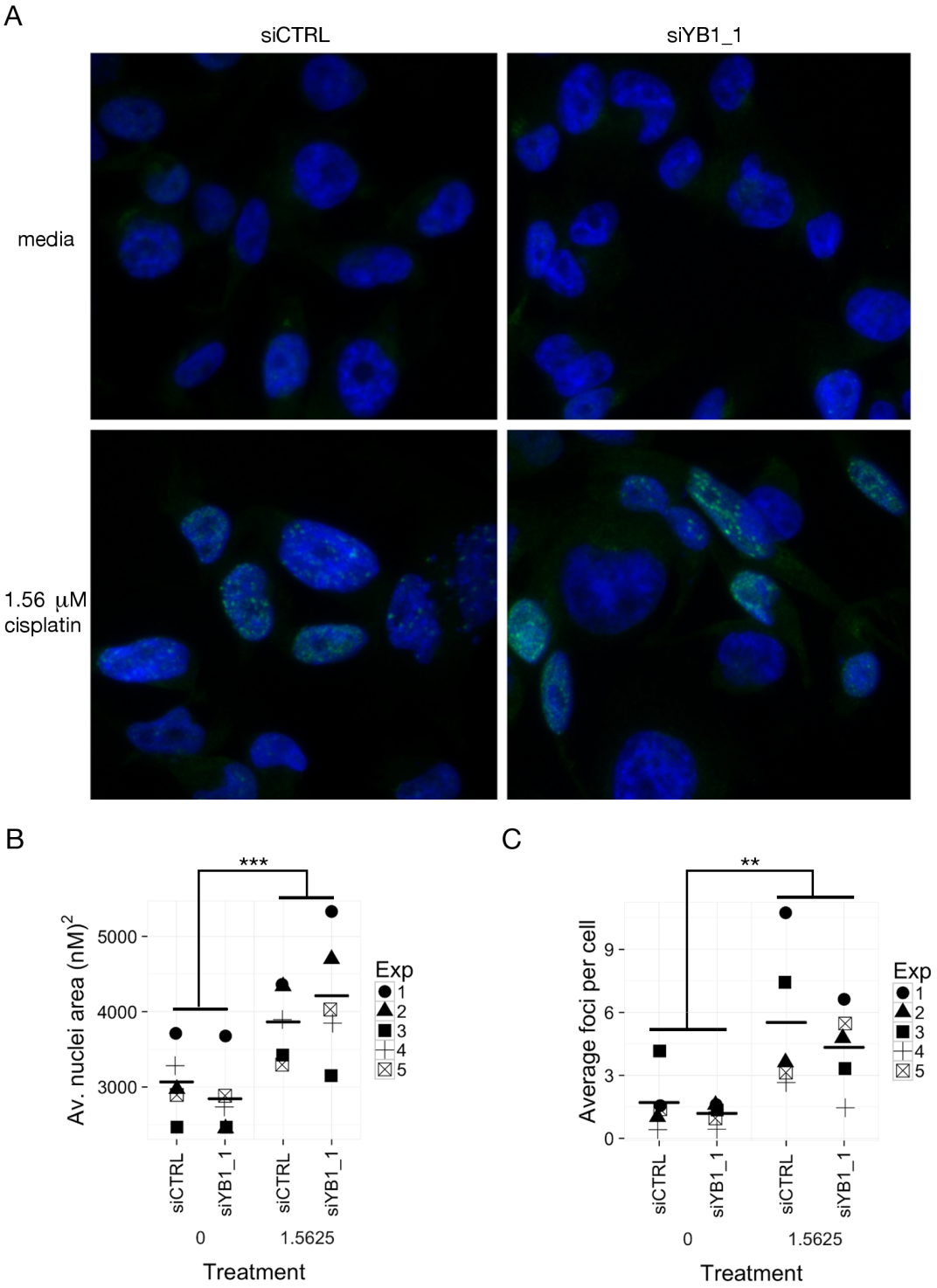

Figure 7.12: Depleting YB-1 has no effect on the size of MDA-MB231 nuclei or the number γH2AX foci during cisplatin exposure. MDA-MB231 cells were fixed with 2% paraformaldehyde and IF performed (n = 5). **A**, representative images from IF of MDA-MB231 cells where anti-γH2AX was labelled with AlexaFluor 488 and DNA labelled with Hoechst is represented as blue. **B**, the average size of the nuclei of MDA-MB231 cells following 48 hrs of media or 1.56 μM cisplatin in media. **C**, the average number of γH2AX foci per MDA-MB231 cell with and without YB1 protein present. Two-way ANOVA was used to assess how siRNA duplex, cisplatin, and experiment (covariate) alter the number of γH2AX foci per MDA-MB231 cell. ** = p <0.005, *** = p <0.001.

growth reduction that normally accompanies the depletion of YB-1 in MDA-MB231 cells;

- There was no support for the hypothesis that YB-1 participates in the repair of double-strand DNA breaks during cisplatin exposure.

7.3.1 The interaction of YB-1 and TRIM28 or C1QBP is unlikely to positively influence cell survival

The experiments provided no support for the involvement of either TRIM28 or C1QBP in the cisplatin resistance of MDA-MB231 cells. C1QBP was selected due to its reported function as a survival factor during cisplatin exposure rather than increased levels of C1QBP copurifying with YB-1 during cisplatin exposure (reviewed in **Chapter 7.1**). The results presented here contradict another study that showed depleting C1QBP in MDA-MB231 cells reduced cell proliferation and cell migration (McGee et al. 2011).

Prior to the commencement of this work TRIM28 appeared to be the strongest candidate (**Chapter 6**) as it is well connected to functions that would be appropriate for YB-1; repairing DNA damage and the repression of transcription. One hypothesis stated that the interaction of the two proteins facilitated a transcriptional response to cisplatin exposure; most likely as a down-regulation of E2F-family gene targets (Wang et al. 2007, Hu et al. 2012, Chen et al. 2012). The second hypothesis held that YB-1 and TRIM28 interact to repair double-strand DNA breaks in regions of heterochromatin. The results from the experiments in this chapter showed that depleting TRIM28 has no effect on the survival of MDA-MB231 cells during cisplatin exposure. Depleting TRIM28 failed to render MDA-MB231 cells more sensitive to chronic cisplatin exposure or, to reduce their survival following a 2 hr exposure to cisplatin. This is sufficient evidence to reject both hypotheses relating to the functional significance of TRIM28 and YB-1 interactions in MDA-MB231 cells during cisplatin exposure.

Indirect support for rejecting the latter hypothesis came from the quantification of γH2AX foci in MDA-MB231 cells. Depleting YB-1 had no effect on the number of γH2AX foci in MDA-MB231 cells. Therefore, YB-1 does not appear to be involved in the repair of double-strand DNA breaks during cisplatin exposure, irrespective of any interaction with TRIM28. Variation between experiments was evident for the γH2AX foci quantifications. This may be explained by variations in the number of

γH2AX foci during the cell cycle as the number of γH2AX foci is elevated during the later stage of cell division (Löbrich et al. 2010). Therefore, variations in the cell cycle profile may explain some of the variation. The intensity of the signal from nuclei can be used to identify cells that are yet to begin S-phase. However, plotting the intensity of individual nuclei did not provide sufficient resolution to separate cells that were yet to begin S-phase of the mitotic cycle. There is also a further reason why these experiments may have missed a real alteration to the number of γH2AX foci following the depletion of YB-1. The hypothesised targets for these experiments, double-strand DNA breaks in regions of heterochromatin, were outnumbered by the predominance of double-strand DNA breaks in euchromatin which comprise $\sim 75\%$ of double-strand DNA breaks in primary human fibroblasts (Goodarzi et al. 2008). Furthermore, γH2AX foci can provide reliable estimates of double-strand DNA breaks but deregulated DNA repair mechanisms may lead to γH2AX foci failing to accurately represent these breaks and their repair (Löbrich et al. 2010).

An alternative approach is to accept the null hypothesis for the γH2AX experiments, that is, the ability of YB-1 to promote the survival of MDA-MB231 cells during cisplatin exposure is unrelated to the repair of double-strand DNA breaks. Double-strand DNA break repair proteins, besides TRIM28, were detected in LC-MS/MS of cross-linked YB-1. XRCC5 and XRCC6 participate in the repair of double-strand breaks. However, both proteins appear to interact with RNA in addition to roles in DNA repair (Britton et al. 2013). Therefore, their presence in IP of YB-1 may be explained via RNA binding rather than DNA binding. Furthermore, quantification of XRCC6 in **Chapter 6.2.6** indicates that its interaction with YB-1 was unaffected or reduced during cisplatin exposure and this is inconsistent with increased rates of DNA repair.

Further indirect evidence against the importance of double-strand DNA breaks comes via the observation that YB-1 is important to the survival of MDA-MB231 cells following a brief exposure to cisplatin. The shorter period of exposure should reduce the potential for double-strand DNA breaks to occur following the cisplatin exposure. Many of the cells that in the growth phase of mitosis when the cisplatin is added will have more time to remove cisplatin adducts before double-strand DNA breaks are introduced during S-phase. However, the sensitisation that is elicited by depleting YB-1 remains strong despite the reduction in the potential for double-strand DNA breaks to be produced. Therefore, the null hypothesis that YB-1 promotes the survival of MDA-MB231 cells during cisplatin exposure, without relying

on the repair of double-strand DNA breaks, is accepted.

Double-strand DNA breaks are not the primary form of DNA damage from cisplatin exposure and γH2AX foci are not general markers of DNA damage or repair. The repair pathways that can remove platinum adducts and cross-links from DNA do not necessarily lead to γH2AX foci (Revet et al. 2011).

The question of whether YB-1 participates in DNA repair remains interesting. During cisplatin exposure, YB-1 increased its interaction with DNA in the nuclei of MDA-MB231 cells (**Chapter 5.2.5**). The ability of YB-1 to preferentially bind to cisplatin-modified DNA, and participate in the main repair pathways for removing cisplatin adducts, still have potential to be relevant to YB-1 function during cisplatin exposure (reviewed in **Chapter 1.8.1**; Gaudreault et al. 2004, Das et al. 2007, Chattopadhyay et al. 2008, Sengupta et al. 2011, Fomina et al. 2015). Further experiments could be designed to use methods that detect cisplatin on DNA. Direct quantification of DNA-cisplatin could confirm whether a continued focus on DNA repair mechanisms is justified. Enzyme linked immunosorbent assays, using antibody preparations directed against cisplatin-DNA, can quantify the amount of cisplatin in purified DNA (Liedert et al. 2006). However, direct assessment of the cisplatin content of DNA using MS, specifically inductively coupled plasma MS, would be the ideal assay for the sensitive quantification of the platinum content of DNA (Bonetti et al. 1996, Brouwers et al. 2006, Hermann et al. 2013).

The work performed here was sufficient to discount the interaction of YB-1 and C1QBP or TRIM28 as a critical component of the function of YB-1 during cisplatin exposure. Furthermore, the interaction of TRIM28 and YB-1 to repair double-strand DNA breaks does not appear to be a central mechanism by which YB-1 promotes the survival of MDA-MB231 cells during cisplatin exposure.

7.3.2 YB-1 and FAM120A during cisplatin exposure

At the beginning of this chapter, FAM120A was hypothesised to promote the survival of MDA-MB231 cells. Formulating a hypothesis about the potential function of any interaction between YB-1 and FAM120A was difficult due to a lack of research into the function of FAM120A. However, the two known functions, the regulation of kinase activity or the ability to influence gene expression by binding to RNA, were both consistent with YB-1 biology. Recent work from Bartolome et al. (2015) has provided further support for the importance of the former function of FAM120A in cell survival.

In MDA-MB231 cells, FAM120A appears to be similar to YB-1 in a number of ways. The subcellular distribution of YB-1 and FAM120A in MDA-MB231 cells is almost indistinguishable. Information about the distribution of FAM120A is scarce. Bartolome et al. (2015) has performed IHC on colorectal tissue samples and IF in a colon carcinoma cell line (KM12SM). The distribution of FAM120A diverged between the IHC and IF. The IHC indicated that FAM120A was present at elevated levels in the cytoplasm of cells in sections from colorectal cancers. The IF signal from FAM120A in KM12SM cells showed that FAM120A was primarily localised to the cell membrane where the authors proposed FAM120A interacted with the IL13 receptor subunit α-2 (IL13Rα2). The results presented in this chapter, show that FAM120A is found throughout MDA-MB231 cells with the majority of signal in the cytoplasm (**Figure 7.6**). Therefore, it is possible that YB-1 and FAM120A interact at the cell membrane. However, the only function that has been attributed to YB-1 at the cell membrane relates to cell movement (Lovett et al. 2010) rather than cell survival. Like YB-1, the subcellular distribution of FAM120A was generally consistent with RNA binding and FAM120A has been shown to associate with PUR-α-containing mRNPs in mouse neuronal tissue (Kobayashi et al. 2008). Human YB-1 also interacts with PUR-α (**Chapter 4**, **Chapter 6**, Kim et al. 2008, Lasham et al. 2000, Chen et al. 1995). Further experiments should focus on the accurate co-localisation of YB-1 and FAM120A. Proximity ligation assays, an imaging technique that only produces signal when two antibodies are adjacent to one another (Gullberg et al. 2003, Söderberg et al. 2008), is ideally suited to this work.

A key finding from this chapter is that depleting FAM120A and YB-1 impairs the survival of MDA-MB231 cells during cisplatin exposure. This is the first report that FAM120A supports cell survival during cisplatin exposure. FAM120A and YB-1 were hypothesised to promote the survival of MDA-MB231 cells via the ability of FAM120A to regulate kinase activity. Tanaka et al. (2009) found that following oxidative stress, the association of FAM120A with Src family kinases led to phosphorylation to tyrosine(s) on FAM120A. The phosphorylated FAM120A was then able to interact with PI3-kinase and Src family kinases to activate the Akt-mediated antiapoptotic pathway. Tanaka et al. (2009) hypothesised that the RNA binding and antiapoptotic activities of FAM120A were separate functions of FAM120A. A recent study from a clinical trial of an AKT inhibitor (GSK2141795) found that AKT inhibition reduced the growth-rate of cells from tumour biopsies while re-sensitising them to cisplatin (Cheraghchi-Bashi et al. 2015). Intruigingly, Cheraghchi-Bashi et al. (2015) also found that biopsies from ovarian cancer patients that received

GSK2141795 had greater levels of YB-1.

Finally, depleting FAM120A, or C1QBP, in conjunction with YB-1 highlighted that FAM120A may have a dual role in MDA-MB231 cells. This observation requires further validation using experiments that directly assess cell division and the cell-cycle. The requirement for MDA-MB231 cells to have FAM120A or C1QBP present, in order for YB-1 depletion to strongly inhibit cell growth, is consistent with the function of C1QBP, which is known to negatively influence cell survival (Meenakshi et al. 2003, Sunayama et al. 2004, Reef et al. 2007). There is currently no research indicating that FAM120A can modulate signals that inhibit cell survival or growth. However, it is possible that when YB-1 is not present in MDA-MB231 cells, FAM120A ceases to be activated, possibly by phosphorylation of tyrosines (Tanaka et al. 2009),

7.3.3 Summary

Two of the three proteins that were the focus of this chapter, TRIM28 and C1QBP, do not appear to have functions that are critical to the survival of MDA-MB231 cells during cisplatin exposure. The results from the experiments that were presented in this chapter, are consistent with FAM120A having a function that supports the survival of MDA-MB231 cells during cisplatin exposure. FAM120A appears to be able to influence kinase signalling (see above). However, whether the effects observed involve kinase signalling has yet to be confirmed. Therefore, future work should focus on the interaction of YB-1 and FAM120A and the involvement of kinase signalling. Another proposition requiring further research is if the RNA binding function that both proteins share is important to the ability of YB-1 and FAM120A to support cell survival during cisplatin exposure.

Chapter 8

Overall summary and conclusions

8.1 Key findings

A number of conclusions can be reached from the research that is outlined in this thesis.

1. Elevated levels of YB-1 in the cytoplasm of breast cancer cells are correlated with high histological grade and ER^{-ve}/PR^{-ve} breast cancers.

2. The binding of antibodies against YB-1 appears to be affected by the tertiary structure or PPI of YB-1.

3. YB-1 from the cytoplasm or nucleus of two cancer cell lines is phosphorylated at multiple sites.

4. Depleting YB-1 impairs the survival of MDA-MB231 cells.

5. Depleting FAM120A or C1QBP, in conjunction with YB-1, counteracts the growth reduction that accompanies YB-1 depletion.

6. Depleting YB-1 impairs the survival of MDA-MB231 cells during cisplatin exposure.

7. The PPI of YB-1 in two cancer cell lines indicates that YB-1 binds to DNA but the molecular function of YB-1 in these cells appears to rely on the ability of YB-1 to bind to RNA.

8. Cisplatin exposure modulates a subset of the PPI of YB-1 that are associated with chromatin assembly.

9. FAM120A is likely to cooperate with YB-1 during cisplatin exposure.

8.2 Introduction

Early research identified the ability of YB-1 to bind to the promoters of known oncogenes; *EGFR*, *ERBB2*, and *ABCB1* (Sakura et al. 1988, Ozer et al. 1990, Asakuno et al. 1994, Kohno et al. 1994). Following this, the levels of YB-1 in breast cancers were positively correlated with *ABCB1* expression (Bargou et al. 1997) and a number of studies have confirmed that YB-1 is elevated in a range of cancers, including breast cancer (reviewed in **Chapter 1.3**). However, the work that has followed Bargou et al. (1997) has also revealed that the role of YB-1 in cancer is more complex than solely promoting drug resistance by acting as a transcription factor for the *ABCB1* gene. Instead, it appears that YB-1 has four main functions in cancer. These functions explain the elevated levels of YB-1 in cancers (**Chapter 1.4**):

- Promoting the early stages of cancer development;
- Having a positive role on mitosis;
- Promoting drug resistance;
- Facilitating an invasive phenotype.

The involvement of YB-1 in these four functions appears to rely on the multifunctionality of YB-1 at the molecular level (**Chapter 1.8**). YB-1 can bind to both DNA and RNA. The ability to bind to DNA allows YB-1 to act as a transcription factor and to participate in DNA repair (**Chapter 1.8.2**). While binding to RNA, YB-1 can modulate the inclusion or exclusion of exons during splicing, stabilise RNA, and either promote or inhibit translation of mRNA transcripts (**Chapter 1.8.3**).

The aim of this thesis was to study the functions of YB-1 in cancer and the mechanisms of drug resistance. IHC was used to examine the levels of YB-1 in breast tumours (**Chapter 3.2.2**). The phosphorylation and PPI of YB-1 from the cytoplasm and nuclei of two cancer cell lines were analysed (**Chapter 4**). The role of YB-1 during cisplatin exposure was also studied (**Chapter 5**). Additionally, this thesis examined the PPI of YB-1 in MDA-MB231 cells during cisplatin exposure. The roles of three proteins that copurify with YB-1 during cisplatin were also assessed.

8.3 YB-1 as a clinical biomarker

IHC was used to reconfirm that YB-1 is elevated in aggressive breast cancers (**Chapter 3.2.2**; Bargou et al. 1997, Lee et al. 2008, Woolley et al. 2011, Stratford et al. 2012, Reipas et al. 2013). The direct comparison of the signals from two antibodies against YB-1, ^{N}YB1 and YB1^{C} , in the same breast tumours was unique. Both antibody preparations have similar affinities for reduced YB-1 (**Chapter 3.2.4**; Cohen et al. 2010) but their sensitivity as prognostic markers differs (**Chapter 3.2.2**; Woolley et al. 2011). The tertiary structure or protein interactions of YB-1 appear to explain the differences in YB-1 detection between ^{N}YB1 and YB1^{C} in IHC and BN-PAGE. The PPI of YB-1 as it binds to RNA, including interactions between two YB-1 molecules, are likely to be the primary initiators of change in epitope availability. These changes are hypothesised to rely on the multimerisation of YB-1 particles that have bound densely to an RNA transcript. This multimerisation is likely to occlude the C-terminus of the YB-1 particles (Izumi et al. 2001, Skabkin et al. 2004, Woolley et al. 2011).

A number of researchers have concluded that YB-1 has potential as a biomarker as well as being a therapeutic target (Habibi et al. 2008, Basaki et al. 2010, Davies et al. 2011, Wang et al. 2015, Lasham et al. 2016). However, the results presented here indicate that there are significant hurdles to overcome before YB-1 can be used in a clinical setting as a biomarker. A biomarker that is useful in the clinic needs to provide reproducible results that also lead to clear clinical outcomes (Taube et al. 2005, Matos et al. 2010). The results presented here highlight that YB-1 is present in almost all tissues and that the levels of YB-1 in normal breast tissue vary greatly between individuals (**Chapter 4**). This variation in subcellular localisation between different studies is another barrier to making a clear assessment of the elevations of YB-1 in cancer (reviewed in **Chapter 3.3**). The results indicate that the signal from antibodies against YB-1 are influenced by factors other than the levels of YB-1, namely the tertiary structure or PPI of YB-1. The importance of this effect is yet to be determined.

If IHC cannot reliably provide the levels of YB-1 in tissues, then *YBX1* mRNA levels may supply a more accurate assessment (Lasham et al. 2012). However, important information which may be relevant to clinical decisions about YB-1 protein characteristics, such as teriary structure, PTM, and subcellular localisation, would be unavailable. Finally, the translation of *YBX1* mRNA appears to be highly regulated by both YB-1 (**Chapter 1.7.1**) and the mTOR pathway (Ilic et al. 2011, Lehmann

et al. 2011, Huober et al. 2013, Vicier et al. 2014, Basho et al. 2016) and both are elevated or activated in some breast cancers. Therefore, it is unclear whether *YBX1* mRNA levels provide an accurate representation of YB-1 levels in all breast tumours.

The usefulness of YB-1 as a clinical biomarker is currently unclear. However, the result that elevated levels of YB-1 are present in aggressive breast cancers is clear and it is supported by multiple studies (**Chapter 3.2.2**; Bargou et al. 1997, Lee et al. 2008, Woolley et al. 2011, Stratford et al. 2012, Reipas et al. 2013). The functional significance of this elevation is less clear.

8.4 Phosphorylation of YB-1

The YB-1 that was purified from the cytoplasm and nuclei of MDA-MB231 and A549 cells was phosphorylated at multiple sites (**Chapter 4.2.2**). YB-1 was phosphorylated at S165, S174, S176, and S314. S167 was also identified as a possible site. Of these phosphorylation sites, only the effect of phosphorylation of YB-1 at S165 has been studied. In this work, phosphorylation of YB-1 at S165 appeared to be associated with YB-1 that is in the cytoplasm (**Chapter 4.2.2**). A single paper has shown that phosphorylation of YB-1 at S165 is necessary for NF-κB activation and it may also be significant to the development of colon cancers (discussed in **Chapter 1.7.2.1**).

YB-1 peptides with phosphorylation at S102 were not identified in this work despite being a known PTM to YB-1 in MDA-MB231 cells (Toulany et al. 2011). This modification appears to be difficult to detect using LC-MS/MS.

The effects of phosphorylation on the molecular function of YB-1 at the other residues (S165, S167, S174, S176, and S314) are yet to be characterised. Further study to examine the importance and function of these phosphorylations is warranted. However, currently the cost of developing antibodies against each phosphorylation site would be prohibitive. The LC-MS/MS analyses that were performed here were optimised to identify phosphorylated peptides without consideration for quantification or the consistent detection of specific peptides. However, the data from this study can be used to establish a quantitative assay that targets the identified peptides (discussed in **Chapter 6.3.2**; Picotti & Aebersold 2012). Using isotopcally labelled peptides, with and without phosphorylation, would provide accurate estimates of the proportion of YB-1 that has each phosphorylation. This assay could be established for all the phosphorylation sites that have been identified

here at a similar price to commercially producing a single phosphorylation specific monoclonal antibody. Refinements to the liquid chromatography and disassociation for MS^2 would also improve the sensitivity of the assay to allow meaningful measurements to be made from less starting material. It would also allow the identification of fragments that can be used to quantify a single phosphorylation in MS^2 spectra that are comprised of two separate peptides; each with a phosphorylation at a different site (an example of this is shown in **Figure 4.8.B**). A quantitative assay for phosphorylated YB-1 peptides would have a number of uses.

The presence and potential importance of these phosphorylation sites may be confirmed by gaining information about their occurrence in other cells. The mutated *K-ras* gene in MDA-MB231 cells leads to constitutive phosphorylation of YB-1 at S102 (Toulany et al. 2011). YB-1 from HEK293 cells was only phosphorylated at S165 following IL-1β exposure while the YB-1 from A549 and MDA-MB231 cells was phosphorylated at S165 with no requirement for external stimulation. Therefore, additional phosphorylation sites may be constitutively active in A549 and MDA-MB231 cells. The phosphorylation state of the YB-1 from cell lines representing normal breast tissue and the subtypes of breast cancer could be assessed using a quantitative LC-MS/MS assay that targets phosphorylated YB-1 peptides (an appropriate list of breast cell lines is shown in **Table 1** of Holliday & Speirs 2011).

Research to date has identified that a function of YB-1 is to support the growth and viability of cancer cells (**Chapter 1.4.2**). The findings in this thesis also support this observation. Depleting YB-1 was seen to reduce the viability of asynchronously dividing MDA-MB231 cells (**Chapter 5**). A LC-MS/MS assay that targets the phosphorylated peptides could also be used to study whether YB-1 phosphorylation changes with the cell cycle. Breast cancer cell lines, including MDA-MB231, could be synchronised to G_1/S-phase using a double thymidine block (Bootsma et al. 1964, Bostock et al. 1971) and the phosphorylation of YB-1 monitored as the cells move through the cell cycle.

8.5 Function of YB-1

The multifunctionality of YB-1 has been extensively reviewed in **Chapter 1**. YB-1 can act as a transcription factor (**Chapter 1.8.2**), modulate the inclusion or exclusion of exons during splicing, stabilise RNA, and promote or inhibit translation of mRNA transcripts (**Chapter 1.8.3**). These functions were generally supported by the results from analysing the proteins that copurified with YB-1 from MDA-

MB231 and A549 cells (**Chapter 4** and **Chapter 6**). Furthermore, the results from **Chapter 4** indicate that most of the YB-1 in the nucleus of these cells was also likely to bind to RNA. Therefore, the results from this thesis imply that the molecular functions of YB-1 that is binding to RNA are important in cancer cells.

YB-1 can bind to RNA and participate in the many steps that separate freshly transcribed pre-mRNA transcripts from the point where a protein is translated (**Chapter 3.2.3**). The PPI of YB-1 are consistent with the literature regarding the interaction of YB-1 with RNA and the biochemical functions that stem from it. The function of the YB-1 that is binding to DNA in MDA-MB231 cells remains less clear (**Chapter 3.2.3 - 3.2.4**).

The ability of YB-1 to act as a transcription factor is well documented (reviewed in **Chapter 1.8.2.1**). In this thesis, YB-1 was shown to interact with DNA (**Figure 3.7** and **Figure 5.10**) and this was consistent with YB-1 participating in transcription. Therefore, prior to performing the immunoprecipitation of YB-1 from the nuclei of two cell lines (reported in **Chapter 4**), the literature and observations from IF and DNA affinity proteins led to an expectation that nuclear YB-1 was acting as a transcription factor. The PPI of YB-1 indicated that, while in the nucleus, YB-1 was binding to both DNA and RNA. The proteins that were associated with RNA binding are consistent with YB-1 influencing RNA splicing, transport, and maturation in the nucleus. However, a subset of the proteins that copurified with YB-1 from the nuclei of the two cancer cell lines, provided further evidence for YB-1 interacting with DNA as proteins that are associated with chromatin, including histones 1 - 3 and TRIM28 among others. However, there was no clear evidence linking this chromatin association with transcriptional machinery.

Studies have highlighted the ability of YB-1 to repress the transcription of genes, including *CD95*, *MMP2*, and *GM-CSF* (see **Table 1.2**). Some of the proteins that copurified with YB-1 are known to repress transcription. TRIM28 has been identified as one of these proteins and it copurified with YB-1 from the nuclei of both MDA-MB231 and A549 cells. However, in addition to the ability to repress transcription of E2F- family target genes, TRIM28 can also participate in DNA repair (Iyengar & Farnham 2011, Neo et al. 2015). Therefore, the function of the interaction between YB-1 and TRIM28 is unclear. The Transcriptional activator protein Pur-alpha (PURA) is another protein that copurifies with YB-1 which can repress transcription (reviewed in Gallia et al. 2000). PURA has been shown to interact with YB-1 to repress the transcription of *CD95* and *TP53* (Lasham et al. 2000, Kim et al. 2008). However, PURA also interacts with RNA to influence

translation (Gallia et al. 2000). In the current study, PURA copurified with YB-1 from the cytoplasm and the nuclei. This is consistent with the interaction of PURA and YB-1 occurring while both proteins are binding to RNA. This study confirms that YB-1 interacts with proteins that associate with chromosomes although the significance of this to the function of YB-1 is yet to be fully defined.

The inferred functions of YB-1 were consistent with the molecular processes in which YB-1 participates (**Chapter 1.8**). However, the significance of some PPI of YB-1 remains less clear. The present work was unable to confirm the importance of the inferred interactions to the molecular functions of YB-1 in the cell lines.

YB-1 is capable of influencing most levels of gene expression. Future work should confirm the molecular functions of YB-1 in these cell lines by testing the effects of depleting YB-1 on all levels of gene expression. To do so, YB-1 can be depleted prior to pulse labelling newly transcribed RNA and proteins in conjunction with sequencing and LC-MS/MS. This protocol, following the approach in Schwanhäusser et al. (2011), provides a model of the rates of mRNA production, mRNA degradation, translation, and protein degradation. Previous research indicates that YB-1 can influence all of these processes except protein degradation (**Chapter 1.8**). This method could confirm whether the molecular functions of YB-1 in A549 and MDA-MB231 cells matches the functions that were strongly inferred by the PPI of YB-1. Specfically, that YB-1 primarily regulates gene expression in A549 and MDA-MB231 cells through post-transcriptional regulation of RNA transcripts and translation.

8.6 YB-1 during cisplatin exposure

The work presented here provides further confirmation that YB-1 can support resistance to a range of drugs (**Chapter 5**; Ohga et al. 1996, Ohga et al. 1998, Shibahara et al. 2004, Shibahara et al. 2004). The conditions used in this thesis ensured that the cisplatin exposure received by MDA-MB231 cells was tolerated. It is not clear that this is true of other papers that explore the role of YB-1 in cisplatin resistance (discussed in **Chapter 5.3**; Guay et al. 2008a, Garand et al. 2011).

The work outlined shows that a subset of proteins interacting with YB-1 increased or decreased in abundance following cisplatin exposure and, that these proteins appeared to have functions in chromatin organisation and DNA binding. Therefore, the modulation of two known functions of YB-1, the repair of DNA damage or a transcriptional response, would be consistent with the protein interactions of YB-1 during cisplatin exposure. The evidence for proteins that are involved in

transcription has been discussed in the preceding chapter. A number of studies have indicated that during cisplatin exposure YB-1 can participate in the repair of DNA (**Chapter 1.8.2.2** and **Chapter 6.3.2**). Proteins from the nucleotide excision repair pathway and the base excision repair pathway, the two DNA repair pathways that YB-1 is known to participate in, did not copurify with YB-1. Instead, more TRIM28 copurified with YB-1 following cisplatin exposure and this interaction was hypothesised to be related to the repair of DNA double strand breaks. However, depleting YB-1 had no effect on the formation of γH2AX foci. Depleting TRIM28 prior to cisplatin exposure did not alter the response of MDA-MB231 cells to the exposure. Therefore, DNA repair via the repair of double strand DNA breaks does not appear to be central to the reduced survival of MDA-MB231 cells accompanying YB-1 depletion. The significance of the interaction between TRIM28 and YB-1 is unknown.

During cisplatin exposure, FAM120A and YB-1 increased their association and depleting FAM120A reduced the growth rate of MDA-MB231 cells. The subcellular distributions of YB-1 and FAM120A were very similar. However, the function of FAM120A is currently poorly defined. The work detailed here is consistent with two previous reports that FAM120A can promote cell survival during stress (Tanaka et al. 2009, Woźniak et al. 2014). This is the first report to show that the presence of FAM120A can improve the growth rate of cells during cisplatin exposure.

One of the novel findings from this thesis is that there is an interaction between YB-1 and FAM120A in A549 and MDA-MB231 cells. This interaction has the potential to promote the survival of cells during cisplatin exposure. Further work is required to confirm the interplay between the two proteins and define the nature of the interaction. However, two alternative models may predict how the proteins interact. The first model pedicts that FAM120A can inhibit cell division but YB-1 represses this function (**Figure 8.1.A**). This is consistent with the depletion of FAM120A rescuing the negative effects of YB-1 depletion on cell division. This model also predicts that FAM120A and YB-1 interact directly to influence cell survival during cisplatin exposure.

The second hypothetical model for the interaction of YB-1 and FAM120A predicts that the two proteins interact to promote the survival of MDA-MB231 cells during stress (**Figure 8.1.B**). In this model, both the depletion of YB-1 and also exposure to cisplatin lead to cell stress and the interaction of YB-1 and FAM120A to promote survival. This second model is the most consistent with reports that FAM120A can promote cell survival (Tanaka et al. 2009, Woźniak et al. 2014).

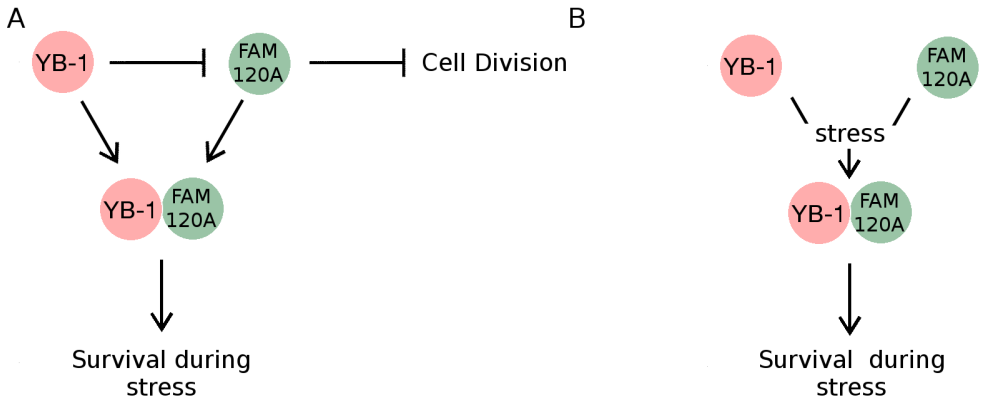

Figure 8.1: Hypothetical models for the interaction of YB-1 and FAM120A. **A**, a model that predicts the interaction of YB-1 and FAM120A. **B**, an alternative model that predicts the interaction of YB-1 and FAM120A.

The molecular function of the interaction between YB-1 and FAM120A was not confirmed in this thesis. However, the work outlined here shows that the association of YB-1 and FAM120A is unlikely to be at the cell membrane. IF indicated that FAM120A was distributed throughout MDA-MB231 cells. FAM120A copurified with YB-1 from the cytoplasm and from the nucleus of MDA-MB231 and A549 cells. Given that both FAM120A and YB-1 can bind to RNA, it appears that these two proteins interact while associating with RNA. However, as was noted in **Chapter 7.3.2**, a proximity ligation assay that tests the colocalisation of YB-1 and FAM120A could confirm where YB-1 and FAM120A interact within cells and how cisplatin exposure influences this interaction. Proximity ligation assays also provide an alternative technique to IP to confirm the interactions of proteins (Gullberg et al. 2003, Söderberg et al. 2008).

On of the assays that was suggested in the preceding sections of this chapter could also be useful to study the role of YB-1 during cisplatin exposure. Phosphorylation has the potential to modulate the molecular function of YB-1. The quantitative assay of YB-1 phosphorylation described in **Chapter 8.4** may also provide useful information about the effects of cisplatin exposure on the phosphorylation of YB-1. FAM120A can influence kinase function, possibly by acting as a scaffold (Tanaka et al. 2009, Bartolome et al. 2015). Therefore, it is possible that the role of FAM120A during cisplatin exposure is to alter the phosphorylation of YB-1. The quantitative assay of YB-1 phosphorylation could also assess whether depleting FAM120A alters the phosphorylation of YB-1 during cisplatin exposure.

8.7 Final remarks

The work presented here indicates that the contribution of different molecular functions of YB-1 may differ from those described in previous reports. It is important to gain an understanding of the relative contribution of the molecular functions of YB-1. The work in this thesis highlights that the role of YB-1 as an RNA binding protein requires greater attention. Many studies that attribute a transcriptional effect to YB-1 may be measuring the effects of YB-1 as an RNA binding protein. The ability of YB-1 to stabilise mRNA transcripts is one mechanism that may lead to increased levels of an mRNA transcript (reviewed in **Chapter 1.8.3.3**). YB-1 may also appear to promote the transcription of a gene via its role as an exonic splicing enhancer during pre-mRNA splicing. Disrupting the interaction of YB-1 with *MDM2* pre-mRNA by camptothecin exposure or depleting YB-1 leads to co-transcriptional exon skipping (Dutertre et al. 2010). Without the intricate assays that were presented by Dutertre et al. (2010), this effect could appear to be a loss of YB-1 transcriptional promotion.

The dominance of proteins that are involved in RNA amongst those that copurify with YB-1 was consistent with the results from IHC and IF. However, the function of YB-1 while it is binding to DNA remains an interesting focus, particularly if this focus confirms that the DNA binding functions of YB-1 are of secondary importance to the RNA binding functions. As noted above this question should receive further attention.

Phosphorylation of YB-1 was more extensive than expected. Given the potential for these phosphorylations to partition the molecular function of YB-1 they also warrant further study. Finally, FAM120A appears to be an important binding partner for YB-1. The handful of papers highlight important functions of its own. It is difficult to study because of the small amount that is currently known about it but this is also a strength of its identification.

Finally, FAM120A appears to be an important binding partner for YB-1. It is currently challenging to study FAM120A as there is a limited body of work characterising this protein. The potential to contribute knowledge regarding the function of both proteins by further defining the interaction of YB-1 and FAM120A, highlights that this should be a focus for future research.

Bibliography

Al Jabry, T. S. H. (2016). *Characterising the phosphorylation of YB-1*, PhD thesis, Sydney Medical School, Children's Medical Research Institute, The university of Sydney, Australia.

Alemasova, E. E., Pestryakov, P. E., Sukhanova, M. V., Kretov, D. A., Moor, N. A., Curmi, P. A., Ovchinnikov, L. P. & Lavrik, O. I. (2015). Poly(ADP-ribosyl)ation as a new posttranslational modification of YB-1, *Biochimie* **119**: 36–44.

Alidousty, C., Rauen, T., Hanssen, L., Wang, Q., Alampour-Rajabi, S., Mertens, P. R., Bernhagen, J., Floege, J., Ostendorf, T. & Raffetseder, U. (2014). Calcineurin-mediated YB-1 dephosphorylation regulates CCL5 expression during monocyte differentiation, *J Biol Chem* **289**(31): 21401–12.

Anderson, P., Kedersha, N. & Ivanov, P. (2015). Stress granules, P-bodies and cancer, *Biochim Biophys Acta* **1849**(7): 861–70.

André, F. & Zielinski, C. C. (2012). Optimal strategies for the treatment of metastatic triple-negative breast cancer with currently approved agents, *Ann Oncol* **23 Suppl 6**: vi46–51.

Andreassi, C. & Riccio, A. (2009). To localize or not to localize: mRNA fate is in 3'UTR ends, *Trends Cell Biol* **19**(9): 465–74.

Arnér, E. S. J. (2010). Selenoproteins-What unique properties can arise with selenocysteine in place of cysteine?, *Exp Cell Res* **316**(8): 1296–303.

Aronchik, I., Appleton, B. A., Basham, S. E., Crawford, K., Del Rosario, M., Doyle, L. V., Estacio, W. F., Lan, J., Lindvall, M. K., Luu, C. A., Ornelas, E., Venetsanakos, E., Shafer, C. M. & Jefferson, A. B. (2014). Novel potent and selective inhibitors of p90 ribosomal S6 kinase reveal the heterogeneity of RSK function in MAPK-driven cancers, *Mol Cancer Res* **12**(5): 803–12.

Asakuno, K., Kohno, K., Uchiumi, T., Kubo, T., Sato, S., Isono, M. & Kuwano, M. (1994). Involvement of a DNA binding protein, MDR-NF1/YB-1, in human MDR1 gene expression by actinomycin D, *Biochem Biophys Res Commun* **199**(3): 1428–35.

Ashburner, M., Ball, C. A., Blake, J. A., Botstein, D., Butler, H., Cherry, J. M., Davis, A. P., Dolinski, K., Dwight, S. S., Eppig, J. T., Harris, M. A., Hill,

D. P., Issel-Tarver, L., Kasarskis, A., Lewis, S., Matese, J. C., Richardson, J. E., Ringwald, M., Rubin, G. M. & Sherlock, G. (2000). Gene ontology: tool for the unification of biology. The Gene Ontology Consortium, *Nat Genet* **25**(1): 25–9.

Astanehe, A., Finkbeiner, M. R., Hojabrpour, P., To, K., Fotovati, A., Shadeo, A., Stratford, A. L., Lam, W. L., Berquin, I. M., Duronio, V. & Dunn, S. E. (2009). The transcriptional induction of PIK3CA in tumor cells is dependent on the oncoprotein Y-box binding protein-1, *Oncogene* **28**(25): 2406–18.

Astanehe, A., Finkbeiner, M. R., Krzywinski, M., Fotovati, A., Dhillon, J., Berquin, I. M., Mills, G. B., Marra, M. A. & Dunn, S. E. (2012). MKNK1 is a YB-1 target gene responsible for imparting trastuzumab resistance and can be blocked by RSK inhibition, *Oncogene* **31**(41): 4434–46.

Baba, T. W. & Humphries, E. H. (1984). Differential response to avian leukosis virus infection exhibited by two chicken lines, *Virology* **135**(1): 181–8.

Bader, A. G., Felts, K. A., Jiang, N., Chang, H. W. & Vogt, P. K. (2003). Y box-binding protein 1 induces resistance to oncogenic transformation by the phosphatidylinositol 3-kinase pathway, *Proc Natl Acad Sci U S A* **100**(21): 12384–9.

Bader, A. G. & Vogt, P. K. (2004). An essential role for protein synthesis in oncogenic cellular transformation, *Oncogene* **23**(18): 3145–50.

Bader, A. G. & Vogt, P. K. (2005). Inhibition of protein synthesis by Y box-binding protein 1 blocks oncogenic cell transformation, *Mol Cell Biol* **25**(6): 2095–106.

Bader, A. G. & Vogt, P. K. (2008). Phosphorylation by Akt disables the anti-oncogenic activity of YB-1, *Oncogene* **27**(8): 1179–82.

Baltz, A. G., Munschauer, M., Schwanhäusser, B., Vasile, A., Murakawa, Y., Schueler, M., Youngs, N., Penfold-Brown, D., Drew, K., Milek, M., Wyler, E., Bonneau, R., Selbach, M., Dieterich, C. & Landthaler, M. (2012). The mRNA-bound proteome and its global occupancy profile on protein-coding transcripts, *Mol Cell* **46**(5): 674–90.

Bann, D. V., Beyer, A. R. & Parent, L. J. (2014). A murine retrovirus co-opts YB-1, a translational regulator and stress granule-associated protein, to facilitate virus assembly, *J Virol* **88**(8): 4434–50.

Bargou, R. C., Jürchott, K., Wagener, C., Bergmann, S., Metzner, S., Bommert, K., Mapara, M. Y., Winzer, K. J., Dietel, M., Dörken, B. & Royer, H. D. (1997). Nuclear localization and increased levels of transcription factor YB-1 in primary human breast cancers are associated with intrinsic MDR1 gene expression, *Nat Med* **3**(4): 447–50.

Bartolome, R. A., Garcia-Palmero, I., Torres, S., Lopez-Lucendo, M., Balyasnikova, I. V. & Casal, J. I. (2015). IL13 receptor alpha2 signaling requires a scaffold protein, FAM120A, to activate the FAK and PI3K pathways in colon cancer metastasis, *Cancer Res* **75**(12): 2434–44.

Basaki, Y., Hosoi, F., Oda, Y., Fotovati, A., Maruyama, Y., Oie, S., Ono, M., Izumi, H., Kohno, K., Sakai, K., Shimoyama, T., Nishio, K. & Kuwano, M. (2007). Akt-dependent nuclear localization of Y-box-binding protein 1 in acquisition of malignant characteristics by human ovarian cancer cells, *Oncogene* **26**(19): 2736–46.

Basaki, Y., Taguchi, K.-I., Izumi, H., Murakami, Y., Kubo, T., Hosoi, F., Watari, K., Nakano, K., Kawaguchi, H., Ohno, S., Kohno, K., Ono, M. & Kuwano, M. (2010). Y-box binding protein-1 (YB-1) promotes cell cycle progression through CDC6-dependent pathway in human cancer cells, *Eur J Cancer* **46**(5): 954–65.

Basho, R. K., Gilcrease, M., Murthy, R. K., Helgason, T., Karp, D. D., Meric-Bernstam, F., Hess, K. R., Herbrich, S. M., Valero, V., Albarracin, C., Litton, J. K., Chavez-MacGregor, M., Ibrahim, N. K., Murray, 3rd, J. L., Koenig, K. B., Hong, D., Subbiah, V., Kurzrock, R., Janku, F. & Moulder, S. L. (2016). Targeting the PI3K/AKT/mTOR pathway for the treatment of mesenchymal triple-negative breast cancer: evidence from a phase 1 trial of mTOR inhibition in combination with liposomal doxorubicin and bevacizumab, *JAMA Oncol* **Online**.
URL: *http://dx.doi.org/10.1001/jamaoncol.2016.5281*

Benore-Parsons, M., Seidah, N. G. & Wennogle, L. P. (1989). Substrate phosphorylation can inhibit proteolysis by trypsin-like enzymes, *Arch Biochem Biophys* **272**(2): 274–80.

Bergmann, S., Royer-Pokora, B., Fietze, E., Jürchott, K., Hildebrandt, B., Trost, D., Leenders, F., Claude, J.-C., Theuring, F., Bargou, R., Dietel, M. & Royer, H.-D. (2005). YB-1 provokes breast cancer through the induction of chromosomal instability that emerges from mitotic failure and centrosome amplification, *Cancer Res* **65**(10): 4078–87.

Bieging, K. T., Mello, S. S. & Attardi, L. D. (2014). Unravelling mechanisms of p53-mediated tumour suppression, *Nat Rev Cancer* **14**(5): 359–70.

Biemann, K. (1990). Appendix 5. Nomenclature for peptide fragment ions (positive ions), *Methods Enzymol* **193**: 886–7.

Bisio, A., Latorre, E., Andreotti, V., Bressac-de Paillerets, B., Harland, M., Scarra, G. B., Ghiorzo, P., Spitale, R. C., Provenzani, A. & Inga, A. (2015). The 5'-untranslated region of p16INK4a melanoma tumor suppressor acts as a cellular IRES, controlling mRNA translation under hypoxia through YBX1 binding, *Oncotarget* **6**(37): 39980–94.

Blagosklonny, M. V. & Fojo, T. (1999). Molecular effects of paclitaxel: myths and reality (a critical review), *Int J Cancer* **83**(2): 151–6.

Blenkiron, C., Hurley, D. G., Fitzgerald, S., Print, C. G. & Lasham, A. (2013). Links between the oncoprotein YB-1 and small non-coding RNAs in breast cancer, *PLoS One* **8**(11): e80171.

Blows, F. M., Driver, K. E., Schmidt, M. K., Broeks, A., van Leeuwen, F. E., Wesseling, J., Cheang, M. C., Gelmon, K., Nielsen, T. O., Blomqvist, C., Heikkilä, P., Heikkinen, T., Nevanlinna, H., Akslen, L. A., Bégin, L. R., Foulkes, W. D., Couch, F. J., Wang, X., Cafourek, V., Olson, J. E., Baglietto, L., Giles, G. G., Severi, G., McLean, C. A., Southey, M. C., Rakha, E., Green, A. R., Ellis, I. O., Sherman, M. E., Lissowska, J., Anderson, W. F., Cox, A., Cross, S. S., Reed, M. W. R., Provenzano, E., Dawson, S.-J., Dunning, A. M., Humphreys, M., Easton, D. F., García-Closas, M., Caldas, C., Pharoah, P. D. & Huntsman, D. (2010). Subtyping of breast cancer by immunohistochemistry to investigate a relationship between subtype and short and long term survival: a collaborative analysis of data for 10,159 cases from 12 studies, *PLoS Med* **7**(5): e1000279.

Bommert, K. S., Effenberger, M., Leich, E., Küspert, M., Murphy, D., Langer, C., Moll, R., Janz, S., Mottok, A., Weissbach, S., Rosenwald, A., Bargou, R. & Bommert, K. (2013). The feed-forward loop between YB-1 and MYC is essential for multiple myeloma cell survival, *Leukemia* **27**(2): 441–50.

Bonetti, A., Apostoli, P., Zaninelli, M., Pavanel, F., Colombatti, M., Cetto, G. L., Franceschi, T., Sperotto, L. & Leone, R. (1996). Inductively coupled plasma mass spectroscopy quantitation of platinum-DNA adducts in peripheral blood leukocytes of patients receiving cisplatin- or carboplatin-based chemotherapy, *Clin Cancer Res* **2**(11): 1829–35.

Boothby, M. & Williams, C. L. (2012). The Goldilocks effect, *Sci Transl Med* **4**(163): 163fs42.

Bootsma, D., Budke, L. & Vos, O. (1964). Studies on synchronous division of tissue culture cells initiated by excess thymidine, *Exp Cell Res* **33**: 301–9.

Bosco, E. E., Mayhew, C. N., Hennigan, R. F., Sage, J., Jacks, T. & Knudsen, E. S. (2004). RB signaling prevents replication-dependent DNA double-strand breaks following genotoxic insult, *Nucleic Acids Res* **32**(1): 25–34.

Bostock, C. J., Prescott, D. M. & Kirkpatrick, J. B. (1971). An evaluation of the double thymidine block for synchronizing mammalian cells at the g1-s border, *Exp Cell Res* **68**(1): 163–8.

Bounedjah, O., Desforges, B., Wu, T.-D., Pioche-Durieu, C., Marco, S., Hamon, L., Curmi, P. A., Guerquin-Kern, J.-L., Piétrement, O. & Pastré, D. (2014). Free mRNA in excess upon polysome dissociation is a scaffold for protein multimerization to form stress granules, *Nucleic Acids Res* **42**(13): 8678–91.

Bouvet, P., Matsumoto, K. & Wolffe, A. P. (1995). Sequence-specific RNA recognition by the Xenopus Y-box proteins. An essential role for the cold shock domain, *J Biol Chem* **270**(47): 28297–303.

Braithwaite, A. W., Royds, J. A. & Jackson, P. (2005). The p53 story: layers of complexity, *Carcinogenesis* **26**(7): 1161–9.

Braun, J. E., Huntzinger, E. & Izaurralde, E. (2013). The role of GW182 proteins in miRNA-mediated gene silencing, *Adv Exp Med Biol* **768**: 147–63.

Brill, L. M., Xiong, W., Lee, K.-B., Ficarro, S. B., Crain, A., Xu, Y., Terskikh, A., Snyder, E. Y. & Ding, S. (2009). Phosphoproteomic analysis of human embryonic stem cells, *Cell Stem Cell* **5**(2): 204–13.

Britton, S., Coates, J. & Jackson, S. P. (2013). A new method for high-resolution imaging of Ku foci to decipher mechanisms of DNA double-strand break repair, *J Cell Biol* **202**(3): 579–95.

Brouwers, E. E. M., Tibben, M. M., Rosing, H., Hillebrand, M. J. X., Joerger, M., Schellens, J. H. M. & Beijnen, J. H. (2006). Sensitive inductively coupled plasma mass spectrometry assay for the determination of platinum originating from cisplatin, carboplatin, and oxaliplatin in human plasma ultrafiltrate, *J Mass Spectrom* **41**(9): 1186–94.

Brozovic, A., Damrot, J., Tsaryk, R., Helbig, L., Nikolova, T., Hartig, C., Osmak, M., Roos, W. P., Kaina, B. & Fritz, G. (2009). Cisplatin sensitivity is related to late DNA damage processing and checkpoint control rather than to the early DNA damage response, *Mutat Res* **670**(1-2): 32–41.

Byrski, T., Huzarski, T., Dent, R., Marczyk, E., Jasiowka, M., Gronwald, J., Jakubowicz, J., Cybulski, C., Wisniowski, R., Godlewski, D., Lubinski, J. & Narod, S. A. (2014). Pathologic complete response to neoadjuvant cisplatin in BRCA1-positive breast cancer patients, *Breast Cancer Res Treat* **147**(2): 401–5.

Caiola, E., Salles, D., Frapolli, R., Lupi, M., Rotella, G., Ronchi, A., Garassino, M. C., Mattschas, N., Colavecchio, S., Broggini, M., Wiesmüller, L. & Marabese, M. (2015). Base excision repair-mediated resistance to cisplatin in KRAS(G12C) mutant NSCLC cells, *Oncotarget* **6**(30): 30072–87.

Capowski, E. E., Esnault, S., Bhattacharya, S. & Malter, J. S. (2001). Y box-binding factor promotes eosinophil survival by stabilizing granulocyte-macrophage colony-stimulating factor mRNA, *J Immunol* **167**(10): 5970–6.

Carey, L. A., Perou, C. M., Livasy, C. A., Dressler, L. G., Cowan, D., Conway, K., Karaca, G., Troester, M. A., Tse, C. K., Edmiston, S., Deming, S. L., Geradts, J., Cheang, M. C. U., Nielsen, T. O., Moorman, P. G., Earp, H. S. & Millikan, R. C. (2006). Race, breast cancer subtypes, and survival in the Carolina Breast Cancer Study, *JAMA* **295**(21): 2492–502.

Carroll, A. G., Voeller, H. J., Sugars, L. & Gelmann, E. P. (1993). p53 oncogene mutations in three human prostate cancer cell lines, *Prostate* **23**(2): 123–34.

Castella, S., Bernard, R., Corno, M., Fradin, A. & Larcher, J.-C. (2015). Ilf3 and NF90 functions in RNA biology, *Wiley Interdiscip Rev RNA* **6**(2): 243–56.

Castellana, B., Aasen, T., Moreno-Bueno, G., Dunn, S. E. & Ramón y Cajal, S. (2015). Interplay between YB-1 and IL-6 promotes the metastatic phenotype in breast cancer cells, *Oncotarget* **6**(35): 38239–56.

Chaikam, V. & Karlson, D. T. (2010). Comparison of structure, function and regulation of plant cold shock domain proteins to bacterial and animal cold shock domain proteins, *BMB Rep* **43**(1): 1–8.

Chalfie, M., Tu, Y., Euskirchen, G., Ward, W. W. & Prasher, D. C. (1994). Green fluorescent protein as a marker for gene expression, *Science* **263**(5148): 802–5.

Chansky, H. A., Hu, M., Hickstein, D. D. & Yang, L. (2001). Oncogenic TLS/ERG and EWS/Fli-1 fusion proteins inhibit RNA splicing mediated by YB-1 protein, *Cancer Res* **61**(9): 3586–90.

Chatterjee, M., Rancso, C., Stühmer, T., Eckstein, N., Andrulis, M., Gerecke, C., Lorentz, H., Royer, H.-D. & Bargou, R. C. (2008). The Y-box binding protein YB-1 is associated with progressive disease and mediates survival and drug resistance in multiple myeloma, *Blood* **111**(7): 3714–22.

Chattopadhyay, R., Das, S., Maiti, A. K., Boldogh, I., Xie, J., Hazra, T. K., Kohno, K., Mitra, S. & Bhakat, K. K. (2008). Regulatory role of human AP-endonuclease (APE1/Ref-1) in YB-1-mediated activation of the multidrug resistance gene MDR1, *Mol Cell Biol* **28**(23): 7066–80.

Chen, C. Y., Gherzi, R., Andersen, J. S., Gaietta, G., Jürchott, K., Royer, H. D., Mann, M. & Karin, M. (2000). Nucleolin and YB-1 are required for JNK-mediated interleukin-2 mRNA stabilization during T-cell activation, *Genes Dev* **14**(10): 1236–48.

Chen, L., Chen, D. T., Kurtyka, C., Rawal, B., Fulp, W. J., Haura, E. B. & Cress, W. D. (2012). Tripartite motif containing 28 (Trim28) can regulate cell proliferation by bridging HDAC1/E2F interactions, *J Biol Chem* **287**(48): 40106–18.

Chen, M. & Manley, J. L. (2009). Mechanisms of alternative splicing regulation: insights from molecular and genomics approaches, *Nat Rev Mol Cell Biol* **10**(11): 741–54.

Chen, N. N., Chang, C. F., Gallia, G. L., Kerr, D. A., Johnson, E. M., Krachmarov, C. P., Barr, S. M., Frisque, R. J., Bollag, B. & Khalili, K. (1995). Cooperative action of cellular proteins YB-1 and Pur alpha with the tumor antigen of the human JC polyomavirus determines their interaction with the viral lytic control element, *Proc Natl Acad Sci U S A* **92**(4): 1087–91.

Cheraghchi-Bashi, A., Parker, C. A., Curry, E., Salazar, J.-F., Gungor, H., Saleem, A., Cunnea, P., Rama, N., Salinas, C., Mills, G. B., Morris, S. R., Kumar, R., Gabra, H. & Stronach, E. A. (2015). A putative biomarker signature for clinically effective AKT inhibition: correlation of in vitro, in vivo and clinical data identifies the importance of modulation of the mTORC1 pathway, *Oncotarget* **6**(39): 41736–49.

Chernov, K. G., Barbet, A., Hamon, L., Ovchinnikov, L. P., Curmi, P. A. & Pastré, D. (2009). Role of microtubules in stress granule assembly: microtubule dynamical instability favors the formation of micrometric stress granules in cells, *J Biol Chem* **284**(52): 36569–80.

Chernov, K. G., Curmi, P. A., Hamon, L., Mechulam, A., Ovchinnikov, L. P. & Pastré, D. (2008a). Atomic force microscopy reveals binding of mRNA to microtubules mediated by two major mRNP proteins YB-1 and PABP, *FEBS Lett* **582**(19): 2875–81.

Chernov, K. G., Mechulam, A., Popova, N. V., Pastre, D., Nadezhdina, E. S., Skabkina, O. V., Shanina, N. A., Vasiliev, V. D., Tarrade, A., Melki, J., Joshi, V., Baconnais, S., Toma, F., Ovchinnikov, L. P. & Curmi, P. A. (2008b). YB-1 promotes microtubule assembly in vitro through interaction with tubulin and microtubules, *BMC Biochem* **9**: 23.

Chibi, M., Meyer, M., Skepu, A., G Rees, D. J., Moolman-Smook, J. C. & Pugh, D. J. R. (2008). RBBP6 interacts with multifunctional protein YB-1 through its RING finger domain, leading to ubiquitination and proteosomal degradation of YB-1, *J Mol Biol* **384**(4): 908–16.

Choudhary, C., Kumar, C., Gnad, F., Nielsen, M. L., Rehman, M., Walther, T. C., Olsen, J. V. & Mann, M. (2009). Lysine acetylation targets protein complexes and co-regulates major cellular functions, *Science* **325**(5942): 834–40.

Ciardiello, F. & Tortora, G. (2008). EGFR antagonists in cancer treatment, *N Engl J Med* **358**(11): 1160–74.

Classon, M. & Harlow, E. (2002). The retinoblastoma tumour suppressor in development and cancer, *Nat Rev Cancer* **2**(12): 910–7.

Cobbold, L. C., Spriggs, K. A., Haines, S. J., Dobbyn, H. C., Hayes, C., de Moor, C. H., Lilley, K. S., Bushell, M. & Willis, A. E. (2008). Identification of internal ribosome entry segment (IRES)-trans-acting factors for the Myc family of IRESs, *Mol Cell Biol* **28**(1): 40–9.

Cobbold, L. C., Wilson, L. A., Sawicka, K., King, H. A., Kondrashov, A. V., Spriggs, K. A., Bushell, M. & Willis, A. E. (2010). Upregulated c-myc expression in multiple myeloma by internal ribosome entry results from increased interactions with and expression of PTB-1 and YB-1, *Oncogene* **29**(19): 2884–91.

Cohen, J. C., Lundblad, L. K. A., Bates, J. H. T., Levitzky, M. & Larson, J. E. (2004). The "Goldilocks effect" in cystic fibrosis: identification of a lung phenotype in the cftr knockout and heterozygous mouse, *BMC Genet* **5**: 21.

Cohen, S. B., Ma, W., Valova, V. A., Algie, M., Harfoot, R., Woolley, A. G., Robinson, P. J. & Braithwaite, A. W. (2010). Genotoxic stress-induced nuclear localization of oncoprotein YB-1 in the absence of proteolytic processing, *Oncogene* **29**(3): 403–10.

Coles, L. S., Bartley, M. A., Bert, A., Hunter, J., Polyak, S., Diamond, P., Vadas, M. A. & Goodall, G. J. (2004). A multi-protein complex containing cold shock domain (Y-box) and polypyrimidine tract binding proteins forms on the vascular endothelial growth factor mRNA. Potential role in mRNA stabilization, *Eur J Biochem* **271**(3): 648–60.

Coles, L. S., Lambrusco, L., Burrows, J., Hunter, J., Diamond, P., Bert, A. G., Vadas, M. A. & Goodall, G. J. (2005). Phosphorylation of cold shock domain/Y-box proteins by ERK2 and GSK3beta and repression of the human VEGF promoter, *FEBS Lett* **579**(24): 5372–8.

Dahl, E., En-Nia, A., Wiesmann, F., Krings, R., Djudjaj, S., Breuer, E., Fuchs, T., Wild, P. J., Hartmann, A., Dunn, S. E. & Mertens, P. R. (2009). Nuclear detection of Y-box protein-1 (YB-1) closely associates with progesterone receptor negativity and is a strong adverse survival factor in human breast cancer, *BMC Cancer* **9**: 410.

Das, S., Chattopadhyay, R., Bhakat, K. K., Boldogh, I., Kohno, K., Prasad, R., Wilson, S. H. & Hazra, T. K. (2007). Stimulation of NEIL2-mediated oxidized base excision repair via YB-1 interaction during oxidative stress, *J Biol Chem* **282**(39): 28474–84.

Davies, A. H., Barrett, I., Pambid, M. R., Hu, K., Stratford, A. L., Freeman, S., Berquin, I. M., Pelech, S., Hieter, P., Maxwell, C. & Dunn, S. E. (2011). YB-1 evokes susceptibility to cancer through cytokinesis failure, mitotic dysfunction and HER2 amplification, *Oncogene* **30**(34): 3649–60.

Davies, A. H., Reipas, K. M., Pambid, M. R., Berns, R., Stratford, A. L., Fotovati, A., Firmino, N., Astanehe, A., Hu, K., Maxwell, C., Mills, G. B. & Dunn, S. E. (2014). YB-1 transforms human mammary epithelial cells through chromatin remodeling leading to the development of basal-like breast cancer, *Stem Cells* **32**(6): 1437–50.

Davis, A. J. & Chen, D. J. (2013). DNA double strand break repair via non-homologous end-joining, *Transl Cancer Res* **2**(3): 130–43.

Davydova, E. K., Evdokimova, V. M., Ovchinnikov, L. P. & Hershey, J. W. (1997). Overexpression in COS cells of p50, the major core protein associated with mRNA, results in translation inhibition, *Nucleic Acids Res* **25**(14): 2911–6.

de Souza-Pinto, N. C., Mason, P. A., Hashiguchi, K., Weissman, L., Tian, J., Guay, D., Lebel, M., Stevnsner, T. V., Rasmussen, L. J. & Bohr, V. A. (2009). Novel DNA mismatch-repair activity involving YB-1 in human mitochondria, *DNA Repair (Amst)* **8**(6): 704–19.

Deckert, J., Hartmuth, K., Boehringer, D., Behzadnia, N., Will, C. L., Kastner, B., Stark, H., Urlaub, H. & Lührmann, R. (2006). Protein composition and electron microscopy structure of affinity-purified human spliceosomal B complexes isolated under physiological conditions, *Mol Cell Biol* **26**(14): 5528–43.

Dedio, J., Jahnen-Dechent, W., Bachmann, M. & Muller-Esterl, W. (1998). The multiligand-binding protein gC1qR, putative C1q receptor, is a mitochondrial protein, *J Immunol* **160**(7): 3534–42.

Dent, R., Trudeau, M., Pritchard, K. I., Hanna, W. M., Kahn, H. K., Sawka, C. A., Lickley, L. A., Rawlinson, E., Sun, P. & Narod, S. A. (2007). Triple-negative breast cancer: clinical features and patterns of recurrence, *Clin Cancer Res* **13**(15 Pt 1): 4429–34.

Dephoure, N., Zhou, C., Villén, J., Beausoleil, S. A., Bakalarski, C. E., Elledge, S. J. & Gygi, S. P. (2008). A quantitative atlas of mitotic phosphorylation, *Proc Natl Acad Sci U S A* **105**(31): 10762–7.

Dessauvagie, B. F., Zhao, W., Heel-Miller, K. A., Harvey, J. & Bentel, J. M. (2007). Characterization of columnar cell lesions of the breast: immunophenotypic analysis of columnar alteration of lobules with prominent apical snouts and secretions, *Hum Pathol* **38**(2): 284–92.

Diamond, P., Shannon, M. F., Vadas, M. A. & Coles, L. S. (2001). Cold shock domain factors activate the granulocyte-macrophage colony-stimulating factor promoter in stimulated Jurkat T cells, *J Biol Chem* **276**(11): 7943–51.

Didier, D. K., Schiffenbauer, J., Woulfe, S. L., Zacheis, M. & Schwartz, B. D. (1988). Characterization of the cDNA encoding a protein binding to the major histocompatibility complex class II Y box, *Proc Natl Acad Sci U S A* **85**(19): 7322–6.

Dolfini, D. & Mantovani, R. (2013a). Targeting the Y/CCAAT box in cancer: YB-1 (YBX1) or NF-Y?, *Cell Death Differ* **20**(5): 676–85.

Dolfini, D. & Mantovani, R. (2013b). YB-1 (YBX1) does not bind to Y/CCAAT boxes in vivo, *Oncogene* **32**(35): 4189–90.

Donaubauer, E. M. & Hunzicker-Dunn, M. E. (2016). Extracellular signal-regulated kinase (ERK)-dependent phosphorylation of Y-Box-binding protein 1 (YB-1) enhances gene expression in granulosa cells in response to follicle-stimulating hormone (FSH), *J Biol Chem* **291**(23): 12145–60.

Dong, J., Akcakanat, A., Stivers, D. N., Zhang, J., Kim, D. & Meric-Bernstam, F. (2009). RNA-binding specificity of Y-box protein 1, *RNA Biol* **6**(1): 59–64.

Dorn, A., Bollekens, J., Staub, A., Benoist, C. & Mathis, D. (1987). A multiplicity of CCAAT box-binding proteins, *Cell* **50**(6): 863–72.

Dunker, A. K., Cortese, M. S., Romero, P., Iakoucheva, L. M. & Uversky, V. N. (2005). Flexible nets. The roles of intrinsic disorder in protein interaction networks, *FEBS J* **272**(20): 5129–48.

Dürnberger, G., Bürckstümmer, T., Huber, K., Giambruno, R., Doerks, T., Karayel, E., Burkard, T. R., Kaupe, I., Müller, A. C., Schönegger, A., Ecker, G. F., Lohninger, H., Bork, P., Bennett, K. L., Superti-Furga, G. & Colinge, J. (2013). Experimental characterization of the human non-sequence-specific nucleic acid interactome, *Genome Biol* **14**(7): R81.

Dutertre, M., Sanchez, G., De Cian, M.-C., Barbier, J., Dardenne, E., Gratadou, L., Dujardin, G., Le Jossic-Corcos, C., Corcos, L. & Auboeuf, D. (2010). Co-transcriptional exon skipping in the genotoxic stress response, *Nat Struct Mol Biol* **17**(11): 1358–66.

Early Breast Cancer Trialists' Collaborative Group (EBCTCG), Dowsett, M., Forbes, J. F., Bradley, R., Ingle, J., Aihara, T., Bliss, J., Boccardo, F., Coates, A., Coombes, R. C., Cuzick, J., Dubsky, P., Gnant, M., Kaufmann, M., Kilburn, L., Perrone, F., Rea, D., Thürlimann, B., van de Velde, C., Pan, H., Peto, R., Davies, C. & Gray, R. (2015). Aromatase inhibitors versus tamoxifen in early breast cancer: patient-level meta-analysis of the randomised trials, *Lancet* **386**(10001): 1341–52.

Eckert, M. A., Lwin, T. M., Chang, A. T., Kim, J., Danis, E., Ohno-Machado, L. & Yang, J. (2011). Twist1-induced invadopodia formation promotes tumor metastasis, *Cancer Cell* **19**(3): 372–86.

Elmore, L. W., Rehder, C. W., Di, X., McChesney, P. A., Jackson-Cook, C. K., Gewirtz, D. A. & Holt, S. E. (2002). Adriamycin-induced senescence in breast tumor cells involves functional p53 and telomere dysfunction, *J Biol Chem* **277**(38): 35509–15.

Enright, A. J., Van Dongen, S. & Ouzounis, C. A. (2002). An efficient algorithm for large-scale detection of protein families, *Nucleic Acids Res* **30**(7): 1575–84.

Essen Bioscience (2009). IncuCyte technical note; media fluorescence, *Technical Report 8000-0055-B*, Essen Bioscience.

Evdokimova, V. M., Kovrigina, E. A., Nashchekin, D. V., Davydova, E. K., Hershey, J. W. & Ovchinnikov, L. P. (1998). The major core protein of messenger ribonucleoprotein particles (p50) promotes initiation of protein biosynthesis in vitro, *J Biol Chem* **273**(6): 3574–81.

Evdokimova, V. M., Wei, C. L., Sitikov, A. S., Simonenko, P. N., Lazarev, O. A., Vasilenko, K. S., Ustinov, V. A., Hershey, J. W. & Ovchinnikov, L. P. (1995). The major protein of messenger ribonucleoprotein particles in somatic cells is a member of the Y-box binding transcription factor family, *J Biol Chem* **270**(7): 3186–92.

Evdokimova, V., Ovchinnikov, L. P. & Sorensen, P. H. B. (2006a). Y-box binding protein 1: providing a new angle on translational regulation, *Cell Cycle* **5**(11): 1143–7.

Evdokimova, V., Ruzanov, P., Anglesio, M. S., Sorokin, A. V., Ovchinnikov, L. P., Buckley, J., Triche, T. J., Sonenberg, N. & Sorensen, P. H. B. (2006b). Akt-mediated YB-1 phosphorylation activates translation of silent mRNA species, *Mol Cell Biol* **26**(1): 277–92.

Evdokimova, V., Ruzanov, P., Imataka, H., Raught, B., Svitkin, Y., Ovchinnikov, L. P. & Sonenberg, N. (2001). The major mRNA-associated protein YB-1 is a potent 5' cap-dependent mRNA stabilizer, *EMBO J* **20**(19): 5491–502.

Evdokimova, V., Tognon, C., Ng, T., Ruzanov, P., Melnyk, N., Fink, D., Sorokin, A., Ovchinnikov, L. P., Davicioni, E., Triche, T. J. & Sorensen, P. H. B. (2009a). Translational activation of snail1 and other developmentally regulated transcription factors by YB-1 promotes an epithelial-mesenchymal transition, *Cancer Cell* **15**(5): 402–15.

Evdokimova, V., Tognon, C., Ng, T. & Sorensen, P. H. B. (2009b). Reduced proliferation and enhanced migration: two sides of the same coin? Molecular mechanisms of metastatic progression by YB-1, *Cell Cycle* **8**(18): 2901–6.

Familari, M., Almouzni, G. & Wolffe, A. P. (1994). Isolation of a potentially functional Y-box protein (MSY-1) processed pseudogene from mouse: evolutionary relationships within the EF1A/dbpB/YB-1 gene family, *Gene* **141**(2): 255–9.

Fomina, E. E., Pestryakov, P. E., Maltseva, E. A., Petruseva, I. O., Kretov, D. A., Ovchinnikov, L. P. & Lavrik, O. I. (2015). Y-box binding protein 1 (YB-1) promotes detection of DNA bulky lesions by XPC-HR23B factor, *Biochemistry (Mosc)* **80**(2): 219–27.

Foulkes, W. D., Smith, I. E. & Reis-Filho, J. S. (2010). Triple-negative breast cancer, *N Engl J Med* **363**(20): 1938–48.

Fox, A. H., Bond, C. S. & Lamond, A. I. (2005). P54nrb forms a heterodimer with PSP1 that localizes to paraspeckles in an RNA-dependent manner, *Mol Biol Cell* **16**(11): 5304–15.

Franceschini, A., Szklarczyk, D., Frankild, S., Kuhn, M., Simonovic, M., Roth, A., Lin, J., Minguez, P., Bork, P., von Mering, C. & Jensen, L. J. (2013). STRING v9.1: protein-protein interaction networks, with increased coverage and integration, *Nucleic Acids Res* **41**(Database issue): D808–15.

Frankenberg-Schwager, M., Kirchermeier, D., Greif, G., Baer, K., Becker, M. & Frankenberg, D. (2005). Cisplatin-mediated DNA double-strand breaks in replicating but not in quiescent cells of the yeast Saccharomyces cerevisiae, *Toxicology* **212**(2-3): 175–84.

Fraser, D. J., Phillips, A. O., Zhang, X., van Roeyen, C. R., Muehlenberg, P., En-Nia, A. & Mertens, P. R. (2008). Y-box protein-1 controls transforming growth factor-beta1 translation in proximal tubular cells, *Kidney Int* **73**(6): 724–32.

Friedman, J. R., Fredericks, W. J., Jensen, D. E., Speicher, D. W., Huang, X. P., Neilson, E. G. & Rauscher, F. J. (1996). KAP-1, a novel corepressor for the highly conserved KRAB repression domain, *Genes Dev* **10**(16): 2067–78.

Frye, B. C., Halfter, S., Djudjaj, S., Muehlenberg, P., Weber, S., Raffetseder, U., En-Nia, A., Knott, H., Baron, J. M., Dooley, S., Bernhagen, J. & Mertens, P. R.

(2009). Y-box protein-1 is actively secreted through a non-classical pathway and acts as an extracellular mitogen, *EMBO Rep* **10**(7): 783–9.

Fujii, R., Mutoh, M., Niwa, K., Yamada, K., Aikou, T., Nakagawa, M., Kuwano, M. & Akiyama, S. (1994). Active efflux system for cisplatin in cisplatin-resistant human KB cells, *Jpn J Cancer Res* **85**(4): 426–33.

Fujita, T., Ito, K.-i., Izumi, H., Kimura, M., Sano, M., Nakagomi, H., Maeno, K., Hama, Y., Shingu, K., Tsuchiya, S.-i., Kohno, K. & Fujimori, M. (2005). Increased nuclear localization of transcription factor Y-box binding protein 1 accompanied by up-regulation of P-glycoprotein in breast cancer pretreated with paclitaxel, *Clin Cancer Res* **11**(24 Pt 1): 8837–44.

Fukada, T. & Tonks, N. K. (2003). Identification of YB-1 as a regulator of PTP1B expression: implications for regulation of insulin and cytokine signaling, *EMBO J* **22**(3): 479–93.

Fukuda, T., Ashizuka, M., Nakamura, T., Shibahara, K., Maeda, K., Izumi, H., Kohno, K., Kuwano, M. & Uchiumi, T. (2004). Characterization of the 5'-untranslated region of YB-1 mRNA and autoregulation of translation by YB-1 protein, *Nucleic Acids Res* **32**(2): 611–22.

Gallia, G. L., Johnson, E. M. & Khalili, K. (2000). Puralpha: a multifunctional single-stranded DNA- and RNA-binding protein, *Nucleic Acids Res* **28**(17): 3197–205.

Garand, C., Guay, D., Sereduk, C., Chow, D., Tsofack, S. P., Langlois, M., Perreault, E., Yin, H. H. & Lebel, M. (2011). An integrative approach to identify YB-1 interacting proteins required for cisplatin resistance in MCF7 and MDA-MB-231 breast cancer cells, *Cancer Sci* **102**(7): 1410–7.

Gasser, S. M. (2002). Visualizing chromatin dynamics in interphase nuclei, *Science* **296**(5572): 1412–6.

Gately, D. P. & Howell, S. B. (1993). Cellular accumulation of the anticancer agent cisplatin: a review, *Br J Cancer* **67**(6): 1171–6.

Gauci, S., Helbig, A. O., Slijper, M., Krijgsveld, J., Heck, A. J. R. & Mohammed, S. (2009). Lys-N and trypsin cover complementary parts of the phosphoproteome in a refined SCX-based approach, *Anal Chem* **81**(11): 4493–501.

Gaudreault, I., Guay, D. & Lebel, M. (2004). YB-1 promotes strand separation in vitro of duplex DNA containing either mispaired bases or cisplatin modifications, exhibits endonucleolytic activities and binds several DNA repair proteins, *Nucleic Acids Res* **32**(1): 316–27.

Ge, H., Liu, Z., Church, G. M. & Vidal, M. (2001). Correlation between transcriptome and interactome mapping data from Saccharomyces cerevisiae, *Nat Genet* **29**(4): 482–6.

Gessner, C., Woischwill, C., Schumacher, A., Liebers, U., Kuhn, H., Stiehl, P., Jürchott, K., Royer, H. D., Witt, C. & Wolff, G. (2004). Nuclear YB-1 expression as a negative prognostic marker in nonsmall cell lung cancer, *Eur Respir J* **23**(1): 14–9.

Giménez-Bonafé, P., Fedoruk, M. N., Whitmore, T. G., Akbari, M., Ralph, J. L., Ettinger, S., Gleave, M. E. & Nelson, C. C. (2004). YB-1 is upregulated during prostate cancer tumor progression and increases P-glycoprotein activity, *Prostate* **59**(3): 337–49.

Goodarzi, A. A., Jeggo, P. & Lobrich, M. (2010). The influence of heterochromatin on DNA double strand break repair: getting the strong, silent type to relax, *DNA Repair (Amst)* **9**(12): 1273–82.

Goodarzi, A. A., Noon, A. T., Deckbar, D., Ziv, Y., Shiloh, Y., Lobrich, M. & Jeggo, P. A. (2008). ATM signaling facilitates repair of DNA double-strand breaks associated with heterochromatin, *Mol Cell* **31**(2): 167–77.

Goodarzi, A. A., Noon, A. T. & Jeggo, P. A. (2009). The impact of heterochromatin on DSB repair, *Biochem Soc Trans* **37**(Pt 3): 569–76.

Goodarzi, H., Liu, X., Nguyen, H. C. B., Zhang, S., Fish, L. & Tavazoie, S. F. (2015). Endogenous tRNA-derived fragments suppress breast cancer progression via YBX1 displacement, *Cell* **161**(4): 790–802.

Gorgoni, B., Richardson, W. A., Burgess, H. M., Anderson, R. C., Wilkie, G. S., Gautier, P., Martins, J. P. S., Brook, M., Sheets, M. D. & Gray, N. K. (2011). Poly(A)-binding proteins are functionally distinct and have essential roles during vertebrate development, *Proc Natl Acad Sci U S A* **108**(19): 7844–49.

Griffiths, C. L. & Olin, J. L. (2012). Triple negative breast cancer: a brief review of its characteristics and treatment options, *J Pharm Pract* **25**(3): 319–23.

Gronostajski, R. M., Nagata, K. & Hurwitz, J. (1984). Isolation of human DNA sequences that bind to nuclear factor I, a host protein involved in adenovirus DNA replication, *Proc Natl Acad Sci U S A* **81**(13): 4013–7.

Grover, R., Ray, P. S. & Das, S. (2008). Polypyrimidine tract binding protein regulates IRES-mediated translation of p53 isoforms, *Cell Cycle* **7**(14): 2189–98.

Gu, C., Oyama, T., Osaki, T., Kohno, K. & Yasumoto, K. (2001). Expression of Y box-binding protein-1 correlates with DNA topoisomerase IIalpha and proliferating cell nuclear antigen expression in lung cancer, *Anticancer Res* **21**(4A): 2357–62.

Guay, D., Evoy, A.-A., Paquet, E., Garand, C., Bachvarova, M., Bachvarov, D. & Lebel, M. (2008a). The strand separation and nuclease activities associated with YB-1 are dispensable for cisplatin resistance but overexpression of YB-1 in MCF7 and MDA-MB-231 breast tumor cells generates several chemoresistance signatures, *Int J Biochem Cell Biol* **40**(11): 2492–507.

Guay, D., Garand, C., Reddy, S., Schmutte, C. & Lebel, M. (2008b). The human endonuclease III enzyme is a relevant target to potentiate cisplatin cytotoxicity in Y-box-binding protein-1 overexpressing tumor cells, *Cancer Sci* **99**(4): 762–9.

Guay, D., Gaudreault, I., Massip, L. & Lebel, M. (2006). Formation of a nuclear complex containing the p53 tumor suppressor, YB-1, and the Werner syndrome gene product in cells treated with UV light, *Int J Biochem Cell Biol* **38**(8): 1300–13.

Gullberg, M., Fredriksson, S., Taussig, M., Jarvius, J., Gustafsdottir, S. & Landegren, U. (2003). A sense of closeness: protein detection by proximity ligation, *Curr Opin Biotechnol* **14**(1): 82–6.

Gunasekaran, V. P. & Ganeshan, M. (2014). Inverse correlation of ribosomal protein S27A and multifunctional protein YB-1 in hepatocellular carcinoma, *Clin Biochem* **47**(13-14): 1262–4.

Guryanov, S. G., Selivanova, O. M., Nikulin, A. D., Enin, G. A., Melnik, B. S., Kretov, D. A., Serdyuk, I. N. & Ovchinnikov, L. P. (2012). Formation of amyloid-like fibrils by Y-box binding protein 1 (YB-1) is mediated by its cold shock domain and modulated by disordered terminal domains, *PLoS One* **7**(5): e36969.

Habibi, G., Leung, S., Law, J. H., Gelmon, K., Masoudi, H., Turbin, D., Pollak, M., Nielsen, T. O., Huntsman, D. & Dunn, S. E. (2008). Redefining prognostic factors for breast cancer: YB-1 is a stronger predictor of relapse and disease-specific survival than estrogen receptor or HER-2 across all tumor subtypes, *Breast Cancer Res* **10**(5): R86.

Han, G., Ye, M., Liu, H., Song, C., Sun, D., Wu, Y., Jiang, X., Chen, R., Wang, C., Wang, L. & Zou, H. (2010). Phosphoproteome analysis of human liver tissue by long-gradient nanoflow LC coupled with multiple stage MS analysis, *Electrophoresis* **31**(6): 1080–9.

Hanahan, D. & Weinberg, R. A. (2000). The hallmarks of cancer, *Cell* **100**(1): 57–70.

Hanahan, D. & Weinberg, R. A. (2011). Hallmarks of cancer: the next generation, *Cell* **144**(5): 646–74.

Hanssen, L., Alidousty, C., Djudjaj, S., Frye, B. C., Rauen, T., Boor, P., Mertens, P. R., van Roeyen, C. R., Tacke, F., Heymann, F., Tittel, A. P., Koch, A., Floege, J., Ostendorf, T. & Raffetseder, U. (2013). YB-1 is an early and central mediator of bacterial and sterile inflammation in vivo, *J Immunol* **191**(5): 2604–13.

Harada, M., Kotake, Y., Ohhata, T., Kitagawa, K., Niida, H., Matsuura, S., Funai, K., Sugimura, H., Suda, T. & Kitagawa, M. (2014). YB-1 promotes transcription of cyclin D1 in human non-small-cell lung cancers, *Genes Cells* **19**(6): 504–16.

Hartmuth, K., Urlaub, H., Vornlocher, H.-P., Will, C. L., Gentzel, M., Wilm, M. & Lührmann, R. (2002). Protein composition of human prespliceosomes isolated by a tobramycin affinity-selection method, *Proc Natl Acad Sci U S A* **99**(26): 16719–24.

Hasegawa, S. L., Doetsch, P. W., Hamilton, K. K., Martin, A. M., Okenquist, S. A., Lenz, J. & Boss, J. M. (1991). DNA binding properties of YB-1 and dbpA: binding to double-stranded, single-stranded, and abasic site containing DNAs, *Nucleic Acids Res* **19**(18): 4915–20.

Hermann, G., Heffeter, P., Falta, T., Berger, W., Hann, S. & Koellensperger, G. (2013). In vitro studies on cisplatin focusing on kinetic aspects of intracellular chemistry by LC-ICP-MS, *Metallomics* **5**(6): 636–47.

Heyd, F., Carmo-Fonseca, M. & Moroy, T. (2008). Differential isoform expression and interaction with the P32 regulatory protein controls the subcellular localization of the splicing factor U2AF26, *J Biol Chem* **283**(28): 19636–45.

Higashi, K., Inagaki, Y., Suzuki, N., Mitsui, S., Mauviel, A., Kaneko, H. & Nakatsuka, I. (2003). Y-box-binding protein YB-1 mediates transcriptional repression of human alpha 2(I) collagen gene expression by interferon-gamma, *J Biol Chem* **278**(7): 5156–62.

Hollestelle, A., Elstrodt, F., Nagel, J. H. A., Kallemeijn, W. W. & Schutte, M. (2007). Phosphatidylinositol-3-OH kinase or RAS pathway mutations in human breast cancer cell lines, *Mol Cancer Res* **5**(2): 195–201.

Holliday, D. L. & Speirs, V. (2011). Choosing the right cell line for breast cancer research, *Breast Cancer Res* **13**(4): 215.

Holm, P. S., Bergmann, S., Jurchott, K., Lage, H., Brand, K., Ladhoff, A., Mantwill, K., Curiel, D. T., Dobbelstein, M., Dietel, M., Gansbacher, B. & Royer, H.-D. (2002). YB-1 relocates to the nucleus in adenovirus-infected cells and facilitates viral replication by inducing E2 gene expression through the E2 late promoter, *J Biol Chem* **277**(12): 10427–34.

Homer, C., Knight, D. A., Hananeia, L., Sheard, P., Risk, J., Lasham, A., Royds, J. A. & Braithwaite, A. W. (2005). Y-box factor YB1 controls p53 apoptotic function, *Oncogene* **24**(56): 8314–25.

Horwitz, E. M., Maloney, K. A. & Ley, T. J. (1994). A human protein containing a "cold shock" domain binds specifically to H-DNA upstream from the human gamma-globin genes, *J Biol Chem* **269**(19): 14130–9.

Horwitz, K. B. & McGuire, W. L. (1975). Specific progesterone receptors in human breast cancer, *Steroids* **25**(4): 497–505.

Hsieh, A. C., Liu, Y., Edlind, M. P., Ingolia, N. T., Janes, M. R., Sher, A., Shi, E. Y., Stumpf, C. R., Christensen, C., Bonham, M. J., Wang, S., Ren, P., Martin, M., Jessen, K., Feldman, M. E., Weissman, J. S., Shokat, K. M., Rommel, C. &

Ruggero, D. (2012). The translational landscape of mTOR signalling steers cancer initiation and metastasis, *Nature* **485**(7396): 55–61.

Hu, C., Zhang, S., Gao, X., Gao, X., Xu, X., Lv, Y., Zhang, Y., Zhu, Z., Zhang, C., Li, Q., Wong, J., Cui, Y., Zhang, W., Ma, L. & Wang, C. (2012). Roles of Kruppel-associated box (KRAB)-associated co-repressor KAP1 Ser-473 phosphorylation in DNA damage response, *J Biol Chem* **287**(23): 18937–52.

Hu, M., Crawford, S. A., Henstridge, D. C., Ng, I. H. W., Boey, E. J. H., Xu, Y., Febbraio, M. A., Jans, D. A. & Bogoyevitch, M. A. (2013). p32 protein levels are integral to mitochondrial and endoplasmic reticulum morphology, cell metabolism and survival, *Biochem J* **453**(3): 381–91.

Huang, D. W., Sherman, B. T. & Lempicki, R. A. (2009a). Bioinformatics enrichment tools: paths toward the comprehensive functional analysis of large gene lists, *Nucleic Acids Res* **37**(1): 1–13.

Huang, D. W., Sherman, B. T. & Lempicki, R. A. (2009b). Systematic and integrative analysis of large gene lists using DAVID bioinformatics resources, *Nat Protoc* **4**(1): 44–57.

Huang, J., Tan, P.-H., Li, K.-B., Matsumoto, K., Tsujimoto, M. & Bay, B.-H. (2005). Y-box binding protein, YB-1, as a marker of tumor aggressiveness and response to adjuvant chemotherapy in breast cancer, *Int J Oncol* **26**(3): 607–13.

Huang, X., Okafuji, M., Traganos, F., Luther, E., Holden, E. & Darzynkiewicz, Z. (2004b). Assessment of histone H2AX phosphorylation induced by DNA topoisomerase I and II inhibitors topotecan and mitoxantrone and by the DNA cross-linking agent cisplatin, *Cytometry A* **58**(2): 99–110.

Huang, X., Ushijima, K., Komai, K., Takemoto, Y., Motoshima, S., Kamura, T. & Kohno, K. (2004a). Co-expression of Y box-binding protein-1 and P-glycoprotein as a prognostic marker for survival in epithelial ovarian cancer, *Gynecol Oncol* **93**(2): 287–91.

Hui, L., Zheng, Y., Yan, Y., Bargonetti, J. & Foster, D. A. (2006). Mutant p53 in MDA-MB-231 breast cancer cells is stabilized by elevated phospholipase D activity and contributes to survival signals generated by phospholipase D, *Oncogene* **25**(55): 7305–10.

Huober, J., Fasching, P. A., Hanusch, C., Rezai, M., Eidtmann, H., Kittel, K., Hilfrich, J., Schwedler, K., Blohmer, J.-U., Tesch, H., Gerber, B., Höß, C., Kümmel, S., Mau, C., Jackisch, C., Khandan, F., Costa, S. D., Krabisch, P., Loibl, S., Nekljudova, V., Untch, M. & Minckwitz, G. v. (2013). Neoadjuvant chemotherapy with paclitaxel and everolimus in breast cancer patients with non-responsive tumours to epirubicin/cyclophosphamide (EC) ± bevacizumab - results of the randomised GeparQuinto study (GBG 44), *Eur J Cancer* **49**(10): 2284–93.

Hutchins, J. R. A., Toyoda, Y., Hegemann, B., Poser, I., Hériché, J.-K., Sykora, M. M., Augsburg, M., Hudecz, O., Buschhorn, B. A., Bulkescher, J., Conrad, C., Comartin, D., Schleiffer, A., Sarov, M., Pozniakovsky, A., Slabicki, M. M., Schloissnig, S., Steinmacher, I., Leuschner, M., Ssykor, A., Lawo, S., Pelletier, L., Stark, H., Nasmyth, K., Ellenberg, J., Durbin, R., Buchholz, F., Mechtler, K., Hyman, A. A. & Peters, J.-M. (2010). Systematic analysis of human protein complexes identifies chromosome segregation proteins, *Science* **328**(5978): 593–9.

Ignatiadis, M. & Sotiriou, C. (2008). Understanding the molecular basis of histologic grade, *Pathobiology* **75**(2): 104–11.

Ilic, N., Utermark, T., Widlund, H. R. & Roberts, T. M. (2011). PI3K-targeted therapy can be evaded by gene amplification along the MYC-eukaryotic translation initiation factor 4E (eIF4E) axis, *Proc Natl Acad Sci U S A* **108**(37): E699–E708.

Isaacs, W. B., Carter, B. S. & Ewing, C. M. (1991). Wild-type p53 suppresses growth of human prostate cancer cells containing mutant p53 alleles, *Cancer Res* **51**(17): 4716–20.

Ise, T., Nagatani, G., Imamura, T., Kato, K., Takano, H., Nomoto, M., Izumi, H., Ohmori, H., Okamoto, T., Ohga, T., Uchiumi, T., Kuwano, M. & Kohno, K. (1999). Transcription factor Y-box binding protein 1 binds preferentially to cisplatin-modified DNA and interacts with proliferating cell nuclear antigen, *Cancer Res* **59**(2): 342–6.

Ivanov, P., Emara, M. M., Villen, J., Gygi, S. P. & Anderson, P. (2011). Angiogenin-induced tRNA fragments inhibit translation initiation, *Mol Cell* **43**(4): 613–23.

Ivanov, P., O'Day, E., Emara, M. M., Wagner, G., Lieberman, J. & Anderson, P. (2014). G-quadruplex structures contribute to the neuroprotective effects of angiogenin-induced tRNA fragments, *Proc Natl Acad Sci U S A* **111**(51): 18201–6.

Iwanami, T., Uramoto, H., Nakagawa, M., Shimokawa, H., Yamada, S., Kohno, K. & Tanaka, F. (2014). Clinical significance of epithelial-mesenchymal transition-associated markers in malignant pleural mesothelioma, *Oncology* **86**(2): 109–16.

Iyengar, S. & Farnham, P. J. (2011). KAP1 protein: an enigmatic master regulator of the genome, *J Biol Chem* **286**(30): 26267–76.

Izumi, H., Imamura, T., Nagatani, G., Ise, T., Murakami, T., Uramoto, H., Torigoe, T., Ishiguchi, H., Yoshida, Y., Nomoto, M., Okamoto, T., Uchiumi, T., Kuwano, M., Funa, K. & Kohno, K. (2001). Y box-binding protein-1 binds preferentially to single-stranded nucleic acids and exhibits 3'5' exonuclease activity, *Nucleic Acids Res* **29**(5): 1200–7.

Jackson, R. J., Hellen, C. U. T. & Pestova, T. V. (2010). The mechanism of eukaryotic translation initiation and principles of its regulation, *Nat Rev Mol Cell Biol* **11**(2): 113–27.

Jackson, V. (1999). Formaldehyde cross-linking for studying nucleosomal dynamics, *Methods* **17**(2): 125–39.

Janz, M., Harbeck, N., Dettmar, P., Berger, U., Schmidt, A., Jürchott, K., Schmitt, M. & Royer, H.-D. (2002). Y-box factor YB-1 predicts drug resistance and patient outcome in breast cancer independent of clinically relevant tumor biologic factors HER2, uPA and PAI-1, *Int J Cancer* **97**(3): 278–82.

Jevtić, P. & Levy, D. L. (2014). Mechanisms of nuclear size regulation in model systems and cancer, *Adv Exp Med Biol* **773**: 537–69.

Jurchott, K., Bergmann, S., Stein, U., Walther, W., Janz, M., Manni, I., Piaggio, G., Fietze, E., Dietel, M. & Royer, H.-D. (2003). YB-1 as a cell cycle-regulated transcription factor facilitating cyclin A and cyclin B1 gene expression, *J Biol Chem* **278**(30): 27988–96.

Jürchott, K., Kuban, R.-J., Krech, T., Blüthgen, N., Stein, U., Walther, W., Friese, C., Kiełbasa, S. M., Ungethüm, U., Lund, P., Knösel, T., Kemmner, W., Morkel, M., Fritzmann, J., Schlag, P. M., Birchmeier, W., Krueger, T., Sperling, S., Sers, C., Royer, H.-D., Herzel, H. & Schäfer, R. (2010). Identification of Y-box binding protein 1 as a core regulator of MEK/ERK pathway-dependent gene signatures in colorectal cancer cells, *PLoS Genet* **6**(12): e1001231.

Kahm, M., Hasenbrink, G., Lichtenberg-Fraté, H., Ludwig, J. & Kschischo, M. (2010). grofit: fitting biological growth curves with R, *J Stat Softw* **33**(7): 1–21.

Käll, L., Canterbury, J. D., Weston, J., Noble, W. S. & MacCoss, M. J. (2007). Semi-supervised learning for peptide identification from shotgun proteomics datasets, *Nat Methods* **4**(11): 923–5.

Kalluri, R. (2009). EMT: when epithelial cells decide to become mesenchymal-like cells, *J Clin Invest* **119**(6): 1417–9.

Kamal, A. & Datta, K. (2006). Upregulation of hyaluronan binding protein 1 (HABP1/p32/gC1qR) is associated with cisplatin induced apoptosis, *Apoptosis* **11**(5): 861–74.

Kaminski, R., Darbinyan, A., Merabova, N., Deshmane, S. L., White, M. K. & Khalili, K. (2008). Protective role of Puralpha to cisplatin, *Cancer Biol Ther* **7**(12): 1926–35.

Kamura, T., Yahata, H., Amada, S., Ogawa, S., Sonoda, T., Kobayashi, H., Mitsumoto, M., Kohno, K., Kuwano, M. & Nakano, H. (1999). Is nuclear expression of Y box-binding protein-1 a new prognostic factor in ovarian serous adenocarcinoma?, *Cancer* **85**(11): 2450–4.

Kang, S., Lee, T. A., Ra, E. A., Lee, E., Choi, H. j., Lee, S. & Park, B. (2014). Differential control of interleukin-6 mRNA levels by cellular distribution of YB-1, *PLoS One* **9**(11): e112754.

Kang, Y., Hu, W., Ivan, C., Dalton, H. J., Miyake, T., Pecot, C. V., Zand, B., Liu, T., Huang, J., Jennings, N. B., Rupaimoole, R., Taylor, M., Pradeep, S., Wu, S. Y., Lu, C., Wen, Y., Huang, J., Liu, J. & Sood, A. K. (2013). Role of focal adhesion kinase in regulating YB-1-mediated paclitaxel resistance in ovarian cancer, *J Natl Cancer Inst* **105**(19): 1485–95.

Kapust, R. B. & Waugh, D. S. (1999). Escherichia coli maltose-binding protein is uncommonly effective at promoting the solubility of polypeptides to which it is fused, *Protein Sci* **8**(8): 1668–74.

Kashihara, M., Azuma, K., Kawahara, A., Basaki, Y., Hattori, S., Yanagawa, T., Terazaki, Y., Takamori, S., Shirouzu, K., Aizawa, H., Nakano, K., Kage, M., Kuwano, M. & Ono, M. (2009). Nuclear Y-box binding protein-1, a predictive marker of prognosis, is correlated with expression of HER2/ErbB2 and HER3/ErbB3 in non-small cell lung cancer, *J Thorac Oncol* **4**(9): 1066–74.

Kaszubiak, A., Kupstat, A., Müller, U., Hausmann, R., Holm, P. S. & Lage, H. (2007). Regulation of MDR1 gene expression in multidrug-resistant cancer cells is independent from YB-1, *Biochem Biophys Res Commun* **357**(1): 295–301.

Katano, K., Kondo, A., Safaei, R., Holzer, A., Samimi, G., Mishima, M., Kuo, Y.-M., Rochdi, M. & Howell, S. B. (2002). Acquisition of resistance to cisplatin is accompanied by changes in the cellular pharmacology of copper, *Cancer Res* **62**(22): 6559–65.

Kato, M., Wang, L., Putta, S., Wang, M., Yuan, H., Sun, G., Lanting, L., Todorov, I., Rossi, J. J. & Natarajan, R. (2010). Post-transcriptional up-regulation of Tsc-22 by Ybx1, a target of miR-216a, mediates TGF-beta-induced collagen expression in kidney cells, *J Biol Chem* **285**(44): 34004–15.

Kawaguchi, A., Asaka, M. N., Matsumoto, K. & Nagata, K. (2015). Centrosome maturation requires YB-1 to regulate dynamic instability of microtubules for nucleus reassembly, *Sci Rep* **5**: 8768.

Kedersha, N. & Anderson, P. (2007). Mammalian stress granules and processing bodies, *Methods Enzymol* **431**: 61–81.

Kelland, L. (2007). The resurgence of platinum-based cancer chemotherapy, *Nat Rev Cancer* **7**(8): 573–84.

Khan, M. I., Adhami, V. M., Lall, R. K., Sechi, M., Joshi, D. C., Haidar, O. M., Syed, D. N., Siddiqui, I. A., Chiu, S.-Y. & Mukhtar, H. (2014). YB-1 expression promotes epithelial-to-mesenchymal transition in prostate cancer that is inhibited by a small molecule fisetin, *Oncotarget* **5**(9): 2462–74.

Khandelwal, P., Padala, M. K., Cox, J. & Guntaka, R. V. (2009). The N-terminal domain of Y-box binding protein-1 induces cell cycle arrest in G2/M phase by binding to Cyclin D1, *Int J Cell Biol* **2009**: 243532.

Kick, D., Barrett, P., Cummings, A. & Sommerville, J. (1987). Phosphorylation of a 60 kDa polypeptide from Xenopus oocytes blocks messenger RNA translation, *Nucleic Acids Res* **15**(10): 4099–109.

Kim, E. R., Selyutina, A. A., Buldakov, I. A., Evdokimova, V., Ovchinnikov, L. P. & Sorokin, A. V. (2013). The proteolytic YB-1 fragment interacts with DNA repair machinery and enhances survival during DNA damaging stress, *Cell Cycle* **12**(24): 3791–803.

Kim, K., Choi, J., Heo, K., Kim, H., Levens, D., Kohno, K., Johnson, E. M., Brock, H. W. & An, W. (2008). Isolation and characterization of a novel H1.2 complex that acts as a repressor of p53-mediated transcription, *J Biol Chem* **283**(14): 9113–26.

King, H. A., Cobbold, L. C., Pichon, X., Pöyry, T., Wilson, L. A., Booden, H., Jukes-Jones, R., Cain, K., Lilley, K. S., Bushell, M. & Willis, A. E. (2014). Remodelling of a polypyrimidine tract-binding protein complex during apoptosis activates cellular IRESs, *Cell Death Differ* **21**(1): 161–71.

Klockenbusch, C. & Kast, J. (2010). Optimization of formaldehyde cross-linking for protein interaction analysis of non-tagged integrin beta1, *J Biomed Biotechnol* **2010**: 927585.

Kloks, C. P. A. M., Spronk, C. A. E. M., Lasonder, E., Hoffmann, A., Vuister, G. W., Grzesiek, S. & Hilbers, C. W. (2002). The solution structure and DNA-binding properties of the cold-shock domain of the human Y-box protein YB-1, *J Mol Biol* **316**(2): 317–26.

Knudson, Jr, A. G. (1986). Genetics of human cancer, *J Cell Physiol Suppl* **4**: 7–11.

Kobayashi, Y., Suzuki, K., Kobayashi, H., Ohashi, S., Koike, K., Macchi, P., Kiebler, M. & Anzai, K. (2008). C9orf10 protein, a novel protein component of Puralpha-containing mRNA-protein particles (Puralpha-mRNPs): characterization of developmental and regional expressions in the mouse brain, *J Histochem Cytochem* **56**(8): 723–31.

Kohno, K., Izumi, H., Uchiumi, T., Ashizuka, M. & Kuwano, M. (2003). The pleiotropic functions of the Y-box-binding protein, YB-1, *Bioessays* **25**(7): 691–8.

Kohno, K., Tanimura, H., Sato, S., Nakayama, Y., Makino, Y., Wada, M., Fojo, A. T. & Kuwano, M. (1994). Cellular control of human multidrug resistance 1 (mdr-1) gene expression in absence and presence of gene amplification in human cancer cells, *J Biol Chem* **269**(32): 20503–8.

Koike, K., Uchiumi, T., Ohga, T., Toh, S., Wada, M., Kohno, K. & Kuwano, M. (1997). Nuclear translocation of the Y-box binding protein by ultraviolet irradiation, *FEBS Lett* **417**(3): 390–4.

Kolluri, R., Torrey, T. A. & Kinniburgh, A. J. (1992). A CT promoter element binding protein: definition of a double-strand and a novel single-strand DNA binding motif, *Nucleic Acids Res* **20**(1): 111–6.

Kotake, Y., Ozawa, Y., Harada, M., Kitagawa, K., Niida, H., Morita, Y., Tanaka, K., Suda, T. & Kitagawa, M. (2013). YB1 binds to and represses the p16 tumor suppressor gene, *Genes Cells* **18**(11): 999–1006.

Kothandapani, A., Dangeti, V. S. M. N., Brown, A. R., Banze, L. A., Wang, X.-H., Sobol, R. W. & Patrick, S. M. (2011). Novel role of base excision repair in mediating cisplatin cytotoxicity, *J Biol Chem* **286**(16): 14564–74.

Kovrigina, E. A., Nashchekin, D. V., Evdokimova, V. M. & Ovchinnikov, L. P. (1996). The major cytoplasmic mRNP protein, p50, is required for efficient mRNA translation in vitro, *Biokhimiia* **61**(12): 2173–80.

Krupp, M., Marquardt, J. U., Sahin, U., Galle, P. R., Castle, J. & Teufel, A. (2012). RNA-Seq Atlas–a reference database for gene expression profiling in normal tissue by next-generation sequencing, *Bioinformatics* **28**(8): 1184–5.

Kudo, S., Mattei, M. G. & Fukuda, M. (1995). Characterization of the gene for dbpA, a family member of the nucleic-acid-binding proteins containing a cold-shock domain, *Eur J Biochem* **231**(1): 72–82.

Kyono, Y., Sugiyama, N., Imami, K., Tomita, M. & Ishihama, Y. (2008). Successive and selective release of phosphorylated peptides captured by hydroxy acid-modified metal oxide chromatography, *J Proteome Res* **7**(10): 4585–93.

Ladomery, M. & Sommerville, J. (1994). Binding of Y-box proteins to RNA: involvement of different protein domains, *Nucleic Acids Res* **22**(25): 5582–9.

Ladomery, M. & Sommerville, J. (1995). A role for Y-box proteins in cell proliferation, *Bioessays* **17**(1): 9–11.

Laemmli, U. K. (1970). Cleavage of Structural Proteins during the Assembly of the Head of Bacteriophage T4, *Nature* **227**(5259): 680–685.

Landsman, D. (1992). RNP-1, an RNA-binding motif is conserved in the DNA-binding cold shock domain, *Nucleic Acids Res* **20**(11): 2861–4.

Larson, C. A., Blair, B. G., Safaei, R. & Howell, S. B. (2009). The role of the mammalian copper transporter 1 in the cellular accumulation of platinum-based drugs, *Mol Pharmacol* **75**(2): 324–30.

Lasham, A., Lindridge, E., Rudert, F., Onrust, R. & Watson, J. (2000). Regulation of the human fas promoter by YB-1, Puralpha and AP-1 transcription factors, *Gene* **252**(1-2): 1–13.

Lasham, A., Mehta, S. Y., Fitzgerald, S. J., Woolley, A. G., Hearn, J. I., Hurley, D. G., Ruza, I., Algie, M., Shelling, A. N., Braithwaite, A. W. & Print, C. G. (2016). A novel EGR-1 dependent mechanism for YB-1 modulation of paclitaxel response in a triple negative breast cancer cell line, *Int J Cancer* **139**(5): 1157–70.

Lasham, A., Moloney, S., Hale, T., Homer, C., Zhang, Y. F., Murison, J. G., Braithwaite, A. W. & Watson, J. (2003). The Y-box-binding protein, YB1, is a potential negative regulator of the p53 tumor suppressor, *J Biol Chem* **278**(37): 35516–23.

Lasham, A., Samuel, W., Cao, H., Patel, R., Mehta, R., Stern, J. L., Reid, G., Woolley, A. G., Miller, L. D., Black, M. A., Shelling, A. N., Print, C. G. & Braithwaite, A. W. (2012). YB-1, the E2F pathway, and regulation of tumor cell growth, *J Natl Cancer Inst* **104**(2): 133–46.

Law, J. H., Li, Y., To, K., Wang, M., Astanehe, A., Lambie, K., Dhillon, J., Jones, S. J. M., Gleave, M. E., Eaves, C. J. & Dunn, S. E. (2010). Molecular decoy to the Y-box binding protein-1 suppresses the growth of breast and prostate cancer cells whilst sparing normal cell viability, *PLoS One* **5**(9): e12661.

Lee, C., Dhillon, J., Wang, M. Y. C., Gao, Y., Hu, K., Park, E., Astanehe, A., Hung, M.-C., Eirew, P., Eaves, C. J. & Dunn, S. E. (2008). Targeting YB-1 in HER-2 overexpressing breast cancer cells induces apoptosis via the mTOR/STAT3 pathway and suppresses tumor growth in mice, *Cancer Res* **68**(21): 8661–6.

Lehmann, B. D., Bauer, J. A., Chen, X., Sanders, M. E., Chakravarthy, A. B., Shyr, Y. & Pietenpol, J. A. (2011). Identification of human triple-negative breast cancer subtypes and preclinical models for selection of targeted therapies, *J Clin Invest* **121**(7): 2750–67.

Leitner, A., Walzthoeni, T., Kahraman, A., Herzog, F., Rinner, O., Beck, M. & Aebersold, R. (2010). Probing native protein structures by chemical cross-linking, mass spectrometry, and bioinformatics, *Mol Cell Proteomics* **9**(8): 1634–49.

Lemaitre, C. & Soutoglou, E. (2014). Double strand break (DSB) repair in heterochromatin and heterochromatin proteins in DSB repair, *DNA Repair (Amst)* **19**: 163–8.

Levenson, V. V., Davidovich, I. A. & Roninson, I. B. (2000). Pleiotropic resistance to DNA-interactive drugs is associated with increased expression of genes involved in DNA replication, repair, and stress response, *Cancer Res* **60**(18): 5027–30.

Levine, A. J. & Oren, M. (2009). The first 30 years of p53: growing ever more complex, *Nat Rev Cancer* **9**(10): 749–58.

Levine, A. J. & Puzio-Kuter, A. M. (2010). The control of the metabolic switch in cancers by oncogenes and tumor suppressor genes, *Science* **330**(6009): 1340–4.

Li, C. I., Anderson, B. O., Daling, J. R. & Moe, R. E. (2003a). Trends in incidence rates of invasive lobular and ductal breast carcinoma, *JAMA* **289**(11): 1421–4.

Li, J., Hawkins, I. C., Harvey, C. D., Jennings, J. L., Link, A. J. & Patton, J. G. (2003b). Regulation of alternative splicing by SRrp86 and its interacting proteins, *Mol Cell Biol* **23**(21): 7437–47.

Li, X., Wang, W., Wang, J., Malovannaya, A., Xi, Y., Li, W., Guerra, R., Hawke, D. H., Qin, J. & Chen, J. (2015). Proteomic analyses reveal distinct chromatin-associated and soluble transcription factor complexes, *Mol Syst Biol* **11**(1): 775.

Liedert, B., Pluim, D., Schellens, J. & Thomale, J. (2006). Adduct-specific monoclonal antibodies for the measurement of cisplatin-induced DNA lesions in individual cell nuclei, *Nucleic Acids Res* **34**(6): e47.

Liggett, Jr, W. H. & Sidransky, D. (1998). Role of the p16 tumor suppressor gene in cancer, *J Clin Oncol* **16**(3): 1197–206.

Liu, L. F., Desai, S. D., Li, T. K., Mao, Y., Sun, M. & Sim, S. P. (2000). Mechanism of action of camptothecin, *Ann N Y Acad Sci* **922**: 1–10.

Liu, T. T., Arango-Argoty, G., Li, Z., Lin, Y., Kim, S. W., Dueck, A., Ozsolak, F., Monaghan, A. P., Meister, G., DeFranco, D. B. & John, B. (2015). Noncoding RNAs that associate with YB-1 alter proliferation in prostate cancer cells, *RNA* **21**(6): 1159–72.

Löbrich, M., Shibata, A., Beucher, A., Fisher, A., Ensminger, M., Goodarzi, A. A., Barton, O. & Jeggo, P. A. (2010). gammaH2AX foci analysis for monitoring DNA double-strand break repair: strengths, limitations and optimization, *Cell Cycle* **9**(4): 662–9.

Lovett, D. H., Cheng, S., Cape, L., Pollock, A. S. & Mertens, P. R. (2010). YB-1 alters MT1-MMP trafficking and stimulates MCF-7 breast tumor invasion and metastasis, *Biochem Biophys Res Commun* **398**(3): 482–8.

Lowndes, N. F. & Toh, G. W.-L. (2005). DNA repair: the importance of phosphorylating histone H2AX, *Curr Biol* **15**(3): R99–R102.

Lu, J. & Holmgren, A. (2009). Selenoproteins, *J Biol Chem* **284**(2): 723–27.

Lu, Z. H., Books, J. T. & Ley, T. J. (2005). YB-1 is important for late-stage embryonic development, optimal cellular stress responses, and the prevention of premature senescence, *Mol Cell Biol* **25**(11): 4625–37.

Lutz, M., Wempe, F., Bahr, I., Zopf, D. & von Melchner, H. (2006). Proteasomal degradation of the multifunctional regulator YB-1 is mediated by an F-Box protein induced during programmed cell death, *FEBS Lett* **580**(16): 3921–30.

Lyabin, D. N., Doronin, A. N., Eliseeva, I. A., Guens, G. P., Kulakovskiy, I. V. & Ovchinnikov, L. P. (2014). Alternative forms of Y-box binding protein 1 and YB-1 mRNA, *PLoS One* **9**(8): e104513.

Lyabin, D. N., Eliseeva, I. A. & Ovchinnikov, L. P. (2012). YB-1 synthesis is regulated by mTOR signaling pathway, *PLoS One* **7**(12): e52527.

Lyabin, D. N., Eliseeva, I. A., Skabkina, O. V. & Ovchinnikov, L. P. (2011). Interplay between Y-box-binding protein 1 (YB-1) and poly(A) binding protein (PABP) in specific regulation of YB-1 mRNA translation, *RNA Biol* **8**(5): 883–92.

Lyabin, D. N., Nigmatullina, L. F., Doronin, A. N., Eliseeva, I. A. & Ovchinnikov, L. P. (2013). Identification of proteins specifically interacting with YB-1 mRNA 3' UTR and the effect of hnRNP Q on YB-1 mRNA translation, *Biochemistry (Mosc)* **78**(6): 651–9.

Lyabin, D. N. & Ovchinnikov, L. P. (2016). Selective regulation of YB-1 mRNA translation by the mTOR signaling pathway is not mediated by 4E-binding protein, *Sci Rep* **6**: 22502.

Lyons, S. M., Achorn, C., Kedersha, N. L., Anderson, P. J. & Ivanov, P. (2016). YB-1 regulates tiRNA-induced stress granule formation but not translational repression, *Nucleic Acids Res* **Online**.
URL: *http://dx.doi.org/10.1093/nar/gkw418*

MacDonald, G. H., Itoh-Lindstrom, Y. & Ting, J. P. (1995). The transcriptional regulatory protein, YB-1, promotes single-stranded regions in the DRA promoter, *J Biol Chem* **270**(8): 3527–33.

Maere, S., Heymans, K. & Kuiper, M. (2005). BiNGO: a Cytoscape plugin to assess overrepresentation of gene ontology categories in biological networks, *Bioinformatics* **21**(16): 3448–9.

Maher-Laporte, M., Berthiaume, F., Moreau, M., Julien, L.-A., Lapointe, G., Mourez, M. & DesGroseillers, L. (2010). Molecular composition of staufen2-containing ribonucleoproteins in embryonic rat brain, *PLoS One* **5**(6): e11350.

Makino, Y., Ohga, T., Toh, S., Koike, K., Okumura, K., Wada, M., Kuwano, M. & Kohno, K. (1996). Structural and functional analysis of the human Y-box binding protein (YB-1) gene promoter, *Nucleic Acids Res* **24**(10): 1873–8.

Manning, A. L. & Dyson, N. J. (2012). RB: mitotic implications of a tumour suppressor, *Nat Rev Cancer* **12**(3): 220–6.

Marenstein, D. R., Chan, M. K., Altamirano, A., Basu, A. K., Boorstein, R. J., Cunningham, R. P. & Teebor, G. W. (2003). Substrate specificity of human endonuclease III (hNTH1). Effect of human APE1 on hNTH1 activity, *J Biol Chem* **278**(11): 9005–12.

Marenstein, D. R., Ocampo, M. T., Chan, M. K., Altamirano, A., Basu, A. K., Boorstein, R. J., Cunningham, R. P. & Teebor, G. W. (2001). Stimulation of human endonuclease III by Y box-binding protein 1 (DNA-binding protein B). Interaction between a base excision repair enzyme and a transcription factor, *J Biol Chem* **276**(24): 21242–9.

Marko, M., Leichter, M., Patrinou-Georgoula, M. & Guialis, A. (2010). hnRNP M interacts with PSF and p54(nrb) and co-localizes within defined nuclear structures, *Exp Cell Res* **316**(3): 390–400.

Marullo, R., Werner, E., Degtyareva, N., Moore, B., Altavilla, G., Ramalingam, S. S. & Doetsch, P. W. (2013). Cisplatin induces a mitochondrial ROS response that contributes to cytotoxicity depending on mitochondrial redox status and bioenergetic functions, *PLoS One* **8**(11).

Matos, L. L. d., Trufelli, D. C., de Matos, M. G. L. & da Silva Pinhal, M. A. (2010). Immunohistochemistry as an important tool in biomarkers detection and clinical practice, *Biomark Insights* **5**: 9–20.

Matsumoto, K., Meric, F. & Wolffe, A. P. (1996). Translational repression dependent on the interaction of the Xenopus Y-box protein FRGY2 with mRNA. Role of the cold shock domain, tail domain, and selective RNA sequence recognition, *J Biol Chem* **271**(37): 22706–12.

Mauri, D., Pavlidis, N. & Ioannidis, J. P. A. (2005). Neoadjuvant versus adjuvant systemic treatment in breast cancer: a meta-analysis, *J Natl Cancer Inst* **97**(3): 188–94.

Mauri, D., Pavlidis, N., Polyzos, N. P. & Ioannidis, J. P. A. (2006). Survival with aromatase inhibitors and inactivators versus standard hormonal therapy in advanced breast cancer: meta-analysis, *J Natl Cancer Inst* **98**(18): 1285–91.

McGee, A. M., Douglas, D. L., Liang, Y., Hyder, S. M. & Baines, C. P. (2011). The mitochondrial protein C1qbp promotes cell proliferation, migration and resistance to cell death., *Cell Cycle* **10**(23): 4119–4127.

Meenakshi, J., Anupama, Goswami, S. K. & Datta, K. (2003). Constitutive expression of hyaluronan binding protein 1 (HABP1/p32/gC1qR) in normal fibroblast cells perturbs its growth characteristics and induces apoptosis, *Biochem Biophys Res Commun* **300**(3): 686–93.

Mellacheruvu, D., Wright, Z., Couzens, A. L., Lambert, J.-P., St-Denis, N. A., Li, T., Miteva, Y. V., Hauri, S., Sardiu, M. E., Low, T. Y., Halim, V. A., Bagshaw, R. D., Hubner, N. C., Al-Hakim, A., Bouchard, A., Faubert, D., Fermin, D., Dunham, W. H., Goudreault, M., Lin, Z.-Y., Badillo, B. G., Pawson, T., Durocher, D., Coulombe, B., Aebersold, R., Superti-Furga, G., Colinge, J., Heck, A. J. R., Choi, H., Gstaiger, M., Mohammed, S., Cristea, I. M., Bennett, K. L., Washburn, M. P., Raught, B., Ewing, R. M., Gingras, A.-C. & Nesvizhskii, A. I. (2013). The CRAPome: a contaminant repository for affinity purification-mass spectrometry data, *Nat Methods* **10**(8): 730–6.

Mermoud, J. E., Cohen, P. & Lamond, A. I. (1992). Ser/Thr-specific protein phosphatases are required for both catalytic steps of pre-mRNA splicing, *Nucleic Acids Res* **20**(20): 5263–9.

Mertens, P. R., Harendza, S., Pollock, A. S. & Lovett, D. H. (1997). Glomerular mesangial cell-specific transactivation of matrix metalloproteinase 2 transcription is mediated by YB-1, *J Biol Chem* **272**(36): 22905–12.

Mertens, P. R., Steinmann, K., Alfonso-Jaume, M. A., En-Nia, A., Sun, Y. & Lovett, D. H. (2002). Combinatorial interactions of p53, activating protein-2, and YB-1 with a single enhancer element regulate gelatinase A expression in neoplastic cells, *J Biol Chem* **277**(28): 24875–82.

Minich, W. B., Maidebura, I. P. & Ovchinnikov, L. P. (1993). Purification and characterization of the major 50-kDa repressor protein from cytoplasmic mRNP of rabbit reticulocytes, *Eur J Biochem* **212**(3): 633–8.

Minich, W. B. & Ovchinnikov, L. P. (1992). Role of cytoplasmic mRNP proteins in translation, *Biochimie* **74**(5): 477–83.

Moasser, M. M. (2007). The oncogene HER2: its signaling and transforming functions and its role in human cancer pathogenesis, *Oncogene* **26**(45): 6469–87.

Modok, S., Mellor, H. R. & Callaghan, R. (2006). Modulation of multidrug resistance efflux pump activity to overcome chemoresistance in cancer, *Curr Opin Pharmacol* **6**(4): 350–4.

Mohammed, H., D'Santos, C., Serandour, A. A., Ali, H. R., Brown, G. D., Atkins, A., Rueda, O. M., Holmes, K. A., Theodorou, V., Robinson, J. L. L., Zwart, W., Saadi, A., Ross-Innes, C. S., Chin, S.-F., Menon, S., Stingl, J., Palmieri, C., Caldas, C. & Carroll, J. S. (2013). Endogenous purification reveals GREB1 as a key estrogen receptor regulatory factor, *Cell Rep* **3**(2): 342–9.

Molina, H., Horn, D. M., Tang, N., Mathivanan, S. & Pandey, A. (2007). Global proteomic profiling of phosphopeptides using electron transfer dissociation tandem mass spectrometry, *Proc Natl Acad Sci U S A* **104**(7): 2199–204.

Moore, M. J. & Proudfoot, N. J. (2009). Pre-mRNA processing reaches back to transcription and ahead to translation, *Cell* **136**(4): 688–700.

Moraes, K. C. M., Quaresma, A. J. C., Maehnss, K. & Kobarg, J. (2003). Identification and characterization of proteins that selectively interact with isoforms of the mRNA binding protein AUF1 (hnRNP D), *Biol Chem* **384**(1): 25–37.

Morin, J. G. & Hastings, J. W. (1971). Energy transfer in a bioluminescent system, *J Cell Physiol* **77**(3): 313–8.

Moron, M. S., Depierre, J. W. & Mannervik, B. (1979). Levels of glutathione, glutathione reductase and glutathione S-transferase activities in rat lung and liver, *BBA-Gen Subjects* **582**(1): 67–78.

Muñoz, M. J., Pérez Santangelo, M. S., Paronetto, M. P., de la Mata, M., Pelisch, F., Boireau, S., Glover-Cutter, K., Ben-Dov, C., Blaustein, M., Lozano, J. J., Bird, G., Bentley, D., Bertrand, E. & Kornblihtt, A. R. (2009). DNA damage

regulates alternative splicing through inhibition of RNA polymerase II elongation, *Cell* **137**(4): 708–20.

Murakami, K., Elmlund, H., Kalisman, N., Bushnell, D. A., Adams, C. M., Azubel, M., Elmlund, D., Levi-Kalisman, Y., Liu, X., Gibbons, B. J., Levitt, M. & Kornberg, R. D. (2013). Architecture of an RNA polymerase II transcription pre-initiation complex, *Science* **342**(6159): 1238724.

Murray, M. T., Krohne, G. & Franke, W. W. (1991). Different forms of soluble cytoplasmic mRNA binding proteins and particles in Xenopus laevis oocytes and embryos, *J Cell Biol* **112**(1): 1–11.

Murray, M. T., Schiller, D. L. & Franke, W. W. (1992). Sequence analysis of cytoplasmic mRNA-binding proteins of Xenopus oocytes identifies a family of RNA-binding proteins, *Proc Natl Acad Sci U S A* **89**(1): 11–5.

Murre, C., McCaw, P. S. & Baltimore, D. (1989). A new DNA binding and dimerization motif in immunoglobulin enhancer binding, daughterless, MyoD, and myc proteins, *Cell* **56**(5): 777–83.

Muta, T., Kang, D., Kitajima, S., Fujiwara, T. & Hamasaki, N. (1997). p32 protein, a splicing factor 2-associated protein, is localized in mitochondrial matrix and is functionally important in maintaining oxidative phosphorylation, *J Biol Chem* **272**(39): 24363–70.

Mylona, E., Melissaris, S., Giannopoulou, I., Theohari, I., Papadimitriou, C., Keramopoulos, A. & Nakopoulou, L. (2014). Y-box-binding protein 1 (YB1) in breast carcinomas: relation to aggressive tumor phenotype and identification of patients at high risk for relapse, *Eur J Surg Oncol* **40**(3): 289–96.

Nagano, K., Shinkawa, T., Mutoh, H., Kondoh, O., Morimoto, S., Inomata, N., Ashihara, M., Ishii, N., Aoki, Y. & Haramura, M. (2009). Phosphoproteomic analysis of distinct tumor cell lines in response to nocodazole treatment, *Proteomics* **9**(10): 2861–74.

Nasrin, F., Rahman, M. A., Masuda, A., Ohe, K., Takeda, J.-I. & Ohno, K. (2014). HnRNP C, YB-1 and hnRNP L coordinately enhance skipping of human MUSK exon 10 to generate a Wnt-insensitive MuSK isoform, *Sci Rep* **4**: 6841.

Nekrasov, M. P., Ivshina, M. P., Chernov, K. G., Kovrigina, E. A., Evdokimova, V. M., Thomas, A. A. M., Hershey, J. W. B. & Ovchinnikov, L. P. (2003). The mRNA-binding protein YB-1 (p50) prevents association of the eukaryotic initiation factor eIF4G with mRNA and inhibits protein synthesis at the initiation stage, *J Biol Chem* **278**(16): 13936–43.

Neo, S. H., Itahana, Y., Alagu, J., Kitagawa, M., Guo, A. K., Lee, S. H., Tang, K. & Itahana, K. (2015). TRIM28 is an E3 ligase for ARF-mediated NPM1/B23 SUMOylation that represses centrosome amplification, *Mol Cell Biol* **35**(16): 2851–63.

Nielsen, T. O., Hsu, F. D., Jensen, K., Cheang, M., Karaca, G., Hu, Z., Hernandez-Boussard, T., Livasy, C., Cowan, D., Dressler, L., Akslen, L. A., Ragaz, J., Gown, A. M., Gilks, C. B., van de Rijn, M. & Perou, C. M. (2004). Immunohistochemical and clinical characterization of the basal-like subtype of invasive breast carcinoma, *Clin Cancer Res* **10**(16): 5367–74.

Noon, A. T., Shibata, A., Rief, N., Lobrich, M., Stewart, G. S., Jeggo, P. A. & Goodarzi, A. A. (2010). 53BP1-dependent robust localized KAP-1 phosphorylation is essential for heterochromatic DNA double-strand break repair, *Nat Cell Biol* **12**(2): 177–84.

O'Clair, L. & Appledorn, D. M. (2011). Application Note; CellPlayer 96-Well Cytotoxicity Assay, *Application Note 8000-0093-B00*, Essen Bioscience.

Oda, Y., Ohishi, Y., Saito, T., Hinoshita, E., Uchiumi, T., Kinukawa, N., Iwamoto, Y., Kohno, K., Kuwano, M. & Tsuneyoshi, M. (2003). Nuclear expression of Y-box-binding protein-1 correlates with P-glycoprotein and topoisomerase II alpha expression, and with poor prognosis in synovial sarcoma, *J Pathol* **199**(2): 251–8.

Ohashi, S., Fukumura, R., Higuchi, T. & Kobayashi, S. (2009). YB-1 transcription in the postnatal brain is regulated by a bHLH transcription factor Math2 through an E-box sequence in the 5'-UTR of the gene, *Mol Cell Biochem* **327**(1-2): 267–75.

Ohga, T., Koike, K., Ono, M., Makino, Y., Itagaki, Y., Tanimoto, M., Kuwano, M. & Kohno, K. (1996). Role of the human Y box-binding protein YB-1 in cellular sensitivity to the DNA-damaging agents cisplatin, mitomycin C, and ultraviolet light, *Cancer Res* **56**(18): 4224–8.

Ohga, T., Uchiumi, T., Makino, Y., Koike, K., Wada, M., Kuwano, M. & Kohno, K. (1998). Direct involvement of the Y-box binding protein YB-1 in genotoxic stress-induced activation of the human multidrug resistance 1 gene, *J Biol Chem* **273**(11): 5997–6000.

Olsen, J. V., Vermeulen, M., Santamaria, A., Kumar, C., Miller, M. L., Jensen, L. J., Gnad, F., Cox, J., Jensen, T. S., Nigg, E. A., Brunak, S. & Mann, M. (2010). Quantitative phosphoproteomics reveals widespread full phosphorylation site occupancy during mitosis, *Sci Signal* **3**(104): ra3.

Onishi, H., Kino, Y., Morita, T., Futai, E., Sasagawa, N. & Ishiura, S. (2008). MBNL1 associates with YB-1 in cytoplasmic stress granules, *J Neurosci Res* **86**(9): 1994–2002.

Ozer, J., Chalkley, R. & Sealy, L. (1993a). Characterization of rat pseudogenes for enhancer factor I subunit A: ripping provides clues to the evolution of the EFIA/dbpB/YB-1 multigene family, *Gene* **133**(2): 187–95.

Ozer, J., Chalkley, R. & Sealy, L. (1993b). Isolation of the CCAAT transcription factor subunit EFIA cDNA and a potentially functional EFIA processed pseudogene from Bos taurus: insights into the evolution of the EFIA/dbpB/YB-1 gene family, *Gene* **124**(2): 223–30.

Ozer, J., Faber, M., Chalkley, R. & Sealy, L. (1990). Isolation and characterization of a cDNA clone for the CCAAT transcription factor EFIA reveals a novel structural motif, *J Biol Chem* **265**(36): 22143–52.

Pan, C., Olsen, J. V., Daub, H. & Mann, M. (2009). Global effects of kinase inhibitors on signaling networks revealed by quantitative phosphoproteomics, *Mol Cell Proteomics* **8**(12): 2796–808.

Pan, Q., Shai, O., Lee, L. J., Frey, B. J. & Blencowe, B. J. (2008). Deep surveying of alternative splicing complexity in the human transcriptome by high-throughput sequencing, *Nat Genet* **40**(12): 1413–15.

Panchaud, A., Singh, P., Shaffer, S. A. & Goodlett, D. R. (2010). xComb: a cross-linked peptide database approach to protein-protein interaction analysis, *J Proteome Res* **9**(5): 2508–15.

Pauletti, G., Godolphin, W., Press, M. F. & Slamon, D. J. (1996). Detection and quantitation of HER-2/neu gene amplification in human breast cancer archival material using fluorescence in situ hybridization, *Oncogene* **13**(1): 63–72.

Paull, T. T., Rogakou, E. P., Yamazaki, V., Kirchgessner, C. U., Gellert, M. & Bonner, W. M. (2000). A critical role for histone H2AX in recruitment of repair factors to nuclear foci after DNA damage, *Curr Biol* **10**(15): 886–95.

Peerschke, E. I. B. & Ghebrehiwet, B. (2014). cC1qR/CR and gC1qR/p33: observations in cancer, *Mol Immunol* **61**(2): 100–9.

Pellettieri, J. & Sánchez Alvarado, A. (2007). Cell turnover and adult tissue homeostasis: from humans to planarians, *Annu Rev Genet* **41**: 83–105.

Perou, C. M., Sørlie, T., Eisen, M. B., van de Rijn, M., Jeffrey, S. S., Rees, C. A., Pollack, J. R., Ross, D. T., Johnsen, H., Akslen, L. A., Fluge, O., Pergamenschikov, A., Williams, C., Zhu, S. X., Lønning, P. E., Børresen-Dale, A. L., Brown, P. O. & Botstein, D. (2000). Molecular portraits of human breast tumours, *Nature* **406**(6797): 747–52.

Pestryakov, P., Zharkov, D. O., Grin, I., Fomina, E. E., Kim, E. R., Hamon, L., Eliseeva, I. A., Petruseva, I. O., Curmi, P. A., Ovchinnikov, L. P. & Lavrik, O. I. (2012). Effect of the multifunctional proteins RPA, YB-1, and XPC repair factor on AP site cleavage by DNA glycosylase NEIL1, *J Mol Recognit* **25**(4): 224–33.

Petersen-Mahrt, S. K., Estmer, C., Ohrmalm, C., Matthews, D. A., Russell, W. C. & Akusjarvi, G. (1999). The splicing factor-associated protein, p32, regulates RNA splicing by inhibiting ASF/SF2 RNA binding and phosphorylation, *EMBO J* **18**(4): 1014–24.

Petrelli, F., Coinu, A., Borgonovo, K., Cabiddu, M., Ghilardi, M., Lonati, V. & Barni, S. (2014). The value of platinum agents as neoadjuvant chemotherapy in triple-negative breast cancers: a systematic review and meta-analysis, *Breast Cancer Res Treat* **144**(2): 223–32.

Picotti, P. & Aebersold, R. (2012). Selected reaction monitoring-based proteomics: workflows, potential, pitfalls and future directions, *Nat Methods* **9**(6): 555–66.

Pisarev, A. V., Skabkin, M. A., Thomas, A. A., Merrick, W. C., Ovchinnikov, L. P. & Shatsky, I. N. (2002). Positive and negative effects of the major mammalian messenger ribonucleoprotein p50 on binding of 40 S ribosomal subunits to the initiation codon of beta-globin mRNA, *J Biol Chem* **277**(18): 15445–51.

Popp, S. L., Joffroy, C., Stope, M. B., Buck, M. B., Fritz, P. & Knabbe, C. (2013). Antiestrogens suppress effects of transforming growth factor-beta in breast cancer cells via the signaling axis estrogen receptor-alpha and Y-box binding protein-1, *Anticancer Res* **33**(6): 2473–80.

Prabhu, L., Mundade, R., Wang, B., Wei, H., Hartley, A.-V., Martin, M., McElyea, K., Temm, C. J., Sandusky, G., Liu, Y. & Lu, T. (2015). Critical role of phosphorylation of serine 165 of YBX1 on the activation of NF-B in colon cancer, *Oncotarget* **6**(30): 29396–412.

Prochazka, L., Tesarik, R. & Turanek, J. (2014). Regulation of alternative splicing of CD44 in cancer, *Cell Signal* **26**(10): 2234–9.

Qian, F., Kruse, U., Lichter, P. & Sippel, A. E. (1995). Chromosomal localization of the four genes (NFIA, B, C, and X) for the human transcription factor nuclear factor I by FISH, *Genomics* **28**(1): 66–73.

Raffetseder, U., Frye, B., Rauen, T., Jürchott, K., Royer, H.-D., Jansen, P. L. & Mertens, P. R. (2003). Splicing factor SRp30c interaction with Y-box protein-1 confers nuclear YB-1 shuttling and alternative splice site selection, *J Biol Chem* **278**(20): 18241–8.

Raffetseder, U., Liehn, E. A., Weber, C. & Mertens, P. R. (2012). Role of cold shock Y-box protein-1 in inflammation, atherosclerosis and organ transplant rejection, *Eur J Cell Biol* **91**(6-7): 567–75.

Rakoff-Nahoum, S., Chen, H., Kraus, T., George, I., Oei, E., Tyorkin, M., Salik, E., Beuria, P. & Sperber, K. (2001). Regulation of class II expression in monocytic cells after HIV-1 infection, *J Immunol* **167**(4): 2331–42.

Rapp, T. B., Yang, L., Conrad, 3rd, E. U., Mandahl, N. & Chansky, H. A. (2002). RNA splicing mediated by YB-1 is inhibited by TLS/CHOP in human myxoid liposarcoma cells, *J Orthop Res* **20**(4): 723–9.

Rausch, T., Jones, D. T. W., Zapatka, M., Stütz, A. M., Zichner, T., Weischenfeldt, J., Jäger, N., Remke, M., Shih, D., Northcott, P. A., Pfaff, E., Tica, J., Wang, Q., Massimi, L., Witt, H., Bender, S., Pleier, S., Cin, H., Hawkins, C., Beck,

C., von Deimling, A., Hans, V., Brors, B., Eils, R., Scheurlen, W., Blake, J., Benes, V., Kulozik, A. E., Witt, O., Martin, D., Zhang, C., Porat, R., Merino, D. M., Wasserman, J., Jabado, N., Fontebasso, A., Bullinger, L., Rücker, F. G., Döhner, K., Döhner, H., Koster, J., Molenaar, J. J., Versteeg, R., Kool, M., Tabori, U., Malkin, D., Korshunov, A., Taylor, M. D., Lichter, P., Pfister, S. M. & Korbel, J. O. (2012). Genome sequencing of pediatric medulloblastoma links catastrophic DNA rearrangements with TP53 mutations, *Cell* **148**(1-2): 59–71.

Ray, D., Kazan, H., Chan, E. T., Peña Castillo, L., Chaudhry, S., Talukder, S., Blencowe, B. J., Morris, Q. & Hughes, T. R. (2009). Rapid and systematic analysis of the RNA recognition specificities of RNA-binding proteins, *Nat Biotechnol* **27**(7): 667–70.

Rayess, H., Wang, M. B. & Srivatsan, E. S. (2012). Cellular senescence and tumor suppressor gene p16, *Int J Cancer* **130**(8): 1715–25.

Reef, S., Shifman, O., Oren, M. & Kimchi, A. (2007). The autophagic inducer smARF interacts with and is stabilized by the mitochondrial p32 protein, *Oncogene* **26**(46): 6677–83.

Reipas, K. M., Law, J. H., Couto, N., Islam, S., Li, Y., Li, H., Cherkasov, A., Jung, K., Cheema, A. S., Jones, S. J. M., Hassell, J. A. & Dunn, S. E. (2013). Luteolin is a novel p90 ribosomal S6 kinase (RSK) inhibitor that suppresses Notch4 signaling by blocking the activation of Y-box binding protein-1 (YB-1), *Oncotarget* **4**(2): 329–45.

Renan, M. J. (1993). How many mutations are required for tumorigenesis? Implications from human cancer data, *Mol Carcinog* **7**(3): 139–46.

Renart, J., Reiser, J. & Stark, G. R. (1979). Transfer of proteins from gels to diazobenzyloxymethyl-paper and detection with antisera: a method for studying antibody specificity and antigen structure, *Proc Natl Acad Sci U S A* **76**(7): 3116–20.

Revet, I., Feeney, L., Bruguera, S., Wilson, W., Dong, T. K., Oh, D. H., Dankort, D. & Cleaver, J. E. (2011). Functional relevance of the histone H2Ax in the response to DNA damaging agents, *Proc Natl Acad Sci U S A* **108**(21): 8663–7.

Riley, K. J. & Steitz, J. A. (2013). The "Observer Effect" in genome-wide surveys of protein-RNA interactions, *Mol Cell* **49**(4): 601–4.

Ritz, C., Baty, F., Streibig, J. C. & Gerhard, D. (2015). Dose-Response Analysis Using R, *PLoS One* **10**(12): e0146021.

Ritz, C. & Streibig, J. C. (2005). Bioassay Analysis Using R, *J Stat Softw* **12**(5): 1–22.

Ross, J. S. & Fletcher, J. A. (1998). The HER-2/neu oncogene in breast cancer: prognostic factor, predictive factor, and target for therapy, *Stem Cells* **16**(6): 413–28.

Roy, R., Chun, J. & Powell, S. N. (2012). BRCA1 and BRCA2: different roles in a common pathway of genome protection, *Nat Rev Cancer* **12**(1): 68–78.

Rubin, C. S. & Rosen, O. M. (1975). Protein phosphorylation, *Annu Rev Biochem* **44**: 831–87.

Ruse, C. I., McClatchy, D. B., Lu, B., Cociorva, D., Motoyama, A., Park, S. K. & Yates, 3rd, J. R. (2008). Motif-specific sampling of phosphoproteomes, *J Proteome Res* **7**(5): 2140–50.

Rusk, N. (2011). From pseudogenes to proteins, *Nat Meth* **8**(6): 448–9.

Sabath, D. E., Podolin, P. L., Comber, P. G. & Prystowsky, M. B. (1990). cDNA cloning and characterization of interleukin 2-induced genes in a cloned T helper lymphocyte, *J Biol Chem* **265**(21): 12671–8.

Sager, R. (1989). Tumor suppressor genes: the puzzle and the promise, *Science* **246**(4936): 1406–12.

Sakura, H., Maekawa, T., Imamoto, F., Yasuda, K. & Ishii, S. (1988). Two human genes isolated by a novel method encode DNA-binding proteins containing a common region of homology, *Gene* **73**(2): 499–507.

Salleron, L., Magistrelli, G., Mary, C., Fischer, N., Bairoch, A. & Lane, L. (2014). DERA is the human deoxyribose phosphate aldolase and is involved in stress response, *Biochim Biophys Acta* **1843**(12): 2913–25.

Samimi, G., Varki, N. M., Wilczynski, S., Safaei, R., Alberts, D. S. & Howell, S. B. (2003). Increase in expression of the copper transporter ATP7A during platinum drug-based treatment is associated with poor survival in ovarian cancer patients, *Clin Cancer Res* **9**(16 Pt 1): 5853–9.

Sancar, A., Lindsey-Boltz, L. A., Unsal-Kaçmaz, K. & Linn, S. (2004). Molecular mechanisms of mammalian DNA repair and the DNA damage checkpoints, *Annu Rev Biochem* **73**: 39–85.

Satya-Prakash, K. L., Pathak, S., Hsu, T. C., Olivé, M. & Cailleau, R. (1981). Cytogenetic analysis on eight human breast tumor cell lines: high frequencies of 1q, 11q and HeLa-like marker chromosomes, *Cancer Genet Cytogenet* **3**(1): 61–73.

Saupe, M., Rauschenberger, L., Preuß, M., Oswald, S., Fussek, S., Zimmermann, U., Walther, R., Knabbe, C., Burchardt, M. & Stope, M. B. (2014). Differential expression of the multidrug resistance 1 (MDR1) protein in prostate cancer cells is independent from anticancer drug treatment and Y box binding protein 1 (YB-1) activity, *World J Urol* **33**(10): 1481–6.

Schilling, B., Rardin, M. J., MacLean, B. X., Zawadzka, A. M., Frewen, B. E., Cusack, M. P., Sorensen, D. J., Bereman, M. S., Jing, E., Wu, C. C., Verdin, E., Kahn, C. R., MacCoss, M. J. & Gibson, B. W. (2012). Platform-independent

and label-free quantitation of proteomic data using MS1 extracted ion chromatograms in Skyline, *Mol Cell Proteomics* **11**(5): 202–14.

Schindelin, J., Arganda-Carreras, I., Frise, E., Kaynig, V., Longair, M., Pietzsch, T., Preibisch, S., Rueden, C., Saalfeld, S., Schmid, B., Tinevez, J.-Y., White, D. J., Hartenstein, V., Eliceiri, K., Tomancak, P. & Cardona, A. (2012). Fiji: an open-source platform for biological-image analysis, *Nat Methods* **9**(7): 676–82.

Schittek, B., Psenner, K., Sauer, B., Meier, F., Iftner, T. & Garbe, C. (2007). The increased expression of Y box-binding protein 1 in melanoma stimulates proliferation and tumor invasion, antagonizes apoptosis and enhances chemoresistance, *Int J Cancer* **120**(10): 2110–8.

Schubbert, S., Shannon, K. & Bollag, G. (2007). Hyperactive Ras in developmental disorders and cancer, *Nat Rev Cancer* **7**(4): 295–308.

Schwanhäusser, B., Busse, D., Li, N., Dittmar, G., Schuchhardt, J., Wolf, J., Chen, W. & Selbach, M. (2011). Global quantification of mammalian gene expression control, *Nature* **473**(7347): 337–42.

Selivanova, O. M., Guryanov, S. G., Enin, G. A., Skabkin, M. A., Ovchinnikov, L. P. & Serdyuk, I. N. (2010). YB-1 is capable of forming extended nanofibrils, *Biochemistry (Mosc)* **75**(1): 115–20.

Sena, L. & Chandel, N. (2012). Physiological roles of mitochondrial reactive oxygen species, *Molecular Cell* **48**(2): 158 – 167.

Sengupta, S., Mantha, A. K., Mitra, S. & Bhakat, K. K. (2011). Human AP endonuclease (APE1/Ref-1) and its acetylation regulate YB-1-p300 recruitment and RNA polymerase II loading in the drug-induced activation of multidrug resistance gene MDR1, *Oncogene* **30**(4): 482–93.

Shah, S. P., Roth, A., Goya, R., Oloumi, A., Ha, G., Zhao, Y., Turashvili, G., Ding, J., Tse, K., Haffari, G., Bashashati, A., Prentice, L. M., Khattra, J., Burleigh, A., Yap, D., Bernard, V., McPherson, A., Shumansky, K., Crisan, A., Giuliany, R., Heravi-Moussavi, A., Rosner, J., Lai, D., Birol, I., Varhol, R., Tam, A., Dhalla, N., Zeng, T., Ma, K., Chan, S. K., Griffith, M., Moradian, A., Cheng, S.-W. G., Morin, G. B., Watson, P., Gelmon, K., Chia, S., Chin, S.-F., Curtis, C., Rueda, O. M., Pharoah, P. D., Damaraju, S., Mackey, J., Hoon, K., Harkins, T., Tadigotla, V., Sigaroudinia, M., Gascard, P., Tlsty, T., Costello, J. F., Meyer, I. M., Eaves, C. J., Wasserman, W. W., Jones, S., Huntsman, D., Hirst, M., Caldas, C., Marra, M. A. & Aparicio, S. (2012). The clonal and mutational evolution spectrum of primary triple-negative breast cancers, *Nature* **486**(7403): 395–9.

Shen, Q., Fan, L. & Newburger, P. E. (2006). Nuclease sensitive element binding protein 1 associates with the selenocysteine insertion sequence and functions in mammalian selenoprotein translation, *J Cell Physiol* **207**(3): 775–83.

Shen, Q., Wu, R., Leonard, J. L. & Newburger, P. E. (1998). Identification and molecular cloning of a human selenocysteine insertion sequence-binding protein. A bifunctional role for DNA-binding protein B, *J Biol Chem* **273**(10): 5443–6.

Shevchenko, A., Jensen, O. N., Podtelejnikov, A. V., Sagliocco, F., Wilm, M., Vorm, O., Mortensen, P., Shevchenko, A., Boucherie, H. & Mann, M. (1996). Linking genome and proteome by mass spectrometry: large-scale identification of yeast proteins from two dimensional gels, *Proc Natl Acad Sci U S A* **93**(25): 14440–5.

Shi, S. R., Cote, R. J. & Taylor, C. R. (2001). Antigen retrieval techniques: current perspectives, *J Histochem Cytochem* **49**(8): 931–7.

Shibahara, K., Sugio, K., Osaki, T., Uchiumi, T., Maehara, Y., Kohno, K., Yasumoto, K., Sugimachi, K. & Kuwano, M. (2001). Nuclear expression of the Y-box binding protein, YB-1, as a novel marker of disease progression in non-small cell lung cancer, *Clin Cancer Res* **7**(10): 3151–5.

Shibahara, K., Uchiumi, T., Fukuda, T., Kura, S., Tominaga, Y., Maehara, Y., Kohno, K., Nakabeppu, Y., Tsuzuki, T. & Kuwano, M. (2004). Targeted disruption of one allele of the Y-box binding protein-1 (YB-1) gene in mouse embryonic stem cells and increased sensitivity to cisplatin and mitomycin C, *Cancer Sci* **95**(4): 348–53.

Shibao, K., Takano, H., Nakayama, Y., Okazaki, K., Nagata, N., Izumi, H., Uchiumi, T., Kuwano, M., Kohno, K. & Itoh, H. (1999). Enhanced coexpression of YB-1 and DNA topoisomerase II alpha genes in human colorectal carcinomas, *Int J Cancer* **83**(6): 732–7.

Shinkai, K., Nakano, K., Cui, L., Mizuuchi, Y., Onishi, H., Oda, Y., Obika, S., Tanaka, M. & Katano, M. (2016). Nuclear expression of Y-box binding protein-1 is associated with poor prognosis in patients with pancreatic cancer and its knockdown inhibits tumor growth and metastasis in mice tumor models, *Int J Cancer* **139**(2): 433–45.

Shiota, M., Itsumi, M., Yokomizo, A., Takeuchi, A., Imada, K., Kashiwagi, E., Inokuchi, J., Tatsugami, K., Uchiumi, T. & Naito, S. (2014). Targeting ribosomal S6 kinases/Y-box binding protein-1 signaling improves cellular sensitivity to taxane in prostate cancer, *Prostate* **74**(8): 829–38.

Shiota, M., Izumi, H., Onitsuka, T., Miyamoto, N., Kashiwagi, E., Kidani, A., Hirano, G., Takahashi, M., Naito, S. & Kohno, K. (2008b). Twist and p53 reciprocally regulate target genes via direct interaction, *Oncogene* **27**(42): 5543–53.

Shiota, M., Izumi, H., Onitsuka, T., Miyamoto, N., Kashiwagi, E., Kidani, A., Yokomizo, A., Naito, S. & Kohno, K. (2008a). Twist promotes tumor cell growth through YB-1 expression, *Cancer Res* **68**(1): 98–105.

Shiota, M., Izumi, H., Tanimoto, A., Takahashi, M., Miyamoto, N., Kashiwagi, E., Kidani, A., Hirano, G., Masubuchi, D., Fukunaka, Y., Yasuniwa, Y., Naito, S., Nishizawa, S., Sasaguri, Y. & Kohno, K. (2009). Programmed cell death protein 4 down-regulates Y-box binding protein-1 expression via a direct interaction with Twist1 to suppress cancer cell growth, *Cancer Res* **69**(7): 3148–56.

Shiota, M., Yokomizo, A., Itsumi, M., Uchiumi, T., Tada, Y., Song, Y., Kashiwagi, E., Masubuchi, D. & Naito, S. (2010b). Twist1 and Y-box-binding protein-1 promote malignant potential in bladder cancer cells, *BJU Int* **108**(2 Pt 2): E142–9.

Shiota, M., Yokomizo, A., Tada, Y., Uchiumi, T., Inokuchi, J., Tatsugami, K., Kuroiwa, K., Yamamoto, K., Seki, N. & Naito, S. (2010a). P300/CBP-associated factor regulates Y-box binding protein-1 expression and promotes cancer cell growth, cancer invasion and drug resistance, *Cancer Sci* **101**(8): 1797–806.

Shiota, M., Zoubeidi, A., Kumano, M., Beraldi, E., Naito, S., Nelson, C. C., Sorensen, P. H. B. & Gleave, M. E. (2011). Clusterin is a critical downstream mediator of stress-induced YB-1 transactivation in prostate cancer, *Mol Cancer Res* **9**(12): 1755–66.

Shnyreva, M., Schullery, D. S., Suzuki, H., Higaki, Y. & Bomsztyk, K. (2000). Interaction of two multifunctional proteins. Heterogeneous nuclear ribonucleoprotein K and Y-box-binding protein, *J Biol Chem* **275**(20): 15498–503.

Shortt, J. & Johnstone, R. W. (2012). Oncogenes in cell survival and cell death, *Cold Spring Harb Perspect Biol* **4**(12): a009829.

Siddik, Z. H. (2003). Cisplatin: mode of cytotoxic action and molecular basis of resistance, *Oncogene* **22**(47): 7265–79.

Silva, J. C., Gorenstein, M. V., Li, G.-Z., Vissers, J. P. C. & Geromanos, S. J. (2006). Absolute quantification of proteins by LCMSE: a virtue of parallel MS acquisition, *Mol Cell Proteomics* **5**(1): 144–56.

Singh, A. & Settleman, J. (2010). EMT, cancer stem cells and drug resistance: an emerging axis of evil in the war on cancer, *Oncogene* **29**(34): 4741–51.

Sinnberg, T., Sauer, B., Holm, P., Spangler, B., Kuphal, S., Bosserhoff, A. & Schittek, B. (2012). MAPK and PI3K/AKT mediated YB-1 activation promotes melanoma cell proliferation which is counteracted by an autoregulatory loop, *Exp Dermatol* **21**(4): 265–70.

Skabkin, M. A., Evdokimova, V., Thomas, A. A. & Ovchinnikov, L. P. (2001). The major messenger ribonucleoprotein particle protein p50 (YB-1) promotes nucleic acid strand annealing, *J Biol Chem* **276**(48): 44841–7.

Skabkin, M. A., Kiselyova, O. I., Chernov, K. G., Sorokin, A. V., Dubrovin, E. V., Yaminsky, I. V., Vasiliev, V. D. & Ovchinnikov, L. P. (2004). Structural organization of mRNA complexes with major core mRNP protein YB-1, *Nucleic Acids Res* **32**(18): 5621–35.

Skabkina, O. V., Lyabin, D. N., Skabkin, M. A. & Ovchinnikov, L. P. (2005). YB-1 autoregulates translation of its own mRNA at or prior to the step of 40S ribosomal subunit joining, *Mol Cell Biol* **25**(8): 3317–23.

Skabkina, O. V., Skabkin, M. A., Popova, N. V., Lyabin, D. N., Penalva, L. O. & Ovchinnikov, L. P. (2003). Poly(A)-binding protein positively affects YB-1 mRNA translation through specific interaction with YB-1 mRNA, *J Biol Chem* **278**(20): 18191–8.

Skalweit, A., Doller, A., Huth, A., Kähne, T., Persson, P. B. & Thiele, B.-J. (2003). Posttranscriptional control of renin synthesis: identification of proteins interacting with renin mRNA 3'-untranslated region, *Circ Res* **92**(4): 419–27.

Skoko, N., Baralle, M., Buratti, E. & Baralle, F. E. (2008). The pathological splicing mutation c.6792C>G in NF1 exon 37 causes a change of tenancy between antagonistic splicing factors, *FEBS Lett* **582**(15): 2231–6.

Smith, D. & Johnson, K. (1988). Single-step purification of polypeptides expressed in Escherichia coli as fusions with glutathione S-transferase, *Gene* **67**(1): 31–40.

Smyth, D. R., Mrozkiewicz, M. K., McGrath, W. J., Listwan, P. & Kobe, B. (2003). Crystal structures of fusion proteins with large-affinity tags, *Protein Sci* **12**(7): 1313–22.

Snel, B., Lehmann, G., Bork, P. & Huynen, M. A. (2000). STRING: a web-server to retrieve and display the repeatedly occurring neighbourhood of a gene, *Nucleic Acids Res* **28**(18): 3442–4.

Söderberg, O., Leuchowius, K.-J., Gullberg, M., Jarvius, M., Weibrecht, I., Larsson, L.-G. & Landegren, U. (2008). Characterizing proteins and their interactions in cells and tissues using the in situ proximity ligation assay, *Methods* **45**(3): 227–32.

Somasekharan, S. P., El-Naggar, A., Leprivier, G., Cheng, H., Hajee, S., Grunewald, T. G. P., Zhang, F., Ng, T., Delattre, O., Evdokimova, V., Wang, Y., Gleave, M. & Sorensen, P. H. (2015). YB-1 regulates stress granule formation and tumor progression by translationally activating G3BP1, *J Cell Biol* **208**(7): 913–29.

Song, Y. H., Shiota, M., Yokomizo, A., Uchiumi, T., Kiyoshima, K., Kuroiwa, K., Oda, Y. & Naito, S. (2014). Twist1 and Y-box-binding protein-1 are potential prognostic factors in bladder cancer, *Urol Oncol* **32**(1): 31.e1–7.

Soop, T., Nashchekin, D., Zhao, J., Sun, X., Alzhanova-Ericsson, A. T., Björkroth, B., Ovchinnikov, L. & Daneholt, B. (2003). A p50-like Y-box protein with a putative translational role becomes associated with pre-mRNA concomitant with transcription, *J Cell Sci* **116**(Pt 8): 1493–503.

Sorokin, A. V., Selyutina, A. A., Skabkin, M. A., Guryanov, S. G., Nazimov, I. V., Richard, C., Th'ng, J., Yau, J., Sorensen, P. H. B., Ovchinnikov, L. P. & Evdokimova, V. (2005). Proteasome-mediated cleavage of the Y-box-binding protein 1 is linked to DNA-damage stress response, *EMBO J* **24**(20): 3602–12.

Spitkovsky, D. D., Royer-Pokora, B., Delius, H., Kisseljov, F., Jenkins, N. A., Gilbert, D. J., Copeland, N. G. & Royer, H. D. (1992). Tissue restricted expression and chromosomal localization of the YB-1 gene encoding a 42 kD nuclear CCAAT binding protein, *Nucleic Acids Res* **20**(4): 797–803.

Stein, U., Bergmann, S., Scheffer, G. L., Scheper, R. J., Royer, H.-D., Schlag, P. M. & Walther, W. (2005). YB-1 facilitates basal and 5-fluorouracil-inducible expression of the human major vault protein (MVP) gene, *Oncogene* **24**(22): 3606–18.

Stein, U., Jürchott, K., Walther, W., Bergmann, S., Schlag, P. M. & Royer, H. D. (2001). Hyperthermia-induced nuclear translocation of transcription factor YB-1 leads to enhanced expression of multidrug resistance-related ABC transporters, *J Biol Chem* **276**(30): 28562–9.

Stenina, O. I., Poptic, E. J. & DiCorleto, P. E. (2000). Thrombin activates a Y box-binding protein (DNA-binding protein B) in endothelial cells, *J Clin Invest* **106**(4): 579–87.

Stenina, O. I., Shaneyfelt, K. M. & DiCorleto, P. E. (2001). Thrombin induces the release of the Y-box protein dbpB from mRNA: a mechanism of transcriptional activation, *Proc Natl Acad Sci U S A* **98**(13): 7277–82.

Stickeler, E., Fraser, S. D., Honig, A., Chen, A. L., Berget, S. M. & Cooper, T. A. (2001). The RNA binding protein YB-1 binds A/C-rich exon enhancers and stimulates splicing of the CD44 alternative exon v4, *EMBO J* **20**(14): 3821–30.

Stratford, A. L., Fry, C. J., Desilets, C., Davies, A. H., Cho, Y. Y., Li, Y., Dong, Z., Berquin, I. M., Roux, P. P. & Dunn, S. E. (2008). Y-box binding protein-1 serine 102 is a downstream target of p90 ribosomal S6 kinase in basal-like breast cancer cells, *Breast Cancer Res* **10**(6): R99.

Stratford, A. L., Reipas, K., Hu, K., Fotovati, A., Brough, R., Frankum, J., Takhar, M., Watson, P., Ashworth, A., Lord, C. J., Lasham, A., Print, C. G. & Dunn, S. E. (2012). Targeting p90 ribosomal S6 kinase eliminates tumor-initiating cells by inactivating Y-box binding protein-1 in triple-negative breast cancers, *Stem Cells* **30**(7): 1338–48.

Subkhankulova, T., Mitchell, S. A. & Willis, A. E. (2001). Internal ribosome entry segment-mediated initiation of c-Myc protein synthesis following genotoxic stress, *Biochem J* **359**(Pt 1): 183–92.

Sugiyama, N., Masuda, T., Shinoda, K., Nakamura, A., Tomita, M. & Ishihama, Y. (2007). Phosphopeptide enrichment by aliphatic hydroxy acid-modified metal

oxide chromatography for nano-LC-MS/MS in proteomics applications, *Mol Cell Proteomics* **6**(6): 1103–9.

Sui, S., Wang, J., Yang, B., Song, L., Zhang, J., Chen, M., Liu, J., Lu, Z., Cai, Y., Chen, S., Bi, W., Zhu, Y., He, F. & Qian, X. (2008). Phosphoproteome analysis of the human Chang liver cells using SCX and a complementary mass spectrometric strategy, *Proteomics* **8**(10): 2024–34.

Sunayama, J., Ando, Y., Itoh, N., Tomiyama, A., Sakurada, K., Sugiyama, A., Kang, D., Tashiro, F., Gotoh, Y., Kuchino, Y. & Kitanaka, C. (2004). Physical and functional interaction between BH3-only protein Hrk and mitochondrial pore-forming protein p32, *Cell Death Differ* **11**(7): 771–81.

Sutherland, B. W., Kucab, J., Wu, J., Lee, C., Cheang, M. C. U., Yorida, E., Turbin, D., Dedhar, S., Nelson, C., Pollak, M., Leighton Grimes, H., Miller, K., Badve, S., Huntsman, D., Blake-Gilks, C., Chen, M., Pallen, C. J. & Dunn, S. E. (2005). Akt phosphorylates the Y-box binding protein 1 at Ser102 located in the cold shock domain and affects the anchorage-independent growth of breast cancer cells, *Oncogene* **24**(26): 4281–92.

Sutherland, B. W., Toews, J. & Kast, J. (2008). Utility of formaldehyde cross-linking and mass spectrometry in the study of protein-protein interactions, *J Mass Spectrom* **43**(6): 699–715.

Svitkin, Y. V., Evdokimova, V. M., Brasey, A., Pestova, T. V., Fantus, D., Yanagiya, A., Imataka, H., Skabkin, M. A., Ovchinnikov, L. P., Merrick, W. C. & Sonenberg, N. (2009). General RNA-binding proteins have a function in poly(A)-binding protein-dependent translation, *EMBO J* **28**(1): 58–68.

Svitkin, Y. V., Ovchinnikov, L. P., Dreyfuss, G. & Sonenberg, N. (1996). General RNA binding proteins render translation cap dependent, *EMBO J* **15**(24): 7147–55.

Swamy, M., Siegers, G. M., Minguet, S., Wollscheid, B. & Schamel, W. W. A. (2006). Blue native polyacrylamide gel electrophoresis (BN-PAGE) for the identification and analysis of multiprotein complexes, *Sci. STKE* **2006**(345): pl4.

Swamynathan, S. K., Nambiar, A. & Guntaka, R. V. (1998). Role of single-stranded DNA regions and Y-box proteins in transcriptional regulation of viral and cellular genes, *FASEB J* **12**(7): 515–22.

Swamynathan, S. K., Varma, B. R., Weber, K. T. & Guntaka, R. V. (2002). Targeted disruption of one allele of the Y-box protein gene, Chk-YB-1b, in DT40 cells results in major defects in cell cycle, *Biochem Biophys Res Commun* **296**(2): 451–7.

Szklarczyk, D., Franceschini, A., Wyder, S., Forslund, K., Heller, D., Huerta-Cepas, J., Simonovic, M., Roth, A., Santos, A., Tsafou, K. P., Kuhn, M., Bork, P.,

Jensen, L. J. & von Mering, C. (2015). STRING v10: protein-protein interaction networks, integrated over the tree of life, *Nucleic Acids Res* **43**(Database issue): D447–52.

Tacar, O., Sriamornsak, P. & Dass, C. R. (2013). Doxorubicin: an update on anticancer molecular action, toxicity and novel drug delivery systems, *J Pharm Pharmacol* **65**(2): 157–70.

Tafuri, S. R. & Wolffe, A. P. (1992). DNA binding, multimerization, and transcription stimulation by the Xenopus Y box proteins in vitro, *New Biol* **4**(4): 349–59.

Tafuri, S. R. & Wolffe, A. P. (1993). Selective recruitment of masked maternal mRNA from messenger ribonucleoprotein particles containing FRGY2 (mRNP4), *J Biol Chem* **268**(32): 24255–61.

Tanaka, M., Sasaki, K., Kamata, R., Hoshino, Y., Yanagihara, K. & Sakai, R. (2009). A novel RNA-binding protein, Ossa/C9orf10, regulates activity of Src kinases to protect cells from oxidative stress-induced apoptosis, *Mol Cell Biol* **29**(2): 402–13.

Tanaka, T., Ohashi, S. & Kobayashi, S. (2014). Roles of YB-1 under arsenite-induced stress: translational activation of HSP70 mRNA and control of the number of stress granules, *Biochim Biophys Acta* **1840**(3): 985–92.

Tang, Y., Li, M. & Wang, J. (2015). CytoNCA: a cytoscape plugin for centrality analysis and evaluation of biological network, *Biosystems* **127**: 67–72.

Taube, S. E., Jacobson, J. W. & Lively, T. G. (2005). Cancer diagnostics: decision criteria for marker utilization in the clinic, *Am J Pharmacogenomics* **5**(6): 357–64.

The Open Microscopy Environment (2016). University of dundee and open microscopy environment.
URL: *http://downloads.openmicroscopy.org/bio-formats/5.1.10/*

Thoreen, C. C., Chantranupong, L., Keys, H. R., Wang, T., Gray, N. S. & Sabatini, D. M. (2012). A unifying model for mTORC1-mediated regulation of mRNA translation, *Nature* **485**(7396): 109–13.

To, K., Fotovati, A., Reipas, K. M., Law, J. H., Hu, K., Wang, J., Astanehe, A., Davies, A. H., Lee, L., Stratford, A. L., Raouf, A., Johnson, P., Berquin, I. M., Royer, H.-D., Eaves, C. J. & Dunn, S. E. (2010). Y-box binding protein-1 induces the expression of CD44 and CD49f leading to enhanced self-renewal, mammosphere growth, and drug resistance, *Cancer Res* **70**(7): 2840–51.

To, K., Zhao, Y., Jiang, H., Hu, K., Wang, M., Wu, J., Lee, C., Yokom, D. W., Stratford, A. L., Klinge, U., Mertens, P. R., Chen, C. S., Bally, M., Yapp, D. & Dunn, S. E. (2007). The phosphoinositide-dependent kinase-1 inhibitor 2-amino-N-[4-[5-(2-phenanthrenyl)-3-(trifluoromethyl)-1H-pyrazol-1-yl]phenyl]-acetamide (OSU-03012) prevents Y-box binding protein-1 from inducing epidermal growth factor receptor, *Mol Pharmacol* **72**(3): 641–52.

Toh, S., Nakamura, T., Ohga, T., Koike, K., Uchiumi, T., Wada, M., Kuwano, M. & Kohno, K. (1998). Genomic organization of the human Y-box protein (YB-1) gene, *Gene* **206**(1): 93–7.

Toulany, M., Schickfluß, T.-A., Eicheler, W., Kehlbach, R., Schittek, B. & Rodemann, H. P. (2011). Impact of oncogenic K-RAS on YB-1 phosphorylation induced by ionizing radiation, *Breast Cancer Res* **13**(2): R28.

Towbin, H., Staehelin, T. & Gordon, J. (1979). Electrophoretic transfer of proteins from polyacrylamide gels to nitrocellulose sheets: procedure and some applications, *Proc Natl Acad Sci U S A* **76**(9): 4350–4.

Tsai, C.-F., Wang, Y.-T., Chen, Y.-R., Lai, C.-Y., Lin, P.-Y., Pan, K.-T., Chen, J.-Y., Khoo, K.-H. & Chen, Y.-J. (2008). Immobilized metal affinity chromatography revisited: pH/acid control toward high selectivity in phosphoproteomics, *J Proteome Res* **7**(9): 4058–69.

Tsofack, S. P., Garand, C., Sereduk, C., Chow, D., Aziz, M., Guay, D., Yin, H. H. & Lebel, M. (2011). NONO and RALY proteins are required for YB-1 oxaliplatin induced resistance in colon adenocarcinoma cell lines, *Mol Cancer* **10**(1): 145.

Tsofack, S. P., Meunier, L., Sanchez, L., Madore, J., Provencher, D., Mes-Masson, A.-M. & Lebel, M. (2013). Low expression of the X-linked ribosomal protein S4 in human serous epithelial ovarian cancer is associated with a poor prognosis, *BMC Cancer* **13**: 303.

Turashvili, G., McKinney, S. E., Goktepe, O., Leung, S. C., Huntsman, D. G., Gelmon, K. A., Los, G., Rejto, P. A. & Aparicio, S. A. J. R. (2011). P-cadherin expression as a prognostic biomarker in a 3992 case tissue microarray series of breast cancer, *Mod Pathol* **24**(1): 64–81.

Uramoto, H., Izumi, H., Ise, T., Tada, M., Uchiumi, T., Kuwano, M., Yasumoto, K., Funa, K. & Kohno, K. (2002). p73 Interacts with c-Myc to regulate Y-box-binding protein-1 expression, *J Biol Chem* **277**(35): 31694–702.

Vaiman, A. V., Stromskaya, T. P., Rybalkina, E. Y., Sorokin, A. V., Ovchinnikov, L. P. & Stavrovskaya, A. A. (2007). Development of drug resistance in the population of colon cancer cells under the effect of multifunctional protein YB-1, *Bull Exp Biol Med* **143**(4): 463–6.

Van Dongen, S. (2000). *Graph Clustering by Flow Simulation*, PhD thesis, University of Utrecht.

Van Dongen, S. (2012). Mcl - a cluster algorithm for graphs.
URL: *http://micans.org/mcl/*

Van Hoof, D., Muñoz, J., Braam, S. R., Pinkse, M. W. H., Linding, R., Heck, A. J. R., Mummery, C. L. & Krijgsveld, J. (2009). Phosphorylation dynamics during early differentiation of human embryonic stem cells, *Cell Stem Cell* **5**(2): 214–26.

van Roeyen, C. R. C., Scurt, F. G., Brandt, S., Kuhl, V. A., Martinkus, S., Djudjaj, S., Raffetseder, U., Royer, H.-D., Stefanidis, I., Dunn, S. E., Dooley, S., Weng, H., Fischer, T., Lindquist, J. A. & Mertens, P. R. (2013). Cold shock Y-box protein-1 proteolysis autoregulates its transcriptional activities, *Cell Commun Signal* **11**: 63.

Vicier, C., Dieci, M. V., Arnedos, M., Delaloge, S., Viens, P. & Andre, F. (2014). Clinical development of mtor inhibitors in breast cancer, *Breast Cancer Res* **16**(1): 203.

Vita, M. & Henriksson, M. (2006). The Myc oncoprotein as a therapeutic target for human cancer, *Semin Cancer Biol* **16**(4): 318–30.

Vogel, C., Abreu, R. d. S., Ko, D., Le, S.-Y., Shapiro, B. A., Burns, S. C., Sandhu, D., Boutz, D. R., Marcotte, E. M. & Penalva, L. O. (2010). Sequence signatures and mRNA concentration can explain two-thirds of protein abundance variation in a human cell line, *Mol Syst Biol* **6**: 400.

Vogelstein, B., Papadopoulos, N., Velculescu, V. E., Zhou, S., Diaz, Jr, L. A. & Kinzler, K. W. (2013). Cancer genome landscapes, *Science* **339**(6127): 1546–58.

von Mering, C., Huynen, M., Jaeggi, D., Schmidt, S., Bork, P. & Snel, B. (2003). STRING: a database of predicted functional associations between proteins, *Nucleic Acids Res* **31**(1): 258–61.

von Mering, C., Krause, R., Snel, B., Cornell, M., Oliver, S. G., Fields, S. & Bork, P. (2002). Comparative assessment of large-scale data sets of protein-protein interactions, *Nature* **417**(6887): 399–403.

Wang, C., Rauscher, F. J., Cress, W. D. & Chen, J. (2007). Regulation of E2F1 function by the nuclear corepressor KAP1, *J Biol Chem* **282**(41): 29902–9.

Wang, N., Yamanaka, K. & Inouye, M. (2000). Acquisition of double-stranded DNA-binding ability in a hybrid protein between Escherichia coli CspA and the cold shock domain of human YB-1, *Mol Microbiol* **38**(3): 526–34.

Wang, X., Guo, X.-B., Shen, X.-C., Zhou, H., Wan, D.-W., Xue, X.-F., Han, Y., Yuan, B., Zhou, J., Zhao, H., Zhi, Q.-M. & Kuang, Y.-T. (2015). Prognostic role of YB-1 expression in breast cancer: a meta-analysis, *Int J Clin Exp Med* **8**(2): 1780–91.

Wang, Y., Arribas-Layton, M., Chen, Y., Lykke-Andersen, J. & Sen, G. L. (2015b). DDX6 orchestrates mammalian progenitor function through the mRNA degradation and translation pathways, *Mol Cell* **60**(1): 118–30.

Wang, Y., Chen, Y., Geng, H., Qi, C., Liu, Y. & Yue, D. (2015a). Overexpression of YB1 and EZH2 are associated with cancer metastasis and poor prognosis in renal cell carcinomas, *Tumour Biol* **36**(9): 7159–66.

Wang, Y., Xiao, X., Zhang, J., Choudhury, R., Robertson, A., Li, K., Ma, M., Burge, C. B. & Wang, Z. (2013). A complex network of factors with overlapping affinities represses splicing through intronic elements, *Nat Struct Mol Biol* **20**(1): 36–45.

Ward, E. M., DeSantis, C. E., Lin, C. C., Kramer, J. L., Jemal, A., Kohler, B., Brawley, O. W. & Gansler, T. (2015). Cancer statistics: breast cancer in situ, *CA Cancer J Clin* **65**(6): 481–95.

Warnes, G. R., Bolker, B., Bonebakker, L., Gentleman, R., Huber, W., Liaw, A., Lumley, T., Maechler, M., Magnusson, A., Moeller, S. et al. (n.d.). gplots: various R programming tools for plotting data, *R package version* .
URL: *https://CRAN.R-project.org/package=gplots*

Watermann, D. O., Tang, Y., Zur Hausen, A., Jäger, M., Stamm, S. & Stickeler, E. (2006). Splicing factor Tra2-beta1 is specifically induced in breast cancer and regulates alternative splicing of the CD44 gene, *Cancer Res* **66**(9): 4774–80.

Weber, K. & Osborn, M. (1969). The reliability of molecular weight determinations by dodecyl sulfate-polyacrylamide gel electrophoresis, *J Biol Chem* **244**: 4406–12.

Wehner, K. A., Schütz, S. & Sarnow, P. (2010). OGFOD1, a novel modulator of eukaryotic translation initiation factor 2alpha phosphorylation and the cellular response to stress, *Mol Cell Biol* **30**(8): 2006–16.

Weidensdorfer, D., Stöhr, N., Baude, A., Lederer, M., Köhn, M., Schierhorn, A., Buchmeier, S., Wahle, E. & Hüttelmaier, S. (2009). Control of c-myc mRNA stability by IGF2BP1-associated cytoplasmic RNPs, *RNA* **15**(1): 104–15.

Weigelt, B., Horlings, H. M., Kreike, B., Hayes, M. M., Hauptmann, M., Wessels, L. F. A., de Jong, D., Van de Vijver, M. J., Van't Veer, L. J. & Peterse, J. L. (2008). Refinement of breast cancer classification by molecular characterization of histological special types, *J Pathol* **216**(2): 141–50.

Weigelt, B., Peterse, J. L. & Van't Veer, L. J. (2005). Breast cancer metastasis: markers and models, *Nat Rev Cancer* **5**(8): 591–602.

White, D., Rafalska-Metcalf, I. U., Ivanov, A. V., Corsinotti, A., Peng, H., Lee, S. C., Trono, D., Janicki, S. M. & Rauscher, F. J. (2012). The ATM substrate KAP1 controls DNA repair in heterochromatin: regulation by HP1 proteins and serine 473/824 phosphorylation, *Mol Cancer Res* **10**(3): 401–14.

Wickham, H. (2007). Reshaping Data with the reshape package, *Journal of Statistical Software* **21**(12): 1–20.

Wickham, H. (2009). *ggplot2: elegant graphics for data analysis*, Springer-Verlag New York.

Wickham, H. & Francois, R. (2016). dplyr: a grammar of data manipulation.
URL: *https://github.com/hadley/dplyr*

Wilhelm, M., Schlegl, J., Hahne, H., Moghaddas Gholami, A., Lieberenz, M., Savitski, M. M., Ziegler, E., Butzmann, L., Gessulat, S., Marx, H., Mathieson, T., Lemeer, S., Schnatbaum, K., Reimer, U., Wenschuh, H., Mollenhauer, M., Slotta-Huspenina, J., Boese, J.-H., Bantscheff, M., Gerstmair, A., Faerber, F. & Kuster, B. (2014). Mass-spectrometry-based draft of the human proteome, *Nature* **509**(7502): 582–7.

Wolf, E., Kastner, B., Deckert, J., Merz, C., Stark, H. & Luhrmann, R. (2009). Exon, intron and splice site locations in the spliceosomal B complex, *EMBO J* **28**(15): 2283–92.

Wolf, G., Greenberg, D. & Macfarlan, T. S. (2015). Spotting the enemy within: targeted silencing of foreign DNA in mammalian genomes by the Krüppel-associated box zinc finger protein family, *Mob DNA* **6**: 17.

Wolffe, A. P. (1994). Structural and functional properties of the evolutionarily ancient Y-box family of nucleic acid binding proteins, *Bioessays* **16**(4): 245–51.

Woolley, A. G., Algie, M., Samuel, W., Harfoot, R., Wiles, A., Hung, N. A., Tan, P.-H., Hains, P., Valova, V. A., Huschtscha, L., Royds, J. A., Perez, D., Yoon, H.-S., Cohen, S. B., Robinson, P. J., Bay, B.-H., Lasham, A. & Braithwaite, A. W. (2011). Prognostic association of YB-1 expression in breast cancers: a matter of antibody, *PLoS ONE* **6**(6): 20603.

Woźniak, M., Hotowy, K., Czapińska, E., Duś-Szachniewicz, K., Szczuka, I., Gamian, E., Gamian, A., Terlecki, G. & Ziółkowski, P. (2014). Early induction of stress-associated Src activator/Homo sapiens chromosome 9 open reading frame 10 protein following photodynamic therapy, *Photodiagnosis Photodyn Ther* **11**(1): 27–33.

Wu, J., Lee, C., Yokom, D., Jiang, H., Cheang, M. C. U., Yorida, E., Turbin, D., Berquin, I. M., Mertens, P. R., Iftner, T., Gilks, C. B. & Dunn, S. E. (2006). Disruption of the Y-box binding protein-1 results in suppression of the epidermal growth factor receptor and HER-2, *Cancer Res* **66**(9): 4872–9.

Wu, Y., Wang, K.-y., Li, Z., Liu, Y.-p., Izumi, H., Uramoto, H., Nakayama, Y., Ito, K.-i. & Kohno, K. (2014). Y-box binding protein 1 enhances DNA topoisomerase 1 activity and sensitivity to camptothecin via direct interaction, *J Exp Clin Cancer Res* **33**(1): 112.

Wu, Y., Yamada, S., Izumi, H., Li, Z., Shimajiri, S., Wang, K.-Y., Liu, Y.-P., Kohno, K. & Sasaguri, Y. (2012). Strong YB-1 expression is associated with liver metastasis progression and predicts shorter disease-free survival in advanced gastric cancer, *J Surg Oncol* **105**(7): 724–30.

Xu, W., Zhou, L., Qin, R., Tang, H. & Shen, H. (2009). Nuclear expression of YB-1 in diffuse large B-cell lymphoma: correlation with disease activity and patient outcome, *Eur J Haematol* **83**(4): 313–9.

Yahata, H., Kobayashi, H., Kamura, T., Amada, S., Hirakawa, T., Kohno, K., Kuwano, M. & Nakano, H. (2002). Increased nuclear localization of transcription factor YB-1 in acquired cisplatin-resistant ovarian cancer, *J Cancer Res Clin Oncol* **128**(11): 621–6.

Yan, K.-K., Fang, G., Bhardwaj, N., Alexander, R. P. & Gerstein, M. (2010). Comparing genomes to computer operating systems in terms of the topology and evolution of their regulatory control networks, *Proc Natl Acad Sci U S A* **107**(20): 9186–91.

Yan, X.-B., Zhu, Q.-C., Chen, H.-Q., Peng, J.-Y., Chao, H.-L., Du, H.-X., Wang, Z.-G. & Jin, Z.-M. (2014). Knockdown of Y-box-binding protein-1 inhibits the malignant progression of HT-29 colorectal adenocarcinoma cells by reversing epithelial-mesenchymal transition, *Mol Med Rep* **10**(5): 2720–8.

Yang, J. Y., Ha, S.-A., Yang, Y.-S. & Kim, J. W. (2010). p-Glycoprotein ABCB5 and YB-1 expression plays a role in increased heterogeneity of breast cancer cells: correlations with cell fusion and doxorubicin resistance, *BMC Cancer* **10**: 388.

Yang, W.-H. & Bloch, D. B. (2007). Probing the mRNA processing body using protein macroarrays and "autoantigenomics", *RNA* **13**(5): 704–12.

Yokoyama, H., Harigae, H., Takahashi, S., Takahashi, S., Furuyama, K., Kaku, M., Yamamoto, M. & Sasaki, T. (2003). Regulation of YB-1 gene expression by GATA transcription factors, *Biochem Biophys Res Commun* **303**(1): 140–5.

Yoon, J. S. (2015). AllegroLayout (v2.2.2), AllegoViva.

Yu, H., Kim, P. M., Sprecher, E., Trifonov, V. & Gerstein, M. (2007). The importance of bottlenecks in protein networks: correlation with gene essentiality and expression dynamics, *PLoS Comput Biol* **3**(4): e59.

Yu, Y.-N., Yip, G. W.-C., Tan, P.-H., Thike, A. A., Matsumoto, K., Tsujimoto, M. & Bay, B.-H. (2010). Y-box binding protein 1 is up-regulated in proliferative breast cancer and its inhibition deregulates the cell cycle, *Int J Oncol* **37**(2): 483–92.

Yuan, L., Xiao, Y., Zhou, Q., Yuan, D., Wu, B., Chen, G. & Zhou, J. (2014). Proteomic analysis reveals that MAEL, a component of nuage, interacts with stress granule proteins in cancer cells, *Oncol Rep* **31**(1): 342–50.

Zaccara, S., Tebaldi, T., Pederiva, C., Ciribilli, Y., Bisio, A. & Inga, A. (2014). p53-directed translational control can shape and expand the universe of p53 target genes, *Cell Death Differ* **21**(10): 1522–34.

Zaidi, S., Blanchard, M., Shim, K., Ilett, E., Rajani, K., Parrish, C., Boisgerault, N., Kottke, T., Thompson, J., Celis, E., Pulido, J., Selby, P., Pandha, H., Melcher, A., Harrington, K. & Vile, R. (2015). Mutated BRAF emerges as a major effector of recurrence in a murine melanoma model after treatment with immunomodulatory agents, *Mol Ther* **23**(5): 845–56.

Zasedateleva, O. A., Krylov, A. S., Prokopenko, D. V., Skabkin, M. A., Ovchinnikov, L. P., Kolchinsky, A. & Mirzabekov, A. D. (2002). Specificity of mammalian Y-box binding protein p50 in interaction with ss and ds DNA analyzed with generic oligonucleotide microchip, *J Mol Biol* **324**(1): 73–87.

Zhang, Y. F., Homer, C., Edwards, S. J., Hananeia, L., Lasham, A., Royds, J., Sheard, P. & Braithwaite, A. W. (2003). Nuclear localization of Y-box factor YB1 requires wild-type p53, *Oncogene* **22**(18): 2782–94.

Zheng, Y.-H., Yu, H.-F. & Peterlin, B. M. (2003). Human p32 protein relieves a post-transcriptional block to HIV replication in murine cells, *Nat Cell Biol* **5**(7): 611–8.

Znojek, P. J. (2012). *Investigation of the role of poly (ADP-ribose) polymerase inhibition in topoisomerase I poison-induced cytotoxicity*, PhD thesis, Northern Institute for Cancer Research.

Zou, Y. & Chien, K. R. (1995). EFIA/YB-1 is a component of cardiac HF-1A binding activity and positively regulates transcription of the myosin light-chain 2v gene, *Mol Cell Biol* **15**(6): 2972–82.

Appendices

Appendix A

Analysing peptides using mass spectrometry

A.1 Mass spectrometry; shotgun sequencing

A brief overview of a typical LC-MS/MS experiment is required to better understand the results from LC-MS/MS. Liquid chromatography is used to separate peptides from one another based on alterations to their interaction with the column material as the mobile solvent phase is changed (**Figure A.1.A**). During chromatography, the mass spectrometer cycles between two types of scan. The first is a survey scan (MS^1) of all positively-charged ions that are entering the mass spectrometer at that time. The second type are MS/MS scans (MS^2) that provide information about the structure, or sequence, of the selected precursor. The MS^1 scans measure the mass over charge (m/z) and intensity of all detectable ions that are entering the mass spectrometer at that time (**Figure A.1.B**). The ions detected in the MS^1 scan are referred to as parent or precursor ions. Following the MS^1 scan, MS^2 fragment spectra are generated from the most intense parent ions that were detected in the MS^1 scan (annotated in **Figure A.1.B**). LC-MS/MS programs usually exclude precursors from further MS^2 scans for a short time once 1 - 2 MS^2 scans have been made. The machine uses these rules to collect multiple MS/MS fragment spectra between each MS^1 scan throughout the run. During shotgun mass spectrometry, the machine setup aims produce high quality MS^2 scans of the maximum number of peptides during each run.

The MS^1 scans record the intensity of precursor ions during the LC-MS/MS run. A plot of the intensity of a precursor over sequential MS^1 scans is known

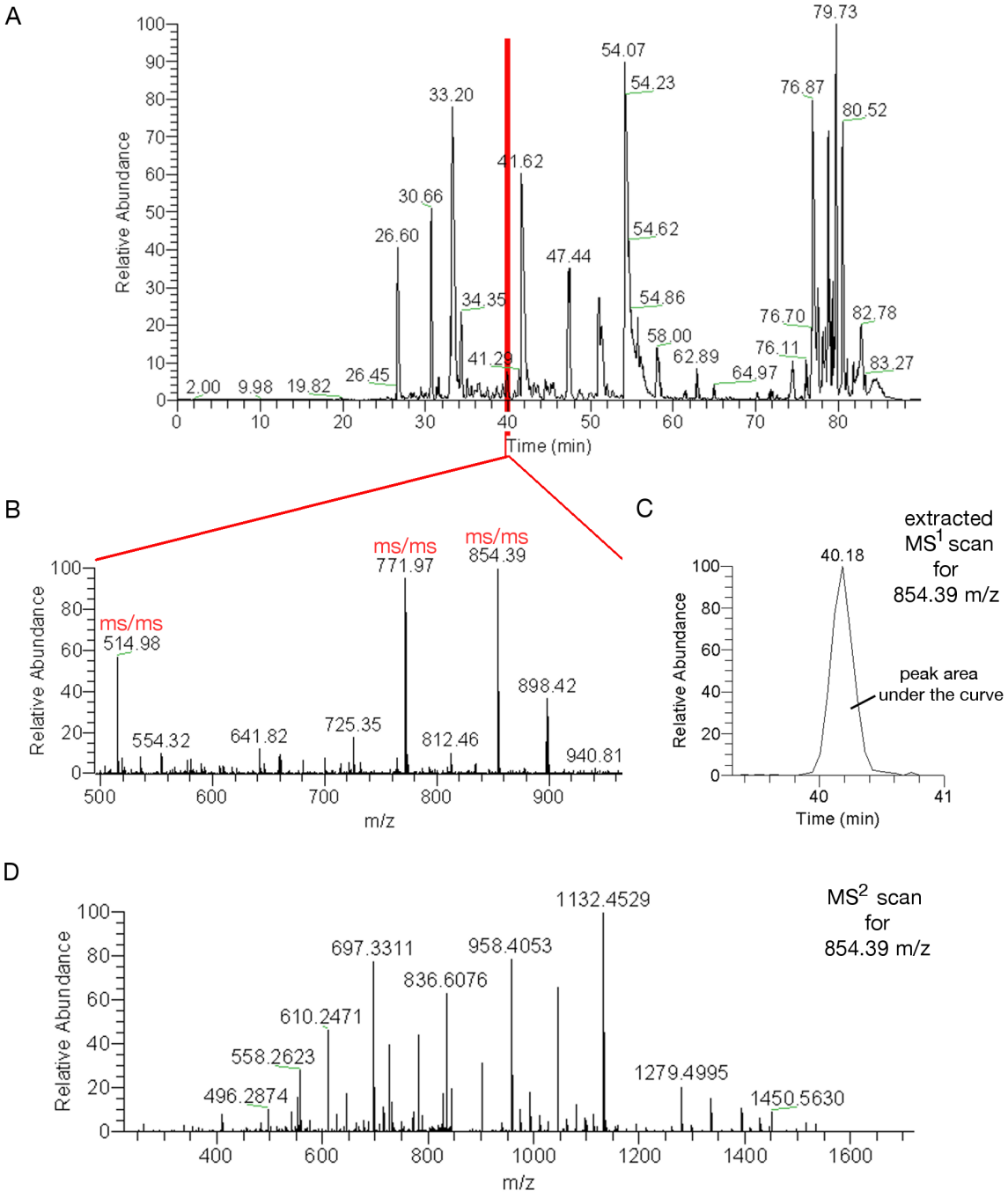

Figure A.1: The basic principles of shotgun sequencing using LC-MS/MS. **A**, a chromatogram showing the material that elutes of a C18 column during an LC-MS/MS run. **B**, MS^1 survey scans provide information about the peptide ions, and other ions, entering the mass spectrometer at a given point in the LC-MS/MS run. **C**, the plotted intensity of the MS^1 survey scans for a peptide (854.39 m/z in the MS^1 scan in **B**). The peak area under the curve (annotated) provides quantitative information for the plotted peptide ion. **D**, MS^2 collision-induced disassociation (CID) spectrum of 854.39 m/z precursor showing the specific fragment ions which reveal amino acid sequence information.

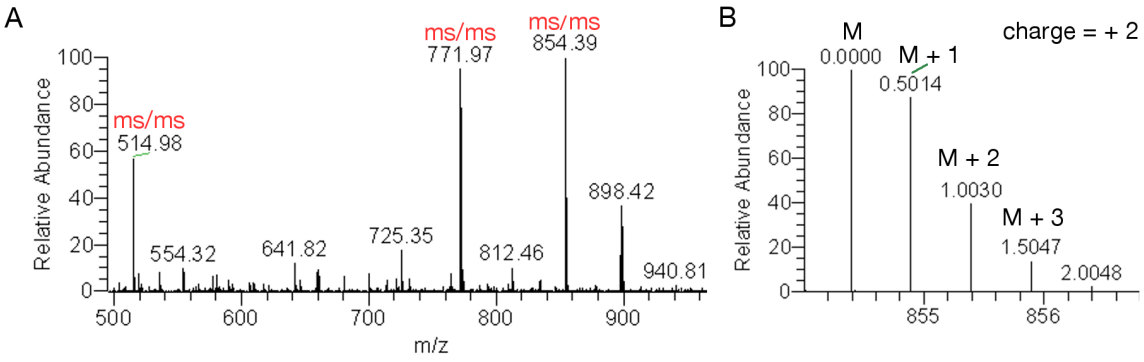

Figure A.2: The isotope peaks in a MS^1 survey scan can be used to gain information about the charge state of ions. **A**, MS^1 survey scans provide information about the peptide ions, and other ions, entering the mass spectrometer at a given point in the LC-MS/MS run. **B**, the isotopic envelope of a peptide (854.39 m/z) from the MS^1 scan (**A**).

as an extracted ion chromatogram (XIC) (**Figure A.1.C**). The area under the elution peak of a precursor in a XIC plot reflects the quantity of the precursor ion. Where an MS^2 spectrum has been attributed to a peptide sequence, the peak area measurements from the corresponding XIC can be assigned to that peptide. The average peak area of the three most abundant peptides assigned to a protein can be used to estimate the amount of a protein that is present (Silva et al. 2006).

Peptides include heavy stable isotopes of the elements, such as C^{13}m N^{15}, O^{17}, and S^{34}, at a rate that reflects the natural abundance of the isotopes. The presence of heavy isotopes in peptides means that precursor ions exist as a monoisotopic peak (M) with no heavy elements followed by other peaks at +1 Da intervals (**Figure A.2.B**). The first peak that follows the monoisotopic peak is the population of peptides with 1 heavy isotope, referred to as M+1. The second peak, referred to as M+2, is comprised of peptides that include 2 heavy isotopes. Thus larger molecules contain more and stronger isotope peaks because there is a higher probability that they contain stable heavy isotopes compared to smaller molecules with less atoms. The intensity of each isotope peak (M, M+1, M+2, ...M+n) can be predicted from the elemental structure of the precursor and the rate at which heavy isotopes occur in nature.

To create the fragment ions, or peptide fragments, that comprise MS^2 spectra, the parent ion is fragmented using collision-induced dissociation (CID). The fragment spectra reveal sequence information for peptide identification. During CID, peptides tend to fragment at amide bonds. Only the fragments that retain the charge can be measured. Peptide fragments that retain the charge on their N-terminus are referred to as b-ions. B-ion fragments are numbered starting at the first amino acid

at the N-terminus (b-1). Peptide fragments that have retained the charge on their C-terminus are known as y-ions and the numbering for y-ion fragments starts at the first amino acid at the C-terminus (the full notation is outlined in Biemann 1990).

A.1.1 Analysis of phosphorylated peptides, neutral losses

The detection of phosphorylated peptides during LC-MS/MS relies on the 80 Da increase in mass that the addition of HPO_3 confers to parent and fragment ions. However, analysis of phosphorylation using LC-MS/MS is complicated by the tendency of the phosphate group to be lost (fragmented) from some parent ions and ion fragments during mass analysis. This process is referred to as neutral loss. Neutral loss from phosphorylated ions have a mass of -80 Da when HPO_3 is lost, or -97.9769 Da when H_3PO_4 is lost. Ions that have lost HPO_3 are problematic as their mass then matches a peptide fragment with no phosphorylation. The neutral loss of H_3PO_4 can be detected as a loss of 97.9769 Da from phosphorylated ions. Following a neutral loss of H_3PO_4, the mass of phosphorylated peptide fragments is shifted by -18.0106 Da relative to unmodified peptide fragments. This leaves a dehydro amino acid at the site of phosphorylation.

Appendix B

Protein interactions of YB-1 in A549 and MDA-MB231 cells.

Table B.1: Proteins that interact with YB-1 in A549 and MDA-MB231 cells.

Accession	Gene	Protein	Sum proteins	SumPSMs	MDA-CYTO	A549-CYTO	MDA-NUC	A559-NUC
P67809	YBX1	Nuclease-sensitive element-binding protein 1	1	2350	1	1	1	1
P04264	KRT1	Keratin, type II cytoskeletal 1	1	4678	1	1	1	1
P11940	PABPC1	Polyadenylate-binding protein 1	2	4059	1	1	1	1
P13645	KRT10	Keratin, type I cytoskeletal 10	1	3119	1	1	1	1
P35527	KRT9	Keratin, type I cytoskeletal 9	1	2623	1	1	1	1
P35908	KRT2	Keratin, type II cytoskeletal 2 epidermal	1	2620	1	1	1	1
Q13310	PABPC4	Isoform 2 of Polyadenylate-binding protein 4	3	2591	1	1	1	1
Q92900	UPF1	Isoform 2 of Regulator of nonsense transcripts 1	4	1380	1	1	1	1
P60709	ACTB	Actin, cytoplasmic 1	2	1101	1	1	1	1
P02533	KRT14	Keratin, type I cytoskeletal 14	1	1090	1	1	1	1
P08779	KRT16	Keratin, type I cytoskeletal 16	1	1067	1	1	1	1
P13647	KRT5	Keratin, type II cytoskeletal 5	1	1056	1	1	1	1
P23396	RPS3	40S ribosomal protein S3	1	1033	1	1	1	1
O00425	IGF2BP3	Insulin-like growth factor 2 mRNA-binding protein 3	1	1011	1	1	1	1
Q6PKG0	LARP1	La-related protein 1	2	997	1	1	1	1
P11142	HSPA8	Heat shock cognate 71 kDa protein	2	853	1	1	1	1
P04259	KRT6B	Keratin, type II cytoskeletal 6B	1	820	1	1	1	1
Q13501	SQSTM1	Sequestosome-1	1	801	1	1	1	1
O60506	SYNCRIP	Isoform 3 of Heterogeneous nuclear ribonucleoprotein Q	5	796	1	1	1	1
P61247	RPS3A	40S ribosomal protein S3a	1	670	1	1	1	1
Q9HCE1	MOV10	Putative helicase MOV-10	1	663	1	1	1	1
Q9NZB2	FAM120A	Constitutive coactivator of PPAR-gamma-like protein 1	3	643	1	1	1	1

P08670	VIM	Vimentin	1	612	1	1	1	1
P68363	TUBA1B	Tubulin alpha-1B chain	3	605	1	1	1	1
P07437	TUBB	Tubulin beta chain	1	604	1	1	1	1
O00571	DDX3X	Isoform 2 of ATP-dependent RNA helicase DDX3X	2	590	1	1	1	1
P46781	RPS9	40S ribosomal protein S9	1	567	1	1	1	1
Q15149	PLEC	Plectin	9	547	1	1	1	1
P15880	RPS2	40S ribosomal protein S2	1	538	1	1	1	1
P05787	KRT8	Keratin, type II cytoskeletal 8	1	534	1	1	1	1
P62701	RPS4X	40S ribosomal protein S4, X isoform	1	528	1	1	1	1
P39023	RPL3	60S ribosomal protein L3	2	509	1	1	1	1
P07910	HNRNPC	Isoform C1 of Heterogeneous nuclear ribonucleoproteins C1/C2	3	502	1	1	1	1
P17844	DDX5	Probable ATP-dependent RNA helicase DDX5	1	482	1	1	1	1
P62249	RPS16	40S ribosomal protein S16	1	475	1	1	1	1
P61978	HNRNPK	Heterogeneous nuclear ribonucleoprotein K	3	468	1	1	1	1
P62979	RPS27A	Ubiquitin-40S ribosomal protein S27a	4	463	1	1	1	1
P62753	RPS6	40S ribosomal protein S6	1	447	1	1	1	1
P62241	RPS8	40S ribosomal protein S8	1	412	1	1	1	1
P52272	HNRNPM	Heterogeneous nuclear ribonucleoprotein M	2	394	1	1	1	1
Q00577	PURA	Transcriptional activator protein Pur-alpha	1	389	1	1	1	1
Q15717	ELAVL1	ELAV-like protein 1	1	356	1	1	1	1
Q7L2E3	DHX30	Isoform 3 of Putative ATP-dependent RNA helicase DHX30	3	355	1	1	1	1
P31943	HNRNPH1	Heterogeneous nuclear ribonucleoprotein H	1	353	1	1	1	1
P43243	MATR3	Matrin-3	1	348	1	1	1	1
P08729	KRT7	Keratin, type II cytoskeletal 7	1	343	1	1	1	1
Q13283	G3BP1	Ras GTPase-activating protein-binding protein 1	1	341	1	1	1	1
P63244	GNB2L1	Guanine nucleotide-binding protein subunit beta-2-like 1	1	340	1	1	1	1
P08865	RPSA	40S ribosomal protein SA	1	326	1	1	1	1
P46782	RPS5	40S ribosomal protein S5	1	322	1	1	1	1
P11021	HSPA5	78 kDa glucose-regulated protein	1	319	1	1	1	1

P26373	RPL13	60S ribosomal protein L13	1	312	1	1	1	1
P05388	RPLP0	60S acidic ribosomal protein P0	2	308	1	1	1	1
P27635	RPL10	60S ribosomal protein L10	1	296	1	1	1	1
P51114	FXR1	Fragile X mental retardation syndrome-related protein 1	2	291	1	1	1	1
P26196	DDX6	Probable ATP-dependent RNA helicase DDX6	1	277	1	1	1	1
P62917	RPL8	60S ribosomal protein L8	1	274	1	1	1	1
P46777	RPL5	60S ribosomal protein L5	1	274	1	1	1	1
P02768	ALB	Serum albumin	2	272	1	1	1	1
P18124	RPL7	60S ribosomal protein L7	1	261	1	1	1	1
P05783	KRT18	Keratin, type I cytoskeletal 18	1	206	1	1	1	1
Q8WWM7	ATXN2L	Ataxin-2-like protein	6	205	1	1	1	1
P38919	EIF4A3	Eukaryotic initiation factor 4A-III	1	202	1	1	1	1
P62280	RPS11	40S ribosomal protein S11	1	183	1	1	1	1
Q15366	PCBP2	Isoform 4 of Poly(rC)-binding protein 2	5	181	1	1	1	1
Q07020	RPL18	60S ribosomal protein L18	1	180	1	1	1	1
P18621	RPL17	60S ribosomal protein L17	1	172	1	1	1	1
Q9UKM9	RALY	Isoform 1 of RNA-binding protein Raly	3	165	1	1	1	1
Q9H2U1	DHX36	Isoform 2 of Probable ATP-dependent RNA helicase DHX36	3	162	1	1	1	1
Q09161	NCBP1	Nuclear cap-binding protein subunit 1	1	149	1	1	1	1
P46778	RPL21	60S ribosomal protein L21	1	141	1	1	1	1
Q96QR8	PURB	Transcriptional activator protein Pur-beta	1	138	1	1	1	1
P51116	FXR2	Fragile X mental retardation syndrome-related protein 2	1	137	1	1	1	1
Q9NUL3	STAU2	Isoform 2 of Double-stranded RNA-binding protein Staufen homolog 2	4	134	1	1	1	1
Q7Z417	NUFIP2	Nuclear fragile X mental retardation-interacting protein 2	1	132	1	1	1	1
Q71RC2	LARP4	La-related protein 4	3	118	1	1	1	1
Q7Z2W4	ZC3HAV1	Zinc finger CCCH-type antiviral protein 1	2	89	1	1	1	1
P30050	RPL12	60S ribosomal protein L12	1	76	1	1	1	1
P62913	RPL11	Isoform 2 of 60S ribosomal protein L11	2	67	1	1	1	1
O43143	DHX15	Putative pre-mRNA-splicing factor ATP-dependent RNA helicase DHX15	1	61	1	1	1	1

Q9NUD5	ZCCHC3	Zinc finger CCHC domain-containing protein 3	1	61	1	1	1	1
Q99700	ATXN2	Isoform 2 of Ataxin-2	3	50	1	1	1	1
Q9NX05	FAM120C	Constitutive coactivator of PPAR-gamma-like protein 2	1	48	1	1	1	1
Q6P2E9	EDC4	Enhancer of mRNA-decapping protein 4	2	42	1	1	1	1
Q14671	PUM1	Isoform 2 of Pumilio homolog 1	2	38	1	1	1	1
P46783	RPS10	40S ribosomal protein S10	1	177	1	1	1	
P16989	CSDA	DNA-binding protein A	2	789	1	1		
P16989	CSDA	Isoform 2 of DNA-binding protein A	1	436	1	1		
P68371	TUBB4B	Tubulin beta-4B chain	2	435	1	1		
P68104	EEF1A1	Elongation factor 1-alpha 1	3	336	1	1		
P10155	TROVE2	60 kDa SS-A/Ro ribonucleoprotein	1	124	1	1		
Q92615	LARP4B	La-related protein 4B	1	119	1	1		
P48200	IREB2	Iron-responsive element-binding protein 2	1	102	1	1		
P52597	HNRNPF	Heterogeneous nuclear ribonucleoprotein F	1	101	1	1		
Q86YZ3	HRNR	Hornerin	1	94	1	1		
P55884	EIF3B	Eukaryotic translation initiation factor 3 subunit B	2	91	1	1		
Q04637	EIF4G1	Isoform E of Eukaryotic translation initiation factor 4 gamma 1	5	88	1	1		
Q14152	EIF3A	Eukaryotic translation initiation factor 3 subunit A	1	81	1	1		
P57678	GEMIN4	Gem-associated protein 4	1	79	1	1		
Q9Y262	EIF3L	Eukaryotic translation initiation factor 3 subunit L	1	71	1	1		
P04183	TK1	Thymidine kinase, cytosolic	1	64	1	1		
Q06787	FMR1	Isoform 8 of Fragile X mental retardation protein 1	8	58	1	1		
Q96I24	FUBP3	Far upstream element-binding protein 3	1	57	1	1		
Q9UKV8	EIF2C2	Isoform 2 of Protein argonaute-2	2	53	1	1		
Q9NSB4	KRT82	Keratin, type II cuticular Hb2	1	43	1	1		
O75534	CSDE1	Isoform Short of Cold shock domain-containing protein E1	2	41	1	1		
Q9Y5A9	YTHDF2	Isoform 2 of YTH domain family protein 2	2	40	1	1		
Q9UHI6	DDX20	Probable ATP-dependent RNA helicase DDX20	1	37	1	1		
Q99613	EIF3C	Eukaryotic translation initiation factor 3 subunit C	1	37	1	1		

Q9BRZ2	TRIM56	E3 ubiquitin-protein ligase TRIM56	1	33	1	1			
O15234	CASC3	Protein CASC3	1	33	1	1			
Q9H6S0	YTHDC2	Probable ATP-dependent RNA helicase YTHDC2	1	28	1	1			
O15371	EIF3D	Eukaryotic translation initiation factor 3 subunit D	1	26	1	1			
Q8IXB1	DNAJC10	Isoform 2 of DnaJ homolog subfamily C member 10	2	25	1	1			
Q9Y5S9	RBM8A	Isoform 2 of RNA-binding protein 8A	2	16	1	1			
P60842	EIF4A1	Eukaryotic initiation factor 4A-I	1	117	1				
Q15365	PCBP1	Poly(rC)-binding protein 1	1	104	1				
Q9Y520	PRRC2C	Isoform 3 of Protein PRRC2C	7	63	1				
Q13347	EIF3I	Eukaryotic translation initiation factor 3 subunit I	1	36	1				
Q8TEQ6	GEMIN5	Gem-associated protein 5	1	34	1				
Q9BYK8	PRIC285	Peroxisomal proliferator-activated receptor A-interacting complex 285 kDa protein	1	33	1				
P48634	PRRC2A	Isoform 2 of Protein PRRC2A	4	26	1				
Q14258	TRIM25	E3 ubiquitin/ISG15 ligase TRIM25	1	23	1				
Q9Y3F4	STRAP	Serine-threonine kinase receptor-associated protein	1	16	1				
P54136	RARS	Isoform Monomeric of Arginine–tRNA ligase, cytoplasmic	2	15	1				
P54687	BCAT1	Isoform 4 of Branched-chain-amino-acid aminotransferase, cytosolic	4	10	1				
Q9H0J9	PARP12	Poly [ADP-ribose] polymerase 12	1	8	1				
Q07021	C1QBP	Complement component 1 Q subcomponent-binding protein, mitochondrial	1	510		1	1	1	
Q92841	DDX17	Probable ATP-dependent RNA helicase DDX17	4	277		1	1	1	
P62906	RPL10A	60S ribosomal protein L10a	1	179		1	1	1	
P84098	RPL19	60S ribosomal protein L19	1	147		1	1	1	
P05091	ALDH2	Aldehyde dehydrogenase, mitochondrial	1	136		1	1	1	
P61254	RPL26	60S ribosomal protein L26	2	117		1	1	1	
P36957	DLST	Dihydrolipoyllysine-residue succinyltransferase component of 2-oxoglutarate dehydrogenase complex, mitochondrial	1	62		1	1	1	
P49406	MRPL19	39S ribosomal protein L19, mitochondrial	1	45		1	1	1	
Q9NYK5	MRPL39	39S ribosomal protein L39, mitochondrial	2	56		1	1		
Q9Y3D9	MRPS23	28S ribosomal protein S23, mitochondrial	1	54		1	1		

Q9NZI8	IGF2BP1	Insulin-like growth factor 2 mRNA-binding protein 1	1	958		1			
P48668	KRT6C	Keratin, type II cytoskeletal 6C	1	644		1			
Q04695	KRT17	Keratin, type I cytoskeletal 17	1	276		1			
P14618	PKM2	Pyruvate kinase isozymes M1/M2	3	208		1			
P08107	HSPA1A	Heat shock 70 kDa protein 1A/1B	1	148		1			
P14923	JUP	Junction plakoglobin	1	98		1			
Q9BPW8	NIPSNAP1	Protein NipSnap homolog 1	1	69		1			
O75323	GBAS	Protein NipSnap homolog 2	1	62		1			
Q13162	PRDX4	Peroxiredoxin-4	1	46		1			
Q8ND56	LSM14A	Protein LSM14 homolog A	2	30		1			
P04792	HSPB1	Heat shock protein beta-1	1	23		1			
P32969	RPL9	60S ribosomal protein L9	1	16		1			
Q9NR30	DDX21	Nucleolar RNA helicase 2	2	702			1	1	
Q00839	HNRNPU	Heterogeneous nuclear ribonucleoprotein U	2	624			1	1	
P16403	HIST1H1C	Histone H1.2	1	613			1	1	
P19338	NCL	Nucleolin	1	546			1	1	
P10412	HIST1H1E	Histone H1.4	2	485			1	1	
Q6P2Q9	PRPF8	Pre-mRNA-processing-splicing factor 8	1	476			1	1	
Q9BUJ2	HNRNPUL1	Isoform 2 of Heterogeneous nuclear ribonucleoprotein U-like protein 1	4	422			1	1	
Q02878	RPL6	60S ribosomal protein L6	1	405			1	1	
P62269	RPS18	40S ribosomal protein S18	1	397			1	1	
P36578	RPL4	60S ribosomal protein L4	1	382			1	1	
P38646	HSPA9	Stress-70 protein, mitochondrial	1	355			1	1	
P26599	PTBP1	Polypyrimidine tract-binding protein 1	9	335			1	1	
O43390	HNRNPR	Heterogeneous nuclear ribonucleoprotein R	2	318			1	1	
O75643	SNRNP200	U5 small nuclear ribonucleoprotein 200 kDa helicase	1	304			1	1	
Q14444	CAPRIN1	Isoform 2 of Caprin-1	2	284			1	1	
P14866	HNRNPL	Heterogeneous nuclear ribonucleoprotein L	1	267			1	1	
Q15029	EFTUD2	116 kDa U5 small nuclear ribonucleoprotein component	1	260			1	1	

Q08211	DHX9	ATP-dependent RNA helicase A	1	253			1	1	
P62424	RPL7A	60S ribosomal protein L7a	1	241			1	1	
P07355	ANXA2	Annexin A2	2	240			1	1	
Q8NC51	SERBP1	Isoform 3 of Plasminogen activator inhibitor 1 RNA-binding protein	4	220			1	1	
P62277	RPS13	40S ribosomal protein S13	1	219			1	1	
O76021	RSL1D1	Ribosomal L1 domain-containing protein 1	1	200			1	1	
Q12905	ILF2	Interleukin enhancer-binding factor 2	1	178			1	1	
P62266	RPS23	40S ribosomal protein S23	1	177			1	1	
P60866	RPS20	40S ribosomal protein S20	2	174			1	1	
P06748	NPM1	Nucleophosmin	3	173			1	1	
P62851	RPS25	40S ribosomal protein S25	1	167			1	1	
P61313	RPL15	60S ribosomal protein L15	1	167			1	1	
Q9BQG0	MYBBP1A	Myb-binding protein 1A	2	165			1	1	
P23246	SFPQ	Splicing factor, proline- and glutamine-rich	1	160			1	1	
P83731	RPL24	60S ribosomal protein L24	1	154			1	1	
P46776	RPL27A	60S ribosomal protein L27a	1	150			1	1	
P40429	RPL13A	60S ribosomal protein L13a	2	124			1	1	
P58876	HIST1H2BD	Histone H2B type 1-D	11	122			1	1	
Q02543	RPL18A	60S ribosomal protein L18a	1	120			1	1	
Q15233	NONO	Non-POU domain-containing octamer-binding protein	1	119			1	1	
P84103	SRSF3	Serine/arginine-rich splicing factor 3	1	117			1	1	
P51991	HNRNPA3	Heterogeneous nuclear ribonucleoprotein A3	2	111			1	1	
P0CW22	RPS17L	40S ribosomal protein S17-like	1	107			1	1	
Q9BZE4	GTPBP4	Nucleolar GTP-binding protein 1	1	104			1	1	
Q9BQ39	DDX50	ATP-dependent RNA helicase DDX50	1	103			1	1	
P50914	RPL14	60S ribosomal protein L14	1	101			1	1	
P22087	FBL	rRNA 2'-O-methyltransferase fibrillarin	1	100			1	1	
P68431	HIST1H3A	Histone H3.1	5	97			1	1	
Q07955	SRSF1	Serine/arginine-rich splicing factor 1	3	87			1	1	

Q3MHD2	LSM12	Protein LSM12 homolog	2	80			1	1
P62841	RPS15	40S ribosomal protein S15	1	78			1	1
P61353	RPL27	60S ribosomal protein L27	1	78			1	1
Q12906	ILF3	Interleukin enhancer-binding factor 3	6	78			1	1
Q9P015	MRPL15	39S ribosomal protein L15, mitochondrial	1	74			1	1
Q9GZR7	DDX24	ATP-dependent RNA helicase DDX24	1	70			1	1
Q96KR1	ZFR	Zinc finger RNA-binding protein	1	66			1	1
Q9UN86	G3BP2	Isoform B of Ras GTPase-activating protein-binding protein 2	2	64			1	1
Q07666	KHDRBS1	KH domain-containing, RNA-binding, signal transduction-associated protein 1	2	64			1	1
Q9BVP2	GNL3	Isoform 2 of Guanine nucleotide-binding protein-like 3	2	64			1	1
P46779	RPL28	60S ribosomal protein L28	2	62			1	1
Q9BUQ8	DDX23	Probable ATP-dependent RNA helicase DDX23	1	61			1	1
P04114	APOB	Apolipoprotein B-100	1	60			1	1
O94906	PRPF6	Isoform 2 of Pre-mRNA-processing factor 6	2	60			1	1
P23527	HIST1H2BO	Histone H2B type 1-O	5	58			1	1
Q9H0D6	XRN2	5'-3' exoribonuclease 2	2	57			1	1
Q13247	SRSF6	Isoform SRP55-3 of Serine/arginine-rich splicing factor 6	3	51			1	1
Q14690	PDCD11	Protein RRP5 homolog	1	51			1	1
Q9UHX1	PUF60	Isoform 4 of Poly(U)-binding-splicing factor PUF60	6	50			1	1
Q9UMS4	PRPF19	Pre-mRNA-processing factor 19	1	50			1	1
P46087	NOP2	Isoform 2 of Putative ribosomal RNA methyltransferase NOP2	2	46			1	1
P10515	DLAT	Dihydrolipoyllysine-residue acetyltransferase component of pyruvate dehydrogenase complex, mitochondrial	1	45			1	1
P51398	DAP3	Isoform 2 of 28S ribosomal protein S29, mitochondrial	2	43			1	1
Q9Y3I0	C22orf28	tRNA-splicing ligase RtcB homolog	1	42			1	1
Q96PK6	RBM14	RNA-binding protein 14	1	39			1	1
Q9H6R4	NOL6	Isoform 4 of Nucleolar protein 6	2	36			1	1
Q15393	SF3B3	Splicing factor 3B subunit 3	1	35			1	1
Q9H0A0	NAT10	N-acetyltransferase 10	1	34			1	1

Q9BXP5	SRRT	Isoform 5 of Serrate RNA effector molecule homolog	5	32			1	1
Q8TDN6	BRIX1	Ribosome biogenesis protein BRX1 homolog	1	32			1	1
Q1KMD3	HNRNPUL2	Heterogeneous nuclear ribonucleoprotein U-like protein 2	1	29			1	1
Q13263	TRIM28	Isoform 2 of Transcription intermediary factor 1-beta	2	27			1	1
P14678	SNRPB	Isoform SM-B of Small nuclear ribonucleoprotein-associated proteins B and B'	4	26			1	1
Q8N163	KIAA1967	DBIRD complex subunit KIAA1967	2	25			1	1
Q99873	PRMT1	Isoform 3 of Protein arginine N-methyltransferase 1	3	21			1	1
Q9NY93	DDX56	Probable ATP-dependent RNA helicase DDX56	1	21			1	1
Q13148	TARDBP	TAR DNA-binding protein 43	2	19			1	1
Q96DV4	MRPL38	39S ribosomal protein L38, mitochondrial	1	19			1	1
Q9BZE1	MRPL37	39S ribosomal protein L37, mitochondrial	1	19			1	1
Q99575	POP1	Ribonucleases P/MRP protein subunit POP1	1	17			1	1
Q8NHQ9	DDX55	ATP-dependent RNA helicase DDX55	1	13			1	1
P39019	RPS19	40S ribosomal protein S19	1	170			1	
P62263	RPS14	40S ribosomal protein S14	1	136			1	
P62854	RPS26	40S ribosomal protein S26	2	131			1	
P62847	RPS24	40S ribosomal protein S24	3	94			1	
P49207	RPL34	60S ribosomal protein L34	1	53			1	
P62888	RPL30	60S ribosomal protein L30	1	48			1	
Q92552	MRPS27	28S ribosomal protein S27, mitochondrial	1	46			1	
Q9BYD3	MRPL4	Isoform 2 of 39S ribosomal protein L4, mitochondrial	2	44			1	
Q96HS1	PGAM5	Serine/threonine-protein phosphatase PGAM5, mitochondrial	2	41			1	
Q99848	EBNA1BP2	Probable rRNA-processing protein EBP2	1	38			1	
P05141	SLC25A5	ADP/ATP translocase 2	1	36			1	
Q96DI7	SNRNP40	U5 small nuclear ribonucleoprotein 40 kDa protein	1	32			1	
P36873	PPP1CC	Serine/threonine-protein phosphatase PP1-gamma catalytic subunit	5	31			1	
Q8N983	MRPL43	Isoform 4 of 39S ribosomal protein L43, mitochondrial	1	27			1	
P82650	MRPS22	28S ribosomal protein S22, mitochondrial	1	25			1	
Q9H9J2	MRPL44	39S ribosomal protein L44, mitochondrial	1	21			1	

O00148	DDX39A	ATP-dependent RNA helicase DDX39A	3	20			1		
P33992	MCM5	DNA replication licensing factor MCM5	1	19			1		
Q9Y2Q9	MRPS28	28S ribosomal protein S28, mitochondrial	1	19			1		
P62318	SNRPD3	Small nuclear ribonucleoprotein Sm D3	1	17			1		
Q9Y265	RUVBL1	RuvB-like 1	1	17			1		
Q8IUX4	APOBEC3F	DNA dC→dU-editing enzyme APOBEC-3F	1	17			1		
P02545	LMNA	Isoform C of Prelamin-A/C	3	15			1		
P52815	MRPL12	39S ribosomal protein L12, mitochondrial	1	14			1		
Q15269	PWP2	Periodic tryptophan protein 2 homolog	1	13			1		
Q8WXF1	PSPC1	Isoform 2 of Paraspeckle component 1	2	12			1		
P45880	VDAC2	Isoform 2 of Voltage-dependent anion-selective channel protein 2	3	11			1		
O95400	CD2BP2	CD2 antigen cytoplasmic tail-binding protein 2	1	11			1		
P42285	SKIV2L2	Superkiller viralicidic activity 2-like 2	1	11			1		
Q9Y3B2	EXOSC1	Exosome complex component CSL4	1	9			1		
Q9BW19	KIFC1	Kinesin-like protein KIFC1	1	8			1		
Q00341	HDLBP	Vigilin	1	717					
P02538	KRT6A	Keratin, type II cytoskeletal 6A	1	350					
P62081	RPS7	40S ribosomal protein S7	1	135					
P22626	HNRNPA2B1	Heterogeneous nuclear ribonucleoproteins A2/B1	2	119					
Q14764	MVP	Major vault protein	1	96					
Q9NUL7	DDX28	Probable ATP-dependent RNA helicase DDX28	1	88					
Q96KK5	HIST1H2AH	Histone H2A type 1-H	7	80					
P68871	HBB	Hemoglobin subunit beta	1	72					
P62750	RPL23A	60S ribosomal protein L23a	1	69					
P38159	RBMX	RNA-binding motif protein, X chromosome	1	69					
P21589	NT5E	5'-nucleotidase	2	65					
O75127	PTCD1	Pentatricopeptide repeat-containing protein 1	1	63					
P04908	HIST1H2AB	Histone H2A type 1-B/E	3	61					
Q06830	PRDX1	Peroxiredoxin-1	1	53					

P69892	HBG2	Hemoglobin subunit gamma-2	2	46						
P04196	HRG	Histidine-rich glycoprotein	1	45						
Q14694	USP10	Ubiquitin carboxyl-terminal hydrolase 10	3	44						
Q9NX00	TMEM160	Transmembrane protein 160	1	38						
P69905	HBA1	Hemoglobin subunit alpha	1	38						
Q9NVP1	DDX18	ATP-dependent RNA helicase DDX18	1	27						
P33993	MCM7	DNA replication licensing factor MCM7	2	27						
Q9Y3B7	MRPL11	39S ribosomal protein L11, mitochondrial	2	24						
P42694	HELZ	Probable helicase with zinc finger domain	1	21						
P15924	DSP	Isoform DPII of Desmoplakin	2	20						
P31942	HNRNPH3	Isoform 3 of Heterogeneous nuclear ribonucleoprotein H3	3	20						
P25205	MCM3	DNA replication licensing factor MCM3	1	19						
P18077	RPL35A	60S ribosomal protein L35a	1	12						
Q8TDD1	DDX54	ATP-dependent RNA helicase DDX54	2	10						

Proteins that interact with YB-1 in A549 and MDA-MB231 cells.

Appendix C

Further *in silico* networks

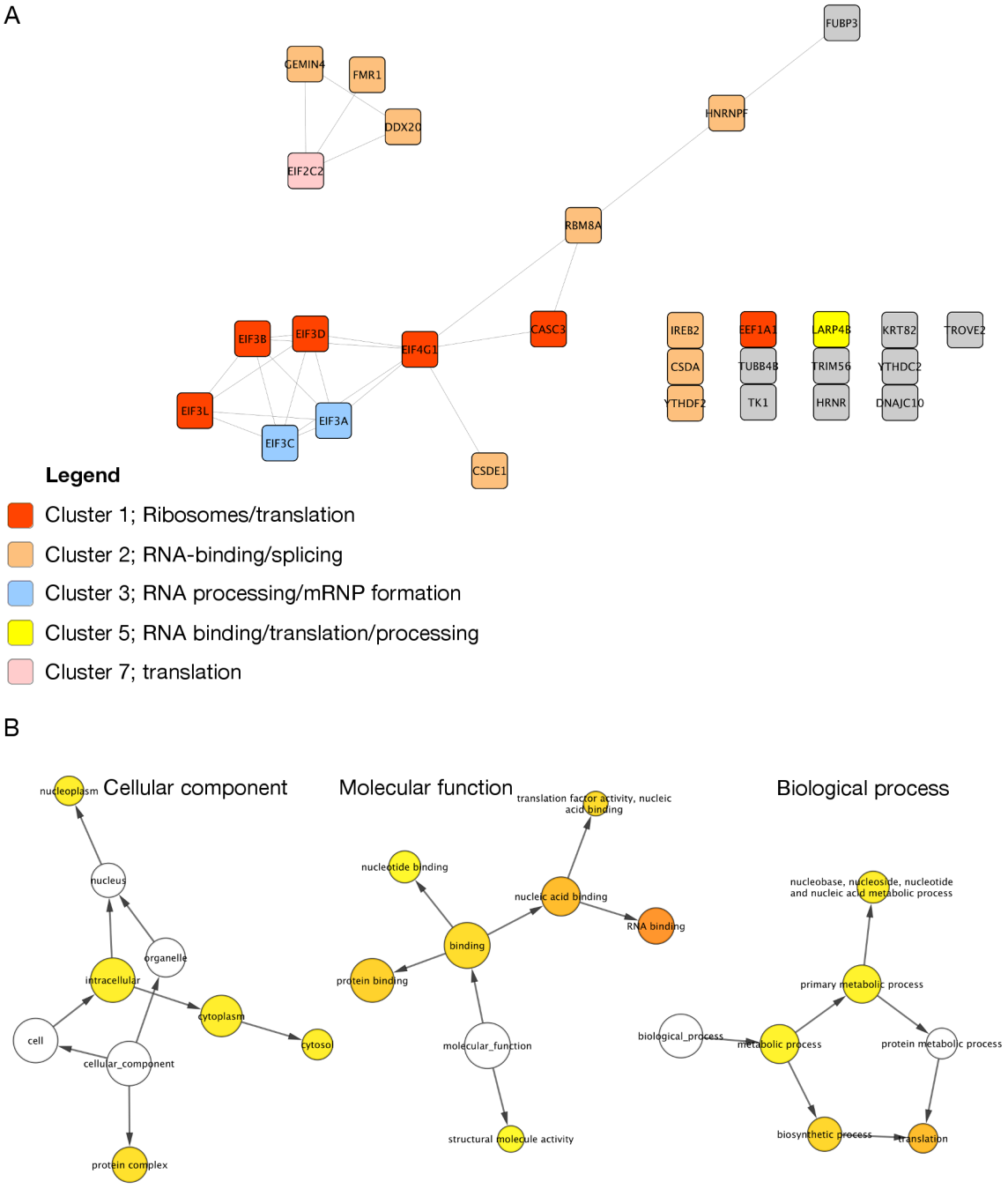

Figure C.1: The binding partners of endogenous YB-1 in the cytoplasm of A549 and MDA-MB231 cells. **A**, a network of *in silico* interactions between the proteins that were identified interacting with YB-1 in the cytoplasm (String, v9.1). Markov clustering (MCL) was applied to the network and the nodes are coloured based on their groupings from the MCL. The terms that summarise the proteins in each cluster are provided in the legend. **B**, enriched terms from gene ontology.

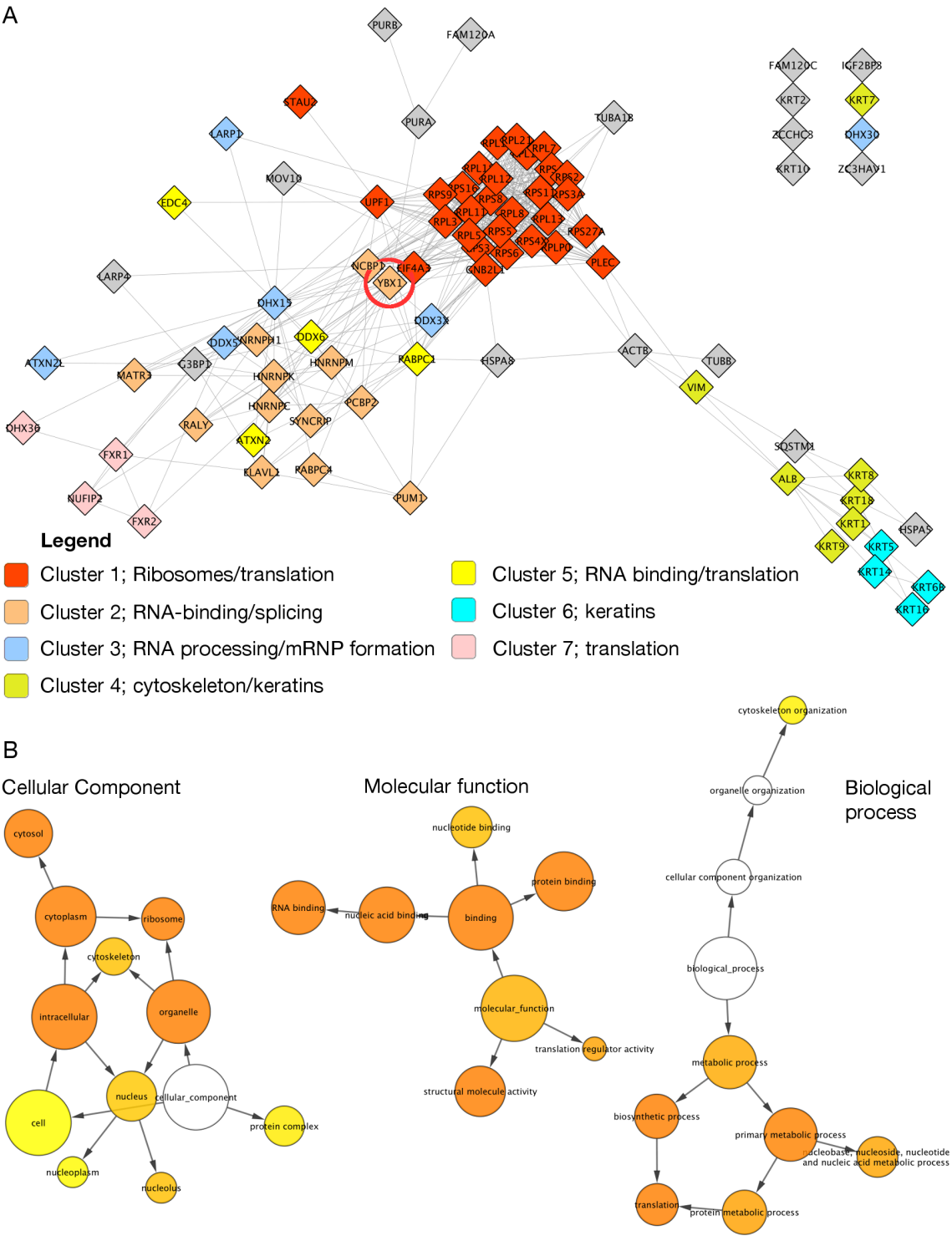

Figure C.2: The binding partners of endogenous YB-1 in the cytoplasm and nucleus of A549 and MDA-MB231 cells. **A**, a network of *in silico* interactions between the proteins that were identified interacting with YB-1 in the cytoplasm and nucleus (String, v9.1). Markov clustering (MCL) was applied to the network and the nodes are coloured based on their groupings from the MCL. The terms that summarise the proteins in each cluster are provided in the legend. **B**, enriched terms from gene ontology.

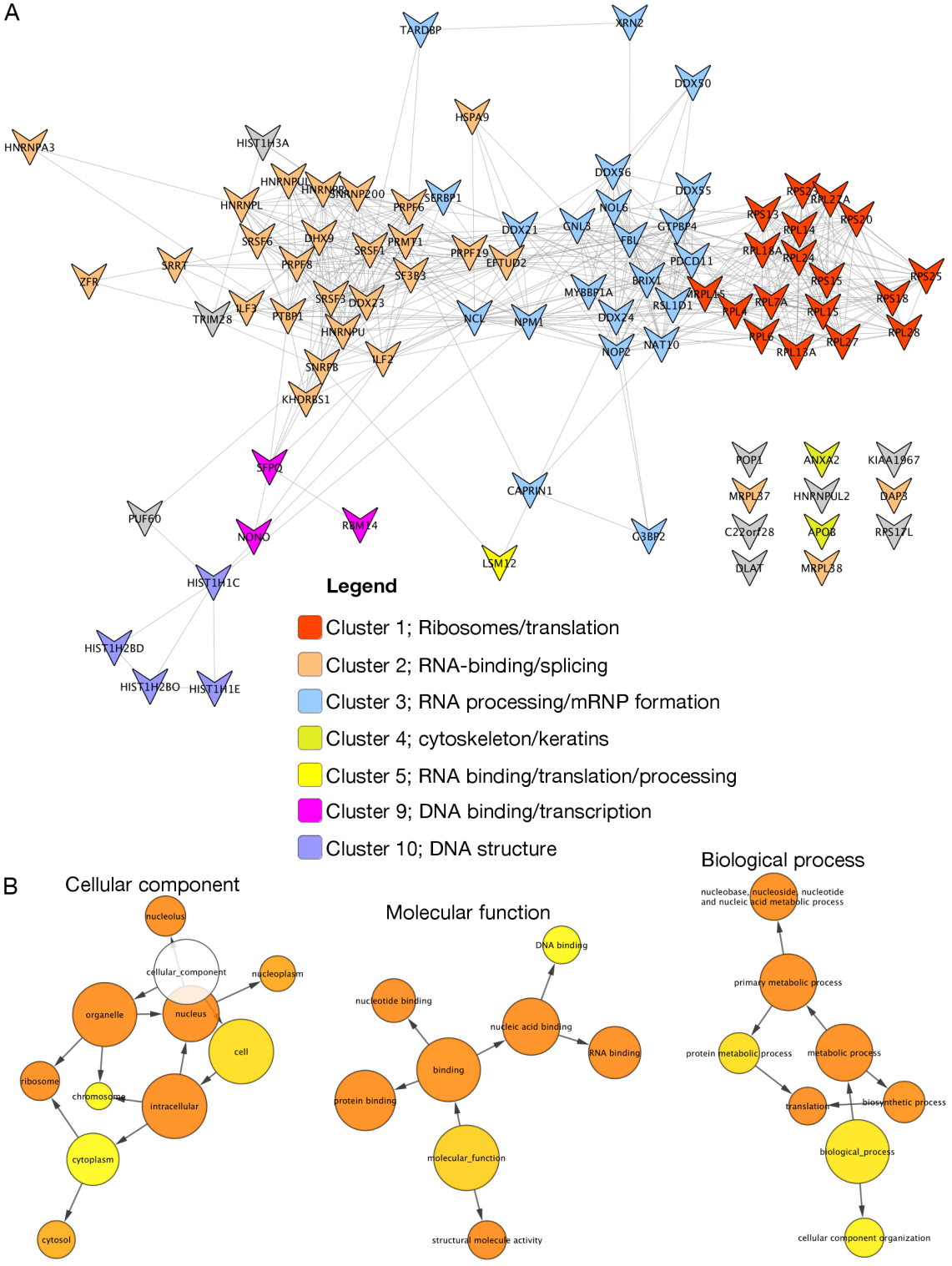

Figure C.3: The binding partners of endogenous YB-1 in the nucleus of A549 and MDA-MB231 cells. **A**, a network of *in silico* interactions between the proteins that were identified interacting with YB-1 in the nucleus (String, v9.1). Markov clustering (MCL) was applied to the network and the nodes are coloured based on their groupings from the MCL. The terms that summarise the proteins in each cluster are provided in the legend. **B**, enriched terms from gene ontology.

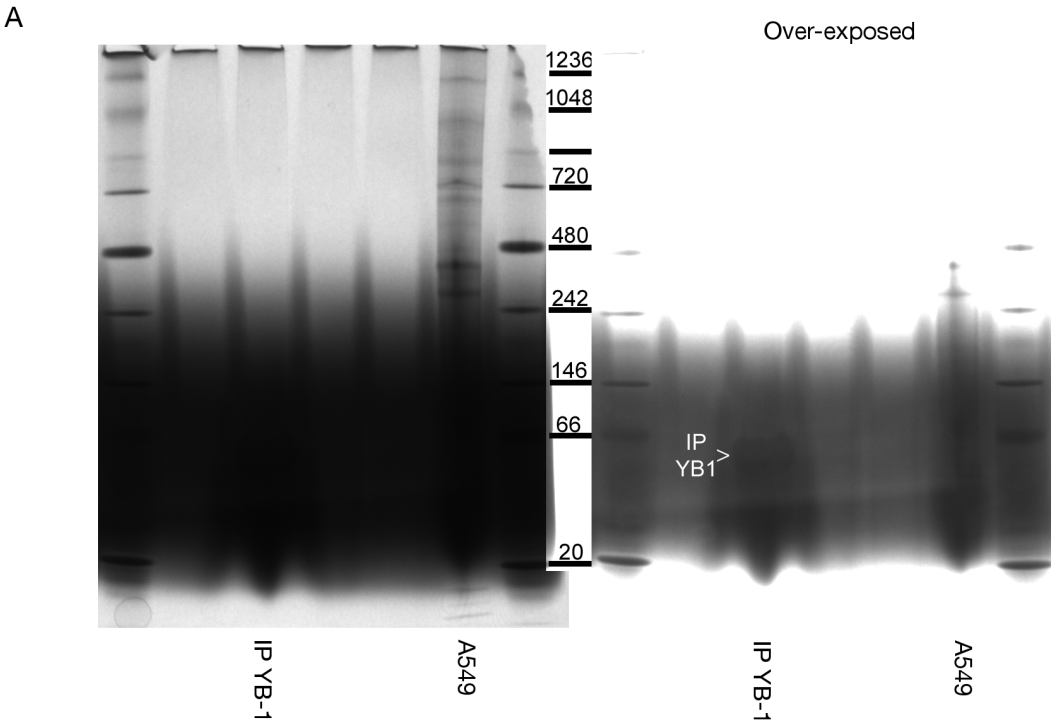

Figure C.4: Purified YB-1 fails to separate on BN-PAGE. Immunopurified YB-1 from 5×10^7 A549 cells was separated using BN-PAGE (**IP-YB-1**). **A549** indicates a lane where a lysate from A549 cells (input) were run. The dark areas on the gel come from coommassie G-250 that could not be destained from the gel. **Over-exposed** provides the clearest image that could be obtained to highlight the presence of purified YB-1 running as a monomer on BN-PAGE (IP YB1>).

Appendix D

Growth plots from drug sensitivity experiments

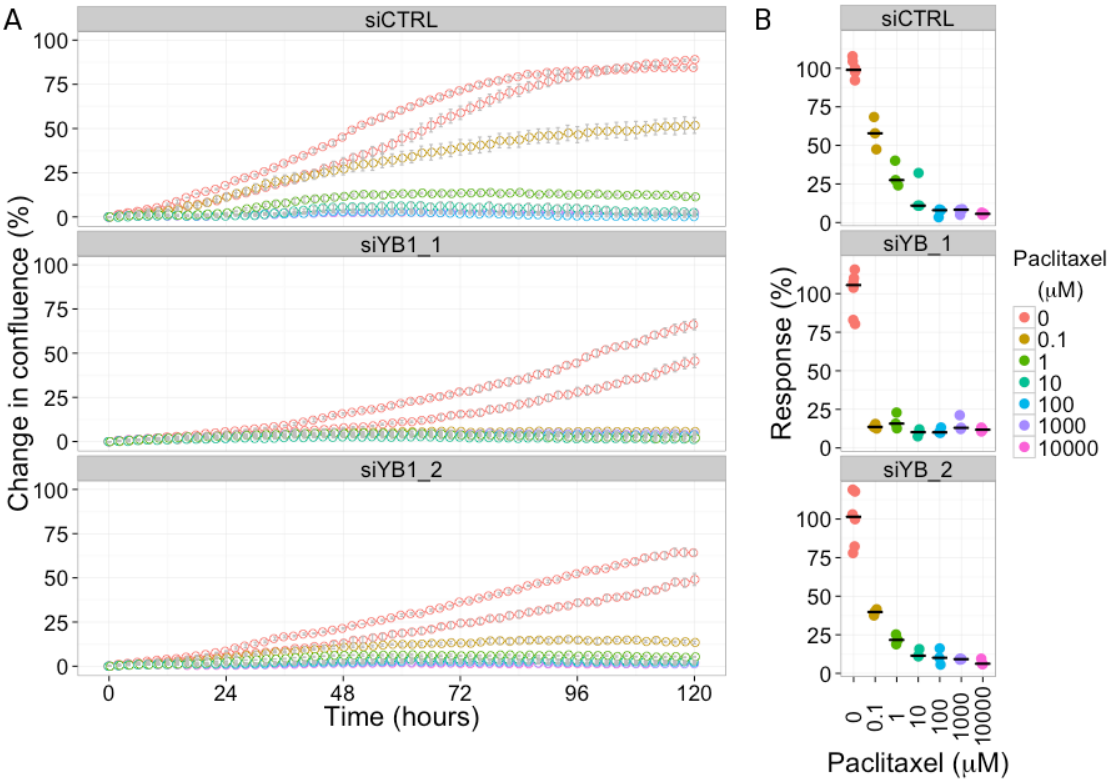

Figure D.1: Depleting YB-1 sensitised MDA-MB231 cells to paclitaxel. MDA-MB231 cells were transfected with a non-targeting siRNA duplex (siCTRL) or one of two siRNA duplexes directed against YB-1 (siYB1_1 and siYB1_2). **A**, media containing paclitaxel (0.1,1,10,100nM, 1, or 10μM) was added and the confluence of the MDA-MB231 cells monitored for 120 hours. **B**, the maximal growth rate (μ) was calculated using the confluence data and for each siRNA duplex, the response to drug was calculated as outlined in **Chapter 2.9**.

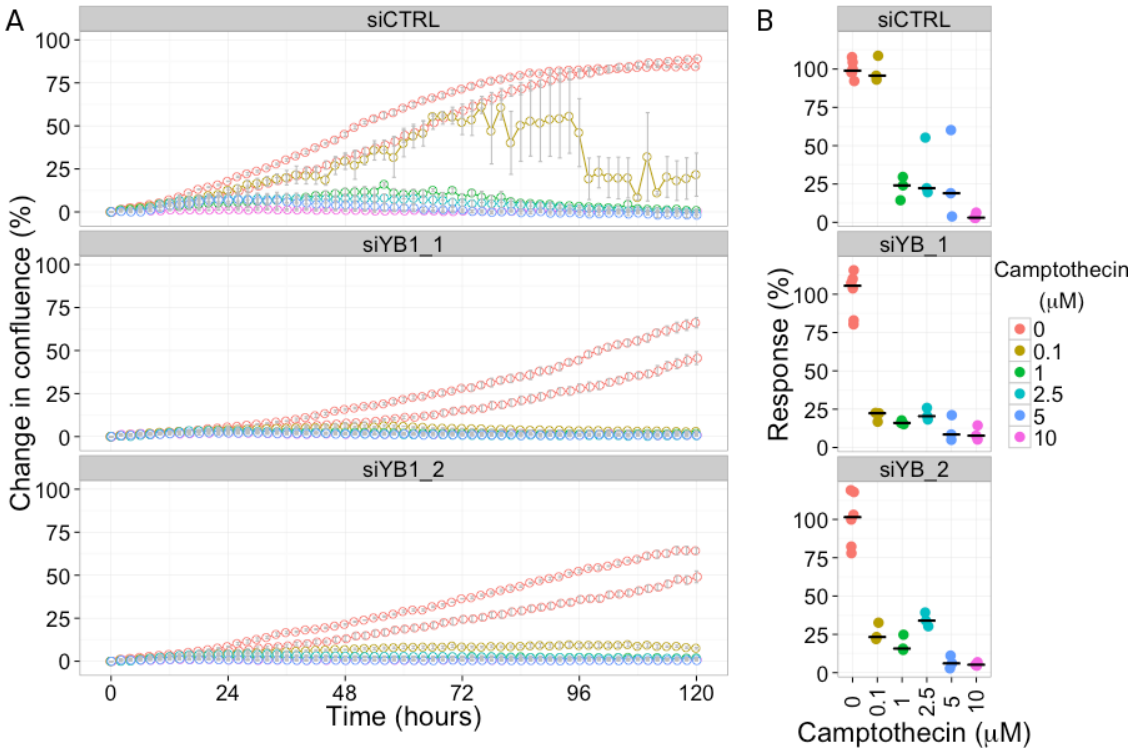

Figure D.2: Depleting YB-1 sensitised MDA-MB231 cells to camptothecin. MDA-MB231 cells were transfected with a non-targeting siRNA duplex (siCTRL) or one of two siRNA duplexes directed against YB-1 (siYB1_1 and siYB1_2). **A**, media containing camptothecin (0.1 - 10 μM) was added and the confluence of the MDA-MB231 cells monitored for 120 hours. The variable measurements of confluence in wells that received siCTRL after 72 hours of exposure to 0.1 μM camptothecin was the result of failed image masking by the confluence algorithm (v1.5). **B**, the maximal growth rate (μ) was calculated using the confluence data and for each siRNA duplex, the response to drug was calculated as outlined in **Chapter 2.9**.

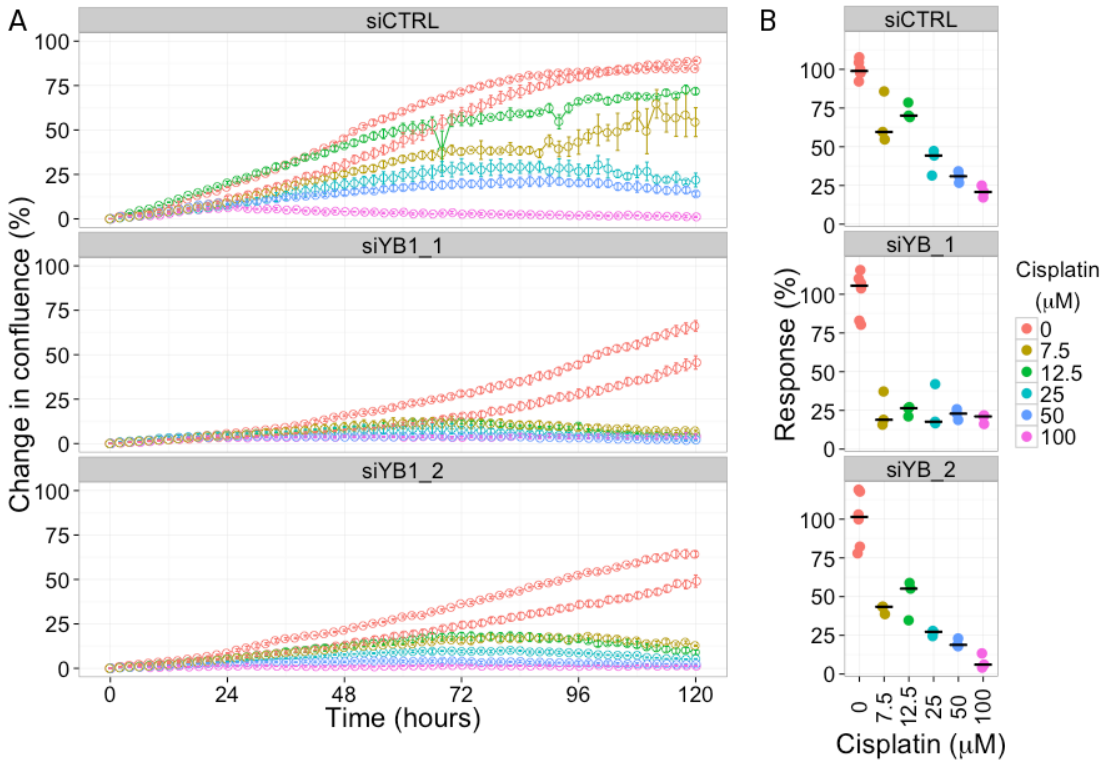

Figure D.3: Depletion of YB-1 sensitised MDA-MB231 cells to cisplatin. MDA-MB231 cells were transfected with a non-targeting siRNA duplex (siCTRL) or one of two siRNA duplexes directed against YB-1 (siYB1_1 and siYB1_2). **A**, media containing cisplatin (7.5 - 100 μM) was added and the confluence of the MDA-MB231 cells monitored for 120 hours. **B**, the maximal growth rate (μ) was calculated using the confluence data and for each siRNA duplex, the response to drug was calculated as outlined in **Chapter 2.9**.

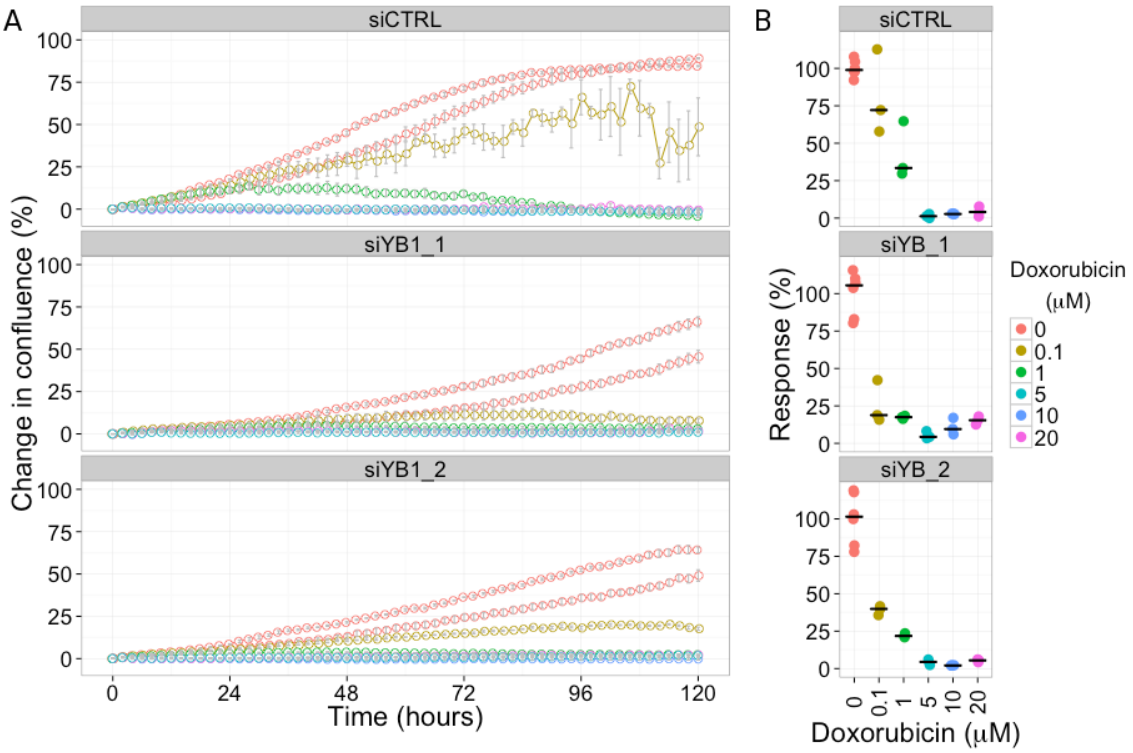

Figure D.4: Depletion of YB-1 sensitised MDA-MB231 cells to doxorubicin. MDA-MB231 cells were transfected with a non-targeting siRNA duplex (siCTRL) or one of two siRNA duplexes directed against YB-1 (siYB1_1 and siYB1_2). **A**, media containing doxorubicin (0.1 - 20 μM) was added and the confluence of the MDA-MB231 cells monitored for 120 hours. **B**, the maximal growth rate (μ) was calculated using the confluence data and for each siRNA duplex, the response to drug was calculated as outlined in **Chapter 2.9**.

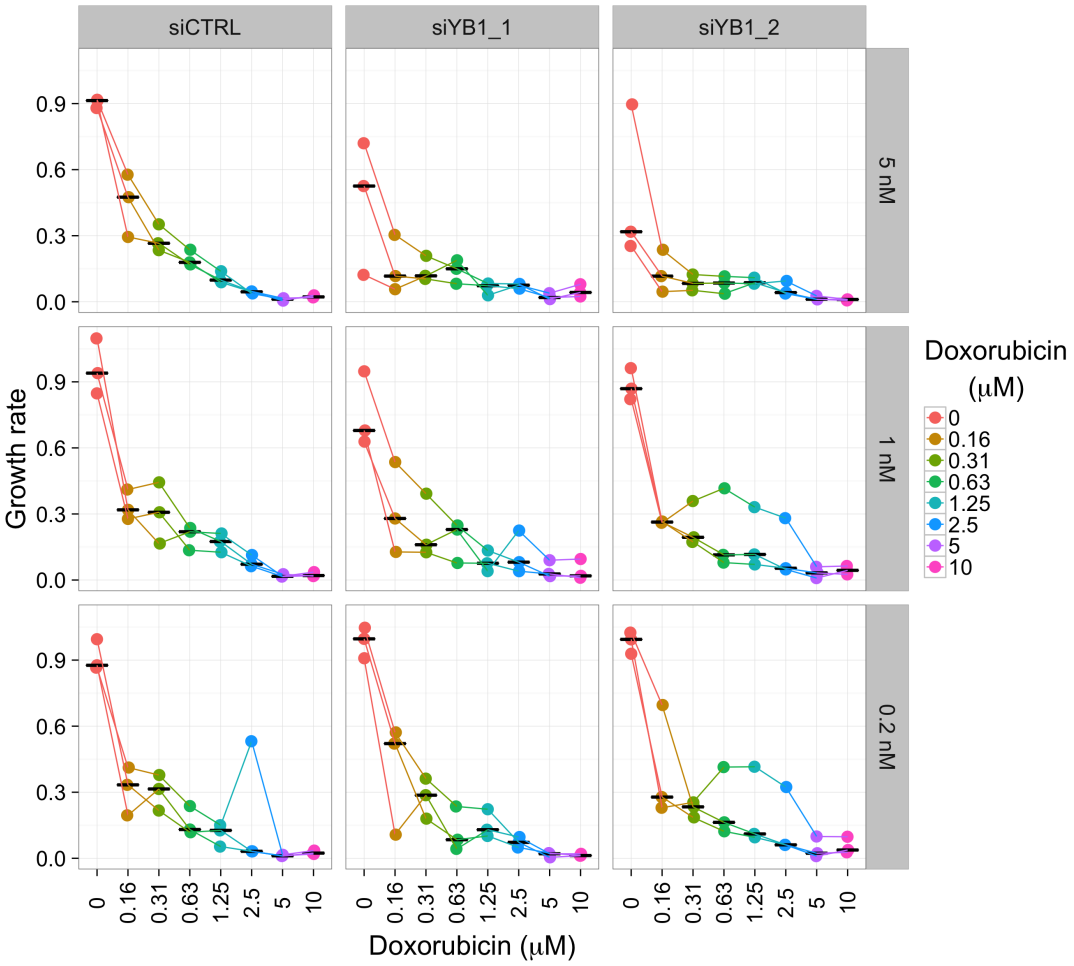

Figure D.5: Depleting YB-1 reduced the confluence of MDA-MB231 cells that are exposed to doxorubicin. The confluence of MDA-MB231 cells in the presence of varying ranges of doxorubicin (0.156 - 10 μM) was monitored for 120 hours. MDA-MB231 cells were transfected with a non-targeting siRNA duplex (siCTRL) or one of two siRNA duplexes directed against YB-1 (siYB1_1 or siYB1_2; **A**). The maximum growth rate for each combination of treatments was calculated from the confluence plots from each well (n = 3).

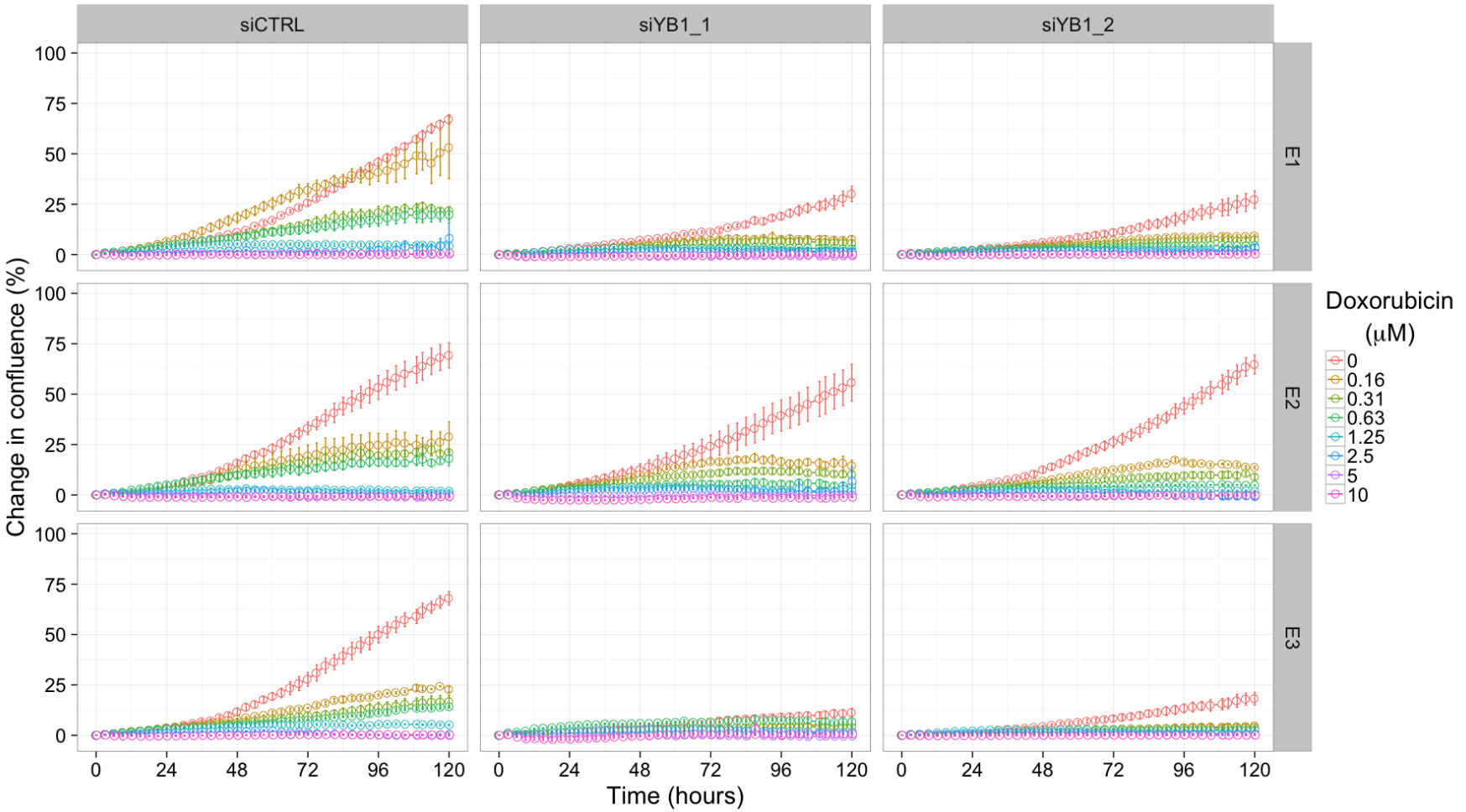

Figure D.6: Growth curves showing the average confluence of wells for all 5 nM siRNA duplexes (siCTRL, siYB1-1, and siYB1-2) during exposure to a range of doxorubicin concentrations (0.165 - 10 μM). The growth plots from individual experiments (E1, E2, and E3) are shown.

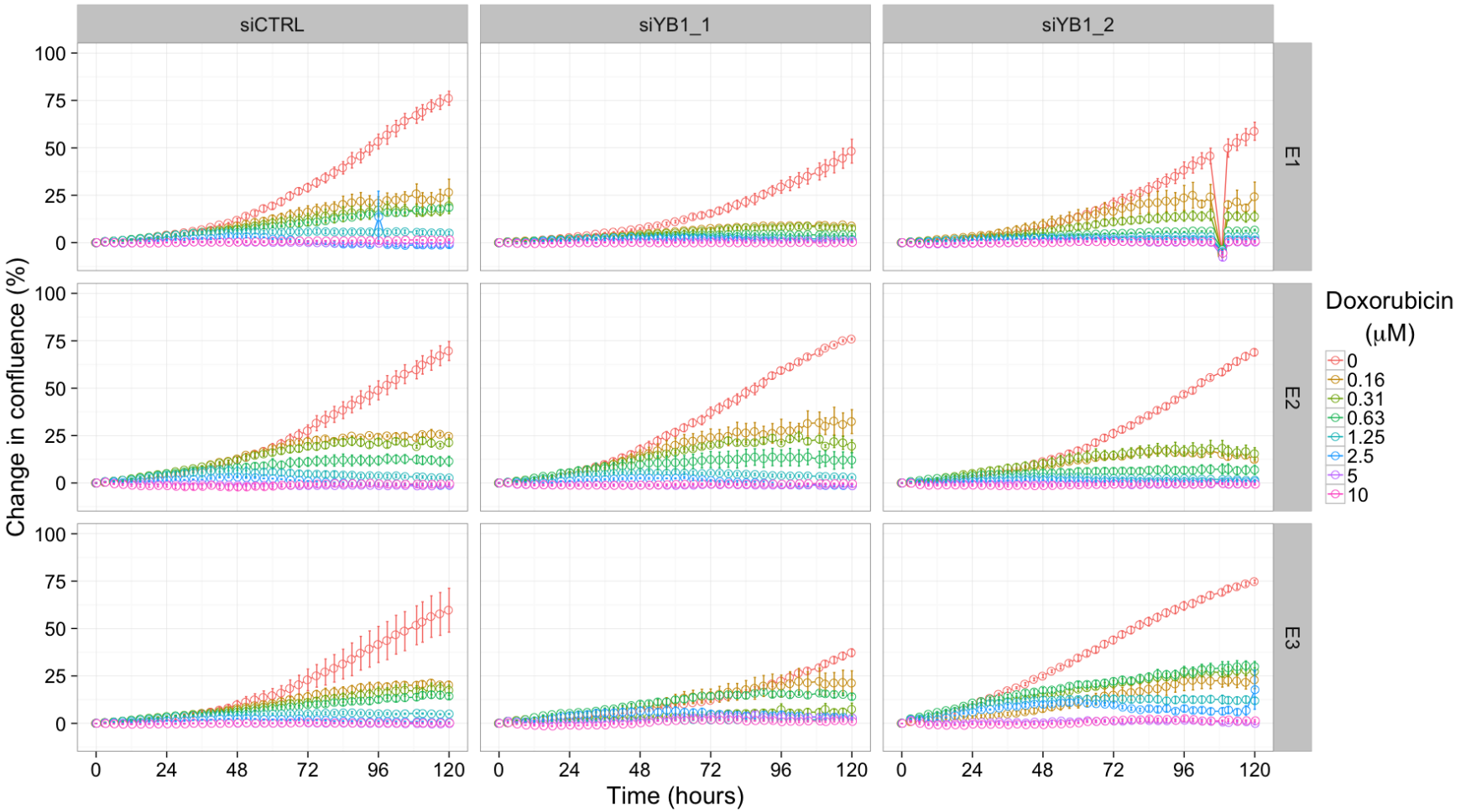

Figure D.7: Growth curves showing the average confluence of wells for all 1 nM siRNA duplexes, siCTRL, siYB1-1, and siYB1-2, during exposure to a range of doxorubicin concentrations (0.165 - 10 μM). The growth plots from individual experiments (E1, E2, and E3) are shown.

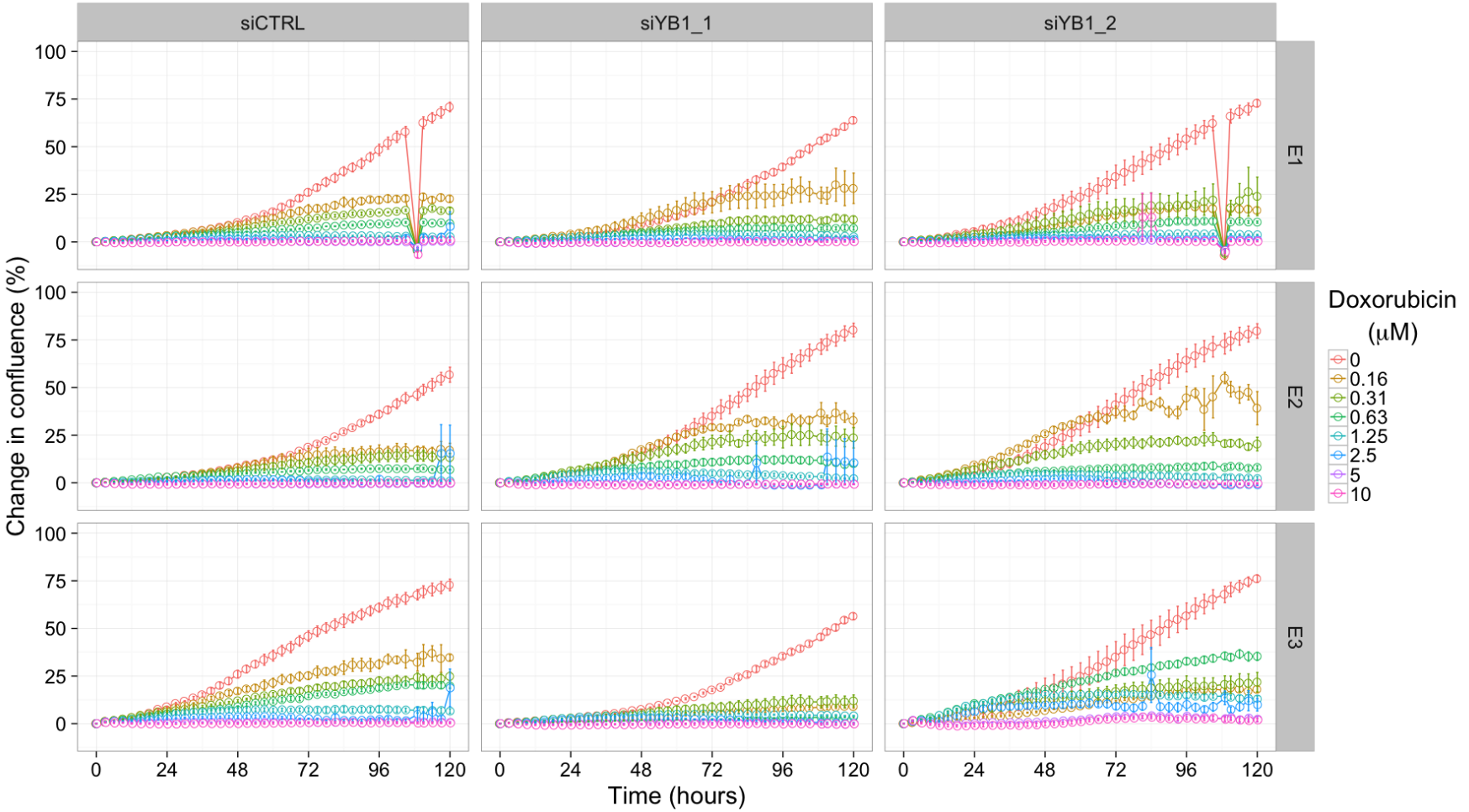

Figure D.8: Growth curves showing the average confluence of wells for all 0.2 nM siRNA duplexes, siCTRL, siYB1-1, and siYB1-2, during exposure to a range of doxorubicin concentrations (0.165 - 10 μM). The growth plots from individual experiments (E1, E2, and E3) are shown. The facet for siYB_2, E3 shows that at 96 hours the Incucyte FLR failed to obtain images. The smoothing parameters in the growth-curve fitting software are essential to ensuring that growth-rate estimates are not perturbed when imaging or image masking fails (**Chapter 2.9**).

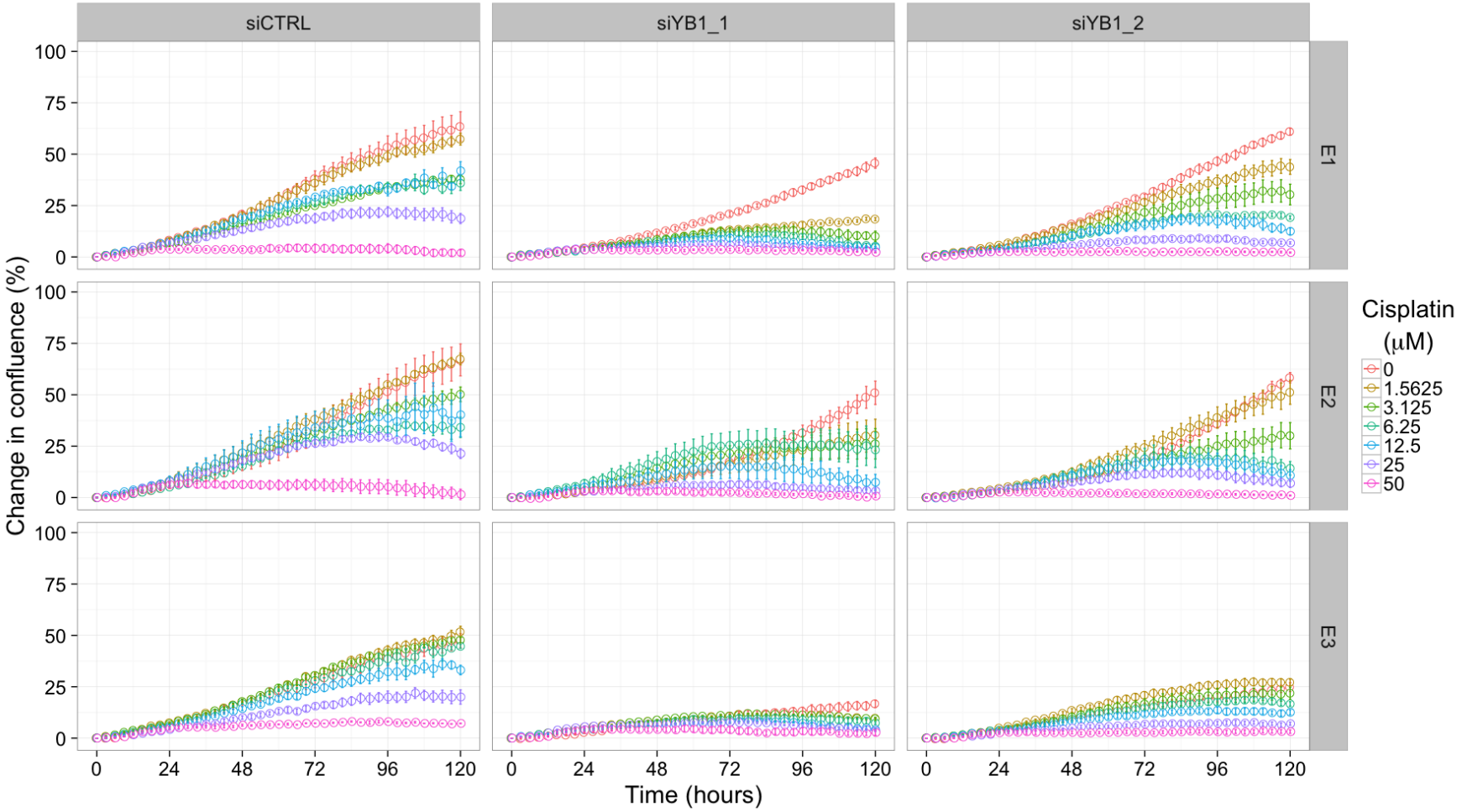

Figure D.9: Growth curves showing the average confluence of wells for all 5 nM siRNA duplexes (siCTRL, siYB1-1, and siYB1-2) during exposure to a range of cisplatin concentrations (0.156 - 50 μM). The growth plots from individual experiments (E1, E2, and E3) are shown.

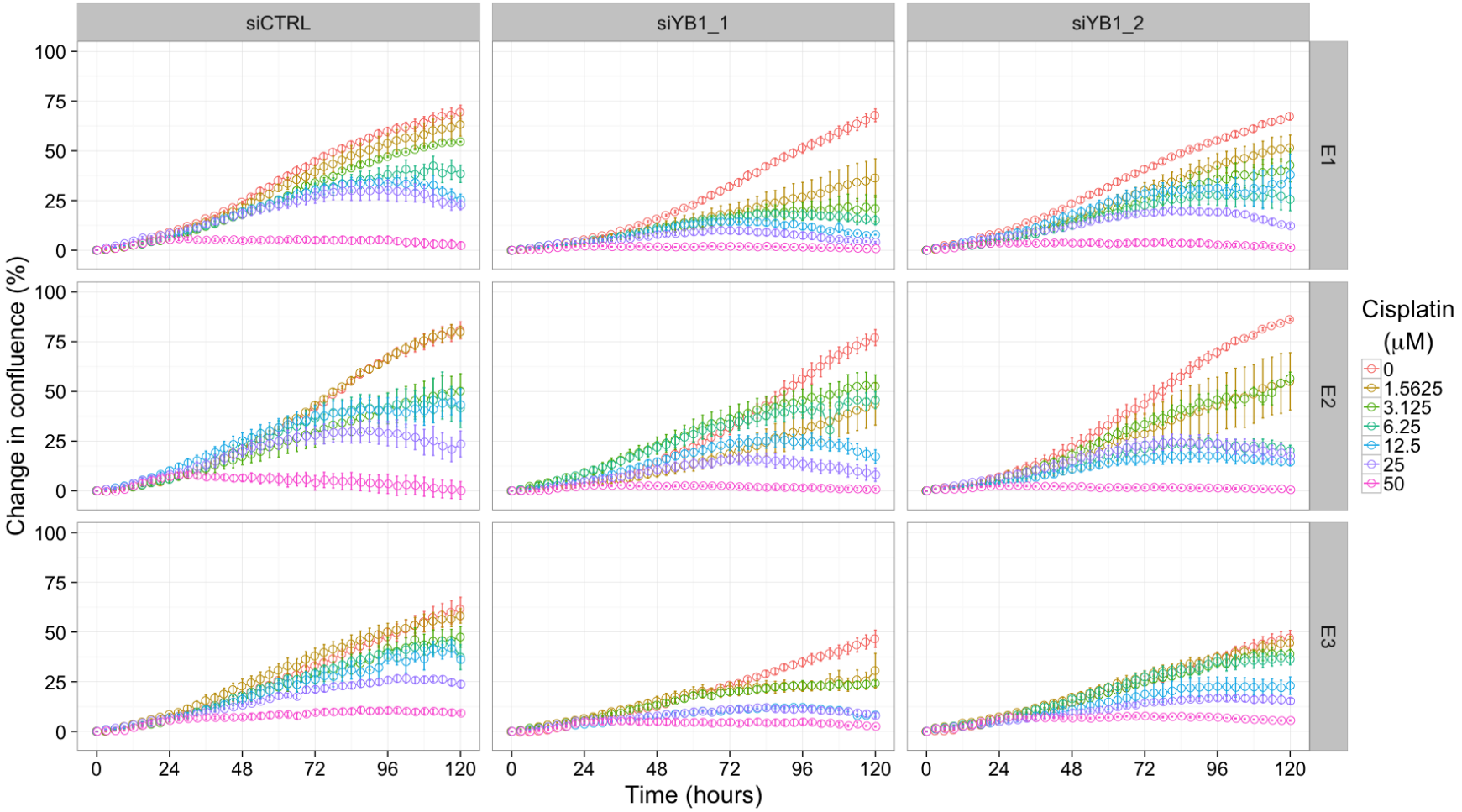

Figure D.10: Growth curves showing the average confluence of wells for all 1 nM siRNA duplexes, siCTRL, siYB1-1, and siYB1-2, during exposure to a range of cisplatin concentrations (0.156 - 50 μM). The growth plots from individual experiments (E1, E2, and E3) are shown.

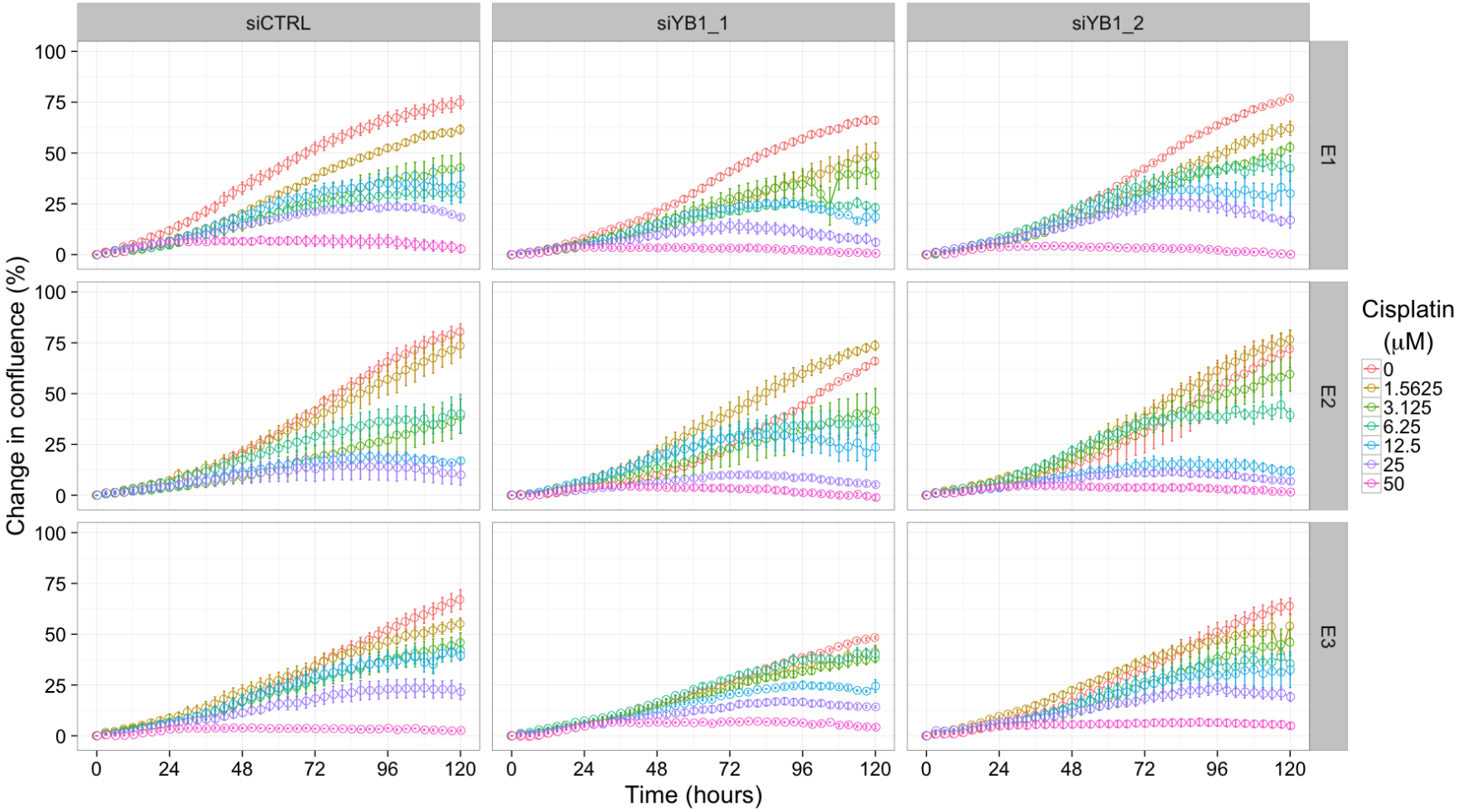

Figure D.11: Growth curves showing the average confluence of wells for all 0.2nM siRNA duplexes, siCTRL, siYB1-1, and siYB1-2, during exposure to a range of cisplatin concentrations (0.156 - 50 μM). The growth plots from individual experiments (E1, E2, and E3) are shown.

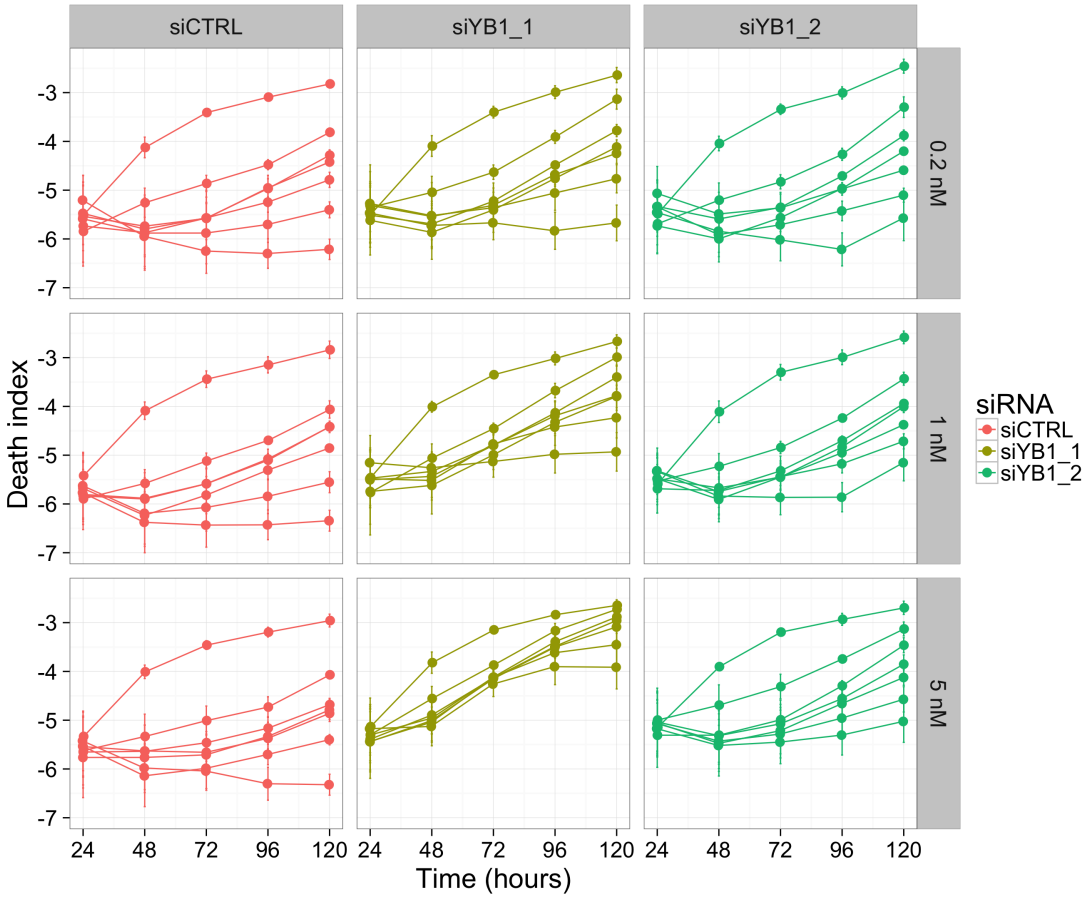

Figure D.12: The viability of MDA-MB231 cells in cisplatin was reduced following the depletion of YB-1. MDA-MB231 cells were transfected with non-targeting siRNA duplex (siCTRL) or one of two siRNA duplexes directed against YB-1 (siYB1_1 or siYB1_2) at 0.2, 1, and 5 nM. The cells were then cultured in media containing 0 - 50 µM cisplatin and YOYO-1 Iodide. The presence of non-viable cells is shown as Death index (see **Chapter 2.9** for details about calculations).

Appendix E

Proteins that interact with crosslinked YB-1 in MDA-MB231 cells.

Table E.1: Proteins that interact with crosslinked YB-1 in MDA-MB231 cells.

Accession	Gene	Protein	SumProteins	Ratio S2/S1	Ratio S3/S1
Q92734	TFG	Protein TFG	1	1.15	0.82
P67809	YBX1	Nuclease-sensitive element-binding protein 1	1	0.82	1.02
P04264	KRT1	Keratin, type II cytoskeletal 1	1	0.75	1.93
P35908	KRT2	Keratin, type II cytoskeletal 2 epidermal	1	0.74	1.77
Q01813	PFKP	6-phosphofructokinase type C	1	0.99	0.63
P11940	PABPC1	Polyadenylate-binding protein 1	1	1.22	0.97
P62241	RPS8	40S ribosomal protein S8	1	1.03	0.78
Q04637	EIF4G1	Isoform E of Eukaryotic translation initiation factor 4 gamma 1	5	0.92	0.9
P23396	RPS3	40S ribosomal protein S3	1	1.17	0.79
P13645	KRT10	Keratin, type I cytoskeletal 10	1	0.83	1.18
Q13310	PABPC4	Isoform 2 of Polyadenylate-binding protein 4	3	1.28	1.02
P35527	KRT9	Keratin, type I cytoskeletal 9	1	0.9	2.43
P15880	RPS2	40S ribosomal protein S2	1	1.26	0.74
Q14444	CAPRIN1	Isoform 2 of Caprin-1	2	1.07	0.75
P16989	CSDA	Isoform 3 of DNA-binding protein A	3	1.01	3.23
P68363	TUBA1B	Tubulin alpha-1B chain	1	1.24	0.73
P62249	RPS16	40S ribosomal protein S16	1	1.11	0.61
P60709	ACTB	Actin, cytoplasmic 1	2	1.04	1.09
O60506	SYNCRIP	Isoform 3 of Heterogeneous nuclear ribonucleoprotein Q	1	1.22	1.02
P17858	PFKL	6-phosphofructokinase, liver type	1	0.84	0.52
Q07021	C1QBP	Complement component 1 Q subcomponent-binding protein, mitochondrial	1	1.45	1.29
P08238	HSP90AB1	Heat shock protein HSP 90-beta	1	0.91	0.74

P68104	EEF1A1	Elongation factor 1-alpha 1	2	1.08	0.56
P07900	HSP90AA1	Heat shock protein HSP 90-alpha	2	0.9	0.73
P55209	NAP1L1	Nucleosome assembly protein 1-like 1	1	0.99	0.47
P61247	RPS3A	40S ribosomal protein S3a	1	1.42	0.75
P46781	RPS9	40S ribosomal protein S9	1	0.98	0.59
O43390	HNRNPR	Heterogeneous nuclear ribonucleoprotein R	1	0.99	0.7
P62851	RPS25	40S ribosomal protein S25	1	1.07	0.61
P11142	HSPA8	Heat shock cognate 71 kDa protein	1	0.95	0.67
P36578	RPL4	60S ribosomal protein L4	1	1.31	0.74
P18621	RPL17	60S ribosomal protein L17	1	1.02	0.42
Q12931	TRAP1	Heat shock protein 75 kDa, mitochondrial	1	1.83	0.62
Q00341	HDLBP	Vigilin	1	1.28	1.13
P10809	HSPD1	60 kDa heat shock protein, mitochondrial	1	1.22	1.33
P19338	NCL	Nucleolin	1	1.34	0.81
P06733	ENO1	Alpha-enolase	1	0.95	0.86
Q00839	HNRNPU	Heterogeneous nuclear ribonucleoprotein U	2	1.65	1.1
P13646	KRT13	Isoform 2 of Keratin, type I cytoskeletal 13	3	0.68	1.4
Q13283	G3BP1	Ras GTPase-activating protein-binding protein 1	1	1.19	0.73
P06576	ATP5B	ATP synthase subunit beta, mitochondrial	1	1.11	0.98
P25705	ATP5A1	ATP synthase subunit alpha, mitochondrial	1	1	0.86
P61978	HNRNPK	Heterogeneous nuclear ribonucleoprotein K	3	1.24	0.88
P62701	RPS4X	40S ribosomal protein S4, X isoform	1	1.2	0.61
P63244	GNB2L1	Guanine nucleotide-binding protein subunit beta-2-like 1	1	1.1	0.67
P62753	RPS6	40S ribosomal protein S6	1	1.09	1.31
P08237	PFKM	6-phosphofructokinase, muscle type	2	0.87	0.57
P62913	RPL11	Isoform 2 of 60S ribosomal protein L11	2	0.56	0.65
P83731	RPL24	60S ribosomal protein L24	1	1.08	0.61
P62979	RPS27A	Ubiquitin-40S ribosomal protein S27a	1	1.98	1.44
P62244	RPS15A	40S ribosomal protein S15a	1	1.18	0.66

Q8NC51	SERBP1	Isoform 3 of Plasminogen activator inhibitor 1 RNA-binding protein	4	1.2	0.68
P07437	TUBB	Tubulin beta chain	1	1.54	0.82
Q00577	PURA	Transcriptional activator protein Pur-alpha	1	1.14	0.89
P34931	HSPA1L	Heat shock 70 kDa protein 1-like	1	1.54	0.79
P48668	KRT6C	Keratin, type II cytoskeletal 6C	1	0.85	1.79
P13647	KRT5	Keratin, type II cytoskeletal 5	1	0.85	1.79
P02533	KRT14	Keratin, type I cytoskeletal 14	1	0.33	0.66
P08779	KRT16	Keratin, type I cytoskeletal 16	1	0.31	0.56
Q96KG9	SCYL1	Isoform 5 of N-terminal kinase-like protein	6	1.17	0.71
P62854	RPS26	40S ribosomal protein S26	1	1.04	0.73
P14618	PKM2	Pyruvate kinase isozymes M1/M2	1	0.67	0.82
P62263	RPS14	40S ribosomal protein S14	1	0.71	0
P46776	RPL27A	60S ribosomal protein L27a	1	1.07	0.71
P38646	HSPA9	Stress-70 protein, mitochondrial	1	1.17	1.27
Q6PKG0	LARP1	La-related protein 1	1	1.34	1.3
P50914	RPL14	60S ribosomal protein L14	1	0.87	0.47
Q96PU5	NEDD4L	Isoform 3 of E3 ubiquitin-protein ligase NEDD4-like	7	0.93	0.79
P62269	RPS18	40S ribosomal protein S18	1	0.97	0.5
P68371	TUBB4B	Tubulin beta-4B chain	1	1.7	0.88
P62280	RPS11	40S ribosomal protein S11	1	1.34	0.78
P46934	NEDD4	Isoform 4 of E3 ubiquitin-protein ligase NEDD4	1	0.94	0.72
Q16555	DPYSL2	Dihydropyrimidinase-related protein 2	1	1.3	1.29
P46782	RPS5	40S ribosomal protein S5	1	1.02	0.51
P16403	HIST1H1C	Histone H1.2	3	0.63	3.52
P62266	RPS23	40S ribosomal protein S23	1	1.12	0.53
P46937	YAP1	Isoform 3 of Yorkie homolog	3	0.8	0.72
P30048	PRDX3	Thioredoxin-dependent peroxide reductase, mitochondrial	1	0.98	1.19
Q9Y6M1	IGF2BP2	Isoform 2 of Insulin-like growth factor 2 mRNA-binding protein 2	2	1.36	1.48

P60866	RPS20	40S ribosomal protein S20	2	0.96	0.38
P39023	RPL3	60S ribosomal protein L3	1	1.28	0.45
P62277	RPS13	40S ribosomal protein S13	1	1.04	0.6
P63104	YWHAZ	14-3-3 protein zeta/delta	1	0.82	0.8
P34897	SHMT2	Serine hydroxymethyltransferase, mitochondrial	1	0.95	0.57
O75521	ECI2	Isoform 2 of Enoyl-CoA delta isomerase 2, mitochondrial	2	1.53	1.23
Q99733	NAP1L4	Nucleosome assembly protein 1-like 4	1	0.9	0.49
O43707	ACTN4	Alpha-actinin-4	1	1.03	1.33
P40926	MDH2	Malate dehydrogenase, mitochondrial	1	1.45	1.38
P08865	RPSA	40S ribosomal protein SA	1	0.99	0.7
P11021	HSPA5	78 kDa glucose-regulated protein	1	1.1	1.04
P62258	YWHAE	Isoform SV of 14-3-3 protein epsilon	2	0.9	0.83
Q02543	RPL18A	60S ribosomal protein L18a	1	1.16	0.51
P12814	ACTN1	Isoform 2 of Alpha-actinin-1	3	1.06	1.31
P00367	GLUD1	Glutamate dehydrogenase 1, mitochondrial	1	1.36	1.64
P26641	EEF1G	Elongation factor 1-gamma	1	1.01	0.56
P46783	RPS10	40S ribosomal protein S10	1	1.11	0.7
P62424	RPL7A	60S ribosomal protein L7a	1	1.14	0.89
P25398	RPS12	40S ribosomal protein S12	1	1.05	0.54
P14625	HSP90B1	Endoplasmin	1	0.73	0.8
P27348	YWHAQ	14-3-3 protein theta	1	0.82	0.76
P60842	EIF4A1	Eukaryotic initiation factor 4A-I	1	1.02	0.95
Q15366	PCBP2	Isoform 4 of Poly(rC)-binding protein 2	5	1.1	0.67
P19013	KRT4	Keratin, type II cytoskeletal 4	1	0.68	1.6
P84103	SRSF3	Serine/arginine-rich splicing factor 3	1	1.12	0.93
O00425	IGF2BP3	Insulin-like growth factor 2 mRNA-binding protein 3	1	1.51	1.66
P21980	TGM2	Protein-glutamine gamma-glutamyltransferase 2	1	0.83	1.15
P29401	TKT	Transketolase	1	0.86	0.98
P27635	RPL10	60S ribosomal protein L10	1	1.43	0.76

P07355	ANXA2	Annexin A2	2	0.95	0.87
P26373	RPL13	60S ribosomal protein L13	1	0.89	0.66
Q02878	RPL6	60S ribosomal protein L6	1	1.31	1.12
Q92598	HSPH1	Isoform Beta of Heat shock protein 105 kDa	3	1.22	0.61
P31946	YWHAB	Isoform Short of 14-3-3 protein beta/alpha	2	1.32	0.96
P04406	GAPDH	Glyceraldehyde-3-phosphate dehydrogenase	1	0.96	0.94
P46778	RPL21	60S ribosomal protein L21	1	1.85	0.78
Q15365	PCBP1	Poly(rC)-binding protein 1	1	0.88	0.66
Q92900	UPF1	Isoform 2 of Regulator of nonsense transcripts 1	2	1.32	1.16
P10155	TROVE2	60 kDa SS-A/Ro ribonucleoprotein	1	0.99	0.23
Q7KZF4	SND1	Staphylococcal nuclease domain-containing protein 1	1	1.03	0.62
Q13765	NACA	Nascent polypeptide-associated complex subunit alpha	1	0.65	0
Q07020	RPL18	60S ribosomal protein L18	1	0.99	1.37
Q9HCE1	MOV10	Putative helicase MOV-10	1	1.43	1.15
Q9BUJ2	HNRNPUL1	Isoform 4 of Heterogeneous nuclear ribonucleoprotein U-like protein 1	4	1.49	0.94
P05388	RPLP0	60S acidic ribosomal protein P0	1	1.04	1.63
P62829	RPL23	60S ribosomal protein L23	1	1.09	0.74
P07954	FH	Isoform Cytoplasmic of Fumarate hydratase, mitochondrial	2	0.55	0.54
P62847	RPS24	Isoform 2 of 40S ribosomal protein S24	3	1.69	0.71
P27824	CANX	Calnexin	1	0.49	0
Q13011	ECH1	Delta(3,5)-Delta(2,4)-dienoyl-CoA isomerase, mitochondrial	1	1.21	0.88
P06748	NPM1	Isoform 2 of Nucleophosmin	2	0.29	0.44
P84098	RPL19	60S ribosomal protein L19	1	1.64	1.22
P61604	HSPE1	10 kDa heat shock protein, mitochondrial	1	1.04	1.02
P09651	HNRNPA1	Isoform 2 of Heterogeneous nuclear ribonucleoprotein A1	4	1.26	0.53
P22314	UBA1	Ubiquitin-like modifier-activating enzyme 1	1	1.03	0.69
Q96QR8	PURB	Transcriptional activator protein Pur-beta	1	1.16	1.23
Q96HN2	AHCYL2	Isoform 2 of Putative adenosylhomocysteinase 3	5	1.04	0.9

P42766	RPL35	60S ribosomal protein L35	1	0.63	0.56
P62081	RPS7	40S ribosomal protein S7	1	1.02	0.54
P13639	EEF2	Elongation factor 2	1	1.02	0.57
P22626	HNRNPA2B1	Isoform A2 of Heterogeneous nuclear ribonucleoproteins A2/B1	2	1.27	0.39
P55072	VCP	Transitional endoplasmic reticulum ATPase	1	0.68	0.5
P61313	RPL15	60S ribosomal protein L15	1	1.08	1.04
Q2M2I8	AAK1	Isoform 2 of AP2-associated protein kinase 1	2	0.61	1
P62917	RPL8	60S ribosomal protein L8	1	1.17	1.31
P23528	CFL1	Cofilin-1	1	1.3	1.33
Q99729	HNRNPAB	Isoform 3 of Heterogeneous nuclear ribonucleoprotein A/B	2	1.09	0.74
P62899	RPL31	Isoform 3 of 60S ribosomal protein L31	3	1.39	0.93
P49207	RPL34	60S ribosomal protein L34	1	0.69	0.89
P62937	PPIA	Peptidyl-prolyl cis-trans isomerase A	1	0.99	0.58
P00505	GOT2	Aspartate aminotransferase, mitochondrial	1	0.92	1.08
P29692	EEF1D	Elongation factor 1-delta	2	0.93	0.83
Q14103	HNRNPD	Isoform 4 of Heterogeneous nuclear ribonucleoprotein D0	4	1.05	0.9
Q06830	PRDX1	Peroxiredoxin-1	1	0.85	0.74
Q14697	GANAB	Neutral alpha-glucosidase AB	2	0.96	1.12
P24752	ACAT1	Acetyl-CoA acetyltransferase, mitochondrial	1	1.01	1.3
P26038	MSN	Moesin	1	1.2	0.7
Q9ULV4	CORO1C	Coronin-1C	1	1.36	1
Q9Y262	EIF3L	Eukaryotic translation initiation factor 3 subunit L	1	1.28	1.13
P42704	LRPPRC	Leucine-rich PPR motif-containing protein, mitochondrial	1	1.38	1.14
P31943	HNRNPH1	Heterogeneous nuclear ribonucleoprotein H	1	1.49	1.08
P41091	EIF2S3	Eukaryotic translation initiation factor 2 subunit 3	1	1.18	1.48
P55884	EIF3B	Eukaryotic translation initiation factor 3 subunit B	2	1.82	1.6
Q86V81	ALYREF	THO complex subunit 4	1	0.77	0
P30050	RPL12	60S ribosomal protein L12	1	1.15	0.93
P26599	PTBP1	Polypyrimidine tract-binding protein 1	3	1.44	1.43

P18206	VCL	Isoform 1 of Vinculin	3	0.88	0.45
Q99623	PHB2	Prohibitin-2	1	1.06	0.61
P50552	VASP	Vasodilator-stimulated phosphoprotein	1	1.1	0.81
P05141	SLC25A5	ADP/ATP translocase 2	2	1.06	0.97
P61254	RPL26	60S ribosomal protein L26	2	1.2	0.82
P11177	PDHB	Isoform 2 of Pyruvate dehydrogenase E1 component subunit beta, mitochondrial	3	1.03	0.94
P0CW22	RPS17L	40S ribosomal protein S17-like	1	1.07	0.9
P46379	BAG6	Isoform 2 of Large proline-rich protein BAG6	3	1.75	0.97
P40429	RPL13A	60S ribosomal protein L13a	2	1.21	0.63
P62750	RPL23A	60S ribosomal protein L23a	1	0.6	0.7
Q13243	SRSF5	Isoform SRP40-4 of Serine/arginine-rich splicing factor 5	2	1.74	1.03
Q9NZB2	FAM120A	Isoform D of Constitutive coactivator of PPAR-gamma-like protein 1	3	1.92	2.96
Q14974	KPNB1	Importin subunit beta-1	1	1.21	0.95
Q8IVD9	NUDCD3	NudC domain-containing protein 3	1	1.09	0.93
O75369	FLNB	Isoform 6 of Filamin-B	6	0.93	0.56
P34932	HSPA4	Heat shock 70 kDa protein 4	1	1.03	0.7
Q9UN86	G3BP2	Isoform B of Ras GTPase-activating protein-binding protein 2	2	1.47	1.11
Q96RD7	PANX1	Isoform 2 of Pannexin-1	2	0.89	1.38
O14874	BCKDK	[3-methyl-2-oxobutanoate dehydrogenase [lipoamide]] kinase, mitochondrial	1	1.69	1.2
Q14694	USP10	Ubiquitin carboxyl-terminal hydrolase 10	3	1.02	0.83
P19474	TRIM21	E3 ubiquitin-protein ligase TRIM21	1	1.75	1.1
P22234	PAICS	Multifunctional protein ADE2	2	0.89	0
P20810	CAST	Isoform 3 of Calpastatin	7	0.76	0.72
P52597	HNRNPF	Heterogeneous nuclear ribonucleoprotein F	1	1.75	1.22
Q08211	DHX9	ATP-dependent RNA helicase A	1	1.7	0.69
Q13263	TRIM28	Isoform 2 of Transcription intermediary factor 1-beta	2	3.05	1.38
P09622	DLD	Dihydrolipoyl dehydrogenase, mitochondrial	1	1.04	0.91
P07910	HNRNPC	Isoform C1 of Heterogeneous nuclear ribonucleoproteins C1/C2	3	1.91	1.07

P12956	XRCC6	X-ray repair cross-complementing protein 6	1	1.17	0.2
P22681	CBL	E3 ubiquitin-protein ligase CBL	1	2.19	0
Q9P015	MRPL15	39S ribosomal protein L15, mitochondrial	1	1.26	1.15
P49411	TUFM	Elongation factor Tu, mitochondrial	1	1.37	1.39
P04181	OAT	Ornithine aminotransferase, mitochondrial	1	1.41	0.98
P48047	ATP5O	ATP synthase subunit O, mitochondrial	1	0.49	1.06
P26196	DDX6	Probable ATP-dependent RNA helicase DDX6	1	1.78	1.31
P46779	RPL28	60S ribosomal protein L28	2	1.95	1.12
Q92615	LARP4B	La-related protein 4B	1	1.38	1.73
Q12906	ILF3	Isoform 5 of Interleukin enhancer-binding factor 3	6	0.48	0.56
P06744	GPI	Glucose-6-phosphate isomerase	2	1.37	0.89
O00571	DDX3X	Isoform 2 of ATP-dependent RNA helicase DDX3X	2	1.17	0.85
P04075	ALDOA	Fructose-bisphosphate aldolase A	1	0	0
P18124	RPL7	60S ribosomal protein L7	1	0.52	0.65
P51398	DAP3	Isoform 2 of 28S ribosomal protein S29, mitochondrial	2	1.15	1.14
P05091	ALDH2	Aldehyde dehydrogenase, mitochondrial	1	1.55	1.85
P35232	PHB	Prohibitin	1	1.15	1.03
P01024	C3	Complement C3	1	0.73	0.52
P11586	MTHFD1	C-1-tetrahydrofolate synthase, cytoplasmic	1	1.12	0
Q9Y295	DRG1	Developmentally-regulated GTP-binding protein 1	1	1.25	0.67
Q96KK5	HIST1H2AH	Histone H2A type 1-H	10	0.97	3.2
P62841	RPS15	40S ribosomal protein S15	1	3.24	0.23
Q9C0C9	UBE2O	Ubiquitin-conjugating enzyme E2 O	1	1.57	0.74
P78371	CCT2	T-complex protein 1 subunit beta	1	0.52	0.58
Q14315	FLNC	Isoform 2 of Filamin-C	2	0.76	0.73
P05455	SSB	Lupus La protein	1	1.39	0.66
P30101	PDIA3	Protein disulfide-isomerase A3	1	1.08	0.67
Q04837	SSBP1	Single-stranded DNA-binding protein, mitochondrial	1	1.38	1.9
P40939	HADHA	Trifunctional enzyme subunit alpha, mitochondrial	1	0	1.34

P48382	RFX5	DNA-binding protein RFX5	1	1.35	2.41
Q6NYC8	PPP1R18	Phostensin	2	0	2.66
P04083	ANXA1	Annexin A1	1	1.44	1
Q9BSJ8	ESYT1	Extended synaptotagmin-1	2	1.43	0.96
O95793	STAU1	Isoform Short of Double-stranded RNA-binding protein Staufen homolog 1	3	1.37	0.87
P21399	ACO1	Cytoplasmic aconitate hydratase	1	0.77	0
P30837	ALDH1B1	Aldehyde dehydrogenase X, mitochondrial	1	1.13	1.39
P61289	PSME3	Proteasome activator complex subunit 3	2	1.48	1.49
P00338	LDHA	Isoform 5 of L-lactate dehydrogenase A chain	5	0.77	0.83
Q92552	MRPS27	28S ribosomal protein S27, mitochondrial	1	1.56	1.16
P41250	GARS	Glycine–tRNA ligase	1	1.63	1.27
P42677	RPS27	40S ribosomal protein S27	1	0.45	0
Q29960	HLA-C	Isoform 2 of HLA class I histocompatibility antigen, Cw-16 alpha chain	25	0	3.05
P23588	EIF4B	Eukaryotic translation initiation factor 4B	1	0.94	2.28
P31040	SDHA	Succinate dehydrogenase [ubiquinone] flavoprotein subunit, mitochondrial	1	1.1	1.07
Q71RC2	LARP4	Isoform 3 of La-related protein 4	3	1.37	1.78
Q9Y305	ACOT9	Isoform 3 of Acyl-coenzyme A thioesterase 9, mitochondrial	4	0	0
Q02218	OGDH	Isoform 2 of 2-oxoglutarate dehydrogenase, mitochondrial	2	0.96	2.23
P49406	MRPL19	39S ribosomal protein L19, mitochondrial	1	0.96	0
P22102	GART	Trifunctional purine biosynthetic protein adenosine-3	1	1.77	0.85
P36957	DLST	Dihydrolipoyllysine-residue succinyltransferase component of 2-oxoglutarate dehydrogenase complex, mitochondrial	1	0	3.67
Q8NBS9	TXNDC5	Thioredoxin domain-containing protein 5	1	0.9	0
P48200	IREB2	Iron-responsive element-binding protein 2	1	0.85	0.84
P08133	ANXA6	Annexin A6	1	0	1.36
Q8N5N7	MRPL50	39S ribosomal protein L50, mitochondrial	1	2.72	1.76
P48643	CCT5	T-complex protein 1 subunit epsilon	1	1.74	0.96
Q9NR30	DDX21	Isoform 2 of Nucleolar RNA helicase 2	2	1.65	0
Q14152	EIF3A	Eukaryotic translation initiation factor 3 subunit A	1	1.46	2.67

O00116	AGPS	Alkyldihydroxyacetonephosphate synthase, peroxisomal	1	1.12	0.97
P36873	PPP1CC	Serine/threonine-protein phosphatase PP1-gamma catalytic subunit	5	1.85	1.41
O43242	PSMD3	26S proteasome non-ATPase regulatory subunit 3	1	1.48	1.24
Q8NE71	ABCF1	Isoform 2 of ATP-binding cassette sub-family F member 1	2	0	0
P25787	PSMA2	Proteasome subunit alpha type-2	1	2.44	1.31
O75390	CS	Citrate synthase, mitochondrial	1	1.35	0.95
Q00610	CLTC	Isoform 2 of Clathrin heavy chain 1	2	0.88	1.26
Q9HC35	EML4	Echinoderm microtubule-associated protein-like 4	1	2514734.53	2814552.93
P10515	DLAT	Dihydrolipoyllysine-residue acetyltransferase component	1	1906005.72	2684224.72
		of pyruvate dehydrogenase complex, mitochondrial	1		
Q8TAA3	PSMA8	Isoform 2 of Proteasome subunit alpha type-7-like	4	1667597.05	1
P49720	PSMB3	Proteasome subunit beta type-3	1	1179805.13	1420907.99
Q6YN16	HSDL2	Hydroxysteroid dehydrogenase-like protein 2	1	1080817.55	1356826.78
P13010	XRCC5	X-ray repair cross-complementing protein 5	1	1041194.36	1
Q07065	CKAP4	Cytoskeleton-associated protein 4	1	918132.09	2320006.64
Q08999	RBL2	Retinoblastoma-like protein 2	1	592091.66	1677832.42
P07305	H1F0	Isoform 2 of Histone H1.0	2	1	3267102.48
Q92522	H1FX	Histone H1x	1	1	3064126.7
O60814	HIST1H2BK	Histone H2B type 1-K	15	1	3052111.41
P35579	MYH9	Myosin-9	1	1	2523520.26
Q7Z6Z7	HUWE1	Isoform 2 of E3 ubiquitin-protein ligase HUWE1	3	1	1859035.7
Q99798	ACO2	Aconitate hydratase, mitochondrial	1	1	1661822.24
P53396	ACLY	Isoform 2 of ATP-citrate synthase	2	1	638738.84

Proteins that interact with crosslinked YB-1 in MDA-MB231 cells.

Appendix F

FAM120A and TRIM28 and their importance to the survival of MDA-MB231 cells during cisplatin exposure.

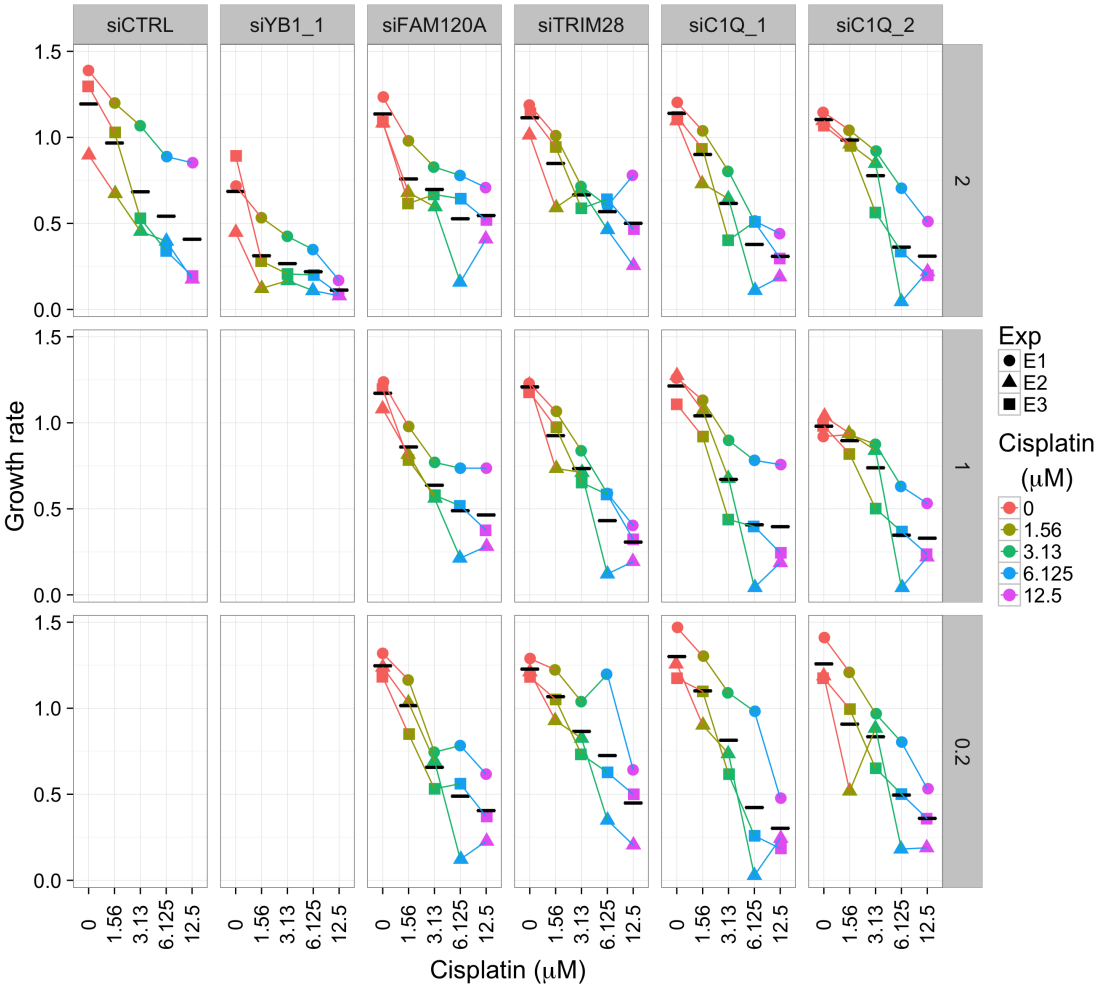

Figure F.1: The maximal growth rates from MDA-MB231 cells during 120 hours of exposure to cisplatin (1.56 - 25 μM; n = 3). MDA-MB231 cells were transfected with siCTRL, siYB1_1, siFAM120A, siTRIM28, siC1Q_1,and siC1Q_2 (0.2 - 5 nM) for 24 hours before the addition of media that contained cisplatin at the indicated concentrations.

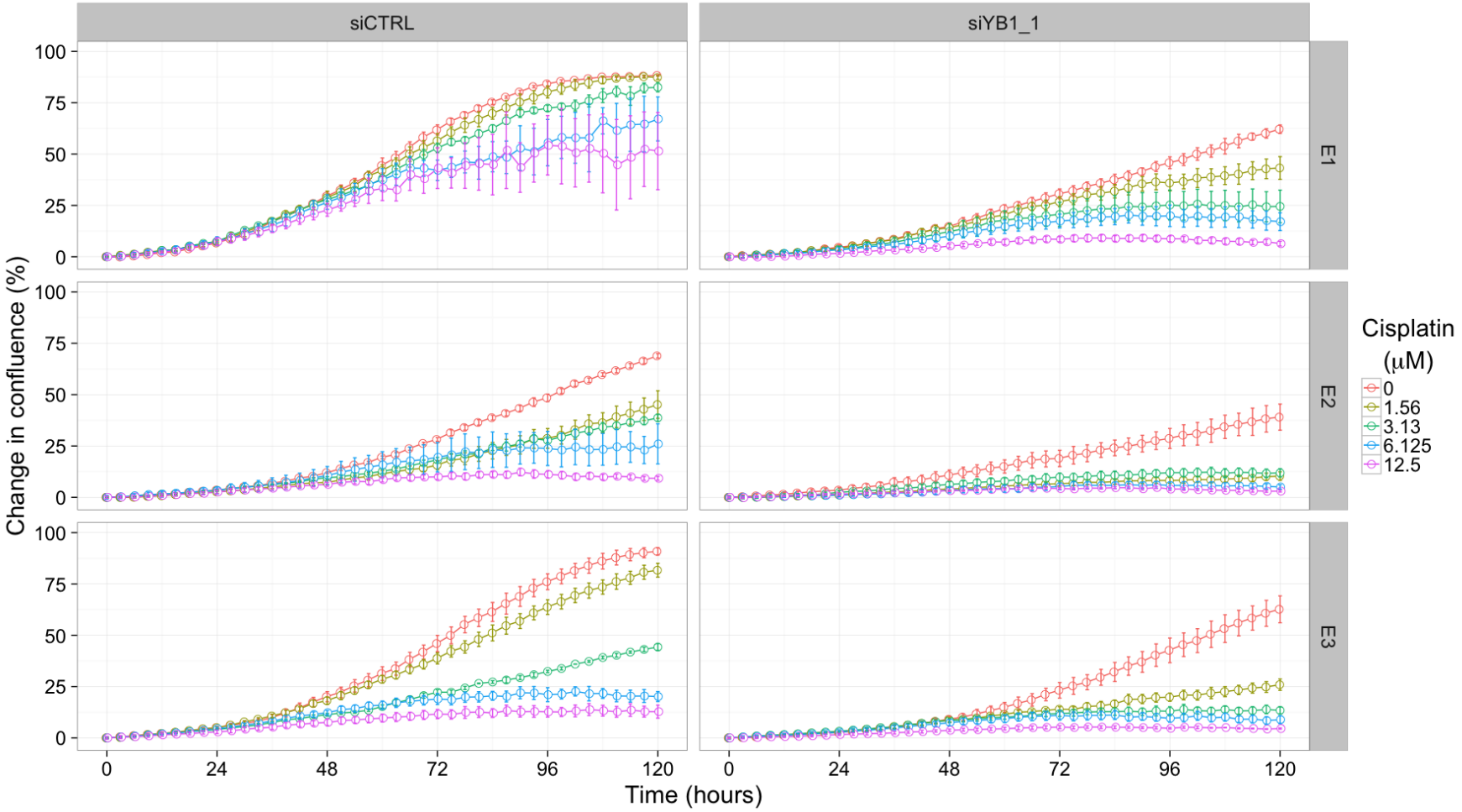

Figure F.2: Growth curves showing the average confluence of wells for all 2 nM siRNA duplexes, siCTRL, siYB1-1 during exposure to a range of cisplatin concentrations (1.56 - 25 μM). The growth plots from individual experiments are shown (n = 3).

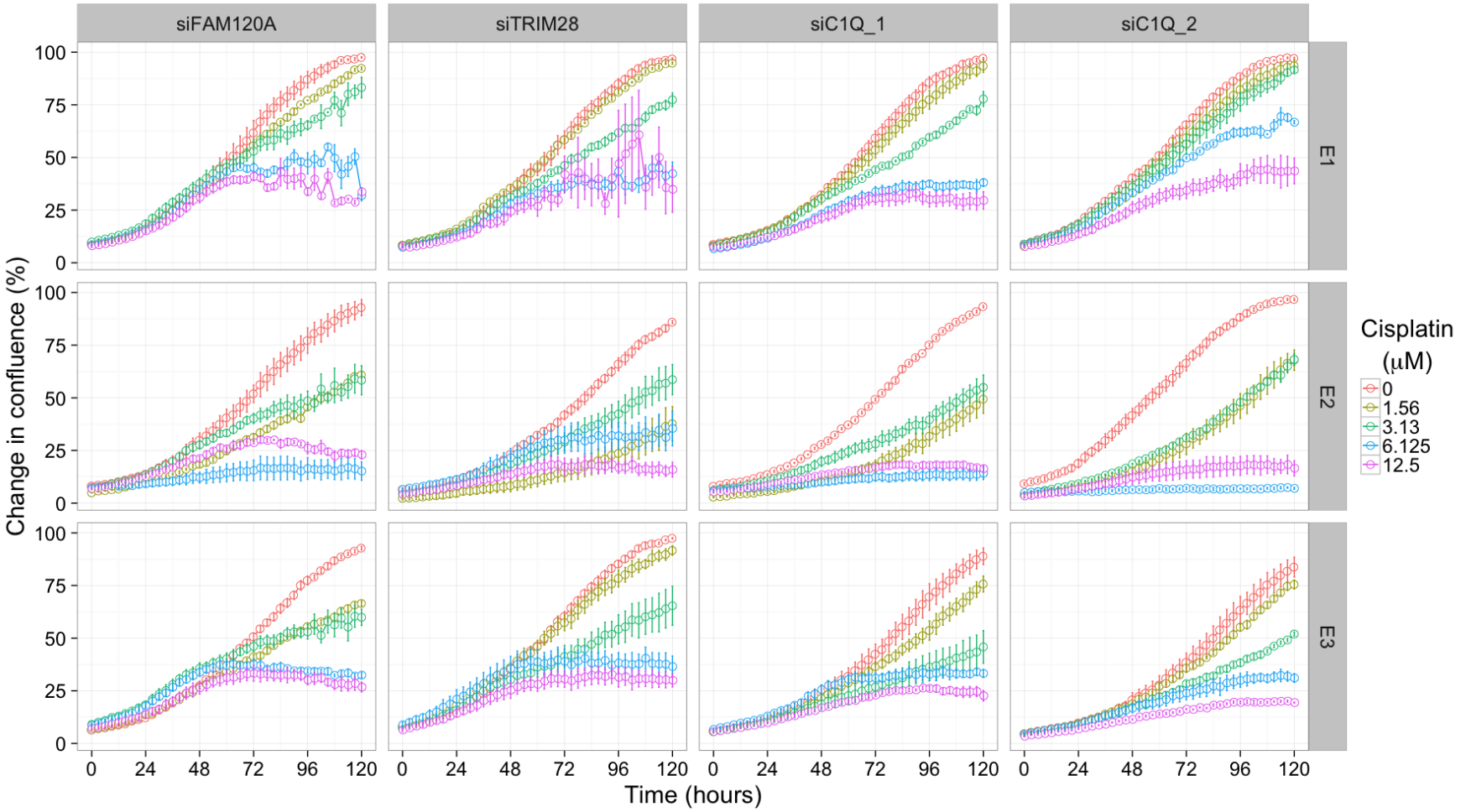

Figure F.3: Growth curves showing the average confluence of wells for all 2 nM siRNA duplexes, siCTRL, siYB1-1, and siYB1-2, during exposure to a range of cisplatin concentrations (1.56 - 12.5 μM). The variable measurements of confluence in wells that received siFAM120A and siTRIM28 after 72 hours of exposure to 12.5 μM cisplatin in E1 were the result of the cells dying the failure of image masking by the confluence algorithm (v1.5). The growth plots from individual experiments are shown (n = 3).

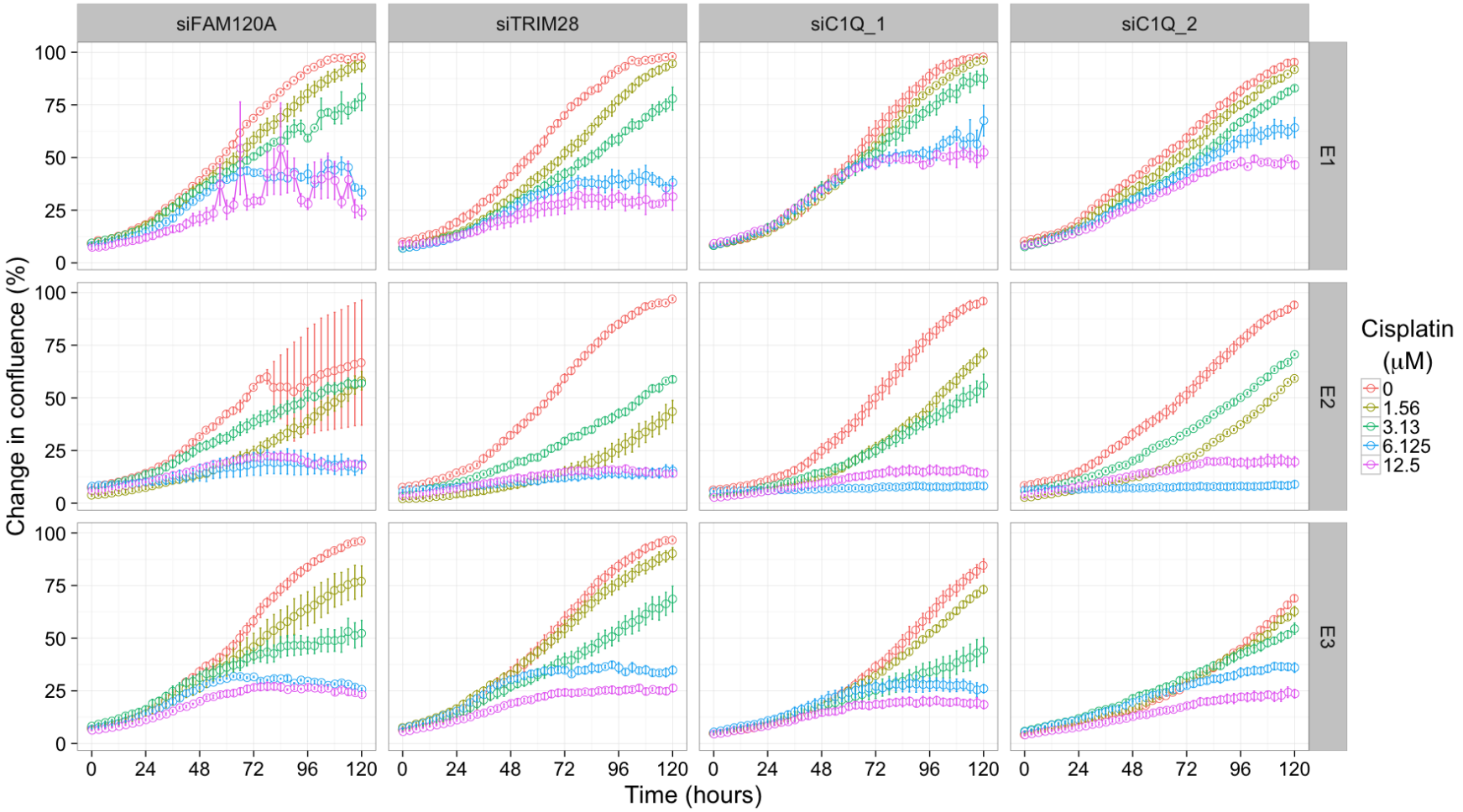

Figure F.4: Growth curves showing the average confluence of wells for all 1 nM siRNA duplexes, siCTRL, siYB1-1, and siYB1-2, during exposure to a range of cisplatin concentrations (1.56 - 12.5 μM). The variable measurements of confluence in wells that received siFAM120A after 72 hours of exposure to 12.5 μM cisplatin in E1 were the result of the cells dying the failure of image masking by the confluence algorithm (v1.5). The growth plots from individual experiments are shown (n = 3).

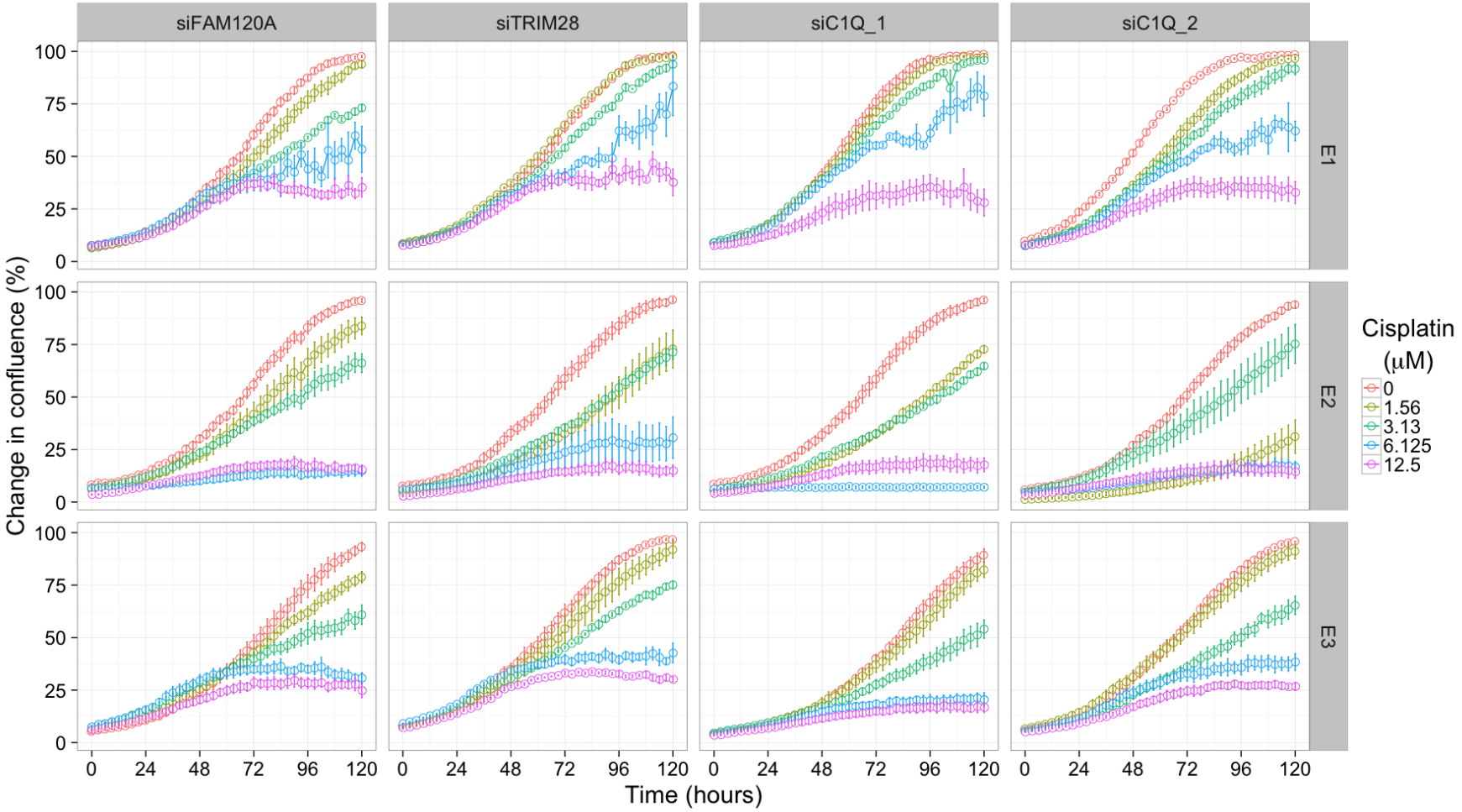

Figure F.5: Growth curves showing the average confluence of wells for all 0.2 nM siRNA duplexes, siC1q-1, siC1q-2, siFAM120A, siTRIM28, during exposure to a range of cisplatin concentrations (1.56 - 12.5 μM). The growth plots from individual experiments are shown (n = 3).